EXPLORATIONS OF HETEROCYCLES AND METAL COMPLEXES AS DRUG CANDIDATES AND INVESTIGATIONS OF LIGAND EFFECTS IN TITANIUM CATALYSIS

By

Zhilin Hou

A DISSERTATION

Submitted to
Michigan State University
in partial fulfillment of the requirements
for the degree of

Chemistry—Doctor of Philosophy

2022

ABSTRACT

EXPLORATIONS OF HETEROCYCLES AND METAL COMPLEXES AS DRUG CANDIDATES AND INVESTIGATIONS OF LIGAND EFFECTS IN TITANIUM CATALYSIS

By

Zhilin Hou

Titanium-catalyzed hydroamination and iminoamination reactions are valuable methods for one-pot syntheses of a variety of nitrogen-containing heterocycles. These synthetic methodologies have significantly shortened the steps to access complex heterocycles. Great potential for heterocycles synthesized by titanium catalysis in drug discovery was demonstrated by the two applications in NRF2 pathway inhibition (chapter 2) and proteasome inhibition (chapter 3). Studies on quantifying ligand effects in titanium catalysis have made great contributions to the improvement of reaction rate, selectivity, and catalyst stability. Computational estimation of ligand donor parameter (LDP) is presented using calculated bonding parameters (chapter 4). Finally, models of the ligand properties as a function of reaction rate are developed to predict catalyst performance and guide future catalyst design. A possible new mechanism with unsubstituted indolyl ligands is investigated. Collectively, these studies demonstrate the importance of titanium catalysis in drug discovery and a deeper understanding of ligand effects.

Copyright by ZHILIN HOU 2022 To my family and friends

ACKNOWLEDGEMENTS

With gratitude, I really want to thank many individuals who I got to meet during my Ph.D. journey. This work would not have been achieved without their guidance and contributions. I would like to begin by thanking my advisor, Aaron. I am beyond grateful to have you as my mentor. You taught me so much in the past five years, not only in chemistry but also the way to think about problems and find ways to solve them. I really appreciate the support and trust you have shown me. Seeing how you work and think about problems motivated me to become a better scientist in the past, and will keep doing so ever since.

I would like to thank all my committee members, Prof. Rob Maleczka, Prof. Kevin Walker, and Prof. Tom Hamann for your guidance in navigating my research. You have given me advice through my second-year seminar and candidacy exam. Many thanks to each committee member, who spent their time reading this dissertation and making corrections. Special thanks to Prof. McCusker for spending time to answer my questions before my seminar and listening to my defense.

I would like to thank my collaborators Prof. Karen Liby, Dr. Di Zhang, Chris Occhiuto, and Liz Lockwood. I really enjoyed working on the medicinal chemistry project and have learned so much about biology from all of you. I would like to thank Prof. Pro. Jetze Tepe and Allison Vanecek for their efforts in testing the bio-activities of ruthenium complexes.

I need to thank my labmates, Seokjoo Lee, Rashmi Jena, Lingqing Mo, and Hannah Barr. You brought so much joy to the lab. It was the conversations about chemistry and chats about everything else that made each failed experiment less frustrating and each successful experiment more enjoyable. I will our friendship could last beyond our time at grad school. Special thanks to

former group members, Dr. Tanner McDaniel, Dr. Brennan Billow, And Dr. Kelly Aldrich. Thank you for still taking the time to offer help even after your graduations. It helped me a lot.

In addition, I would like to thank Dr. Dan Holmes and Dr. Richard Staples for always being there to help with instruments and sharing your knowledge. Thank you for taking the time to listen to my complaints and giving me guidance and advice.

During my graduate studies, I was lucky to meet and make friends with some amazing people. They are there to support and motivate me. Thank you, Dr. Pei Chen, Dr. Daoyang Chen, Dr. Yuting Zhou, Dr. Katarina Keel, Dr. Li Zheng, Dr. Pepe Montero, Kunli Liu, Jiaqi Yao, Fangchun Liang, Mengxia Sun, Yijin Zhang, Amaya Hewage, Ankush Chakraborty, Emmanuel Maloba, Jurick Lahiri, Grace Hubbell, Samantha Houchlei, and TJ Delano.

Finally, I want to thank my parents. Nothing that I have achieved would have been possible without them. They have made a huge sacrifice for letting me achieve my dreams. There is nothing more than the love and support they have shown to encourage me to pursue research as my career. Thank you.

TABLE OF CONTENTS

| LIST OF TABLES | x |
|--|---------|
| LIST OF FIGURES | xi |
| LIST OF SCHEMES | xxiii |
| KEY TO SYMBOLS AND ABBREVIATIONS | XXV |
| CHAPTER 1 INTRODUCTION: TITANIUM-CATALYZED REACTIONS IN | ONE-POT |
| HETEROCYCLIC SYNTHESIS | 1 |
| 1.1 Background | 1 |
| 1.2 Titanium Catalysis in Hydroamination Derived Heterocycle Synthesis | |
| 1.2.1 Intermolecular Hydroamination | |
| 1.2.2 Hydroamination Derived Pyrrolidine Synthesis | |
| 1.2.3 Hydroamination Derived Pyridine Synthesis | |
| 1.3 The Titanium-Catalyzed Multicomponent Coupling Reaction: Iminoamination | 5 |
| 1.4 Titanium Iminoamination in Heterocycle Synthesis | |
| 1.4.1 Type I Products: Pyrazoles, Pyrimidines, and Isoxazoles | |
| 1.4.2 Type II Products: Pyridines and Quinolines | |
| 1.5 Applications and Improvements of Titanium Catalysis by Odom Group | 12 |
| 1.5.1 Substituted Pyridines as NRF2 Pathway Inhibitors | |
| 1.5.2 Substituted Quinolines as Noncovalent Proteasome Inhibitors | 14 |
| 1.5.3 Ligand Effects Modeling in Titanium Catalysis | |
| 1.6 Conclusions | 17 |
| REFERENCES | 18 |
| CHAPTER 2 SYNTHESIS OF SUBSTITUTED PYRIDINES AS NOVEL NRF2 IN | |
| 2.1 Introduction | |
| 2.2 Exploration of Structure-Activity Relationships in MSU382225 Derivatives | |
| 2.2.1 Analog Preparation via Titanium Catalysis | |
| 2.2.2 Analog Preparation via Modification of MSU38225 | |
| 2.2.3 Analog Preparation Incorporating Heterocycles | |
| 2.2.3.1 Installation of Heterocycles on 5-position | |
| 2.2.3.2 Installation of Heterocycles on Amino Group | |
| 2.2.4 Analog Preparation with Core Change | |
| 2.2.4.1 Pyrazine Derivatives | |
| 2.2.4.2 Quinoline and 1,8-naphthyridine Derivatives | |
| 2.2.5 Future Analog Proposals | |
| 2.3 Compounds for Target Identification | |
| 2.3.1 Biotinylation and SAR Analysis | |

| 2.3.2 Synthesis of Biotinylated Compounds | 40 |
|--|--------|
| 2.3.3 Synthesis of Compounds for "Click Chemistry" | |
| 2.4 Improvement of Drug-like Properties | |
| 2.4.1 Solubility | |
| 2.4.2 Metabolic Stability | |
| 2.5 Intramolecular Cyclization Process of ZH-III-71 | |
| 2.6 Conclusions | |
| 2.7 Experimental details. | 50 |
| REFERENCES | 98 |
| CHAPTER 3 SYNTHESIS OF SUBSTITUTED QUINOLINE RUTHENIUM COMI | PLEXES |
| | |
| 3.1 Introduction | |
| 3.2 Synthesis of RuCp ⁺ Complexes | |
| 3.3 Structures and Stabilities of RuCp ⁺ Complexes | |
| 3.4 Biological Activities of RuCp ⁺ Complexes | 112 |
| 3.5 Conclusions | |
| 3.6 Experimental Details | |
| REFERENCES | 131 |
| CHAPTER 4 COMPUTATIONAL ESTIMATION OF LIGAND DONOR PARAMETE | DC 125 |
| 4.1 Introduction | |
| 4.1.1 Electronic Parameterization for Low Oxidation State Late Transition Metals | |
| 4.1.1 Electronic Parameterization for Low Oxidation State Late Transition Metals | |
| 4.1.2 Computational Probes of LDP values | |
| 4.2.1 Bond Distance of Ti–F bonds in XTiF ₃ | |
| 4.2.2 Covalent Bond Order (CBO) Index | |
| 4.2.3 Proton affinity (PA) | |
| 4.2.4 Bond Dissociation Energy (BDE) | |
| 4.2.4 Bolid Dissociation Energy (BDE). | |
| 4.4 Computational Details | |
| REFERENCES | |
| REFERENCES | 100 |
| CHAPTER 5 MODELING COMPLEX LIGANDS FOR TITANIUM-CATA | LYZED |
| HYDROAMINATION | 163 |
| 5.1 Introduction | 163 |
| 5.2 Synthesis of Unsymmetrical Ligands and Titanium Catalysts | 166 |
| 5.3 Modeling Reaction Rate as A Function of Ancillary Ligand Structure | 171 |
| 5.4 Investigation of Indolyl Effect | |
| 5.5 Conclusions | |
| 5.7 Future Work | 186 |
| 5.7 Experimental Details | 187 |
| APPENDICES | 214 |
| APPENDIX A: NMR Spectra (Pyridines) | 215 |
| APPENDIX B: NMR Spectra (Ruthenium Complexes) | |
| APPENDIX C: NMR Spectra (Unsymmetrical Ligands and Titanium Catalysts) | |

| REFERENCES | ~ ~ | ` - | - |
|----------------------|-------|-----|---|
| D 1/1/1/D 1/N/C 1/30 | .,, | 1 | 1 |
| | | | |
| NLI LINLI VCLO | • • • | , | / |

LIST OF TABLES

| Table 2.1. Compounds prepared using titanium-catalyzed one-pot synthesis and their NRF2 activities |
|---|
| Table 2.2. Compounds prepared using titanium-catalyzed one-pot synthesis and their NRF2 activities |
| Table 2.3. Compounds prepared using two-step synthesis and their NRF2 activities33 |
| Table 2.4. Compounds prepared using Buchwald-Hartwig coupling and their NRF2 activities35 |
| Table 2.5. Equilibrium constants and rate constants of cyclization process in different solvents.48 |
| Table 2.6. Energy difference of 5i-o compared to 5i-c from DFT calculation and experiments49 |
| Table 3.1. Comparison of C–C bond distances (Å) in uncoordinated quinoline (Quin1) and in $\eta^6(C_6)$ -complexes $\{Ru(Quin1)Cp\}^+(1)$ |
| Table 3.2. Proteasome inhibition activities for each catalytic site |
| Table 3.3. Cytotoxicity for MC/CAR and RPMI 8226 cell lines |
| Table 4.1. Calculated CBO index with different functionals and basis sets |
| Table 4.2. Comparison of CBO with NRT covalent character using B3PW91 and SDD144 |
| Table 5.1. A library of titanium catalysts with the electronic and steric parameters of the ligands |
| Table 5.2. Rate constants of catalysts and proton affinity with different indole substituents182 |

LIST OF FIGURES

| Figure 1.1. The number of drugs approved by the U.S. FDA in different categories1 |
|---|
| Figure 1.2. Titanium-catalyzed intermolecular hydroamination and proposed Bergman mechanism X ₂ represents one dianionic or two monoanionic ligand(s) |
| Figure 1.3. Examples of titanium catalysts for iminoamination reactions6 |
| Figure 1.4. The titanium-catalyzed multicomponent coupling reaction and proposed imino-amination mechanism, where X_2 represents one dianionic or two monoanionic ligand(s)7 |
| Figure 1.5. Two categories of cyclization of iminoamination products |
| Figure 1.6. Pyrazole synthesis through titanium catalysis |
| Figure 1.7. Pyrimidine and isoxazole synthesis through titanium catalysis |
| Figure 1.8. A summary of heterocycle synthesis using titanium catalysis |
| Figure 1.9. Chromium complex used for the measurement of LDP |
| Figure 1.10. An example of a titanium catalyst and its electronic and steric reporters16 |
| Figure 2.1. NRF2 pathway in normal cells and disrupted NRF2 pathway in certain cancer cells |
| Figure 2.2. The structure of MSU38228 and luciferase assay results after the treatment of MSU38225 with different concentrations by MCF-7 reporter cells stimulated with 20 mmol/L tBHQ |
| Figure 2.3. A xenograft model using A549 cells. Tumors were measured twice a week using a caliper. N = 6 mice/group |
| Figure 2.4. Four different categories on explore SAR |
| Figure 2.5. Strategy to use biotinylation to identify the target |
| Figure 2.6. Summary of structure-activity relationship |
| Figure 2.7. Synthesis of the biotinylated compound |
| Figure 2.8. Analogs with the addition of hetero atoms and their ClogP values43 |

| Figure 2.9. Analogs with decent activities, their ClogP values, and kinetic solubility data44 |
|---|
| Figure 2.10. Analogs with good activities and their microsome stability data45 |
| Figure 2.11. Additional analogs with good activities and their microsome stability data45 |
| Figure 2.12. A picture of the NMR solution of MSU38225 and 5i |
| Figure 2.13. Proposed mechanism of intramolecular cyclization and a crystal structure of the cyclized product. Hydrogens in calculated positions, a second chemically equivalent molecule in the asymmetric unit and CH ₂ Cl ₂ of crystallization are omitted |
| Figure 2.14. Concentration of A (blue dots) and B (red dots) as a function of time in DMSO-d6. Internal standard (ferrocene) was omitted for clarification |
| Figure 2.15. Concentration of A (blue dots) and B (red dots) as a function of time in CDCl ₃ . Internal standard (ferrocene) was omitted for clarification |
| Figure 2.16. Concentration of A (blue dots) and B (red dots) as a function of time in toluene-d8. Internal standard (ferrocene) was omitted for clarification |
| Figure 3.1. Metal-based anti-cancer drugs: cisplatin and carboplatin |
| Figure 3.2. Crystal structure of complex 1. The counter ion PF ₆ -, a molecule of DCM, and hydrogens are emitted for clarity |
| Figure 3.3. Structures of carbocyclic ring and heterocyclic ring bonded ruthenium complexes for DFT calculations. |
| Figure 3.4. Stability of complex 1 and 2 in different coordinating solvents |
| Figure 3.5. From bottom to top, ¹ H NMR of complex 1 with 1.0 equivalent of reduced glutathione in 10% DMSO/D ₂ O after 0, 24, 48, and 72 hours |
| Figure 3.6. Kinetic displacement of quinoline in MeCN-d ₃ on complex 1. The concentration vs. time data are fit to $Y_t = Y_{\infty} + (Y_0 - Y_{\infty})e^{-k_{obs}t}$, where $Y_t = \text{conc.}$ at time t , $Y_0 = \text{conc.}$ at the start of the reaction, $Y_{\infty} = \text{conc.}$ at very long times, and k_{obs} is the observed pseudo-first order rate constant in s ⁻¹ . |
| Figure 3.7. Kinetic displacement of quinoline in DMSO -d ₆ on complex 2. The concentration vs. time data are fit to $Y_t = Y_{\infty} + (Y_0 - Y_{\infty})e^{-k_{obs}t}$, where $Y_t = \text{conc.}$ at time t , $Y_0 = \text{conc.}$ at the start of the reaction, $Y_{\infty} = \text{conc.}$ at very long times, and k_{obs} is the observed pseudo-first order rate constant in s ⁻¹ . |
| Figure 3.8. From bottom to top, ¹ H NMR of 1 in 10% DMSO-d ₆ /D ₂ O after 0 hours, 24 hours, 48 hours, and 72 h |

| Figure 3.9. From bottom to top, ¹ H NMR of 1 in DMSO-d ₆ after 0 hours, 48 hours, and 72 h 125 |
|---|
| Figure 3.10. From bottom to top, ¹ H NMR of 2 in 10% DMSO-d ₆ /D ₂ O after 0, 24, 48, and 72 hours |
| Figure 3.11. From bottom to top, ¹ H NMR of 1 with 1.0 equiv reduced glutathione in 10% DMSO/D ₂ O after 0 hours, 24 hours, 48 hours, and 72 h |
| Figure 3.12 From bottom to top, ¹ H NMR of 1 with 10.0 equiv reduced glutathione in 10% DMSO/D ₂ O after 0 hours, 24 hours, 48 hours, and 72 h |
| Figure 3.13. ¹ H NMR {RuCp(NCMe) ₃ } ⁺ PF ₆ ⁻ after dissolved in DMSO-d ₆ at different time (Y axis) |
| Figure 3.14. From bottom to top, ¹ H NMR of {RuCp(NCMe) ₃ } ⁺ PF ₆ ⁻ in 10% DMSO-d ₆ /D ₂ O after 0 hours and 72 h |
| Figure 4.1. A nickel complex as an electronic reporter for ligand L |
| Figure 4.2. A chromium complex as a LDP reporter for ligand X |
| Figure 4.3. A sample of LDP values from commonly used ligands |
| Figure 4.4. A plot of average Ti-F distance (Å) in XTiF ₃ complexes versus LDP (kcal/mol)140 |
| Figure 4.5. Plot of the Covalent Bond Order (CBO) calculated using Eq 1 from the electron density found using B3PW91 with def2-SVP and NBO7 versus the Ligand Donor Parameter (LDP)143 |
| Figure 4.6. LDP (kcal/mol) versus proton affinity (PA, kcal/mol) for MeNTiX2 calculated using B3PW91 with def2-SVP145 |
| Figure 4.7. Plot of LDP (kcal/mol) versus BDE (kcal/mol) for imide bond cleavage in HN=TiX ₂ . The BDEs shown were calculated using def2-TZVP/M06-2X |
| Figure 4.8. Correlation of LDP and bond length of Ti=N in MeNTiX2 using B3PW91 with def2-SVP |
| Figure 4.9. Correlation of LDP and proton affinity of MeNTiX2 using B3PW91 with def2-TZVPP. |
| Figure 4.10. Correlation of LDP and proton affinity of MeNTiX2 using M06L with def2-TZVPP |
| Figure 5.1. An example of titanium catalyst and its electronic and steric reporter, NCr(NiPr ₂) ₂ (pyr). |

| Figure 5.2. Titanium-catalyzed hydroamination reaction and a library of catalysts | 165 |
|--|------------------|
| Figure 5.3. Two routes to access unsymmetrical ligands | 167 |
| Figure 5.4. Crystal structures of titanium catalysts, 6d and 5b | 170 |
| Figure 5.5. A representative plot with a fit of the kinetics. The loss of alkyne was monitored by NMR using ferrocene as an internal standard | |
| Figure 5.6. The rate constant of example catalysts with symmetrical or unsymmetrical liga | |
| Figure 5.7. A side assignment example with titanium catalyst, 6b. The fragment with a larger L value was assigned to side 1 | |
| Figure 5.8. The plot of k_{obs} vs k_{calc} for catalysts used in the model (black dots). The blue square from catalysts with 3-unsubstituted indole fragments | |
| Figure 5.9. A proposed mechanism with a 5-coordinate titanium species in the transition statement before the Ti–C protonolysis | |
| Figure 5.10. Pictures of the reaction mixture catalyzed by 7c and 7b after hydroamination | 181 |
| Figure 5.11. ² H NMR spectrum of the deuterated ligand from catalyst 5b with aniline-d ₈ . Peak 6.11, 6.17, and 6.28 ppm are from the ligand. Peaks at 6.4, 6.5, and 7.1 ppm are from aniline | e-d ₈ |
| Figure 5.12. ¹ H NMR of the protonated ligand from a reaction between 6b and aniline | 209 |
| Figure 5.13. ¹ H NMR of the deuterated ligand from a reaction between 6b and aniline-d ₈ | 210 |
| Figure 5.14. ¹ H NMR of the deuterated ligand from a reaction between 6b and aniline-d ₈ (exce | |
| Figure 5.15. ² H NMR of the deuterated ligand from a reaction between 6b and aniline-d ₈ | 212 |
| Figure 5.16. ¹ H NMR of the H ₂ dpm ligand from a reaction between Ti(dpm)(NMe ₂) ₂ and MeO d ₄ | |
| Figure 5.17. ¹ H NMR (CDCl ₃ , 500 MHz, 25 °C) | 216 |
| Figure 5.18. ¹³ C NMR (CDCl ₃ , 126 MHz, 25 °C) | 217 |
| Figure 5.19. ¹ H NMR (CDCl ₃ , 500 MHz, 25 °C) | 218 |
| Figure 5.20. ¹³ C NMR (CDCl ₃ , 126 MHz, 25 °C) | 219 |

| Figure 5.21. ¹ H NMR (CDCl ₃ , 500 MHz, 25 °C) | 220 |
|---|-----|
| Figure 5.22. ¹³ C NMR (CDCl ₃ , 126 MHz, 25 °C) | 221 |
| Figure 5.23. ¹ H NMR (CDCl ₃ , 500 MHz, 25 °C) | 222 |
| Figure 5.24. ¹³ C NMR (CDCl ₃ , 126 MHz, 25 °C) | 223 |
| Figure 5.25. ¹ H NMR (CDCl ₃ , 500 MHz, 25 °C) | 224 |
| Figure 5.26. ¹ H NMR (500 MHz, DMSO-d ₆ , 25 °C) | 225 |
| Figure 5.27. ¹³ C NMR (DMSO-d ₆ , 126 MHz, 25 °C) | 226 |
| Figure 5.28. ¹ H NMR (CDCl ₃ , 500 MHz, 25 °C) | 227 |
| Figure 5.29. ¹³ C NMR (CDCl ₃ , 126 MHz, 25 °C) | 228 |
| Figure 5.30. ¹ H NMR (CDCl ₃ , 500 MHz, 25 °C) | 229 |
| Figure 5.31. ¹³ C NMR (CDCl ₃ , 126 MHz, 25 °C) | 230 |
| Figure 5.32. ¹ H NMR (CDCl ₃ , 500 MHz, 25 °C) | 231 |
| Figure 5.33. ¹³ C NMR (CDCl ₃ , 126 MHz, 25 °C) | 232 |
| Figure 5.34. ¹ H NMR (CDCl ₃ , 500 MHz, 25 °C) | 233 |
| Figure 5.35. ¹³ C NMR (CDCl ₃ , 126 MHz, 25 °C) | 234 |
| Figure 5.36. ¹ H NMR (CDCl ₃ , 500 MHz, 25 °C) | 235 |
| Figure 5.37. ¹³ C NMR (CDCl ₃ , 126 MHz, 25 °C) | 236 |
| Figure 5.38. ¹ H NMR (CDCl ₃ , 500 MHz, 25 °C) | 237 |
| Figure 5.39. ¹³ C NMR (CDCl ₃ , 126 MHz, 25 °C) | 238 |
| Figure 5.40. ¹ H NMR (CDCl ₃ , 500 MHz, 25 °C) | 239 |
| Figure 5.41. ¹³ C NMR (CDCl ₃ , 126 MHz, 25 °C) | 240 |
| Figure 5.42. ¹ H NMR (CDCl ₃ , 500 MHz, 25 °C) | 241 |
| Figure 5.43. ¹³ C NMR (CDCl ₃ , 126 MHz, 25 °C) | 242 |

| Figure 5.44. ¹ H NMR (CDCl ₃ , 500 MHz, 25 °C) | 243 |
|---|-----|
| Figure 5.45. ¹³ C NMR (CDCl ₃ , 126 MHz, 25 °C) | 244 |
| Figure 5.46. ¹ H NMR (CDCl ₃ , 500 MHz, 25 °C) | 245 |
| Figure 5.47. ¹³ C NMR (CDCl ₃ , 126 MHz, 25 °C) | 246 |
| Figure 5.48. ¹ H NMR (CDCl ₃ , 500 MHz, 25 °C) | 247 |
| Figure 5.49. ¹³ C NMR (CDCl ₃ , 126 MHz, 25 °C) | 248 |
| Figure 5.50. ¹ H NMR (CDCl ₃ , 500 MHz, 25 °C) | 249 |
| Figure 5.51. ¹³ C NMR (CDCl ₃ , 126 MHz, 25 °C) | 250 |
| Figure 5.52. ¹ H NMR (CDCl ₃ , 500 MHz, 25 °C) | 251 |
| Figure 5.53. ¹³ C NMR (CDCl ₃ , 126 MHz, 25 °C) | 252 |
| Figure 5.54. ¹ H NMR (CDCl ₃ , 500 MHz, 25 °C) | 253 |
| Figure 5.55. ¹³ C NMR (CDCl ₃ , 126 MHz, 25 °C) | 254 |
| Figure 5.56. ¹ H NMR (CDCl ₃ , 500 MHz, 25 °C) | 255 |
| Figure 5.57. ¹³ C NMR (CDCl ₃ , 126 MHz, 25 °C) | 256 |
| Figure 5.58. ¹ H NMR (CDCl ₃ , 500 MHz, 25 °C) | 257 |
| Figure 5.59. ¹³ C NMR (CDCl ₃ , 126 MHz, 25 °C) | 258 |
| Figure 5.60. ¹ H NMR (CDCl ₃ , 500 MHz, 25 °C) | 259 |
| Figure 5.61. ¹ H NMR (CDCl ₃ , 500 MHz, 25 °C) | 260 |
| Figure 5.62. ¹ H NMR (CDCl ₃ , 500 MHz, 25 °C) | 261 |
| Figure 5.63. ¹³ C NMR (CDCl ₃ , 126 MHz, 25 °C) | 262 |
| Figure 5.64. ¹ H NMR (CDCl ₃ , 500 MHz, 25 °C) | 263 |
| Figure 5.65. ¹³ C NMR (CDCl ₃ , 126 MHz, 25 °C) | 264 |
| Figure 5.66. ¹ H NMR (CDCl ₃ , 500 MHz, 25 °C) | 265 |

| Figure 5.67. ¹³ C NMR (CDCl ₃ , 126 MHz, 25 °C) | 266 |
|---|-----|
| Figure 5.68. ¹ H NMR (CDCl ₃ , 500 MHz, 25 °C) | 267 |
| Figure 5.69. ¹³ C NMR (CDCl ₃ , 126 MHz, 25 °C) | 268 |
| Figure 5.70. ¹ H NMR (CDCl ₃ , 500 MHz, 25 °C) | 269 |
| Figure 5.71. ¹³ C NMR (CDCl ₃ , 126 MHz, 25 °C) | 270 |
| Figure 5.72. ¹ H NMR (CDCl ₃ , 500 MHz, 25 °C) | 271 |
| Figure 5.73. ¹³ C NMR (CDCl ₃ , 126 MHz, 25 °C) | 272 |
| Figure 5.74. ¹ H NMR (CDCl ₃ , 500 MHz, 25 °C) | 273 |
| Figure 5.75. ¹³ C NMR (CDCl ₃ , 126 MHz, 25 °C) | 274 |
| Figure 5.76. ¹ H NMR (CDCl ₃ , 500 MHz, 25 °C) | 275 |
| Figure 5.77. ¹³ C NMR (CDCl ₃ , 126 MHz, 25 °C) | 276 |
| Figure 5.78. ¹ H NMR (CDCl ₃ , 500 MHz, 25 °C) | 277 |
| Figure 5.79. ¹³ C NMR (CDCl ₃ , 126 MHz, 25 °C) | 278 |
| Figure 5.80. ¹ H NMR (CDCl ₃ , 500 MHz, 25 °C) | 279 |
| Figure 5.81. ¹³ C NMR (CDCl ₃ , 126 MHz, 25 °C) | 280 |
| Figure 5.82. ¹ H NMR (CDCl ₃ , 500 MHz, 25 °C) | 281 |
| Figure 5.83. ¹³ C NMR (CDCl ₃ , 126 MHz, 25 °C) | 282 |
| Figure 5.84. ¹ H NMR (CDCl ₃ , 500 MHz, 25 °C) | 283 |
| Figure 5.85. ¹³ C NMR (CDCl ₃ , 126 MHz, 25 °C) | 284 |
| Figure 5.86. ¹ H NMR (CDCl ₃ , 500 MHz, 25 °C) | 285 |
| Figure 5.87. ¹³ C NMR (CDCl ₃ , 126 MHz, 25 °C) | 286 |
| Figure 5.88. ¹ H NMR (CDCl ₃ , 500 MHz, 25 °C) | 287 |
| Figure 5.89. ¹³ C NMR (CDCl ₃ , 126 MHz, 25 °C) | 288 |

| Figure 5.90. ¹ H NMR (CDCl ₃ , 500 MHz, 25 °C) | 289 |
|---|-----|
| Figure 5.91. ¹³ C NMR (CDCl ₃ , 126 MHz, 25 °C) | 290 |
| Figure 5.92. ¹ H NMR (CDCl ₃ , 500 MHz, 25 °C) | 291 |
| Figure 5.93. ¹³ C NMR (CDCl ₃ , 126 MHz, 25 °C) | 292 |
| Figure 5.94. ¹ H NMR (CDCl ₃ , 500 MHz, 25 °C) | 293 |
| Figure 5.95. ¹³ C NMR (CDCl ₃ , 126 MHz, 25 °C) | 294 |
| Figure 5.96. ¹ H NMR (CDCl ₃ , 500 MHz, 25 °C) | 295 |
| Figure 5.97. ¹³ C NMR (CDCl ₃ , 126 MHz, 25 °C) | 296 |
| Figure 5.98. ¹ H NMR (CDCl ₃ , 500 MHz, 25 °C) | 297 |
| Figure 5.99. ¹³ C NMR (CDCl ₃ , 126 MHz, 25 °C) | 298 |
| Figure 5.100. ¹ H NMR (CDCl ₃ , 500 MHz, 25 °C) | 299 |
| Figure 5.101. ¹³ C NMR (CDCl ₃ , 126 MHz, 25 °C) | 300 |
| Figure 5.102. ¹ H NMR (CDCl ₃ , 500 MHz, 25 °C) | 301 |
| Figure 5.103. ¹³ C NMR (CDCl ₃ , 126 MHz, 25 °C) | 302 |
| Figure 5.104. ¹ H NMR (CDCl ₃ , 500 MHz, 25 °C) | 303 |
| Figure 5.105. ¹³ C NMR (CDCl ₃ , 126 MHz, 25 °C) | 304 |
| Figure 5.106. ¹ H NMR (CDCl ₃ , 500 MHz, 25 °C) | 305 |
| Figure 5.107. ¹³ C NMR (CDCl ₃ , 126 MHz, 25 °C) | 306 |
| Figure 5.108. ¹ H NMR (500 MHz, DMSO-d ₆ , 25 °C) | 307 |
| Figure 5.109. ¹ H NMR (CDCl ₃ , 500 MHz, 25 °C) | 308 |
| Figure 5.110. ¹ H NMR (CDCl ₃ , 500 MHz, 25 °C) | 309 |
| Figure 5.111. ¹³ C NMR (CDCl ₃ , 126 MHz, 25 °C) | 310 |
| Figure 5.112. ¹ H NMR (CDCl ₃ , 500 MHz, 25 °C) | 311 |

| Figure 5.113. ¹³ C NMR (CDCl ₃ , 126 MHz, 25 °C) | 312 |
|--|-----|
| Figure 5.114. ¹ H NMR (CDCl ₃ , 500 MHz, 25 °C) | 313 |
| Figure 5.115. ¹³ C NMR (CDCl ₃ , 126 MHz, 25 °C) | 314 |
| Figure 5.116. ¹ H NMR (CDCl ₃ , 500 MHz, 25 °C) | 316 |
| Figure 5.117. ¹³ C NMR (CDCl ₃ , 126 MHz, 25 °C) | 317 |
| Figure 5.118. ¹⁹ F NMR (CDCl ₃ , 470 MHz, 25 °C) | 318 |
| Figure 5.119. ¹ H NMR (CDCl ₃ , 500 MHz, 25 °C) | 319 |
| Figure 5.120. ¹³ C NMR (CDCl ₃ , 126 MHz, 25 °C) | 320 |
| Figure 5.121. ¹⁹ F NMR (CDCl ₃ , 470 MHz, 25 °C) | 321 |
| Figure 5.122. ¹ H NMR (CDCl ₃ , 500 MHz, 25 °C) | 322 |
| Figure 5.123. ¹³ C NMR (CDCl ₃ , 126 MHz, 25 °C) | 323 |
| Figure 5.124. ¹⁹ F NMR (CDCl ₃ , 470 MHz, 25 °C) | 324 |
| Figure 5.125. ¹ H NMR (CDCl ₃ , 500 MHz, 25 °C) | 325 |
| Figure 5.126. ¹³ C NMR (CDCl ₃ , 126 MHz, 25 °C) | 326 |
| Figure 5.127. ¹⁹ F NMR (CDCl ₃ , 470 MHz, 25 °C) | 327 |
| Figure 5.128. ¹ H NMR (CDCl ₃ , 500 MHz, 25 °C) | 329 |
| Figure 5.129. ¹ H NMR (CDCl ₃ , 500 MHz, 25 °C) | 330 |
| Figure 5.130. ¹³ C NMR (CDCl ₃ , 126 MHz, 25 °C) | 331 |
| Figure 5.131. ¹ H NMR (CDCl ₃ , 500 MHz, 25 °C) | 332 |
| Figure 5.129. ¹ H NMR (CDCl ₃ , 500 MHz, 25 °C) | 330 |
| Figure 5.130. ¹³ C NMR (CDCl ₃ , 126 MHz, 25 °C) | 331 |
| Figure 5.131. ¹ H NMR (CDCl ₃ , 500 MHz, 25 °C) | 332 |
| Figure 5.132. ¹ H NMR (CDCl ₃ , 500 MHz, 25 °C) | 333 |

| Figure 5.133. ¹ H NMR (CDCl ₃ , 500 MHz, 25 °C) | 334 |
|--|-----|
| Figure 5.134. ¹ H NMR (CDCl ₃ , 500 MHz, 25 °C) | 335 |
| Figure 5.135. ¹³ C NMR (CDCl ₃ , 126 MHz, 25 °C) | 336 |
| Figure 5.136. ¹ H NMR (CDCl ₃ , 500 MHz, 25 °C) | 337 |
| Figure 5.137. ¹³ C NMR (CDCl ₃ , 126 MHz, 25 °C) | 338 |
| Figure 5.138. ¹ H NMR (CDCl ₃ , 500 MHz, 25 °C) | 339 |
| Figure 5.139. ¹³ C NMR (CDCl ₃ , 126 MHz, 25 °C) | 340 |
| Figure 5.140. ¹ H NMR (CDCl ₃ , 500 MHz, 25 °C) | 341 |
| Figure 5.141. ¹³ C NMR (CDCl ₃ , 126 MHz, 25 °C) | 342 |
| Figure 5.142. ¹ H NMR (CDCl ₃ , 500 MHz, 25 °C) | 343 |
| Figure 5.143. ¹³ C NMR (CDCl ₃ , 126 MHz, 25 °C) | 344 |
| Figure 5.144. ¹¹ B NMR (CDCl ₃ , 160 MHz, 25 °C) | 345 |
| Figure 5.145. ¹ H NMR (CDCl ₃ , 500 MHz, 25 °C) | 346 |
| Figure 5.146. ¹³ C NMR (CDCl ₃ , 126 MHz, 25 °C) | 347 |
| Figure 5.147. ¹ H NMR (CDCl ₃ , 500 MHz, 25 °C) | 348 |
| Figure 5.148. ¹³ C NMR (CDCl ₃ , 126 MHz, 25 °C) | 349 |
| Figure 5.149. ¹ H NMR (CDCl ₃ , 500 MHz, 25 °C) | 350 |
| Figure 5.150. ¹³ C NMR (CDCl ₃ , 126 MHz, 25 °C) | 351 |
| Figure 5.151. ¹⁹ F NMR (CDCl ₃ , 470 MHz, 25 °C) | 352 |
| Figure 5.152. ¹ H NMR (CDCl ₃ , 500 MHz, 25 °C) | 353 |
| Figure 5.153. ¹³ C NMR (CDCl ₃ , 126 MHz, 25 °C) | 354 |
| Figure 5.154. ¹⁹ F NMR (CDCl ₃ , 470 MHz, 25 °C) | 355 |
| Figure 5.155. ¹ H NMR (CDCl ₃ , 500 MHz, 25 °C) | 356 |

| Figure 5.156. ¹³ C NMR (CDCl ₃ , 126 MHz, 25 °C) | 357 |
|--|-----|
| Figure 5.157. ¹⁹ F NMR (CDCl ₃ , 470 MHz, 25 °C) | 358 |
| Figure 5.158. ¹ H NMR (CDCl ₃ , 500 MHz, 25 °C) | 359 |
| Figure 5.159. ¹³ C NMR (CDCl ₃ , 126 MHz, 25 °C) | 360 |
| Figure 5.160. ¹⁹ F NMR (CDCl ₃ , 470 MHz, 25 °C) | 361 |
| Figure 5.161. ¹ H NMR (CDCl ₃ , 500 MHz, 25 °C) | 362 |
| Figure 5.162. ¹³ C NMR (CDCl ₃ , 126 MHz, 25 °C) | 363 |
| Figure 5.163. ¹⁹ F NMR (CDCl ₃ , 470 MHz, 25 °C) | 364 |
| Figure 5.164. ¹ H NMR (CDCl ₃ , 500 MHz, 25 °C) | 365 |
| Figure 5.165. ¹ H NMR (CDCl ₃ , 500 MHz, 25 °C) | 366 |
| Figure 5.166. ¹³ C NMR (CDCl ₃ , 126 MHz, 25 °C) | 367 |
| Figure 5.167. ¹ H NMR (CDCl ₃ , 500 MHz, 25 °C) | 368 |
| Figure 5.168. ¹³ C NMR (CDCl ₃ , 126 MHz, 25 °C) | 369 |
| Figure 5.169. ¹ H NMR (DMSO-d ₆ , 500 MHz, 25 °C) | 370 |
| Figure 5.170. ¹³ C NMR (DMSO-d ₆ , 126 MHz, 25 °C) | 371 |
| Figure 5.171. ¹ H NMR (C ₆ D ₆ , 500 MHz, 25 °C) | 372 |
| Figure 5.172. ¹³ C NMR (C ₆ D ₆ , 126 MHz, 25 °C) | 373 |
| Figure 5.173. ¹ H NMR (C ₆ D ₆ , 500 MHz, 25 °C) | 374 |
| Figure 5.174. ¹³ C NMR (C ₆ D ₆ , 126 MHz, 25 °C) | 375 |
| Figure 5.175. ¹⁹ F NMR (470 MHz, C ₆ C ₆ , 25 °C) | 376 |
| Figure 5.176. ¹ H NMR (C ₆ D ₆ , 500 MHz, 25 °C) | 377 |
| Figure 5.177. ¹³ C NMR (C ₆ D ₆ , 126 MHz, 25 °C) | 378 |
| Figure 5.178. ¹ H NMR (C ₆ D ₆ , 500 MHz, 25 °C) | 379 |

| Figure 5.179. ¹³ C NMR (C ₆ D ₆ , 126 MHz, 25 °C) | 380 |
|--|-----|
| Figure 5.180. ¹ H NMR (C ₆ D ₆ , 500 MHz, 25 °C) | 381 |
| Figure 5.181. ¹³ C NMR (C ₆ D ₆ , 126 MHz, 25 °C) | 382 |
| Figure 5.182. ¹ H NMR (C ₆ D ₆ , 500 MHz, 25 °C) | 383 |
| Figure 5.183. ¹³ C NMR (C ₆ D ₆ , 126 MHz, 25 °C) | 384 |
| Figure 5.184. ¹ H NMR (C ₆ D ₆ , 500 MHz, 25 °C) | 385 |
| Figure 5.185. ¹³ C NMR (C ₆ D ₆ , 126 MHz, 25 °C) | 386 |
| Figure 5.186. ¹ H NMR (C ₆ D ₆ , 500 MHz, 25 °C) | 387 |
| Figure 5.187. ¹³ C NMR (C ₆ D ₆ , 126 MHz, 25 °C) | 388 |
| Figure 5.188. ¹⁹ F NMR (470 MHz, C ₆ C ₆ , 25 °C) | 389 |
| Figure 5.189. ¹ H NMR (C ₆ D ₆ , 500 MHz, 25 °C) | 390 |
| Figure 5.190. ¹³ C NMR (C ₆ D ₆ , 126 MHz, 25 °C) | 391 |
| Figure 5.191. ¹⁹ F NMR (470 MHz, C ₆ C ₆ , 25 °C) | 392 |
| Figure 5.192. ¹ H NMR (C ₆ D ₆ , 500 MHz, 25 °C) | 393 |
| Figure 5.193. ¹³ C NMR (C ₆ D ₆ , 126 MHz, 25 °C) | 394 |
| Figure 5.194. ¹ H NMR (C ₆ D ₆ , 500 MHz, 25 °C) | 395 |
| Figure 5.195. ¹³ C NMR (C ₆ D ₆ , 126 MHz, 25 °C) | 396 |

LIST OF SCHEMES

| Scheme 1.1. One-pot synthesis of pyrrolidines using titanium catalysis by Doye group4 |
|--|
| Scheme 1.2. Synthesis of substituted pyridine by titanium catalysis |
| Scheme 1.3. One-pot synthesis of heterocycles using 1,3-diimines as intermediate |
| Scheme 1.4. Quinoline synthesis through titanium catalysis |
| Scheme 1.5. Pyridine synthesis through titanium catalysis |
| Scheme 1.6. Synthesis of MSU38225 by a titanium-catalyzed multicomponent coupling13 |
| Scheme 1.7. Synthesis of the human 20S proteasome inhibitor, Quin1 |
| Scheme 2.1. Synthesis of MSU38225 by Ti(NMe ₂) ₂ (dpm)-catalyzed multicomponent coupling in a one-pot reaction |
| Scheme 2.2. Proposed mechanism of pyridine synthesis. B: a base, e.g., DBU26 |
| Scheme 2.3. Synthesis of 2-aminonicotonitriles by Ti(NMe ₂) ₂ (dpm)-catalyzed multicomponent coupling in a one-pot reaction |
| Scheme 2.4. Modifications of MSU38225 |
| Scheme 2.5. Synthesis of 5-aryl pyridine derivatives |
| Scheme 2.6. Synthesis of 2-bromo pyridine derivative |
| Scheme 2.7. Synthesis of pyrazine derivative |
| Scheme 2.8. Synthesis of quinoline and 1,8-naphthyridine derivative |
| Scheme 2.9. Proposed synthesis of 4-chloropyridine derivative |
| Scheme 2.10. Proposed synthesis of 4-substituted pyridine derivatives |
| Scheme 2.11. Proposed mechanism of "halogen dance" |
| Scheme 2.12. Example of copper-catalyzed Click reaction |
| Scheme 2.13. Synthesis of a pyridine derivative with a terminal alkyne |

| Scheme 2.14. Synthesis of a pyridine derivative with a terminal alkyne | 42 |
|--|--------|
| Scheme. 2.15. Synthesis of analogs with higher benzylic stability | 45 |
| Scheme 3.1. Synthesis of substituted quinoline derivatives by Ti(NMe ₂) ₂ (dpm)-c multicomponent coupling in a one-pot reaction | |
| Scheme 3.2. Proposed mechanism for the second step of titanium catalyzed quinoline s | - |
| Scheme 3.3. Synthesis of the human 20S proteasome inhibitor, Quin1 | 105 |
| Scheme 3.4. Synthesis of {CpRu(NCMe ₃) ₃ } ⁺ PF ₆ ⁻ by Gill and coworkers | 106 |
| Scheme 3.5. Synthesis of {CpRu(NCMe ₃) ₃ } ⁺ PF ₆ ⁻ by Monnier and coworkers | 106 |
| Scheme 3.6. Synthesis of complexes 1 and 2 | 107 |
| Scheme 3.7. Synthesis of {CpRu(Quin1)}+BArF ₂₄ | 107 |
| Scheme 3.8. Proposed synthesis of {CpRu(DMSO) ₃ }+PF ₆ | 108 |
| Scheme 3.9. Synthesis of {CpRu(DMSO) ₃ } ⁺ PF ₆ ⁻ | 108 |
| Scheme 3.10. Potential enantiomers of complex 1 | 113 |
| Scheme 5.1. Unsymmetrical ligand synthesis using Route 1 | 168 |
| Scheme 5.2. An example of unsymmetrical ligand synthesis using Route 2 | 168 |
| Scheme 5.3. Examples of unsymmetrical ligand synthesis using Route 2 | 169 |
| Scheme 5.4. Complexation of titanium catalyst 5a | 170 |
| Scheme 5.5. Conditions of titanium-catalyzed intermolecular hydroamination | 171 |
| Scheme 5.6. A proposed proton transfer through 3-position on indole fragment of the liga | ınd180 |
| Scheme 5.7. Synthesis of catalyst 7c | 181 |
| Scheme 5.8. Synthesis of titanium catalysts 7b | 182 |
| Scheme 5.9. Labeling experiment between titanium catalysts and aniline-ds | 184 |

KEY TO SYMBOLS AND ABBREVIATIONS

FDA food and drug administration

NRF2 nuclear factor erythroid-2-related factor 2

KAEP1 kelch-like ECH-associated protein 1

DFT density functional theory

LDP ligand donor parameter

%V_{bur} percent buried volume

COD cyclooctadiene

H₂dpm 5,5'-dimethyldipyrrolylmethane

 H_2 dpma $N,N-di(pyrrolyl-\alpha-methyl)-N-methylamine$

IC₅₀ half maximal inhibitory concentration

BArF₂₄ tetrakis(3,5-(trifluoromethyl)phenyl)borane

DCM dichloromethane

THF tetrahydrofuran

GC-MS gas chromatography-mass spectrometry

NMR nuclear magnetic resonance (spectroscopy)

EI electronic ionization

EA elemental analysis

FID flame ionization detector

CHAPTER 1. INTRODUCTION: TITANIUM-CATALYZED REACTIONS IN ONE-POT HETEROCYCLIC SYNTHESIS

1.1 Background

Nitrogen-containing heterocycles are one of the most important structural components of pharmaceuticals. A study of a database of all U.S. FDA-approved pharmaceuticals analyzed the frequency of substructures that are present in these drugs. This study of 1994 pharmaceuticals including small molecules and biologics revealed that about 40% of small-molecule drugs contain a nitrogen-based heterocycle (Figure 1.1), which reflects the central role of nitrogen-containing heterocycles in modern drug design. The increasing presence of these heterocycles in drugs illustrates the need for synthetic methodologies to access a diverse class of heterocycles with short steps.

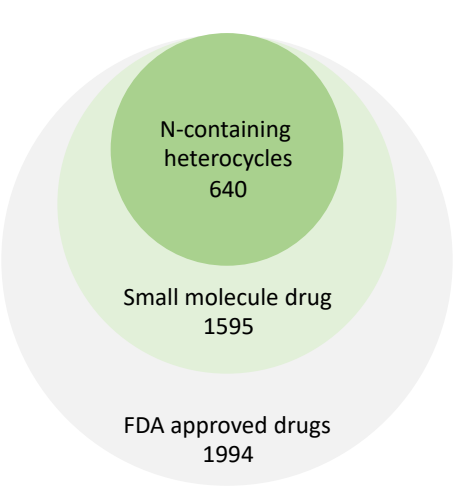


Figure 1.1. The number of drugs approved by the U.S. FDA in different categories.¹

Many frequently used coupling reactions in heterocyclic synthesis involve transition metals (e.g., Pd, Ir, Ru, Rh, etc.) that are exiguous in the Earth's crust. Due to their low production and high costs, replacements of these catalysts with Earth-abundant and cheap metal catalysts are needed. Titanium is the second most abundant transition metal and the ninth most abundant

element among all elements in crustal rocks.² In the past few decades, researchers have been exploring the use of titanium-based catalysts in many different chemical transformations as titanium catalysts are generally considered nontoxic and inexpensive. In fact, they are found in many important chemical reactions in both industry and academia, notably olefin polymerization and Sharpless asymmetric epoxidation.³ Relevant to this study, the use of titanium catalysts for nitrogen-containing small molecule synthesis is discussed. These catalysts have shown great contributions to fast nitrogen-containing heterocycle synthesis via the formation of new C–N bonds and C–C bonds.

1.2 Titanium Catalysis in Hydroamination Derived Heterocycle Synthesis

1.2.1 Intermolecular Hydroamination

One of the most useful reactions in C–N bond formation is hydroamination. Hydroamination is the formal addition of an N–H bond across an unsaturated C–C bond. This transformation is a 100% atom-economical route to generate amines and imines from alkenes and alkynes. Many main group and late transition metal catalysts have been developed with improved functional group tolerance, milder conditions, and higher regioselectivity over the years. However, titanium catalysts for hydroamination were not explored until the late 90s. In 1999, the Doye group published a dimethyltitanocene-catalyzed intermolecular hydroamination reaction that gives anti-Markovnikov products. In 2001, the Odom group discovered that the commercially available reagent Ti(NMe₂)₄ is an effective catalyst for hydroamination of alkynes, which is cheaper and more stable than the titanocene-based catalysts. The reaction time was shortened to 2 h for terminal alkynes and arylamines as compared to the titanocene-based catalysts that take 36 h in many cases. It was proposed that the precatalyst initially reacts with an amine to give the active catalyst, a titanium(IV) imido complex entering the catalytic cycle (Figure 1.2). The titanium

imido complex undergoes [2 + 2]-cycloaddition with an alkyne in a reversible reaction where the slow step in the catalytic cycle is believed to be the Ti–C protonolysis step. Final proton transfer releases the enamine product and restores the active catalyst. Like many other titanium-catalyzed hydroamination reactions that were developed later, this mechanism was originally established by Bergman and coworkers for zirconocene-based catalysts.⁸

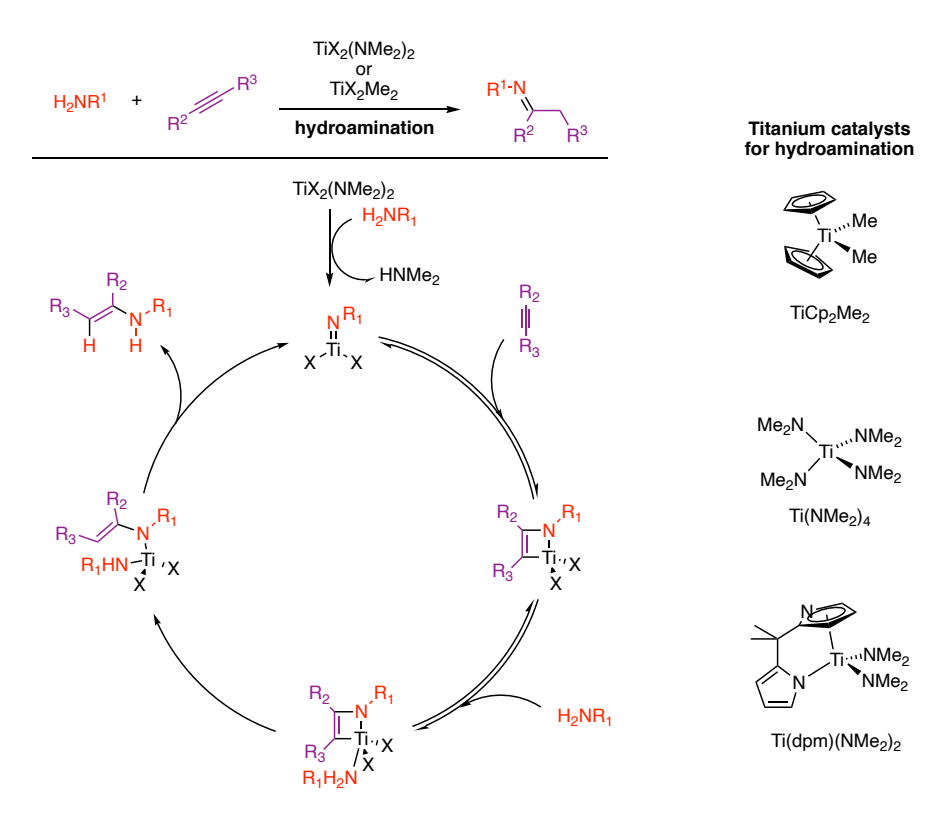


Figure 1.2. Titanium-catalyzed intermolecular hydroamination and proposed Bergman mechanism. X₂ represents one dianionic or two monoanionic ligand(s).⁷

Advances were made in catalysts prepared using a protonolysis reaction of Ti(NMe₂)₄ with suitably protic ligands (Eq. 1).⁹ For example, the reaction of Ti(NMe₂)₄ with a dipyrrole-based ancillary ligand, H₂dpm, produces Ti(dpm)(NMe₂)₂ and 2 equivalents of dimethylamine. The resulting TiX₂(NMe₂)₂ catalysts, where X₂ represents one dianionic or two monoanionic ligand(s), are relatively mild and competent catalysts with a wide substrate scope.⁹ The hydroamination products are useful small building blocks that can be incorporated into syntheses of more complex

heterocycles. These products have been used to prepare five- or six-membered rings, such as pyrrolidines, pyrroles, pyridines, and tetrahydroisoquinolines. 10,11,12

1.2.2 Hydroamination Derived Pyrrolidine Synthesis

Based on the analysis of U.S. FDA-approved drugs, pyrrolidine was ranked the most frequently used core among all categories and was more present than the other four structures combined in the top five, five-membered nonaromatic nitrogen heterocycles.¹ Given the importance of pyrrolidine in drug discovery, titanium catalysts were developed for the synthesis of pyrrolidines by the Doye group in 2009 (Scheme 1.1).¹¹ The synthesis proceeded through a titanium-catalyzed regioselective hydroamination of a 1-aryl-2-cyclopropylalkyne using a primary amine. The resulting product underwent a cyclopropylimine rearrangement in the presence of catalytic amounts of NH₄Cl to yield the 2-pyrroline product. Subsequent reduction by NaBH₃CN and ZnCl₂ afforded the final 2-(arylmethyl)pyrrolidines in one pot. One limitation was the accessibility of different 1-aryl-2-cyclopropylalkynes, which needed to be synthesized by Sonogoshira coupling. This synthesis afforded thirty examples with yields up to 95%. Low yields were found with electron-deficient aryl groups.

Scheme 1.1. One-pot synthesis of pyrrolidines using titanium catalysis by Doye group.¹¹

1.2.3 Hydroamination Derived Pyridine Synthesis

Pyridine is the second most commonly used nitrogen-containing heterocycle among all U.S. FDA-approved drugs and number 1 among aromatics. Traditional methods like condensation using 1,3- or 1,5-dicarbonyl derivatives, e.g., Hantzsch and Kröhnke pyridine synthesis, a can afford pyridine derivatives, but offer restricted substitution patterns and low yields. The Schafer group reported a pyridine synthesis using N-silylenamines as reactive intermediates (Scheme 1.2). A regioselective hydroamination reaction of alkynes with N-silylamine was catalyzed by a titanium catalyst. The addition of α , β -unsaturated carbonyls to the crude reaction mixtures followed by oxidation afforded substituted pyridines in one pot. This methodology was used in 47 examples with yields up to 96%.

Scheme 1.2. Synthesis of substituted pyridine by titanium catalysis. ¹²

1.3 The Titanium-Catalyzed Multicomponent Coupling Reaction: Iminoamination

The examples above used the titanium-catalyzed hydroamination products as intermediates to afford heterocycles. Other than the hydroamination reaction, titanium catalysts have also been developed for other reactions in the Odom group, such as hydrohydrazination, iminoamination, and iminohydrazination. According to the proposed mechanism, the slow step in titanium-catalyzed hydroamination reaction was proposed to be the protonolysis step. ¹⁴ Our group's strategy was to trap the azatitanacyclobutene intermediate before protonolysis using isonitriles as they were discovered as an interesting reagent to react with the azatitanacyclobutene intermediate faster than

proton transfer. This led to the discovery of a new multi-component coupling reaction, iminoamination, which forms a new C–C and C–N bond by coupling a primary amine, alkyne, and isonitrile.¹⁵ Typical catalysts for iminoamination reactions are Ti(dpm)(NMe₂)₂ and Ti(dpma)(NMe₂)₂ with yields around 70% (Figure 1.3). Side reactions including hydroamination, formamidine formation, and four-component coupling contribute to lower yields in comparison to titanium-catalyzed hydroamination reactions.¹⁶

Figure 1.3. Examples of titanium catalysts for iminoamination reactions. 16

The mechanism of the three-component coupling reaction was proposed to involve an azatitanacyclobutene intermediate. The 1,1-insertion of isonitrile to the Ti–C bond occurs before the hydrolysis of the product (Figure 1.4). The final product arises from the formal addition of an iminyl and amino group across the C–C triple bond, resulting in tautomers of 1,3-diimines.

Figure 1.4. The titanium-catalyzed multicomponent coupling reaction and proposed iminoamination mechanism, where X₂ represents one dianionic or two monoanionic ligand(s).¹⁵

1.4 Titanium Iminoamination in Heterocycle Synthesis

The 1,3-diimines products from the iminoamination reaction exhibit great electrophilicity toward nucleophilic reagents with reactivity similar to 1,3-dicarbonyl compounds in heterocycle synthesis. The Odom group developed one-pot strategies by using the iminoamination product to afford a variety of heterocycle derivatives that usually take multiple steps to synthesize with respect to other reported methods. In general, the first step includes a mixture of three-component substrates, catalyst, solvent, and heating to form the diimine products. The diimine products are

not isolated and instead treated directly with a mixture of reagents in the second step to afford the final cyclized products (Scheme 1.3).

Scheme 1.3. One-pot synthesis of heterocycles using 1,3-diimines as intermediate.

This procedure can be used in the synthesis of heterocycles, such as pyrazoles, pyrimidines, isoxazoles, pyridines, and quinolines. The cyclization step involving the diimine product can be divided into two categories depending on the number of atoms used in the final product (Figure 1.5). Type I products contain three carbons from the iminoamination product, whereas Type II products contain one nitrogen and three carbon atoms giving one primary amine as a byproduct. The first Type is exemplified by the synthesis of isoxazoles, pyrazoles, and pyrimidines. The second Type is exemplified by the synthesis of quinolines and pyridines.

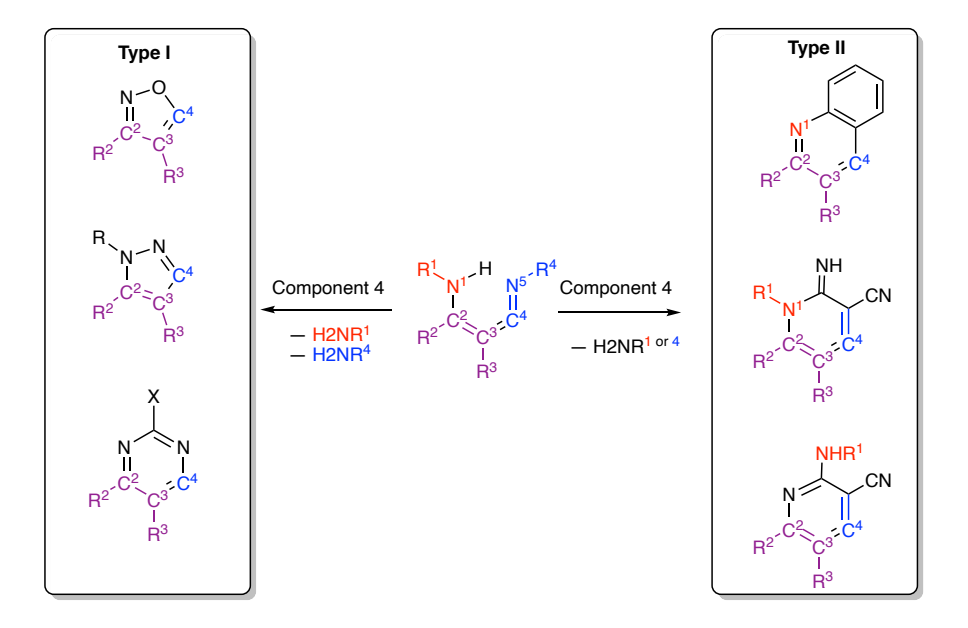


Figure 1.5. Two categories of cyclization of iminoamination products. 16

1.4.1 Type I Products: Pyrazoles, Pyrimidines, and Isoxazoles

Pyrazoles are found in important pharmaceuticals such as celecoxib (Celebrex®), sildenafil (Viagra®), and rimonabant (Acomplia®) and are also found in a few natural products such as withasomnine. In 2009, the Odom group developed a titanium-catalyzed one-pot synthesis of substituted pyrazoles from commercially available primary amines, alkynes, and isonitriles. The three-component coupling products are produced *in situ* and then undergo cyclization with hydrazine and hydrazine derivatives in a one-pot procedure. Interestingly, the regioselectivity of diimine products can be controlled in some cases with catalyst architecture if the substituent on the terminal alkyne is an alkyl (Figure 1.6). For example, 1,4-pyrazoles were found as preferred products by using Ti(dpm)(NMe₂)₂, while 1,5-pyrazoles were found as preferred products if Ti(dpma)(NMe₂)₂ was used as a catalyst. The addition of monosubstituted hydrazines to unsymmetrical 1,3-diimines favors the addition to the less hindered aldimine carbon by the unsubstituted NH₂-group of the hydrazine. Seventeen examples of pyrazoles were synthesized using this procedure with modest yields (27-50%). This multi-component coupling strategy was also applied to the synthesis of withasomnine in an efficient procedure. Is

Figure 1.6. Pyrazole synthesis through titanium catalysis.¹⁸

The condensation of iminoamination products with nucleophilic reagents was applied to the synthesis of pyrimidines¹⁹ and isoxazoles.²⁰ Amidines or hydroxylamine hydrochloride were reacted with the three-component coupling products to afford pyrimidines or isoxazoles, accordingly (Figure 1.7).

Figure 1.7. Pyrimidine and isoxazole synthesis through titanium catalysis.¹⁹

1.4.2 Type II Products: Pyridines and Quinolines

The synthesis of bicyclic substructures such as quinolines has been studied as well. The Odom group developed a one-pot strategy for the synthesis of substituted quinolines using titanium-catalyzed iminoamination.²¹ An aromatic amine with an *ortho*-hydrogen needs to be used in this method. Once the diimine products are formed, the simple addition of acetic acid and heating promotes electrophilic cyclization onto the aromatic ring to afford quinoline derivatives (Scheme 1.4). This synthesis can be employed to synthesize substituted anilines, aminonaphthalenes, or even heterocyclic amines with yields varying from 25-71%.

Scheme 1.4. Quinoline synthesis through titanium catalysis.²¹

In 2014, the Odom group developed a one-pot strategy for 2-amino-3-cyanopyridines.²² The reaction of iminoamination products with malononitrile and DBU produces a 1,2-dihydro-2-imino-3-pyridinecarbonitrile intermediate and proceeds through a Dimroth rearrangement²³ to afford 2-amino-5-cyanopyridines as the final products (Scheme 1.5). It was also found that the 1,2-dihydro-2-imino-3-pyridinecarbonitrile intermediate can be isolated by using a less nucleophilic base, Et₃N. Twenty four 2-amino-3-cyanopyridines were synthesized in moderate to good yields (42-76%).

Scheme 1.5. Pyridine synthesis through titanium catalysis.²²

In summary, titanium-catalyzed iminoamination products were incorporated into one-pot syntheses of a variety of heterocycles. These one-pot syntheses use commercially available starting materials and easily prepared catalysts to access complex molecules that would require multi-step syntheses with other methods. The practical advantage of these syntheses has also been demonstrated by the regioselectivity of the products in some cases. A summary of current one-pot heterocycle syntheses using titanium catalysis is shown in Figure 1.8.

$$\begin{array}{c} \text{H}_2\text{NR}^1\\ \text{H}_2\text{NR}^1\\ \text{H}_2\text{NR}^1\\ \text{H}_2\text{NR}^1\\ \text{H}_2\text{NR}^1\\ \text{H}_2\text{NR}^1\\ \text{H}_2\text{NR}^1\\ \text{H}_2\text{NR}^1\\ \text{Iminoamination} \\ \text{Iminoamination} \\$$

Figure 1.8. A summary of heterocycle synthesis using titanium catalysis. 16

1.5 Applications and Improvements of Titanium Catalysis by Odom Group

Given fast access to so many types of nitrogen-containing heterocycles, many synthetic products can be screened and tested for their biological activities in drug discovery. Two applications discussed in this thesis are NRF2 pathway inhibition and human proteasome inhibition by nitrogen-containing heterocycles. The activities and properties of these compounds as drug candidates were studied in collaboration with other research groups at MSU. These applications also demonstrated the importance of designing new catalysts with improved yields, broader substrate scopes, and higher regioselectivity. In this study, models of ligand properties and reaction rate were generated as tools for guiding future catalyst design.

1.5.1 Substituted Pyridines as NRF2 Pathway Inhibitors

NRF2 is a transcription factor that induces a gene transcription program that renders cells resistant to oxidative stress. This pathway plays a key role in the growth, survival, and aggressiveness of cancer. A constitutively activated NRF2 pathway was found in several different

cancers resulting in low sensitivity to chemo- and radiotherapy.²⁴ NRF2 pathway inhibition is a prevalent area of research due to the lack of treatment options for cancers with a constructively activated NRF2 pathway. In collaboration with the Liby group at MSU, we reported a novel, selective NRF2 pathway inhibitor, MSU38225, which was synthesized using a titanium-catalyzed one-pot synthesis (Scheme 1.6).²⁵ Both *in vitro* and *in vivo* studies found that MSU38225 reduced the NRF2 activity selectively without inhibiting general protein expression. It was also found that this NRF2 inhibitor enhanced the sensitivity of cancer cells to chemotherapeutics, which opens a new therapeutic window for cancers with constructively activated NRF2.

Scheme 1.6. Synthesis of MSU38225 by a titanium-catalyzed multicomponent coupling.

With titanium catalysis, a library of compounds can be synthesized to place a variety of functional groups at different positions. This library of compounds can help us understand the structural effects on the inhibition activity and guide the design of new drugs with higher potency and better "drug-like" properties. Even though titanium catalysis can enable a one-pot synthesis of many pyridine analogs from simple starting materials, certain analogs are not accessible through this methodology. For example, substrates containing heterocycles usually give low TOF in titanium catalysis and functionalizing the *para* position on the pyridine ring requires additional steps. Therefore, other synthetic methodologies to access pyridine analogs were explored to expand the scope of the library. The structure-activity relationship and improvement of "drug-like" properties are discussed in Chapter 2.

1.5.2 Substituted Quinolines as Noncovalent Proteasome Inhibitors

Regulation of proteasome activity has shown to be an important method for treating multiple myeloma and mantle cell lymphoma because these cancer cells have higher proteasome activities compared to non-transformed cells.²⁶ These cancer cells are more sensitive to proteasome inhibitors, and as a result, proteasome inhibition causes rapid apoptosis due to the higher levels of metabolism and growth factors.²⁷ In collaboration with the Tepe group at MSU, the structure-activity relationship of substituted quinolines and their human proteasome inhibition activities was reported by the Odom group in 2016.²⁸ A library of substituted quinolines prepared by titanium catalysis was screened in this study with the discovery of **Quin1**, which has a single-digit micromolar half maximal inhibitory concentration (IC₅₀). The substituted quinolines were found as nonpeptidic and noncovalent inhibitors which could be used to overcome the inevitable resistance of competitive inhibitors. **Quin1** was synthesized by an olefin hydrogenation of a quinoline product from the titanium-catalyzed one-pot strategy methodology (Scheme 1.7).

Scheme 1.7. Synthesis of the human 20S proteasome inhibitor, Quin1.²⁸

Combination drugs with ruthenium-based compounds have been incorporated with other drugs for their multitargeting properties in cancer treatment.²⁹ Incorporating a proteasome inhibitor to ruthenium complexes could lead to potential anti-cancer drug candidates with a broader range of targets. The synthesis and biological activities of such a ruthenium complex as a potential drug were conducted in Chapter 3.

1.5.3 Ligand Effects Modeling in Titanium Catalysis

One of the most common methods to improve catalyst performance is to modify ancillary ligand properties. However, the electronic and steric profiles of ligands can be difficult to analyze without a tool to quantify these properties. Our group developed an experimental system to parameterize the electronic donation of a ligand towards a high oxidation state transition metal center.³⁰ A chromium(VI) complex, NCr(NiPr₂)₂X, was designed for measuring the electronic donation from a mono-anionic ligand X (Figure 1.9). The Ligand Donor Parameter, LDP, uses the rotation barrier of a Cr-N bond in the chromium(VI) complex to represent the donor ability to high oxidation state transition metal centers. A better donor results in a higher single bond character in the Cr-N bond, which increases the rate of rotation along this bond. Therefore, a good donor ligand results in a high LDP value. Despite the quantitive measurement of the electronic donation in this system, a reliable computational method to estimate LDP values could bypass the challenges in chromium complex syntheses and reduce the costs and hazards associated with the syntheses. In Chapter 4, a computational study to estimate LDP values was explored by establishing correlations of calculated metal-ligand bonding properties with LDP.

Figure 1.9. Chromium complex used for the measurement of LDP.

With tools to quantify the electronic and steric effects of the ligands in titanium catalysis, a study on modeling hydroamination rate as a function of ancillary ligand properties was published by our group in 2017.³¹ A library of titanium catalysts with a large range of electronic and steric profiles were synthesized. The electronic (LDP) and steric (%V_{bur}) parameters of the ligands were

modeled with the experimental hydroamination rate constant (Eq. 2). The model suggests that catalysts with electron-deficient and small ligands faster than those with electron-rich and big ligands. It also indicated that the contribution of steric effects is slightly more important than the electronic effects. With this model, a prediction of reaction rates can be made prior to the catalyst synthesis.

$$k_{obs}(\times 10^4) = 1.34 + 1.61(LDP) - 2.25(\%V_{bur})$$
 (2)

Here, a more complex ligand system was investigated to be generated since all ancillary ligands in the previous study were symmetrical. Studies on similar systems have shown that unsymmetrical ligands can contribute to higher reaction rates in high oxidation state metal catalysis.³² In Chapter 5, unsymmetrical ligands in titanium catalysis are explored and the ligand effects were modeled with more parameters of the ligands. The electronic and steric parameters of the two parts of the ligands (Figure 1.10) were measured using the chromium reporter and modeled with the experimental rate of hydroamination catalysis using Eq.3. In this study, an unexpected effect on catalysis rate due to having indoles with specific substitution patterns was discovered.

$$k_{obs}(\times 10^4) = a + b(LDP)_1 + c(LDP)_2 + d(\%V_{bur})_1 + e(\%V_{bur})_2$$

$$\text{Me} \qquad \qquad \text{NMe}_2 \qquad \qquad \text{Pri} \qquad \qquad \text{Pri} \qquad \qquad \text{NMe}_2 \qquad \qquad \text{Pri} \qquad \qquad \text{P$$

Figure 1.10. An example of a titanium catalyst and its electronic and steric reporters.

1.6 Conclusions

Titanium-catalyzed hydroamination and iminoamination reactions have been developed for one-pot syntheses of a variety of nitrogen-containing heterocycles. These synthetic methodologies have significantly shortened the steps to access complex heterocycles. Great potential for heterocycles synthesized by titanium catalysis in drug discovery was demonstrated by the two applications in proteasome inhibition and NRF2 pathway inhibition. Studies on quantifying ligand effects in titanium catalysis have made great contributions to the improvement of reaction rate, selectivity, and catalyst stability. Models of the ligand properties as a function of reaction rate were developed to predict catalyst performance and guide future catalyst design.

REFERENCES

REFERENCES

- 1. Vitaku, E.; Smith, D. T.; Njardarson, J. T. Analysis of the Structural Diversity, Substitution Patterns, and Frequency of Nitrogen Heterocycles among U.S. FDA Approved Pharmaceuticals. *Journal of Medicinal Chemistry* **2014**, *57* (24), 10257-10274.
- 2. Greenwood, N. N.; Earnshaw, A. Chemistry of the Elements; Elsevier, 2012.
- 3. Katsuki, T.; Sharpless, K. B. The first practical method for asymmetric epoxidation. *Journal of the American Chemical Society* **1980**, *102* (18), 5974-5976. Alt, H. G.; Köppl, A. Effect of the Nature of Metallocene Complexes of Group IV Metals on Their Performance in Catalytic Ethylene and Propylene Polymerization. *Chemical Reviews* **2000**, *100* (4), 1205-1222.
- 4. Müller, T. E.; Beller, M. Metal-Initiated Amination of Alkenes and Alkynes. *Chemical Reviews* **1998**, *98* (2), 675-704.
- 5. Bender, C. F.; Widenhoefer, R. A. Platinum-Catalyzed Intramolecular Hydroamination of Unactivated Olefins with Secondary Alkylamines. *Journal of the American Chemical Society* **2005**, *127* (4), 1070-1071. Huang, L.; Arndt, M.; Gooßen, K.; Heydt, H.; Gooßen, L. J. Late Transition Metal-Catalyzed Hydroamination and Hydroamidation. *Chemical Reviews* **2015**, *115* (7), 2596-2697.
- 6. Haak, E.; Bytschkov, I.; Doye, S. Intermolecular hydroamination of alkynes catalyzed by dimethyltitanocene. *Angewandte Chemie International Edition* **1999**, *38* (22), 3389-3391.
- 7. Shi, Y.; Ciszewski, J. T.; Odom, A. L. Ti(NMe2)4 as a Precatalyst for Hydroamination of Alkynes with Primary Amines. *Organometallics* **2001**, *20* (19), 3967-3969.
- 8. Walsh, P. J.; Baranger, A. M.; Bergman, R. G. Stoichiometric and catalytic hydroamination of alkynes and allene by zirconium bisamides Cp2Zr(NHR)2. *Journal of the American Chemical Society* **1992**, *114* (5), 1708-1719.
- 9. Shi, Y.; Hall, C.; Ciszewski, J. T.; Cao, C.; Odom, A. L. Titanium dipyrrolylmethane derivatives: rapid intermolecular alkyne hydroamination. *Chemical Communications* **2003**, (5), 586-587.
- 10. Zhang, Z.; Leitch, D. C.; Lu, M.; Patrick, B. O.; Schafer, L. L. An Easy-To-Use, Regioselective, and Robust Bis(amidate) Titanium Hydroamination Precatalyst: Mechanistic and Synthetic Investigations toward the Preparation of Tetrahydroisoquinolines and Benzoquinolizine Alkaloids. *Chemistry A European Journal* **2007**, *13* (7), 2012-2022. Ackermann, L.; Sandmann, R.; Kaspar, L. T. Two Titanium-Catalyzed Reaction Sequences for Syntheses of Pyrroles from (E/Z)-Chloroenynes or α-Haloalkynols. *Organic Letters* **2009**, *11* (9), 2031-2034.

- 11. Gräbe, K.; Zwafelink, B.; Doye, S. One-Pot Procedure for the Synthesis of N-Substituted 2-(Arylmethyl)pyrrolidines from 1-Aryl-2-cyclopropylalkynes and Primary Amines by a Hydroamination/Cyclopropylimine Rearrangement/Reduction Sequence. *European Journal of Organic Chemistry* **2009**, 2009 (32), 5565-5575.
- 12. Lui, E. K. J.; Hergesell, D.; Schafer, L. L. N-Silylenamines as Reactive Intermediates: Hydroamination for the Modular Synthesis of Selectively Substituted Pyridines. *Organic Letters* **2018**, *20* (21), 6663-6667.
- 13. Hantzsch, A. Condensationsprodukte aus Aldehydammoniak und ketonartigen Verbindungen. *Berichte der deutschen chemischen Gesellschaft* **1881**, *14* (2), 1637-1638. KRÖHNKE, F. The Specific Synthesis of Pyridines and Oligopyridines. *Synthesis* **1976**, (1), 1-24.
- 14. Pohlki, F.; Doye, S. The Mechanism of the [Cp2TiMe2]-Catalyzed Intermolecular Hydroamination of Alkynes. *Angewandte Chemie International Edition* **2001**, *40* (12), 2305-2308.
- 15. Cao, C. S.; Shi, Y. H.; Odom, A. L. A titanium-catalyzed three-component coupling to generate alpha, beta-unsaturated beta-iminoamines. *Journal of the American Chemical Society* **2003**, *125* (10), 2880-2881.
- 16. Odom, A. L.; McDaniel, T. J. Titanium-Catalyzed Multicomponent Couplings: Efficient One-Pot Syntheses of Nitrogen Heterocycles. *Accounts of Chemical Research* **2015**, *48* (11), 2822-2833.
- 17. Naim, M. J.; Alam, O.; Nawaz, F.; Alam, M. J.; Alam, P. Current status of pyrazole and its biological activities. *J Pharm Bioallied Sci* **2016**, *8* (1), 2-17.
- 18. Majumder, S.; Gipson, K. R.; Staples, R. J.; Odom, A. L. Pyrazole Synthesis Using a Titanium-Catalyzed Multicomponent Coupling Reaction and Synthesis of Withasomnine. *Advanced Synthesis & Catalysis* **2009**, *351* (11-12), 2013-2023.
- 19. Majumder, S.; Odom, A. L. Titanium catalyzed one-pot multicomponent coupling reactions for direct access to substituted pyrimidines. *Tetrahedron* **2010**, *66* (17), 3152-3158.
- 20. Dissanayake, A. A.; Odom, A. L. Regioselective conversion of alkynes to 4-substituted and 3,4-disubstituted isoxazoles using titanium-catalyzed multicomponent coupling reactions. *Tetrahedron* **2012**, *68* (3), 807-812.
- 21. Majumder, S.; Gipson, K. R.; Odom, A. L. A Multicomponent Coupling Sequence for Direct Access to Substituted Quinolines. *Organic Letters* **2009**, *11* (20), 4720-4723.
- 22. Dissanayake, A. A.; Staples, R. J.; Odom, A. L. Titanium-Catalyzed, One-Pot Synthesis of 2-Amino-3-cyano- pyridines. *Advanced Synthesis & Catalysis* **2014**, *356* (8), 1811-1822.

- 23. Dimroth, O. Ueber intramolekulare Umlagerungen. Umlagerungen in der Reihe des 1, 2, 3-Triazols. *Justus Liebigs Annalen der Chemie* **1909**, *364* (2), 183-226.
- 24. Sporn, M. B.; Liby, K. T. NRF2 and cancer: the good, the bad and the importance of context. *Nature Reviews Cancer* **2012**, *12* (8), 564-571.
- 25. Zhang, D.; Hou, Z.; Aldrich, K. E.; Lockwood, L.; Odom, A. L.; Liby, K. T. A Novel Nrf2 Pathway Inhibitor Sensitizes Keap1-Mutant Lung Cancer Cells to Chemotherapy. *Molecular Cancer Therapeutics* **2021**, *20* (9), 1692-1701.
- 26. Sterz, J.; Metzler, I. v.; Hahne, J.-C.; Lamottke, B.; Rademacher, J.; Heider, U.; Terpos, E.; Sezer, O. The potential of proteasome inhibitors in cancer therapy. *Expert Opinion on Investigational Drugs* **2008**, *17* (6), 879-895.
- 27. Goldberg, A. L. Bortezomib's Scientific Origins and Its Tortuous Path to the Clinic. In *Bortezomib in the Treatment of Multiple Myeloma*, 2011; pp 1-27.
- 28. McDaniel, T. J.; Lansdell, T. A.; Dissanayake, A. A.; Azevedo, L. M.; Claes, J.; Odom, A. L.; Tepe, J. J. Substituted quinolines as noncovalent proteasome inhibitors. *Bioorganic & Medicinal Chemistry* **2016**, *24* (11), 2441-2450.
- 29. Golbaghi, G.; Castonguay, A. Rationally Designed Ruthenium Complexes for Breast Cancer Therapy. *Molecules* **2020**, *25*, 265.
- 30. DiFranco, S. A.; Maciulis, N. A.; Staples, R. J.; Batrice, R. J.; Odom, A. L. Evaluation of Donor and Steric Properties of Anionic Ligands on High Valent Transition Metals. *Inorganic Chemistry* **2012**, *51* (2), 1187-1200.
- 31. Billow, B. S.; McDaniel, T. J.; Odom, A. L. Quantifying ligand effects in high-oxidation-state metal catalysis. *Nat Chem* **2017**, *9* (9), 837-842.
- 32. Poater, A.; Solans-Monfort, X.; Clot, E.; Copéret, C.; Eisenstein, O. Understanding d0-Olefin Metathesis Catalysts: Which Metal, Which Ligands? *Journal of the American Chemical Society* **2007**, *129* (26), 8207-8216. Sinha, A.; Schrock, R. R. Reactions of Mo(NAr)(CH-t-Bu)(CH2-t-Bu)2 with Alcohols To Give Metathesis Catalysts of the Type Mo(NAr)(CH-t-Bu)(CH2-t-Bu)(OR). *Organometallics* **2004**, *23* (8), 1643-1645.

CHAPTER 2 SYNTHESIS OF SUBSTITUTED PYRIDINES AS NOVEL NRF2 INHIBITORS

2.1 Introduction

Nuclear factor erythroid-2-related factor 2 (NRF2)-Keap1-ARE plays important roles in various cellular processes including redox-balancing, detoxification, proliferation, inflammation, and metabolism.¹ Activation of the NRF2 pathway is closely controlled by its negative regulator, Kelch-like ECH-associated protein 1 (KEAP1). When the cells get exposed to cellular stress or reactive species such as hydrogen peroxide, reactive nitrogen species, and alkylating agents, the NRF2 protein gets released from KEAP1 protein and translocates into the nucleus to activate the expression of a series of cytoprotective proteins.² Because of this cytoprotective role of the NRF2 pathway, NRF2 regulation was considered a very attractive strategy for cancer prevention.

Evidence has been gathered that NRF2 activation contributes to the suppression of carcinogenesis. ^{1,3} A greater susceptibility to tumor formation was found in genetic NRF2 knockout mice. ⁴ The expression of many transporters and metabolic enzymes regulated by the NRF2 pathway was found responsible for the detoxification of normal cells. ⁵ Results from the epidemiological studies have suggested NRF2 activators, like sulforaphane, can be a complementary or alternative chemotherapeutic. ⁶ The most cited natural product NRF2 activator, sulforaphane, was found in broccoli and Brussels sprouts. ⁷ This is also why we should keep a healthy diet.

On the other hand, NRF2 pathway inhibition may be important in some cancer treatments. A constitutively activated NRF2 pathway was found in several different cancers resulting in low sensitivity to chemo- and radiotherapy.³ This means many chemotherapeutics do not have the same efficiency for these cancers. Loss-of-function mutations of KEAP1 and gain-of-function mutations

of NFE2L2 (the gene that codes for NRF2) were found in many human cancers, especially lung cancers, approximately 28% of lung cancers contain mutations relevant to the disrupted NRF2 pathway.⁸ With the increased concentration of NRF2 protein, the expression of efflux transporters, which show affinity toward several kinase inhibitors, can significantly reduce drug sensitivity and confer drug resistance.^{9,10} Recent studies also suggest the activation of the NRF2 pathway promotes the proliferation and detoxification processes of tumor cells (Figure 2.1).¹⁰ This makes cancers with these mutations very hard to treat.

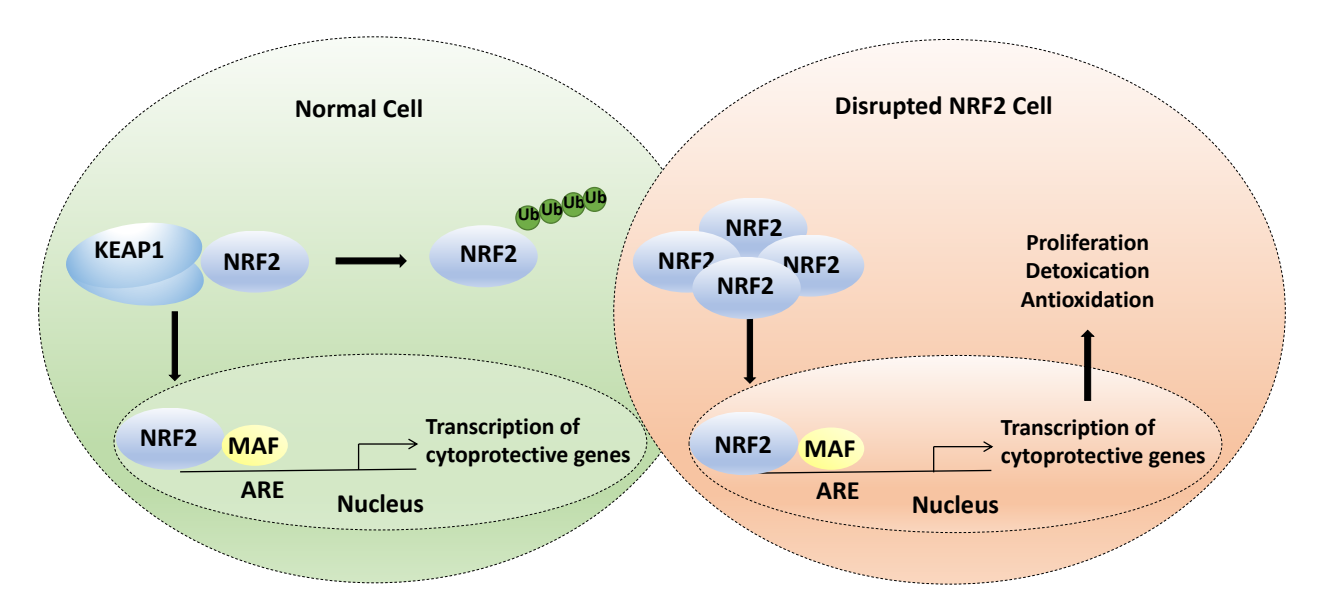


Figure 2.1. NRF2 pathway in normal cells and disrupted NRF2 pathway in certain cancer cells. Ub: Ubiquitination.

Unfortunately, there are only a few known NRF2 pathway inhibitors. However, their exact mechanisms are unclear, or the inhibitions are nonspecific. 11 Due to the lack of selective NRF2 inhibitors as drugs, these cancer mutations reduce patient survival rates. There is an urgent need for selective NRF2 inhibitors to treat cancers with constitutively activated NRF2 pathway.

In 2021, the Liby and Odom group at MSU published a study on the discovery of a new NRF2 inhibitor.¹² The small molecule synthesized in the Odom group, MSU38225, can suppress the NRF2 pathway selectively. A luciferase assay with MCF-7 reporter cells transfected with a

NRF2/ARE luciferase construct showed that 5 mM of MSU38225 reduces NRF2 activity by about 50% (Figure 2.2). Additionally, MSU38225 reduced NRF2 transcriptional activities and decreases the expression of NRF2 downstream targets, including NQO1, GCLC, GCLM, AKR1C2, and UGT1A6, but it did not inhibit protein expression in other cellular processes, such as in the NF-kB pathway, which has a similar mechanism of regulation as NRF2. It was found that the cellular NRF2 protein level is significantly reduced after treatment with MSU38225. More excitingly, MSU38225 increased the sensitivity of human lung cancer cells to chemotherapies, like carboplatin, both *in vitro* and *in vivo*.

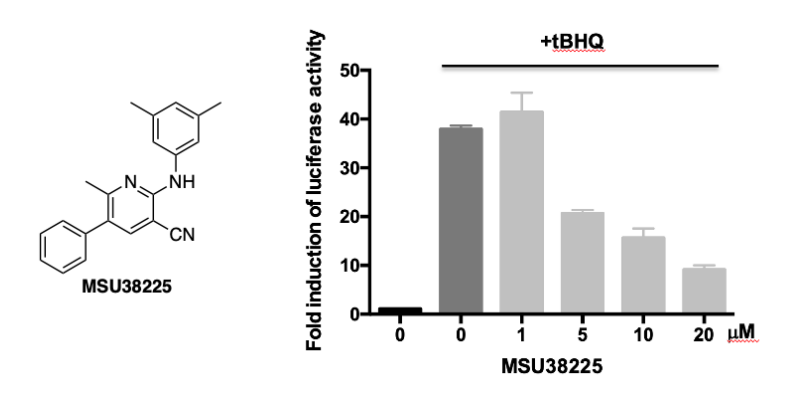


Figure 2.2. The structure of MSU38228 and luciferase assay results after the treatment of MSU38225 with different concentrations by MCF-7 reporter cells stimulated with 20 mmol/L tBHQ.¹²

The xenograft study showed low dose carboplatin was not able to slow down tumor growth due to the constructively activated NRF2 pathway in A549 (Figure 2.3). MSU38225 itself reduced tumor growth. Because activated NRF2 promoted proliferation and metabolism of cancer cells, the treatment with a NRF2 inhibitor slowed tumor growth. A combination of MSU38225 and carboplatin significantly reduced tumor growth and showed synergistic inhibition, which means the NRF2 inhibitor enhances the sensitivity of tumors to chemotherapeutics. In addition, MSU38225 was well-tolerated in mice without inducing any changes in body weight over time.

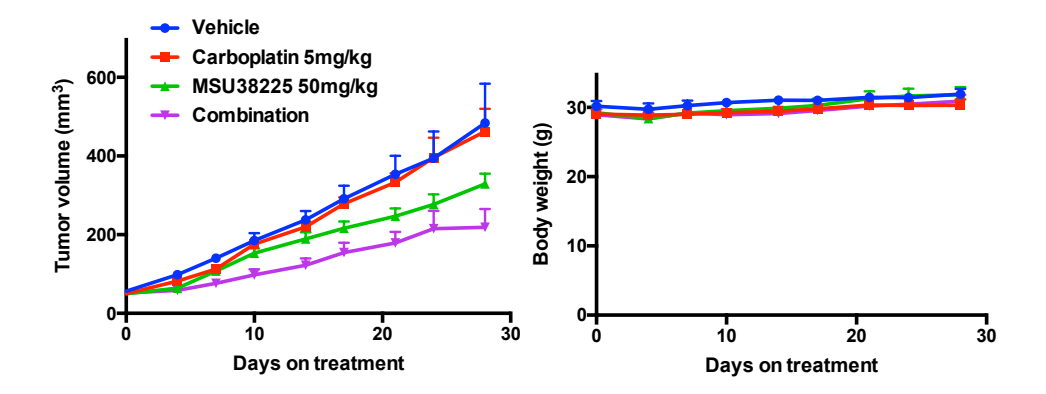


Figure 2.3. A xenograft model using A549 cells. Tumors were measured twice a week using a caliper. N = 6 mice/group.¹²

Compound MSU38225 was identified as a "hit" compound during the high-throughput screening of small molecules from an MSU compound library. It was synthesized using a novel titanium-catalyzed multicomponent coupling reaction developed by the Odom group (Scheme 2.1).¹³ In this two-step one-pot strategy, a commercially available primary amine, alkyne, and isonitrile were used to form a new C–C and C–N bond through a Ti(NMe₂)₂(dpm)-catalyzed alkyne iminoamination reaction (see Chapter 1). The iminoamination product, a 1,3-diimine derivative, was directly treated with malononitrile and DBU in ethanol without the need for purification or isolation to achieve a 34% yield.

Scheme 2.1. Synthesis of MSU38225 by Ti(NMe₂)₂(dpm)-catalyzed multicomponent coupling in a one-pot reaction.

This methodology can be used for many different starting materials with a variety of functional groups including olefin, ether, amide, etc. The mechanism of the cyclization process

was proposed as in Scheme 2.2. It was proposed that malononitrile attacks the multicomponent coupling product first in the presence of a base. After the loss of amine, a Dimroth rearrangement affords 2-amino-5-cyano pyridine derivatives, a reaction thermodynamically driven by the aromatization of the pyridine ring.¹³

Scheme 2.2. Proposed mechanism of pyridine synthesis. B: a base, e.g., DBU.

This promising result suggested a therapeutic window for treating cancers with a constructively activated NRF2 pathway, even though it is unclear how this molecule inhibits the NRF2 pathway. The identification of the binding target can greatly help us understand the mechanism of the inhibition and guide the design of new inhibitors. In addition, the physicochemical properties and biological activities of this molecular need to be optimized to further explore the drug candidacy. This chapter discussed the follow-up efforts in target identification and lead optimization. First, MSU38225 derivatives need to be tested to establish a structure-activity relationship (SAR). With the SAR study, a labeled compound can be used to determine the direct binding partner for the inhibition. Second, "drug-like" properties, such as water solubility and metabolic stability, need to be modified for the success of drug candidates. Third, a search for a more potent molecule will be conducted.

2.2 Exploration of Structure-Activity Relationships in MSU382225 Derivatives

After a new class of selective NRF inhibitors was identified, an exploration of the structureactivity relationship was in need. Without identification of the direct binding partner of the small
molecule inhibitor, tools like molecular docking cannot be used to guide the design of the new
compounds. To expand the scope of the analogs and gather useful information from a variety of
different structures as fast as possible, I developed 4 different categories of the syntheses to explore
SAR (Figure 2.4): (1) Install functional groups at different positions using the titanium-catalyzed
one-pot strategy from commercially available/prefunctionalized amines and alkynes. (2)
Functionalize MSU38225 to explore the importance of hydrogen bonding donors and acceptors.
(3) Explore the compatibility of heterocycles in the replacement of phenyl rings. (4) Explore the
flexibility of pyridine core structure with other heterocycles. With both peripheral and core
changes, the tolerance of changes will guide us to design molecules for target identification.

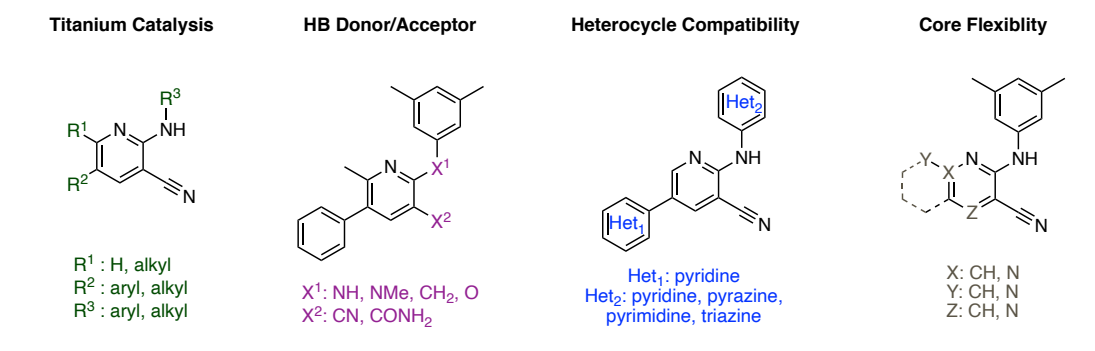


Figure 2.4. Four different categories on explore SAR.

All activities were reported by using a NRF2/ARE luciferase reporter construct stably expressed in MCF-7 cells in collaboration with the Liby group at MSU. MCF-7 cells (human breast cancer cells), stably transfected with a NRF2 binding site and firefly luciferase coding region, were treated with different compounds at 5 mM for 24 hours. The luciferase activities were reported as the representation of NRF2 activity. The reduction of luciferase activity was reported as inhibition

activity, and activation activities were reported as negative inhibition activities. All compounds were purified to >98% purity by GC-FID.

All activity data was collected by Dr. Di Zhang, Beth Lockwood, and Chris Occhiuto in Prof. Karen Liby's lab in the department of pharmacology and toxicology at MSU. Solubility and microsome stability data were collected by Dr. Matt Giletto in the medicinal chemistry facility at MSU. A few analog syntheses were conducted with the help of Dr. Kelly Aldrich and Linqing Mo.

2.2.1 Analog Preparation via Titanium Catalysis

As mentioned earlier, a titanium-catalyzed one-pot strategy can be used to access 2-aminonicotonitriles rapidly. Substituent R¹ is from a primary amine, whereas R² and R³ are from an alkyne (Scheme 2.3). The titanium catalysis can tolerate many functional groups including tertiary and secondary amines, ethers, halides, olefins, and silyl groups. Amines or alcohols tend to compete with substrates to bind to titanium. For functional groups that are not tolerated by titanium catalysis, protecting groups were used and later removed from the pyridine products.

Scheme 2.3. Synthesis of 2-aminonicotonitriles by Ti(NMe₂)₂(dpm)-catalyzed multicomponent coupling in a one-pot reaction.

For the purpose of investigating SAR at the R¹ position, different aniline derivatives were used (Table 2.1). MSU38225 is the original "hit" compound with an inhibition activity of 51% at 5 μM. ¹² All activity data shown later in the tables is at 5 μM. In comparison with MSU38225, moving one *meta* methyl group to the *ortho* position (**1a**) or removing one methyl group (**1c**) did not alter inhibition activity. The construction of heteroatoms like O (**1f**, **1g**) or N (**1d**) at the benzylic carbon resulted in a reduction of inhibition activity whereas replacing the benzylic methyl

with an isopropyl group (1b) retained inhibition activity. Di-halo substituted aniline (1h, 1i) also resulted in lower activities.

Table 2.1. Compounds prepared using titanium-catalyzed one-pot synthesis and their NRF2 activities.

| Compound | % Yield ^a | % Activity | Compound | % Yield | % Activity |
|------------------------------|----------------------|--|---------------------|---------------------|---|
| N NH Ph CN 1a | 15 | 51 ± 4.5 | HO NH NH CN | 45 | 16.7 ± 21.5 |
| N NH Ph CN | 18 | 55.2 ± 4.0 | OH NH NH CN 1g | 33, 54 ^b | $26.0 \pm 10.4^{\circ}$ 5.2 ± 13.0 |
| N NH Ph CN | 29 | 40.9 ± 9 | CI CI CI N NH CN 1h | 28 | 0.2 ± 26.9 |
| Ph CN 1d | 19 | 58.4 ± 10.8 | Br Br Br N NH CN 1i | 19 | 7.7 ± 8.1 |
| H ₂ N NH Ph CN 1e | 53, 86 ^b | -151.34±55.37 58.8 ± 7.6 ^d | N NH Ph CN | 38 | 51.8 ± 4.0 |

^aYields are of the purified compound after two synthetic steps, except as specified. ^bDeprotection Yield. ^cActivity before deprotection. ^dConcentration was increased to 10 μM.

SAR at R^2 and R^3 was explored by using different alkyne substrates (Table 2.2). The activities of these compounds showed that the proton at R^2 has slightly reduced activity in comparison to the methyl group, MSU38225 vs 2a, 2c vs 2d, 2e vs 2f.

Table 2.2. Compounds prepared using titanium-catalyzed one-pot synthesis and their NRF2 activities.

| Compound | % Yield ^a | % Activity | Compound | % Yield | % Activity |
|------------------|----------------------|------------------|---------------|---------------------|-----------------|
| N NH CN 2a | 19 | 38.4 ± 2.6 | 2g Sg | 22 | 17.7 ± 4.0 |
| N NH CN 2b | 34 | -11.8 ± 31.4 | N NH CN CN 2h | 17 | -4.9 ± 36.5 |
| N NH CN 2c | 15 | 37.2 ± 0.9 | Zi Zi | 10 | -29.6 ± 7.1 |
| N NH CN 2d | 14 | -32.3 ± 13.4 | N NH CN 2j | 12 | -1.5 ± 20.9 |
| CI N NH CN 2e | 19 | 49.2 ± 7.3 | N NH CN 2k | 17, 35 ^b | -6.3 ± 23.5 |
| CI N NH CN 2f | 23 | 18.2 ± 22.4 | | | |

^aYields are of the purified compound after two synthetic steps, except as specified. ^bHydrogenation Yield.

Long alkyl substitution like n-propyl group (2b) diminished inhibition activity. The position of substitution on the phenyl ring at R^3 was also explored (2f-h). meta (2f) or ortho (2g) substitutions seem to retain some activities, but para substitution diminished activity (2h-j). Replacement of the aromatic group with alkyl at R^3 (2k) also resulted in no activity.

The 2-step one-pot synthesis achieved decent yields overall (10-50%). The low yield can be reasoned from minor side products (*e.g.*, hydroamination product, formamidine product) or leftover starting materials (isonitrile) from the first step interfering with the second step. Higher yields should be achievable with the purification of iminoamination product. For the purposes of this study, the optimization of reaction conditions was not explored.

2.2.2 Analog Preparation via Modification of MSU38225

Hydrogen bonding donors and acceptors can highly influence the "drug-like" properties of the molecule according to Lipinski's rule of 5.¹⁴ Modifications of MSU38225 were conducted to explore the importance of hydrogen bonding donors and acceptors (Scheme 2.4). When the hydrogen bonding donor NH was replaced by NMe (3a) or NCOMe (3b), the analogs showed reduced inhibition activities. Base-catalyzed hydration (3c) of the nitrile to an amide resulted in a compound as an activator. This suggested that the hydrogen bonding donors and acceptors may play an important role in the inhibition mechanism. Simple bromination (3d) on the electron-rich site, *para* to N on the phenyl ring, gives an analog with reduced activity.

Scheme 2.4. Modifications of MSU38225.

2.2.3 Analog Preparation Incorporating Heterocycles

As mentioned earlier, titanium catalysis is not compatible with basic heterocycles since they bind to the catalysts and slow down the turnover frequency. In order to explore the activities of compounds incorporating heterocycles, different synthetic methodologies were explored to expand the scope of the compound library.

2.2.3.1 Installation of Heterocycles on 5-position

A selective chloride functionalization in the Pd-catalyzed amination of pyridines bearing traditionally more reactive bromides was used on 5-bromo-2-chloronicotinonitrile (Scheme 2.5).
DMAPF was used as a ligand to install dimethylaniline in 71% yield. The product, the 5-bromo-2-((3,5-dimethylphenyl)amino)nicotinonitrile, was treated with Suzuki-Miyaura coupling conditions to access analogs with different aromatic groups on the 5-position.

Scheme 2.5. Synthesis of 5-aryl pyridine derivatives.

Adding dialkyl substitution to the *meta* position (**4a**) on the phenyl ring slightly reduced activity (Table 2.3). For example, 3,5-dimethoxyl substitutions (**4b**) diminished inhibition activity. Dichloro substitution (**4c**) did not retain good inhibition activity either. One conclusion that can be drawn is that *meta* di-substitution reduces inhibition activity. Replacement of phenyl with a 3- or 4-pyridinyl group gave activation (**4d-f**).

Table 2.3. Compounds prepared using two-step synthesis and their NRF2 activities.

| Compound | % Yield | % Activity |
|------------------|---------|------------------|
| N NH CN 4a | 74 | 25.1 ± 12.3 |
| N NH CN 4b | 84 | -23.3 ± 4.6 |
| CI N NH CN CN 4c | 20 | 2.9 ± 4.2 |
| N NH CN 4d | 81 | -63.8 ± 32.0 |
| N NH CN 4f | 79 | -23.1 ± 32.0 |

Other boronic acids, such as 2-pyridinyl, and 2-furanyl boronic acid, did not give the desired product. The reason that 2-pyridinyl boronic acid gave no yield could be due to the undesired reaction, protodeboronation in the presence of a base.

2.2.3.2 Installation of Heterocycles on Amino group

Aniline derivatives incorporating heterocycles are known for good chelating ligands.¹⁶ However, once the substrate chelates to titanium catalysts, the iminoamination reaction proceeds very slow.¹⁷ To install different heterocycles on the amino group, a different synthetic route was proposed that uses bromopyridine to couple amino-heterocycles via Buchwald-Hartwig coupling.¹⁸ The bromopyridine derivative was accessed through a 3-step synthesis (Scheme 2.6). First, 3-dimethylamino-2-phenylacrylaldehyde, synthesized by Vilsmeier-Haack formylation of phenylacetaldehyde dimethyl acetal, was condensed with cyanoacetamide to access a pyridone derivative, which was later converted to a bromopyridine upon the treatment with P₂O₅ and NBu₄Br (Scheme 2.6).

Scheme 2.6. Synthesis of 2-bromo pyridine derivative.

The Buchwald-Hartwig coupling reaction of different aniline derivatives gave good yields overall (Table 2.4). Having a nitrogen atom on the ring *para* to the amino group (**5a**, **5c**, **5g**) seems harmful to the inhibition activity. Nitrogen at the *meta* or *ortho* position with no adjacent alkyl substituents can retain decent inhibition activities (**5h**, **5i**).

Table 2.4. Compounds prepared using Buchwald-Hartwig coupling and their NRF2 activities.

| Compound | % Yield | % Activity | Compound | % Yield | % Activity |
|---------------|---------|------------------|---------------|---------|------------------|
| N NH NH CN 5a | 12 | -4.8 ± 25.0 | Ph CN | 63 | -13.8 ± 9.8 |
| Ph Sb | 69 | 11.2 ± 9.9 | Ph Sg | 68 | -28.4 ± 34.5 |
| N NH NH CN 5c | 21 | -29.9 ± 11.2 | Ph Sh | 68 | 25.3 ± 9.1 |
| Ph Sd CN | 50 | 8.0 ± 20.2 | N NH NH CN 5i | 42 | 46.7 ± 6.9 |
| Ph CN 5e | 35 | 13.2 ± 12.5 | | | |

2.2.4 Analog Preparation with Core Change

Changes in the pyridine core structure were also explored. While pyridine was recognized as the first commonly used 6-membered aromatic nitrogen heterocycles among U.S. FDA-approved pharmaceuticals, quinoline and pyrazine are very commonly found and ranked 4th and 5th in all 6-membered aromatic nitrogen heterocycles.¹⁹

2.2.4.1 Pyrazine Derivatives

An analog with the replacement of pyridine with pyrazine was synthesized. The condensation of aminomalononitrile with phenylglyoxal oxime in isopropanol yielded 2-amino-3-cyano-5-phenylpyrazine N-oxide, which was later reduced by the treatment of triethyl phosphite to afford the amino pyrazine (Scheme 2.7).²⁰

The initial attempts by using the Buchwald-Hartwig coupling were not successful. Conditions using Pd(OAc)₂ or Pd₂dba₃ with JohnPhos, CyJohnPhos, Xantphos, and BINAP gave 0% yield. Chan-Lam coupling with dimethylphenylboronic acid achieved a 9% yield. The reaction conditions were further explored by screening different copper sources (CuCl₂, Cu(acac)₂, CuI, Cu₂O), base (TEA, pyridine, KO^tBu, Na₂CO₃), and solvents (DMF, DCM, MeCN, THF, EtOAc). However, the yield did not improve.

Scheme 2.7. Synthesis of pyrazine derivative.

Interestingly, even with such a small change in the core structure, the pyrazine derivative showed no inhibition activity (% inhibition: -7.8 ± 9.1). The reason could be that the polarity of

the molecule could contribute to the activity, and an additional hydrogen bonding acceptor on the pyridine ring was not favorable.

2.2.4.2 Quinoline and 1,8-naphthyridine Derivatives

Other than a pyrazine core structure, the quinoline and 1,8-naphthyridine derivatives were explored by using 2-aminoarylaldehydes and malononitrile (Scheme 2.8). Buchwald-Hartwig coupling catalyzed by $Pd(OAc)_2$ and Xantphos with aryl bromide yielded desired products in decent yields. The quinoline derivative showed some inhibition activity (% inhibition: 21.2 ± 23.9), while the naphthyridine derivative turned out to be an activator (% inhibition: -42.7 ± 28.7).

Scheme 2.8. Synthesis of quinoline and 1,8-naphthyridine derivative.

2.2.5 Future Analog Proposals

One of the limitations of using titanium-catalyzed one-pot pyridine synthesis is that no substitutions can be installed in the *para* position. For the construction of different functional groups at the *para* position, the following synthesis was proposed.

One can use mCPBA to convert MSU38225 into pyridine N-oxide derivative (Scheme 2.9), which is more electrophilic to nucleophilic attack. With POCl₃, Cl should attack the most electron-deficient site, *para* position of the pyridine N-oxide ring, to install the chloride.

Scheme 2.9. Proposed synthesis of 4-chloropyridine derivative.

Other than modification of MSU38225, a more general synthesis to install nucleophiles or electrophiles on the *para* position was proposed by using a *para* bromopyridine derivative.

To install OMe, nucleophilic aromatic substitution can be used (Scheme 2.10). The para methoxyl group can later be used as a directing group for directed lithiation at 5-position by using 2 equivalents of *n*BuLi. Quenching the reaction with 1 equivalent of NBS should yield the 5-bromopyridine derivative, which can be used for Suzuki coupling later.

Scheme 2.10. Proposed synthesis of 4-substituted pyridine derivatives.

To install electrophiles, halogen dance can be used to place the halogen in the desired position. LDA can deprotonate the 5-position directed by Br. After the formation of aryl lithium, halogen metal exchange happens to form the dibromopyridine derivative and the *para*-lithiated pyridine derivative (Scheme 2.11). The second halogen metal exchange should be selective because the *para*-bromine is directed by the cyano and bromo groups. After quenching with the desired electrophile, Suzuki coupling and deprotection should yield desired products.

Scheme 2.11. Proposed mechanism of "halogen dance".²¹

2.3 Compounds for Target Identification

2.3.1 Biotinylation and SAR Analysis

The strong interaction between biotin and avidin/streptavidin has been used in protein purification, detection, immobilization, labeling, and drug targeting systems.²² For identifying a target, a biotinylated small molecule drug can be used to pull down the interacting protein. If the small molecule can covalently bind to the target after treating the cells with biotinylated compounds, the target protein in the cell lysate can be purified using streptavidin due to the high affinity of streptavidin for biotin. The rest of the cellular proteins that do not bind to streptavidin can be washed away resulting in the separation of the target protein. The targeted protein can then be identified using mass spectroscopy.



Figure 2.5. Strategy to use biotinylation to identify the target.

As mentioned earlier, a structure-activity relationship can guide the structural design for the biotinylated small molecule due to the high sensitivity of the inhibitory activity to structural change. It was found that both peripheral and core structure changes can alter the inhibition activity (Figure 2.5). Core structural changes including replacing the pyridine ring with pyrazine, the hydration of the cyano-group, or the replacement of NH with other groups all diminished the inhibitory activity. Peripheral substitutions at R², R⁴, or R⁶ also reduced activity. However, a few

structural changes did not result in a reduction of inhibition activity, for example, compounds with substitutions at R³ or R⁵. Alkyl or halo substitutions at R³ or R⁵ retained similar inhibition activity with MSU38225.

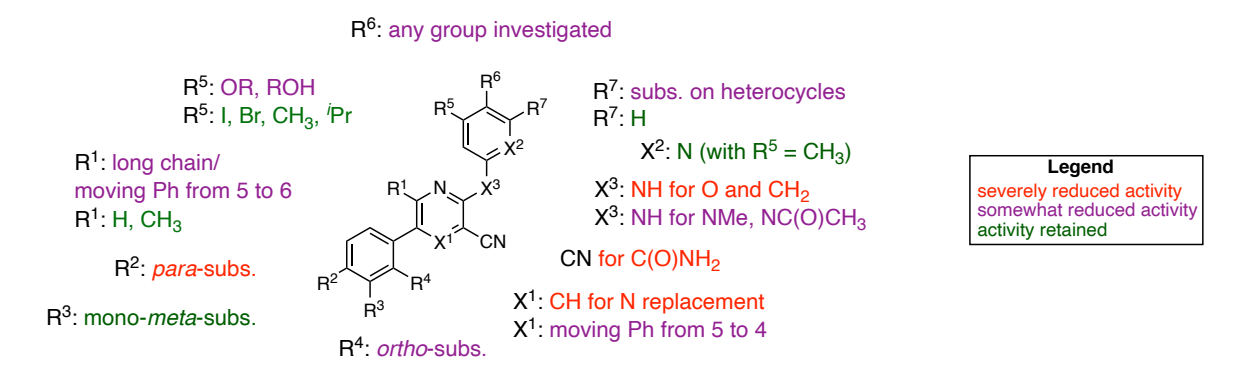


Figure 2.6. Summary of structure-activity relationship.

2.3.2 Synthesis of Biotinylated Compounds

With the SAR analysis, the possible positions that could accommodate PEG linker and biotin are R³ or R⁵. A synthetic route to install a PEG linker and biotin at R⁵ was developed using the commercially available 3-cyano-6-methyl-2-pyridone. The dihalo pyridine, 2-chloro-3-cyano-5-bromo-6-methyl-pyridine, was synthesized using NBS, followed by POCl₃.²³ A mixture of 5-bromo coupled and 2-chloro coupled products were observed after treating the dihalo pyridine with standard Suzuki condition. The desired product can be separated by column chromatography. The aniline derivative with a protected amine was coupled with 2-chloro-pyridine, followed by TFA deprotection to afford the product that showed 59% inhibition at 10 μM. The amide formation was achieved by using the activated biotin ester in the presence of a base.

Figure 2.7. Synthesis of the biotinylated compound.

However, the biotinylated compound did not present any inhibitory activity after multiple trials. One of the possible reasons could be the low permeability of the biotinylated compound. To solve this problem, "Click Chemistry" was proposed as an alternative to identify the target protein.

2.3.3 Synthesis of Compounds for "Click Chemistry"

The term "Click chemistry" was introduced by Karl Sharpless in 2001.²⁴ It refers to a class of biocompatible small molecule reactions commonly used in bioconjugation.²⁵ The classic click reaction is a copper-catalyzed cycloaddition of an azide and a terminal alkyne to form a 1,4-disubstituted triazole selectively. This type of reaction has been widely used for its biocompatibility and high yields with a large substrate scope.²⁵

Scheme 2.12. Example of copper-catalyzed Click reaction.

How we would like to apply click chemistry for our purpose is to treat the cancer cells with a small molecule with a terminal alkyne group first. After the small molecule binds to the target, a biotin-azide can be used to react with the alkyne via a copper catalyst. Then, streptavidin can be used to pull down the target.

Scheme 2.13. Synthesis of a pyridine derivative with a terminal alkyne.

As mentioned earlier, there are two positions that can accommodate substitutions without losing the inhibition activity. Due to the high reactivity of terminal alkyne in the presence of Pd catalyst,²⁶ the alkyne was protected with TMS groups before the Buchwald-Hartwig cross-coupling. Propargyl bromide was treated with benzyl alcohol in the presence of a base, followed by Buchwald-Hartwig coupling and deprotection to afford the desired product in 12% yield after 3 steps (Scheme 2.13).

Scheme 2.14. Synthesis of a pyridine derivative with a terminal alkyne.

A different synthetic route was developed by using the selective chloride functionalization in the Pd-catalyzed amination of pyridines,¹⁵ followed by Suzuki coupling and deprotection to afford the final product in 32% yield. Target identification with these two compounds is under investigation.

2.4 Improvement of Drug-like Properties

There are many important physicochemical properties of a small molecule drug to be considered, such as molecular weight, lipophilicity, hydrogen bonding, and ionization state.²⁷ These properties highly influence the ADMET profiles (absorption, distribution, metabolism,

elimination, toxicity) of the drug candidate.²⁸ Lipinski's "rule of 5" was often used to guide the design of small molecule drugs to balance property-associated parameters of potency, permeability, and metabolic clearance.²⁹ Over the years, the "rule of 5" has been optimized into the "rule of 3": (1) Octanol-water partition coefficient log P (ClogP) not greater than 3. (2) Molecular weight less than 300 daltons. (3) No more than 3 hydrogen bond donors.³⁰

Looking at MSU38225 (ClogP = 4.6; molecular weight = 313; Hydrogen bond donor = 1), the partition coefficient was far from ideal, making MSU38225 not very water-soluble.

2.4.1 Solubility

In order to solve the solubility problem of MSU38225, the calculated ClogP values were used as an estimate for the water solubility. The strategy to reduce the ClogP value was to incorporate heteroatoms like oxygen or nitrogen into the structure. In many cases, adding hetero atoms did reduce the ClogP values under 3. Unfortunately, many analogs with lower ClogP values do not have good inhibition activities including changes in aromatic rings or peripheral substituents (Figure 2.8).

Figure 2.8. Analogs with the addition of hetero atoms and their ClogP values.

A few compounds that showed similar inhibition activities with MSU38225 were tested for kinetic solubility (Figure 2.9). Compound 5i with promising ClogP value show much better kinetic solubility (209 μ M in 1× PBS), 70 times more soluble than MSU38225 (3 μ M).

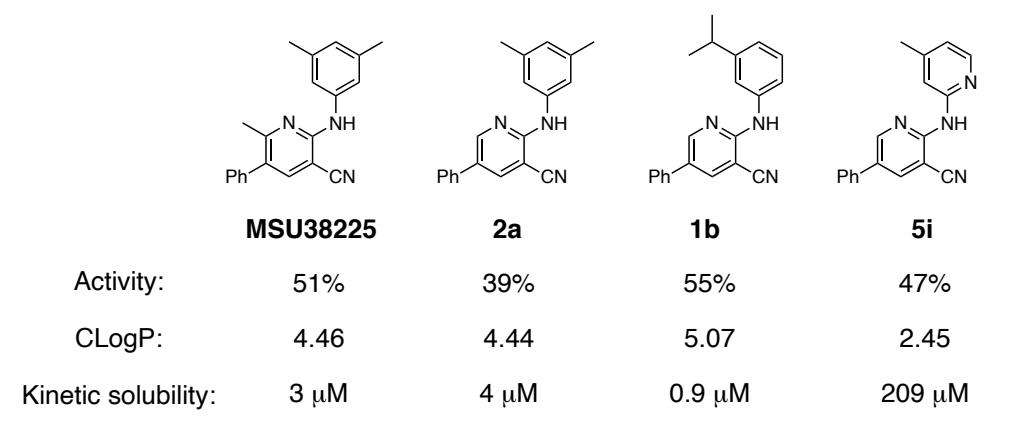


Figure 2.9. Analogs with decent activities, their ClogP values, and kinetic solubility data.

Solubility of 5i in DMSO was limited to about 20 μ M possibly due to the high lattice energy of the intramolecular cyclization product. The low solubility of this molecule attributes to H-bonding and possible large conjugation of the cyclization product with π stacking. The hydrogen chloride salt of 5i was synthesized and showed no greater solubility in DMSO. The mesylate salt of 5i showed improved solubility in DMSO, but seems unstable in pure water. The decomposition product is under investigation.

2.4.2 Metabolic Stability

Another important "drug-like" property is metabolic stability. The drug should stay in the body long enough to interact with the target. One strategy to increase metabolic stability is to reduce the overall lipophilicity of the structure because the binding sites of metabolizing enzymes are generally lipophilic in nature.

MSU drug discovery core facility tests rat microsomal stability in rats and reports the percentage of remaining compounds after 30 min. By comparing the microsomal stability of these analogs, a few sites of cellular oxidation were proposed (Figure 2.10). One site can be the benzylic C–H bond because benzylic C–H bonds are in general easily oxidized.

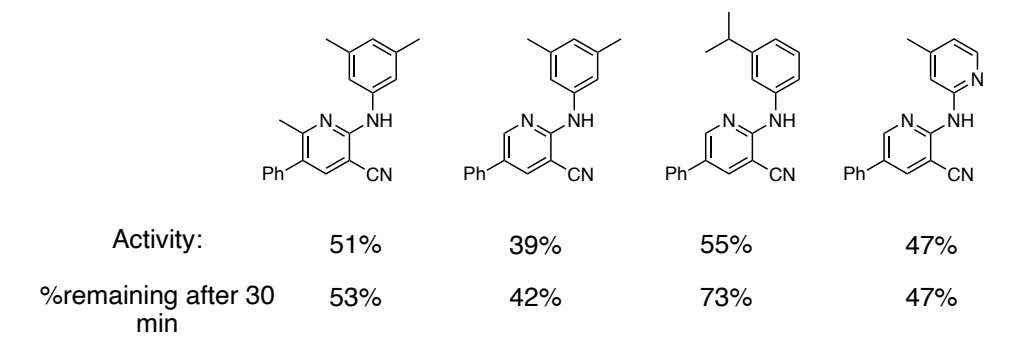


Figure 2.10. Analogs with good activities and their microsome stability data.

To test this hypothesis, a few analogs with no benzylic C–H bonds were synthesized using the Buchwald-Hartwig coupling. The benzylic methyl group was replaced by CF₃ or a cyclopropyl group, which makes the benzylic position harder to oxidize (Scheme 2.15).

Scheme. 2.15. Synthesis of analogs with higher benzylic stability.

Another possible site for cellular oxidation is the *para* position of the 5-phenyl group. To test this hypothesis, compound **2h** will be tested for microsome stability regardless of the low inhibition activity. Other methods, for example, testing the PK properties of possible metabolites, are being investigated.

Figure 2.11. Additional analogs with good activities and their microsome stability data.

The results from the second batch of compounds showed that the CF₃ replacement of benzylic methyl groups increased the microsomal stability. It also indicated that the addition of electron-withdrawing groups on the 5-phenyl group results in an improvement in stability. However, all tested compounds were considered moderate stable (40-75%). A better stability result is expected with the CF₃ substitution on pyridine and electron-withdrawing groups on the phenyl group.

2.5 Intramolecular Cyclization Process of ZH-III-71

A very interesting feature of compound **5i** caught my attention once it was synthesized. Not only does it show an unusually yellow color in solid-state and solution (Figure 2.12), but growing peaks were found upon sitting in NMR solvents over a few hours. These findings led to further investigation of this compound.

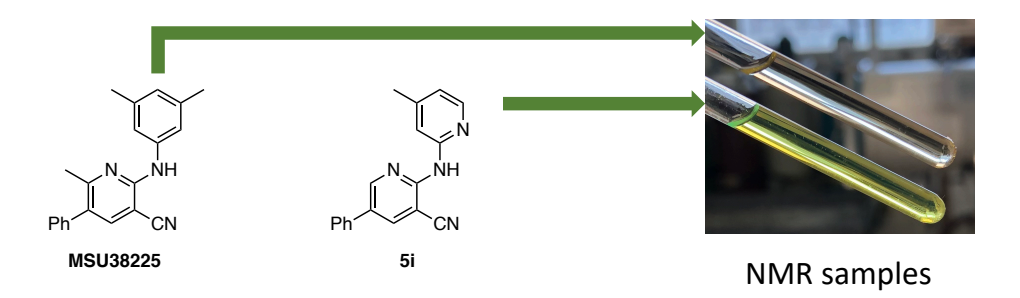


Figure 2.12. A picture of the NMR solution of MSU38225 and 5i.

Single crystals were grown by layering hexanes on the top of a DCM solution of **5i**. A single crystal XRD revealed an intramolecular cyclization product, which contributed to the yellow color due to its large aromatic conjugation. The compound undergoes a nucleophilic attack of the pyridine nitrogen on the nitrile as shown in Figure 2.13. This process was found reversible by dissolving the compound in solvents like chloroform. The open form (**5i-o**) and the closed form(**5i-c**) exist in equilibrium. The NMR peaks of the two isomers were assigned with the assumption that the major isomer is closed. Once the solid is dissolved, the incoming peaks are from the open form.

Figure 2.13. Proposed mechanism of intramolecular cyclization and a crystal structure of the cyclized product. Hydrogens in calculated positions, a second chemically equivalent molecule in the asymmetric unit and CH₂Cl₂ of crystallization are omitted.

The kinetics of the isomerization process were monitored by NMR with ferrocene as the internal standard (Table 2.5). The forward and back rate constants were calculated by fitting the proton NMR-derived concentrations as a function of time in these solvents (see experimental for the plots). The rate of the equilibrium is not a function of the polarity of the solvents. The isomerization took about 1.5 h in chloroform and 14 h in toluene to reach completion. The equilibrium process in DMSO seems to be the slowest among the three solvents that were tested, taking about 36 hours. The NMR experiments showed that the major isomer in toluene is in the open form, and the major isomer in chloroform and DMSO is in the closed form. The final ratio of the two isomers after reaching equilibrium were calculated by dividing the concentration of the open form by the concentration of the closed form.

Table 2.5. Equilibrium constants and rate constants of cyclization process in different solvents.

$$\begin{array}{c|c}
N & N & N \\
N & N & NH \\
N & NH & NH \\
Si-c & Si-o & Si-$$

| Solvents | $K_{ m eq}$ | $(\times 10^{-5} \text{ s}^{-1})$ | $(\times 10^{-5} \text{ s}^{-1})$ |
|-------------------|-------------|-----------------------------------|-----------------------------------|
| toluene | 1.48 | 4.8 | 3.3 |
| CHCl ₃ | 0.77 | 39 | 51 |
| DMSO | 0.49 | 1.5 | 3.0 |

The equilibrium constant, k_{eq}, was then converted to free energy by Van't Hoff equation (Table 2.6). The energy difference between the closed form and the open form was found as a function of the polarity of the solvents. It showed that polar solvents favor the closed form and non-polar solvents favor the open form. The energy difference was also calculated by DFT studies with B3LYP functional, cc-pvTZ basis set, and SMD solvent models. It showed that the open form is about 2 kcal/mol lower in energy when using toluene in the solvent model.

Due to the isomerization of **5i**, the potency of the active species may be higher than the assay result. The mixture of the two isomers could also cause off-target binding, which was supported by the much higher cytotoxicity of **5i** compared to MSU38225. The inhibition mechanism studies of MSU388225 and **5i** are under way.

Table 2.6. Energy difference of **5i-o** compared to **5i-c** from DFT calculation and experiments.

| | DFT calculation | Experimental |
|----------------------------|------------------|--------------|
| 5i-o : ΔE(kcal/mol) | (B3LYP, cc-pvTZ) | (25 °C) |
| toluene | -2.16 | -0.5 |
| CHCl ₃ | -0.43 | 0.01 |
| DMSO | -0.09 | 0.5 |
| H ₂ O | 1.10 | NR |

The equilibrium constants were calculated using the Van't Hoff equation, $\Delta G^{\circ} = -RT \ln K_{eq}$, where $R = 1.987 \times 10^{-3}$ kcal/mol and T = 298 K. The "Experimental" values are from ¹H NMR spectroscopy in the solvent after several days.

2.6 Conclusions

A novel NRF2 selective inhibitor, MSU38225, was synthesized by a titanium-catalyzed one-pot reaction. The effects of structural changes on MSU38225 were explored using 4 main categories of synthesis including titanium catalysis, Pd- and Cu-based coupling reactions. A few slightly more potent analogs were found through the SAR study. The inhibition activity seems very sensitive to structural changes, many minor peripheral or core structure changes cause the loss of inhibition activity.

Drug-like properties like solubility and metabolic properties were optimized from the lead compound resulting in a compound with improved solubility and high cytotoxicity. An isomerization of this compound was also discovered and studied, which could lead to a different inhibition mechanism.

2.7 Experimental details

General Considerations

All manipulations were carried out under an inert dinitrogen atmosphere in an MBraun glovebox or using standard Schlenk techniques. Toluene was sparged with dinitrogen and passed over an activated alumina column prior to use. Tetrahydrofuran, n-hexane, and 1,4-dioxane were dried over sodium-benzophenone radical, refluxed, and distilled under dinitrogen prior to use. Ethanol was dried over magnesium, refluxed, and distilled under dinitrogen prior to use. p-Cymene was sparged with dinitrogen and distilled from CaH₂ prior to use. All deuterated NMR solvents were purchased from Cambridge Isotope Laboratories. Benzene-d₆ was dried over CaH2 and distilled under dinitrogen. CDCl₃ was dried over P₂O₅ and distilled under dinitrogen. Synthesis of tert-butylisonitrile was made according to the literature procedure and purified by distillation under dry dinitrogen. Synthesis of Ti(dpm)(NMe₂)₂ and Ti(NMe₂)₃/SiO₂⁷⁰⁰ was done according to the literature procedures.³¹

Ti(NMe₂)₄ was purchased from Gelest and used as received. Palladium acetate was purchased from Strem and used as received. Tris(dibenzylideneacetone)dipalladium was purchased from Oakwood and used as received. BINAP was purchased from Alfa Aesar Chemicals and used as received. DMAPF was purchased from Sigma Aldrich and used as received. 1-phenyl-1-propyne and phenylacetylene were purchased from Combi-block and distilled from barium oxide prior to use.

General procedure A: Synthesis of 2-amino-nicotinonitrile derivatives via Titanium-catalyzed multicomponent coupling

In a glovebox, a 15 mL pressure tube equipped with a stir bar was loaded with Ti(dpm)(NMe₂)₂ (32 mg, 0.1 mmol, 10 mol%) in dry toluene (2 mL). To the solution was added arylamine (1.0 mmol, 1.0 equiv), alkyne (1.0 mmol, 1.0 equiv), and tert-butylisonitrile (1.5 mmol, 1.5 equiv). The pressure tube was sealed with a Teflon screw cap and taken out of the glovebox. With stirring, the solution was heated for 48 h at 100 °C in a silicone oil bath. The pressure tube was cooled to room temperature. Then, the tube was charged with malononitrile (132 mg, 2.0 mmol), DBU (76 mg, 0.5 mmol), molecular sieves (200 mg), and ethanol (2 mL). The mixture was heated for 2-12 h at 80 °C in an oil bath. The reaction was cooled to room temperature and diluted with ethyl acetate (50 mL). The reaction was washed with brine (50 mL × 3). The organic layer was separated and dried over Na₂SO₄. After the solvent was evaporated, the crude product was purified by column chromatography (silica gel, hexanes:EtOAc 10:1) to afford the desired products.

2-((2,5-dimethylphenyl)amino)-6-methyl-5-phenylnicotinonitrile (1a)

General procedure A was followed using 2,5-xylidine (249 μ L, 2.0 mmol, 1.0 equiv), 1-phenyl-1-propyne (250 μ L, 2.0 mmol, 1.0 equiv), tert-butylisonitrile (340 μ L, 3.0 mmol, 1.5 equiv), Ti(dpm)(NMe₂)₂ (62 mg, 0.2 mmol, 10 mol%), and 5 mL of dry toluene. The second step used

malononitrile (264 mg, 4.0 mmol, 2.0 equiv), DBU (152 mg, 1.0 mmol, 0.5 equiv), molecular sieves (400 mg), 4 mL of ethanol and was heated for 2 h. Removal of solvent afforded product as a white powder (96 mg, 15%). M.p.: 128-129°C. ¹H NMR (CDCl₃, 500 MHz, 25 °C): δ 7.81 (s, 1H), 7.62 (s, 1H), 7.44 (t, *J*=7.3 Hz, 2H), 7.41-7.35 (m, 1H), 7.30-7.26 (m, 2H), 7.13 (d, *J*=7.7 Hz, 1H), 6.92 (d, *J*=8.4 Hz, 1H), 6.79 (s, 1H), 2.43 (s, 3H), 2.36 (s, 3H), 2.31 (s, 3H). ¹³C³² NMR (CDCl₃, 126 MHz, 25 °C): δ 160.48, 154.88, 142.24, 138.39, 136.92, 136.36, 130.57, 129.24, 128.73, 127.95, 127.73, 126.91, 125.43, 123.25, 116.89, 90.25, 24.29, 21.44, 17.81. LRMS (EI): calc'd: 313; found: 312.

2-((3-isopropylphenyl)amino)-6-methyl-5-phenylnicotinonitrile (1b)

General procedure A was followed using 3-isopropylaniline (281 μL, 2.0 mmol, 1.0 equiv), 1-phenyl-1-propyne (250 μL, 2.0 mmol, 1.0 equiv), *tert*-butylisonitrile (340 μL, 3.0 mmol, 1.5 equiv), Ti(dpm)(NMe₂)₂ (62 mg, 0.2 mmol, 10 mol%), and 5 mL of dry toluene. The second step used malononitrile (264 mg, 4.0 mmol, 2.0 equiv), DBU (152 mg, 1.0 mmol, 0.5 equiv), molecular sieves (400 mg), 4 mL of ethanol and was heated for 2 h. Removal of solvent afforded product as a white powder (120 mg, 18%). M.p.: 114-115 °C ¹H NMR (CDCl₃, 500 MHz, 25 °C): δ 7.64 (s, 1H), 7.59-7.51 (m, 2H), 7.44 (app t, *J*=7.3 Hz, 2H), 7.38 (app t, *J*=7.3 Hz, 1H), 7.32-7.27 (m, 3H), 7.26 (s, 1H), 6.99 (s, 1H), 6.97 (s, 1H), 2.93 (hept, *J*=7.5 Hz, 1H), 2.47 (s, 3H), 1.29 (d, *J*=6.9 Hz, 6H). ¹³C {¹H} NMR (CDCl₃, 126 MHz, 25 °C): δ 154.30, 149.95, 142.24, 139.00, 138.32, 130.13, 129.23, 128.96, 128.76, 128.15, 127.78, 121.93, 118.35, 117.70, 116.88, 90.42, 34.30, 24.28, 24.11. LRMS (EI): calc'd: 327; found: 326.

6-methyl-5-phenyl-2-(m-tolylamino)nicotinonitrile (1c)

General procedure A was followed using *m*-toluidine (214 μL, 2.0 mmol, 1.0 equiv), 1-phenyl-1-propyne (250 μL, 2.0 mmol, 1.0 equiv), *tert*-butylisonitrile (340 μL, 3.0 mmol, 1.5 equiv), Ti(dpm)(NMe₂)₂ (62 mg, 0.2 mmol, 10 mol%), and 5 mL of dry toluene. The second step used malononitrile (264 mg, 4.0 mmol, 2.0 equiv), DBU (152 mg, 1.0 mmol, 0.5 equiv), molecular sieves (400 mg), 4 mL of ethanol and was heated for 2 h. Removal of solvent afforded product as a white powder (155 mg, 29%). M.p.:117-118 °C ¹H NMR (CDCl₃, 500 MHz, 25 °C): δ 7.64 (s, 1H), 7.59 (app d, *J*=8.1 Hz, 1H), 7.49-7.42 (m, 3H), 7.39 (app t, *J*=8.0 Hz, 1H), 7.31-7.23 (m, 4H), 6.94 (s, 1H), 6.93 (s, 1H), 2.49 (s, 3H), 2.39 (s, 3H). ¹³C {¹H} NMR (CDCl₃, 126 MHz, 25 °C): δ 160.36, 154.29, 142.23, 139.00, 138.95, 138.31, 129.23, 128.95, 128.75, 128.18, 127.78, 124.40, 120.85, 117.36, 116.85, 90.48, 24.28, 21.74. LRMS (EI): calc'd: 299; found: 298.

2-((3-bromo-5-methylphenyl)amino)-6-methyl-5-phenylnicotinonitrile (1d)

The general procedure A was followed using 3-bromo-5-methylaniline (370 mg, 2.0 mmol, 1.0 equiv), 1-phenyl-1-propyne (250 μL, 2.0 mmol, 1.0 equiv), *tert*-butylisonitrile (340 μL, 3.0 mmol, 1.5 equiv), Ti(dpm)(NMe₂)₂ (62 mg, 0.2 mmol, 10 mol%), and 5 mL of dry toluene. The second step used malononitrile (264 mg, 4.0 mmol, 2.0 equiv), DBU (152 mg, 1.0 mmol, 0.5 equiv), molecular sieves (400 mg), 4 mL of ethanol and was heated for 12 h. Removal of solvent afforded

product as a white powder (168 mg, 19%). M.p.: 161-162 °C. ¹H NMR (CDCl₃, 500 MHz, 25 °C): δ 7.63 (s, 1H), 7.46 (s, 2H), 7.44 (t, J=7.4 Hz, 2H), 7.38 (t, J=7.3 Hz, 1H), 7.27 (d, J=8.5 Hz, 2H), 6.87 (s, 1H), 2.78 (s, 3H), 2.47 (s, 3H). 13 C { 1 H} NMR (CDCl₃, 126 MHz, 25 °C): δ 160.36, 154.07, 142.26, 138.87, 138.18, 137.55, 130.20, 129.20, 128.79, 128.42, 127.86, 121.36, 119.96, 116.73, 90.67, 29.71, 24.25. LRMS (EI): calc'd: 377; found: 378.

tert-butyl (3-((3-cyano-6-methyl-5-phenylpyridin-2-yl)amino)benzyl)carbamate

General procedure was followed using 2-chloro-6-methyl-5-phenylnicotinonitrile (200 mg1.0 equiv), tert-butyl (3-aminobenzyl)carbamate (213 mg, 1.2 equiv), palladium(II) acetate (9 mg, 4 mol%), Xantphos (24 mg, 4.4 mol%), cesium carbonate (1146 mg, 4.0 equiv), and 3 mL of dry toluene. Column condition: 5% of EtOAc in hexanes. Removal of solvent afforded product as a colorless oil (220 mg, 53%). ¹H NMR (CDCl₃, 500 MHz, 25 °C): δ 7.67 (s, 1H), 7.64 (s, 1H), 7.61 (app d, *J*=8.1 Hz, 1H), 7.45 (app t, *J*=7.2 Hz, 2H), 7.39 (app t, *J*=7.4 Hz, 1H), 7.33 (app t, *J*=7.9 Hz, 1H), 7.28 (app d, *J*=6.8 Hz, 2H), 7.02 (app d, *J*=8.4 Hz, 1H), 7.01 (s, 1H), 4.91 (s, 1H), 4.36 (d, *J*=6.1 Hz, 2H), 2.49 (s, 3H), 1.47 (s, 9H). ¹³C{¹H} NMR (CDCl₃, 126 MHz, 25 °C): δ 160.21, 155.90, 154.01, 142.15, 139.87, 139.31, 138.10, 129.22, 129.09, 128.65, 128.30, 127.71, 122.39, 119.10, 116.61, 90.53, 79.55, 53.46, 44.68, 28.45, 24.14.

2-((3-(aminomethyl)phenyl)amino)-6-methyl-5-phenylnicotinonitrile (1e)

Tert-butyl (3-((3-cyano-6-methyl-5-phenylpyridin-2-yl)amino)benzyl)carbamate was dissolved in 5 mL of DCM in a 20 mL glass vial. To the solution, a 1 mL of TFA (1 mL) was added dropwise and let stir under room temperature overnight. The solution was neutralized by saturated Na₂CO₃ solution. The organic phase was separated, dried over Na₂SO₄, and then evaporated. The crude product was purified by column chromatography on silica gel (60% EtOAc in hexanes). Removal of solvent afforded product as a colorless oil (144 mg, 86%). ¹H NMR (CDCl₃, 500 MHz, 25 °C): δ 7.65 (app d, J=7.9 Hz, 1H), 7.63 (s, 1H), 7.63 (s, 1H), 7.44 (app t, J=7.3 Hz, 2H), 7.38 (app t, J=7.4 Hz, 1H), 7.33 (app t, J=7.8 Hz, 1H), 7.30 – 7.25 (m, 2H), 7.10 (s, 1H), 7.05 (app d, J=7.6 Hz, 1H), 3.90 (s, 2H), 2.48 (s, 3H). ¹³C{¹H} NMR (CDCl₃, 126 MHz, 25 °C): δ 160.17, 154.10, 144.22, 142.16, 139.25, 138.11, 129.13, 129.08, 128.63, 128.17, 127.67, 122.06, 118.71, 118.54, 116.67, 90.46, 46.46, 24.16.

2-((3-(((tert-butyldimethylsilyl)oxy)methyl)phenyl)amino)-6-methyl-5-phenylnicotinonitrile

General procedure A was followed using 3-(((tert-butyldimethylsilyl)oxy)methyl)aniline (474 mg, 2.0 mmol, 1.0 equiv), 1-phenyl-1-propyne (250 μ L, 2.0 mmol, 1.0 equiv), *tert*-butylisonitrile (340 μ L, 3.0 mmol, 1.5 equiv), Ti(dpm)(NMe₂)₂ (64 mg, 0.2 mmol, 10 mol%), and 4 mL of dry toluene. The second step used malononitrile (264 mg, 4 mmol, 2.0 equiv), DBU (152 mg, 1.0 mmol, 0.5 equiv), molecular sieves (400 mg), 4 mL of ethanol and was heated for 2 h. Removal of solvent afforded product as light yellow oil (384 mg, 45%). ¹H NMR (CDCl₃, 500 MHz, 25 °C): δ 7.64 (s, 2H), 7.61 (app d, J=7.6 Hz, 1H), 7.44 (app t, J=7.3 Hz, 2H), 7.38 (app t, J=7.4 Hz, 1H), 7.32 (app t, J=7.8 Hz, 1H), 7.28 (app d, J=6.8 Hz, 2H), 7.06 (d, J=7.6 Hz, 1H), 7.00 (s, 1H), 4.77

(s, 2H), 2.47 (s, 3H), 0.96 (s, 9H), 0.13 (s, 6H). The NMR shows a compound with modest purity, that was used without further purification in the next step.

2-((3-(1-hydroxyethyl)phenyl)amino)-6-methyl-5-phenylnicotinonitrile (1f)

In a 20 mL glass vial, 2-((3-(((tert-butyldimethylsilyl)oxy)methyl)phenyl)amino)-6-methyl-5-phenylnicotinonitrile (**1u-I**) (400 mg, 0.93 mmol) was dissolved in 5 mL of THF with a stir bar. To this solution, 3 mL of 1 M TBAF solution (3.0 mmol) in THF was added dropwise under room temperature. The colorless solution became bright orange. After 1 h of stirring, the solvent was removed and crude product was purified by column chromatography (silica hexanes:EtOAc 4:1), which afforded the desired compound as colorless crystals (54%, 163 mg). M.p.: 114-115 °C. ¹H NMR (DMSO-d₆, 500 MHz, 25 °C): δ 8.34 (s, 1H), 8.20 (s, 1H), 8.13 (app d, *J*=9.6 Hz, 1H), 8.02 (app t, *J*=7.2 Hz, 3H), 7.95 (app t, *J*=7.4 Hz, 1H), 7.94-7.90 (m, 2H), 7.87 (app t, *J*=7.8 Hz, 1H), 7.62 (app d, *J*=8.6 Hz, 1H), 5.22-5.09 (m, 2H), 3.77 (t, *J*=6.0 Hz, 1H), 2.94 (s, 3H). ¹³C {¹H} NMR (DMSO-d₆, 126 MHz, 25 °C): δ 159.72, 154.42, 143.04, 142.86, 139.61, 138.32, 129.18, 128.55, 127.99, 127.56, 121.52, 119.81, 119.41, 116.35, 90.76, 63.68, 23.28.

2-((3-(1-((tert-butyldimethylsilyl)oxy)ethyl)phenyl)amino)-6-methyl-5-phenylnicotinonitrile

General procedure A was followed using 3-(1-((*tert*-butyldimethylsilyl)oxy)ethyl)aniline (251 mg, 1.0 mmol, 1.0 equiv), 1-phenyl-1-propyne (125 μL, 1.0 mmol, 1.0 equiv), *tert*-butylisonitrile

(170 μL, 1.5 mmol, 1.5 equiv), Ti(dpm)(NMe₂)₂ (32 mg, 0.1 mmol, 10 mol%), and 2 mL of dry toluene. The second step used malononitrile (132 mg, 2 mmol, 2.0 equiv), DBU (76 mg, 0.5 mmol, 0.5 equiv), molecular sieves (200 mg), 2 mL of ethanol and was heated for 2 h. Removal of solvent afforded product as a white powder (146 mg, 33%). M.p.: 69-70 °C. ¹H NMR (CDCl₃, 500 MHz, 25 °C): δ 7.63 (d, *J*=8.4 Hz, 2H), 7.59 (s, 1H), 7.44 (app t, *J*=7.4 Hz, 2H), 7.38 (app t, *J*=7.4 Hz, 1H), 7.31 (app t, *J*=7.9 Hz, 1H), 7.28 (app d, *J*=7.1 Hz, 2H), 7.08 (app d, *J*=7.6 Hz, 1H), 6.98 (s, 1H), 4.89 (q, 1H), 2.47 (s, 3H), 1.44 (d, *J*=6.3 Hz, 3H), 0.91 (s, 9H), 0.08 (s, 3H), 0.01 (s, 3H). ¹³C {¹H} NMR (CDCl₃, 126 MHz, 25 °C): δ 160.34, 154.29, 148.08, 142.24, 138.86, 138.31, 129.23, 128.86, 128.75, 128.20, 127.78, 120.58, 118.58, 117.27, 116.85, 90.48, 70.92, 27.42, 26.06, 24.29, 18.45, –4.56, –4.66.

2-((3-(1-hydroxyethyl)phenyl)amino)-6-methyl-5-phenylnicotinonitrile (1g)

In a 20 mL glass vial, 2-((3-(1-((*tert*-butyldimethylsilyl)oxy)ethyl)phenyl)amino)-6-methyl-5-phenylnicotinonitrile (**1v-I**) (50 mg, 0.11 mmol) was dissolved in 5 mL of THF with a stir bar. To this solution, 1 mL of 1 M TBAF solution (1.0 mmol) in THF was added dropwise under room temperature. The colorless solution became bright orange. After 1 h of stirring, the solvent was removed and crude product was purified by column chromatography (silica hexanes:EtOAc 3:1), which afforded the desired compound as colorless crystals (54%, 20 mg). M.p.: 194-195 °C. ¹H NMR (DMSO-d₆, 500 MHz, 25 °C): δ 11.25 (s, 1H), 8.29 (s, 1H), 8.06 (s, 1H), 7.77 (app d, *J*=8.1 Hz, 1H), 7.63 (s, 2H), 7.50-7.43 (m, 4H), 7.37 (ddd, *J*=8.6, 5.6, 2.3 Hz, 1H), 7.24 (app t, *J*=7.8 Hz, 1H), 6.93 (app d, *J*=7.6 Hz, 1H), 4.70 (q, *J*=6.4 Hz, 1H), 2.42 (s, 3H), 1.34 (d, *J*=6.4 Hz, 3H).

¹³C{¹H} NMR (DMSO-d₆, 126 MHz, 25 °C): δ 170.01, 156.86, 153.28, 148.09, 140.25, 139.06, 138.69, 129.33, 128.37, 127.00, 125.89, 118.60, 117.27, 116.22, 107.79, 68.16, 25.98, 23.47. LRMS (EI): calc'd: 329; found: 328.

2-((3,5-dichlorophenyl)amino)-6-methyl-5-phenylnicotinonitrile (1h)

General procedure A was followed using 3,5-dichloroaniline (324 mg, 2.0 mmol, 1.0 equiv), 1-phenyl-1-propyne (250 μL, 2.0 mmol, 1.0 equiv), *tert*-butylisonitrile (340 μL, 3.0 mmol, 1.5 equiv), Ti(dpm)(NMe₂)₂ (62 mg, 0.2 mmol, 10 mol%), and dry toluene (5 mL). The second step used malononitrile (264 mg, 4.0 mmol, 2.0 equiv), DBU (152 mg, 1.0 mmol, 0.5 equiv), molecular sieves (400 mg), 4 mL of ethanol and was heated for 12 h. Removal of solvent afforded product as a white powder (200 mg, 28%). M.p.: 211-212 °C. ¹H NMR (CDCl₃, 500 MHz, 25 °C): δ 7.72 (d, *J*=1.7 Hz, 2H), 7.68 (s, 1H), 7.45 (t, *J*=7.2 Hz, 2H), 7.40 (t, *J*=7.3 Hz, 1H), 7.28 (d, *J*=6.9 Hz, 2H), 7.08 (t, *J*=1.8 Hz, 1H), 6.98 (s, 1H), 2.52 (s, 3H). ¹³C{¹H} NMR (CDCl₃, 126 MHz, 25 °C): δ 160.36, 153.33, 142.43, 140.94, 137.77, 135.26, 129.50, 129.16, 128.88, 128.10, 123.20, 118.09, 116.21, 91.46, 24.16. LRMS (EI): calc 'd: 353; found: 352.

2-((3,5-dibromophenyl)amino)-6-methyl-5-phenylnicotinonitrile (1i)

General procedure A was followed using 3,5-dibromoaniline (502 mg, 2.0 mmol, 1.0 equiv), 1-phenyl-1-propyne (250 μL, 2.0 mmol, 1.0 equiv), *tert*-butylisonitrile (340 μL, 3.0 mmol, 1.5

equiv), Ti(dpm)(NMe₂)₂ (62 mg, 0.2 mmol, 10 mol%), and dry toluene (5 mL). Then, malononitrile (264 mg, 4.0 mmol, 2.0 equiv), DBU (152 mg, 1.0 mmol, 0.5 equiv), molecular sieves (400 mg), 4 mL of ethanol were added, and the solution was heated for 12 h. Removal of solvent afforded product as a white powder (168 mg, 19%). M.p.: 202-203 °C. ¹H NMR (CDCl₃, 500 MHz, 25 °C): δ 7.91 (d, *J*=1.5 Hz, 2H), 7.68 (s, 1H), 7.45 (t, *J*=7.3 Hz, 2H), 7.40 (t, *J*=7.3 Hz, 1H), 7.37 (t, *J*=1.5 Hz, 1H), 7.28 (d, *J*=6.9 Hz, 2H), 6.98 (s, 1H), 2.51 (s, 3H). ¹³C{¹H} NMR (CDCl₃, 126 MHz, 25 °C): δ 160.44, 153.29, 142.32, 141.33, 137.82, 129.51, 129.16, 128.86, 128.50, 128.07, 123.01, 121.30, 116.25, 91.40, 24.22. LRMS (EI): calc'd: 443; found: 443.

2-((3-iodophenyl)amino)-6-methyl-5-phenylnicotinonitrile (1j)

General procedure A was followed using 3-iodoaniline (438 mg, 2.0 mmol, 1.0 equiv), 1-phenyl-1-propyne (250 μL, 2.0 mmol, 1.0 equiv), *tert*-butylisonitrile (340 μL, 3.0 mmol, 1.5 equiv), Ti(dpm)(NMe₂)₂ (62 mg, 0.2 mmol, 10 mol%), and dry toluene (5 mL). The second step used malononitrile (264 mg, 4.0 mmol, 2.0 equiv), DBU (152 mg, 1.0 mmol, 0.5 equiv), molecular sieves (400 mg), 4 mL of ethanol and was heated for 6 h. Removal of solvent afforded product as a white powder (310 mg, 38%). M.p.: 144-145 °C. ¹H NMR (CDCl₃, 500 MHz, 25 °C): δ 8.25-8.21 (m, 1H), 7.66 (s, 1H), 7.62 (ddd, *J*=8.2, 2.2, 0.8 Hz, 1H), 7.47-7.41 (m, 3H), 7.41-7.37 (m, 1H), 7.30-7.27 (m, 2H), 7.08 (t, *J*=8.0 Hz, 1H), 6.94 (s, 1H), 2.50 (s, 3H). NMR (CDCl₃, 126 MHz, 25 °C): δ 160.39, 153.71, 142.27, 140.30, 138.04, 132.29, 130.50, 129.19, 128.90, 128.81, 128.76, 127.94, 119.18, 116.52, 94.29, 90.94, 24.24.

2-((3,5-dimethylphenyl)amino)-5-phenylnicotinonitrile (2a)

General procedure A was followed using 3,5-dimethylaniline (125 μL, 1.0 mmol, 1.0 equiv), phenylacetylene (110 μL, 1.0 mmol, 1.0 equiv), *tert*-butylisonitrile (170 μL, 1.5 mmol, 1.5 equiv), Ti(dpm)(NMe₂)₂ (32 mg, 0.1 mmol, 10 mol%), and 2 mL of dry toluene. The second step used malononitrile (132 mg, 2.0 mmol, 2.0 equiv), DBU (76 mg, 0.5 mmol, 0.5 equiv), molecular sieves (200 mg), 2 mL of ethanol and was heated for 2 h. Removal of solvent afforded product as a white solid (58 mg, 19%). M.p.: 114-115 °C. ¹H NMR (CDCl₃, 500 MHz, 25 °C): 8.63 (s, 1H), 7.98 (s, 1H), 7.52-7.43 (m, 3H), 7.42-7.38 (m, 1H), 7.23 (s, 2H), 6.95 (s, 1H), 6.80 (s, 1H), 2.35 (s, 6H). ¹³C {¹H} NMR (CDCl₃, 126 MHz, 25 °C): 155.34, 151.00, 139.78, 138.96, 138.71, 136.27, 129.39, 128.07, 127.56, 126.40, 126.22, 118.99, 116.61, 115.71, 21.61. LRMS (EI): calc'd: 299, found: 298.

Alternative method: A 15 mL pressure tube was charged with Ti(NMe₂)₃/SiO₂⁷⁰⁰ (320 mg), 2,6-dimethylphenylamidate (26 mg, 0.10 mmol), p-cymene (1 mL), and a Teflon coated stir bar. This mixture was stirred at room temperature for 5 min. Separately, a solution containing 3,5-dimethylaniline (242 mg, 2.0 mmol), CyNC (218 mg, 2.0 mmol), and phenylacetylene (408 mg, 4.0 mmol) in p-cymene was prepared (with a total volume of ~2 mL). This solution was added to the contents of the pressure tube, which immediately resulted in a color change from pale yelloworange to bright red. The tube was sealed and transferred from the glovebox to a preheated aluminum block (180 °C) where it was heated and stirred for 2 h. GC-FID of the crude 3CC reaction mixture at this point showed ~90% yield of the 3CC product. The tube was removed from

heat and allowed to cool to room temperature before being opened in air. The following reagents were then added: 200 mg of activated 3 Å molecular sieves, 3 mL of dry EtOH, DBU (151 mg, 1 mmol), and malononitrile (264 mg, 4 mmol). The tube was once again sealed and heated to 80 °C in an oil bath, with stirring, for 2 h. After 2 h the reaction was cooled. The crude product could be identified by GC-MS as the targeted pyridine. The contents of the pressure tube were transferred to a round bottom flask, and the volatiles were removed by rotary evaporation. This resulted in ~2 mL of a viscous brown oil, which was purified by column chromatography (hexanes, gradient with 0-10% EtOAc, Al₂O₃ packing, product fluoresces under long-UV, Rf ~0.5). From the column fractions, the solvent was removed by rotary evaporation to yield the product as a waxy tan solid. This waxy solid was washed with hexanes to afford an off-white powder that was pure by several methods of characterization. Yield: 62 mg, 11%. Additionally, from this powder, X-ray quality crystals were grown from a solution of acetone and diethyl ether layered with hexane and stored at ~20 °C overnight.

2-((3,5-dimethylphenyl)amino)-5-phenyl-6-propylnicotinonitrile (2b)

General procedure A was followed using 3,5-dimethylaniline (125 μL, 1.0 mmol, 1.0 equiv), 1-phenyl-1-pentyne (160 μL, 1.0 mmol, 1.0 equiv), *tert*-butylisonitrile (170 μL, 1.5 mmol, 1.5 equiv), Ti(dpm)(NMe₂)₂ (31 mg, 0.1 mmol, 10 mol%), and 2 mL of dry toluene. The second step used malononitrile (132 mg, 2.0 mmol, 2.0 equiv), DBU (76 mg, 0.5 mmol, 0.5 equiv), molecular sieves (200 mg), 2 mL of ethanol and was heated for 2 h. Removal of solvent afforded product as a white powder (113 mg, 34%). M.p.: 126-127°C. ¹H NMR (CDCl₃, 500 MHz, 25 °C): δ 7.60 (s,

1H), 7.43 (t, J=7.2 Hz, 2H), 7.38 (t, J=7.3 Hz, 1H), 7.36 (s, 2H), 7.26 (d, 2H), 6.92 (s, 1H), 6.75 (s, 1H), 2.70 (t, J=7.6 Hz, 2H), 2.34 (s, 6H), 1.79 (h, J=7.4 Hz, 2H), 0.90 (t, J=7.4 Hz, 3H). 13 C{ 1 H} NMR (CDCl₃, 126 MHz, 25 °C): δ 163.60, 154.38, 142.28, 138.96, 138.61, 138.39, 129.35, 128.67, 128.15, 127.69, 125.10, 117.95, 116.90, 90.13, 37.73, 21.78, 21.59, 14.08. LRMS (EI): calc'd: 341; found: 340.

6-methyl-5-phenyl-2-((3,4,5-trimethylphenyl)amino)nicotinonitrile (2c)

General procedure A was followed using 3,4,5-trimethylaniline (280 μL, 2.0 mmol, 1.0 equiv), 1-phenyl-1-propyne (250 μL, 2.0 mmol, 1.0 equiv), *tert*-butylisonitrile (340 μL, 3.0 mmol, 1.5 equiv), Ti(dpm)(NMe₂)₂ (62 mg, 0.2 mmol, 10 mol%), and 5 mL of dry toluene. The second step used malononitrile (264 mg, 4.0 mmol, 2.0 equiv), DBU (152 mg, 1.0 mmol, 0.5 equiv), molecular sieves (400 mg), 4 mL of ethanol and was heated for 2 h. Removal of solvent afforded product as a white powder (98 mg, 15%). M.p.: 167-177 °C ¹H NMR (CDCl₃, 500 MHz, 25 °C): δ 7.61 (s, 1H), 7.48-7.42 (m, 2H), 7.41-7.36 (m, 1H), 7.34 (s, 2H), 7.29-7.27 (m, 2H), 6.84 (s, 1H), 2.52 (s, 3H), 2.31 (s, 6H), 2.17 (s, 3H). ¹³C{¹H} NMR (CDCl₃, 126 MHz, 25 °C): δ 160.38, 154.55, 142.20, 138.44, 137.13, 135.96, 130.65, 129.24, 128.72, 127.79, 127.69, 119.89, 116.99, 90.10, 24.29, 20.99, 15.08. LRMS (EI): calc'd: 327; found: 326.

5-phenyl-2-((3,4,5-trimethylphenyl)amino)nicotinonitrile (2d)

General procedure A was followed using 3,4,5-trimethylaniline (140 μL, 1.0 mmol, 1.0 equiv), phenylacetylene (110 μL, 1.0 mmol, 1.0 equiv), *tert*-butylisonitrile (170 μL, 1.5 mmol, 1.5 equiv), Ti(dpm)(NMe₂)₂ (32 mg, 0.1 mmol, 10 mol%), and 2 mL of dry toluene. The second step used malononitrile (132 mg, 2.0 mmol, 2.0 equiv), DBU (76 mg, 0.5 mmol, 0.5 equiv), molecular sieves (200 mg), 2 mL of ethanol and was heated for 2 h. Removal of solvent afforded product as a white solid (43 mg, 14%). ¹H NMR (CDCl₃, 500 MHz, 25 °C): δ 8.61 (s, 1H), 7.96 (s, 1H), 7.54-7.43 (m, 4H), 7.39 (t, *J*=7.7 Hz, 1H), 7.23 (s, 2H), 6.91 (s, 1H), 2.32 (s, 6H), 2.17 (s, 3H). ¹³C { ¹H } NMR (CDCl₃, 126 MHz, 25 °C): δ 155.58, 151.00, 139.62, 137.25, 136.23, 135.18, 131.60, 129.24, 127.85, 127.10, 126.22, 121.06, 116.61, 92.73, 20.83, 15.04. LRMS (EI): calc'd: 313; found: 312. 5-(3-chlorophenyl)-2-((3.5-dimethylphenyl)amino)-6-methylnicotinonitrile (2e)

General procedure A was followed using 3,5-dimethylaniline (250 μL, 2.0 mmol, 1.0 equiv), 1-chloro-3-(prop-1-yn-1-yl)benzene (300 mg, 2.0 mmol, 1.0 equiv), *tert*-butylisonitrile (340 μL, 3.0 mmol, 1.5 equiv), Ti(dpm)(NMe₂)₂ (64 mg, 0.2 mmol, 10 mol%), and 4 mL of dry toluene. The second step used malononitrile (264 mg, 4.0 mmol, 2.0 equiv), DBU (152 mg, 1.0 mmol, 0.5 equiv), molecular sieves (400 mg), 4 mL of ethanol and was heated for 2 h. Removal of solvent afforded product as a white solid (127 mg, 18%). M.p.: 136-137 °C. ¹H NMR (CDCl₃, 500 MHz,

25 °C): δ 7.60 (s, 1H), 7.38-7.34 (m, 2H), 7.31 (s, 2H), 7.29-7.27 (m, 1H), 7.19-7.13 (m, 1H), 6.92 (s, 1H), 6.77 (s, 1H), 2.46 (s, 3H), 2.34 (s, 7H). ¹³C{¹H} NMR (CDCl₃, 126 MHz, 25 °C): δ 154.56, 142.24, 140.06, 138.80, 138.63, 134.63, 130.03, 129.32, 127.96, 127.48, 126.59, 125.64, 118.27, 116.60, 90.52, 24.19, 21.65.

5-(3-chlorophenyl)-2-((3,5-dimethylphenyl)amino)nicotinonitrile (2f)

General procedure A was followed using 3,5-dimethylaniline (125 μL, 1.0 mmol, 1.0 equiv), 1-chloro-3-ethynylbenzene (136 mg, 1.0 mmol, 1.0 equiv), *tert*-butylisonitrile (170 μL, 1.5 mmol, 1.5 equiv), Ti(dpm)(NMe₂)₂ (32 mg, 0.1 mmol, 10 mol%), and 2 mL of dry toluene. The second step used malononitrile (132 mg, 2.0 mmol, 2.0 equiv), DBU (76 mg, 0.5 mmol, 0.5 equiv), molecular sieves (200 mg), 2 mL of ethanol and was heated for 2 h. Removal of solvent afforded product as a white solid (76 mg, 23%). M.p.: 125-126 °C. ¹H NMR (CDCl₃, 500 MHz, 25 °C): δ 8.60 (s, 1H), 7.96 (s, 1H), 7.53-7.46 (m, 1H), 7.45-7.32 (m, 3H), 7.23 (s, 2H), 6.99 (s, 1H), 6.81 (s, 1H), 2.35 (s, 6H). ¹³C {¹H} NMR (CDCl₃, 126 MHz, 25 °C): δ 155.47, 150.82, 139.62, 138.87, 137.99, 137.94, 130.50, 127.95, 126.37, 126.27, 125.98, 124.35, 118.96, 116.22, 93.18, 21.47. LRMS (EI): calc'd: 333; found: 332.

5-(2-chlorophenyl)-2-((3,5-dimethylphenyl)amino)nicotinonitrile (2g)

General procedure A was followed using 3,5-dimethylaniline (250 μL, 1.0 mmol, 1.0 equiv), 1-chloro-3-ethynylbenzene (272 mg, 2.0 mmol, 1.0 equiv), *tert*-butylisonitrile (340 μL, 3.0 mmol, 1.5 equiv), Ti(dpm)(NMe₂)₂ (64 mg, 0.2 mmol, 10 mol%), and 5 mL of dry toluene. The second step used malononitrile (264 mg, 4.0 mmol, 2.0 equiv), DBU (152 mg, 1.0 mmol, 0.5 equiv), molecular sieves (400 mg), 4 mL of ethanol and was heated for 2 h. Removal of solvent afforded product as a white solid (149 mg, 22%). M.p.: 139-140°C. ¹H NMR (CDCl₃, 500 MHz, 25 °C): δ 8.46 (d, *J*=1.9 Hz, 1H), 7.99-7.85 (m, 1H), 7.53-7.47 (m, 1H), 7.39-7.28 (m, 3H), 7.24 (s, 2H), 6.99 (s, 1H), 6.81 (s, 1H), 2.35 (s, 6H). ¹³C{¹H} NMR (CDCl₃, 126 MHz, 25 °C): δ 155.26, 152.76, 142.17, 138.85, 138.03, 135.24, 134.99, 130.90, 130.32, 129.49, 127.37, 126.24, 119.04, 116.33, 109.53, 92.40, 21.47. LRMS (EI): calc 'd: 333; found: 332.

5-(4-chlorophenyl)-2-((3,5-dimethylphenyl)amino)nicotinonitrile (2h)

General procedure A was followed using 3,5-dimethylaniline (125 μ L, 1.0 mmol, 1.0 equiv), 1-chloro-4-ethynylbenzene (136 mg, 1.0 mmol, 1.0 equiv), *tert*-butylisonitrile (170 μ L, 1.5 mmol, 1.5 equiv), Ti(dpm)(NMe₂)₂ (32 mg, 0.1 mmol, 10 mol%), and dry toluene (2 mL). The second step used malononitrile (132 mg, 2.0 mmol, 2.0 equiv), DBU (76 mg, 0.5 mmol, 0.5 equiv), molecular sieves (200 mg), 2 mL of ethanol and was heated for 2 h. Removal of solvent afforded product as light yellow crystals (55 mg, 17%). M.p.: 147-148 °C. ¹H NMR (CDCl₃, 500 MHz, 25 °C): δ 8.59 (d, J=2.5 Hz, 1H), 7.93 (d, J=2.5 Hz, 1H), 7.47-7.38 (m, 4H), 7.23 (s, 2H), 6.99 (s, 1H), 6.80 (s, 1H), 2.35 (s, 6H). 13 C{ 1 H} NMR (CDCl₃, 126 MHz, 25 °C): δ 155.42, 150.78, 139.58,

138.95, 138.17, 134.69, 134.20, 129.56, 127.57, 126.32, 126.28, 119.03, 116.40, 93.27, 21.59. LRMS (EI): calc'd: 333; found: 332.

2-((3,5-dimethylphenyl)amino)-5-(p-tolyl)nicotinonitrile (2i)

General procedure A was followed using 3,5-dimethylaniline (125 μL, 1.0 mmol, 1.0 equiv), 4-ethynyltoluene (127 μL, 1.0 mmol, 1.0 equiv), *tert*-butylisonitrile (170 μL, 1.5 mmol, 1.5 equiv), Ti(dpm)(NMe₂)₂ (32 mg, 0.1 mmol, 10 mol%), and dry toluene (2 mL). The second step used malononitrile (132 mg, 2.0 mmol, 2.0 equiv), DBU (76 mg, 0.5 mmol, 0.5 equiv), molecular sieves (200 mg), 2 mL of ethanol and was heated for 2 h. Removal of solvent afforded product as a white solid (31 mg, 10%). M.p.: 112-113 °C. ¹H NMR (CDCl₃, 500 MHz, 25 °C): δ 8.62 (d, *J*=2.5 Hz, 1H), 7.95 (d, *J*=2.5 Hz, 1H), 7.39 (d, *J*=8.1 Hz, 2H), 7.28 (d, *J*=7.9 Hz, 2H), 7.23 (s, 2H), 6.94 (s, 1H), 6.79 (s, 1H), 2.41 (s, 3H), 2.35 (s, 6H). ¹³C {¹H} NMR (CDCl₃, 126 MHz, 25 °C): δ 150.79, 139.53, 138.41, 137.99, 133.34, 130.07, 127.53, 126.21, 126.09, 118.88, 116.66, 21.60, 21.27. LRMS (EI): calc'd: 313; found: 312.

2-((3,5-dimethylphenyl)amino)-5-(4-methoxyphenyl)nicotinonitrile (2j)

General procedure A was followed using 3,5-dimethylaniline (125 μ L, 1.0 mmol, 1.0 equiv), 4-ethynylanisole (130 μ L, 1.0 mmol, 1.0 equiv), *tert*-butylisonitrile (170 μ L, 1.5 mmol, 1.5 equiv), Ti(dpm)(NMe₂)₂ (32 mg, 0.1 mmol, 10 mol%), and dry toluene (2 mL). The second step used

malononitrile (132 mg, 2.0 mmol, 2.0 equiv), DBU (76 mg, 0.5 mmol, 0.5 equiv), molecular sieves (200 mg), 2 mL of ethanol and was heated for 2 h. Removal of solvent afforded product as a white solid (39 mg, 12%). M.p.: 141-142°C. ¹H NMR (CDCl₃, 500 MHz, 25 °C): δ 8.59 (d, *J*=2.4 Hz, 1H), 7.92 (d, *J*=2.9 Hz, 1H), 7.42 (d, *J*=8.5 Hz, 2H), 7.23 (s, 2H), 7.00 (d, *J*=8.6 Hz, 2H), 6.92 (s, 1H), 6.79 (s, 1H), 3.86 (s, 3H), 2.34 (s, 6H). ¹³C { ¹H } NMR (CDCl₃, 126 MHz, 25 °C): δ 159.71, 154.94, 150.59, 139.32, 138.94, 138.46, 128.73, 127.54, 127.37, 126.07, 118.85, 116.70, 114.82, 93.19, 55.55, 21.61. LRMS (EI): calc 'd: 329; found: 328.

2-((3,5-dimethylphenyl)amino)-6-methyl-5-(prop-1-en-2-yl)nicotinonitrile

General procedure A was followed using 3,5-dimethylaniline (125 μL, 1.0 mmol, 1.0 equiv), 2-methyl-1-penten-3-yne **1c-I** (106 μL, 1.0 mmol, 1.0 equiv), *tert*-butylisonitrile (170 μL, 1.5 mmol, 1.5 equiv), Ti(dpm)(NMe₂)₂ (31 mg, 0.1 mmol, 10 mol%), and 2 mL of dry toluene. The second step used malononitrile (132 mg, 2.0 mmol, 2.0 equiv), DBU (76 mg, 0.5 mmol, 0.5 equiv), molecular sieves (200 mg), 2 mL of ethanol and was heated for 2 h. Removal of solvent afforded product as a yellow oil (47 mg, 17%). ¹H NMR (CDCl3, 500 MHz, 25 °C): δ 7.50 (s, 1H), 7.28 (s, 2H), 6.82 (s, 1H), 6.74 (s, 1H), 5.28-5.22 (m, 1H), 4.91 (dd, *J*=1.6, 0.8 Hz, 1H), 2.50 (s, 3H), 2.33 (s, 6H), 2.02-2.01 (m, 3H). LRMS (EI): calc'd: 277; found: 276. The NMR shows a compound with modest purity, that was used without further purification in the next step.

6-Methyl-2-[(3,5-dimethylphenyl)amino]-5-(isopropyl)nicotinonitrile (2k)

6-Methyl-2-[(3,5-dimethylphenyl)amino]-5-(prop-1-en-2-yl)nicotinonitrile (80 mg, 0.28 mmol) was dissolved in dry ethanol (6 mL) in a 100 mL Schlenk flask. Palladium on carbon (10%, 100 mg) was added. The flask was flushed with purified dinitrogen, then with dihydrogen gas. The joint was fit with an adaptor for a hydrogen-filled balloon and was stirred at room temperature (25 °C) for 30 min. Purification was accomplished by filtration through neutral alumina, followed by column chromatography (neutral alumina, hexanes:EtOAc 10:1), which afforded the desired compound as a yellow liquid (35%, 28 mg, 0.1 mmol). ¹H NMR (CDCl₃, 500 MHz, 25 °C): 7.59 (s, 1H), 7.29 (s, 2H), 6.77 (s, 1H), 6.73 (s, 1H), 3.06 (hept, *J*=6.9 Hz, 1H), 2.54 (s, 3H), 2.34 (s, 6H), 1.22 (d, *J*=6.9 Hz, 6H). ¹³C{¹H} NMR (CDCl₃, 126 MHz, 25 °C): 160.1, 153.4, 139.2, 138.6, 138.1, 132.5, 124.9, 117.7, 117.3, 90.6, 29.8, 28.5, 23.0, 21.6. LRMS (EI): calc'd: 279; found: 279.

Category 2: Post functionalization of MSU38225

2-((3,5-dimethylphenyl)(methyl)amino)-6-methyl-5-phenylnicotinonitrile (3a)

In a 20 mL glass vial, 2-((3,5-dimethylphenyl)amino)-6-methyl-5-phenylnicotinonitrile (80 mg, 1.0 equiv), potassium *tert*-butoxide (32 mg, 1.1 equiv), and 3 mL of DMF were loaded with a stir bar. The mixture was stirred under room temperature for 10 min before methyl iodide (40 mg, 1.1 equiv) was added dropwise. The mixture was stirred for another 2 h under room temperature. The reaction mixture was poured onto water and extracted with 20 mL of EtOAc. The organic layer was washed with brine, dried with sodium sulfate, and evaporated. The crude product was purified by column chromatography on silica gel (hexane/ethyl acetate) to afford pure product as a white solid (46 mg, 55%). M.p.: 106-107 °C. ¹H NMR (CDCl₃, 500 MHz, 25 °C): δ 7.52 (s, 1H), 7.42 (t, *J*=7.6 Hz, 2H), 7.35 (t, *J*=7.3 Hz, 1H), 7.28 (d, *J*=7.9 Hz, 2H), 6.94 (s, 1H), 6.89 (s, 2H), 3.52

(d, J=1.5 Hz, 3H), 2.47 (d, J=1.5 Hz, 3H), 2.33 (s, 6H). 13 C{ 1 H} NMR (CDCl₃, 126 MHz, 25 $^{\circ}$ C): δ 159.35, 157.10, 146.51, 144.88, 139.60, 138.52, 129.21, 128.65, 128.56, 127.53, 127.29, 124.04, 116.72, 92.44, 40.73, 24.15, 21.53. LRMS (EI): calc'd: 327; found: 327.

N-(3-cyano-6-methyl-5-phenylpyridin-2-yl)-N-(3,5-dimethylphenyl)acetamide (3b)

In a 15 mL pressure tube, 2-((3,5-dimethylphenyl)amino)-6-methyl-5-phenylnicotinonitrile (100 mg, 0.32 mmol) and acetic anhydride (2 mL, 21 mmol) were loaded with a stir bar. The tube was sealed and heated in an oil bath at 80 °C for 2 h. After the reaction was cooled to room temperature, the reaction mixture was poured onto water and extracted with 20 mL of EtOAc. The organic layer was washed with brine, dried with sodium sulfate, and evaporated. The crude product was purified by column chromatography on silica gel (hexane/ethyl acetate) to afford pure product as a white solid (78 mg, 69%). M.p.: 161-162 °C. ¹H NMR (CDCl₃, 500 MHz, 25 °C): δ 7.83 (s, 1H), 7.51-7.43 (m, 3H), 7.32-7.28 (m, 2H), 7.18 (s, 2H), 7.02 (s, 1H), 2.51 (s, 3H), 2.36 (s, 6H), 2.15 (s, 3H). ¹³C (¹H) NMR (CDCl₃, 126 MHz, 25 °C): δ 171.42, 161.32, 154.59, 142.53, 140.61, 139.55, 137.22, 136.30, 130.42, 128.95, 128.60, 126.50, 115.94, 106.44, 24.14, 22.99, 21.38. LRMS (EI): calc 'd: 355; found: 355.

2-((3,5-dimethylphenyl)amino)-6-methyl-5-phenylnicotinamide (3c)

2-((3,5-dimethylphenyl)amino)-6-methyl-5-phenylnicotinonitrile (110 mg, 0.35 mmol) was placed in a 50 mL round bottom flask with a stir bar and 4 mL of EtOH. This solution was stirred,

and tetrabutylammonium hydroxide solution (0.5 mL, 40% in water) was added. An air condenser was attached to the flask, and the solution was heated, in air, until it was actively refluxing. The solution was sampled at 30 min intervals and checked by TLC for completion (watched the starting pyridine disappear). When the starting material no longer appeared by TLC, the reaction was removed from heat and allowed to cool (~4 h). Once cooled, the solution was neutralized with ammonium chloride until the pH was between 7 and 8. The crude solution was then extracted with DCM several times (5 mL × 5). The combined organic fractions were dried over Na₂SO₄, filtered to remove the drying agent, and concentrated by rotary evaporation. This provided the crude product as a sticky orange oil. This oil was washed with water to remove excess NⁿBu₄Cl generated during neutralization. The resulting residue was rinsed with hexanes and dried once more by rotary evaporation. This provided the product as a yellow powder (yield: 27 mg, 23%). From this powder, X-ray quality crystals were grown from a solution of CHCl₃ layered with n-pentane at -20 °C for 3 d. The crystals contain CHCl₃ in the lattice, so this method of purification is undesirable for biological samples due to this solvation. ¹H NMR (CDCl₃, 500 MHz, 25 °C): 10.52 (s, 1H), 7.54 (s, 1H), 7.47-7.40 (m, 4H), 7.39-7.34 (m, 1H), 7.34-7.29 (m, 2H), 6.67 (s, 1H), 5.77 (s (br), 2H), 2.47 (s, 3H), 2.33 (s, 6H). ¹³C NMR (126 MHz, CDCl₃) δ 170.48, 159.57, 154.20, 140.25, 139.65, 138.34, 137.73, 129.38, 128.63, 127.32, 126.31, 124.07, 118.08, 106.60, 23.88, 21.70. LRMS (EI): calc'd: 331; found: 331.

2-((4-bromo-3,5-dimethylphenyl)amino)-6-methyl-5-phenylnicotinonitrile (3d)

In a 50 mL round bottom flask, freshly recrystallized N-bromosuccinimide (66 mg, 0.37 mmol, 1.0 equiv) and benzoyl peroxide (5.0 mg, 0.05 equiv) was dissolved in 3 mL of CCl₄ with a stir bar. A solution of 2-((3,5-dimethylphenyl)amino)-6-methyl-5-phenylnicotinonitrile (115 mg, 0.37 mmol, 1.0 equiv) in 3 mL of CCl₄ was added. The round bottom flask was fixed with a condenser and heated in an oil bath at 78 °C for 18 h. After the reaction was cooled to room temperature, the reaction mixture was diluted by adding 50 mL of EtOAc, then washed with brine. The organic layer was dried with sodium sulfate and evaporated. The crude product was purified by column chromatography on silica gel (hexane/ethyl acetate) to afford pure product as an off-white solid (124 mg, 86%). ¹H NMR (CDCl₃, 500 MHz, 25 °C): δ 7.63 (s, 1H), 7.46 (s, 2H), 7.44 (t, *J*=7.5 Hz, 2H), 7.38 (t, *J*=7.3 Hz, 1H), 7.28 (s, 1H), 6.87 (s, 1H), 2.47 (s, 3H), 2.43 (s, 6H). ¹³C{¹H} NMR (CDCl₃, 126 MHz, 25 °C): δ 160.36, 154.07, 142.26, 138.87, 138.18, 137.55, 129.20, 128.78, 128.40, 127.86, 121.36, 119.96, 116.73, 90.67. LRMS (EI): calc 'd: 391; found: 392.

Category 3: Analog Preparation Incorporating Heterocycles

Synthesis of 5-bromo-2-((3,5-dimethylphenyl)amino)nicotinonitrile

In a glove box, tris(dibenzylideneacetone)dipalladium(0) (23 mg, 0.05 mmol, 2.5 mol%) and DMAPF (25.3 mg, 0.06 mmol, 6 mol%) were dissolved in 2 mL of dry dioxane in a 35 mL pressure tube. The mixture was stirred for 2 min before 5-bromo-2-chloronicotinonitrile (217 mg, 1.0 mmol, 1.0 equiv), 3,5-dimethylaniline (125 μL, 1.0 mmol, 1.0 equiv), and sodium *tert*-butoxide (119 mg, 1.25 mmol, 1.25 equiv) were added to the pressure tube. Then, another 2 mL of dry dioxane was added. The reaction was then removed from the glovebox and heated in an oil bath at 70 °C for 15 h. After the reaction was cooled to room temperature, the reaction mixture was filtered through

Celite and rinsed with ethyl acetate. The filtrate was evaporated, and the crude product was purified by column chromatography on silica gel (hexane/ethyl acetate) to afford pure product as an off-white solid (214 mg, 71%). M.p.: 145-147 °C. ¹H NMR (CDCl₃, 500 MHz, 25 °C): δ 8.39 (s, 1H), 7.84 (s, 1H), 7.15 (s, 2H), 6.90 (s, 1H), 6.81 (s, 1H), 2.33 (s, 7H). ¹³C{¹H} NMR (CDCl₃, 126 MHz, 25 °C): δ 154.89, 153.56, 143.17, 139.02, 137.80, 126.62, 119.20, 115.31, 107.29, 94.52, 21.57. LRMS (EI): calc'd: 301; found: 302.

General procedure B: synthesis of 3-cyano-pyridine derivatives via Suzuki coupling

In a glove box, tetrakis(triphenylphosphine)palladium(0) (10 mol%), potassium carbonate (2.0 equiv), 5-bromo-2-((3,5-dimethylphenyl)amino)nicotinonitrile **6-I** (1.0 equiv), aryl boronic acid (1.0 equiv), and 3 mL of dioxane were added in a 50 mL Schlenk tube. The reaction was then removed from the glovebox and charged with water under a constant flow of dry dinitrogen. Then, the Schlenk tube was sealed and heated in an oil bath at 110 °C for 12 h. After the reaction was cooled to room temperature, the reaction mixture was filtered through Celite and rinsed with ethyl acetate. The filtrate was evaporated, and the crude product was purified by column chromatography on silica gel (hexane/ethyl acetate) to afford pure product.

5-(3,5-dimethylphenyl)-2-((3,5-dimethylphenyl)amino)nicotinonitrile (4a)

General procedure B was followed using 5-bromo-2-((3,5-dimethylphenyl)amino)nicotinonitrile **6-I** (50 mg, 1.0 equiv), (3,5-dimethylphenyl)boronic acid (25 mg, 1.0 equiv), tetrakis(triphenylphosphine)palladium(0) (19 mg, 10 mol%), potassium carbonate (69 mg, 3.0 equiv), 2 mL of dioxane, and 0.5 mL of water. Removal of solvent afforded product as a white powder (40 mg, 74 %). M.p.: 162-163 °C. 1 H NMR (CDCl₃, 500 MHz, 25 °C): δ 8.61 (d, J=2.4 Hz, 1H), 7.96 (d, J=2.5 Hz, 1H), 7.23 (s, 2H), 7.11 (s, 2H), 7.03 (s, 1H), 6.94 (s, 1H), 6.79 (s, 1H), 2.38 (s, 6H), 2.34 (s, 6H). 13 C{ 1 H} NMR (CDCl₃, 126 MHz, 25 °C): δ 155.10, 150.61, 140.02, 139.03, 138.96, 138.30, 136.08, 129.75, 127.79, 126.23, 124.27, 119.01, 116.54, 93.27, 21.60, 21.53. LRMS (EI): calc'd: 327; found: 326.

5-(3,5-dimethoxyphenyl)-2-((3,5-dimethylphenyl)amino)nicotinonitrile (4b)

General procedure B was followed using 5-bromo-2-((3,5-dimethylphenyl)amino)nicotinonitrile (80 mg, 1.0 equiv), (3,5-dimethoxyphenyl)boronic acid (25 mg, 1.0 equiv), tetrakis(triphenylphosphine)palladium(0) (30 mg, 10 mol%), potassium carbonate (110 mg, 3.0 equiv), 2 mL of dioxane, and 0.5 mL of water. Removal of solvent afforded product as a white powder (80 mg, 84 %). M.p.: 169-170 °C. ¹H NMR (CDCl₃, 500 MHz, 25 °C): δ 8.61 (d, *J*=2.3 Hz, 1H), 7.95 (d, *J*=2.4 Hz, 1H), 7.23 (s, 2H), 6.96 (s, 1H), 6.80 (s, 1H), 6.61 (s, 2H), 6.48 (s, 1H), 3.85 (s, 6H), 2.35 (s, 6H). ¹³C{¹H} NMR (CDCl₃, 126 MHz, 25 °C): δ 161.57, 155.46, 151.01, 139.86, 138.96, 138.29, 127.46, 126.23, 118.98, 116.57, 104.67, 99.76, 93.11, 55.62, 21.61. LRMS (EI): calc 'd: 359; found: 358.

5-(3,5-dichlorophenyl)-2-((3,5-dimethylphenyl)amino)nicotinonitrile (4c)

General procedure B was followed using 5-bromo-2-((3,5-dimethylphenyl)amino)nicotinonitrile (80 mg, 1.0 equiv), (3,5-dichlorophenyl)boronic acid (51 mg, 1.0 equiv), tetrakis(triphenylphosphine)palladium(0) (30 mg, 10 mol%), potassium carbonate (110 mg, 3.0 equiv), 2 mL of dioxane, and 0.5 mL of water. Removal of solvent afforded product as a white powder (25 mg, 20 %). M.p.: 191-192 °C. ¹H NMR (CDCl₃, 500 MHz, 25 °C): δ 8.57 (d, *J*=2.4 Hz, 1H), 7.93 (d, *J*=2.5 Hz, 1H), 7.37 (s, 3H), 7.22 (s, 2H), 7.03 (s, 1H), 6.82 (s, 1H), 2.35 (s, 7H). ¹³C {¹H} NMR (CDCl₃, 126 MHz, 25 °C): δ 211.98, 155.85, 150.92, 139.73, 139.22, 139.04, 137.92, 136.02, 127.95, 126.60, 124.80, 119.21, 116.13, 93.40, 21.60. LRMS (EI): calc'd: 367; found: 366.

6-((3,5-dimethylphenyl)amino)-[3,4'-bipyridine]-5-carbonitrile (4d)

General procedure b was followed using 5-bromo-2-((3,5-dimethylphenyl)amino)nicotinonitrile (100 mg, 1.0 equiv), pyridin-4-ylboronic acid (41 mg, 1.0 equiv), tetrakis(triphenylphosphine)palladium(0) (38 mg, 10 mol%), potassium carbonate (137 mg, 3.0 equiv), 3 mL of dioxane, and 0.75 mL of water. Removal of solvent afforded product as a white powder (80 mg, 81 %). M.p.: 185-186 °C. ¹H NMR (CDCl₃, 500 MHz, 25 °C): δ 8.71-8.67 (m, 3H), 8.04 (d, *J*=2.5 Hz, 1H), 7.47-7.38 (m, 2H), 7.23 (s, 2H), 7.08 (s, 1H), 6.83 (s, 1H), 2.35 (s,

6H). ¹³C{¹H} NMR (CDCl₃, 126 MHz, 25 °C): δ 156.27, 151.04, 150.84, 143.50, 139.74, 139.06, 137.81, 126.76, 124.19, 120.46, 119.39, 116.12, 93.52, 21.59. LRMS (EI): calc'd: 300; found: 299. 6-((3,5-dimethylphenyl)amino)-[3,3'-bipyridine]-5-carbonitrile (4e)

General procedure b was followed using 5-bromo-2-((3,5-dimethylphenyl)amino)nicotinonitrile (71 mg, 1.0 equiv), pyridin-3-ylboronic acid (29 mg, 1.0 equiv), tetrakis(triphenylphosphine)palladium(0) (27 mg, 10 mol%), potassium carbonate (97 mg, 3.0 equiv), 2 mL of dioxane, and 0.5 mL of water. Removal of solvent afforded product as a yellow powder (mg, 79 %). M.p.: 93-95°C. ¹H NMR (CDCl₃, 500 MHz, 25 °C): δ 8.81 (s, 1H), 8.65 (d, *J*=4.6 Hz, 1H), 8.64 (s, 1H), 8.00 (s, 1H), 7.87 (d, *J*=7.9 Hz, 1H), 7.46 (t, *J*=6.7 Hz, 1H), 7.24 (s, 2H), 7.05 (s, 1H), 6.84 (app t, 1H), 2.36 (s, 6H).¹³C {¹H} NMR (CDCl₃, 126 MHz, 25 °C): δ 155.75, 150.83, 148.31, 146.64, 139.67, 138.92, 137.78, 134.18, 132.34, 126.51, 124.17, 123.62, 119.16, 116.04, 93.42, 21.46. LRMS (EI): calc'd: 300; found: 299.

Synthesis of 3-(dimethylamino)-2-phenylacrylaldehyde

The procedure was adapted from a literature procedure.³³ A 250 mL Schlenk flask was loaded with POCl₃ (41.39 g, 0.27 mol, 3 equiv) and a magnetic stir bar. Then, the flask was flushed with dry dinitrogen for 5 min and set in a room temperature water bath. With vigorous stirring, dimethylformamide (24 g, 0.33 mol, 3.67 equiv) was then added dropwise to POCl₃. The mixture

was stirred under room temperature for 5 min. After 5 min, phenylacetaldehyde dimethyl acetal (15 g, 0.09 mol, 1 equiv) in 45 mL dimethylformamide was added dropwise for about 5 min. The resulting solution was stirred at 70 °C for 18 h before it was poured into 375 mL ice and neutralized by the addition of anhydrous potassium carbonate till pH is around 7. Then the solution was slowly added sodium hydroxide (50 g, 1.25 mol), and 50 mL of water and heated at 50 °C with stirring for 1 h. The mixture was cooled and extracted with DCM (50 mL × 2) and washed with water thoroughly (50 mL × 3). The excess solvent was removed *in vacuo*, resulting a red-brown oil. The crude product was used in the next step without further purification. Further purification can be achieved by cooling concentrated ether solution in a freezer (-30 °C) overnight to afford a red-brown oil (12.79 g, 0.073 mol, 81.2%). 1H NMR (CDCl₃, 500 MHz, 25 °C): δ 9.10 (s, 1H), 7.31-7.35 (m, 2H), 7.22-7.25 (m, 1H), 7.16-7.20 (m, 2H), 6.78 (s, 1H, br), 2.81 (s, 1H, br). 13C{1H} NMR (CDCl₃, 126 MHz, 25 °C): δ188.96, 158.60, 133.73, 130.81, 127.45, 126.36, 125.23, 114.86. LRMS (EI): calc'd: 175; found: 175.

Synthesis of 2-hydroxy-5-phenylnicotinonitrile

The procedure was adapted from a literature procedure.³⁴ A 500 mL Schlenk flask was loaded with NaH (3.22 g, 0.134 mol, 2.35 equiv) and a magnetic stir bar before 130 mL of MeOH slowly was added. After 10 min of stirring at room temperature, cyanoacetamide (13.78 g, 0.164 mol, 2.88 equiv), and 3-(dimethylamino)-2-phenylprop-2-enal (10 g, 0.0571 mol, 1.0 equiv) was added. The mixture was stirred at room temperature for 1.5 h and then refluxed overnight. After cooling to room temperature, 100 mL of water was added, and the mixture was acidified with 1 M HCl solution. While adding acid, a large amount of yellow solid precipitated out. The solid was filtered

and washed with water (20 mL × 3), methanol (5mL × 3), ether (5mL × 3) and hexane (5mL × 3) to afford a light-yellow product. (5.91 g, 0.03 mol, 52.7%). M.p.: 226-227 °C. ¹H NMR (CDCl₃, 500 MHz, 25 °C): δ 13.61 (s, 1H, br), 8.23 (s, 1H), 7.99 (s, 1H), 7.45-7.51 (m, 2H), 7.38-7.45 (m, 3H). ¹³C{¹H} NMR (CDCl₃, 126 MHz, 25 °C): δ162.11, 147.96, 137.47, 134.04, 129.55, 128.54, 125.88, 121.76, 115.21, 105.35. LRMS (EI): calc'd: 196; found: 196.

Synthesis of 2-bromo-5-phenylnicotinonitrile

A 250 mL Schlenk flask was charged with 2-hydroxy-5-phenylnicotinonitrile (2.14 g, 10.9 mmol), Bu₄NBr (4.8 g, 14.9 mmol), P₂O₅ (4.1 g, 28.8 mmol), toluene (110 mL), and a magnetic stir bar. The mixture was heated for 14 h under reflux. Then, the toluene layer was decanted and washed with 30 mL of saturated NaHCO₃ solution and then 50 mL of water. 50 mL of water and powered NaHCO₃ was added till no gas was evolved. The mixture was extracted with 250 mL DCM, washed with 2 × 50 mL of brine, and washed with 30 mL of water. The organic layers were combined and dried with MgSO₄. Removal of the solvent in vacuo afforded a light-yellow power. Further purification can be achieved by chromatography (1:10 EtOAc:hexane). (2.48 g, 9.61 mmol, 88.2%). M.p.: 139-140 °C. ¹H NMR (CDCl₃, 500 MHz, 25 °C): δ 8.76 (s, 1H), 8.10 (s, 1H), 7.48-7.57 (m, 5H). ¹³C (¹¹H) NMR (CDCl₃, 126 MHz, 25 °C): δ151.33, 142.07, 140.50, 136.33, 134.41, 129.76, 129.73, 127.15, 115.90, 114.29, 24.99. LRMS (EI): calc'd: 258; found: 257.

General procedure B: synthesis of 2-amino-5-phenylnicotinonitrile derivatives via Buchwald-Hartwig coupling

In a glove box, palladium(II) acetate (9.0 mg, 0.04 mmol, 4 mol%) and Xantphos (25.4 mg, 0.044 mmol, 4.4 mol%) were dissolved in 2 mL of dry toluene in a 35 mL pressure tube. The mixture was stirred for 2 min before 2-bromo-5-phenylnicotinonitrile (259 mg, 1.0 mmol, 1.0 equiv), aryl amine (1.2 mmol, 1.2 equiv), and cesium carbonate (1312 mg, 4.0 mmol, 4.0 equiv) were added to the pressure tube. Then, another 3 mL of dry toluene were added. The reaction was then removed from the glovebox and heated in an oil bath at 110 °C for 14 h. After the reaction was cooled to room temperature, the reaction mixture was filtered through Celite and rinsed with ethyl acetate. The filtrate was evaporated, and the crude product was purified by column chromatography on silica gel (hexane/ethyl acetate).

2-((4,6-dimethyl-1,3,5-triazin-2-yl)amino)-5-phenylnicotinonitrile (5a)

General procedure B was followed using 2-bromo-5-phenylnicotinonitrile (300 mg, 1.16 mmol, 1.0 equiv), 4,6-dimethyl-1,3,5-triazin-2-amine (172 mg, 1.2 equiv), palladium(II) acetate (10.4 mg, 4 mol%), xantphos (29.5 mg, 4.4 mol%), cesium carbonate (1520 mg, 4.0 equiv), and 5 mL of dry toluene. Removal of solvent afforded product as an off-white powder (42 mg, 12%). M.p.: 225-226 °C. ¹H NMR (CDCl₃, 500 MHz, 25 °C): 9.36 (br s, 1H), 8.97 (d, *J*=2.3 Hz, 1H), 8.22 (d, *J*=2.3 Hz, 1H), 7.59 (d, *J*=7.4 Hz, 2H), 7.53 (t, *J*=7.5 Hz, 2H), 7.47 (t, *J*=7.3 Hz, 1H), 2.57 (s, 6H). ¹³C{¹H} NMR (CDCl₃, 126 MHz, 25 °C): 176.94, 163.43, 150.75, 150.34, 140.75, 135.21, 133.29, 129.46, 128.93, 126.85, 115.77, 103.84, 25.50. LRMS (EI): calc'd: 302; found: 301.

2-((4,6-dimethylpyrimidin-2-yl)amino)-5-phenylnicotinonitrile (5b)

General procedure B was followed using 2-bromo-5-phenylnicotinonitrile (200 mg, 1.0 equiv), 4,6-dimethylpyrimidin-2-amine (114 mg, 1.2 equiv), palladium(II) acetate (7 mg, 4 mol%), xantphos (19.6 mg, 4.4 mol%), cesium carbonate (1013 mg, 4.0 equiv), and 4 mL of dry toluene. Removal of solvent afforded product as an off-white powder (207 mg, 69%). M.p.: 215-216 °C. ¹H NMR (CDCl₃, 500 MHz, 25 °C): δ 8.82 (d, *J*=2.4 Hz, 1H), 8.25 (s, 1H), 8.13 (d, *J*=2.4 Hz, 1H), 7.56 (d, *J*=7.5 Hz, 2H), 7.50 (t, *J*=7.6 Hz, 2H), 7.43 (t, *J*=7.3 Hz, 1H), 6.69 (s, 1H), 2.44 (s, 6H). ¹³C{¹H} NMR (CDCl₃, 126 MHz, 25 °C): δ 168.18, 157.97, 152.43, 150.58, 140.78, 135.86, 131.52, 129.47, 128.61, 126.84, 116.40, 114.81, 101.06, 23.99. LRMS (EI): calc'd: 301; found: 300.

2-((2,6-dimethylpyrimidin-4-yl)amino)-5-phenylnicotinonitrile (5c)

General procedure B was followed using 2-bromo-5-phenylnicotinonitrile (300 mg, 1.16 mmol, 1.0 equiv), 2,6-dimethylpyrimidin-4-amine (170 mg, 1.2 equiv), palladium(II) acetate (10.4 mg, 4 mol%), xantphos (29.5 mg, 4.4 mol%), cesium carbonate (1520 mg, 4.0 equiv), and 5 mL of dry toluene. Removal of solvent afforded product as an off-white powder (74 mg, 21%). M.p.: 154-155 °C. ¹H NMR (CDCl₃, 500 MHz, 25 °C): 8.77 (d, *J*=2.3 Hz, 1H), 8.11 (s, 1H), 8.09 (d, *J*=2.5 Hz, 1H), 7.86 (s, 1H), 7.41-7.57 (m, 5H), 2.61 (s, 3H), 2.53 (s, 3H). ¹³C{¹H} NMR (CDCl₃, 126

MHz, 25 °C): 151.33, 142.07, 140.50, 136.34, 134.42, 129.76, 129.73, 129.51, 128.70, 127.84, 127.15, 126.89, 119.25, 115.91, 114.30, 21.49. LRMS (EI): calc'd: 301; found: 300.

2-((4,6-dimethylpyridin-2-yl)amino)-5-phenylnicotinonitrile (5d)

General procedure B was followed using 2-bromo-5-phenylnicotinonitrile (160 mg, 0.62 mmol, 1.0 equiv), 4,6-dimethylpyridin-2-amine (91 mg, 1.2 equiv), palladium(II) acetate (5.5 mg, 4 mol%), xantphos (15.7 mg, 4.4 mol%), cesium carbonate (810 mg, 4.0 equiv), and 4 mL of dry toluene. The compound was purified by column chromatography on silica gel using40% EtOAc in hexanes. Removal of solvent afforded product as an off-white powder (93 mg, 50%). M.p.: 112-113 °C. ¹H NMR (CDCl₃, 500 MHz, 25 °C): δ 8.70 (d, *J*=2.4 Hz, 1H), 8.03 (d, *J*=2.4 Hz, 1H), 8.02 (s, 1H), 7.76 (s, 1H), 7.56-7.46 (m, 4H), 7.41 (t, *J*=7.2 Hz, 1H), 6.72 (s, 1H), 2.45 (s, 3H), 2.37 (s, 3H). ¹³C{¹H} NMR (CDCl₃, 126 MHz, 25 °C): δ 156.85, 153.80, 151.44, 150.41, 149.74, 140.08, 136.05, 129.44, 128.48, 128.28, 126.51, 119.63, 116.03, 110.74, 94.59, 24.06, 21.59.. LRMS (EI): calc'd: 300; found: 299.

2-((6-methylpyrazin-2-yl)amino)-5-phenylnicotinonitrile (5e)

General procedure B was followed using 2-bromo-5-phenylnicotinonitrile (200 mg, 1.0 equiv), 6-methylpyrazin-2-amine (101 mg, 1.2 equiv), palladium(II) acetate (7 mg, 4 mol%), xantphos (19.6 mg, 4.4 mol%), cesium carbonate (1013 mg, 4.0 equiv), and 4 mL of dry toluene. Removal

of solvent afforded product as a white powder (77 mg, 35%). M.p.: 160-161 °C. ¹H NMR (CDCl₃, 500 MHz, 25 °C): δ 9.59 (s, 1H), 8.74 (d, *J*=2.5 Hz, 1H), 8.18 (s, 1H), 8.08 (d, *J*=2.5 Hz, 1H), 7.72 (s, 1H), 7.54 (d, *J*=7.0 Hz, 2H), 7.50 (t, *J*=7.6 Hz, 2H), 7.45-7.41 (m, 1H), 2.51 (s, 3H). ¹³C{¹H} NMR (CDCl₃, 126 MHz, 25 °C): δ 152.87, 152.09, 150.51, 148.05, 140.08, 138.13, 135.66, 132.55, 129.74, 129.53, 128.60, 126.65, 115.69, 94.97, 21.32. LRMS (EI): calc'd: 287; found: 286.

2-((6-methylpyridin-2-yl)amino)-5-phenylnicotinonitrile (5f)

General procedure B was followed using 2-bromo-5-phenylnicotinonitrile (259 mg, 1.0 equiv), 6-methylpyridin-2-amine (130 mg, 1.2 equiv), palladium(II) acetate (9 mg, 4 mol%), xantphos (25.5 mg, 4.4 mol%), cesium carbonate (1312 mg, 4.0 equiv), and 4 mL of dry toluene. Removal of solvent afforded product as a yellow powder (180 mg, 63%). M.p.: 145-146 °C. ¹H NMR (CDCl₃, 500 MHz, 25 °C): δ 8.68 (dd, *J*=2.3, 0.9 Hz, 1H), 8.20 (d, *J*=8.3 Hz, 1H), 8.04 (dd, *J*=2.4, 1.0 Hz, 1H), 7.81 (s, 1H), 7.61 (t, *J*=7.7 Hz, 1H), 7.56-7.45 (m, 4H), 7.41 (t, *J*=7.6 Hz, 1H), 6.87 (d, *J*=7.5 Hz, 1H), 2.49 (s, 3H). ¹³C{¹H} NMR (CDCl₃, 126 MHz, 25 °C): δ 157.32, 153.75, 151.36, 150.39, 140.05, 138.43, 135.99, 129.45, 128.63, 128.31, 126.52, 118.31, 116.00, 110.14, 94.62, 24.26. LRMS (EI): calc 'd: 286; found: 285.

2-((2-methylpyridin-4-yl)amino)-5-phenylnicotinonitrile (5g)

General procedure B was followed using 2-bromo-5-phenylnicotinonitrile (147 mg, 1.0 equiv), 2-methylpyridin-4-amine (74 mg, 1.2 equiv), palladium(II) acetate (5 mg, 4 mol%), xantphos (15 mg, 4.4 mol%), cesium carbonate (744 mg, 4.0 equiv), and 3 mL of dry toluene. Removal of solvent afforded product as white crystals (110 mg, 68%). M.p.: 133-134 °C. ¹H NMR (CDCl₃, 500 MHz, 25 °C): 8.74 (d, *J*=2.4 Hz, 1H), 8.42 (d, *J*=6.1 Hz, 1H), 8.06 (d, *J*=2.4 Hz, 1H), 7.55-7.46 (m, 6H), 7.43 (t, *J*=7.0 Hz, 1H), 7.16 (s, 1H), 2.58 (s, 3H). ¹³C (¹H) NMR (CDCl₃, 126 MHz, 25 °C): δ 159.63, 154.02, 150.55, 150.10, 146.21, 139.89, 135.69, 129.54, 129.45, 128.59, 126.62, 115.93, 112.64, 110.93, 95.02, 24.83. LRMS (EI): calc 'd: 286; found: 285.

2-((5-methylpyridin-3-yl)amino)-5-phenylnicotinonitrile (5h)

General procedure B was followed using 2-bromo-5-phenylnicotinonitrile (147 mg, 1.0 equiv), 5-methylpyridin-3-amine (74 mg, 1.2 equiv), palladium(II) acetate (5 mg, 4 mol%), xantphos (15 mg, 4.4 mol%), cesium carbonate (744 mg, 4.0 equiv), and 3 mL of dry toluene. Removal of solvent afforded product as white crystals (110 mg, 68%). M.p.: 180-181 °C. ¹H NMR (CDCl₃, 500 MHz, 25 °C): 8.64 (d, *J*=2.4 Hz, 2H), 8.21 (s, 1H), 8.02 (d, *J*=2.5 Hz, 1H), 7.95 (s, 1H), 7.56-7.44 (m, 4H), 7.40 (t, *J*=7.7 Hz, 1H), 7.10 (s, 1H), 2.39 (s, 3H). ¹³C{¹H} NMR (CDCl₃, 126 MHz, 25 °C): δ ¹³C NMR (126 MHz, CDCl₃) δ 154.76, 150.73, 145.65, 139.94, 139.80, 135.92, 135.11, 133.48, 129.44, 128.56, 128.38, 128.31, 126.46, 116.24, 93.84, 18.63. LRMS (EI): calc'd: 286; found: 285.

2-((4-methylpyridin-2-yl)amino)-5-phenylnicotinonitrile (5i)

General procedure B was followed using 2-bromo-5-phenylnicotinonitrile (259 mg, 1.0 equiv), 4-methylpyridin-2-amine (9 mg, 1.2 equiv), palladium(II) acetate (5 mg, 4 mol%), xantphos (25.5 mg, 4.4 mol%), cesium carbonate (1312 mg, 4.0 equiv), and 5 mL of dry toluene. Removal of solvent afforded product as an orange powder (109 mg, 42%). M.p.: 149-150 °C. ¹H NMR (CDCl₃, 500 MHz, 25 °C): δ 9.12 (s, 1H), 8.99 (d, *J*=7.0 Hz, 1H), 8.31 (s, 1H), 7.66 (d, *J*=7.8 Hz, 2H), 7.51 (t, *J*=7.6 Hz, 3H), 7.42 (t, *J*=7.1 Hz, 1H), 7.22 (s, 1H), 6.64 (d, *J*=7.5 Hz, 1H), 2.40 (s, 3H). ¹³C{¹H} NMR (CDCl₃, 126 MHz, 25 °C): δ 154.66, 154.27, 150.45, 147.79, 137.17, 132.38, 131.13, 129.43, 129.37, 128.24, 127.31, 127.06, 126.50, 124.17, 115.35, 109.66, 21.54. ¹H NMR (500 MHz, DMSO-d₆, 25 °C) δ 10.03 (s, 1H), 9.12 (d, *J*=2.6 Hz, 1H), 9.07 (d, *J*=2.6 Hz, 1H), 8.97 (d, *J*=7.5 Hz, 1H), 7.90 (d, *J*=7.2 Hz, 2H), 7.54 (t, *J*=7.7 Hz, 2H), 7.43 (t, *J*=7.4 Hz, 1H), 7.14 (s, 1H), 6.82 (dd, *J*=7.5, 2.0 Hz, 1H), 2.37 (s, 3H). uncyclized form: ¹H NMR (CDCl₃, 500 MHz, 25 °C): δ 8.71 (d, *J*=2.4 Hz, 1H), 8.22 (s, 1H), 8.17 (d, *J*=5.1 Hz, 1H), 8.04 (d, *J*=2.6 Hz, 1H), 7.81 (s, 1H), 7.65 (s, 2H), 7.47 (d, *J*=7.9 Hz, 2H), 7.40 (d, *J*=7.6 Hz, 1H), 6.84 (d, *J*=4.2 Hz, 1H), 2.41 (s, 3H). LRMS (EI): cale'd: 286; found: 285.

Category 4: Analog Preparation With Core Change

3-((3,5-dimethylphenyl)amino)-6-phenylpyrazine-2-carbonitrile

In a 50 mL round bottom flask, 3-amino-6-phenylpyrazine-2-carbonitrile (392 mg, 2.0 mmol, 1.0 equiv), (3,5-dimethylphenyl)boronic acid (300 mg, 2.0 mmol, 1.0 equiv), copper(II) acetate monohydrate (800 mg, 4.0 mmol, 2.0 equiv), potassium phosphate monohydrate (920 mg, 4.0 mmol, 2.0 equiv), and 10 mL of DMSO were loaded with a stir bar. The solution has a dark green color. The reaction was heated in an oil bath at 120 °C for 12 h. After the reaction was cooled to room temperature, the reaction mixture was diluted by adding 50 mL of EtOAc, then washed with brine. The organic layer was dried with sodium sulfate and evaporated. The crude product was purified by column chromatography on silica gel (hexane/ethyl acetate) to afford pure product as an off-white solid (53 mg, 9%). 1 H NMR (CDCl₃, 500 MHz, 25 °C): δ 8.78 (s, 1H), 7.92 (d, J=7.1 Hz, 2H), 7.49 (t, J=7.4 Hz, 2H), 7.44 (t, J=7.3 Hz, 1H), 7.21 (s, 2H), 7.03 (s, 1H), 6.84 (s, 1H), 2.36 (s, 6H). 13 C (1 H) NMR (CDCl₃, 126 MHz, 25 °C): δ 152.40, 143.95, 143.03, 139.16, 137.42, 135.17, 129.48, 129.24, 126.80, 125.95, 119.06, 115.31, 114.41, 21.59. LRMS (EI): calc'd: 300; found: 299.

2-((3,5-dimethylphenyl)amino)quinoline-3-carbonitrile

In a glove box, palladium(II) acetate (9.0 mg, 0.04 mmol, 4 mol%) and xantphos (25.4 mg, 0.044 mmol, 4.4 mol%) were dissolved in 2 mL of dry toluene in a 35 mL pressure tube. The mixture was stirred for 2 min before 2-aminoquinoline-3-carbonitrile (169 mg, 1.0 mmol, 1.0 equiv), 1-bromo-3,5-dimethylbenzene (185 mg, 1.0 mmol, 1.0 equiv), and cesium carbonate (1312 mg, 4.0 mmol, 4.0 equiv) were added to the pressure tube. Then, another 3 mL of dry toluene were added. The reaction was then removed from the glovebox and heated in an oil bath at 100 °C for 12 h. After the reaction was cooled to room temperature, the reaction mixture was filtered through

Celite and rinsed with ethyl acetate. The filtrate was evaporated, and the crude product was purified by column chromatography on silica gel (hexane/ethyl acetate) to afford pure product as an off-white powder (253 mg, 93 %). M.p.: 141-142 °C. ¹H NMR (CDCl₃, 500 MHz, 25 °C): δ 8.34 (s, 1H), 7.82 (d, *J*=8.5 Hz, 1H), 7.70 (t, *J*=7.6 Hz, 1H), 7.66 (d, *J*=8.0 Hz, 1H), 7.47 (s, 2H), 7.36 (t, *J*=7.5 Hz, 1H), 7.05 (s, 1H), 6.79 (s, 1H), 2.37 (s, 7H). ¹³C{¹H} NMR (CDCl₃, 126 MHz, 25 °C): δ 151.25, 144.31, 138.83, 133.26, 128.14, 127.67, 125.70, 124.59, 121.90, 118.18, 96.74, 21.69. LRMS (EI): calc'd: 273; found: 272.

tert-butyl (3-((3-cyano-6-methyl-5-phenylpyridin-2-yl)amino)benzyl)carbamate

In a glove box, palladium(II) acetate (9.0 mg, 0.04 mmol, 4 mol%) and Xantphos (25.4 mg, 0.044 mmol, 4.4 mol%) were dissolved in 2 mL of dry toluene in a 35 mL pressure tube. The mixture was stirred for 2 min before 2-chloro-6-methyl-5-phenylnicotinonitrile (200 mg1.0 equiv), tert-butyl (3-aminobenzyl)carbamate (213 mg, 1.2 equiv) and cesium carbonate (1146 mg, 4.0 equiv) were added to the pressure tube. Then, another 3 mL of dry toluene were added. The reaction was then removed from the glovebox and heated in an oil bath at 110 °C for 14 h. After the reaction was cooled to room temperature, the reaction mixture was filtered through Celite and rinsed with ethyl acetate. The filtrate was evaporated, and the crude product was purified by column chromatography on silica gel (hexane/ethyl acetate). Column condition: 5% of EtOAc in hexanes. Removal of solvent afforded product as a colorless oil (220 mg, 53%). ¹H NMR (CDCl₃, 500 MHz, 25 °C): δ 7.67 (s, 1H), 7.64 (s, 1H), 7.61 (d, *J*=8.1 Hz, 1H), 7.45 (t, *J*=7.2 Hz, 2H), 7.39 (t, *J*=7.4 Hz, 1H), 7.33 (t, *J*=7.9 Hz, 1H), 7.28 (d, *J*=6.8 Hz, 2H), 7.02 (d, *J*=8.4 Hz, 1Hz, 1Hz, 7.01 (s,

1H), 4.91 (s, 1H), 4.36 (d, *J*=6.1 Hz, 2H), 2.49 (s, 3H), 1.47 (s, 9H). ¹³C{¹H} NMR (CDCl₃, 126 MHz, 25 °C): δ 160.21, 155.90, 154.01, 142.15, 139.87, 139.31, 138.10, 129.22, 129.09, 128.65, 128.30, 127.71, 122.39, 119.10, 116.61, 90.53, 79.55, 53.46, 44.68, 28.45, 24.14.

2-((3-(aminomethyl)phenyl)amino)-6-methyl-5-phenylnicotinonitrile

Tert-butyl (3-((3-cyano-6-methyl-5-phenylpyridin-2-yl)amino)benzyl)carbamate was dissolved in 5 mL of DCM in a 20 mL glass vial. To the solution, a 1 mL of TFA (1 mL) was added dropwise and let stir under room temperature overnight. The solution was neutralized by saturated Na₂CO₃ solution. The organic phase was separated, dried over Na₂SO₄, and then evaporated. The crude product was purified by column chromatography on silica gel (60% EtOAc in hexanes). Removal of solvent afforded product as a colorless oil (144 mg, 86%). ¹H NMR (CDCl₃, 500 MHz, 25 °C): δ 7.65 (d, J=7.9 Hz, 1H), 7.63 (s, 1H), 7.63 (s, 1H), 7.44 (t, J=7.3 Hz, 2H), 7.38 (t, J=7.4 Hz, 1H), 7.33 (t, J=7.8 Hz, 1H), 7.30-7.25 (m, 2H), 7.10 (s, 1H), 7.05 (d, J=7.6 Hz, 1H), 3.90 (s, 2H), 2.48 (s, 3H). ¹³C{¹H} NMR (CDCl₃, 126 MHz, 25 °C): δ 160.17, 154.10, 144.22, 142.16, 139.25, 138.11, 129.13, 129.08, 128.63, 128.17, 127.67, 122.06, 118.71, 118.54, 116.67, 90.46, 46.46, 24.16.

2-((3-(aminomethyl)phenyl)amino)-6-methyl-5-phenylnicotinonitrile (30 mg, 1.0 equiv) and DIPEA (50 μL, 3.0 equiv) was dissolved in 5 mL of DMF in a 20 mL glass vial. To the solution, a solution of biotin-PEG2-NHS (47.8 mg, 2.0 equiv) in 5 mL of DMF was added dropwise and let stir under room temperature overnight. The solution was diluted with 50 mL of EtOAc and washed with brine for 3 times. The organic phase was separated, dried over Na₂SO₄, and then evaporated. The crude product was purified by column chromatography on silica gel (90% MeOH in DCM). Removal of solvent afforded product as a colorless oil (25 mg, 38%). ¹H NMR (CD₃OD, 600 MHz, 25 °C): δ 7.63 (s, 1H), 7.50 (d, *J*=8.6 Hz, 2H), 7.34 (t, *J*=7.4 Hz, 2H), 7.27 (t, *J*=7.4 Hz, 1H), 7.22 (d, *J*=6.9 Hz, 2H), 7.18 (t, *J*=7.7 Hz, 1H), 6.90 (d, *J*=7.7 Hz, 1H), 4.35 (dd, *J*=8.4, 4.5 Hz, 1H), 4.31 (s, 2H), 4.15 (dd, *J*=7.9, 4.5 Hz, 1H), 3.67 (t, *J*=6.0 Hz, 2H), 3.54-3.43 (m, 4H), 3.38 (t, *J*=5.4 Hz, 2H), 3.25 (s, 1H), 3.19 (t, *J*=5.5 Hz, 2H), 3.09-3.00 (m, 1H), 2.78 (dd, *J*=12.7, 5.0 Hz, 1H), 2.57 (d, *J*=12.7 Hz, 1H), 2.42 (t, *J*=6.0 Hz, 2H), 2.30 (s, 3H), 2.13-2.03 (m, 2H), 1.64-1.41 (m, 4H), 1.29 (p, *J*=7.5 Hz, 2H). ¹³C{¹H} NMR (CD₃OD, 126 MHz, 25 °C): δ 176.10, 173.86, 166.05, 161.10, 155.75, 144.23, 141.37, 140.56, 139.60, 130.26, 129.78, 129.68, 129.57, 128.69, 123.17,

120.79, 117.50, 92.05, 71.25, 71.13, 70.60, 68.23, 63.31, 61.58, 56.97, 44.09, 41.04, 40.29, 37.74, 36.68, 29.74, 29.46, 26.81, 24.13. HR-MS (EI): cal'c for M+H+: 700.32029, found: 700.32269. 4-(((3-(trimethylsilyl)prop-2-yn-1-yl)oxy)methyl)pyridin-2-amine

In 100 mL Schlenk flask, (2-aminopyridin-4-yl)methanol (248 mg, 1.0 equiv) was dissolved in 20 mL of dry THF, followed by the addition of LiHMDS (367 mg, 2.2 equiv). The mixture was stirred overnight at room temperature. Propargyl bromide (392 μ L, 1.2 equiv) was added. The reaction was heated in oil bath at 60 °C for 24 h. After the reaction was cooled to room temperature, 20 mL of water was added to quench the reaction. Ethyl acetate (20 mL) used to extract the product. The organic layer was separated, dried over sodium sulfate, then evaporated. The crude product was purified by column chromatography on silica gel (60% EtOAc in hexanes) to afford pure product as light yellow solid (45 mg, 10%), and deprotected acetylene product separately (64 mg, 20%). ¹H NMR (CDCl₃, 500 MHz, 25 °C): δ δ 8.02 (d, J=5.4 Hz, 1H), 6.61 (d, J=5.3 Hz, 1H), 6.51 (s, 1H), 4.50 (s, 2H), 4.43 (s, 2H), 4.20 (s, 2H), 0.19 (s, 9H). The NMR shows a compound with modest purity, that was used without further purification in the next step.

5-phenyl-2-((4-(((3-(trimethylsilyl)prop-2-yn-1-yl)oxy)methyl)pyridin-2-yl)amino) nicotinonitrile

General procedure A was followed using 2-bromo-5-phenylnicotinonitrile (177 mg, 1.0 equiv), 4-(((3-(trimethylsilyl)prop-2-yn-1-yl)oxy)methyl)pyridin-2-amine (160 mg, 1.0 equiv),

palladium(II) acetate (6 mg, 4 mol%), xantphos (19 mg, 4.4 mol%), cesium carbonate (897 mg, 4.0 equiv), and 4 mL of dry toluene. Removal of solvent afforded product as an orange powder (108 mg, 38%). M.p.: 102-103 °C. ¹H NMR (CDCl₃, 500 MHz, 25 °C): δ 9.12 (d, *J*=2.4 Hz, 1H), 9.05 (d, *J*=7.5 Hz, 1H), 8.32 (d, *J*=2.6 Hz, 1H), 7.66 (d, *J*=7.2 Hz, 2H), 7.51 (t, *J*=7.6 Hz, 2H), 7.42 (t, *J*=7.3 Hz, 1H), 7.37 (s, 1H), 6.80 (dd, *J*=7.6, 2.0 Hz, 1H), 4.61 (s, 2H), 4.27 (s, 2H), 0.20 (s, 9H). LRMS (EI): calc'd: 412; found: 412. The NMR shows a compound with modest purity, that was used without further purification in the next step.

5-phenyl-2-((4-((prop-2-yn-1-yloxy)methyl)pyridin-2-yl)amino)nicotinonitrile

5-phenyl-2-((4-((trimethylsilyl)ethynyl)pyridin-2-In 20 mL glass vial, yl)amino)nicotinonitrile (40 mg, 0.11 mmol) was dissolved in 5 mL of THF with a stir bar. To this solution, 1 mL of 1 M TBAF solution (1.0 mmol) in THF was added dropwise under room temperature. The colorless solution became bright orange. After 1 h of stirring, the solvent was removed and crude product was purified by column chromatography (silica hexanes:EtOAc 5:1), which afforded the desired compound as colorless crystals (mg, 63%). M.p.: 137-138 °C. ¹H NMR (CDCl₃, 500 MHz, 25 °C): δ 9.14 (s, 1H), 9.06 (d, *J*=7.9 Hz, 1H), 8.58 (s, 1H), 8.32 (s, 1H), 7.67 (d, J=7.8 Hz, 2H), 7.52 (t, J=7.1 Hz, 2H), 7.44 (t, J=7.4 Hz, 1H), 7.39 (s, 1H), 6.80 (d, J=7.5 Hz, 1H), 7.52 (t, J=7.1 Hz, 2H), 7.44 (t, J=7.4 Hz, 1H), 7.39 (s, 1H), 6.80 (d, J=7.5 Hz, 1H), 7.39 (s, 1H1H), 4.64 (s, 2H), 4.29 (s, 2H), 2.52 (s, 1H).). ${}^{13}C\{{}^{1}H\}$ NMR (CDCl₃, 126 MHz, 25 °C): δ 154.45, 154.38, 150.25, 148.38, 146.89, 140.05, 137.14, 132.92, 131.16, 129.45, 128.40, 128.17, 127.16, 126.58, 123.14, 111.62, 78.89, 75.73, 75.28, 70.40, 69.43, 58.21. ¹H NMR (CDCl₃, 500 MHz, 25 °C): δ 10.08 (s, 1H), 9.14 (s, 1H), 9.08 (s, 1H), 9.02 (d, J=6.7 Hz, 1H), 7.90 (d, J=7.8 Hz, 2H),

7.54 (t, *J*=7.7 Hz, 2H), 7.43 (t, *J*=7.7 Hz, 1H), 7.21 (s, 1H), 6.87 (d, *J*=9.3 Hz, 1H), 4.61 (s, 2H), 4.33 (s, 2H), 3.57 (s, 1H).

3-bromo-9-methyl-5H-dipyrido[1,2-a:2',3'-d]pyrimidin-5-imine

In a glove box, tris(dibenzylideneacetone)dipalladium(0) (23 mg, 2.5 mol%) and DMAPF (25 mg, 6 mol%) were dissolved in 2 mL of dry dioxane in a 35 mL pressure tube. The mixture was stirred for 2 min before 5-bromo-2-chloro-nicotinonitrile (217 mg, 1.0 equiv), 4-methylpyridin-2-amine (108 mg, 1.0 equiv), and sodium *tert*-butoxide (116 mg, 1.25 equiv) were added to the pressure tube. Then, another 3 mL of dry dioxane was added. The reaction was then removed from the glovebox and heated in an oil bath at 80 °C for 15 h. After the reaction was cooled to room temperature, the reaction mixture was filtered through Celite and rinsed with ethyl acetate. The filtrate was evaporated, and the crude product was purified by column chromatography on silica gel (85% EtOAc in hexanes) to afford pure product as a red solid (160 mg, 55%). ¹H NMR (CDCl₃, 500 MHz, 25 °C): δ 8.96 (d, *J*=6.4 Hz, 1H), 8.85 (s, 1H), 8.48 (d, *J*=13.7 Hz, 1H), 8.27 (s, 1H), 7.20 (s, 1H), 6.66 (d, *J*=7.6 Hz, 1H), 2.40 (s, 3H). LRMS (EI): calc'd:288; found: 289. The NMR shows a compound with modest purity, that was used without further purification in the next step. 5-(3-ethynylphenyl)-2-((4-methylpyridin-2-yl)amino)nicotinonitrile

In a glove box, tetrakis(triphenylphosphine)palladium(0) (32 mg, 10 mol%), potassium carbonate (115 mg, 3.0 equiv), 3-bromo-9-methyl-5H-dipyrido[1,2-a:2',3'-d]pyrimidin-5-imine (800 mg, 1.0 equiv) (1.0 equiv), 3-[(trimethylsilyl)ethynyl]phenylboronic acid pinacol ester (83 mg, 1.0 equiv), and 3mL of toluene were added in a 50 mL Schlenk tube. The reaction was then removed from glovebox and charged with water under a constant flow of dry dinitrogen. Then, the Schlenk tube was sealed and heated in an oil bath at 110 °C for 24 hours. After the reaction was cooled to room temperature, the reaction mixture was filtered through celite and rinsed with ethyl acetate. The filtrate was evaporated, and the crude product was purified by column chromatography on silica gel (hexane/ethyl acetate). The resulting yellow solid was dissolved in 5 mL of THF with a stir bar in a 20 mL glass vial. To this solution, 1 mL of 1 M TBAF solution (1.0 equiv) in THF was added dropwise under room temperature. The colorless solution became bright orange. After 1 h of stirring, the solvent was removed and crude product was purified by column chromatography (silica hexanes:EtOAc 5:1), which afforded the desired compound as colorless crystals (50 mg, 58%). M.p.: 170-171 °C. ¹H NMR (CDCl₃, 500 MHz, 25 °C): δ 9.09 (d, J=2.4 Hz, 1H), 9.00 (d, J=6.3 Hz, 1H), 8.56 (s, 1H), 8.30 (s, 1H), 7.80 (s, 1H), 7.65 (dt, J=7.8, 1.6 Hz, 1H), 7.55 (dt, J=7.8, 1.4 Hz, 1H), 7.48 (t, J=7.7 Hz, 1H), 7.23 (s, 1H), 6.66 (dd, J=7.5, 2.0 Hz, 1H), 3.16 (s, 1H), 2.40 (s, 3H). 13 C { 1 H} NMR (CDCl₃, 126 MHz, 25 °C): δ 155.00, 154.12, 150.67, 146.20, 145.50, 137.52, 131.80, 131.37, 131.29, 130.70, 129.47, 127.46, 124.25, 123.40, 120.05, 115.50, 78.19, 21.57. ¹H NMR (DMSO-d₆, 600 MHz, 25 °C): δ 10.06 (s, 1H), 9.15-9.06 (m, 2H), 8.97 (d, J=7.5 Hz, 1H), 8.03 (s, 1H), 7.94 (d, J=7.4 Hz, 1H), 7.57-7.49 (m, 2H), 7.13 (s, 1H), 7.94 (d, J=7.5 Hz, 1H), 7.57-7.49 (m, 2H), 7.13 (s, 1H), 7.94 (d, J=7.4 Hz, 1H), 7.57-7.49 (m, 2H), 7.13 (s, 1H), 7.94 (d, J=7.4 Hz, 1H), 7.57-7.49 (m, 2H), 7.13 (s, 1H), 7.94 (d, J=7.4 Hz, 1H), 7.57-7.49 (m, 2H), 7.13 (s, 1H), 7.94 (d, J=7.4 Hz, 1H), 7.57-7.49 (m, 2H), 7.13 (s, 1H), 7.94 (d, J=7.4 Hz, 1H), 7.57-7.49 (m, 2H), 7.13 (s, 1H), 7.94 (d, J=7.4 Hz, 1H), 7.57-7.49 (m, 2H), 7.13 (s, 1H), 7.94 (d, J=7.4 Hz, 1H), 7.57-7.49 (m, 2H), 7.13 (s, 1H), 7.94 (d, J=7.4 Hz, 1H), 7.57-7.49 (m, 2H), 7.13 (s, 1H), 7.94 (d, J=7.4 Hz, 1H), 7.57-7.49 (m, 2H), 7.13 (s, 1H), 7.57-7.49 (m, 2H), 7.13 (s, 1H), 7.13 (s1H), 6.82 (dd, J=7.5, 2.0 Hz, 1H), 4.30 (s, 1H), 2.36 (s, 3H).

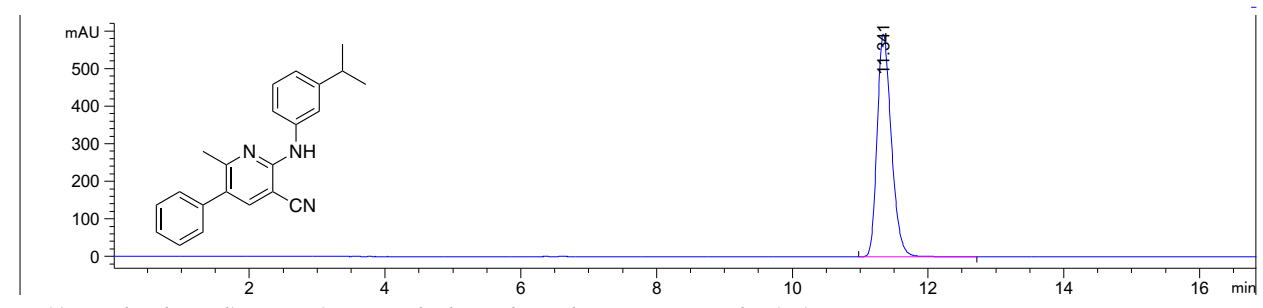
5-(3-chlorophenyl)-2-((4-methylpyridin-2-yl)amino)nicotinonitrile

In a glove box, tetrakis(triphenylphosphine)palladium(0) (19 mg, 10 mol%), potassium carbonate (46 mg, 2.0 equiv), 3-bromo-9-methyl-5H-dipyrido[1,2-a:2',3'-d]pyrimidin-5-imine (50 mg, 1.0 equiv), 3-chlorophenyl boronic acid (33 mg, 1.2 equiv), and 3 mL of dioxane were added in a 50 mL Schlenk tube. The reaction was then removed from the glovebox and charged with water (0.5 mL) under a constant flow of dry dinitrogen. Then, the Schlenk tube was sealed and heated in an oil bath at 110 °C for 12 h. After the reaction was cooled to room temperature, the reaction mixture was filtered through Celite and rinsed with ethyl acetate. The filtrate was evaporated, and the crude product was purified by column chromatography on silica gel (hexane/ethyl acetate) to afford pure product. Removal of solvent afforded product as a white powder (21 mg, 38 %). M.p.: 177-178 °C. ¹H NMR (CDCl₃, 500 MHz, 25 °C): δ 9.08 (d, *J*=2.4 Hz, 1H), 9.02 (d, *J*=6.4 Hz, 1H), 8.57 (s, 1H), 8.28 (s, 1H), 7.65 (s, 1H), 7.55 (d, *J*=7.6 Hz, 1H), 7.45 (t, *J*=7.7 Hz, 1H), 7.40 (d, *J*=8.9 Hz, 1H), 7.24 (s, 1H), 6.67 (dd, *J*=7.5, 2.0 Hz, 1H), 2.41 (s, 3H).. ¹³C (¹H) NMR (CDCl₃, 126 MHz, 25 °C): δ 178.31, 153.94, 135.26, 133.29, 132.37, 130.53, 129.52, 128.16, 127.05, 125.10, 115.41, 85.24, 77.27, 77.02, 76.77, 21.45.

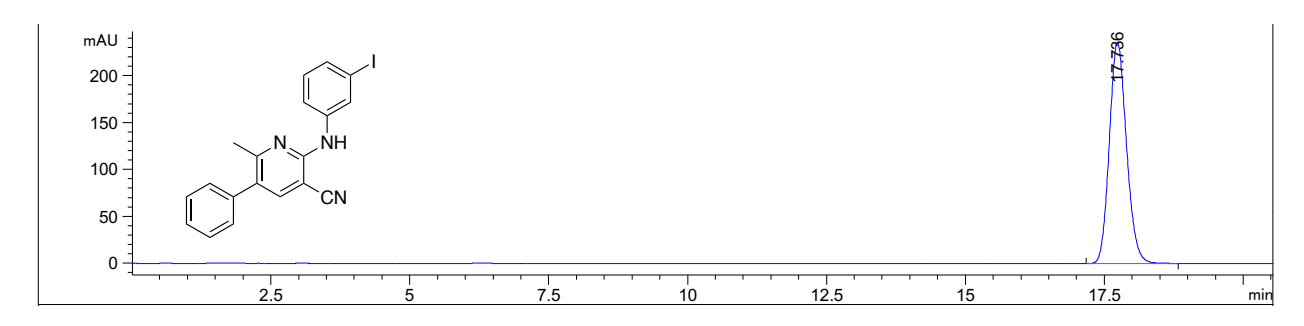
Representative HPLC traces of in vitro tested compounds

HPLC data was collected using AD-H column on Agilent 1260 HPLC. A mixture of hexanes and isopropanol (90:10) were used with 360 nm wavelength.

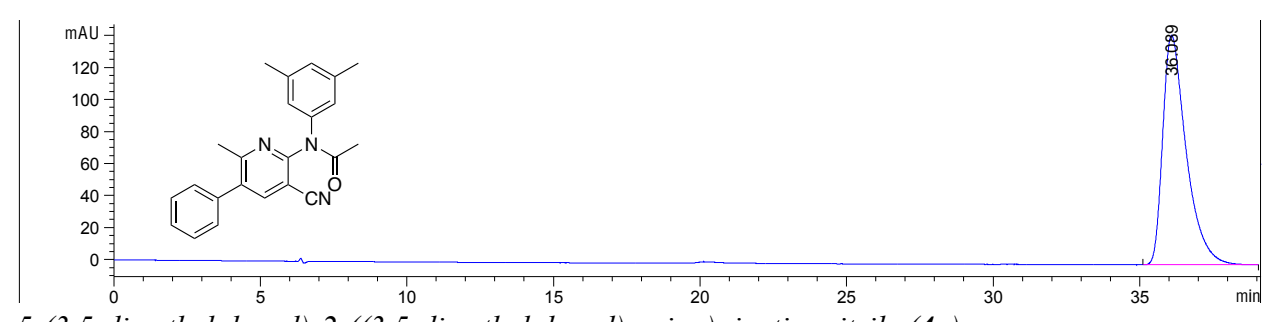
2-((3-isopropylphenyl)amino)-6-methyl-5-phenylnicotinonitrile (1b).



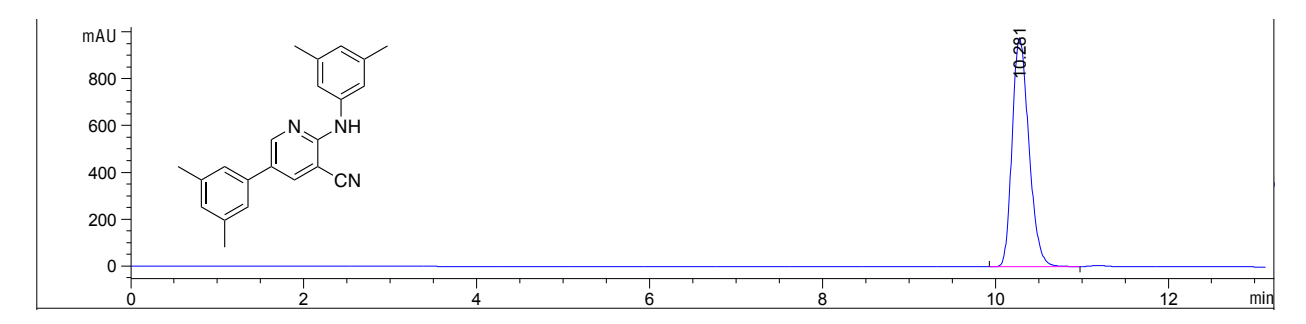
2-((3-iodophenyl)amino)-6-methyl-5-phenylnicotinonitrile (1j).



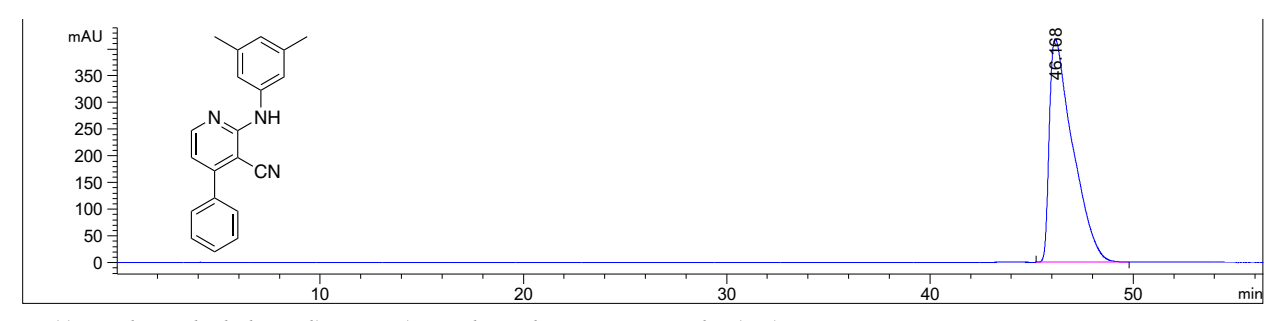
N-(3-cyano-6-methyl-5-phenylpyridin-2-yl)-N-(3,5-dimethylphenyl)acetamide (3 \boldsymbol{b}).



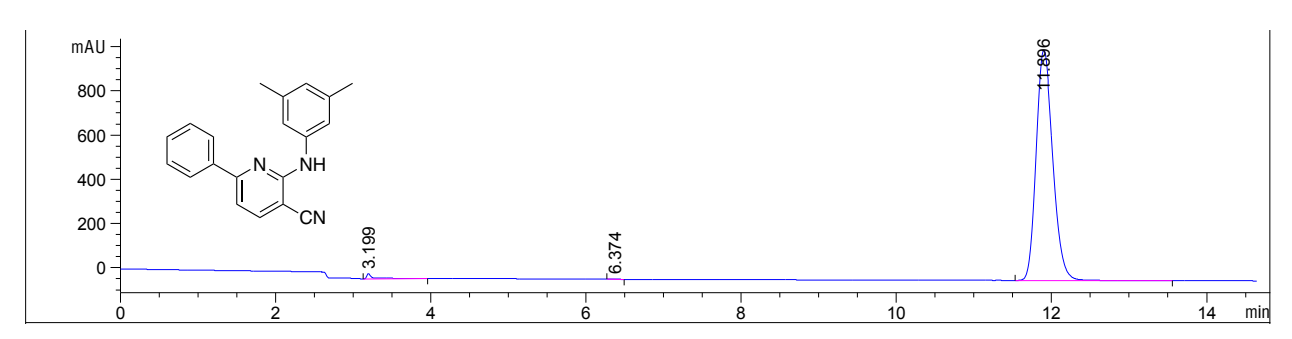
5-(3,5-dimethylphenyl)-2-((3,5-dimethylphenyl)amino)nicotinonitrile (4a).



$2\hbox{-}((3,5\hbox{-}dimethylphenyl)amino)\hbox{-}4\hbox{-}phenylnicotinonitrile \eqref{8a}).$



 $2\hbox{-}((3,5\hbox{-}dimethylphenyl)amino)\hbox{-}6\hbox{-}phenylnicotinonitrile~(\textbf{9b}).$



Kinetic Studies

To a 20 mL glass vial, 5i (2.2 mg) and ferrocene (1.0 mg) were added. The deuterated solvent (1.0 mL) was added using a volumetric syringe. The sample was made homogeneous by a glass pipette mixing, i.e., the solution was drawn up into the pipette and pushed back into the volumetric flask, until all solids were completely dissolved. The sample was filtered and transferred into an NMR tube. An array ¹H NMR experiment was set over a gradient range of time with 16 scans and 10 s of relaxation time. The relative concentrations of isomers vs internals standard ferrocene were monitored as a function of time. The fits of the exponential decay of $\bf A$ and growth of $\bf B$ were done using Kaleidagraph. The expression used to fit the data is shown in Eq S1, where $\bf Y$ = concentration of isomer $\bf A$ or $\bf B$ at time t ($\bf Y_1$), infinity ($\bf Y_{\infty}$), or at the start of the reaction ($\bf Y_0$). The rate constants were calculated by averaging the values of the decay of isomer $\bf A$ and the growth of isomer $\bf B$. The forward and backward rate constants, $\bf k_1$ and $\bf k_{-1}$, were calculated from Eq S3 and Eq S4.³⁵

$$Y_t = Y_{\infty} + (Y_0 - Y_{\infty})e^{-(k_1 + k_{-1})t}$$
 Eq S1
$$k_e = k_1 + k_{-1}$$
 Eq S2
$$k_1 = \frac{k_e}{1 + K^{-1}}$$
 Eq S3
$$k_{-1} = \frac{k_e}{1 + K}$$
 Eq S4

| Solvent | k ₁ | k ₋₁ | Keq |
|------------------------|-----------------------|-----------------------|------|
| toluene-d ₈ | 4.82×10^{-5} | 3.25×10^{-5} | 1.48 |
| CDCl ₃ | 3.94×10^{-4} | 5.06×10^{-4} | 0.77 |
| DMSO-d ₆ | 1.49×10^{-5} | 3.03×10^{-5} | 0.49 |

 k_1 and k_{-1} are from the fit of Eq S1, which provided $k_1 + k_{-1}$ (= k_e), then Eq S3 and S4 were used to separate the forward (k_1) and backward (k_{-1}) rate constants. The equilibrium constant (K) is measured from ¹H NMR spectroscopy on the equilibrium mixture at long times (after several days) in the solvent at room temperature.

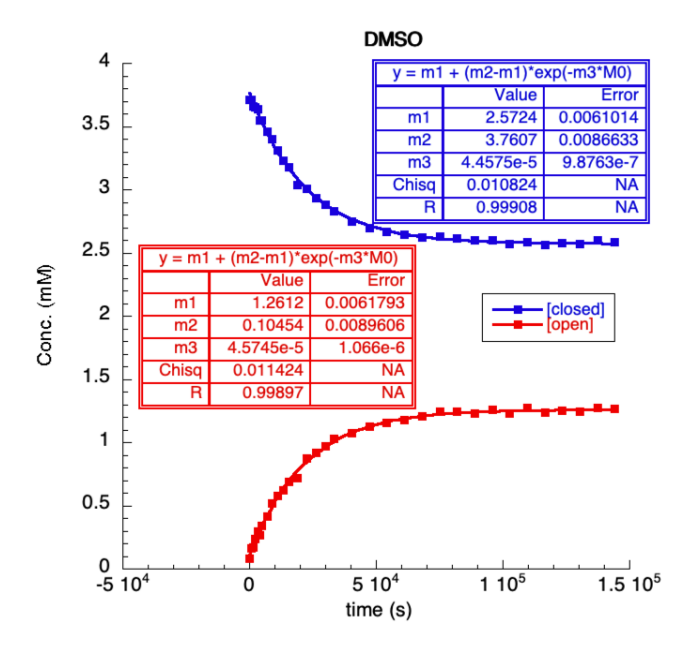


Figure 2.14. Concentration of **A** (blue dots) and **B** (red dots) as a function of time in DMSO-d6. Internal standard (ferrocene) was omitted for clarification.

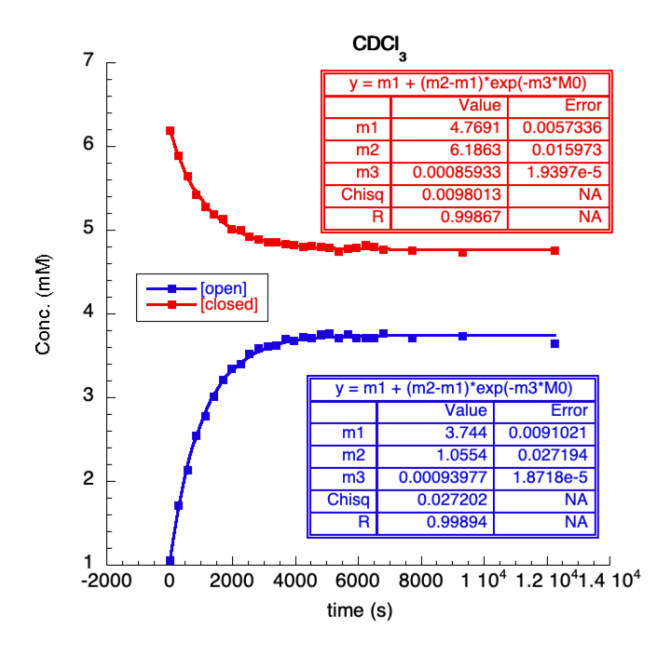


Figure 2.15. Concentration of A (blue dots) and B (red dots) as a function of time in CDCl₃. Internal standard (ferrocene) was omitted for clarification.

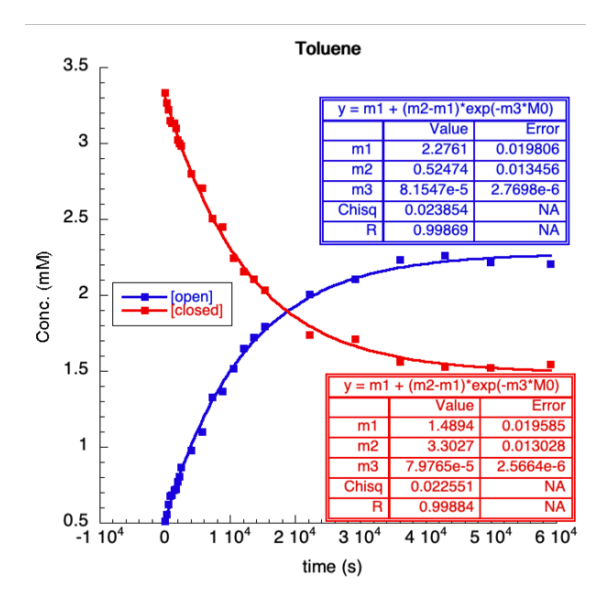


Figure 2.16. Concentration of **A** (blue dots) and **B** (red dots) as a function of time in toluene-d8. Internal standard (ferrocene) was omitted for clarification.

DFT Calculations for Equilibrium Constants for 5i in Various Media

| Column4 | ΔG (kcal/mol) | |
|-------------------|---------------|---------------|
| Solvent | cc-pvTZ | 6-311G++(p,d) |
| gas phase | -4.68 | -6.04 |
| toluene | -2.16 | -2.72 |
| CHCl ₃ | -0.43 | -1.91 |
| DMSO | -0.09 | -0.64 |
| H_2O | 1.10 | 0.49 |

The compound structures were optimized using DFT with B3PW91 functional and 6-311G+(d,p) basis set on all atoms with Gaussian16. Energy calculations were conducted using optimized geometry with 6-311G+(d,p) and cc-pvTZ basis set on all atoms. $\Delta G = Gibbs$ free energy of **B** minus the Gibbs free energy of **A**.

REFERENCES

REFERENCES

- 1. Menegon, S.; Columbano, A.; Giordano, S. The Dual Roles of NRF2 in Cancer. *Trends in Molecular Medicine* **2016**, *22* (7), 578-593.
- 2. Khor, T. O.; Huang, M. T.; Prawan, A.; Liu, Y.; Hao, X.; Yu, S.; Cheung, W. K.; Chan, J. Y.; Reddy, B. S.; Yang, C. S.; et al. Increased susceptibility of Nrf2 knockout mice to colitis-associated colorectal cancer. *Cancer Prev Res (Phila)* **2008**, *I* (3), 187-191.
- 3. Sporn, M. B.; Liby, K. T. NRF2 and cancer: the good, the bad and the importance of context. *Nature Reviews Cancer* **2012**, *12* (8), 564-571.
- 4. Khor, T. O.; Huang, M. T.; Prawan, A.; Liu, Y.; Hao, X. P.; Yu, S. W.; Cheung, W. K. L.; Chan, J. Y.; Reddy, B. S.; Yang, C. S.; et al. Increased Susceptibility of Nrf2 Knockout Mice to Colitis-Associated Colorectal Cancer. *Cancer Prevention Research* **2008**, *1* (3), 187-191.
- 5. Mitsuishi, Y.; Taguchi, K.; Kawatani, Y.; Shibata, T.; Nukiwa, T.; Aburatani, H.; Yamamoto, M.; Motohashi, H. Nrf2 redirects glucose and glutamine into anabolic pathways in metabolic reprogramming. *Cancer Cell* **2012**, *22* (1), 66-79.
- 6. Nandini, D. B.; Rao, R. S.; Deepak, B. S.; Reddy, P. B. Sulforaphane in broccoli: The green chemoprevention!! Role in cancer prevention and therapy. *J Oral Maxillofac Pathol* **2020**, *24* (2), 405-405.
- 7. Yagishita, Y.; Fahey, J. W.; Dinkova-Kostova, A. T.; Kensler, T. W. Broccoli or Sulforaphane: Is It the Source or Dose That Matters? *Molecules* **2019**, *24* (19).
- 8. Collisson, E. A.; Campbell, J. D.; Brooks, A. N.; Berger, A. H.; Lee, W.; Chmielecki, J.; Beer, D. G.; Cope, L.; Creighton, C. J.; Danilova, L.; et al. Comprehensive molecular profiling of lung adenocarcinoma. *Nature* **2014**, *511* (7511), 543-550. Hammerman, P. S.; Lawrence, M. S.; Voet, D.; Jing, R.; Cibulskis, K.; Sivachenko, A.; Stojanov, P.; McKenna, A.; Lander, E. S.; Gabriel, S.; et al. Comprehensive genomic characterization of squamous cell lung cancers. *Nature* **2012**, *489* (7417), 519-525.
- 9. Krall, E. B.; Wang, B.; Munoz, D. M.; Ilic, N.; Raghavan, S.; Niederst, M. J.; Yu, K.; Ruddy, D. A.; Aguirre, A. J.; Kim, J. W.; et al. KEAP1 loss modulates sensitivity to kinase targeted therapy in lung cancer. *eLife* **2017**, *6*, e18970.
- 10. Lignitto, L.; LeBoeuf, S. E.; Homer, H.; Jiang, S. W.; Askenazi, M.; Karakousi, T. R.; Pass, H. I.; Bhutkar, A. J.; Tsirigos, A.; Ueberheide, B.; et al. Nrf2 Activation Promotes Lung Cancer Metastasis by Inhibiting the Degradation of Bach1. *Cell* **2019**, *178* (2), 316-+.

- 11. Cuadrado, A.; Rojo, A. I.; Wells, G.; Hayes, J. D.; Cousin, S. P.; Rumsey, W. L.; Attucks, O. C.; Franklin, S.; Levonen, A. L.; Kensler, T. W.; et al. Therapeutic targeting of the NRF2 and KEAP1 partnership in chronic diseases. *Nat Rev Drug Discov* **2019**.
- 12. Zhang, D.; Hou, Z.; Aldrich, K. E.; Lockwood, L.; Odom, A. L.; Liby, K. T. A Novel Nrf2 Pathway Inhibitor Sensitizes Keap1-Mutant Lung Cancer Cells to Chemotherapy. *Molecular Cancer Therapeutics* **2021**, *20* (9), 1692-1701.
- 13. Dissanayake, A. A.; Staples, R. J.; Odom, A. L. Titanium-Catalyzed, One-Pot Synthesis of 2-Amino-3-cyano- pyridines. *Advanced Synthesis & Catalysis* **2014**, *356* (8), 1811-1822.
- 14. Mullard, A. Re-assessing the rule of 5, two decades on. *Nature Reviews Drug Discovery* **2018**, *17* (11), 777-777.
- 15. Cuny, G. D.; Yu, P. B.; Laha, J. K.; Xing, X. C.; Liu, J. F.; Lai, C. S.; Deng, D. Y.; Sachidanandan, C.; Bloch, K. D.; Peterson, R. T. Structure-activity relationship study of bone morphogenetic protein (BMP) signaling inhibitors. *Bioorganic & Medicinal Chemistry Letters* **2008**, *18* (15), 4388-4392.
- 16. Hafeez, M.; Riaz, M. Aminopyridine stabilized group-IV metal complexes and their applications. *Applied Petrochemical Research* **2016**, *6* (4), 307-340.
- 17. Odom, A. L.; McDaniel, T. J. Titanium-Catalyzed Multicomponent Couplings: Efficient One-Pot Syntheses of Nitrogen Heterocycles. *Accounts of Chemical Research* **2015**, *48* (11), 2822-2833.
- 18. Rauws, T. R. M.; Biancalani, C.; De Schutter, J. W.; Maes, B. U. W. Synthesis of new tetracyclic azaheteroaromatic cores via auto-tandem Pd-catalyzed and one-pot Pd- and Cucatalyzed double C-N bond formation. *Tetrahedron* **2010**, *66* (34), 6958-6964.
- 19. Vitaku, E.; Smith, D. T.; Njardarson, J. T. Analysis of the Structural Diversity, Substitution Patterns, and Frequency of Nitrogen Heterocycles among U.S. FDA Approved Pharmaceuticals. *Journal of Medicinal Chemistry* **2014**, *57* (24), 10257-10274.
- 20. Haight, A. R.; Bailey, A. E.; Baker, W. S.; Cain, M. H.; Copp, R. R.; DeMattei, J. A.; Ford, K. L.; Henry, R. F.; Hsu, M. C.; Keyes, R. F.; et al. A scaleable synthesis of fiduxosin. *Organic Process Research & Development* **2004**, *8* (6), 897-902.
- 21. Schnürch, M.; Spina, M.; Khan, A. F.; Mihovilovic, M. D.; Stanetty, P. Halogen dance reactions—A review. *Chemical Society Reviews* **2007**, *36* (7), 1046-1057.
- 22. Livnah, O.; Bayer, E. A.; Wilchek, M.; Sussman, J. L. Three-dimensional structures of avidin and the avidin-biotin complex. *Proceedings of the National Academy of Sciences* **1993**, *90* (11), 5076-5080.

- 23. Kumar, M. R.; Park, K.; Lee, S. Synthesis of Amido-N-imidazolium Salts and their Applications as Ligands in Suzuki–Miyaura Reactions: Coupling of Hetero- aromatic Halides and the Synthesis of Milrinone and Irbesartan. *Advanced Synthesis & Catalysis* **2010**, *352* (18), 3255-3266. Zhao, Y.; Li, M.; Li, B.; Zhang, S.; Su, A.; Xing, Y.; Ge, Z.; Li, R.; Yang, B. Discovery and optimization of thienopyridine derivatives as novel urea transporter inhibitors. *European Journal of Medicinal Chemistry* **2019**, *172*, 131-142.
- 24. Kolb, H. C.; Finn, M. G.; Sharpless, K. B. Click Chemistry: Diverse Chemical Function from a Few Good Reactions. *Angewandte Chemie International Edition* **2001**, *40* (11), 2004-2021.
- 25. Kolb, H. C.; Sharpless, K. B. The growing impact of click chemistry on drug discovery. *Drug Discovery Today* **2003**, *8* (24), 1128-1137.
- 26. Gelman, D.; Buchwald, S. L. Efficient Palladium-Catalyzed Coupling of Aryl Chlorides and Tosylates with Terminal Alkynes: Use of a Copper Cocatalyst Inhibits the Reaction. *Angewandte Chemie International Edition* **2003**, *42* (48), 5993-5996.
- 27. Meanwell, N. A. Improving Drug Candidates by Design: A Focus on Physicochemical Properties As a Means of Improving Compound Disposition and Safety. *Chemical Research in Toxicology* **2011**, *24* (9), 1420-1456.
- 28. Gleeson, M. P.; Hersey, A.; Montanari, D.; Overington, J. Probing the links between in vitro potency, ADMET and physicochemical parameters. *Nature Reviews Drug Discovery* **2011**, *10* (3), 197-208.
- 29. Lipinski, C. A. Drug-like properties and the causes of poor solubility and poor permeability. *Journal of Pharmacological and Toxicological Methods* **2000**, *44* (1), 235-249.
- 30. Jhoti, H.; Williams, G.; Rees, D. C.; Murray, C. W. The 'rule of three' for fragment-based drug discovery: where are we now? *Nature Reviews Drug Discovery* **2013**, *12* (8), 644-644.
- 31. Cao, C. S.; Shi, Y. H.; Odom, A. L. A titanium-catalyzed three-component coupling to generate alpha,beta-unsaturated beta-iminoamines. *Journal of the American Chemical Society* **2003**, *125* (10), 2880-2881. Aldrich, K. E.; Odom, A. L. A silica-supported titanium catalyst for heterogeneous hydroamination and multicomponent coupling reactions. *Dalton Transactions* **2019**, *48* (30), 11352-11360.
- 32. Mo, L.; Barr, H. I.; Odom, A. L. Investigation of phosphine donor properties to vanadium(V) nitrides. *Results in Chemistry* **2022**, *4*, 100344.
- 33. Coppola, G. M.; Hardtmann, G. E.; Huegi, B. S. Synthesis and reactions of 2-aryl-3-(dimethylamino)acroleins. *Journal of Heterocyclic Chemistry* **1974**, *11* (1), 51-56.
- 34. Church, R.; Trust, R.; Albright, J. D.; Powell, D. W. New synthetic routes to 3-aryl-2-chloropyridines, 5-aryl-2-chloropyridines, and 6-aryl-2-chloropyridines. *Journal of Organic Chemistry* **1995**, *60* (12), 3750-3758.

| 35. | Espenson, J. H. Chemical kinetics and reaction mechanisms; McGraw Hill, 2002. |
|-----|---|
| | |
| | |
| | |
| | |
| | |

CHAPTER 3 SYNTHESIS OF SUBSTITUTED QUINOLINE RUTHENIUM COMPLEXES

3.1 Introduction

Metal complexes have been an important class of drugs for many different diseases including cancers. Cisplatin, the first metal-based anti-cancer drug, is widely used for the treatment of various solid cancers such as testicular, ovarian, head and neck, bladder, lung, cervical cancer, melanoma, lymphomas and many others.¹ In the 1960s, Barney Rosenberg and coworkers discovered some late transition metal complexes, like platinum and ruthenium, can inhibit cell division when they investigated the impact of electric fields on bacterial growth.² This discovery quickly led to the application of these platinum complexes in cancer treatment.³ Today, platinum complexes, like carboplatin, are still recommended therapeutics to patients for many type of cancers.⁴ Even though ruthenium complexes were discovered together with the platinum complexes to inhibit cell division, they are not as widely used as their platinum analogs. Nevertheless, they also display important activity in cancer treatment.⁵

$$H_3N$$
 Pt Cl O Pt NH_3 cisplatin carboplatin

Figure 3.1. Metal-based anti-cancer drugs: cisplatin and carboplatin.

The combination of drugs with different targets has also attracted a lot of attention in cancer treatment. In 2021, the Liby group and Odom group reported that a combination treatment of MSU38225 and carboplatin showed a great improvement on slowing tumor growth compared to either individual drug.⁶ Combination drugs with ruthenium-based compounds have also been incorporated with other drugs on different systems, for example, a kinase or P450 inhibitor.⁷ In

particular, a synergistic effect between cisplatin and the proteasome inhibitor, bortezomib, has been observed for human bladder cancer.⁸

The 26S proteasome is a complex, multi-subunit threonine protease responsible for degradation of redundant, misfolded, or damaged proteins in cells. The 26S proteasome consists of a barrel-shaped proteolytic core structure, the 20S proteasome, and one or two regulatory 19S particles. The 20S proteasome is comprised of four stacked heptameric rings; two α-rings and two β-rings that house three unique catalytic sites responsible for their caspase-like, trypsin-like, and chymotrypsin-like activity. These three different catalytic sites differ based on the amino acids they cleave, where the caspase-like site cleaves following acidic residues, the trypsin-like site following basic residues, and the chymotrypsin-like site following large, hydrophobic residues. The role of the 19S regulatory particle is to recognize and unfold ubiquitinylated proteins, and then transfer the unfolded substrate protein into the 20S proteolytic core.

Regulation of proteasome activity has shown to be an important method in cancer treatment. Proteasome inhibitors are used for treating multiple myeloma and mantle cell lymphoma because these cancer cells have higher proteasome activities compared to non-transformed cells.¹² Due to the higher levels of metabolism and growth factors, the cancer cells are more sensitive to proteasome inhibitors, and as a result, proteasome inhibition in these cancer cells causes rapid apoptosis.¹³ Proteasome inhibitors can be divided into two groups (competitive and non-competitive inhibitors) depending on if they interact with the active sites or another allosteric site. Studies have found that substituted quinolines represent a new class of non-competitive proteasome inhibitors (e.g., chloroquine and 5AHQ).¹⁴

In 2009, the Odom group reported a rapid synthesis for substituted quinolines using a titanium-catalyzed one-pot two-step strategy.¹⁵ In this synthesis, the titanium catalyst,

Ti(NMe₂)₂(dpm), was used to couple an aniline, alkyne, and isonitrile to form a 1,3-diimine product with a new C–C bond and C–N bond. The iminoamination product, the 1,3-diimine derivative, was then directly treated with an excess of acetic acid, without the need for any additional purification or isolation, to afford substituted quinoline products (Scheme 3.1).

Scheme 3.1. Synthesis of substituted quinoline derivatives by Ti(NMe₂)₂(dpm)-catalyzed multicomponent coupling in a one-pot reaction.

The mechanism of the second step was proposed to go through a 6π -electrocyclic cyclization process (Scheme 3.2). After proton transfer and amine loss, the aromatization of the ring affords substituted quinolines. This methodology can be applied to many different substituted anilines, aminonaphthalenes, or even heterocyclic amines.¹⁵

Scheme 3.2. Proposed mechanism for the second step of titanium catalyzed quinoline synthesis.

In collaboration with the Tepe group at MSU, the structure-activity relationship of substituted quinolines and their human proteasome inhibition activities was reported by the Odom group in 2016.¹⁶ A library of substituted quinolines prepared by titanium catalysis was screened in this study. **Quin1** was identified as a promising human 20S proteasome inhibitor, with a single

digit micromolar half maximal inhibitory concentration (IC₅₀). **Quin1** was synthesized by an olefin hydrogenation of a quinoline product from the titanium-catalyzed one-pot strategy (Scheme 3.3).

Scheme 3.3. Synthesis of the human 20S proteasome inhibitor, Quin1.

These studies inspired us to design a ruthenium complex, incorporating a proteasome inhibitor, as a potential drug with synergistic targets. The hope for this complex is to be stable before administration, but separate into a proteasome inhibitor and a ruthenium drug in cancer cells. The dissociated quinoline could target proteasome activity, while the resulting ruthenium complex could potentially induce intrinsic apoptosis of these cancer cells.¹⁷ A synergistic effect of the two targets is expected, as these cancer cells are sensitive to proteasome inhibitors.

Furthermore, there is only one crystal structure found in the CCDC database with a η^6 -quinoline complex with any transition metal center, ((quinoline)Mo(PMe₃)₃ discovered by Parkin and coworkers in 2002). A study on the structures and activities of η^6 -quinoline complexes with other transition metal center is of interest.

3.2 Synthesis of RuCp⁺ Complexes

 ${CpRu(quinoline)}^+PF_6^-$ and ${CpRu(2-Me-quinoline)}^+PF_6^-$ are two reported complexes synthesized from ${CpRu(NCMe_3)_3}^+PF_6^-$, reported by Fish and coworkers. ¹⁹ The three-step syntheses of ${CpRu(NCMe_3)_3}^+PF_6^-$ was reported in 1982 by Gill and coworkers (Scheme 3.4). ²⁰ A substitution of chloride in $[Ru(C_6H_6)Cl_2]_2$ with cyclopentadiene was achieved by using freshly cracked HCp in the presence of base. A photolytic cleavage of the ruthenium arene bond was used

to afford the product. The problem with the photolysis step is that the rate of the reaction is sensitive to the concentration and purity of the ruthenium benzene product; it could take a very long time for large scale reactions.

Scheme 3.4. Synthesis of {CpRu(NCMe₃)₃}+PF₆⁻ by Gill and coworkers.²⁰

A different synthesis of $\{CpRu(NCMe_3)_3\}^+PF_6^-$, developed by Monnier and coworkers, was followed and scaled up successfully (Scheme 3.5).²¹ In contrast to the previous method, the cyclopentadienyl ligand was introduced prior to the η^6 -arene. After the formation of ruthenocene by reducing ruthenium chloride hydrate, $\{CpRu(naphthalene)\}^+PF_6^-$ was synthesized with TiCl₄ as an additive to trap cyclodienyl ligands. The naphthalene complex can undergo haptotropic slipping and kinetic displacement by acetonitrile to afford $\{CpRu(NCMe_3)_3\}^+PF_6^-$.

Scheme 3.5. Synthesis of {CpRu(NCMe₃)₃}+PF₆- by Monnier and coworkers.²¹

Complex 1 and 2 were successfully synthesized through simple addition of the respective quinolines to {CpRu(NCMe₃)₃}+PF₆-in dichloromethane at room temperature. Recrystallization from a dichloromethane and diethyl ether mixture afforded modest yields of the desired ruthenium complexes (Scheme 3.6).

$$+ \underbrace{\begin{array}{c} \bigoplus_{\substack{P \in \mathbb{N} \\ P \neq 0 \\ N}} \mathbb{P}_{R_{0}} \\ \mathbb{P}_{R_{0}}$$

Scheme 3.6. Synthesis of complexes 1 and 2.

Complexes 1 and 2 are formed as a pair of enantiomers because the ruthenium can bond to the carbocyclic ring on either side. One of the methods to separate two cationic enantiomers is to replace the achiral anion with a chiral anion, since the resulting two diastereomers will have a different stabilities, allowing selective crystallization of one diastereomer. Here we decided to study the racemic mixture and an achiral BArF₂₄ anion was used to explore the anion exchange reactivity (Scheme 3.7). The resulting salt was purified by recrystallization and characterized by NMR. This complex could also be used for other purposes with a higher solubility in organic solvents.

Scheme 3.7. Synthesis of {CpRu(Quin1)}⁺BArF₂₄⁻.

The synthesis of {CpRu(DMSO)₃}⁺PF₆⁻ was of interest because it is the decomposition product of complex **2** in DMSO (See Chapter 3.3). The initial proposal was to use a similar strategy as the synthesis for {CpRu(NCMe)₃}⁺PF₆⁻. Due to the difficulty of separating the desired product from the naphthalene side product and excess DMSO, DMSO was not used as a solvent in the design of this synthesis. However, a treatment of 10 equivalents of DMSO in THF or H₂O resulted in a recovery of starting materials (Scheme 3.8).

Scheme 3.8. Proposed synthesis of {CpRu(DMSO)₃}+PF₆-.

A different approach was developed by using {CpRu(NCMe₃)₃}⁺PF₆⁻ (Scheme 3.9). Dissolving {CpRu(NCMe₃)₃}⁺PF₆⁻ in DMSO resulted incomplete substitution. A trituration using a DMSO/H₂O mixture afforded the tris-DMSO complex in high yield. The recrystallization from DMSO/ether and water/THF mixture was not successful.

Scheme 3.9. Synthesis of {CpRu(DMSO)₃}⁺PF₆⁻.

3.3 Structures and Stabilities of RuCp⁺ Complexes

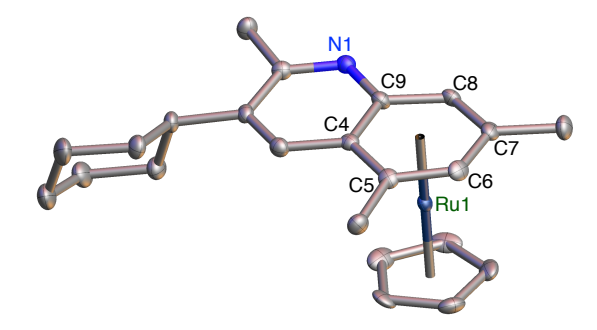


Figure 3.2. Crystal structure of complex **1**. The counter ion PF₆-, a molecule of DCM, and hydrogens are emitted for clarity.

Single crystal XRD of complex 1 was obtained by layering diethyl ether on top of a dichloromethane solution. Complex 1 has a typical sandwich geometry with the ruthenium center between a cyclopentadiene ring and carbocyclic ring of substituted quinoline (Figure 3.2); the centroid-Ru-centroid angle is 177.33(3)°. The five carbons of the cyclopentadienyl ligand are nearly equidistant from the ruthenium center, whereas the C–C bond distances on the bonded quinoline are slightly lengthened (Table 3.1). A few C–C bonds are lengthened more significantly (beyond 3 times estimated standard deviation): 1–2, 4–9, 4–5, 5–6, and 7–8 (Table 3.1).

Table 3.1. Comparison of C–C bond distances (Å) in uncoordinated quinoline (**Quin1**) and in $\eta^6(C_6)$ -complexes $\{Ru(Quin1)Cp\}^+$ (1).

| Bond Position | Quin1 | 1 | 1-Quin1 ^a |
|------------------|----------|----------|----------------------|
| 1-2 | 1.406(2) | 1.461(5) | 0.055 |
| 2-3 | 1.359(2) | 1.360(5) | 0.001 |
| 3-4 | 1.411(2) | 1.432(5) | 0.021 |
| 4-9 | 1.418(2) | 1.441(5) | 0.023 |
| 4-5 | 1.410(2) | 1.440(5) | 0.030 |
| 5-6 | 1.360(2) | 1.417(5) | 0.057 |
| 6-7 | 1.405(2) | 1.423(5) | 0.018 |
| 7-8 | 1.358(2) | 1.420(5) | 0.062 |
| 8-9 | 1.417(2) | 1.425(5) | 0.008 |

^aDifferences in the distances between coordinated and uncoordinated quinolines outside of three standard deviations are shown in red.

The energy difference between the structures with ruthenium bonded to the heterocyclic ring and carbocyclic ring was calculated by density functional theory (DFT) using Gaussian16 from B3PW91 with LANL2DZ basis set. The unsubstituted quinoline was used as a ligand for simplicity (Figure 3.3). It was found that the structure bonded with the carbocyclic ring has an

energy 10.4 kcal/mol lower than the structure with the heterocyclic ring bonded, and adding strong electron-withdrawing groups was not able to change the preference for the carbocyclic ring. For example, 5,7-bis(trifluoromethyl)quinoline and 5,6,7,8-tetrafluoroquinoline both prefer bonding to the carbocyclic ring over the heterocyclic ring, with 7.2 kcal/mol and 3.9 kcal/mol difference, respectively.

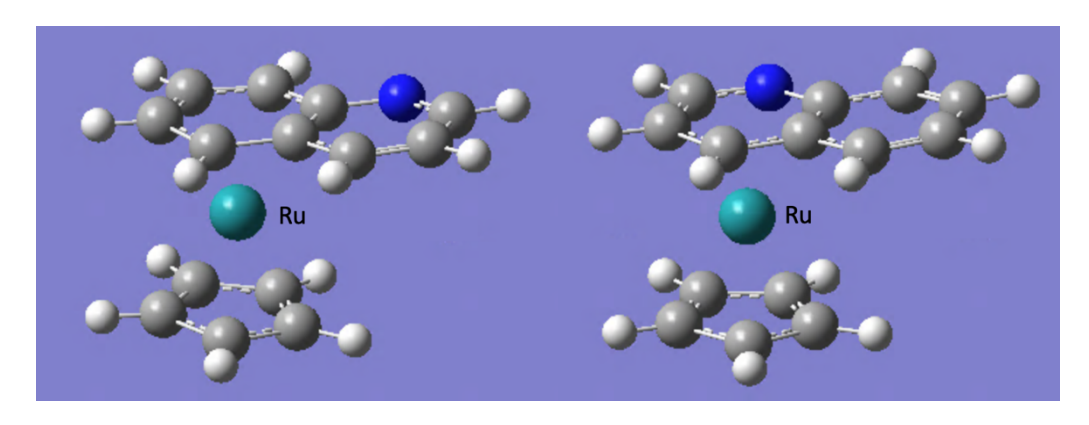


Figure 3.3. Structures of carbocyclic ring and heterocyclic ring bonded ruthenium complexes for DFT calculations.

The stability of $(\eta^6$ -arene)Ru(II) species has been noted by Fish and coworkers previously. They reported that $\{(\eta^6-2\text{-Me-quinoline})\text{Ru}(\text{Cp})\}^+$ in the presence of excess MeCN results in free quinoline and $\{\text{Ru}(\text{Cp})(\text{NCMe})_3\}^+$ after two days at ambient temperature.²² The stability of complexes 1 and 2 in different coordinating solvents was investigated in this study.

Complexes 1 and 2 share a similar structure and were expected to have similar stability to different coordinating solvents. It was found that both complexes 1 and 2 are unstable in an excess of acetonitrile. Dissolving complex 1 or 2 in acetonitrile resulted in the formation of free quinoline and tris(acetonitrile)RuCp⁺. A plot of [Quin1] vs time MeCN-d₃ can be found in the supporting information. Similarly, complexes 1 and 2 are both stable in 1:9 DMSO-d₆:D₂O for days (Figure 3.4). This suggested that water is a worse ligand compared to acetonitrile.

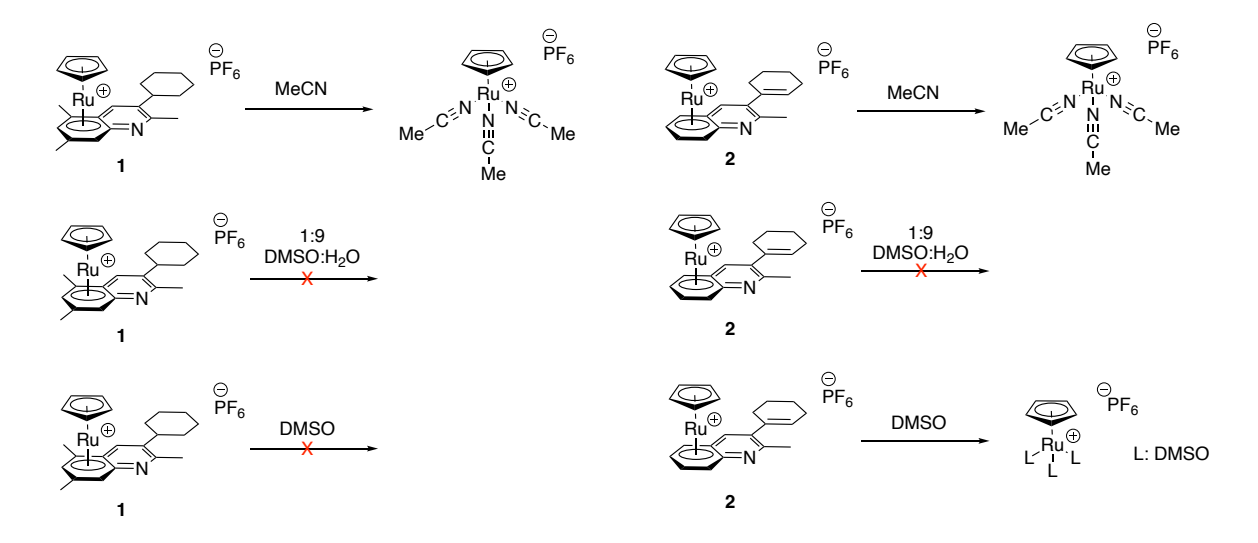


Figure 3.4. Stability of complex 1 and 2 in different coordinating solvents.

However, 1 and 2 showed different stabilities in DMSO. The reaction of 2 with DMSO-d₆ resulted in free **Quin2** and a new ruthenium species, {Ru(Cp)(DMSO-d₆)₃}⁺; whereas, 1 appears to be stable in DMSO-d₆ for days. This suggested that the quinoline ring can be displaced by solvents with the kinetic ability going as acetonitrile > DMSO > water. A few reasons can be proposed to explain why complex 1 exhibits higher stability in coordinating solvents than complex 2. Having electron-donating groups on the quinoline can make it a better ligand and form stronger metal-ligand bonds. Multiple methyl groups could also increase the steric bulk of the ligand and attenuate the intermolecular interaction between the metal center and other free ligands. Nolan and coworkers studied the thermodynamics of hydrocarbon- π -systems binding to {Ru(Cp)(NCMe)₃}⁺.²³ They stated that the addition of electron-donating groups (e.g., Me, SiMe₃, OMe, and NMe₂) thermodynamically significantly stabilizes the η^6 -arene complex.

The stability of 1 in the presence of a common reductant in cells, glutathione, was also investigated (Figure 3.5). Since a higher level of glutathione is found in cancer cells compared to normal cells,²⁴ glutathione could be a potential reductant that can free the quinoline from metal center in cancer cells. However, no significant change was observed after a 72 h incubation with

1 equivalent of glutathione at ambient temperature. However, this experiment does not rule out the possibility of potential dissociation of the proteasome inhibitor, **Quin1**, from the metal center in cancer cells through other mechanisms.

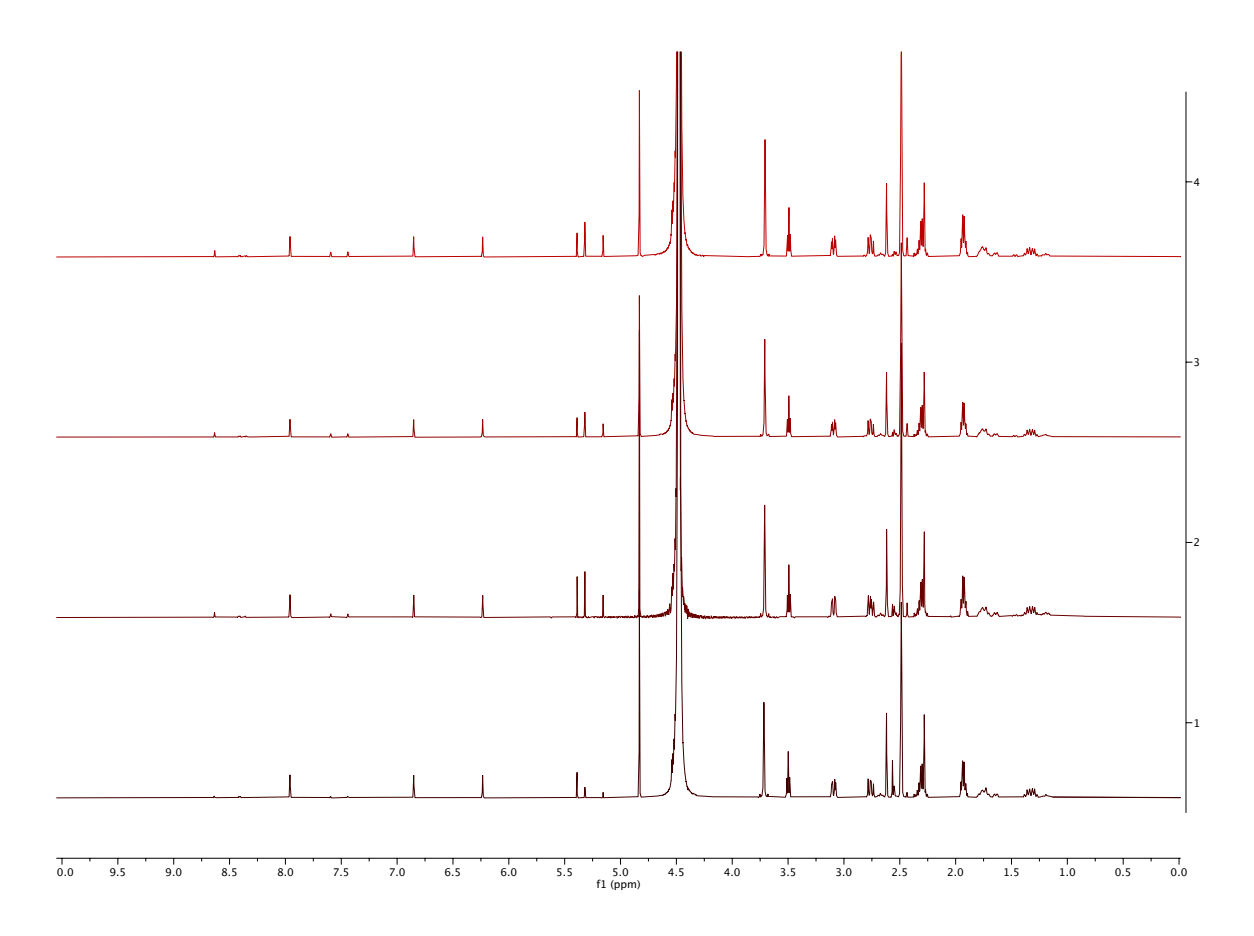


Figure 3.5. From bottom to top, ¹H NMR of complex **1** with 1.0 equivalent of reduced glutathione in 10% DMSO/D₂O after 0, 24, 48, and 72 hours.

3.4 Biological Activities of RuCp⁺ Complexes

In collaboration with Prof. Tepe's group, the *in vitro* proteasome activities of **Quin1**, **Quin2**, and their Ru complexes, **1** and **2**, were tested using fluorogenic peptide substrates. The rate of hydrolysis was determined by monitoring the increase in fluorescence at 37 °C over 30 minutes. The curve was then used to calculate the half maximal inhibitory concentration (IC₅₀). The IC₅₀

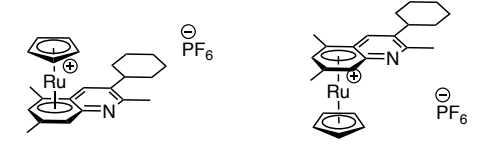
values represent the concentration of the drug that is required to inhibit the proteasome activity by half; more potent drugs (lower IC₅₀ values) are desirable for this study.

Quin1 and Quin2 were tested previously, where Quin1 was found to be a potent proteasome inhibitor (CT-L: $IC_{50}=9 \mu M$), while Quin2 was not identified as a proteasome inhibitor since its IC_{50} is greater than 80 μM . Quin1's ruthenium complex, 1, showed reduced inhibition activity in comparison with unbonded Quin1. In order to rule out the possibility of the ruthenium metal center inhibiting the proteasome activity, Quin2's ruthenium complex, complex 2, was also tested, but it showed no inhibition of proteasome activity (Table 3.2). This suggested the ruthenium complexes do not dissociate in proteasome or in the buffer used for testing.

Table 3.2. Proteasome inhibition activities for each catalytic site.

| Compound | CT-L IC ₅₀ (μM) | Casp-L IC ₅₀ (μM) | 3 sites IC ₅₀ (μM) |
|--------------------------|----------------------------|------------------------------|-------------------------------|
| Quin1 | 9 | 9 | 14 |
| Quin2 | >80 | >80 | >80 |
| CpRu(Quin1) ⁺ | 15 | 16 | 30 |
| CpRu(Quin2) ⁺ | >80 | >80 | >80 |

One possible reason why complex 1 showed lower inhibition activity is that the formation of the ruthenium complexes resulted in a mixture of two enantiomers (Scheme 3.10); separation of the two enantiomers on HPLC was not successful. An alternative strategy using a chiral anion is possible, but was not explored for this study.



Scheme 3.10. Potential enantiomers of complex 1.

Cyclopentadienyl ruthenium complexes have been studied for their anti-cancer activity for many different cancer types (e.g., HL-60 (human leukemia), LoVo (human colon adenocarcinoma), MiaPaCa (pancreatic cancer), A2780 (cisplatin resistant human ovarian), MCF7 (human breast cancer), PC3 (human prostate cancer), MM96L (human skin carcinoma), MDA-MB-231 (hormone-independent breast cancer), and HeLa (cervical carcinoma)),²⁵ and their cytotoxicity has shown to be dependent upon the ligands on the metal center. In our system, a proteasome inhibitor as the ligand has the potential to enhance cytotoxic effects in cancer cells.

Therefore, two different multiple myeloma cell lines, MC/CAR and RPMI 8226, were used to check the cytotoxicity of the ruthenium complexes. **Quin1**, **Quin2**, and their ruthenium complexes, **1** and **2**, were tested for cytotoxicity (Table 3.3). The extract concentration that reduced the cell viability by 50% when compared to untreated controls was reported as CC₅₀. As expected, **Quin1** being a proteasome inhibitor showed cytotoxicity toward these two cell lines. Complex **2**, the ruthenium complex of the inactive quinoline, also showed cytotoxicity. What is most promising, is that complex **1**, a combination of ruthenium and a proteasome inhibitor, showed the highest toxicity in the two cell lines. The combination index (0.7 for MC/CAR and 0.6 for RPMI 8226) indicated a synergistic effect of the ruthenium complex with the proteasome inhibitor.

Table 3.3. Cytotoxicity for MC/CAR and RPMI 8226 cell lines.

| Compound | MC/CAR CC ₅₀ (µM) | RPMI CC ₅₀ (μM) |
|---|------------------------------|----------------------------|
| Quin1 | 19.5 | 11.8 |
| Quin2 + CpRu(DMSO ₃) ⁺ | 19.1 | 36.6 |
| CpRu(Quin1) ⁺ | 3.4 | 2.0 |
| CpRu(Quin2) ⁺ | 6.8 | 5.0 |

Currently, the cytotoxicity of {CpRu(DMSO)₃}⁺PF₆⁻ is being tested. It is expected to show the same or lower cytotoxicity than complex **2** in DMSO (dissociate to **Quin2** + CpRu(DMSO₃)⁺), because **Quin2** is not a proteasome inhibitor and is not expected to show cytotoxicity in these cell lines.

Proteosome inhibition activities and cytotoxic activities of all compounds were tested by our collaborator Allison Vanecek from Prof. Tepe' group at MSU.

3.5 Conclusions

Examples of ruthenium quinoline complexes being prepared and structurally characterized are rare. The metal center binds to the more electron-rich arene side of the quinoline ligand in an η^6 fashion. The energy difference of binding on the arene and heterocycle was investigated by DFT. The energy difference could be reduced by installing electron-withdrawing substituents, but was not inverted. The lengthened C–C bonds within the heterocycle suggests a significant backbonding to the quinoline ring from the metal center. The stability study has led to the discovery of an increased stability of the ruthenium complex with a methyl substituted quinoline. The kinetic ability of solvent to replace quinoline ring goes acetonitrile > DMSO > water.

The proteosome inhibition activity of the ruthenium quinoline complexes was investigated in this study. Coordination of the **Quin1** to ruthenium reduces its ability to inhibit proteasome activity; however, it showed higher cytotoxicity towards multiple myeloma cell lines than **Quin1**. A synergistic activity between proteasome inhibitor **Quin1** and a highly reactive $\{Ru(Cp)(OH_2)_3\}^+$ was determined by a combination index of ~0.6 for two different multiple myeloma cell lines with the assumption that complex 2 could be a surrogate for the reactive ruthenium complex $\{Ru(Cp)(OH_2)_3\}^+$.

The study on the biological activity of the ruthenium complex presented an outstanding therapeutic opportunity for the development of metal complexes with tandem pharmacological activities.

3.6 Experimental details

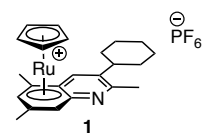
General Considerations

All manipulations were carried out under an inert dinitrogen atmosphere in an MBraun glovebox or using standard Schlenk techniques. The solvents toluene, acetonitrile, and diethyl ether were sparged with dinitrogen and passed over an activated alumina column prior to use. *n*-hexane was dried by refluxing with sodium-benzophenone ketyl and distilled under dinitrogen prior to use. Ethanol was dried by refluxing over magnesium and distilled under dinitrogen prior to use. CDCl₃ was purchased from Cambridge Isotope Laboratories, dried over P₂O₅, and distilled under dinitrogen. All solvents were stored over 3 Å molecular sieves in an inert atmosphere glove box after purification. Synthesis of *tert*-butylisonitrile was done according to the literature procedure and purified by distillation under dry dinitrogen.²⁶ Syntheses of Ti(dpm)(NMe₂)₂ was done according to the literature procedure.²⁷ {CpRu(CH₃CN)₃}PF₆ was prepared by a modification of the literature procedure, and the details of the modifications can be found in the SI.²⁸ Quin1 and Quin2 were prepared using the literature procedures.^{15,16}

All NMR spectra were recorded in the Max T. Rogers NMR Facility at Michigan State University using an Agilent DDR2 500 MHz NMR spectrometer equipped with a 5 mm PFG OneProbe operating at 500 MHz (¹H), 126 MHz (¹³C), and 460 MHz (¹⁹F).

All crystallographic data were collected at the Michigan State University Center for X-ray Crystallography. Single crystal diffraction data were collected from Rigaku Synergy S dual source single crystal diffractometer using CuKα. Single crystals were mounted on glass fiber loops using N-paratone oil. Data collection was done at 173 K under a liquid nitrogen cold stream. The structures were solved with the ShelXT solution program using intrinsic phasing and refined with the XL refinement package using least squares minimization in Olex 2.

Synthesis of $(\eta^6(C6)-3-cyclohexyl-2,5,7-trimethylquinoline)(\eta^5-cyclopentadienyl)ruthenium(II)$ hexafluorophosphate (1):



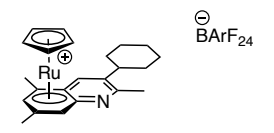
This procedure was adapted from a literature synthesis.²⁹ In a glove box, tris(acetonitrile)(η^5 -cyclopentadienyl)ruthenium(II) hexafluorophosphate (43.4 mg, 0.1 mmol, 1.0 equiv) was dissolved in 2 mL of dry CH₂Cl₂ in a 20 mL glass vial. In a separate 20 mL vial, 3-cyclohexyl-2,5,7-trimethylquinoline (25.3 mg, 0.1 mmol, 1.0 equiv) was dissolved in 2 mL of CH₂Cl₂. The quinoline solution was added dropwise to the stirring solution of the acetonitrile complex to form a clear, yellow solution that was stirred for 1 h after addition. The solution was then layered with approximately 4 mL of OEt₂ and put in a freezer at –35 °C overnight. The next morning, off white crystals and powder (29.0 mg, 50%) were collected of 1. M.p.: 226-227 °C. ¹H NMR (CDCl₃, 500 MHz, 25 °C): δ 7.96 (s, 1H), 6.85 (s, 1H), 6.43 (s, 1H), 4.92 (s, 5H), 2.83 (s, 3H), 2.71 (s, 3H), 2.48 (s, 3H), 2.03-1.77 (m, 5H), 1.53-1.43 (m, 5H). ¹³C{¹H} NMR (CDCl₃, 126 MHz, 25 °C): δ 169.92, 145.24, 130.08, 111.10, 102.45, 97.27, 92.09, 90.03, 84.41, 80.61, 40.72, 33.31, 33.16, 26.89, 26.85, 25.78, 24.24, 20.48, 18.00. ¹⁹F NMR (CDCl₃, 470 MHz, 25 °C): -71.52 (d, J=713.3

Hz). Elemental analysis (with one equivalent dichloromethane in the lattice): calc'd for C₂₄H₃₀NF₆Cl₂PRu: C, 44.39; H, 4.66; N, 2.16. Found: C, 44.01; H, 4.68; N, 2.19. HRMS: QTOF EI (positive ion) calc'd for C₂₃H₂₈NRu: 420.1271; found: 420.1276.

Synthesis of $(\eta^6(C6)-3-(cyclohex-1-en-1-yl)-2-methylquinoline)(\eta^5-cyclopentadienyl)$ ruthenium(II) hexafluorophosphate (2).

In a glove box, tris(acetonitrile)(η^5 -cyclopentadienyl)ruthenium(II) hexafluorophosphate (20 mg, 1.0 equiv) was dissolved in 2 mL of dry dichloromethane in a 20 mL glass vial. In a separate 20 mL vial, 3-(cyclohex-1-en-1-yl)-2-methylquinoline (10.3 mg, 1.0 equiv) was dissolved in 2 mL of dichloromethane. The quinoline solution was added dropwise to the stirring solution of the acetonitrile complex to form a clear, yellow solution that was allowed to stir for 1 h. The solution was then layered with approximately 4 mL of diethyl ether and put in a freezer at -35 °C overnight. The next morning, off white crystals and powder (19.0 mg, 77%) were collected of **2**. M.p.: 185-187 °C. ¹H NMR (CDCl₃, 500 MHz, 25 °C): δ 7.84 (s, 1H), 7.12-7.04 (m, 1H), 7.04-6.95 (m, 1H), 6.38-6.28 (m, 2H), 5.75 (s, 1H), 5.08 (s, 5H), 2.65 (s, 3H), 2.27-2.18 (m, 4H), 1.84-1.70 (m, 4H). 13 C (1 H) NMR (CDCl₃, 126 MHz, 25 °C): δ 170.30, 143.28, 136.04, 135.11, 130.37, 112.41, 92.79, 86.68, 86.15, 84.09, 84.02, 80.31, 29.62, 25.47, 25.18, 22.70, 21.71. 19 F NMR (CDCl₃, 470 MHz, 25 °C): -72.50 (d, J = 712.2 Hz). HRMS: QTOF EI (positive ion) calc'd for C₂₁H₂₂NRu: 390.0801; found: 390.0802.

Synthesis of $(\eta^6(C6)-3-cyclohexyl-2,5,7-trimethylquinoline)(\eta^5-cyclopentadienyl)ruthenium(II)$ tetrakis $\{3,5-bis(trifluoromethyl)phenyl\}borate.$



In a glove box, $(\eta^6(C6)\text{-}3\text{-}\mathrm{cyclohexyl-}2,5,7\text{-}\mathrm{trimethylquinoline})(\eta^5\text{-}\mathrm{cyclopentadienyl})$ ruthenium(II) hexafluorophosphate (20 mg, 1.0 equiv) was dissolved in 2 mL of dry ether in a 20 mL glass vial. To this vial, sodium tetrakis {3,5-bis(trifluoromethyl)phenyl} borate (50 mg, 1.2 equiv) was added. The mixture was stirred at room temperature for 24 h. The solution was then layered with approximately 3 mL of n-hexane and put in a freezer at -35 °C overnight. The next morning, white solid (31.0 mg, 70%) was collected. ¹H NMR (CDCl₃, 500 MHz, 25 °C): δ 7.78 (s, 1H), 7.69 (s, 8H), 7.52 (s, 4H), 6.88 (s, 1H), 5.90 (s, 1H), 4.65 (s, 5H), 2.76 (s, 1H), 2.72 (s, 3H), 2.58 (s, 3H), 2.34 (s, 3H), 1.96-1.82 (m, 4H), 1.43-1.25 (m, 4H). ¹³C{¹H} NMR (CDCl₃, 126 MHz, 25 °C): 134.75, 128.51, 125.59, 117.50, 102.03, 88.60, 84.95, 79.71, 40.47, 33.41, 33.34, 26.51, 26.46, 25.62, 24.10, 20.41, 18.13. ¹⁹F NMR (CDCl₃, 470 MHz, 25 °C): -62.30 (s).

Synthesis of tris(dimethyl sulfoxide)(η^5 -cyclopentadienyl)ruthenium(II) hexafluorophosphate.

In 20 mL glass vial, tris(acetonitrile)(η^5 -cyclopentadienyl)ruthenium(II) hexafluorophosphate (20 mg, 1.0 equiv) was loaded with a stir bar. To the solid, 84 μ L of DMSO (12 equiv) was added, followed by 1 mL of H₂O. The reaction was kept stirring under vacuum at 60°C for 12 h. The product was collected as an off white solid (50 mg, 93%). M.p.: °C. ¹H NMR (DMSO-d₆, 500 MHz, 25 °C): δ 5.47 (s, 5H), 3.50 (s, 18H). ¹³C{¹H} NMR (DMSO-d₆, 126 MHz, 25 °C): δ 85.74, 52.45. ¹9F NMR (DMSO-d₆, 470 MHz, 25 °C): δ -70.12 (d, J = 711.5 Hz). HRMS: QTOF EI (positive ion) calc'd for C₁₁H₂₃O₃S₃Ru: 400.9854; found: 400.9855.

Measurement of the kinetics of quinoline replacement by acetonitrile-d₃. In an inert atmosphere glove box, a 20 mL glass vial was loaded 1 (6.0 mg, 10.3 μmol), ferrocene (as a reference, 2.0 mg, 10.75 μmol), and acetonitrile-d₃ (600 μL). The solution was mixed by drawing in and out of a pipette until homogeneous. The reaction was transferred into an NMR tube, which was carefully capped and sealed with electrical tape. Then, the NMR tube was removed from the glovebox and placed in a room temperature silicon oil bath. Periodically, an NMR tube was removed from the oil bath, and a ¹H NMR spectrum was measured. The relative concentration of 1 vs ferrocene was monitored as a function of time. The fits of the exponential decay of 1 were done using the scientific program KaleidaGraph v5.0.1. The expression used to fit the data was $Y_t = Y_\infty + (Y_0 - Y_\infty)e^{-k_{obs}t}$, where Y = concentration at time t (Y_t), infinity (Y_∞), or at the start of the reaction (Y₀).³⁰ An example of a plot of concentration vs time and its fit is shown in Figure 3.5.

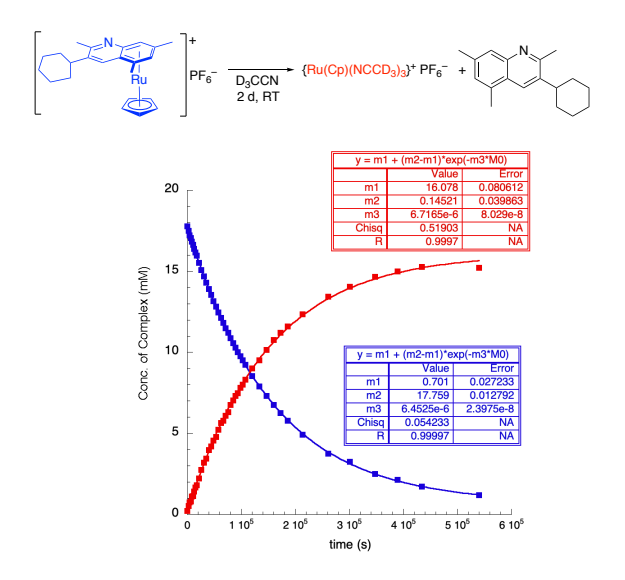


Figure 3.6. Kinetic displacement of quinoline in MeCN-d₃ on complex 1. The concentration vs. time data are fit to $Y_t = Y_{\infty} + (Y_0 - Y_{\infty})e^{-k_{obs}t}$, where $Y_t = \text{conc.}$ at time t, $Y_0 = \text{conc.}$ at the start of the reaction, $Y_{\infty} = \text{conc.}$ at very long times, and k_{obs} is the observed pseudo-first order rate constant in s⁻¹.

Measurement of the kinetics of quinoline replacement by DMSO-d₆: In an inert atmosphere glove box, a 20 mL glass vial was loaded **2** (3.1 mg, 5.8 μmol), ferrocene (3.7 mg, 19.9 μmol), and DMSO-d₆ (600 μL). The solution was mixed by drawing in and out of a pipette until homogeneous. The reaction was transferred into an NMR tube, which was carefully capped and sealed with electrical tape. Then, the NMR tube was removed from the glovebox and placed in a room temperature silicon oil bath. Periodically, an NMR tube was removed from the oil bath, and a ¹H NMR spectrum was measured. The relative concentration of **2** vs ferrocene was monitored as a function of time. The fits of the exponential decay of **2** were done using the scientific program KaleidaGraph v4.1.3. The expression used to fit the data was $Y_t = Y_\infty + (Y_0 - Y_\infty)e^{-k_{obs}t}$, where Y = concentration at time t (Y_t), infinity (Y_∞), or at the start of the reaction (Y_0). An example of a plot of concentration vs time and its fit is shown in Figure. 3.6. The plots and fits for the other trials, along with tabulated data, can be found in the SI.

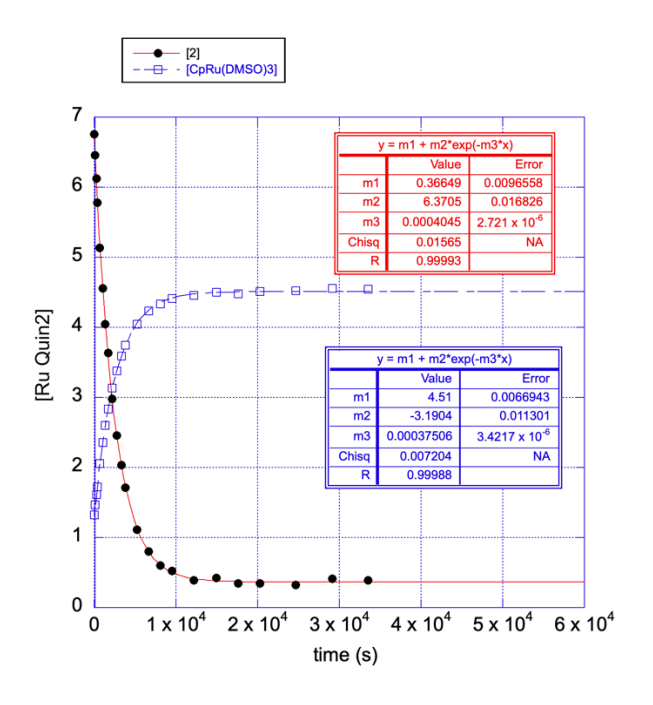


Figure 3.7. Kinetic displacement of quinoline in DMSO -d₆ on complex **2**. The concentration vs. time data are fit to $Y_t = Y_{\infty} + (Y_0 - Y_{\infty})e^{-k_{obs}t}$, where $Y_t = \text{conc.}$ at time t, $Y_0 = \text{conc.}$ at the start of the reaction, $Y_{\infty} = \text{conc.}$ at very long times, and k_{obs} is the observed pseudo-first order rate constant in s⁻¹.

Procedure for the 20S Proteasome Inhibition Activity Assay: The activity assay was conducted in a 100 μL reaction volume in a black, clear-bottom 96-well plate. Purified human 20S proteasome (1 nM) and stock solutions of the test compound were added to final concentrations ranging from 1.25-80 μM in assay buffer (50 mM Tris-HCl buffer, 0.03% SDS, pH 7.5), and the plate was incubated at 37 °C for 15 min. The fluorogenic substrates (Suc-LLVY-AMC, Boc-LRR-AMC, and Z-LLE-AMC) were added to a final concentration of 50 μM. Fluorescence was measured at 37 °C on a SpectraMax M5e spectrometer taking kinetic readings every 1 min for 30 min (380/460 nm).

Cell viability assay. MC/CAR cells (5,000/well) were seeded in a white, opaque 96-well plate in 100 μL of Iscove's Modified Dulbecco's Medium (IMDM) supplemented with 20% FBS and 1% penicillin/streptomycin. RPMI 8226 cells (25,000/well) were seeded in a white, opaque 96-well plate in 100 μL of RPMI-1640 Medium supplemented with 10% FBS and 1% penicillin/streptomycin. Drug stock solutions were made in 100% DMSO-d₆ or 9:1 water/ DMSO-d₆. The cells were then treated with the test compound at concentrations ranging from 1.25-40 μM (0.5% DMSO-d₆ final concentration) for 72 hours at 37 °C and 5% CO₂. For samples in 100% d-DMSO, a total volume of 0.5 μL drug stock was added; for samples in 9:1 water/DMSO-d₆, a total volume of 5 μL drug stock was added. Cells were equilibrated to room temperature and CellTiter-Glo (Promega) solution (100 μL) was added and incubated with shaking for 2 minutes at room temperature. Assay plate was then allowed to equilibrate for 10 more minutes at room temperature and luminescence readings were taken on a SpectraMax M5e. Statistical analyses were performed with GraphPad Prism 8.1; Brown-Forsythe and Welch ANOVA with a post hoc Dunnett's T3 test was used for multiple comparisons of group means (*p \leq 0.05; **p \leq 0.01).

Stability of 1 in DMSO-d₆/D2O

In a 20 mL glass vial, 1 (1.2 mg) was dissolved in DMSO- d_6 (60 μ L), which was then diluted with D_2O (540 μ L). The solution was mixed via pipet and transferred to an NMR tube. Proton NMR was taken after 0 hours, 24 hours, 48 hours, and 72 hours. No appreciable change was observed in the spectra over this time period.

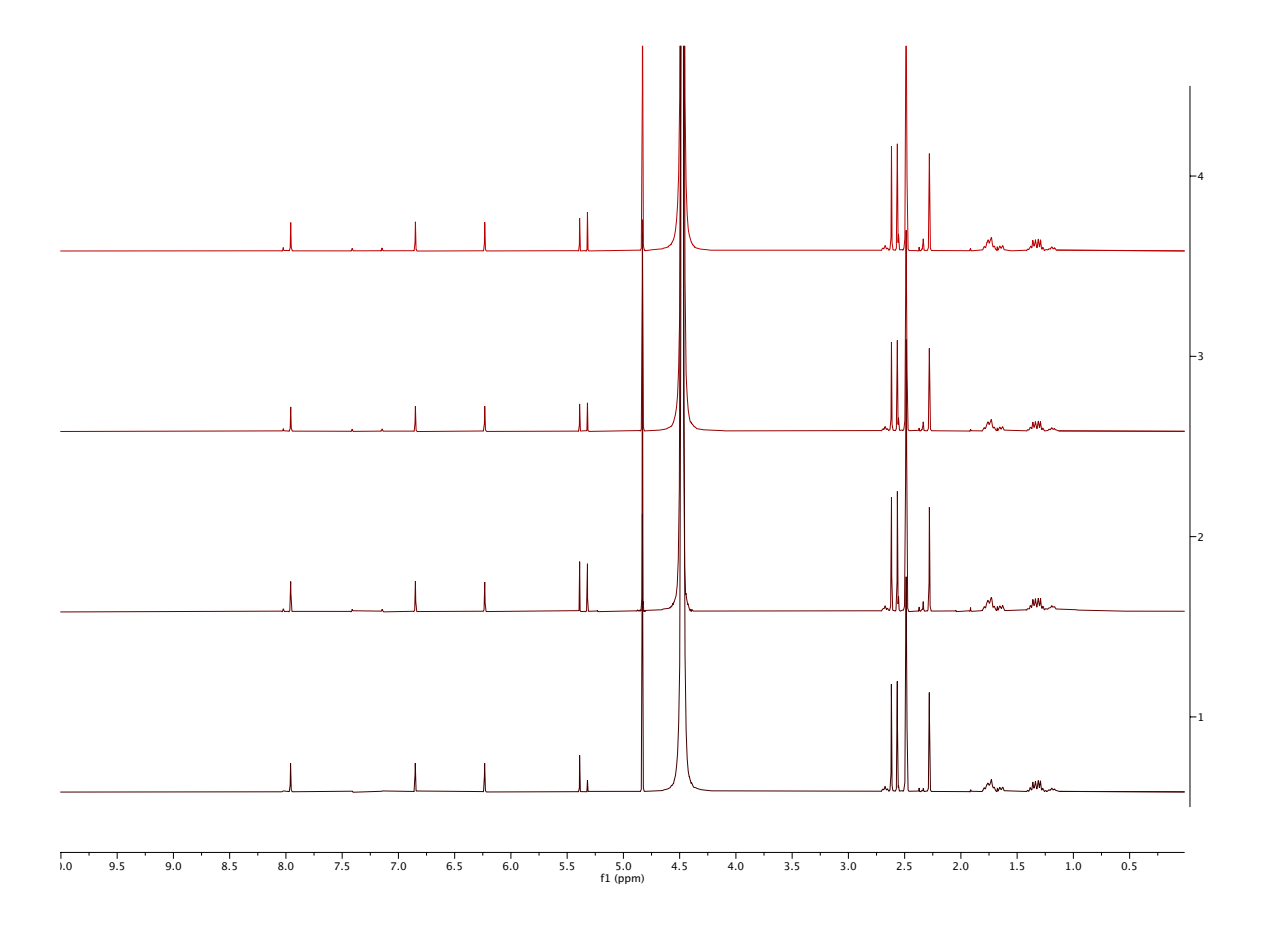


Figure 3.8. From bottom to top, ¹H NMR of **1** in 10% DMSO-d₆/D₂O after 0 hours, 24 hours, 48 hours, and 72 h.

Stability of 1 in DMSO-d₆

In a 20 mL glass vial, 1 (1.3 mg) was dissolved in DMSO-d₆ (600 μ L). The solution was mixed via pipet and transferred to an NMR tube. Proton NMR was taken d₆ after 0 hours, 48 hours, and 72 h.

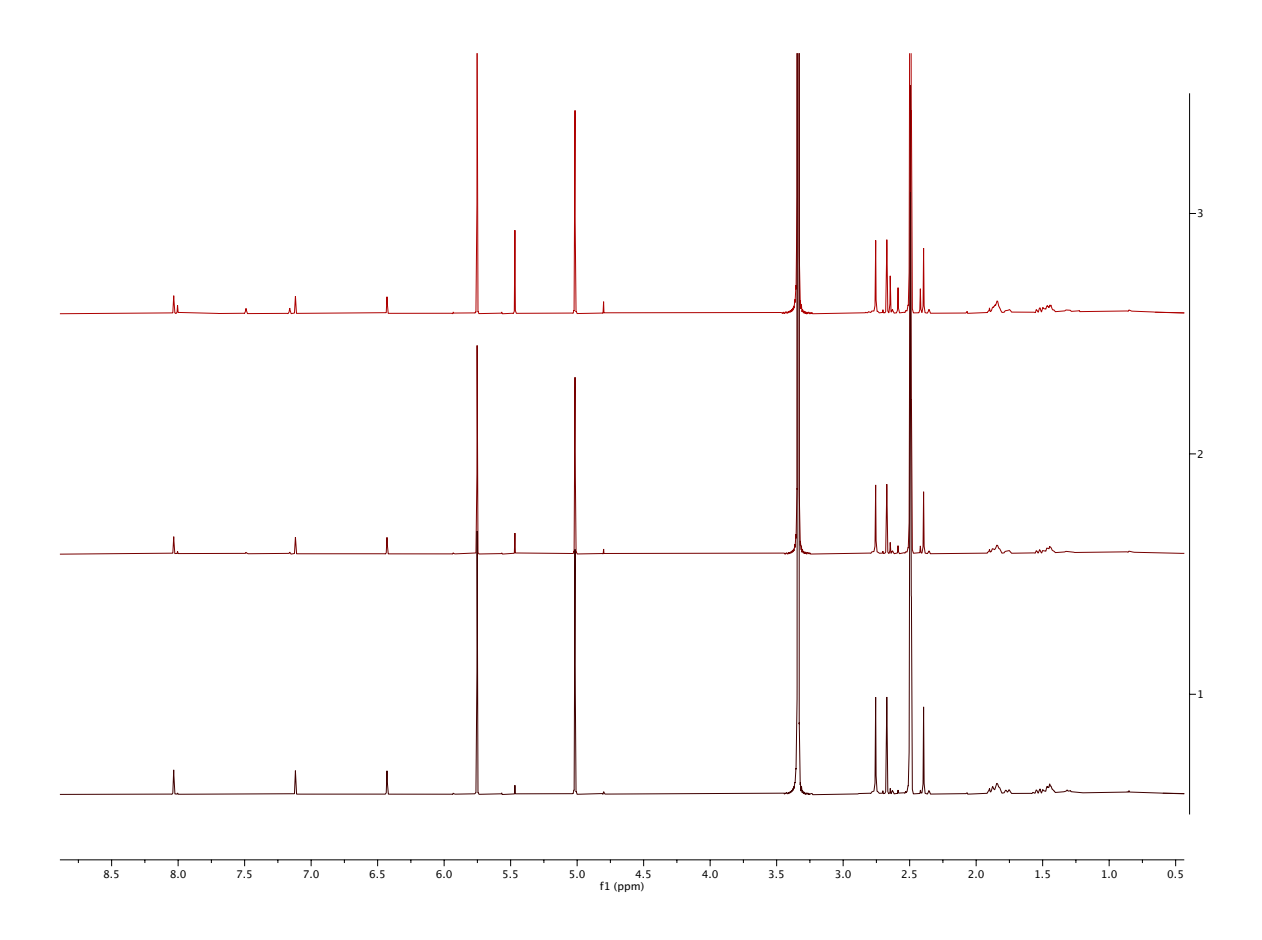


Figure 3.9. From bottom to top, ¹H NMR of 1 in DMSO-d₆ after 0 hours, 48 hours, and 72 h.

Stability of 2 in DMSO- d_6/D_2O

In a 20 mL glass vial, **2** (3.8 mg) was dissolved in DMSO-d₆ (60 μ L), which was then diluted with D₂O (540 μ L). The solution was mixed via pipet and transferred to an NMR tube. Proton NMR was taken after 0, 24, 48, and 72 hours. No appreciable change was observed in the spectra over this time period.

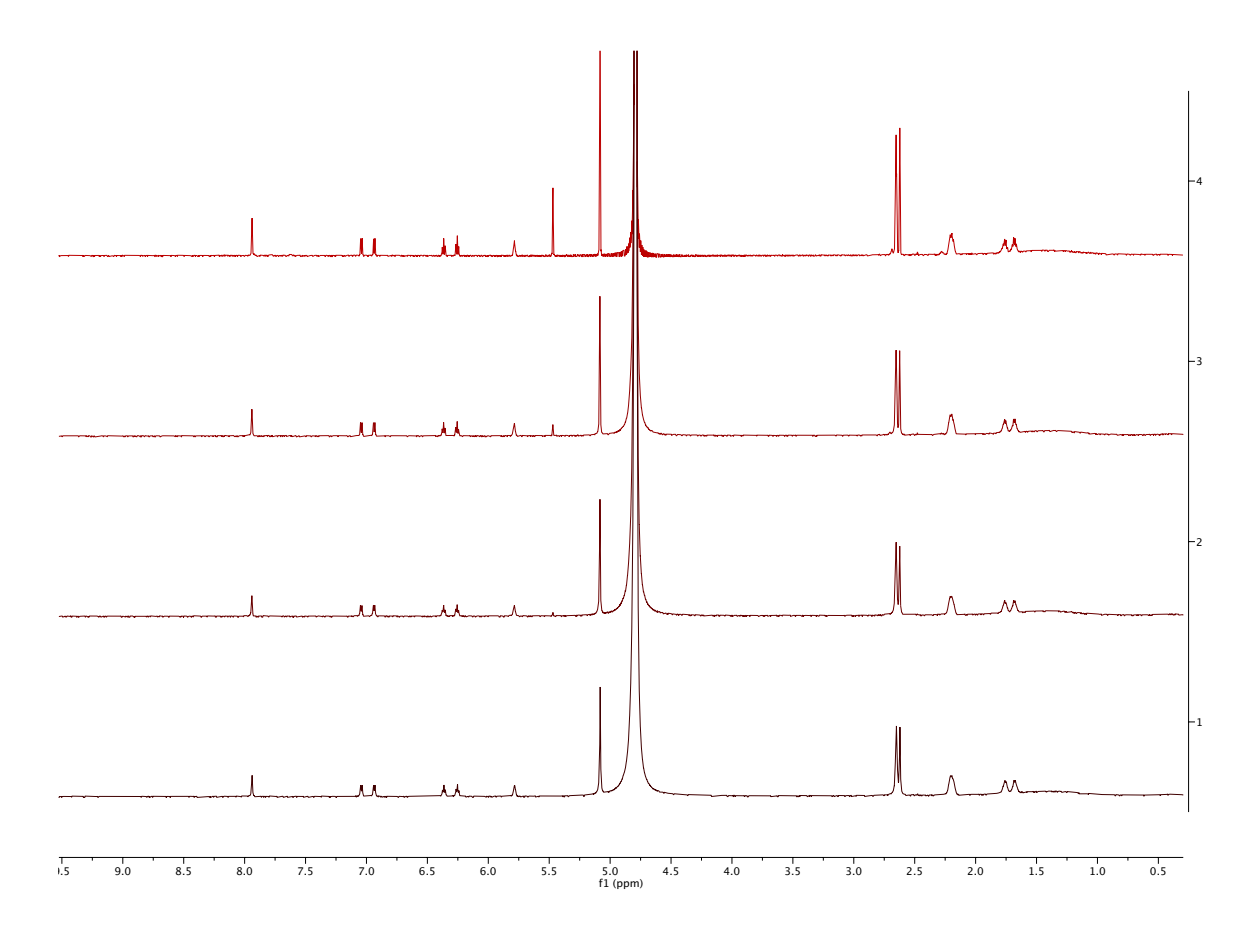


Figure 3.10. From bottom to top, ¹H NMR of **2** in 10% DMSO-d₆/D₂O after 0, 24, 48, and 72 hours.

Stability of 1 in DMSO- d_6/D_2O with reduced glutathione

In a 20 mL glass vial, **1** (2.0 mg) and reduced L-glutathione (1.1 mg for 1.0 equiv, 11.5 mg for 10 equiv) were dissolved in DMSO-d₆ (60 μ L), which was then diluted with D₂O (540 μ L). The solution was mixed via pipet and transferred to an NMR tube. Proton NMR was taken after 0 hours, 24 hours, 48 hours, and 72 hours.

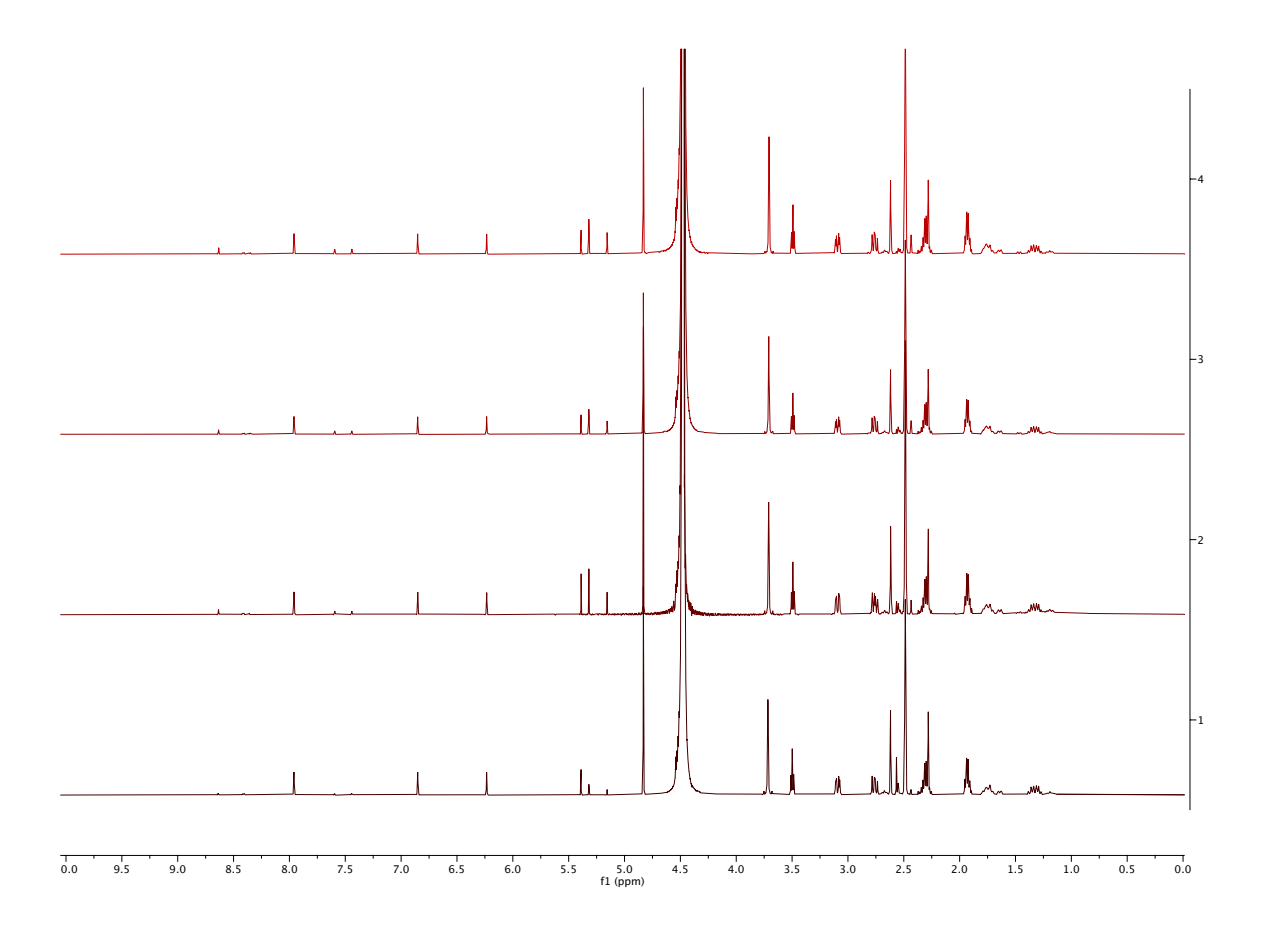


Figure 3.11. From bottom to top, ¹H NMR of **1** with 1.0 equiv reduced glutathione in 10% DMSO/D₂O after 0 hours, 24 hours, 48 hours, and 72 h.

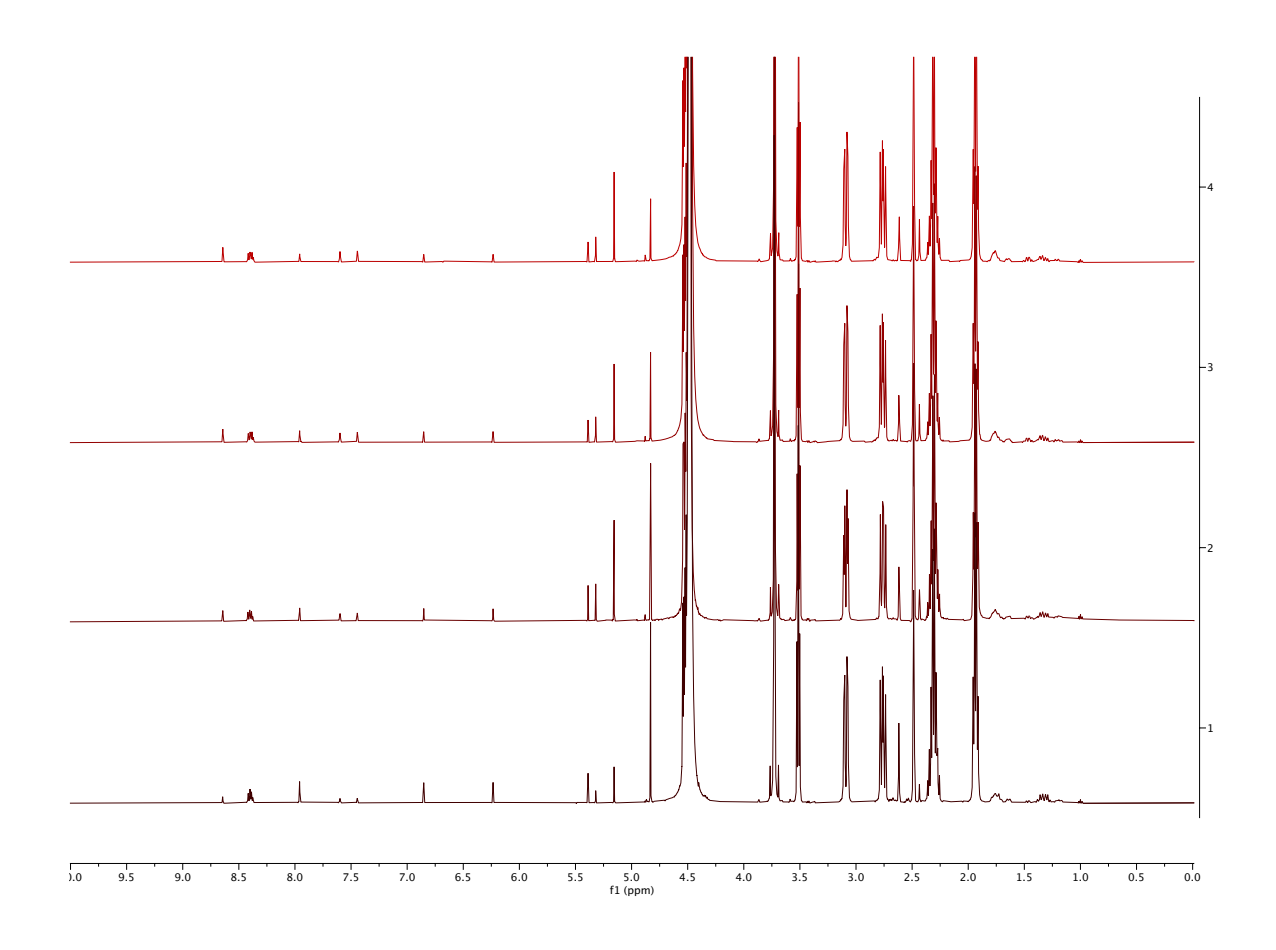
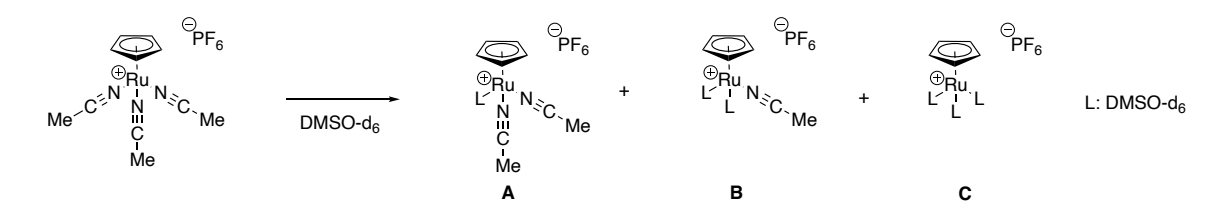


Figure 3.12 From bottom to top, ¹H NMR of **1** with 10.0 equiv reduced glutathione in 10% DMSO/D₂O after 0 hours, 24 hours, 48 hours, and 72 h.

Stability of $\{RuCp(NCMe)_3\}^+ PF_6^-$ in DMSO- d_6



In a 20 mL glass vial, {RuCp(NCMe)₃}⁺ PF₆⁻ (1.0 mg) was dissolved in DMSO-d₆ (600 μ L). The solution was mixed via pipet and transferred to an NMR tube. Proton NMR was taken periodically. According to NMR integration, chemical shifts of products were assigned as following: **A**: ¹H NMR (DMSO-d₆, 500 MHz, 25 °C): δ 4.76 (s, 5H), 2.54 (s, 6H). **B**: ¹H NMR (DMSO-d₆, 500 MHz, 25 °C): δ 5.13 (s, 5H), 2.58 (s, 3H). **C**: ¹H NMR (DMSO-d₆, 500 MHz, 25 °C): δ 5.47 (s, 5H).

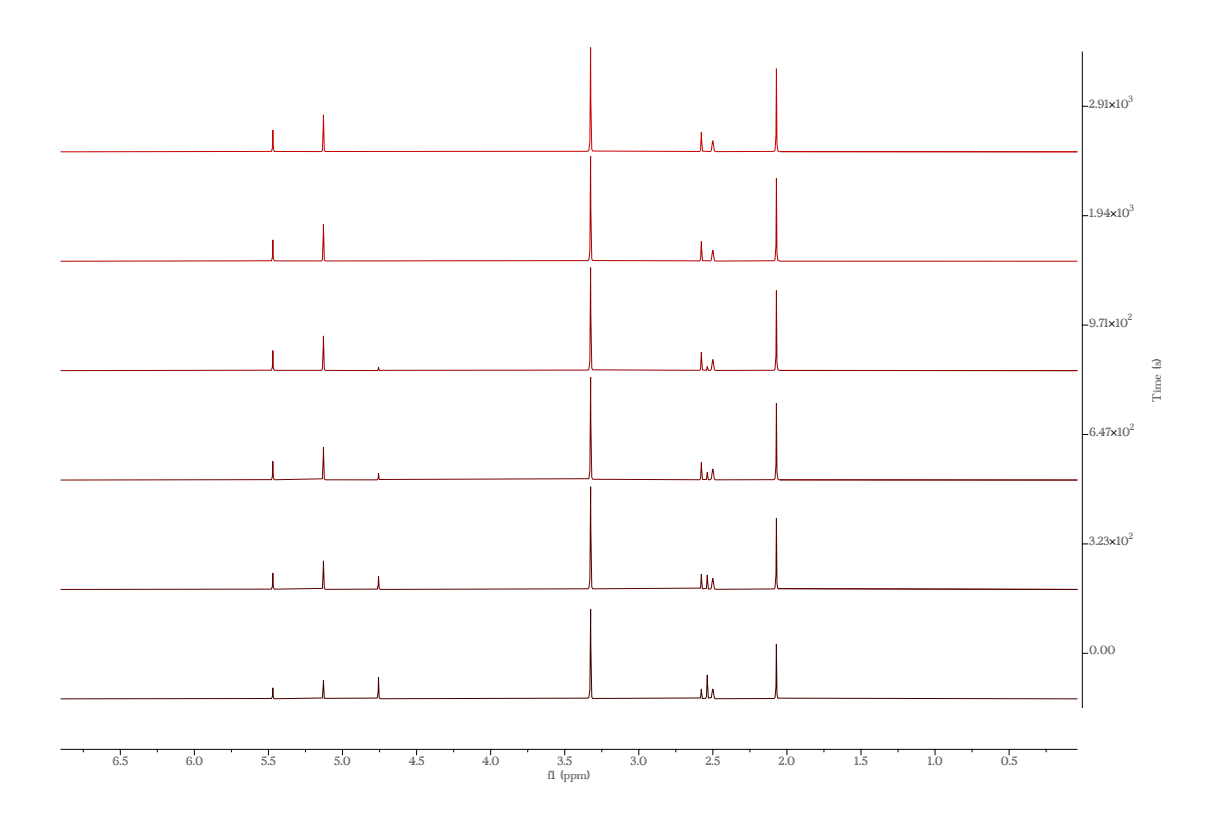


Figure 3.13. ¹H NMR {RuCp(NCMe)₃}⁺ PF₆⁻ after dissolved in DMSO-d₆ at different time (Y axis).

Stability of $\{RuCp(NCMe)_3\}^+ PF_6^-$ in DMSO-d₆/D₂O

In a 20 mL glass vial, $\{RuCp(NCMe)_3\}^+ PF_6^-$ (1.1 mg) was dissolved in pre-mixed 10% DMSO-d₆/D₂O (600 μ L). The solution was mixed via pipet and transferred to an NMR tube. A, B, and C were observed at 0 hours. B and C were observed at time 72 hours.

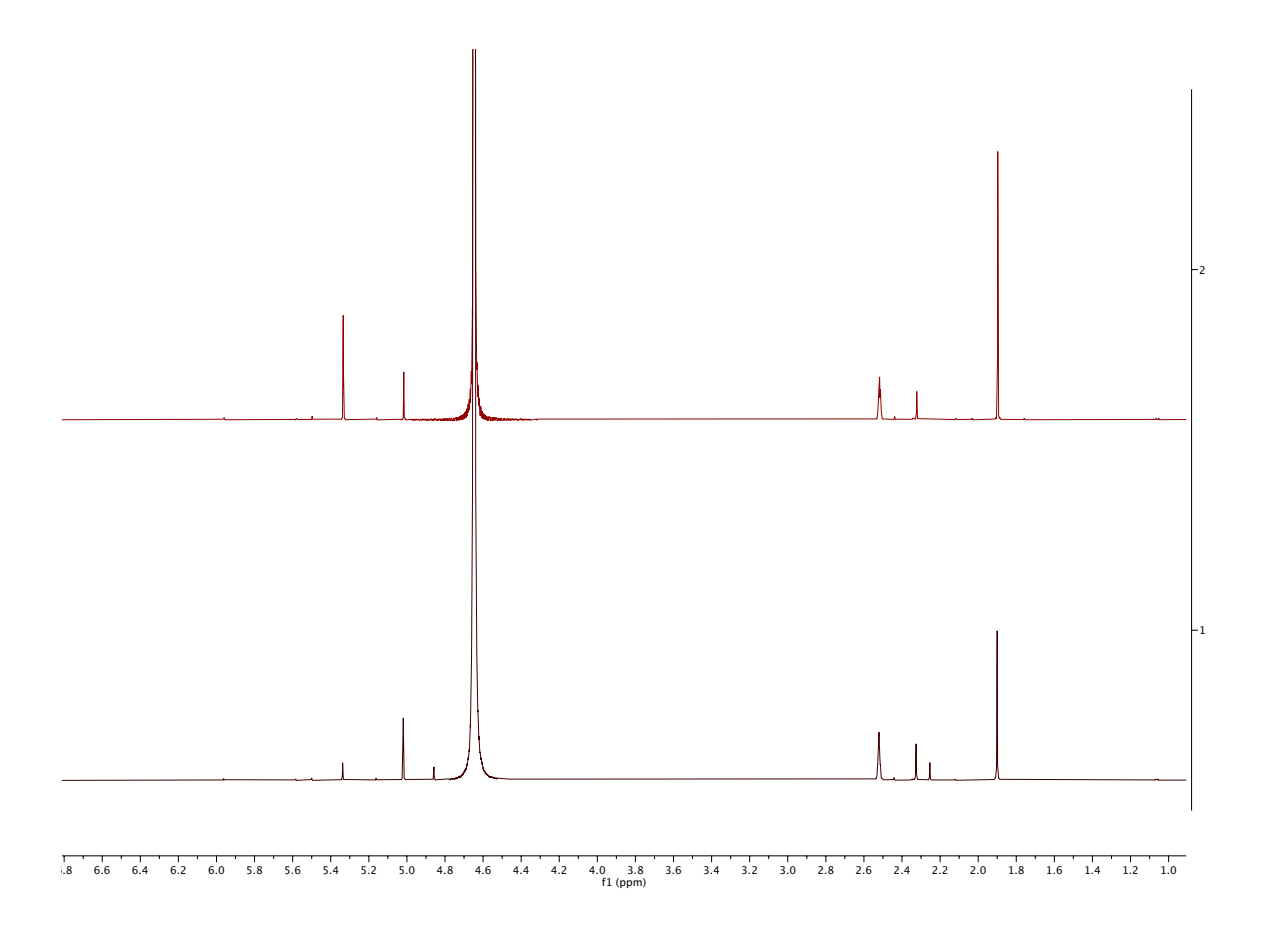


Figure 3.14. From bottom to top, ¹H NMR of {RuCp(NCMe)₃}⁺ PF₆⁻ in 10% DMSO-d₆/D₂O after 0 hours and 72 h.

REFERENCES

REFERENCES

- 1. Ghosh, S. Cisplatin: The first metal based anticancer drug. *Bioorganic Chemistry* **2019**, *88*, 102925.
- 2. Rosenberg, B.; Vancamp, L.; Krigas, T. Inhibition of cell division in escherichia coli by electrolysis products from a platinum electrode. *Nature* **1965**, *205* (4972), 698.
- 3. Rosenberg, B.; Vancamp, L.; Trosko, J. E.; Mansour, V. H. Platinum compounds a new class of potent antitumour agents. *Nature* **1969**, *222* (5191), 385.
- 4. Johnstone, T. C.; Suntharalingam, K.; Lippard, S. J. The Next Generation of Platinum Drugs: Targeted Pt(II) Agents, Nanoparticle Delivery, and Pt(IV) Prodrugs. *Chemical Reviews* **2016**, *116* (5), 3436-3486.
- 5. Kumar, P.; Mondal, I.; Kulshreshtha, R.; Patra, A. K. Development of novel ruthenium(II)-arene complexes displaying potent anticancer effects in glioblastoma cells. *Dalton Transactions* **2020**, *49* (38), 13294-13310. Wang, H. R.; Wei, J. H.; Jiang, H.; Zhang, Y.; Jiang, C. N.; Ma, X. L. Design, Synthesis and Pharmacological Evaluation of Three Novel Dehydroabietyl Piperazine Dithiocarbamate Ruthenium(II) Polypyridyl Complexes as Potential Antitumor Agents: DNA Damage, Cell Cycle Arrest and Apoptosis Induction. *Molecules* **2021**, *26* (5).
- 6. Zhang, D.; Hou, Z.; Aldrich, K. E.; Lockwood, L.; Odom, A. L.; Liby, K. T. A Novel Nrf2 Pathway Inhibitor Sensitizes Keap1-Mutant Lung Cancer Cells to Chemotherapy. *Molecular Cancer Therapeutics* **2021**, *20* (9), 1692-1701.
- 7. Golbaghi, G.; Castonguay, A. Rationally Designed Ruthenium Complexes for Breast Cancer Therapy. *Molecules* **2020**, *25*, 265.
- 8. Konac, E.; Varol, N.; Kiliccioglu, I.; Bilen, C. Y. Synergistic effects of cisplatin and proteasome inhibitor bortezomib on human bladder cancer cells. *Oncology Letters* **2015**, *10* (1), 560-564.
- 9. Ben-Nissan, G.; Sharon, M. Regulating the 20S Proteasome Ubiquitin-Independent Degradation Pathway. *Biomolecules* **2014**, *4* (3), 862-884.
- 10. Groll, M.; Heinemeyer, W.; Jäger, S.; Ullrich, T.; Bochtler, M.; Wolf, D. H.; Huber, R. The catalytic sites of 20S proteasomes and their role in subunit maturation: A mutational and crystallographic study. *Proceedings of the National Academy of Sciences* **1999**, *96* (20), 10976-10983.
- 11. Tanaka, K. The proteasome: Overview of structure and functions. *Proceedings of the Japan Academy Series B-Physical and Biological Sciences* **2009**, *85* (1), 12-36.

- 12. Sterz, J.; Metzler, I. v.; Hahne, J.-C.; Lamottke, B.; Rademacher, J.; Heider, U.; Terpos, E.; Sezer, O. The potential of proteasome inhibitors in cancer therapy. *Expert Opinion on Investigational Drugs* **2008**, *17* (6), 879-895.
- 13. Goldberg, A. L. Bortezomib's Scientific Origins and Its Tortuous Path to the Clinic. In *Bortezomib in the Treatment of Multiple Myeloma*, 2011; pp 1-27.
- 14. Harnessing Proteasome Dynamics and Allostery in Drug Design. *Antioxidants & Redox Signaling* **2014**, *21* (17), 2286-2301.
- 15. Majumder, S.; Gipson, K. R.; Odom, A. L. A Multicomponent Coupling Sequence for Direct Access to Substituted Quinolines. *Organic Letters* **2009**, *11* (20), 4720-4723.
- 16. McDaniel, T. J.; Lansdell, T. A.; Dissanayake, A. A.; Azevedo, L. M.; Claes, J.; Odom, A. L.; Tepe, J. J. Substituted quinolines as noncovalent proteasome inhibitors. *Biorg. Med. Chem.* **2016**, *24* (11), 2441-2450.
- 17. Jan, R.; Chaudhry, G. E. S. Understanding Apoptosis and Apoptotic Pathways Targeted Cancer Therapeutics. *Advanced Pharmaceutical Bulletin* **2019**, *9* (2), 205-218.
- 18. Zhu, G.; Tanski, J. M.; Churchill, D. G.; Janak, K. E.; Parkin, G. The Reactivity of Mo(PMe₃)₆ Towards Heterocyclic Nitrogen Compounds: Transformations Relevant to Hydrodenitrogenation. *Journal of the American Chemical Society* **2002**, *124* (46), 13658-13659.
- 19. Fish, R. H.; Fong, R. H.; Tran, A.; Baralt, E. Heteroaromatic nitrogen ligand studies with the (η^5 -pentamethylcyclopentadienyl)ruthenium cation η^1 -(N) and η^6 -(π) bonding modes and factors that influence a nitrogen to π -rearrangement. *Organometallics* **1991**, 10 (4), 1209-1212.
- 20. Gill, T. P.; Mann, K. R. Photochemical properties of the cyclopentadienyl(.eta.6-benzene)ruthenium(II) cation. The synthesis and reactions of a synthetically useful intermediate: the cyclopentadienyltris(acetonitrile)ruthenium(II) cation. *Organometallics* **1982**, *I* (3), 485-488.
- 21. Kündig, E. P.; Monnier, F. R. Efficient Synthesis of Tris(acetonitrile)-(η5-cyclopentadienyl)- ruthenium(II) Hexafluorophosphate via Ruthenocene. *Advanced Synthesis & Catalysis* **2004**, *346* (8), 901-904.
- 22. Fish, R. H.; Kim, H. S.; Fong, R. H. Bonding studies of nitrogen heterocyclic ligands to $(\eta^5$ -cyclopentadienyl)ruthenium cation a novel nitrogen to π -rearrangement. *Organometallics* **1989**, 8 (5), 1375-1377.
- 23. Nolan, S. P.; Martin, K. L.; Stevens, E. D.; Fagan, P. J. Enthalpies of Reaction of $Cp*Ru(CH_3CN)_3^+O_3SCF_3^-(Cp*=\eta^5-C_5Me_5)$ With Arenes—Solution Thermochemical Study Of Arene Binding To The $Cp*Ru^+$ Fragment. *Organometallics* **1992**, *11* (12), 3947-3953.
- 24. Estrela, J. M.; Ortega, A.; Obrador, E. Glutathione in Cancer Biology and Therapy. *Critical Reviews in Clinical Laboratory Sciences* **2006**, *43* (2), 143-181.

- 25. Busto, N.; Valladolid, J.; Aliende, C.; Jalon, F. A.; Manzano, B. R.; Rodriguez, A. M.; Gaspar, J. F.; Martins, C.; Biver, T.; Espino, G.; et al. Preparation of Organometallic Ruthenium-Arene-Diaminotriazine Complexes as Binding Agents to DNA. *Chemistry-an Asian Journal* **2012**, 7 (4), 788-801. Clavel, C. M.; Paunescu, E.; Nowak-Sliwinska, P.; Griffioen, A. W.; Scopelliti, R.; Dyson, P. J. Modulating the Anticancer Activity of Ruthenium(II)-Arene Complexes. *Journal of Medicinal Chemistry* **2015**, *58* (8), 3356-3365. Florindo, P. R.; Pereira, D. M.; Borralho, P. M.; Rodrigues, C. M. P.; Piedade, M. F. M.; Fernandes, A. C. Cyclopentadienyl-Ruthenium(II) and Iron(II) Organometallic Compounds with Carbohydrate Derivative Ligands as Good Colorectal Anticancer Agents. *Journal of Medicinal Chemistry* **2015**, *58* (10), 4339-4347.
- 26. Gokel, G. W.; Widera, R. P.; Weber, W. P. Phase-transfer hofmann carbylamine reaction *tert*-butyl isocyanide. *Organic Syntheses* **1976**, *55*, 96.
- 27. Shi, Y. H.; Hall, C.; Ciszewski, J. T.; Cao, C. S.; Odom, A. L. Titanium dipyrrolylmethane derivatives: rapid intermolecular alkyne hydroamination. *Chemical Communications* **2003**, (5), 586-587.
- 28. Gill, T. P.; Mann, K. R. Photochemical properties of the cyclopentadienyl(η^6 -benzene)ruthenium(II) cation the synthesis and reactions of a synthetically useful intermediate the cyclopentadienyltris(acetonitrile)ruthenium(II) cation. *Organometallics* **1982**, *I* (3), 485-488.
- 29. Fish, R. H.; Kim, H. S.; Fong, R. H. Bonding mode of nitrogen heterocyclic ligands to (η^5 -cyclopentadienyl)ruthenium cation and reactivity studies of the nitrogen and π -bonded complexes mechanistic aspects of a nitrogen to π rearrangement. *Organometallics* **1991**, *10* (3), 770-777.
- 30. Espenson, J. H. Chemical kinetics and reaction mechanisms; McGraw Hill, 2002.

CHAPTER 4 COMPUTATIONAL ESTIMATION OF LIGAND DONOR PARAMETERS

4.1 Introduction

Transition metal catalysis plays an incomparable role in modern chemical transformations. There are many approaches that are used to modify and optimize transition metal catalysts. One of the most important methods is to modify ligands and study the ligand effects on catalysis. Modifying the electronic and steric profiles of the ligands can contribute to an improvement in reaction yields, rates, selectivity, substrate scopes, and catalyst stability. However, understanding ligand effects in catalysts can be very difficult without quantification of ligand properties. Metrics for the electronic and steric properties can greatly help establish relationships between the measurable outcomes (yields, rates, selectivity) and ancillary ligand properties. Such models can guide the discovery, optimization, and design of new catalysts. Therefore, these tools are of great interest and the subject of active investigations by researchers.

4.1.1 Electronic parameterization for low oxidation state late transition metals

Palladium-based catalysts are heavily used in the drug discovery industry. A survey conducted on the frequency of different reaction types used in drug discovery found that the Suzuki-Miyaura coupling reaction was the second most frequently used reaction of all types of chemical transformations.¹ Phosphines are the most important ligands in late transition metal catalysis, especially for palladium catalysis, due to their special electronic donor and acceptor properties.² A parameterization tool of phosphine ligands was developed by Chadwick Tolman and coworkers in 1970s to measure the electronic donation from phosphine ligands to low valent late transition metals.³ The nickel complex LNi(CO)₃, with L being a variety of phosphine ligands, was used to measure the electronic donation of the phosphine ligand L by comparing the CO

stretching frequencies (Figure 4.1). The symmetric stretching (A₁) frequencies of the CO ligands in LNi(CO)₃ were to define Tolman's electronic parameter of ligand L.⁴ A more electron-donating phosphine ligand results in a higher electronic occupation in the antibonding orbital of CO ligands, giving a lower CO stretching frequency. The CO stretching frequencies of the nickel complexes with different phosphine ligands were measured by infrared spectroscopy and can now be compared directly with each other. In later work, tri-*tert*-butylphosphine, as the most electron donating ligand, was scaled to 0 cm⁻¹.³ This reporter can be used to measure many different phosphine ligands for late transition metal catalysis. Yet, ligands with high oxidation state early transition metals are not measurable or comparable in this system.

Figure 4.1. A nickel complex as an electronic reporter for ligand L.

4.1.2 Electronic parameterization for high oxidation state transition metals

Even though Tolman's electronic parameter successfully describes the ligand donation to late transition metal centers, ligands for high oxidation state early transition metals do not have such a measuring system. The differences in ligand-metal interactions lead to a very different group of ancillary ligands in high oxidation state metal catalysts. The ligands for high oxidization state metals cover a large set of structures, including amides (e.g., ethylene polymerization catalysts),⁵ nitrogen-containing heterocycles (e.g., titanium multicomponent coupling catalysts),⁶ alkoxides (e.g., olefin metathesis catalysts and Sharpless epoxidation catalysts),⁷ and more. Despite the fact that these ancillary ligands are used extensively in both industry and academia, ligand electronic parameterization tools for high oxidation state metals are very limited. Traditionally, pKa's or Hammett parameters are often used to quantify the electronic parameter of

organic ligands. However, such metrics do not represent accurate electronic interactions between high oxidation metals and ligands. For example, π -donation is not taken into account when comparing pKa values.

In 2012, the Odom group developed an experimental system to parameterize the electronic donation towards high oxidation state transition metal catalysts.⁸ A chromium(VI) complex NCr(NⁱPr₂)₂X, was designed for measuring the electronic donation from a mono-anionic ligand X to a high oxidation state metal center (Figure 4.2). The Ligand Donor Parameter, LDP, is a measurement system that could be considered as an analog to Tolman's electronic parameter. Instead of measuring the carbonyl stretching frequency as in the Tolman system, our LDP system uses the rotation barrier of a Cr-N bond in the chromium(VI) complex to represent the donor ability to high oxidation state transition metal centers.

Figure 4.2. A chromium complex as a LDP reporter for ligand X.

The LDP reporter, $NCr(N^iPr_2)_2X$, was designed based on the an electronic competition between the diisopropylamide ligands and a mono-anionic ligand X. Because the highly electronegative chromium center is accessible for σ and π donation, the electronic donation from different ligands changes the bond order of the Cr-N amide bond. For example, if the X ligand is a poor donor, this results in a higher electronic donation from amide nitrogen lone pairs, which increases the double bond character of the C-N bond and hinders rotation. The rotation barrier can be measured by 1H NMR spectroscopy. First, the rate of Cr-N bond rotation is measured by SST experiment. Second, the rate is converted to free energy using Eyring equation. Lastly, the enthalpy of the rotation is calculated using Gibbs equation with an assumption of constant entropy (ΔS^{\ddagger} = –

9 e.u.). The enthalpy is used as the LDP value in kcal/mol. Therefore, a poorly donating ligand results in a higher LDP value.

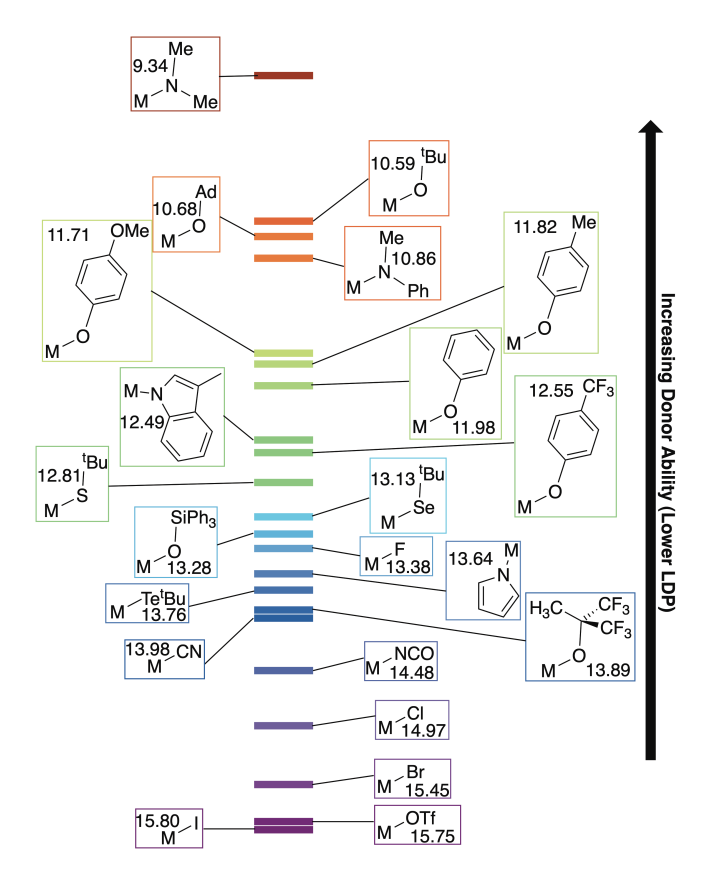


Figure 4.3. A sample of LDP values from commonly used ligands.⁹

A variety of mono-ionic ligands were measured for their LDP values, including phenoxides, alkoxides, amides, halides, and heterocycles (Figure 4.3). The experimental LDP values range from 9 to 16 kcal/mol. These LDP values have strong correlation with many different experimental data, including ¹³C NMR chemical shifts in a tungsten system, Hammett parameters for aryloxides, and reaction rate of a titanium-catalyzed hydroamination reaction. ^{8,10}

4.2 Computational probes of LDP values

In addition to the reliable LDP values, a computational method to access these values is desirable to predict LDP values of ligands whose chromium complexes have synthetic challenges. Furthermore, if the calculated LDP values could represent the experimental LDP values accurately, the costs, time, and hazards associated with the chromium complex syntheses could be avoided. The study on NCr(NiPr₂)₂X to compare the enthalpy differences between the ground state of and transition state for the amide bond rotation found that more than one local minimum were associated with the amide rotation. Herein, a series of different correlations between experimental LDP values and computational data were investigated. These correlations are expected as complementary tools to quickly estimate the LDP value for a given ligand without the need to synthesize the chromium complexes. The LDP values were able to be measured experimentally because the change of bonding between metal center and ligand X ultimately affects the bonding between metal center and the diisopropylamide ligands. This means the influence of ligand X can be measured by analyzing the bonding properties of the metal center. Therefore, a rapid computational method to study the properties of M-X bond, while the other ligands remain constant, would be useful for probing the relative impact of various X ligands. In this study, different bonding properties of metal ligand bonds under the influence of ligand X are investigated by computational studies.

4.2.1 Bond distance of Ti-F bonds in XTiF₃

Bond distance is often used as a measurement to represent electronic properties of ligands in transition metal catalysis. ¹¹ For this study, XTiF₃ was used as a computational reporter to analyze the correlation of the Ti–F bond distance and LDP values. Fluoride was used as the reporting ligand because it has σ and π donating properties and is readily calculated. The titanium

system provides a low steric interference allowing a high oxidation state metal environment accessible for σ and π donation. In addition, bond distance calculation does not require finding a transition state, greatly simplifying the calculations. As a result, the calculated Ti–F bond distance was compared with LDP of ligand X in XTiF₃. The Ti–F bond distance is reported as an average of the three Ti–F bonds after geometry optimizations.

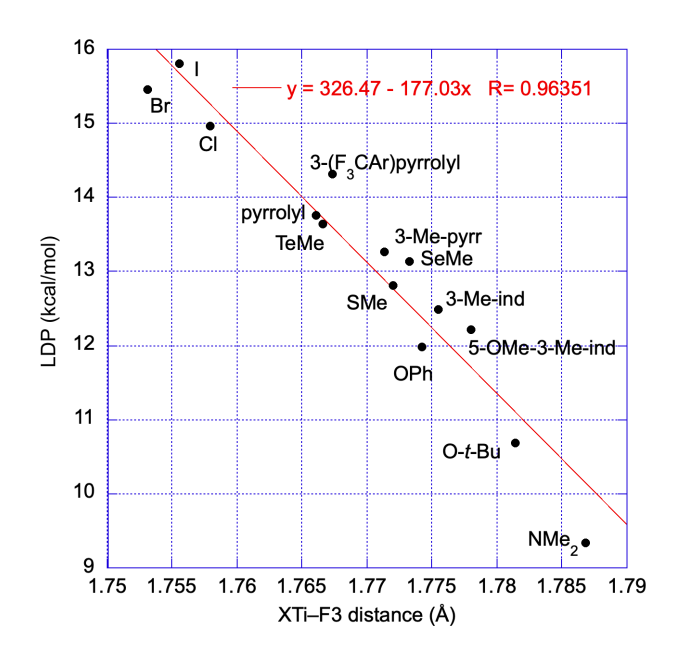


Figure 4.4. A plot of average Ti–F distance (Å) in XTiF₃ complexes versus LDP (kcal/mol).

A variety of commonly used ligands were studied in the bond distance calculations, including phenoxides, alkoxides, amides, halides, and nitrogen-containing heterocycles. The LDP values of the ligands range from 9 to 16 kcal/mol, and the calculated bond distances differ from 1.75 to 1.79 Å (Figure 4.4). There is a strong linear relationship (R=0.96) between the bond distance and LDP values. As expected, a more electron-donating ligand results a longer Ti–F bond. A general formula can be used to calculate LDP values simply by computing the Ti–F bond distance with the desired ligand X. Other than the Ti–F bond distance in XTiF₃ system, the Ti=N bond distance in MeNTiX₂ was also investigated and showed similar correlation: a more donating ligand results in a longer Ti=N bond (see supporting information Figure 4.8). The distances range

from 1.64 to 1.68 Å, but a weaker linear correlation compared to what was found in the XTiF₂ system.

4.2.2 Covalent bond order (CBO) index

Covalent bond order (CBO) index is a useful tool for understanding the bonding interaction between ligands and metal centers. In 2011, Occhipinti and Jensen used a comparative density functional theory (DFT) study to analyze the nature of the metal-carbene bond in Grubbs olefin metathesis catalysts. 12 A series of bonding analyses, including the CBO index, was used to classify the Grubbs catalysts as "electrophilic covalent", a different category than the traditional Fisher- or Schrock-type metal carbene complexes. The CBO index uses natural bond orbital (NBO) analysis to quantify the covalent character in metal-ligand bonds. 13 The calculation of CBO index uses the number of electrons in each of the natural bonding ($n_{\text{occ},i}$) and antibonding ($n_{\text{occ},j}$) orbitals and the amount of metal character in each of these orbitals ($f_{\text{M,i}}$ and $f_{\text{M,j}}^*$), where i is the overall bonding and j is overall antibonding orbitals between the metal and ligand (Eq. 1).

$$CBO = \sum_{i} n_{occ,i} \left(\frac{1}{2} - \left| f_{M,i} - \frac{1}{2} \right| \right) - \sum_{i} n_{occ,j}^* \left(\frac{1}{2} - \left| f_{M,j}^* - \frac{1}{2} \right| \right)$$
 (1)

Titanium imido complexes are considered as important active catalysts for hydroamination and iminoaminiation reactions. The ligand effects of these titanium catalysts are of great interest to guide future catalyst design. A correlation between the LDP value of ancillary ligands for titanium hydroamination catalysts and the rate of catalysis was established by our group recently. The titanium imido complexes used for this study are MeNTiX2, where X is a mono-anionic ligand of interest. These complexes were used to analyze the CBO index of Ti=N bond. The structures of the MeNTiX2 complexes were optimized at first with NBO analysis, then the CBO index of each ligand was calculated by using Eq. 1. Different combinations of functionals and basis sets were explored for geometry optimization with a series of mono-anionic ligands. It was found that the

CBO index values are not overly sensitive to changes in different functional and basis set. A comparison of CBO values from different functional and basis set combinations can be found in Table 4.1.

Table 4.1. Calculated CBO index with different functionals and basis sets.

| | | B3W91 | | M06 | WB97XD |
|------------------|----------------|---------|-------|-------|--------|
| X | LDP (kcal/mol) | Def2SVP | SDD | SDD | SDD |
| I | 15.8 | 1.547 | 1.500 | 1.485 | 1.495 |
| Br | 15.45 | 1.533 | 1.522 | 1.505 | 1.513 |
| C1 | 14.97 | 1.512 | 1.525 | 1.516 | 1.334 |
| pyr | 13.64 | 1.487 | 1.406 | 1.446 | 1.397 |
| F | 13.38 | 1.377 | 1.380 | 1.443 | 1.384 |
| OMe | 10.59 | 1.321 | 1.341 | 1.305 | 1.288 |
| NMe ₂ | 9.34 | 1.292 | 1.288 | 1.302 | 1.387 |

The CBO index of commonly used ligands for titanium catalysis, including amides, phenoxides, pyrrolides, and halides, was calculated by using B3PW91 with def2-SVP basis set. The CBO index was reported as a function of LDP. The LDP values of these ligands differ from 9 to 16 kcal/mol, affording a difference in CBO index from 1.25 to 1.55 (Figure 4.5). The correlation shows a strong linear relationship (R = 0.98) between CBO index and LDP. As expected, more electron-donating ligands result in a less covalent Ti=N bond. A general formula can be used to estimate LDP values simply by calculating the Ti=N CBO index for desired ligand X.

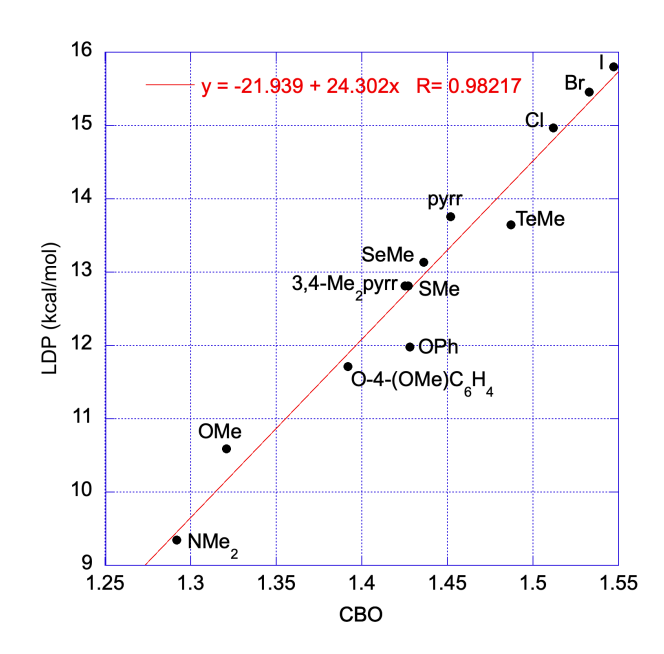


Figure 4.5. Plot of the Covalent Bond Order (CBO) calculated using Eq 1 from the electron density found using B3PW91 with def2-SVP and NBO7 versus the Ligand Donor Parameter (LDP).

Other than the CBO index, the covalent and ionic character of the Ti=N bond was analyzed by natural resonance theory (NRT) and compared with CBO index (Table 4.2). The CBO index agree well with covalent bond order from NRT analysis. The correlation between LDP and covalent bond order from NRT analysis gives a slightly weaker linear relationship (R = 0.88). Therefore, bond order from NRT seems to be less accurate than CBO index.

Table 4.2. Comparison of CBO with NRT covalent character using B3PW91 and SDD.

| X | LDP | CBO index | CBO(NRT) | Ionic BO(NRT) | BO (NRT) |
|------|-------|-----------|----------|------------------|----------|
| I | 15.8 | 1.500 | 1.342 | 1.090 | 2.433 |
| Br | 15.45 | 1.522 | 1.369 | 1.086 | 2.455 |
| Cl | 14.97 | 1.525 | 1.373 | 1.096 | 2.469 |
| Pyr | 13.64 | 1.406 | 1.345 | 1.318 | 2.663 |
| F | 13.38 | 1.380 | 1.234 | 1.195 | 2.428 |
| OMe | 10.59 | 1.341 | 1.164 | 1.282 | 2.446 |
| NMe2 | 9.34 | 1.288 | 1.133 | 1.278 | 2.411 |

4.2.3 Proton affinity (PA)

Proton affinity (PA) is also an important computational descriptor that is used to guide the discovery, optimization, and design of catalysts.¹⁵ Despite the correlations of Ti–F bond distance and Ti=N CBO index with LDP being fairly strong, the range of these values from different ligand X is quite small. Therefore, proton affinity of the nitrogen on MeN=TiX₂ on nitrogen was investigated as a function of LDP and was expected to have a larger difference. PA is calculated as the difference between the energy of the neutral titanium complex, MeN=TiX₂, and protonated singlet complex, Me(H)N=TiX₂⁺. The proton affinity of MeN=TiX₂ range from -240 to -190 kcal/mol. A linear correlation (R = 0.97) was found between proton affinity on nitrogen and LDP (Figure 4.6). Due to the difficulty of structure optimization of the protonated species, some ligands were not accessible for such a calculation. Lizbeth Lockwood, Di Zhang2, Christopher J.

Occhiuto2, Linqing Mo1, Kelly Aldrich1‡, Hayden Stoub3, Kathleen A. Gallo3, Karen T. Liby2*, and Aaron L. Odom1

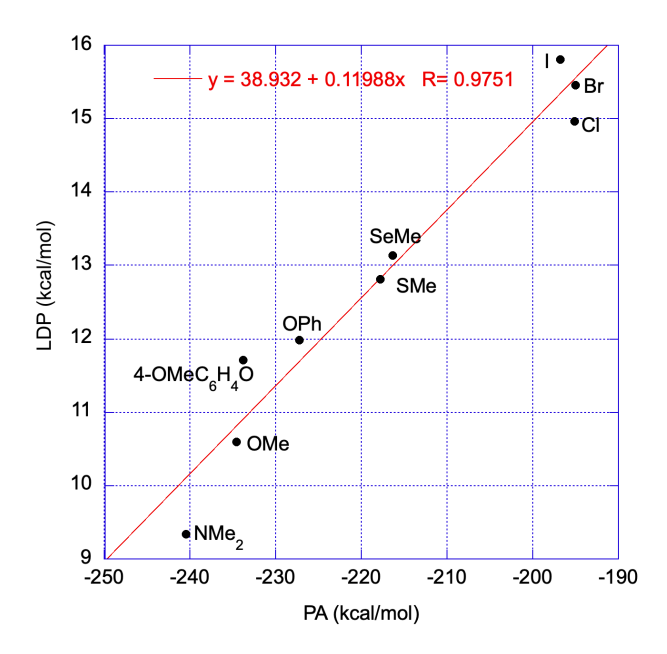


Figure 4.6. LDP (kcal/mol) versus proton affinity (PA, kcal/mol) for MeNTiX2 calculated using B3PW91 with def2-SVP.

Unlike of CBO index for MeNTiX₂, the correlation of PA versus LDP was impacted by the choice of functional and basis set. Lower R values for the fits were obtained when def2TZVPP/B3PW91 and def2TZVPP/M06L were employed (see supporting information). Overall, using calculated PA values to estimate LDP gives moderate accuracy. In fact, PA was found to correlate well with the eigenvalues of the σ lone pair orbitals in carbenes.¹⁶ The poor correlation between PA and LDP may be due PA's higher dependance on the σ bonding with a proton. In contrast, the LDP values take both σ and π bonding into account.

4.2.4 Bond dissociation energy (BDE)

Bond dissociation energy (BDE) provides the most quantitative description of the bond. While BDEs of light main group elements are generally well-known and readily calculated by

modern computational chemistry, bonds involving the transition metals remain extremely challenging through computation in some cases.¹⁷ This is partly due to the simultaneous importance of electron correlation, spin-orbit interaction, and other effects. These are coupled with a large numbers of low-lying states that are accessible in systems with an open d subshell.¹⁷ Regardless of the challenges, Occhipinti and Jensen were able to analyze the singlet-triplet gaps of metal fragments and ligand fragments to compare Grubbs catalysts with traditional Fisher- or Schrock-type metal carbene complexes using DFT calculations.¹² We decided to explore if the BDEs of N=Ti bonds in HN=TiX₂ correlate with experimental LDP values. The BDEs were calculated by summing the excited state energies of the optimized geometries for the NH fragment and the TiX₂ fragments, then subtracting the energies of the optimized molecules from the sum of the fragments. The NH fragment and the TiX₂ fragments can both be singlets to give a singlet BDE or both triplets to give a triplet BDE. In many cases with a different ligand X, the singlet BDEs are higher in energy than the triplet BDEs. Therefore, the triplet BDEs were used to investigate the correlation with LDP values.

The optimization of the metal fragment's triplet state was faced with a few problems. The low coordinate metal center, TiX_2 , gains additional interaction from hydrogen in some cases (e.g. agostic interactions). This results in a deviation from the desired coordination geometries of metal fragment, which limited the ligand selection. Optimized geometries that cannot truly represent the interaction between the metal and ligands are omitted for correlation. Many of the potential energy calculations for open-shell metal fragments require long calculation times due to multiple local minima geometries. Starting a DFT calculation from a density matrix provided by Hartree-Fock optimization with def2-TZVP was found to be helpful for solving the problems of getting self-consistent field (SCF) errors.

Despite the challenges, a few BDEs were calculated and plotted as a function of LDP values. The correlation of LDP and BDEs is fairly weak. However, strong correlations were found within the elements in the same group. Linear correlations were found for halogens and chalcogens (Figure 4.7). This is similar to the trend observed in the previous study with BDEs of Cr-X bonds in NCr(NiPr2)2X using DFT calculation. The different correlation lines could be due to a more important role of metal-ligand orbital overlap in BDE calculations. As the elements go down the column, the decrease in overlap causes lower BDE values.

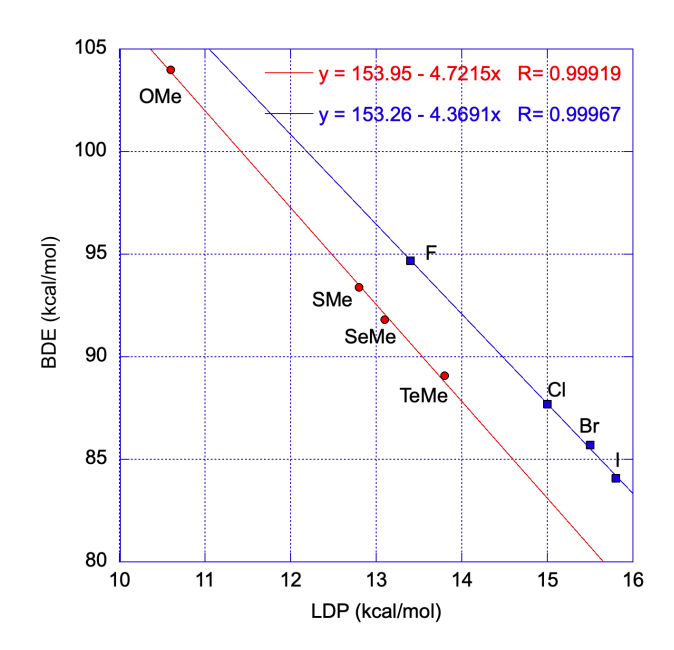


Figure 4.7. Plot of LDP (kcal/mol) versus BDE (kcal/mol) for imide bond cleavage in HN=TiX₂. The BDEs shown were calculated using def2-TZVP/M06-2X.

Three different functionals (B3PW91, M06-2X, and M06L) were tested with def2-TZVP basis set. All three functionals gave reasonable correlations with reasonable R^2 -values (> 0.99) when X = a halide; meanwhile only M06-2X gave a good correlation for the chalcogenides. As a consequence of the halides and chalcogenides reside on different lines with different slopes, the prediction of LDP from plotting ligand X into resulted formula is limited.

All BDE calculations were contributed by Sean Walsh.

4.3 Conclusions

Our lab created an experimental descriptor that uses the complex NCr(NiPr2)2X to report the ligand donor ability of mono-anionic ligand X in high oxidation state metal catalysis. A reliable computational method to estimate LDP values could bypass the challenges in chromium complex syntheses and reduce the costs and hazards associated with the syntheses. In this study, a computational study to estimate LDP values was explored by establishing correlations of calculated metal-ligand bonding properties with LDP. Calculating the Ti–F bond distance of the XTiF3 system was found as an easy method for the estimation of LDP with a linear correlation (R = 0.96). CBO index calculation can also be used to estimate LDP values (Eq. 1). The CBO index calculation was also found insensitive to functional and basis set change. Proton affinity calculation gave a moderate correlation with experimental LDP values and seems sensitive to different functionals and basis sets. In addition, BDE calculations can be challenging due to the additional interactions of metal fragments and SCF errors; they also gave two separate correlation lines for halogens and chalcogens. The BDEs of metal-ligand bonds could also be affected by metal-ligand overlap.

Overall, this study provided several easy, complementary methods to access LDP values of ligands for high oxidation state metals using computational studies. Different bonding properties in different systems were investigated. We hope the reported results will contribute to the parameterization tool database to guide future catalyst design. Future work is in progress to explore other computational methods for estimating donor ability of neutral ligands to high oxidation metals.¹⁸

4.4 Computational Details

All calculations were done at the High-Performance Computing Center (HPCC) and was supported in part through computational resources and services provided by the Institute for Cyber-Enable Research (ICER) at Michigan State University. Molecular optimizations, electron densities, and thermochemistry were calculated using the Gaussian16-B01 software package. Natural bond orbital (NBO) and natural resonance theory (NRT) calculations were conducted using NBO7.

For the XTiF₃ molecules, the structure optimizations were done using M06L with the TZVP basis set for atoms smaller than Kr and with def2-qzvp for atoms larger than Kr using the Gaussian16 software package.

For the MeNTiX₂ molecules in LDP correlation, the structure optimizations were done using B3PW91 with def2-SVP basis set for all atoms. The CBO index was calculated using Eq. 1. The number of electron and the amount of metal character in natural bonding and antibonding orbitals are derived from NBO analysis. For cases when the N=Ti bond was not found as a triple bond, a CHOOSE commend was used to freeze the triple bond geometry.

For the MeNTiX₂ and Me(H)NTiX₂⁺, the structure optimizations and frequency calculations were done using B3PW91 with def2-SVP basis set for atoms. The electronic energies with thermal free energy correction were used to calculate the proton affinity energy of each compound. Proton affinity was reported as the subtraction of the energy of MeNTiX₂⁺ from the energy of Me(H)NTiX₂⁺. Proton affinity calculations with both B3PW91 with def2-TZVPP and M06L with def2-TZVPP were conducted the same way.

For the $HNTiX_2$ in BDE calculations, the geometry optimizations were performed by using M06-2X and def2svp. The energy calculations of triplet metal or NH fragments used the frozen

geometries from optimized structure of $HNTiX_2$. The triplet BDEs were calculated by summing the energies of the NH fragment and the TiX_2 fragments, then subtracting the energies of the optimized molecules from the sum of the fragments.

Correlation of LDP and Bond length in MeNTiX2 complexes

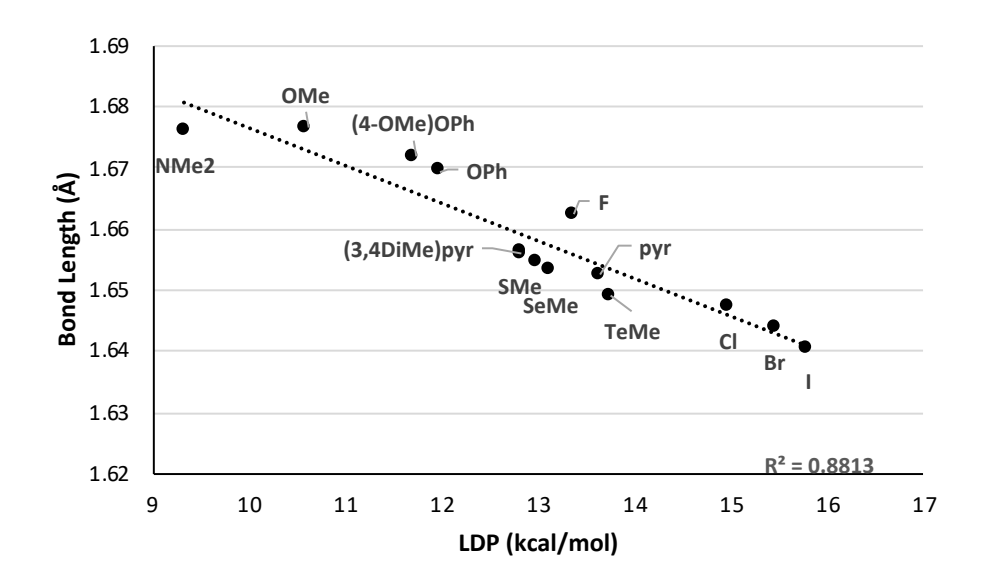


Figure 4.8. Correlation of LDP and bond length of Ti=N in MeNTiX2 using B3PW91 with def2-SVP.

Additional correlation of LDP and proton affinity of MeNTiX2 complexes

B3PW91 with def2-TZVPP

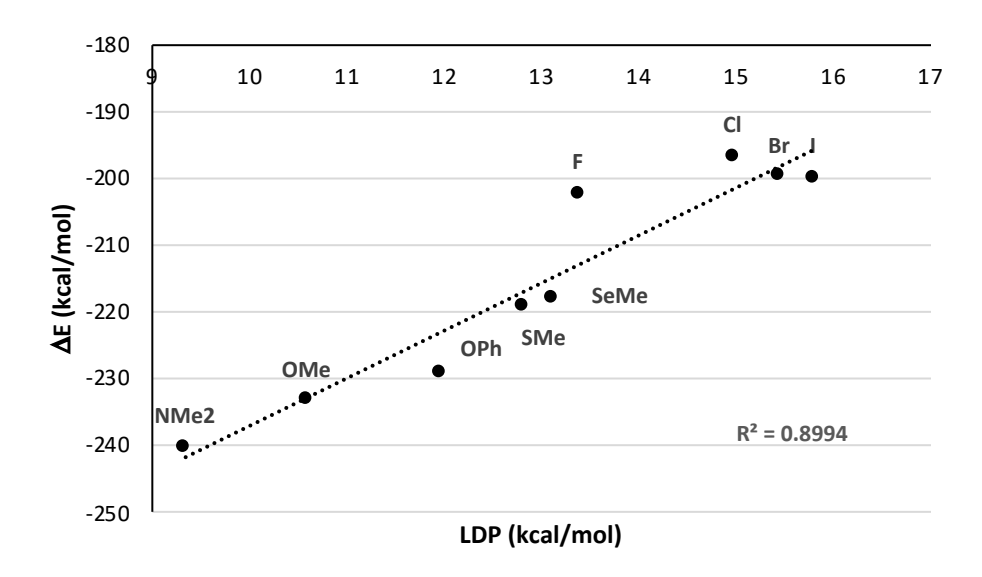


Figure 4.9. Correlation of LDP and proton affinity of MeNTiX2 using B3PW91 with def2-TZVPP.

M06L with def2-TZVPP

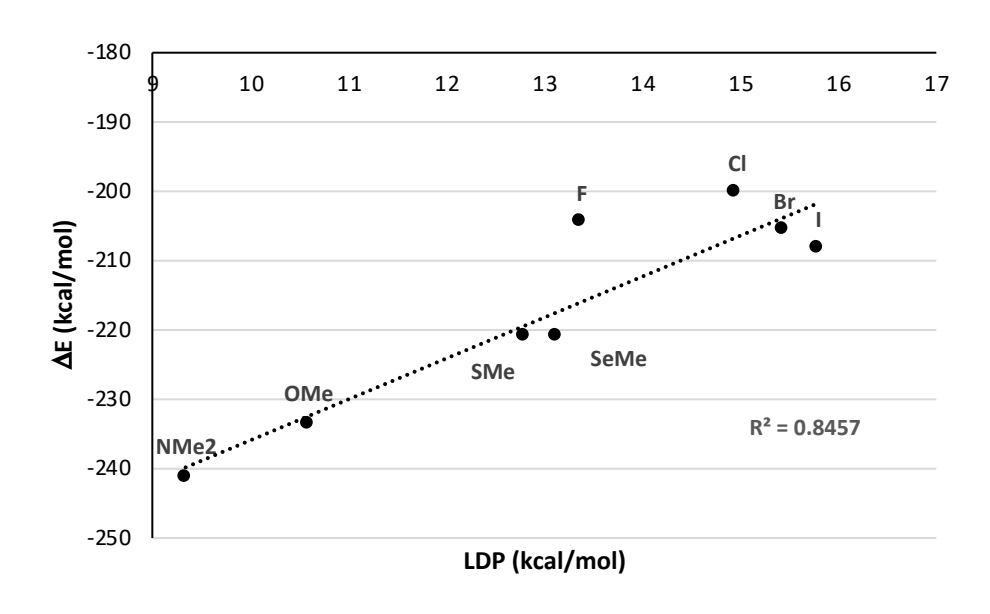


Figure 4.10. Correlation of LDP and proton affinity of MeNTiX2 using M06L with def2-TZVPP.

Example Input Files

Bond length of Ti=N in MeNTiX2

Complex MeNTiBr2

%chk=NTiBr2_def_PW91.chk

opt freq b3pw91 pop=(nbo6,savenbos) geom=connectivity def2svp

Title Card Required

0 1

| Ti | 0.00004000 | 0.26316400 | 0.15334500 |
|----|-------------|-------------|-------------|
| N | -0.00083000 | 1.90359800 | 0.04553800 |
| C | -0.00236200 | 3.31618200 | -0.10226200 |
| Н | 0.02884400 | 3.80840900 | 0.88610000 |
| Н | 0.87774900 | 3.65835800 | -0.67489400 |
| Н | -0.91324300 | 3.66279900 | -0.62162500 |
| Br | -2.17450300 | -0.71696500 | -0.03811200 |
| Br | 2.17523900 | -0.71564700 | -0.03812800 |

1 2 1.0 7 1.0 8 1.0

2 3 1.0

3 4 1.0 5 1.0 6 1.0

4

5

6

7

8

CBO index

Complex MeNTi(OMe)2

%chk=NTiOMe2_def_PW91.chk

opt=(calcall,tight) freq b3pw91 pop=(nbo6,savenbos) geom=connectivity def2svp

Title Card Required

| 0 1 | | | |
|-----|-------------|-------------|-------------|
| Ti | -0.00119400 | -0.15802400 | -0.29963900 |
| N | 0.00794200 | 1.50541500 | -0.08916800 |
| C | 0.01373200 | 2.89948600 | 0.17644100 |
| Н | 0.79644700 | 3.42977200 | -0.40065200 |
| Н | -0.95374000 | 3.38130900 | -0.06615300 |
| Н | 0.21530300 | 3.10652800 | 1.24519100 |
| O | 1.57537700 | -1.01637600 | -0.04073500 |
| O | -1.58565800 | -1.00161700 | -0.04149900 |
| C | 2.91757800 | -1.01860100 | 0.30204800 |
| Н | 3.52344300 | -1.51001200 | -0.48283600 |
| Н | 3.31528100 | 0.00455400 | 0.44285700 |
| Н | 3.08715500 | -1.57911200 | 1.24075400 |

C -2.92731600 -1.00105000 0.30309400

H -3.53574200 -1.48738000 -0.48296400

Н -3.09738800 -1.56476300 1.23978300

Н -3.32181000 0.02266200 0.44861700

1 2 1.0 7 1.0 8 1.0

2 3 1.0

3 4 1.0 5 1.0 6 1.0

4

5

6

7 9 1.0

8 13 1.0

9 10 1.0 11 1.0 12 1.0

10

11

12

13 14 1.0 15 1.0 16 1.0

14

15

16

Proton affinity

Complex MeNTi(NMe2)2

%chk=NTiNMe2_def_PW91.chk

opt=(calcall,tight) freq b3pw91 pop=(nbo6,savenbos) geom=connectivity def2svp

Title Card Required

| 0 1 | | | |
|-----|-------------|-------------|-------------|
| Ti | 0.00000000 | 0.12664300 | -0.29089800 |
| N | 0.00000000 | 1.79444500 | -0.12357000 |
| C | 0.00000100 | 3.19860600 | 0.07834400 |
| Н | 0.00000100 | 3.74942000 | -0.88302100 |
| Н | -0.89043000 | 3.54483300 | 0.64018400 |
| Н | 0.89043100 | 3.54483300 | 0.64018400 |
| N | 1.75117500 | -0.63222900 | 0.01086900 |
| N | -1.75117500 | -0.63222800 | 0.01086900 |
| C | -1.97004100 | -2.05868300 | 0.02396600 |
| Н | -2.33438200 | -2.42416900 | 1.00702200 |
| Н | -2.72182100 | -2.37600800 | -0.72936400 |
| Н | -1.04314500 | -2.61586600 | -0.19847100 |
| C | -2.96309600 | 0.09986000 | 0.29547800 |
| Н | -3.38401700 | -0.16486800 | 1.28825600 |
| Н | -2.76965900 | 1.18126100 | 0.28758200 |

| Н | -3.75973200 | -0.11079600 | -0.44910900 |
|---|-------------|-------------|-------------|
| C | 1.97004000 | -2.05868400 | 0.02396700 |
| Н | 2.72182000 | -2.37601000 | -0.72936300 |
| Н | 2.33438100 | -2.42417000 | 1.00702300 |
| Н | 1.04314400 | -2.61586600 | -0.19846900 |
| C | 2.96309600 | 0.09985900 | 0.29547800 |
| Н | 3.38401600 | -0.16486800 | 1.28825600 |
| Н | 3.75973200 | -0.11079700 | -0.44910900 |
| Н | 2.76965800 | 1.18126000 | 0.28758100 |

1 2 1.0 7 1.0 8 1.0

2 3 1.0

3 4 1.0 5 1.0 6 1.0

4

5

6

7 17 1.0 21 1.0

8 9 1.0 13 1.0

9 10 1.0 11 1.0 12 1.0

10

11

12

13 14 1.0 15 1.0 16 1.0

```
14
15
16
17 18 1.0 19 1.0 20 1.0
18
19
20
21 22 1.0 23 1.0 24 1.0
22
23
24
Complex Me(H)NTi(NMe2)2+
%chk=HNTiNMe2.chk
# opt=(calcall,tight) freq b3pw91 pop=(nbo6,savenbos) geom=connectivitydef2svp
```

Title Card Required

| 1 1 | | | |
|-----|------------|------------|-------------|
| Ti | 0.00331300 | 0.17980000 | -0.42419500 |
| N | 0.78107700 | 1.80933300 | -0.06077000 |
| C | 2.03289000 | 2.40539000 | 0.36658600 |
| Н | 2.41067800 | 3.12718300 | -0.37732000 |
| Н | 1.91181300 | 2.93820800 | 1.32434000 |

| Н | 2.80006200 | 1.63285300 | 0.51130600 |
|---|-------------|-------------|-------------|
| Н | 0.05662700 | 2.53261200 | -0.15899100 |
| N | -1.79038700 | 0.18264300 | -0.02336400 |
| N | 0.96671400 | -1.30649400 | 0.08317400 |
| C | -2.43262500 | -1.07725800 | -0.36388800 |
| Н | -2.84919400 | -1.58020900 | 0.52663500 |
| Н | -3.25169100 | -0.92235800 | -1.08838000 |
| Н | -1.71336100 | -1.77710800 | -0.83084800 |
| C | 0.65848000 | -2.54816200 | 0.76102300 |
| Н | 0.86681200 | -3.41955000 | 0.11471300 |
| Н | 1.27321900 | -2.65218400 | 1.67225400 |
| Н | -0.39649000 | -2.58010500 | 1.06429600 |
| C | 2.35663200 | -1.15696100 | -0.31536100 |
| Н | 2.50907700 | -0.21596300 | -0.88046000 |
| Н | 3.03634800 | -1.12834400 | 0.55430600 |
| Н | 2.67305700 | -1.98337000 | -0.97640000 |
| C | -2.67439600 | 1.19194800 | 0.52546400 |
| Н | -3.15353500 | 0.82632600 | 1.45057800 |
| Н | -2.11851700 | 2.10547200 | 0.77865900 |
| Н | -3.47550100 | 1.45281600 | -0.18862000 |

1 2 1.0 8 1.0 9 1.0

2 3 1.0 7 1.0

3 4 1.0 5 1.0 6 1.0

8 10 1.0 22 1.0

9 14 1.0 18 1.0

10 11 1.0 12 1.0 13 1.0

14 15 1.0 16 1.0 17 1.0

18 19 1.0 20 1.0 21 1.0

22 23 1.0 24 1.0 25 1.0

REFERENCES

REFERENCES

- 1. Brown, D. G.; Boström, J. Analysis of Past and Present Synthetic Methodologies on Medicinal Chemistry: Where Have All the New Reactions Gone? *Journal of Medicinal Chemistry* **2016**, *59* (10), 4443-4458.
- 2. Martin, R.; Buchwald, S. L. Palladium-Catalyzed Suzuki-Miyaura Cross-Coupling Reactions Employing Dialkylbiaryl Phosphine Ligands. *Accounts of Chemical Research* **2008**, *41* (11), 1461-1473.
- 3. Tolman, C. A. Steric effects of phosphorus ligands in organometallic chemistry and homogeneous catalysis. *Chemical Reviews* **1977**, 77 (3), 313-348.
- 4. Tolman, C. A. Electron donor-acceptor properties of phosphorus ligands. Substituent additivity. *Journal of the American Chemical Society* **1970**, *92* (10), 2953-2956.
- 5. Mason, M. R.; Fneich, B. N.; Kirschbaum, K. Titanium and Zirconium Amido Complexes Ligated by 2,2'-Di(3-methylindolyl)methanes: Synthesis, Characterization, and Ethylene Polymerization Activity. *Inorganic Chemistry* **2003**, *42* (21), 6592-6594.
- 6. Odom, A. L.; McDaniel, T. J. Titanium-Catalyzed Multicomponent Couplings: Efficient One-Pot Syntheses of Nitrogen Heterocycles. *Accounts of Chemical Research* **2015**, *48* (11), 2822-2833.
- 7. Katsuki, T.; Sharpless, K. B. The first practical method for asymmetric epoxidation. *Journal of the American Chemical Society* **1980**, *102* (18), 5974-5976.
- 8. DiFranco, S. A.; Maciulis, N. A.; Staples, R. J.; Batrice, R. J.; Odom, A. L. Evaluation of Donor and Steric Properties of Anionic Ligands on High Valent Transition Metals. *Inorganic Chemistry* **2012**, *51* (2), 1187-1200.
- 9. Billow, B. S.; Bemowski, R. D.; DiFranco, S. A.; Staples, R. J.; Odom, A. L. Synthesis and Structure of Chromium(VI) Nitrido Cyclopentadienyl Complexes. *Organometallics* **2015**, *34* (18), 4567-4573. Beaumier, E. P.; Billow, B. S.; Singh, A. K.; Biros, S. M.; Odom, A. L. A complex with nitrogen single, double, and triple bonds to the same chromium atom: synthesis, structure, and reactivity. *Chemical Science* **2016**, *7* (4), 2532-2536.
- 10. Bemowski, R. D.; Singh, A. K.; Bajorek, B. J.; DePorre, Y.; Odom, A. L. Effective donor abilities of E-t-Bu and EPh (E = O, S, Se, Te) to a high valent transition metal. *Dalton Transactions* **2014**, *43* (32), 12299-12305.
- 11. Jover, J.; Fey, N. Screening substituent and backbone effects on the properties of bidentate P,P-donor ligands (LKB-PPscreen). *Dalton Transactions* **2013**, *42* (1), 172-181.

- 12. Occhipinti, G.; Jensen, V. R. Nature of the Transition Metal–Carbene Bond in Grubbs Olefin Metathesis Catalysts. *Organometallics* **2011**, *30* (13), 3522-3529.
- 13. Sparta, M.; Børve, K. J.; Jensen, V. R. Structure and Stability of Networked Metallofullerenes of the Transition Metals. *The Journal of Physical Chemistry A* **2006**, *110* (41), 11711-11716.
- 14. Billow, B. S.; McDaniel, T. J.; Odom, A. L. Quantifying ligand effects in high-oxidation-state metal catalysis. *Nat Chem* **2017**, *9* (9), 837-842.
- 15. Durand, D. J.; Fey, N. Computational Ligand Descriptors for Catalyst Design. *Chemical Reviews* **2019**, *119* (11), 6561-6594.
- 16. Huynh, H. V.; Frison, G. Electronic Structural Trends in Divalent Carbon Compounds. *The Journal of Organic Chemistry* **2013**, 78 (2), 328-338.
- 17. Morse, M. D. Predissociation Measurements of Bond Dissociation Energies. *Accounts of Chemical Research* **2019**, *52* (1), 119-126.
- 18. Mo, L.; Barr, H. I.; Odom, A. L. Investigation of phosphine donor properties to vanadium(V) nitrides. *Results in Chemistry* **2022**, *4*, 100344.

CHAPTER 5 MODELING COMPLEX LIGANDS FOR TITANIUM-CATALYZED HYDROAMINATION

5.1 Introduction

Catalysis impacts our lives in many aspects from health care to food production, transportation, and energy storage. Scientists have been studying the design, optimization, and discovery of catalysts for improvements in reaction scope, selectivity, efficiency, and sustainability. One of the most effective and commonly used methods to optimize catalysts is to modify ancillary ligands and understand the effects on catalysis. As mentioned in Chapter 4, Tolman's electronic parameter has made great contributions to parameterizing ligands in late transition metal catalysis. This system uses the A₁ carbon monoxide stretching frequency on LNi(CO)₃ to determine phosphine donor ability, which can reveal how ligands affect reactivity in late metal catalyses.³

Early metals in high oxidation states have growing potential in catalysis.⁴ Titanium-catalyzed hydroamination and iminoamination have been incorporated into many important structures (see Chapter 1). For example, the novel, selective NRF2 inhibitor, MSU38225, was synthesized through a titanium-catalyzed iminoamination reaction.⁵ To understand ligand effects in titanium catalysis, parameterization tools for high oxidation state metals are needed. As an analog for high oxidation state early transition metals, our group developed the LDP system to quantitively measure the electronic donation from a mono-anionic ligand X to a metal center.⁶ The chromium(VI) complexes, NCr(NⁱPr₂)₂X where X is the ligand being investigated, were synthesized to measure the rotation barrier of the Cr–N amide bond, which is controlled by the donation of amide nitrogen to the metal center. A better donor results in more single bond character in the Cr–N amide bond, which increases the rotation along this bond giving a lower LDP value.

A variety of mono-anionic ligands were measured for their LDP values, including phenoxides, alkoxides, amides, halides, and heterocycles.⁷ These LDP values have strong correlations with many different experimental data, including ¹³C NMR chemical shifts in a tungsten system and Hammett parameters for aryloxides.^{6,8} The LDP system was also used to study ligand effects in a titanium-catalyzed hydroamination reaction.⁹ A model was designed to correlate the electronic and steric parameters of the ancillary ligands on titanium catalysts with reaction rate (Eq. 1). This model can be used to predict catalyst performance and guide future catalyst design. As the LDP system measures the electronic property of the ligands, a steric parameter for the ligands is also needed.

Reaction rate =
$$a + b(electronic parameter) + c(steric parameter)$$
 (1)

After a comparison of different measurement systems, percent buried volume (${}^{6}V_{bur}$) developed by Cavallo¹⁰ was used as the steric parameter for studying ligand effects in titanium catalysis. The first coordination sphere around the metal center was set as the coordinating space, a sphere with a radius of 3.5 Å. The percentage of the space occupied by the ligands relative to the volume of the sphere is considered percent buried volume (${}^{6}V_{bur}$) of the ligand. The calculation of volume is based on the crystal structure of the metal complex.

Figure 5.1. An example of titanium catalyst and its electronic and steric reporter, $NCr(N^iPr_2)_2(pyr)$.¹¹

Both the electronic and steric parameters of the ligands were measured on the same chromium complex instead of the titanium complexes (Figure 5.1). There is a hapticity difference

in some cases and η^1 in others. Using the chromium complexes, the ligands are forced into η^1 coordination, which was considered a more accurate representation of the active titanium catalyst. On the other hand, due to the nature of the LDP system, only one half of the bidentate ligand can be measured for the electronic parameter. The linkers between the fragments were ignored because they show little influence on catalysis.

$$\begin{array}{c} \text{Ph} & \text{NH}_2 \\ \text{Ph} & \text{Ph} & \text{It cat.} \\ \text{(10 mol}\%) \\ \text{Itoluene-d}_{8}, \\ \text{75 °C} & \text{Ph} & \text{Ph} \\ \text{NMe}_2 & \text{NMe}_2 \\ \text{Me}_2 & \text{NMe}_2 \\ \text{NMe}_2 & \text{NMe$$

Figure 5.2. Titanium-catalyzed hydroamination reaction and a library of catalysts. 11

With the methods to quantitively measure the electronic and steric parameters of the chosen ligands, the kinetics of titanium-catalyzed hydroamination reactions were measured using the catalysts with a large range of electronic and steric profiles (Figure 5.2). The intermolecular hydroamination was run with an excess of aniline to produce pseudo-first order kinetics. The concentration of alkyne was monitored as a function of time and fit into an exponential decay. Modeling the rate constant of the catalysis with the electronic and steric parameters of the ligands produced Eq. 2 with scaled coefficients.

$$k_{obs}(\times 10^4) = 1.34 + 1.61(LDP) - 2.25(\%V_{bur})$$
 (2)

The coefficients in the model suggested that electron deficient and small ligands accelerate the catalysis. This model also indicated that the contribution of the steric effect is slightly more important than the electronic effect. With this model, a prediction of reaction rates can be made prior to the catalyst synthesis, since catalysts with different functional groups on the ligands fit the model very well. As studies have shown that unsymmetrical ligands perform faster catalysis than symmetrical ligands in some cases, ¹² a more complex model with unsymmetrical ligands needs to be studied. In this chapter, the catalyst library is expanded to more complex catalysts with unsymmetrical ligands. A 5-parameter model is generated to study the ligand effects on reaction rate. Along with the exploration, a series of catalysts with 3-unsubstituted indole fragments are proposed to go through a unique hydroamination mechanism, where the indole fragments are involved in proton transfer resulting in faster catalysis.

5.2 Synthesis of Unsymmetrical Ligands and Titanium Catalysts

This project was undertaken in close collaboration with Rashmi Jena, Dr. Tanner McDaniel, and Hannah Barr. Rashmi and Tanner also participated in the syntheses of ligands and catalysts. Their syntheses are not discussed in this chapter; however, the kinetic data of their catalysts is included in the models. Hannah Barr contributed to chromium complex syntheses.

Previous studies have shown that symmetrical bidentate ligands comprised of substituted pyrroles, indoles, and phenols are effective ligands for titanium-catalyzed hydroamination.^{9,13} Pairing different ligands in a bidentate framework is expected to afford a new ancillary ligand that is still effective for titanium-catalyzed hydroamination. For the new ligands, two different strategies for the unsymmetrical bidentate ligands were developed: desymmetrizing symmetrical ligands or combining two different monodentate ligands into a bidentate framework (Figure 5.3).

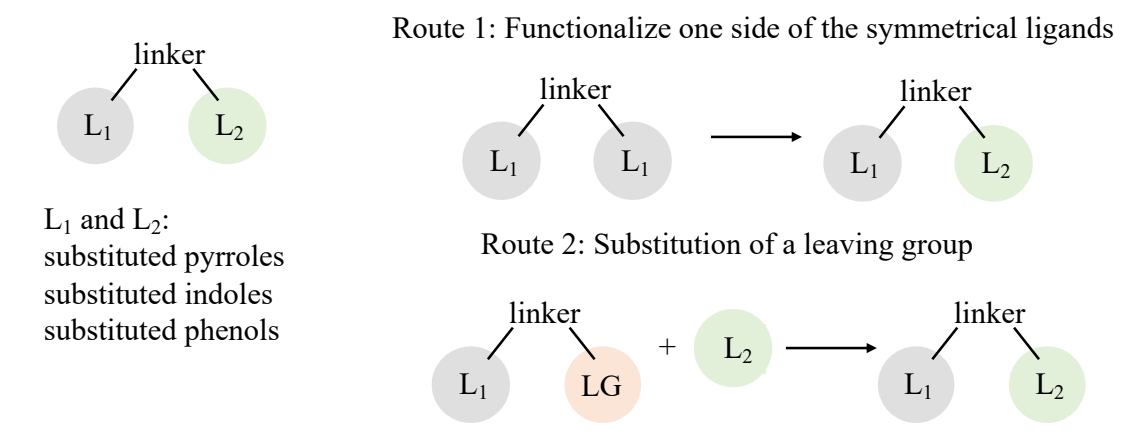


Figure 5.3. Two routes to access unsymmetrical ligands.

The dipyrrolylmethane ligands were discovered as ligands for fast catalysis.¹³ The syntheses of unsymmetrical dipyrrolylmethane derivatives were explored first. The mono borylation of H_2 dpm was achieved in a high yield using a half equivalent of B_2 pin₂ in the presence of iridium catalyst and phenanthroline (Scheme 5.1).¹⁴ The monoborylated product was coupled with aryl bromide using Suzuki-Miyaura coupling conditions to install the aromatic substituents at the α -position of one pyrrole fragment.¹⁵ To expand the range of electronic properties of the ligands, 3,5-dimethyl and 3,5-(bis)trifluoromethyl substituents were chosen to be installed on the dipyrrolylmethane ligands.

Scheme 5.1. Unsymmetrical ligand synthesis using Route 1.

To branch forward with a diverse combination of pyrrolyl, indolyl, and phenoxide ligands, the Route 2 was developed through the substitution of a leaving group with a mono-anionic ligand. Successful substitution of a hydroxyl group was found using a Lewis acid, InCl₃, by Dr. Tanner McDaniel. The synthesis of an unsymmetrical ligand incorporating indole and pyrrole fragments was developed (Scheme 5.2). The reduction of tosyl-protected pyrrole-2-carboxaldehyde by sodium borohydride produced *N*-tosyl-pyrrol-2-ylmethanol. Since the most nucleophilic site of an unsubstituted indole is at the 3-position, 3-methylindole was used to couple with the pyrrolylmethanol product, followed by deprotection to afford the bidentate unsymmetrical ligand.

Scheme 5.2. An example of unsymmetrical ligand synthesis using Route 2.

A different set of unsymmetrical ligands was synthesized using the substitution of a hydroxyl group on indolylmethane derivatives (Scheme 5.3). The indolylmethane precursor was synthesized by the treatment of excess methyllithium with ethyl 1H-indole-2-carboxylate, 18 followed by substitution with pyrrole or pyrrole derivatives in the presence of boron trifluoride etherate. Sequential borylation and Suzuki coupling reactions were used to install different aromatic groups on pyrrole at the α -position. The borylation was selective at the 2-position on the pyrrole ring, which was determined by NMR spectroscopy of the product and the crystal structure of the corresponding titanium catalyst (Figure 5.4).

Scheme 5.3. Examples of unsymmetrical ligand synthesis using Route 2.

Once the unsymmetrical ligands were synthesized, the titanium catalysts were prepared by mixing the ligands with commercially available $Ti(NMe_2)_4$ (Scheme 5.4). The catalysts were purified by recrystallization and characterized by NMR and single-crystal XRD. Generally, a more electron-donating pyrrole ring tends to bond to titanium in an η^5 fashion, since this coordination

donates more electron density to the electron-deficient metal center. For example, the pyrrole fragments with smaller LDP values bond to titanium in η^5 fashion in complex **5d** and **5e** (Table 5.1).

Scheme 5.4. Complexation of titanium catalyst 5a.

Interestingly, the crystal structures of **6d** and **5b** show that titanium bonds to 2-aryl-substituted pyrrole in a η^5 fashion even with electron-deficient pyrroles (Figure 5.4). The energies of titanium complexes with η^1 and η^5 bonded 2-substituted pyrroles are being calculated by DFT. The preference could be due to the steric repulsion of the large substitution on pyrrole with other ligands on titanium.

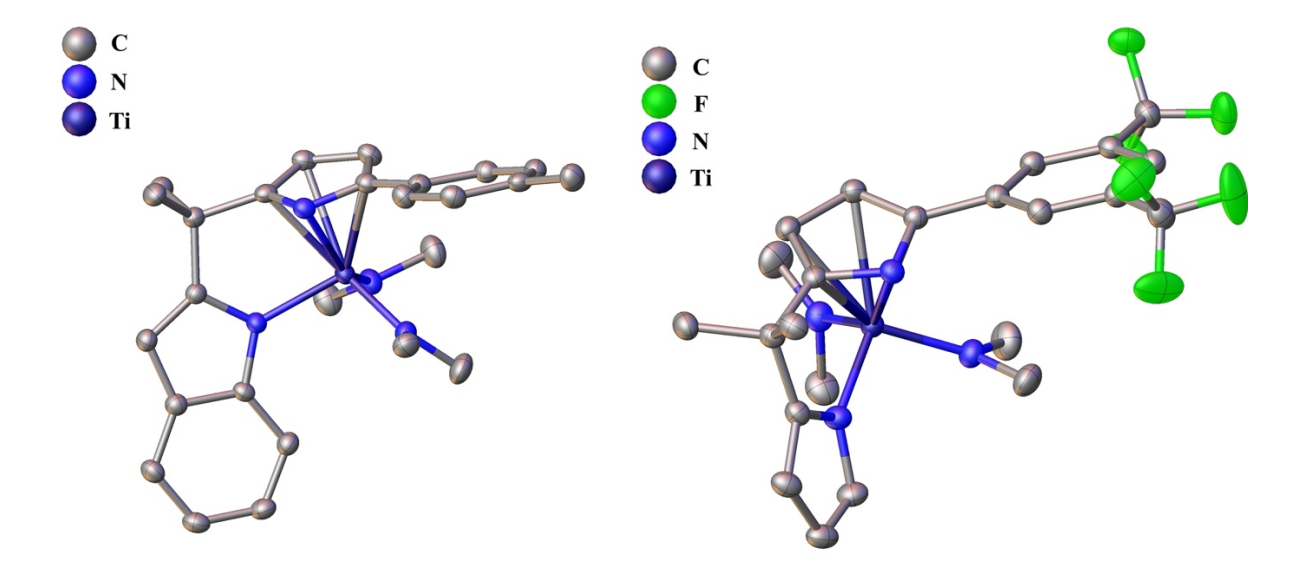


Figure 5.4. Crystal structures of titanium catalysts, 6d and 5b.

5.3 Modeling Reaction Rate as A Function of Ancillary Ligand Structure

After a series of titanium catalysts with unsymmetrical ligands were synthesized, the modeled hydroamination reactions for studying ligand effects were conducted in NMR tubes at 75 °C (Scheme 5.5).

Scheme 5.5. Conditions of titanium-catalyzed intermolecular hydroamination.

The reaction was run under excess of aniline to produce pseudo first order kinetics of alkyne where the concentration of alkyne was monitored as a function of time and fit into an exponential decay (Figure 5.5). The rate constant of the catalyst was reported from the fit.

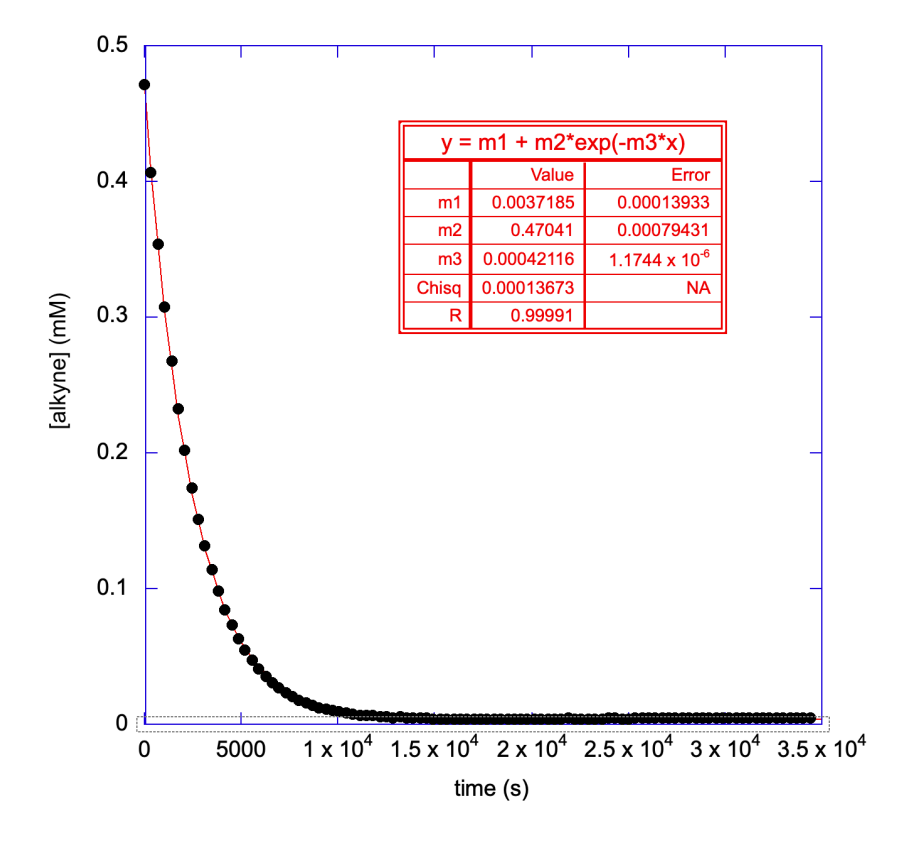


Figure 5.5. A representative plot with a fit of the kinetics. The loss of alkyne was monitored by ¹H NMR using ferrocene as an internal standard.

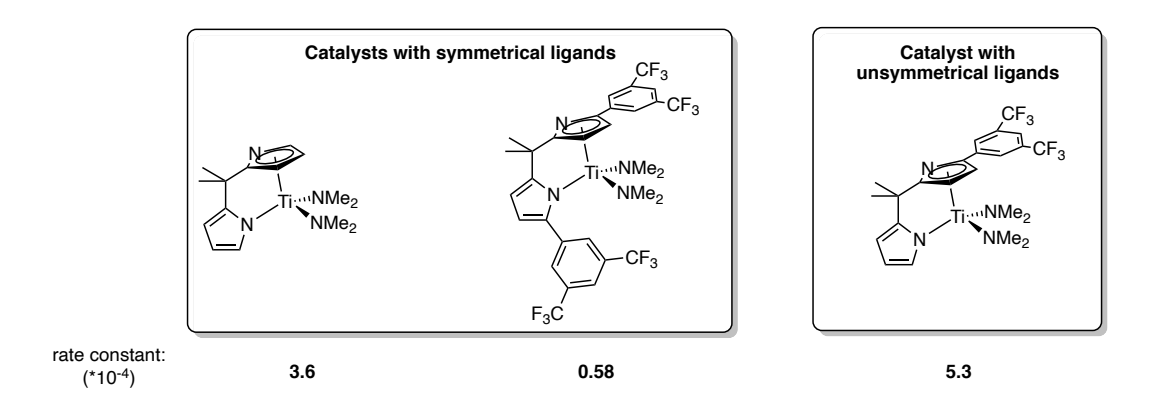


Figure 5.6. The rate constant of example catalysts with symmetrical or unsymmetrical ligands.

The kinetics of the catalysts with symmetrical ligands or unsymmetrical ligands are compared in Figure 5.6. It was found that catalysts with unsymmetrical ligands perform better than their symmetrical derivatives in some cases. This suggests that the ligands could be in an unsymmetrical environment in the key transition state. Containing unsymmetrical ligands can potentially lower the energy of the transition states, resulting in a faster turnover frequency. It was also found that desymmeterizing ligands does not always result in faster catalysis. Therefore, a library of catalysts with unsymmetrical ligands was synthesized to analyze the ligand effects on catalysis rate. The chromium complexes that were used to report the electronic and steric parameters are also shown in Table 5.1 along with the titanium catalysts and their rates.

Table 5.1. A library of titanium catalysts with the electronic and steric parameters of the ligands.

| Titanium | Chromium Complex | LDP | | Rate Constant |
|--|----------------------|------------|-------------------------------|----------------------|
| Catalysts | for parameterization | (kcal/mol) | $\%\mathrm{V}_{\mathrm{bur}}$ | (×10 ⁻⁴) |
| N NMe ₂ NMe ₂ 5a | Pri N N N Pri Pri | 13.91 | 26.7 | 4.2 |

Table 5.1 (cont'd).

| | Pri N N N N N N N N N N N N N N N N N N N | 13.64 | 20.4 | |
|--|---|-------|------|-----|
| CF ₃ CF ₃ T ₁ :NMe ₂ | Pri N Cr N Pri Pri Pri | 14.32 | 27.9 | 5.3 |
| N NMe ₂ | Pri N N Pri Pri | 13.64 | 20.4 | |
| TiNMe ₂ | Pri N N N N N N N N N N N N N N N N N N N | 14.03 | 27.1 | 4.0 |
| 5c | Pri N N Pri Pri Pri | 13.64 | 20.4 | |
| N NMe ₂ | Pri N N Pri N Pri | 13.46 | 23.7 | 3.0 |
| 5d | Pri N N N N N N N N N N Pri N N Pri | 13.64 | 20.4 | |
| N N N N N N N N N N N N N N N N N N N | Pri N N Pri Pri | 13.09 | 23.1 | 1.9 |
| 5e | Pri N III Pri N Pri Pri Pri | 13.46 | 23.7 | |

Table 5.1 (cont'd).

| N TiNMe ₂ | Pri N N N Pri N Pri Pri | 13.64 | 20.4 | 3.5 |
|---------------------------------------|---|-------|------|------|
| 6a | Pri N N Pri Pri | 12.49 | 22.6 | |
| N NMe ₂ NMe ₂ | Pri N N N Pri N Pri Pri | 13.64 | 20.4 | 6.6 |
| | Pri N N Pri Pri | 12.99 | 22.3 | |
| TiNMe ₂ | Pri N III Pri N Pri Pri | 13.46 | 23.7 | 11.5 |
| 6c | Pri N Cr N Pri Pri | 12.99 | 22.3 | |
| N TiNMe ₂ NMe ₂ | Pri N N N N N N N N N N N N N N N N N N N | 13.91 | 26.7 | 6.9 |
| 6d | Pri N N Pri Pri | 12.99 | 22.3 | |

Table 5.1 (cont'd).

| • | | 1 | T | T |
|---|--|-------|--|------|
| N NMe ₂ | Pri N III Pri N Pri Pri | 14.03 | 27.1 | 9.8 |
| 6e | Pri N N Pri Pri Pri | 12.99 | 22.3 | |
| CF ₃ CF ₃ CF ₃ NMMe ₂ | Pri CF ₃ CF ₃ Pri Pr | 14.32 | 27.9 | 15.2 |
| N NMe ₂ | Pri N Cr N Pri Pri | 12.99 | 22.3 | |
| Me_2N $Me_2N-Ti-N$ O | Pri N N Pri Pri Pri | 13.64 | 20.4 | |
| ¹Bu ¹Bu 7a | Pri N Cr O Pri Pri Pri | 11.98 | Pri N tBu Pri N Pri N Pri 21.6 | 0.46 |
| Me ₂ N Me ₂ N TI-N | Pri N Cr N Pri Pri Pri | 12.49 | 22.6 | |
| ¹Bu ¹Bu 7b | Pri N III Pri N Pri Pri | 11.98 | Pri Num Cr O Pri | 0.67 |
| | | | 21.6 | |

Table 5.1 (cont'd).

| Me ₂ N F | Pri N F F Pri Pri Pri | 12.66 | 22.6 | |
|---------------------|----------------------------|-------|--|------|
| ¹Bu ¹Bu 7c | Pri Num Cr Pri / Pri / Pri | 11.98 | Pri N tBu Pri N Pr | 0.67 |

To model a diverse set of ligands, a 5-parameter model (Eq. 2) was employed for the structures using one LDP and one % V_{bur} value for each side of the ligand while the linker in between was ignored. In this model, k is the pseudo first-order rate constant of the reaction, a is a fitting constant, b and c are coefficients for electronic parameters, d and e are coefficients for steric parameters. The superscript l or l refers to side l or l respectively. Even though the model does not reveal the exact structure of the catalysts in the transition state, it gives clues as to whether the two sides of the unsymmetrical ligand are in a different environment.

$$k_{obs}(\times 10^4) = a + b(LDP)_1 + c(LDP)_2 + d(\%V_{bur})_1 + e(\%V_{bur})_2$$
 (2)

In order to assign sides 1 and 2 for all unsymmetrical ligands consistently, the assignments based on electronics and sterics were compared based on their fits. For example, one can assign fragments with larger LDP values to be side 1 (assignment based on electronics), or one can assign fragments with larger %V_{bur} values to be side 1 (assignment based on sterics). It was found that the assignment based on electronics results in a much better model. Therefore, the fragment with a larger LDP value was assigned to side 1 in this study (Figure 5.7).

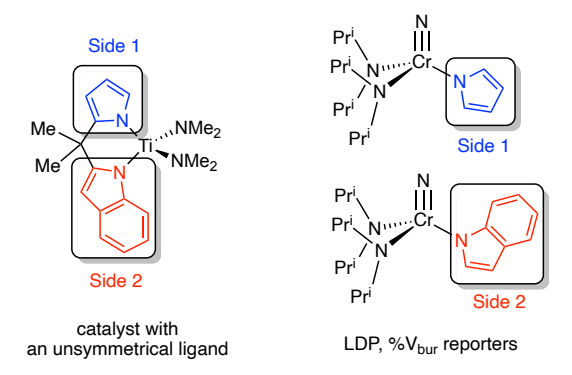


Figure 5.7. A side assignment example with titanium catalyst, **6b**. The fragment with a larger LDP value was assigned to side 1.

The catalysts with symmetrical and unsymmetrical ligands were all included into the model at first. The model shows that precatalysts that contain a 3-unsubstituted indole fragment are noticeably faster than other catalysts in the system, while precatalysts with 3-methylindole fragments fit the model well. The inclusion of the catalysts with 3-unsubstituted indole fragments into the regression analysis results in very poor fits (based on either electronics or sterics). Therefore, the regression analysis was conducted without this class of catalysts. The fit is shown in a red line with black dots as the experimental rates, where the catalysts that were not included in the fit are shown in blue squares in Figure 5.7.

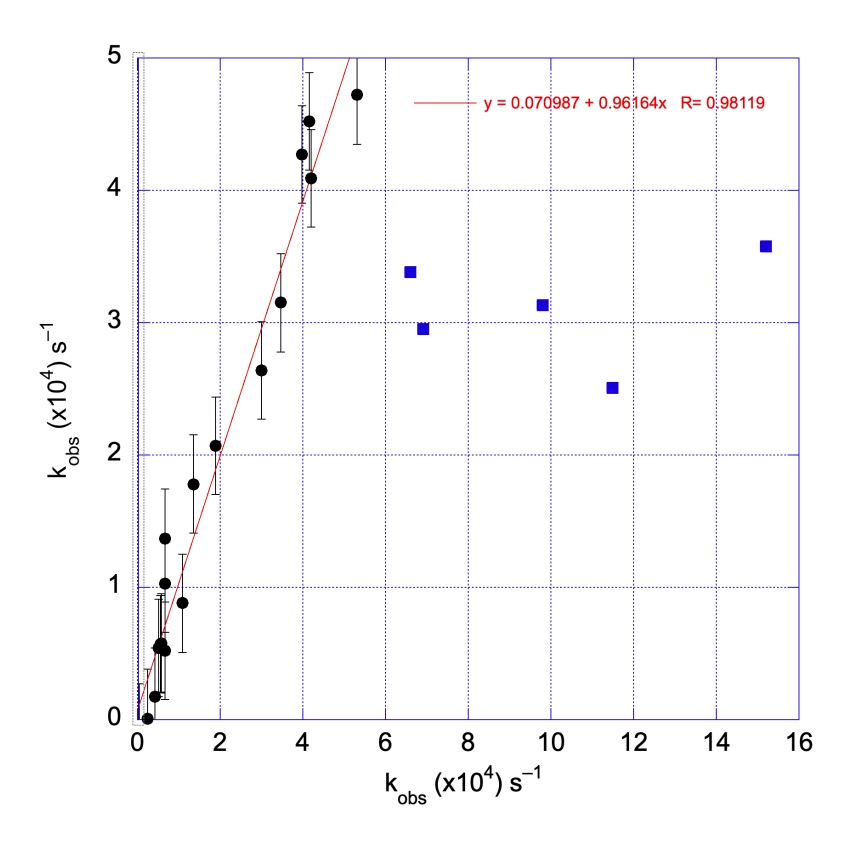


Figure 5.8. The plot of k_{obs} vs k_{calc} for catalysts used in the model (black dots). The blue squares are from catalysts with 3-unsubstituted indole fragments.

The model without inclusion of 3-unsubstituted indolyl catalysts showed a good fit between the experimental and calculated rate constant (Figure 5.8). The model parameters from the regression analysis using natural parameters are shown in Eq. 3. With this model, the rate of a catalyst that was not explored in this study can be predicted by substitution of LDP and %Vbur values into Eq. 3. Based on the model, Side 1 (larger LDP fragment) makes a large contribution to the rate in comparison with Side 2. On the other hand, the sterics of side 2 (smaller LDP fragment) seem to contribute more than Side 1. The signs and magnitudes of the parameters also indicated that a faster catalyst is expected with an unsymmetrical ligand that has one side electron-deficient and the other side very small.

$$k_{obs}(\times\,10^4) = -9.60 + 2.00(LDP)_1 + 0.11(LDP)_2 - 0.15(\%V_{bur})_1 - 0.56(\%V_{bur})_2 \eqno(3)$$

The mechanism of titanium-catalyzed hydroamination reaction was originally established by Bergman and coworkers for zirconocene-based catalysts (Figure 5.9).²⁰ The titanium imido complex, **A**, undergoes [2 + 2]-cycloaddition with an alkyne in a reversible reaction where the slow step in the catalytic cycle is believed to be the Ti–C protonolysis step. Final proton transfer releases the enamine product and restores the active catalyst, **A**. A possible 5-coordinate titanium species, **C**, in the transition state was proposed based on the model. The difference in the parameter coefficients between the two sides suggests that the two sides reside in different environments. Due to the steric repulsion between the substituents on the metal center, small ligands for both sides are favored. Side 2 contributes more to the rate due to the axial position experiencing more steric interaction compared to Side 1. The preference for electron deficient ligands is possibly due to the resulting acidity increase of the titanium amido complexes after the first protonolysis.

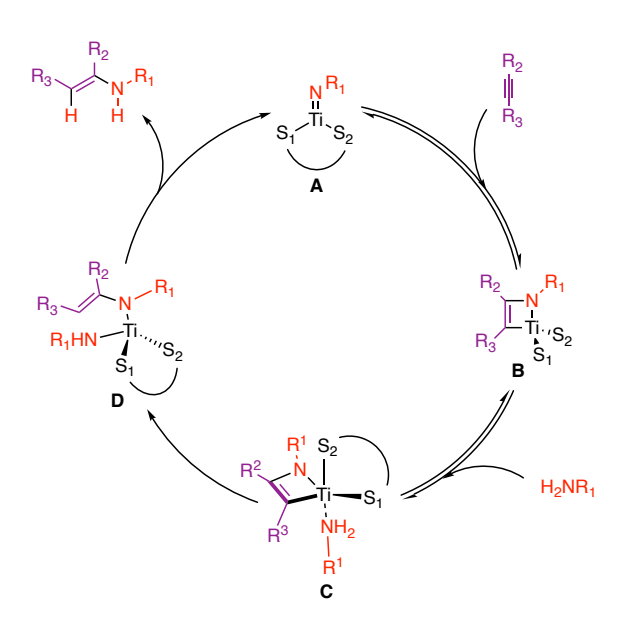


Figure 5.9. A proposed mechanism with a 5-coordinate titanium species in the transition state before the Ti–C protonolysis.

5.4 Investigation of Indolyl Effect

After discovering that the catalysts that did not fit the model all share the same 3-unsubstituted indole fragment, a change in the mechanism associated with this ligand fragment was proposed. The difference in rate between catalysts with 3-methylindole fragments and 3-unsubstituted indole fragments revealed the potential mechanistic importance of the 3-position on indole fragments. A hypothesis was made that the 3-position of the indoles may act as a proton shuttle during the catalysis, which has been proposed in other catalyses (Scheme 5.6).²¹

Scheme 5.6. A proposed proton transfer through 3-position on indole fragment of the ligand.

The rate limiting step of titanium-catalyzed hydroamination is proposed to be the protonolysis of the Ti–C bond in the azatitanacyclobutene intermediate.²² Shuttling the proton through the 3-position of the indole fragment can potentially lower the barrier to the protonolysis. Placing substituents on the 3-position of the indolyl lowers the accessibility of the site resulting in a lower rate of shuttling or perhaps the indolyl ligand does not act as a shuttle in this case.

If this hypothesis is true, the pKa of an appended proton on this site could influence the rate of shuttling significantly. To test this hypothesis, the computational study of the proton affinity at the 3-position of indole fragments was conducted with different substituents at the 5-position. Substituents on 5-position were found to alter the proton affinity by 14 kcal/mol from a methoxy substituent to a trifluoromethyl substituent. This large change in proton affinity was proposed to result in a large difference in rate.

The synthesis of a catalyst containing a 3-unsubstituted indole fragment was conducted (Scheme 5.7). A palladium-catalyzed annulation between iodoanilines and ketones was used to

form the indole derivatives,²³ followed by the sequential esterification and reduction to afford the products with a hydroxyl group as a leaving group. Substitution with pyrrole in the presence of a Lewis acid resulted in the desired unsymmetrical ligand, which was treated with Ti(NMe₂)₄ to afford the precatalyst.

Reagents and conditions: a) pyruvic acid, Pd(OAc)₂, DABCO, DMF, 105 °C, 4 h, 38%; b) H_2SO_4 , EtOH, relux, 12 h, 91%; c) MeLi, THF, r.t., 2 h, 74%; d) $BF_3 \cdot Et_2O$, pyrrole, r.t., 5 min, 47%; e) $Ti(NMe_2)_4$, ether, r.t., 10 h, 29%

Scheme 5.7. Synthesis of catalyst 7c.

Unexpected yellow precipitates were found in the early stage of the catalysis (Figure 5.10). The precipitates were not identified due to the poor solubility in typical solvents like chloroform, benzene, and DMSO. The resulting slow rate was attributed to possible catalyst decomposition and may not be a true representation of the catalysis. An alternative substitution was proposed by using the 4,6-difluoroindole fragment, as the proton affinities between 5-trifluoromethylindole and 4,6-difluoroindole were very close.

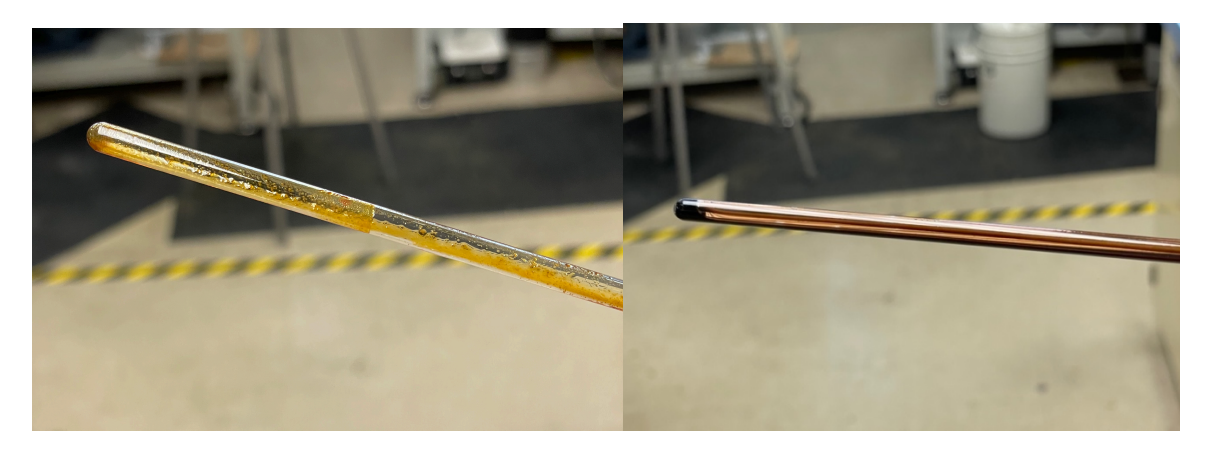


Figure 5.10. Pictures of the reaction mixture catalyzed by 7c and 7b after hydroamination.

The synthesis of the unsymmetrical ligand with 4,6-difluoroindole fragment was conducted through esterification, LAH reduction, pyrrole substitution, and titanium complexation (Scheme 5.8). Because the substitution on the links makes little difference to catalysis, LAH reduction was used instead of methyllithium. In addition, pyrrole substitution took a long time compared to other ligands. Catalyst **7a** was also synthesized by this route.

Reagents and conditions: a) H_2SO_4 , EtOH, relux, 12 h, 96%; b) LAH, THF, r.t., 2 h, 56%; c) $BF_3 \cdot Et_2O$, pyrrole, r.t., 24 h, 28%; d) $Ti(NMe_2)_4$, ether, r.t., 10 h, 30%

Scheme 5.8. Synthesis of titanium catalysts 7b.

Catalysts **7a** and **7b** did not observe obvious catalyst decomposition during the catalysts. However, the catalysts with electron-donating and withdrawing groups on the indole fragment both result in a decrease in rate. No linear correlation was found between the reaction rate and the proton affinity calculated by DFT.

Table 5.2. Rate constants of catalysts and proton affinity with different indole substituents.

| T' | Rate Constant | Structure of PA | PA |
|--|----------------------|-----------------|------------|
| Titanium Catalysts | (×10 ⁻⁴) | calculation | (kcal/mol) |
| N TIINMe ₂ NMe ₂ | 6.6 | | 215.8 |

Table 5.2 (cont'd).

| N N N N N N N N N N N N N N N N N N N | 3.5 | MeO | 222.1 |
|--|-------|------------------|-------|
| N TiNMe ₂ NMe ₂ NMe ₂ | 2.7 | F HZ | 208.0 |
| N NMe ₂ NMe ₂ 7c | 0.017 | F ₃ C | 208.7 |

Labeling experiments were designed to monitor the H/D exchange between the ligands on titanium catalysts and aniline-d₈ by NMR spectroscopy. Titanium catalysts were treated with several equivalents of aniline-d₈ under mild heating for 3 hours before the reactions were quenched with MeOD-d₄ (Scheme 5.9). Then, the integrations of the ligands were compared for changes with those where the catalysts were reacted with aniline. The free ligands were monitored instead of the titanium complexes due to the difficulty in assigning peaks of the multiple titanium species, e.g. titanium imido complexes, and titanium bis-amido complexes. Quenching Ti(dpm)(NMe₂)₂ with MeOD-d₄ as a control experiment did not show deuteration of the dpm ligand, which indicated that the deuteration of the ligands is the result of the interaction between titanium catalysts and aniline-d₈.

Me Me Me
$$\frac{1}{N}$$
 $\frac{1}{N}$ $\frac{1}{$

Scheme 5.9. Labeling experiment between titanium catalysts and aniline-d₈.

Surprisingly, the treatment of catalyst **5b** with 5 equivalents of aniline-d₈ results in deuteration of the 3-position of the indole fragment and 3-, 4-, and 5-position of the pyrrole fragment. A tetra-deuteration product mass was found in the reaction mixture by GC-MS. Further comparison of ¹H NMR spectra revealed that the integrations of these positions at both 3-indolyl and 2-, 3-, and 4-pyrrolyl decreased by about 50% compared to the catalyst treated with protio aniline. The ²H NMR spectrum showed new peaks that can be assigned to the 3-position of the indole fragment and 3-, 4-, and 5-position of the pyrrole fragment. While the deuteration of the pyrrole fragment was unexpected, it does not rule out the potential contribution of the 3-position of the indole fragment in protonolysis. The labeling experiments suggest that H/D exchange on heterocyclic ligands is rapid and occurs under mild conditions relative to the kinetic experiments.

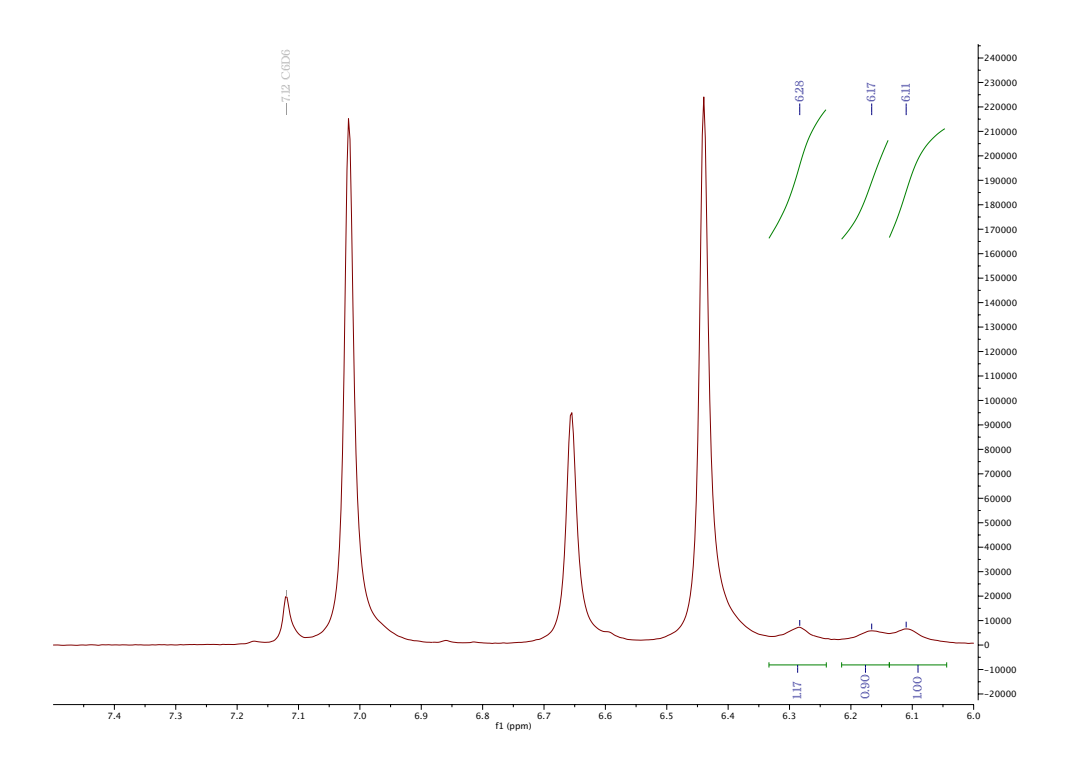


Figure 5.11. ²H NMR spectrum of the deuterated ligand from catalyst **5b** with aniline-d₈. Peaks at 6.11, 6.17, and 6.28 ppm are from the ligand. Peaks at 6.4, 6.5, and 7.1 ppm are from aniline-d₈.

5.5 Conclusions

Homogeneous hydroamination titanium catalysts with bidentate ligands were modeled with the electronic and steric properties of the ligands. The ligand library was expanded to more complex unsymmetrical ligand sets, resulting in a 5-parameter model from multivariate analysis. The model showed a very good fit and can be used to predict the reaction rate of titanium catalysts with symmetrical or unsymmetrical ligands. The coefficients of the model suggest an unsymmetrical environment of the bidentate ligands in the key transition state. In the process of carrying out the study, a series of catalysts with 3-unsubstituted indole fragments were proposed to have a unique hydroamination mechanism, where the indole fragments were involved in proton transfer resulting in faster catalysis. NMR experiments revealed the H/D exchange between aniline and the ligands of titanium catalysts.

5.7 Future Work

Computational studies on the ligand-involved mechanism are under investigation. Even though the correlation between proton affinity at 3-position on indole fragments and catalysis rate did not show a linear relationship, it does not show that this position is mechanistically unimportant. The proton affinity difference between different sites is currently being calculated and correlated with the reaction rate. The energy barriers for proton transfer by the indole fragment could be calculated and compared with those from the Bergman mechanism in the future.

A series of titanium catalysts with 3-unsubstituted indole fragments are being synthesized. With the kinetics of these catalysts, a new model could be generated on this class of ligands to guide the design of titanium catalysts with 3-unsubstituted indole fragments. The new mechanism can lead to a new catalyst design, which might include a 3-unsubstituted indole fragment on both sides of an unsymmetrical ligand.

5.7 Experimental Details

General Considerations

All manipulations were carried out under an inert dinitrogen atmosphere in an MBraun glovebox or using standard Schlenk techniques. Toluene was sparged with dinitrogen and passed over an activated alumina column prior to use. n-Hexane was dried over sodium-benzophenone radical, refluxed, and distilled under dinitrogen prior to use. All deuterated NMR solvents were purchased from Cambridge Isotope Laboratories. Benzene-d₆ was dried over CaH₂ and distilled under dinitrogen. CDCl₃ was dried over P₂O₅ and distilled under dinitrogen.

Ti(NMe₂)₄ was purchased from Gelest and used as received. Tetrakis(triphenylphosphine)palladium(0) was purchased from Strem and used as received. 1-phenyl-1-propyne was purchased from Combi-blocks and distilled from barium oxide prior to use. Aniline was purchased from Sigma-Aldrich and distilled from KOH and passed through dry alumina prior to use. The 5-(trifluoromethyl)-1H-indole-2-carboxylic acid was synthesized using a literature procedure.²³

Synthesis of H₂dpm^{2-Bpin}

In a N₂ glovebox, [Ir(COD)OMe]₂ (7 mg, 0.01 equiv) and phenanthroline (2 mg, 0.1 equiv) were dissolved in THF (2 mL) in a 25 mL Schlenk flask, and the mixture was stirred for 5 min. Then, B₂pin₂ (127 mg, 0.5 equiv) and H₂dpm (174 g, 1.0 equiv) were added dissolved in another portion of THF (3 mL). The reaction was sealed, removed from the glovebox, and heated in oil bath at 80 °C for 15 h. The mixture was allowed to cool to room temperature, and THF was

removed by rotary evaporation. The crude product was diluted with hexane (20 mL) and flushed through a silica plug. Removal of the solvent afforded crude product as a light brown oil (290 mg, 96%). The product was used for the next step without further purification. ¹H NMR (CDCl₃, 500 MHz, 25 °C) δ 8.28 (s, 1H), 7.75 (s, 1H), 6.77 (t, J = 3.0 Hz, 1H), 6.66-6.61 (m, 1H), 6.18-6.14 (m, 1H), 6.14 (d, J = 2.7 Hz, 1H), 6.11-6.07 (m, 1H), 1.66 (s, 6H), 1.29 (s, 12H). LRMS (EI): calc'd: 300, found: 300. The NMR shows a compound with modest purity, that was used without further purification in the next step.

General procedure A for the Synthesis of H₂dpm derivatives

In a glove box, tetrakis(triphenylphosphine)palladium(0) (10 mol%), potassium carbonate (2.0 equiv), H₂dpm^{2Bpin} (1.0 equiv), aryl iodide or aryl bromide (1.0 equiv), and 3 mL (per mmol of H₂dpm^{2Bpin} starting material) of toluene were added in a 50 mL Schlenk tube. The reaction was then removed from the glovebox and charged with 1 mL of water under a constant flow of dry dinitrogen. Then, the Schlenk tube was sealed and heated in an oil bath at 110 °C for 12 h. The organic layer was diluted with EtOAc, separated, and dried over sodium sulfate. The crude product was purified by column chromatography on silica gel (hexane/ethyl acetate) to afford the pure product.

Symnthesis of $H_2dpm^{2-(3,5-diCF3Ph)}$

General procedure A was followed using H_2dpm^{2-Bpin} (600 mg, 1.0 equiv), 1-bromo-3,5-dimethylbenzene (370 mg, 1.0 equiv), tetrakis(triphenylphosphine)palladium(0) (230 mg, 10 mol%), potassium carbonate (828 mg, 3.0 equiv), dry toluene (6 mL), and water (1 mL). Column Chromatography utilized 3% EtOAc in hexanes on silica gel. Removal of solvent afforded the product as a colorless oil (400 mg, 72%). H NMR (CDCl₃, 500 MHz, 25 °C): δ 7.51 (s, 2H), 7.06 (dd, J = 2.6, 1.3 Hz, 1H), 6.71 (s, 1H), 6.67 (d, J = 2.7 Hz, 1H), 6.58-6.55 (m, 1H), 6.51 (d, J = 2.7 Hz, 1H), 6.25 (dd, J = 3.1, 1.2 Hz, 1H), 2.80 (s, 12H), 2.13 (s, 6H), 1.89 (s, 6H). 13 C{ 1 H} NMR (CDCl₃, 126 MHz, 25 °C): δ 163.14, 161.72, 141.57, 137.63, 133.67, 129.98, 124.22, 123.62, 115.14, 112.43, 107.88, 101.79, 47.11, 40.12, 30.10, 21.30. LRMS (EI): calc'd: 278; found: 278. *Synthesis of H*2 $dpm^{2-(3.5-diCF3Ph)}$

General procedure A was followed using H₂dpm^{2-Bpin} (300 mg, 1.0 equiv), 1-bromo-3,5-bis(trifluoromethyl)benzene (293 mg, 1.0 equiv), tetrakis(triphenylphosphine)palladium(0) (164 mg, 4 mol%), potassium carbonate (392 mg, 2.0 equiv), and 3 mL of dry toluene, 1 mL of water. Removal of solvent afforded product as colorless oil (165 mg, 43%). ¹H NMR (CDCl₃, 500 MHz, 25 °C): δ 8.14 (s, 1H), 7.88 (s, 1H), 7.72 (s, 2H), 7.60 (s, 1H), 6.72-6.68 (m, 1H), 6.57 (dd, J = 3.7,

2.8 Hz, 1H), 6.23-6.20 (m, 1H), 6.20-6.18 (m, 1H), 6.17-6.14 (m, 1H), 1.71 (s, 6H). ¹⁹F NMR (CDCl₃, 470 MHz, 25 °C) δ –62.7. LRMS (EI): calc'd: 386; found: 386.

Synthesis of (1-tosyl-1H-pyrrol-2-yl)methanol

The procedure was adapted from a literature procedure. ¹⁶ A 250 mL Schlenk flask equipped with a stir bar was purged with dinitrogen and charged with pyrrole-2-carboxaldehyde (2.0 g, 1.0 equiv) and THF (50 mL). Sodium hydride (0.6 g, 1.1 equiv) was added in 3 portions over 30 min. The mixture was kept stirring under room temperature until no gas was released. Next, a solution of para-toluenesulphonyl chloride (4.4 g, 1.1 equiv) in 15 ml of THF was added to the reaction, and the mixture was stirred at room temperature for 4 h. The reaction was quenched with 50 mL of water. The crude product was extracted with ethyl acetate and washed with brine. Removal of the solvent afforded the crude product as a brown solid (5.4 g). ¹H NMR and ¹³C NMR spectra were consistent with those previously reported. ¹⁶ ¹H NMR (CDCl₃, 500 MHz, 25 °C): δ 9.97 (s, 1H), 7.80 (d, J = 8.4 Hz, 2H), 7.62 (dd, J = 3.1, 1.8 Hz, 1H), 7.33 (s, 2H), 7.15 (dd, J = 3.8, 1.8 Hz, 1H), 6.40 (t, J = 3.4 Hz, 1H), 2.42 (s, 3H). The brown solid was dissolved in 30 mL of MeOH. Sodium borohydride (1.6 g, 2.0 equiv) was added in 3 portions over 10 min, and the resulting mixture was stirred for 2 h. To the reaction was added 20 mL of water and then 20 mL of ethyl acetate. The organic layer was separated, dried over Na₂SO₄, and evaporated to afford a brown solid. The crude product was purified by recrystallization in DCM/hexanes (white solid, 5.14 g, 97%). ¹H NMR and ¹³C NMR spectra were consistent with those previously reported. ¹⁶ ¹H NMR

(CDCl₃, 500 MHz, 25 °C): δ 7.71 (d, J = 8.6 Hz, 2H), 7.31 (d, J = 8.7 Hz, 2H), 7.28-7.25 (m, 1H), 6.25 (dd, J = 3.4, 1.9 Hz, 1H), 6.23 (t, J = 3.3 Hz, 1H), 4.60 (d, J = 5.7 Hz, 2H), 2.41 (s, 3H). *Synthesis of 3-methyl-2-((1-tosyl-pyrrol-2-yl)methyl)-1H-indole*

A 100 mL Schlenk flask was loaded with (1-tosyl-pyrrol-2-yl)methanol (502 mg, 1.0 equiv, 2 mmol), 3-methylindole (262 mg, 1.0 equiv, 2.0 equiv), InCl₃ (88.4 mg, 40 mol%), toluene (10 mL), and a stir bar. The reaction was heated in an oil bath at 75 °C for 12 h. After the removal of solvent, the product was purified by chromatography on silica gel (5% ethyl acetate in hexanes) to obtain the product as light brown solid (290 mg, 40%). H NMR (CDCl₃, 500 MHz, 25 °C): δ 7.70 (s, 1H), 7.47-7.44 (m, 1H), 7.40 (d, J = 8.6 Hz, 2H), 7.33 (dd, J = 3.4, 1.8 Hz, 1H), 7.11-7.04 (m, 3H), 6.97 (d, J = 7.9 Hz, 2H), 6.23 (t, J = 3.4 Hz, 1H), 6.05 (s, 1H), 2.24 (s, 3H), 2.21 (s, 3H). 13 C { 1 H} NMR (CDCl₃, 126 MHz, 25 °C): δ 144.90, 135.85, 135.22, 131.84, 130.71, 129.76, 129.26, 126.45, 123.31, 121.43, 119.10, 118.39, 114.68, 111.63, 110.48, 107.95, 24.50, 21.61, 8.52. LRMS (EI): calc'd: 364; found: 364.

Synthesis of 2-((1H-pyrrol-2-yl)methyl)-3-methylindole

In 100 mL round bottom flask, KOH (178 mg, 4.0 equiv) was dissolved in a mixture of methanol (20 mL) and THF (20 mL). Then, the reaction was charged with 3-methyl-2-((1-tosyl-

pyrrol-2-yl)methyl)indole (290 mg, 1.0 equiv) and heated at 70 °C for 4 h. After cooling the reaction to room temperature, ethyl acetate (20 mL) was added. The organic layer was washed with brine, then, separated, dried over Na₂SO₄, and evaporated to afford product as grey solid (mg, 67%). ¹H NMR (CDCl₃, 500 MHz, 25 °C): δ 7.85 (s, 1H), 7.69 (s, 1H), 7.52 (d, J = 7.5 Hz, 1H), 7.22 (d, J = 7.0 Hz, 1H), 7.16-7.08 (m, 2H), 6.70-6.63 (m, 1H), 6.18 (q, J = 2.9 Hz, 1H), 6.09 (s, 1H), 4.12 (s, 2H), 2.31 (s, 3H). ¹³C{¹H} NMR (CDCl₃, 126 MHz, 25 °C): δ 135.52, 131.58, 129.34, 128.36, 121.70, 119.34, 118.47, 117.56, 110.58, 108.75, 108.02, 106.83, 24.90, 8.62.

Synthesis of 2- $(2-(pyrrol-2-yl)propan-2-yl)indole (H_2pyr-C(CH_3)_2-ind)$

Method A: In a 25 mL Schlenk flask, 2-(indol-2-yl)propan-2-ol (556 mg, 1.0 equiv) was dissolved in an excess of pyrrole (3 mL). Slowly, BF₃·Et₂O (0.2 mL, 0.5 equiv) was added dropwise to the solution under a constant flow of N₂. The reaction rapidly turned purple. The mixture was allowed to stir at room temperature for 5 min. Heat was generated after the addition. The reaction was quenched by adding 20 mL of saturated sodium bicarbonate solution. The product was extracted by adding 20 mL of EtOAc. The organic layer was separated and dried over sodium sulfate. The excess pyrrole was removed under vacuum for 5-8 h. The crude product was purified by column chromatography (silica gel, hexanes:EtOAc 20:1) to afford the desired products. Removal of the solvent afforded the product as a colorless oil (487 mg, 69%). Method B: In a N₂ glovebox, 2-(indol-2-yl)propan-2-ol (556 mg, 1.0 equiv), pyrrole (5 mL), indium(III) chloride (126 mg, 0.2 equiv), and toluene (5 mL) were added to a 35 mL pressure tube. The pressure tube was sealed and removed from the glovebox. The reaction was heated at 70 °C for 12

h. The excess pyrrole was removed under vacuum for 5-8 h. The crude product was purified by column chromatography (silica gel, hexanes: EtOAc 20:1) to afford the desired products. Removal of the solvent afforded the product as a colorless oil (410 mg, 64%). 1 H NMR (CDCl₃, 500 MHz, 25 °C) δ 7.66 (s, 2H), 7.59 (d, J = 6.4 Hz, 1H), 7.18 (d, J = 7.8 Hz, 1H), 7.13 (td, J = 7.5, 1.4 Hz, 1H), 7.09 (td, J = 7.3, 1.3 Hz, 1H), 6.61 (q, J = 2.6 Hz, 1H), 6.44 (d, J = 2.3 Hz, 1H), 6.22-6.15 (m, 2H), 1.74 (s, 6H). 13 C{ 1 H} NMR (CDCl₃, 126 MHz, 25 °C): δ 146.10, 138.32, 136.12, 128.32, 121.76, 120.30, 119.88, 117.61, 110.76, 107.95, 104.19, 98.33, 35.96, 29.04. LRMS (EI): calc'd: 224, found: 224.

Synthesis of 2-(2-(5-methylpyrrol-2-yl)propan-2-yl)indole (H₂pyr^{2Me}-C(CH₃)₂-ind)

In a 25 mL Schlenk flask, 2-(indol-2-yl)propan-2-ol (300 mg, 1.0 equiv) was dissolved in an excess of 2-methylpyrrole (3 mL). Slowly, BF₃·Et₂O (0.1 mL, 0.5 equiv) was added dropwise to the solution under a constant flow of N₂. The reaction rapidly turned purple. The mixture was allowed to stir at room temperature for 5 min. Heat was generated after the addition. The reaction was quenched by adding 20 mL of saturated sodium bicarbonate solution. The product was extracted by adding 20 mL of EtOAc. The organic layer was separated and dried over sodium sulfate. The excess 2-methylpyrrole was removed under vacuum at 70 °C for 12 h. The crude product was purified by column chromatography (silica gel, hexanes: EtOAc 20:1) to afford the desired products. Removal of the solvent afforded the product as a colorless oil (290 mg, 71%). ¹H NMR (CDCl₃, 500 MHz, 25 °C) δ 7.79 (s, 1H), 7.58 (d, J = 7.8 Hz, 1H), 7.44 (s, 1H), 7.24 (d, J = 7.9 Hz, 1H), 7.17-7.05 (m, 2H), 6.42 (s, 1H), 6.03 (s, 1H), 5.80 (s, 1H), 2.15 (s, 3H), 1.73 (s,

6H). ¹³C{¹H} NMR (CDCl₃, 126 MHz, 25 °C): δ 136.87, 136.14, 128.42, 127.70, 121.71, 120.27, 119.84, 110.79, 105.48, 104.24, 98.05, 35.91, 29.02, 13.13. LRMS (EI): calc'd: 238, found: 238. *Synthesis of 2-(2-(5-(boropinacolate)pyrrol-2-yl)propan-2-yl)indole*

In a N_2 glovebox, [Ir(COD)(OMe)]₂ (88 mg, 0.01 equiv) and phenanthroline (241 mg, 0.1 equiv) was dissolved in THF (2 mL) in a 25 mL Schlenk flask, and the mixture was stirred for 5 min. Then, B_2pin_2 (1.7 g, 0.5 equiv) and 2-(2-(pyrrol-2-yl)propan-2-yl)indole (3.0 g, 1.0 equiv) were added together in THF (18 mL). The reaction was removed from the glovebox and heated in an oil bath at 80 °C for 15 h. The mixture was allowed to cool to room temperature, and THF was evaporated. The crude product was diluted with hexane (20 mL) and flush through a silica plug. Removal of solvent afforded the crude product as a light brown oil (mg, 87%). The product was used for the next step without further purification. 1 H NMR (CDCl₃, 500 MHz, 25 °C) δ 8.26 (s, 1H), 7.70 (s, 1H), 7.58 (d, J = 8.4 Hz, 1H), 7.23 (d, J = 7.9 Hz, 1H), 7.13 (td, J = 7.5, 1.4 Hz, 1H), 7.08 (td, J = 7.4, 1.3 Hz, 1H), 6.82-6.76 (m, 1H), 6.43 (d, J = 3.1 Hz, 1H), 6.26-6.22 (m, 1H), 1.76 (s, 6H), 1.27 (s, 12H). 13 C (1 H) NMR (CDCl₃, 126 MHz, 25 °C): δ 136.17, 128.38, 121.72, 120.45, 120.30, 119.87, 117.59, 110.76, 108.01, 106.49, 104.19, 98.29, 83.73, 36.13, 29.12, 24.85. LRMS (ED): calc d: 350, found: 350.

General Procedure B for 2-(2-(pyrrol-2-yl)propan-2-yl)indole Derivatives

In a glove box, tetrakis(triphenylphosphine)palladium(0) (10 mol%), potassium carbonate (2.0 equiv), 2-(2-(5-(boropinacolate)pyrrol-2-yl)propan-2-yl)indole (1.0 equiv), aryl iodide or aryl bromide (1.0 equiv), and 3 mL (per mmol of ind-pyr-Bpin starting material) of toluene were added in a 50 mL Schlenk tube. The reaction was then removed from the glovebox and charged with 1 mL of water under a constant flow of dry dinitrogen. Then, the Schlenk tube was sealed and heated in an oil bath at 110 °C for 12 h. The organic layer was diluted with EtOAc, separated, and dried over sodium sulfate. The crude product was purified by column chromatography on silica gel (hexane/ethyl acetate) to afford the pure product.

Synthesis of 2-(2-(5-phenylpyrrol-2-yl)propan-2-yl)indole (H₂pyr^{2-Ph}-C(CH₃)₂-ind)

General Procedure B was followed using (2-(2-(5-(boropinacolate)pyrrol-2-yl)propan-2yl)indole (1.0)1.0 equiv), iodobenzene (580 1.0 equiv), g, mg, tetrakis(triphenylphosphine)palladium(0) (328 mg, 4 mol%), potassium carbonate (784 mg, 2.0 equiv), dry toluene (5 mL), and water (2 mL). Removal of solvent afforded the product as a colorless oil (620 mg, 73%). H NMR (CDCl₃, 500 MHz, 25 °C): δ 7.98 (s, 1H), 7.83 (s, 1H), 7.60 (d, J = 8.3 Hz, 1H), 7.36 (d, J = 7.1 Hz, 2H), 7.33-7.28 (m, 2H), 7.26-7.22 (m, 1H), 7.18-7.13 (m, 2H), 7.26-7.22 (m,2H), 7.12 (dd, J = 5.0, 1.4 Hz, 1H), 7.11-7.07 (m, 1H), 6.48 (d, J = 1.2 Hz, 1H), 6.48-6.45 (m, 1H), 6.27-6.23 (m, 1H), 1.80 (s, 6H). ¹³C{¹H} NMR (CDCl₃, 126 MHz, 25 °C): δ 145.85, 139.40, 136.19, 132.56, 132.08, 128.93, 128.37, 126.28, 123.76, 121.84, 120.33, 119.93, 110.85, 106.30, 105.70, 98.44, 36.15, 29.12. LRMS (EI): calc'd: 300; found: 300.

Synthesis of 2-(2-(5-(p-tolyl)pyrrol-2-yl)propan-2-yl)indole (H₂pyr^{2-Tol}-C(CH₃)₂-ind)

General procedure B was followed using (2-(2-(5-(boropinacolate)pyrrol-2-yl)propan-2yl)indole (500 1.0 equiv), 4-iodotoluene (311)1.0 mg, mg, equiv), tetrakis(triphenylphosphine)palladium(0) (164 mg, 4 mol%), potassium carbonate (392 mg, 2.0 equiv), dry toluene (3 mL), water (1 mL). Removal of solvent afforded the product as a colorless oil (209 mg, 47%). H NMR (CDCl₃, 500 MHz, 25 °C): δ 7.93 (s, 1H), 7.83 (s, 1H), 7.59 (d, J = 7.7 Hz, 1H), 7.28-7.21 (m, 4H), 7.16-7.07 (m, 4H), 6.47 (s, 1H), 6.41 (s, 1H), 6.23 (s, 1H), 2.31 (s, 3H), 1.79 (s, 6H). ¹³C{¹H} NMR (CDCl₃, 126 MHz, 25 °C): δ 145.97, 138.95, 136.18, 136.02, 132.27, 129.83, 129.60, 128.38, 123.75, 121.81, 120.31, 119.91, 110.85, 106.17, 105.08, 98.37, 36.14, 29.15, 21.23. LRMS (EI): calc'd: 314; found: 314.

Synthesis of ethyl 5-(trifluoromethyl)indole-2-carboxylate

A 100 mL round bottom flask was charged with 5-(trifluoromethyl)indole-2-carboxylic acid (3 g), 50 mL of ethanol, and a stir bar. The reaction was refluxed overnight (\sim 12 h). After the reaction was cooled to room temperature, the reaction was poured into 100 mL cold water. The precipitates were filtered to afford the product as off-white solid (3.06 g, 91%). ¹H NMR (CDCl₃, 500 MHz, 25 °C): δ 9.12 (s, 1H), 8.01 (s, 1H), 7.58-7.49 (m, 2H), 7.30 (s, 1H), 4.44 (q, J = 7.2 Hz, 2H), 1.43

(t, J = 7.2 Hz, 3H). 13 C{ 1 H} NMR (CDCl₃, 126 MHz, 25 °C): δ 161.51, 137.72, 126.71, 121.85, 120.54, 112.33, 109.18, 61.43, 14.38. 19 F NMR (470 MHz, C₆C₆, 25 °C) δ -60.86.

Synthesis of 2-(5-(trifluoromethyl)indol-2-yl)propan-2-ol

A 250 mL Schlenk flask equipped with a stir bar was purged with dinitrogen and charged with ethyl 5-(trifluoromethyl)indole-2-carboxylate (1.4 g, 1.0 equiv) and dry THF (20 mL). The solution was cooled to –78 °C in a dry ice/acetone bath for 15 min. Methyllithium (3.1 M in DME, 8.8 mL, 5.0 equiv) was added dropwise over 15 min. The reaction was stirred at –78 °C for 2 h. Then, water (2 mL) was added dropwise to quench the reaction. The reaction mixture was allowed to warm up to room temperature. Ethyl acetate (50 mL) was added to extract the product. The organic layer was washed with brine (50 mL) and separated from the aqueous layer. The organic layer was separated, dried over Na₂SO₄, and evaporated to afford the product as light yellow solid (980 mg, 74%). ¹H NMR (CDCl₃, 500 MHz, 25 °C): δ 8.70 (s, 1H), 7.85 (s, 1H), 7.45-7.35 (m, 2H), 6.38 (s, 1H), 1.96 (s, 1H), 1.70 (s, 6H). ¹³C{¹H} NMR (CDCl₃, 126 MHz, 25 °C): δ 147.56, 136.88, 127.96, 122.23, 118.63, 118.21, 111.16, 97.91, 69.84, 30.96. ¹⁹F NMR (470 MHz, C₆C₆, 25 °C) δ –60.31.

Synthesis of 2-(2-(pyrrol-2-yl)propan-2-yl)-5-(trifluoromethyl)indole (H2pyr-C(CH3)2-ind^{3-CF3)}

In a 25 mL Schlenk flask, 2-(5-(trifluoromethyl)indol-2-yl)propan-2-ol (500 mg, 1.0 equiv) was dissolved in an excess of pyrrole (3 mL). Slowly, BF₃·Et₂O (0.1 mL, 0.4 equiv) was added dropwise to the solution under a constant flow of N₂. The reaction rapidly turned purple. The

mixture was allowed to stir at room temperature for 5 min. The reaction was quenched by adding 20 mL of saturated sodium bicarbonate solution. The product was extracted by adding EtOAc (20 mL). The organic layer was separated and dried over sodium sulfate. Excess pyrrole was removed under vacuum. The crude product was purified by column chromatography (silica gel, 30% ethyl acetate in hexanes). Removal of solvent afforded the product as a colorless oil (280 mg, 47%). 1 H NMR (CDCl₃, 500 MHz, 25 $^{\circ}$ C): δ 7.91 (s, 1H), 7.85 (s, 1H), 7.80 (s, 1H), 7.35 (dd, J = 8.6, 2.0 Hz, 1H), 7.27 (d, J = 8.6 Hz, 1H), 6.68 (q, J = 2.6 Hz, 1H), 6.50 (d, J = 1.3 Hz, 1H), 6.18 (t, J = 2.9 Hz, 2H), 1.76 (s, 6H). 13 C{ 1 H} NMR (CDCl₃, 126 MHz, 25 $^{\circ}$ C): δ 148.15, 137.60, 127.79, 122.19, 118.57, 117.94, 117.13, 110.91, 108.17, 107.96, 104.58, 103.79, 98.93, 36.04, 29.42, 28.92. 19 F NMR (470 MHz, C₆C₆, 25 $^{\circ}$ C) δ –60.14.

(4,6-difluoro-1H-indol-2-yl)methanol

In a 250 mL flask, LAH (1014 mg, 3.0 equiv) was added to 40 mL of dry THF under a constant flow of N_2 . A solution of ethyl 4,6-difluoro-indole-2-carboxylate (2.0 g, 1.0 equiv) in dry THF (15 mL) was added slowly. The reaction was stirred under room temperature for 1 h. The reaction was slowly quenched with 1 M HCl and extracted with ethyl acetate. The organic layer was washed with brine, separated, and dried over sodium sulfate. The evaporation of the solvent afford ed crude product as an off-white solid (916 mg, 56%). ¹H NMR (CDCl₃, 500 MHz, 25 °C): δ 8.45 (s, 1H), 6.86 (d, J = 8.8 Hz, 1H), 6.60 (td, J = 10.1, 2.0 Hz, 1H), 6.44 (s, 1H), 4.82 (s, 2H¹³C {¹H} NMR (CDCl₃, 126 MHz, 25 °C): δ 171.49, 129.90, 96.15, 92.51, 91.26, 89.73, 89.49, 55.45, 54.54, 17.03. ¹⁹F NMR (CDCl₃, 470 MHz, 25 °C): δ -122.26 (td, J = 9.5, 4.1 Hz), -122.84 (dt, J = 9.9, 3.3 Hz).

2-((1H-pyrrol-2-yl)methyl)-4,6-difluoro-1H-indole (H2pyr-CH2-ind^{4,6-diF})

In a 25 mL Schlenk flask, (4,6-difluoro-1H-indol-2-yl)methanol (900 mg, 1.0 equiv) was dissolved in an excess of pyrrole (3 mL). Slowly, BF₃·Et₂O (0.2 mL, 0.4 equiv) was added dropwise to the solution under a constant flow of N₂. The reaction rapidly turned purple. The mixture was allowed to stir at room temperature for 5 min. The reaction was quenched by adding 20 mL of saturated sodium bicarbonate solution. The product was extracted by adding EtOAc (20 mL). The organic layer was separated and dried over sodium sulfate. Excess pyrrole was removed under vacuum. The crude product was purified by column chromatography (silica gel, 5% ethyl acetate in hexanes). Removal of solvent afforded the product as a colorless oil (320 mg, 28%). 1 H NMR (C₆D₆, 500 MHz, 25 °C): δ 6.64 – 6.59 (m, 2H), 6.28 (d, J = 9.0 Hz, 1H), 6.24 (s, 1H), 6.21 – 6.19 (m, 1H), 6.18 (s, 1H), 5.95 (s, 1H), 3.38 (s, 2H). 13 C{ 1 H} NMR (C₆D₆, 126 MHz, 25 °C): δ 129.34, 127.05, 125.70, 117.76, 108.76, 107.34, 96.92, 95.60, 95.42, 95.37, 95.19, 93.98, 93.94, 93.77, 93.74, 26.69. 19 F NMR (470 MHz, C₆C₆, 25 °C): -119.39 (td, J = 9.1, 3.3 Hz), -119.52 (dt, J = 9.9, 3.3 Hz).

(5-methoxy-1H-indol-2-yl)methanol

In a 250 mL flask, LAH (1104 mg, 3.0 equiv) was added to 40 mL of dry THF under a constant flow of N₂. A solution of ethyl 5-methoxy-indole-2-carboxylate (2.12 g, 1.0 equiv) in dry THF (15 mL) was added slowly. The reaction was stirred under room temperature for 1 h. The reaction was slowly quenched with 1 M HCl and extracted with ethyl acetate. The organic layer was washed

with brine, separated, and dried over sodium sulfate. The evaporation of the solvent afford ed crude product as an off-white solid (820 mg, 46%). 1 H NMR (CDCl₃, 500 MHz, 25 $^{\circ}$ C): δ 8.26 (s, 1H), 7.22 (d, J = 8.7 Hz, 1H), 7.04 (d, J = 2.6 Hz, 1H), 6.84 (dd, J = 8.7, 2.4 Hz, 1H), 6.33 (s, 1H), 4.79 (s, 2H), 3.84 (s, 3H). 1 H NMR and 13 C NMR spectra were consistent with those previously reported. 2-((1H-pyrrol-2-yl)methyl)-5-methoxy-1H-indole

In a 25 mL Schlenk flask, (5-methoxy-1H-indol-2-yl)methanol (450 mg, 1.0 equiv) was dissolved in an excess of pyrrole (3 mL). Slowly, BF₃·Et₂O (0.12 mL, 0.4 equiv) was added dropwise to the solution under a constant flow of N₂. The reaction rapidly turned purple. The mixture was allowed to stir at room temperature for 5 min. The reaction was quenched by adding 20 mL of saturated sodium bicarbonate solution. The product was extracted by adding EtOAc (20 mL). The organic layer was separated and dried over sodium sulfate. Excess pyrrole was removed under vacuum. The crude product was purified by column chromatography (silica gel, 30% ethyl acetate in hexanes). Removal of solvent afforded the product as a colorless oil (387 mg, 67%). 1 H NMR (CDCl₃, 500 MHz, 25 °C): δ 7.94 (s, 1H), 7.75 (s, 1H), 7.14 (d, J = 8.8 Hz, 1H), 7.03 (d, J = 2.4 Hz, 1H), 6.79 (dd, J = 8.7, 2.5 Hz, 1H), 6.73 – 6.65 (m, 1H), 6.28 (s, 1H), 6.18 (q, J = 2.8 Hz, 1H), 6.11 (s, 1H), 4.13 (s, 2H), 3.84 (s, 3H). 13 C (1 H) NMR (CDCl₃, 126 MHz, 25 °C): δ 154.24, 128.34, 117.58, 111.46, 111.29, 108.52, 106.81, 102.12, 100.66, 55.88, 27.15.

(5-methoxy-3-methyl-1H-indol-2-yl)methanol

In a 250 mL flask, LAH (770 mg, 5.0 equiv) was added to 40 mL of dry THF under a constant flow of N_2 . A solution of ethyl 3-formyl-5-methoxy-1H-indole-2-carboxylate (1.0 g, 1.0 equiv) in dry THF (10 mL) was added slowly. The reaction was stirred at 40°C for 12 h. After the reaction cooled to room temperature, the reaction was slowly quenched with 1 M HCl and extracted with ethyl acetate. The organic layer was washed with brine, separated, and dried over sodium sulfate. The evaporation of the solvent afforded crude product as a light yellow solid (710 mg, 92%). Note: the product decomposes in chloroform. 1 H NMR (CDCl₃, 500 MHz, 25 °C): δ 8.06 (s, 1H), 7.20 (d, J = 8.7 Hz, 1H), 6.97 (d, J = 2.6 Hz, 1H), 6.84 (dd, J = 8.7, 2.5 Hz, 1H), 4.79 (s, 2H), 3.87 (s, 3H), 2.25 (s, 3H). 13 C{ 1 H} NMR (CDCl₃, 126 MHz, 25 °C): δ 154.03, 133.90, 130.88, 129.33, 112.44, 111.65, 108.38, 100.90, 56.82, 56.06, 8.58.

2-((1H-pyrrol-2-yl)methyl)-5-methoxy-3-methyl-1H-indole

In a 25 mL Schlenk flask, (5-methoxy-3-methyl-1H-indol-2-yl)methanol (450 mg, 1.0 equiv) was dissolved in an excess of pyrrole (3 mL). Slowly, BF₃·Et₂O (0.12 mL, 0.4 equiv) was added dropwise to the solution under a constant flow of N₂. The reaction rapidly turned purple. The mixture was allowed to stir at room temperature for 5 min. The reaction was quenched by adding 20 mL of saturated sodium bicarbonate solution. The product was extracted by adding EtOAc (20 mL). The organic layer was separated and dried over sodium sulfate. Excess pyrrole was removed under vacuum. The crude product was purified by column chromatography (silica gel, 30% ethyl acetate in hexanes). Removal of solvent afforded the product as a colorless oil (460 mg, 81%). 1 H NMR (DMSO-d₆, 500 MHz, 25 °C): δ 10.52 (s, 1H), 10.40 (s, 1H), 7.13 (d, J = 8.6 Hz, 1H), 6.87 (d, J = 2.4 Hz, 1H), 6.63 (dd, J = 8.7, 2.4 Hz, 1H), 6.60 – 6.55 (m, 1H), 5.88 (q, J = 2.8 Hz, 1H),

5.73 (s, 1H), 3.94 (s, 2H), 3.74 (s, 3H), 2.15 (s, 3H). ¹³C{¹H} NMR (DMSO-d₆, 126 MHz, 25 °C): δ 152.88, 134.22, 130.31, 129.05, 128.91, 116.42, 111.17, 109.93, 107.28, 105.31, 105.08, 99.88, 55.33, 24.44, 8.42. LRMS (EI): calc'd: 240; found: 240.

Synthesis of Titanium Catalysts

General Procedure C for Titanium complexes

In a 20 mL scintillation vial, a stir bar was loaded with Ti(NMe₂)₄ (1.1 equiv.) and ether (5 mL) in an N₂ glovebox. A separate 20 mL scintillation vial was loaded with protic free ligand (1.0 equiv.) and ether (5 mL). Then the solution of ligand was added dropwise to a vigorously stirred solution of Ti(NMe₂)₄ over 15 min. The reaction mixture was stirred at room temperature for 12 h. The volatiles were removed *in vacuo* to give a viscous orange/yellow oil. This oil was taken up by adding toluene (2 mL), followed by layering 2 mL of n-hexane. Standing in a –30 °C freezer overnight generally afforded orange crystals.

Synthesis of $Ti(NMe_2)_2(pyr^{3,5-diMePh}-C(CH_3)_2-pyr)$ (5a)

General procedure C was followed using $H_2dpm^{2-(3,5-diMePh)}$ (362 mg, 1.0 equiv), $Ti(NMe_2)_4$ (292 mg, 1.0 equiv), and dry diethyl ether (3 mL). Recrystallization from ether/n-hexane afforded the product as orange crystals (300 mg, 56%). M.p.: 157-159 °C. 1H NMR (C_6D_6 , 500 MHz, 25 °C): δ 7.51 (s, 2H), 7.06 (dd, J = 2.6, 1.3 Hz, 1H), 6.71 (s, 1H), 6.67 (d, J = 2.7 Hz, 1H), 6.58-6.55 (m, 1H), 6.51 (d, J = 2.7 Hz, 1H), 6.25 (dd, J = 3.1, 1.2 Hz, 1H), 2.80 (s, 12H), 2.13 (s, 6H), 1.89 (s, 6H)... $^{13}C\{^1H\}$ NMR (C_6D_6 , 126 MHz, 25 °C): δ 163.14, 161.72, 141.57, 137.63, 133.67, 129.98,

129.33, 128.57, 125.71, 124.22, 123.62, 115.14, 112.43, 107.88, 101.79, 47.11, 40.12, 30.10, 21.30. Elemental Analysis: Calc'd. C: 66.99; H: 7.82; N: 13.59. Found: C: 66.90; H: 7.92; N: 13.30. *Synthesis of Ti(NMe₂)₂(pyr^{3,5-CF3Ph}-C(CH₃)₂-pyr) (5b)*

General Procedure C was followed using $H_2dpm^{2-(3,5-diCF3Ph)}$ (100 mg, 1.0 equiv), $Ti(NMe_2)_4$ (58 mg, 1.0 equiv), and dry diethyl ether (2 mL). Recrystallization from ether/n-hexane afforded product as orange crystals (60 mg, 45%). M.p.: 143-144 °C. 1H NMR (C_6D_6 , 500 MHz, 25 °C): δ 8.09 (s, 2H), 7.64 (s, 1H), 6.88 (dd, J = 2.3, 1.3 Hz, 1H), 6.37 (s, 2H), 6.31 (dd, J = 3.1, 2.3 Hz, 1H), 6.17 (dd, J = 3.0, 1.3 Hz, 1H), 2.58 (s, 12H), 1.78 (s, 6H). $^{13}C\{^1H\}$ NMR (C_6D_6 , 126 MHz, 25 °C): δ 164.43, 161.08, 137.53, 136.91, 131.78, 131.51, 125.70, 125.25, 120.28, 113.33, 112.74, 109.61, 104.61, 46.81, 39.97, 29.89. ^{19}F NMR (C_6D_6 , 470 MHz, 25 °C) δ -62.58.

Synthesis of $Ti(NMe_2)_2(pyr-CH_2-ind^{3-Me})$ (6a)

25 °C): δ 155.79, 153.42, 143.92, 130.36, 129.33, 120.52, 119.60, 117.14, 116.76, 116.29, 115.31, 105.99, 47.39, 44.06, 29.16, 9.24.

Synthesis of $Ti(NMe_2)_2(pyr-C(CH_3)_2-ind)$ (6b)

General Procedure C was followed using H_2 pyr-C(CH₃)₂-ind (400 mg, 1.0 equiv), Ti(NMe₂)₄ (400 mg, 1.0 equiv), and dry diethyl ether (8 mL). Recrystallization from ether/n-hexane afforded product as orange crystals (440 mg, 69%). M.p.: 99-100 °C. ¹H NMR (C₆D₆, 500 MHz, 25 °C): δ 7.77 (d, J = 8.6 Hz, 1H), 7.59 (d, J = 8.9 Hz, 1H), 7.42-7.36 (m, 1H), 7.32 (t, J = 7.9 Hz, 1H), 6.93 (s, 1H), 6.34 (dd, J = 2.7, 1.3 Hz, 1H), 6.32 (s, 1H), 5.89 (s, 1H), 2.93 (s, 12H), 1.83 (s, 6H). δ 13C {¹H} NMR (C₆D₆, 126 MHz, 25 °C): δ 169.77, 162.08, 143.55, 130.25, 128.50, 120.43, 119.94, 119.30, 115.72, 115.37, 114.63, 97.49, 47.29, 40.06, 29.87.

Synthesis of complex $Ti(NMe_2)_2(pyr^{2-Me}-C(CH_3)_2-ind)$ (6c)

General Procedure C was followed using H_2pyr^{2Me} -C(CH₃)₂-ind (266 mg, 1.0 equiv), $Ti(NMe_2)_4$ (250 mg, 1.0 equiv), and dry diethyl ether (6 mL). Recrystallization from ether/n-hexane afforded product as orange crystals (324 mg, 78%). M.p.: 117-119 °C. 1H NMR (C₆D₆, 500 MHz, 25 °C): δ 7.79 (d, J = 7.6 Hz, 1H), 7.59 (d, J = 8.9 Hz, 1H), 7.37 (td, J = 7.6, 1.5 Hz, 1H), 7.32 (td, J = 7.4, 1.2 Hz, 1H), 6.34 (d, J = 2.4 Hz, 1H), 6.33 (s, 1H), 5.88 (s, 1H), 2.94 (s, 12H), 2.06 (s, 3H), 1.83 (s, 6H). $^{13}C\{^1H\}$ NMR (C₆D₆, 126 MHz, 25 °C): δ 169.81, 159.78, 143.16,

141.67, 130.50, 120.27, 119.86, 119.41, 115.59, 115.03, 114.25, 97.34, 46.95, 39.99, 29.89, 15.43. Elemental Analysis: Calc'd. C: 64.52; H: 7.58; N: 15.05. Found: C: 64.01; H: 7.50; N: 14.58. *Synthesis of Ti(NMe₂)₂(pyr^{2-Ph}-C(CH₃)₂-ind) (6e)*

General Procedure C was followed using H_2pyr^{2-Ph} -C(CH₃)₂-ind (300 mg, 1.0 equiv), $Ti(NMe_2)_4$ (224 mg, 1.0 equiv), and dry diethyl ether (6 mL). Recrystallization from ether/n-hexane afforded product as orange crystals (321 mg, 74%). ¹H NMR (C₆D₆, 500 MHz, 25 °C): δ 7.79 (d, J = 9.0 Hz, 1H), 7.70 (d, J = 8.1 Hz, 2H), 7.55 (d, J = 7.2 Hz, 1H), 7.36-7.27 (m, 2H), 7.09 (t, J = 7.6 Hz, 2H), 7.01 (t, J = 7.4 Hz, 1H), 6.48 (s, 2H), 6.37 (s, 1H), 2.75 (s, 12H), 1.88 (s, 6H). ¹³C{¹H} NMR (C₆D₆, 126 MHz, 25 °C): δ 169.39, 160.80, 142.10, 130.41, 125.94, 120.37, 119.91, 119.34, 115.67, 111.30, 97.46, 46.79, 29.91.

Synthesis of $Ti(NMe_2)_2(pyr^{2-tol}-C(CH_3)_2-ind)$ (6d)

General Procedure C was followed using H_2pyr^{2-tol} -C(CH₃)₂-ind (100 mg, 1.0 equiv), $Ti(NMe_2)_4$ (72 mg, 1.0 equiv), and dry diethyl ether (2 mL). Recrystallization from ether/n-hexane afforded product as orange crystals (50 mg, 35%). M.p.: 135-138 °C. ¹H NMR (C₆D₆, 500 MHz, 25 °C): δ 7.79 (d, J = 9.0 Hz, 1H), 7.68 (d, J = 8.2 Hz, 2H), 7.57 (d, J = 8.9 Hz, 1H), 7.37-7.27 (m, 2H), 6.96 (d, J = 8.2 Hz, 2H), 6.49 (s, 2H), 6.38 (s, 1H), 2.78 (s, 12H), 2.07 (s, 3H), 1.89 (s, 6H).

¹³C {¹H} NMR (C₆D₆, 126 MHz, 25 °C): δ 169.44, 160.57, 143.16, 142.56, 137.99, 131.23, 130.44, 129.06, 125.99, 120.35, 119.87, 119.34, 115.70, 115.67, 110.86, 97.44, 46.82, 40.20, 29.94, 21.23. *Synthesis of Ti(NMe₂)₂(pyr-C(CH₃)₂-ind^{3-CF3}) (7c)*

General Procedure C was followed using H_2 pyr-C(CH₃)₂-ind^{5-CF3} (260 mg, 1.0 equiv), $Ti(NMe_2)_4$ (200 mg, 1.0 equiv), and dry diethyl ether (2 mL). Recrystallization from ether/n-hexane afforded product as orange crystals (170 mg, 49%). ¹H NMR (C₆D₆, 500 MHz, 25 °C): δ 8.05 (s, 1H), 7.59 (dd, J = 8.5, 1.4 Hz, 1H), 7.41 (d, J = 8.6 Hz, 1H), 6.88 (t, J = 1.3 Hz, 1H), 6.30 (dd, J = 2.7, 1.3 Hz, 1H), 6.21 (s, 1H), 5.87 (dd, J = 2.8, 1.4 Hz, 1H), 2.86 (s, 12H), 1.75 (s, 6H).. ¹³C{¹H} NMR (C₆D₆, 126 MHz, 25 °C): δ 171.03, 161.48, 144.27, 129.97, 129.37, 128.36, 125.66, 121.40, 121.15, 116.52, 115.75, 114.68, 97.73, 46.81, 39.69, 29.27. ¹⁹F NMR (470 MHz, C₆C₆, 25 °C) δ –59.24.

Synthesis of $Ti(NMe_2)_2(pyr-CH_2-ind^{4,6-diF})$ (7**b**)

General Procedure C was followed using H_2 pyr- CH_2 -ind^{4,6-diF} (300 mg, 1.0 equiv), $Ti(NMe_2)_4$ (289 mg, 1.0 equiv), and dry diethyl ether (5 mL). Recrystallization from ether/n-hexane afforded product as orange crystals (140 mg, 30%). ¹H NMR (C_6D_6 , 500 MHz, 25 °C): δ 7.07 (dd, J = 10.3, 1.2 Hz, 1H), 6.84-6.77 (m, 2H), 6.45 (d, J = 1.0 Hz, 1H), 5.96 (dd, J = 2.6, 1.3 Hz, 1H), 5.76 (dd, J = 2.7, 1.5 Hz, 1H), 3.90 (s, 2H), 2.82 (s, 12H). ¹³ $C\{^1H\}$ NMR (C_6D_6 , 126 MHz, 25 °C): δ 128.33,

116.93, 116.44, 97.52, 94.46, 94.23, 94.12, 46.74, 29.84, 13.89. 19 F NMR (470 MHz, C₆C₆, 25 $^{\circ}$ C) δ –121.18 (dd, J = 10.0, 2.6 Hz), –122.60 (td, J = 10.2, 2.7 Hz).

Synthesis of $Ti(NMe_2)_2(pyr-CH_2-ind^{5-OMe})$ (7a)

General Procedure C was followed using H_2 pyr- CH_2 -ind^{5-OMe} (380 mg, 1.0 equiv), $Ti(NMe_2)_4$ (380 mg, 1.0 equiv), and dry diethyl ether (5 mL). Recrystallization from ether/n-hexane afforded product as orange crystals (290 mg, 46%). ¹H NMR (C_6D_6 , 500 MHz, 25 °C): δ 7.46 (d, J = 8.6 Hz, 1H), 7.21 (d, J = 2.5 Hz, 1H), 7.16 (d, J = 2.5 Hz, 1H), 6.92 (t, J = 1.5 Hz, 1H), 6.35 (d, J = 1.0 Hz, 1H), 6.09 (dd, J = 2.7, 1.3 Hz, 1H), 5.89 (dd, J = 2.6, 1.5 Hz, 1H), 4.15 (s, 2H), 3.62 (s, 3H), 2.95 (s, 12H). ¹³ $C\{^{1}H\}$ NMR (C_6D_6 , 126 MHz, 25 °C): δ 160.25, 155.24, 153.20, 139.69, 131.19, 129.34, 125.70, 116.60, 116.16, 115.95, 110.09, 101.28, 99.02, 55.46, 47.26, 30.71. *Synthesis of Ti(NMe₂)₂(pyr-CH₂-ind^{3-Me-5-OMe})*

General Procedure C was followed using H₂pyr-CH₂-ind^{3-Me-5-OMe} (400 mg, 1.0 equiv), Ti(NMe₂)₄ (390 mg, 1.0 equiv), and dry diethyl ether (5 mL). Recrystallization from ether/n-hexane afforded product as orange crystals (217 mg, 35%). ¹H NMR (C₆D₆, 500 MHz, 25 °C δ 7.50 (d, J = 8.2 Hz, 1H), 7.18 (d, J = 8.2 Hz, 2H), 6.96 (s, 1H), 6.13 (s, 1H), 5.91 (s, 1H), 4.02 (s, 2H), 3.67 (s, 3H), 2.99 (s, 13H), 2.22 (s, 3H¹³C{¹H} NMR (C₆D₆, 126 MHz, 25 °C): δ 156.96,

155.14, 153.43, 139.26, 130.61, 128.42, 116.66, 116.19, 115.93, 109.94, 105.93, 99.56, 55.52, 47.42, 29.31, 9.36.

General procedure for kinetics

The procedure from the previous study was followed. All manipulations were conducted in an N₂ glovebox. A 2 mL volumetric flask was loaded the catalyst (10 mol%, 0.1 mmol) and ferrocene (56 mg, 0.3 mmol). Toluene-d₈ (~0.75 mL) was added to the volumetric flask, and the solids were dissolved by swirling the flask. Next, aniline (911 μ L, 10 mmol) and 1-phenylpropyne (125 μ L, 1.0 mmol) were added to the volumetric flask. Lastly, the solution was diluted to 2 mL with toluene-d₈. The solution was mixed via a pipette (i.e., the solution was drawn up into the pipette and dispensed back into the volumetric flask) five times to ensure the solution was well-mixed. The solution (~0.75 mL) was loaded into a threaded J. Young tube that was sealed with a Teflon stopper. The tube was removed from the dry box and was heated at 75 °C in the NMR spectrometer (Varian Inova 600). The relative 1-phenylpropyne versus ferrocene concentration was monitored as a function of time. The fits are to the exponential decay of the starting material using the scientific graphing program Origin. The expression used to fit the data was $Y_t = Y_{\infty} + (Y_0 - Y_{\infty})e^{-k_{Obs}t}$, where Y = concentration at time t (Y_t), infinity (Y_∞), or at the start of the reaction (Y_O).²⁴

Labeling Experiment

Me Me NTI::::NMe₂
$$A5 \, ^{\circ}\text{C}, \, \text{C}_6\text{D}_6, \, 2 \, \text{h}$$
 $C \, \text{Me}_2 \, \text{H/D}$ $C \, \text{Me}_2 \, \text{H/D}$

In a glass vial, titanium catalyst (10 mg, 1.0 equiv) was dissolved in 0.75 mL of C₆D₆. To the solution, aniline-d₈ (2.5 μL, 0.5 equiv) was added via a volumetric syringe. The solution was transferred to a threaded J. Young tube with a Teflon stopper. The tube was removed from the dry box and was heated at 45 °C in an oil bath. After 2 h, the tube was removed from heat, and the reaction was quenched with 0.05 mL of MeOD-d₄. The dark orange solution became colorless immediately. The NMR of the resulting solution was taken.

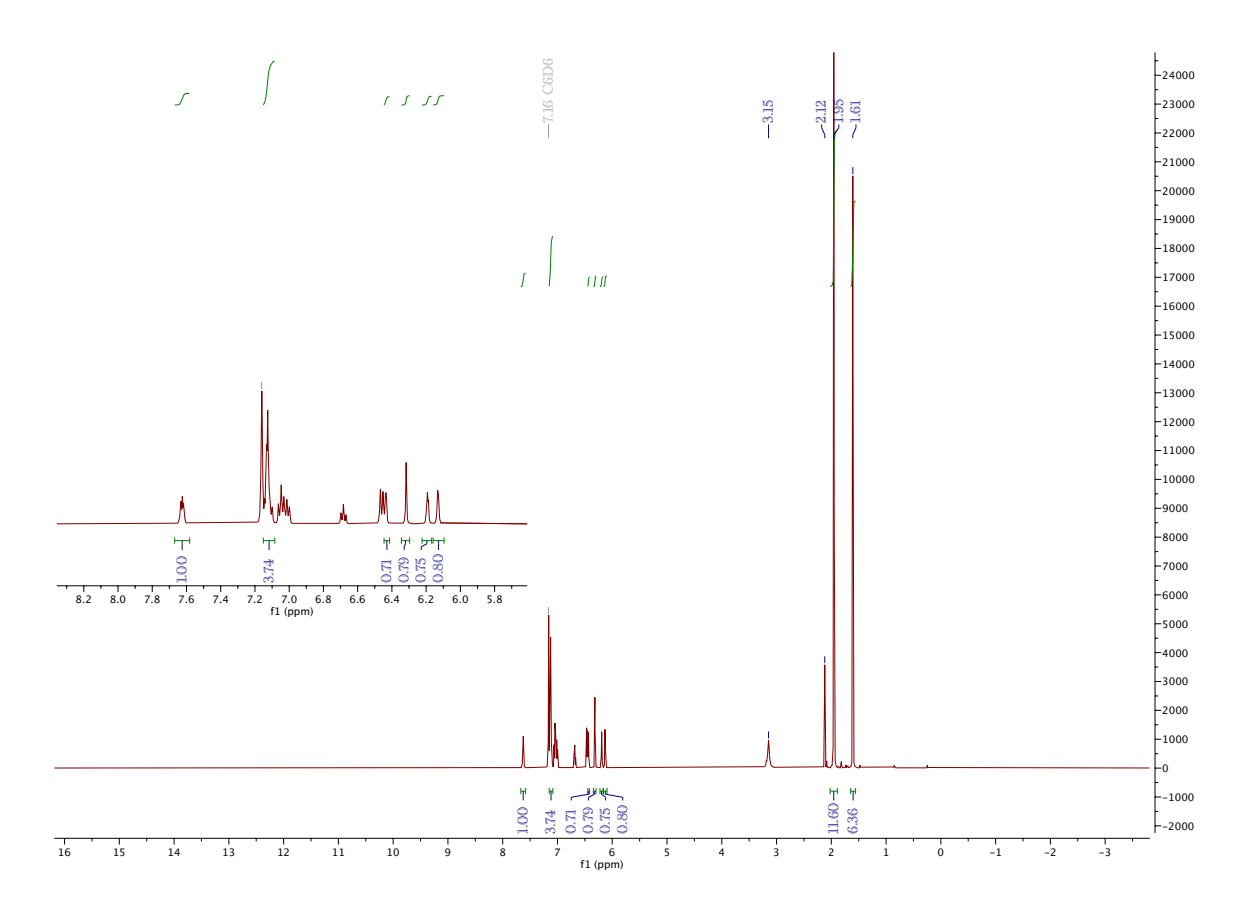


Figure 5.12. ¹H NMR of the protonated ligand from a reaction between **6b** and aniline.

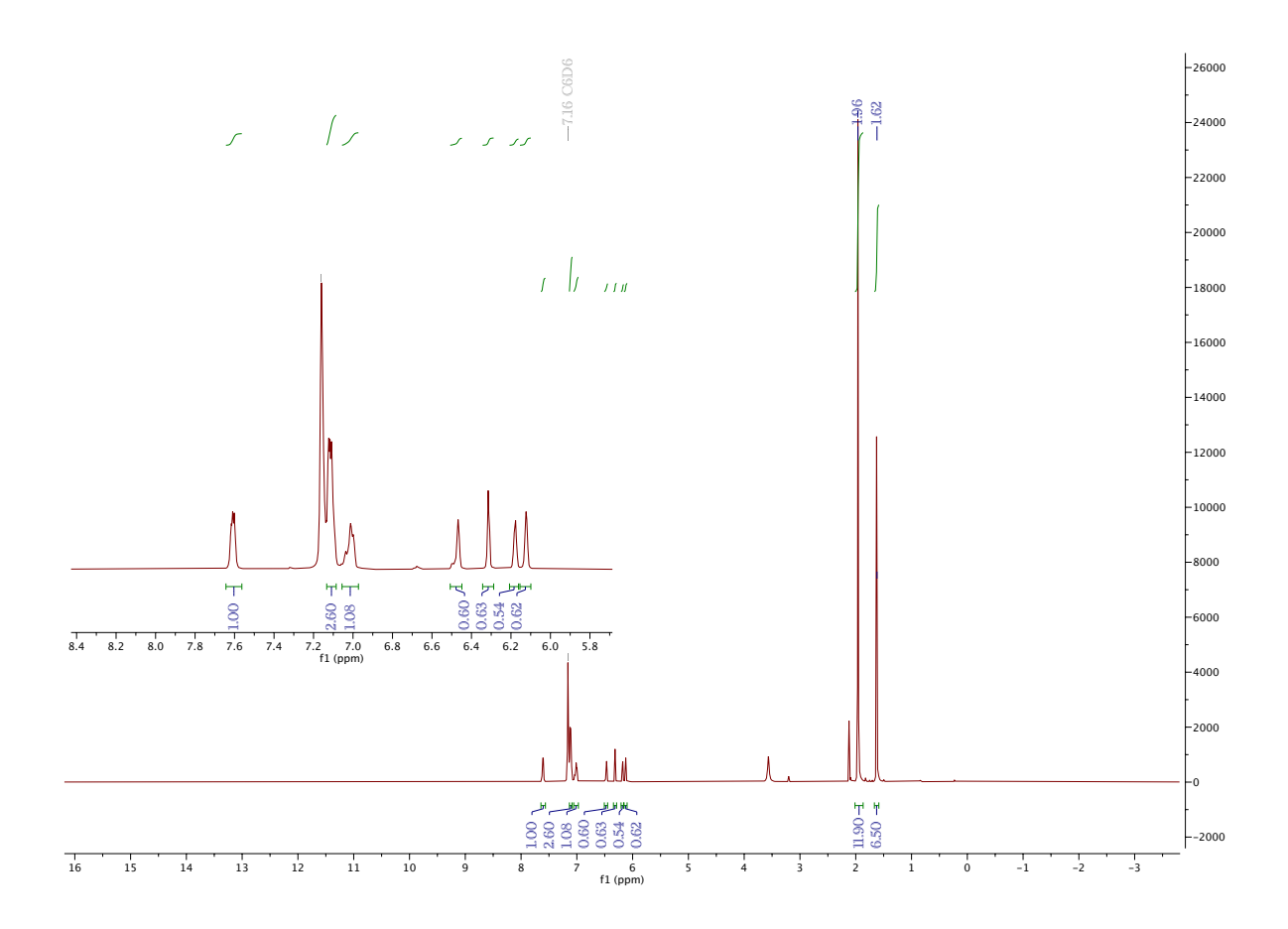


Figure 5.13. ¹H NMR of the deuterated ligand from a reaction between **6b** and aniline-d₈.

$$\begin{array}{c} \text{Me} \\ \text{Me} \\ \text{NMe}_{2} \end{array} \begin{array}{c} \text{4.0 equiv} \\ \text{4.0 equiv} \end{array} \begin{array}{c} \text{ND}_{2} \\ \text{4.0 equiv} \\ \text{NMe}_{2} \end{array} \begin{array}{c} \text{4.0 equiv} \\ \text{45 °C, C}_{6}D_{6}, 3 \text{ h} \\ \text{It} \end{array} \begin{array}{c} \text{D/H} \\ \text{D/H} \end{array} \begin{array}{c} \text{DN} \\ \text{Me}_{2} \\ \text{H/D} \end{array}$$

In a glass vial, titanium catalyst (10 mg, 1.0 equiv) was dissolved in 0.75 mL of C_6D_6 . To the solution, aniline- d_8 (10 μ L, 4.0 equiv) was added via a volumetric syringe. The solution was transferred to a threaded J. Young tube with a Teflon stopper. The tube was removed from the dry box and was heated at 45 °C in an oil bath. After 2 h, the tube was removed from heat, and the reaction was quenched with 0.05 mL of MeOD- d_4 . The dark orange solution became colorless immediately. The NMR spectrum of the resulting solution was taken.

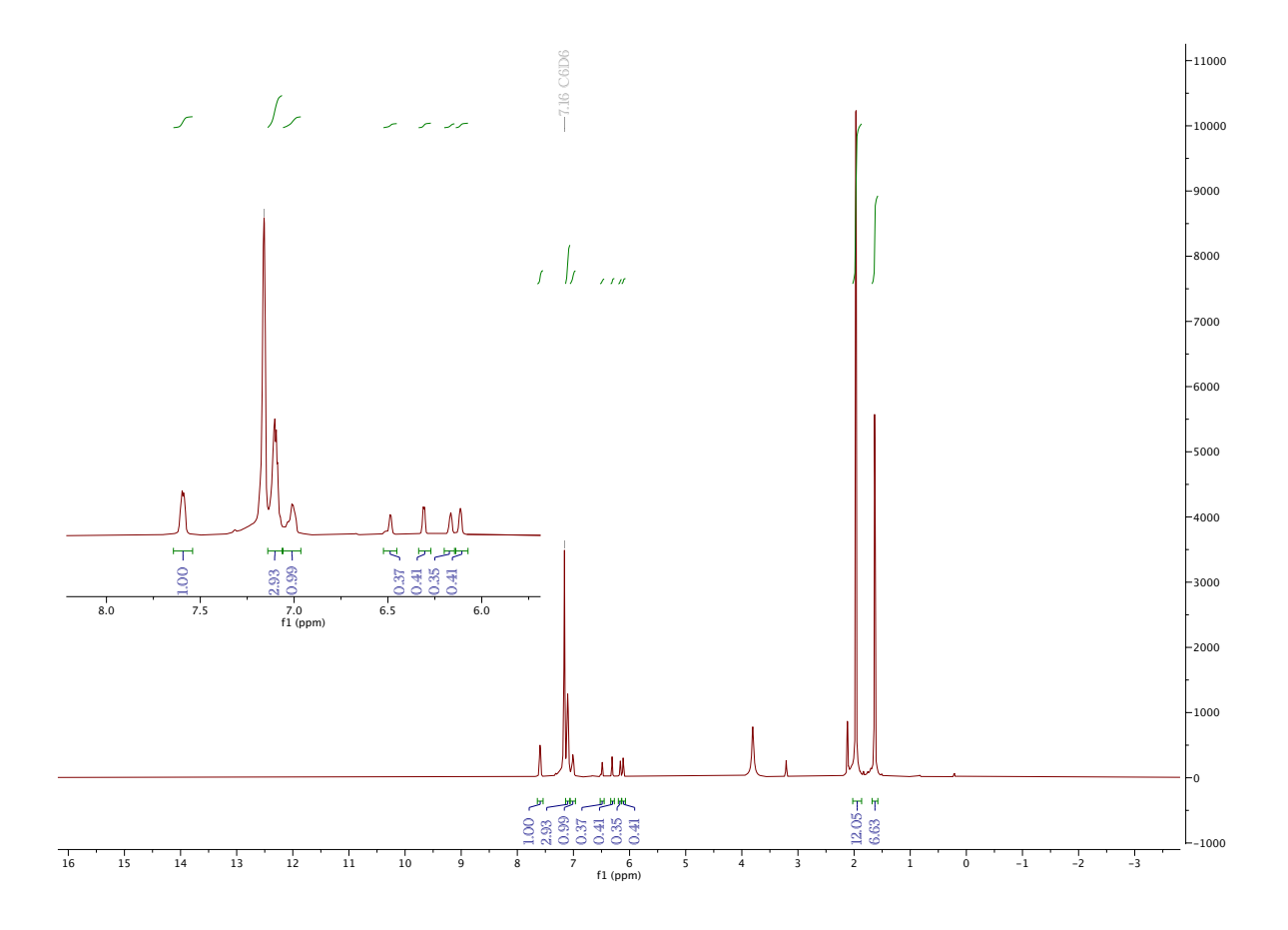


Figure 5.14. ¹H NMR of the deuterated ligand from a reaction between **6b** and aniline-d₈ (excess).

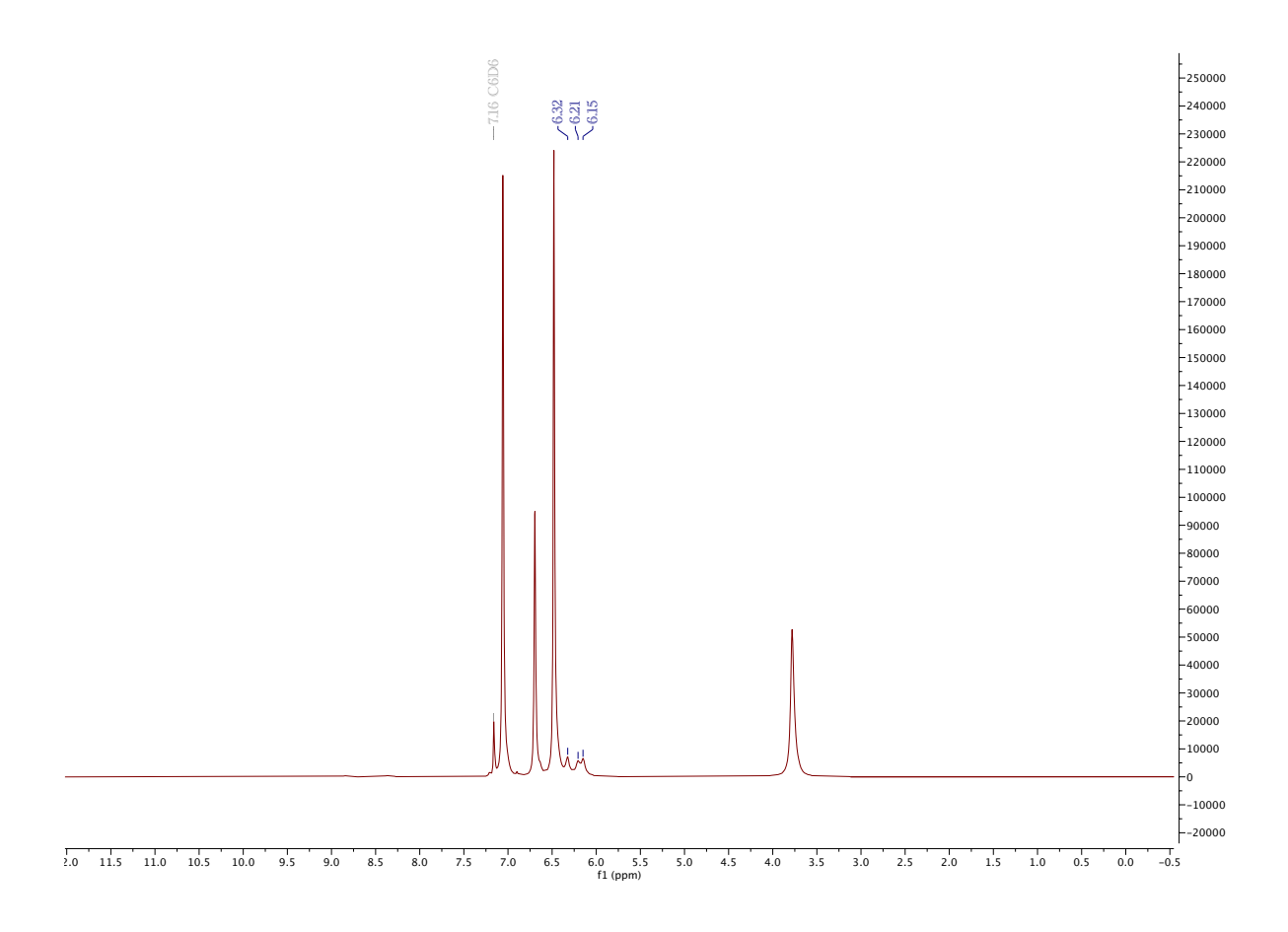


Figure 5.15. ²H NMR of the deuterated ligand from a reaction between **6b** and aniline-d₈.

$$\begin{array}{c} \text{Me} \\ \text{Me} \\ \text{N} \\ \text{Ti} \\ \text{NMe}_2 \end{array} \xrightarrow{\text{xs CD}_3\text{OD}} \begin{array}{c} \text{ND DN} \\ \text{rt} \\ \end{array}$$

In a glass vial, titanium catalyst (10 mg, 1.0 equiv) was dissolved in 0.75 mL of C_6D_6 . To the solution, aniline- d_8 (10 μ L, 4.0 equiv) was added via a volumetric syringe. The solution was transferred to an NMR tube. The tube was removed from the dry box, and the reaction was quenched with 0.05 mL of MeOD- d_4 . The yellow solution became colorless immediately. The NMR of the resulting solution was taken.

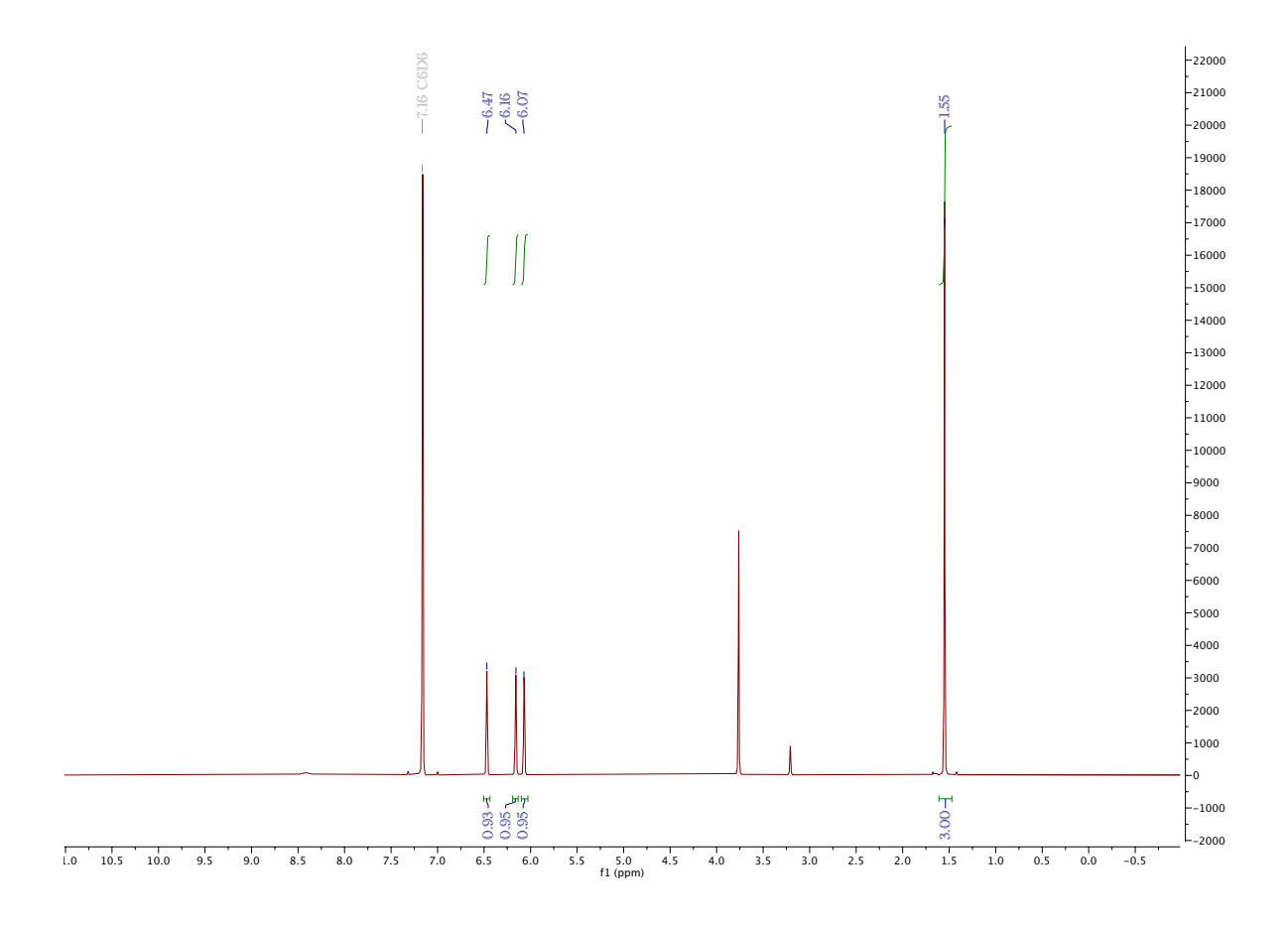


Figure 5.16. ¹H NMR of the H₂dpm ligand from a reaction between Ti(dpm)(NMe₂)₂ and MeOD-d₄.

APPENDICES

APPENDIX A

NMR Spectra (Pyridines)

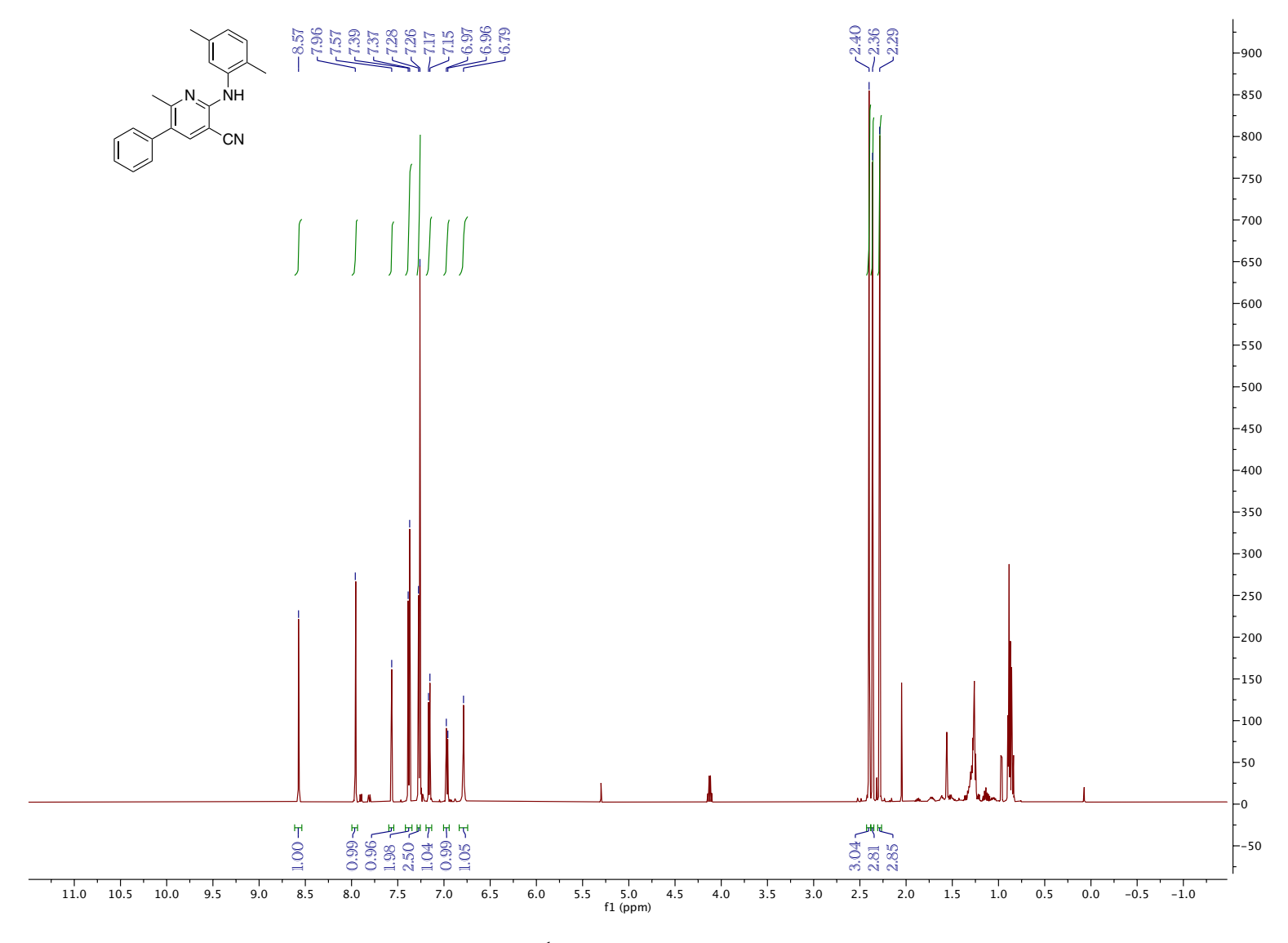


Figure 5.17. ¹H NMR (CDCl₃, 500 MHz, 25 °C)

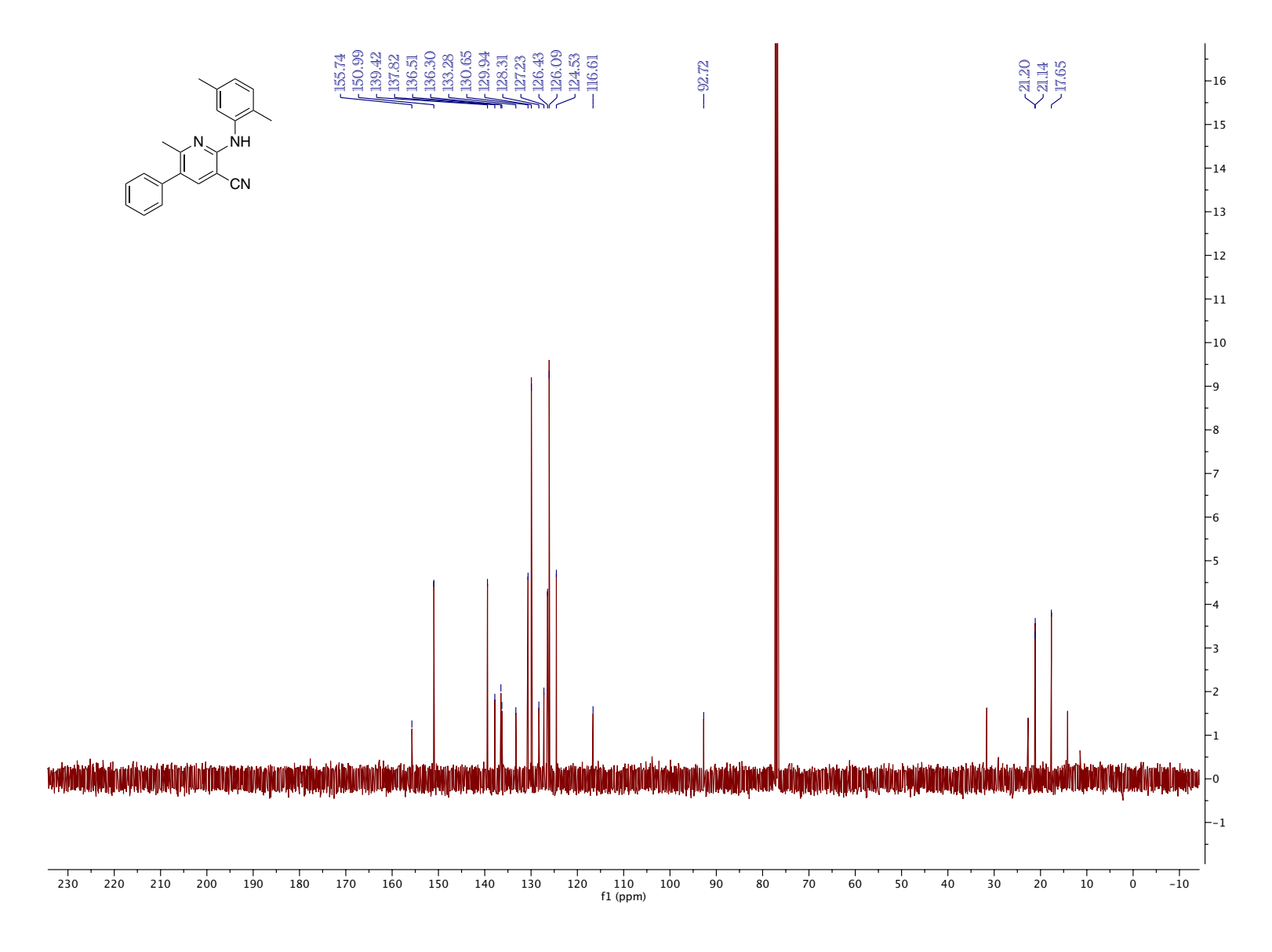


Figure 5.18. ¹³C NMR (CDCl₃, 126 MHz, 25 °C)

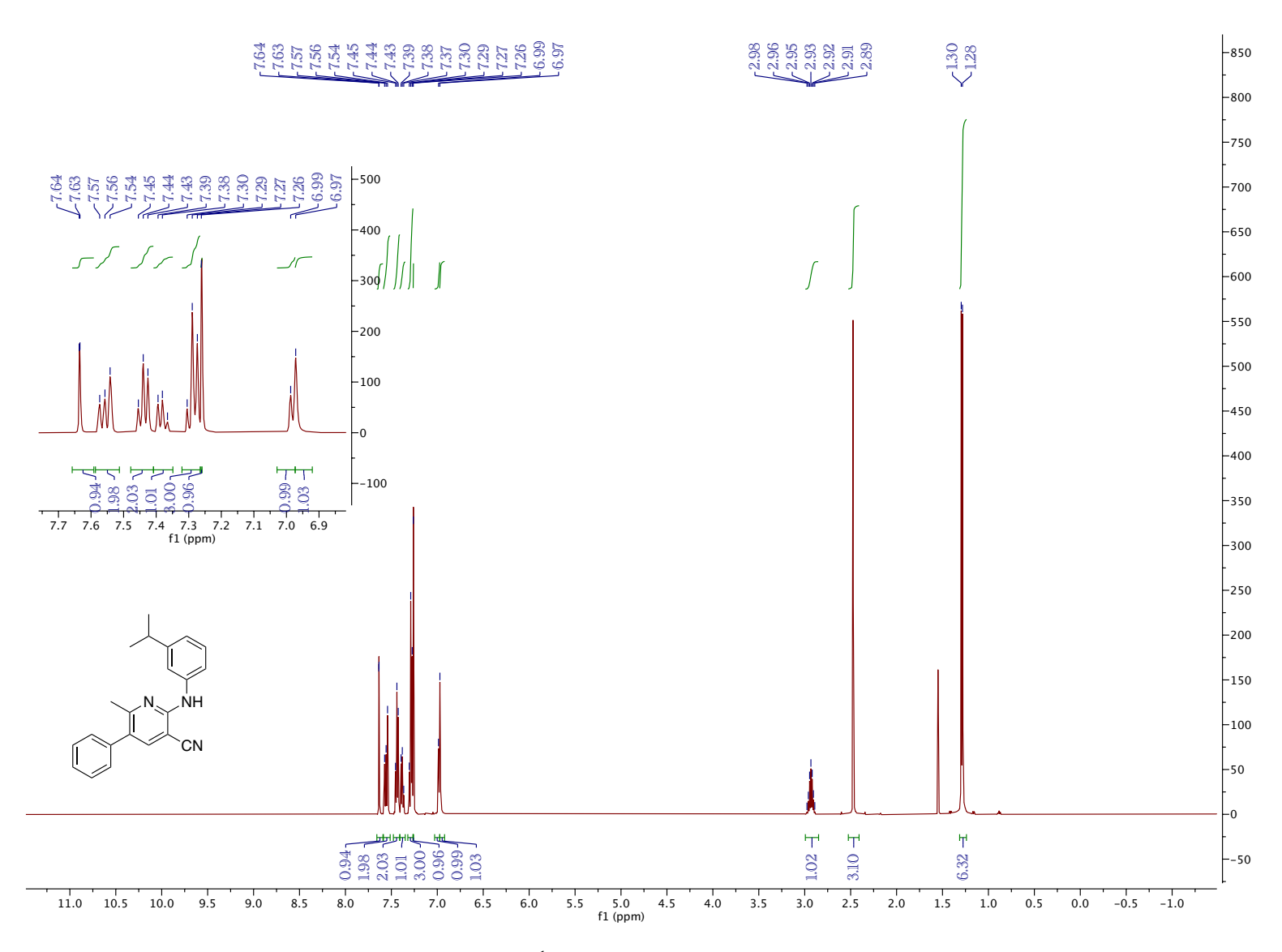


Figure 5.19. ¹H NMR (CDCl₃, 500 MHz, 25 °C)

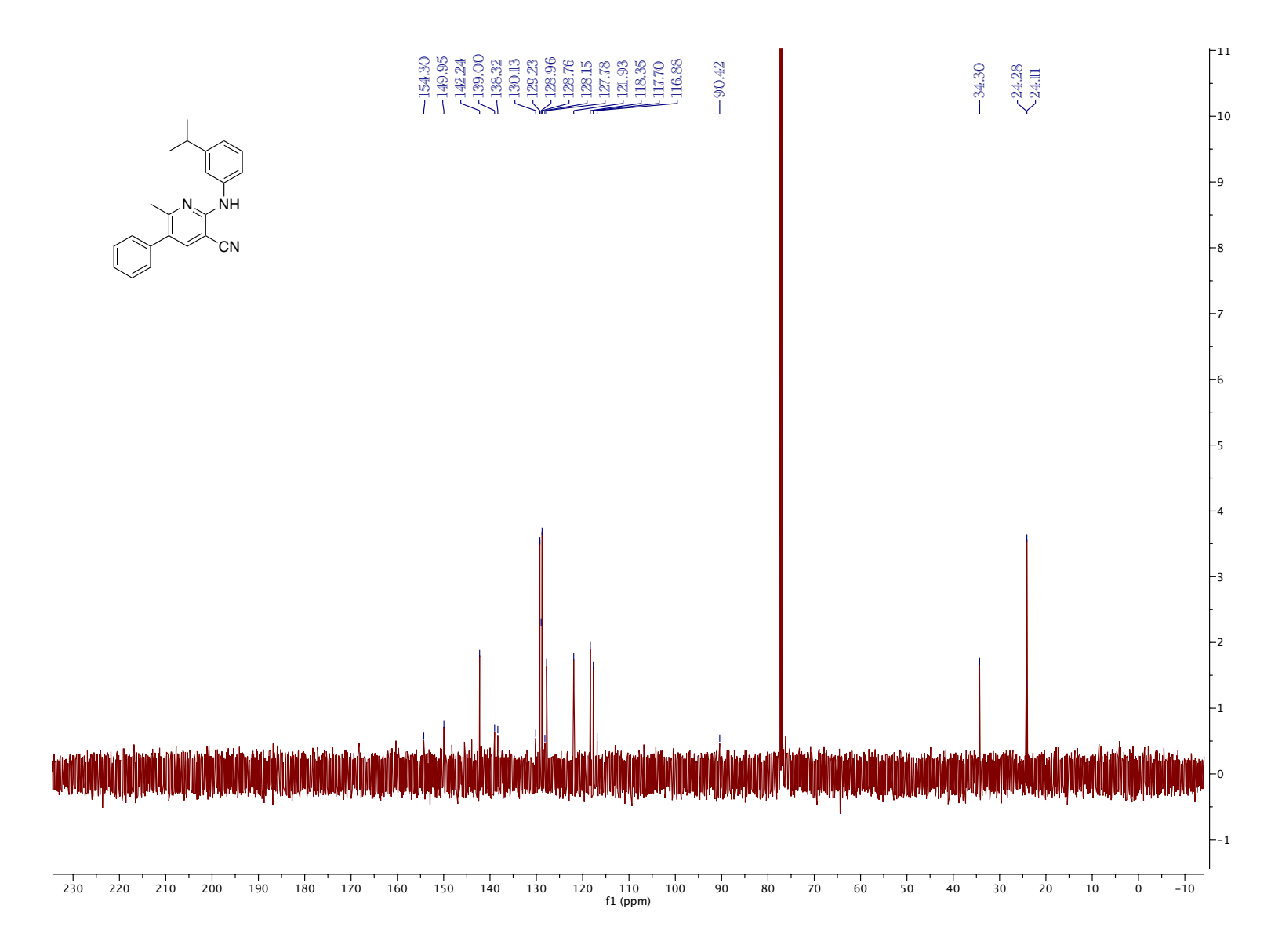


Figure 5.20. 13 C NMR (CDCl₃, 126 MHz, 25 $^{\circ}$ C)

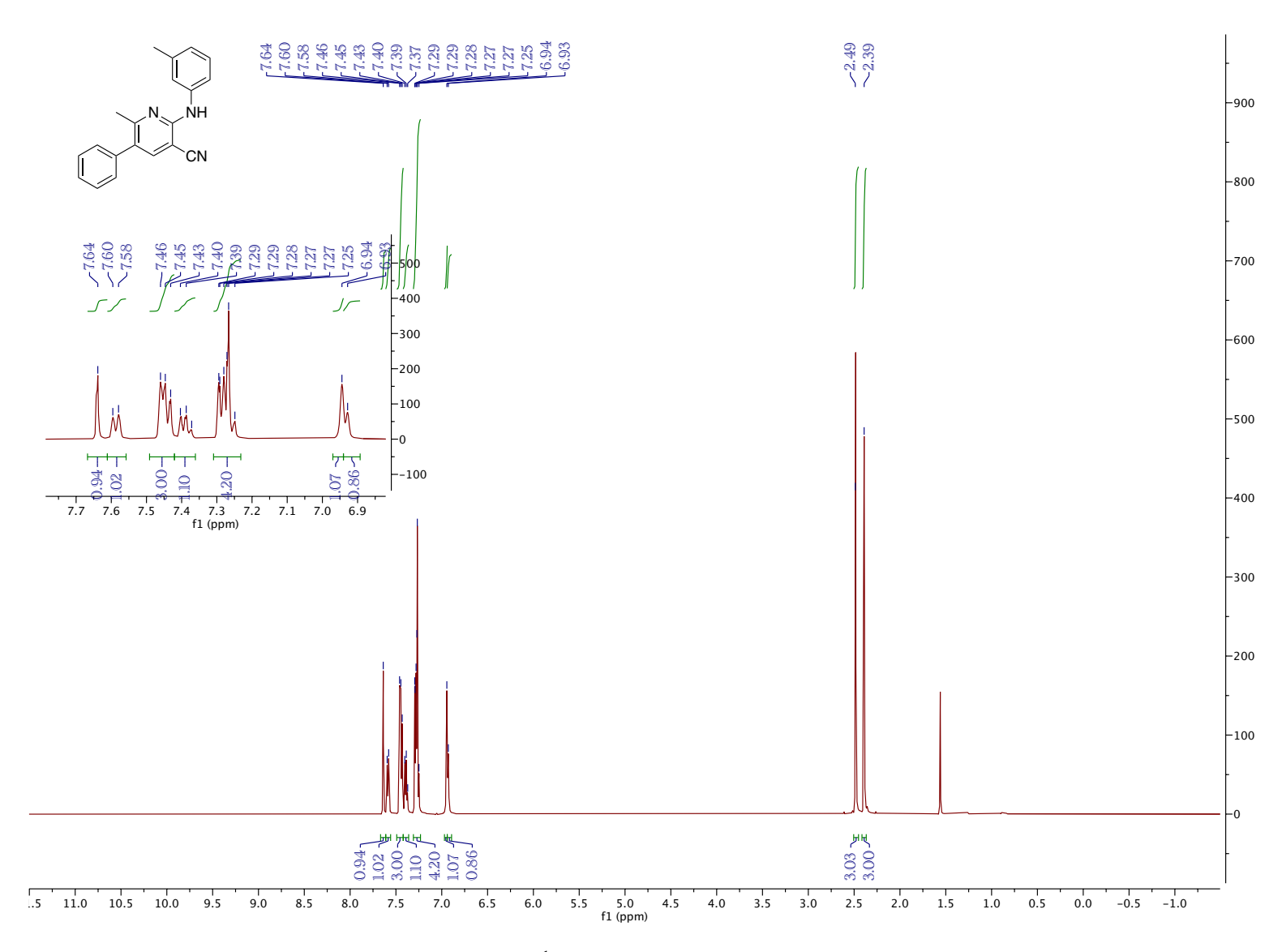


Figure 5.21. ¹H NMR (CDCl₃, 500 MHz, 25 °C)

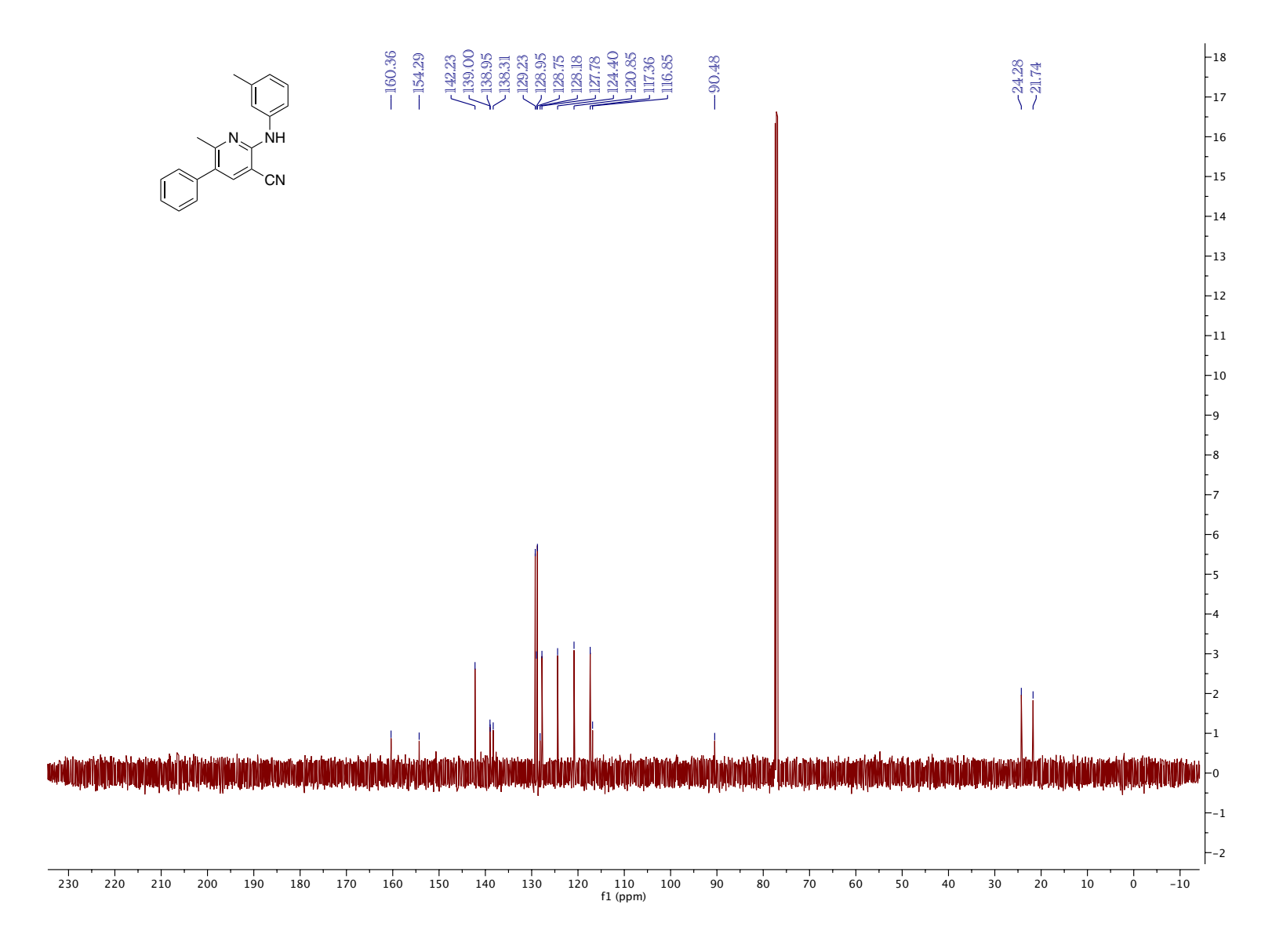


Figure 5.22. ¹³C NMR (CDCl₃, 126 MHz, 25 °C)

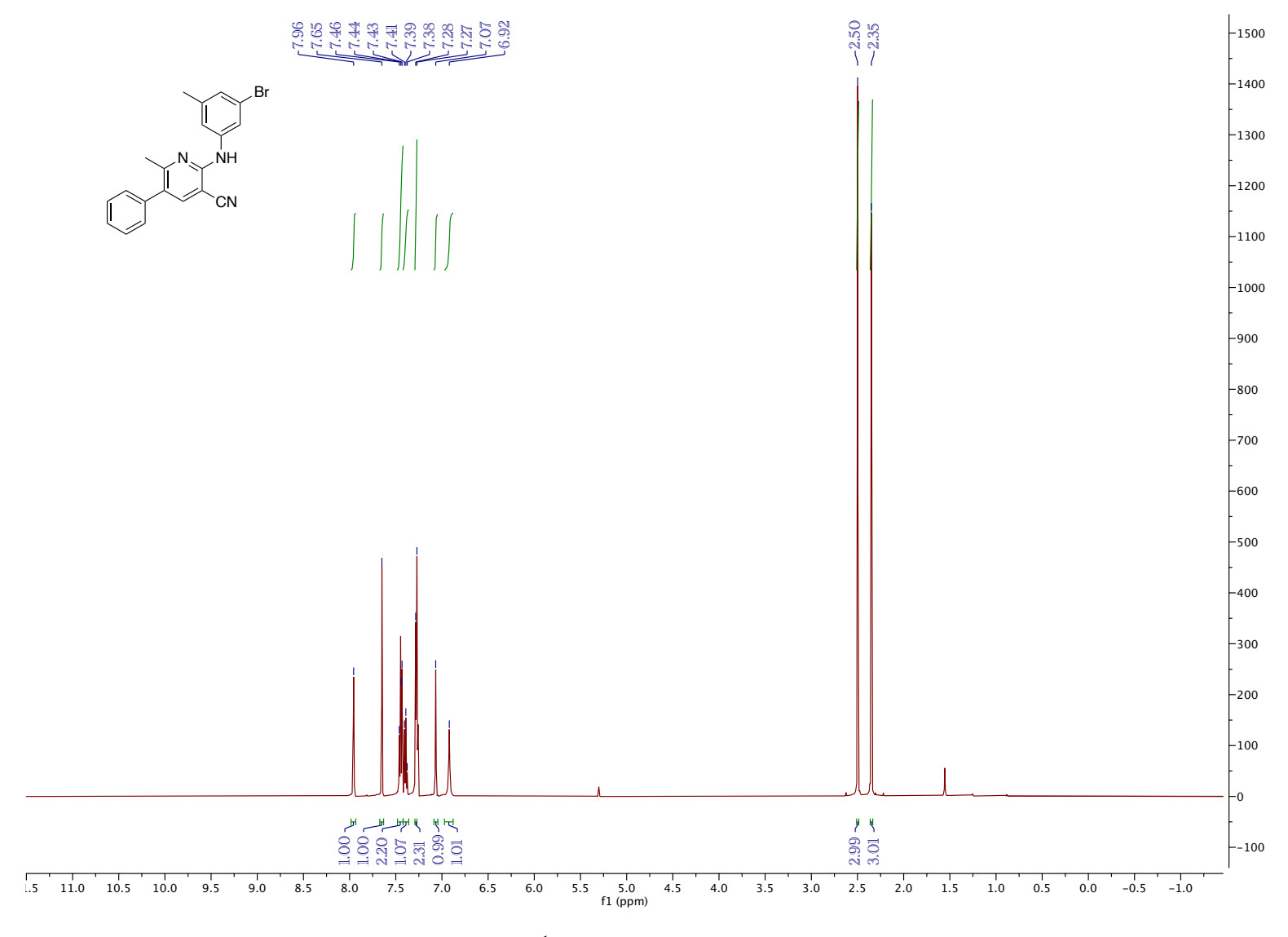


Figure 5.23. ¹H NMR (CDCl₃, 500 MHz, 25 °C)

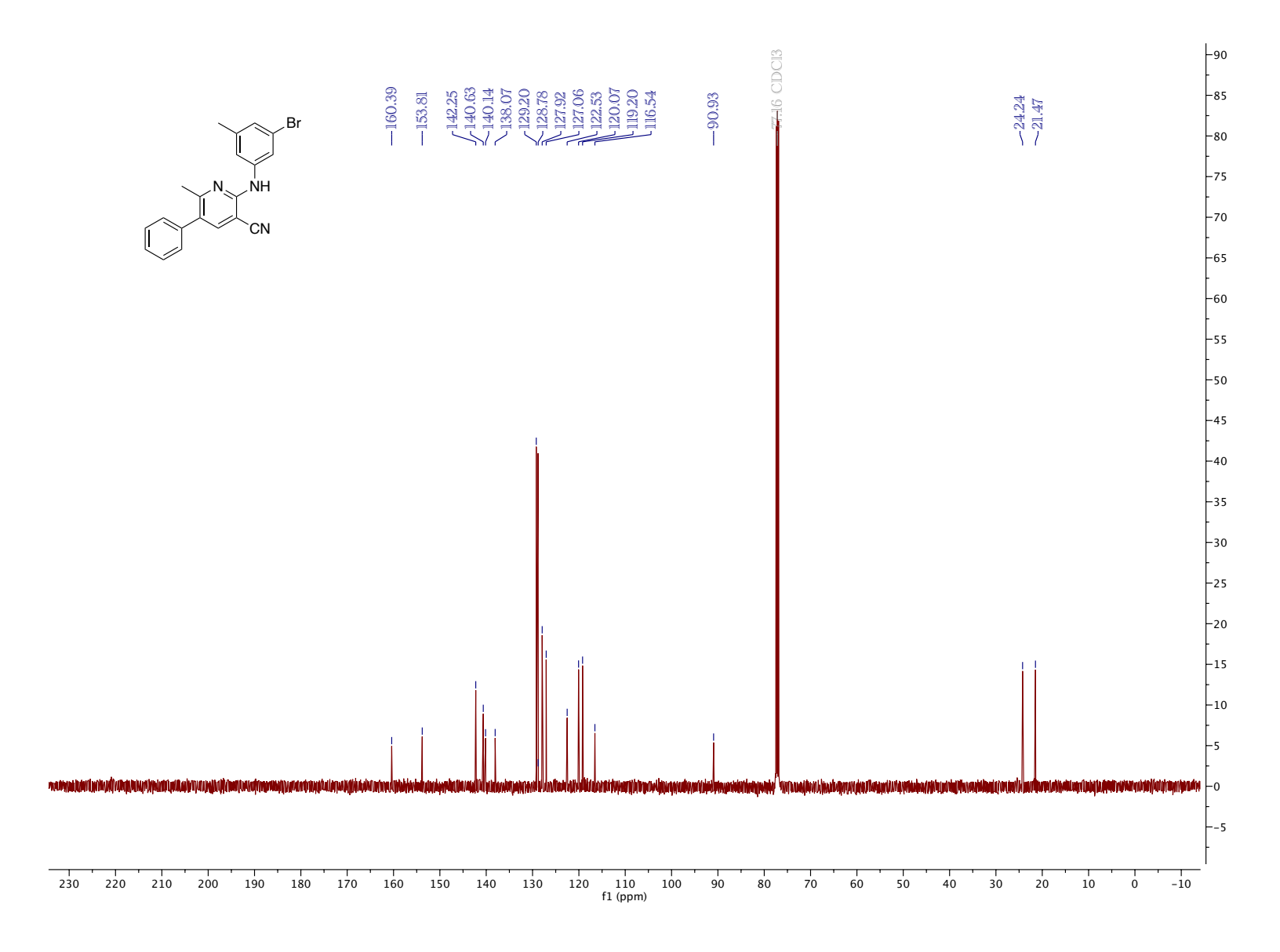


Figure 5.24. ¹³C NMR (CDCl₃, 126 MHz, 25 °C)

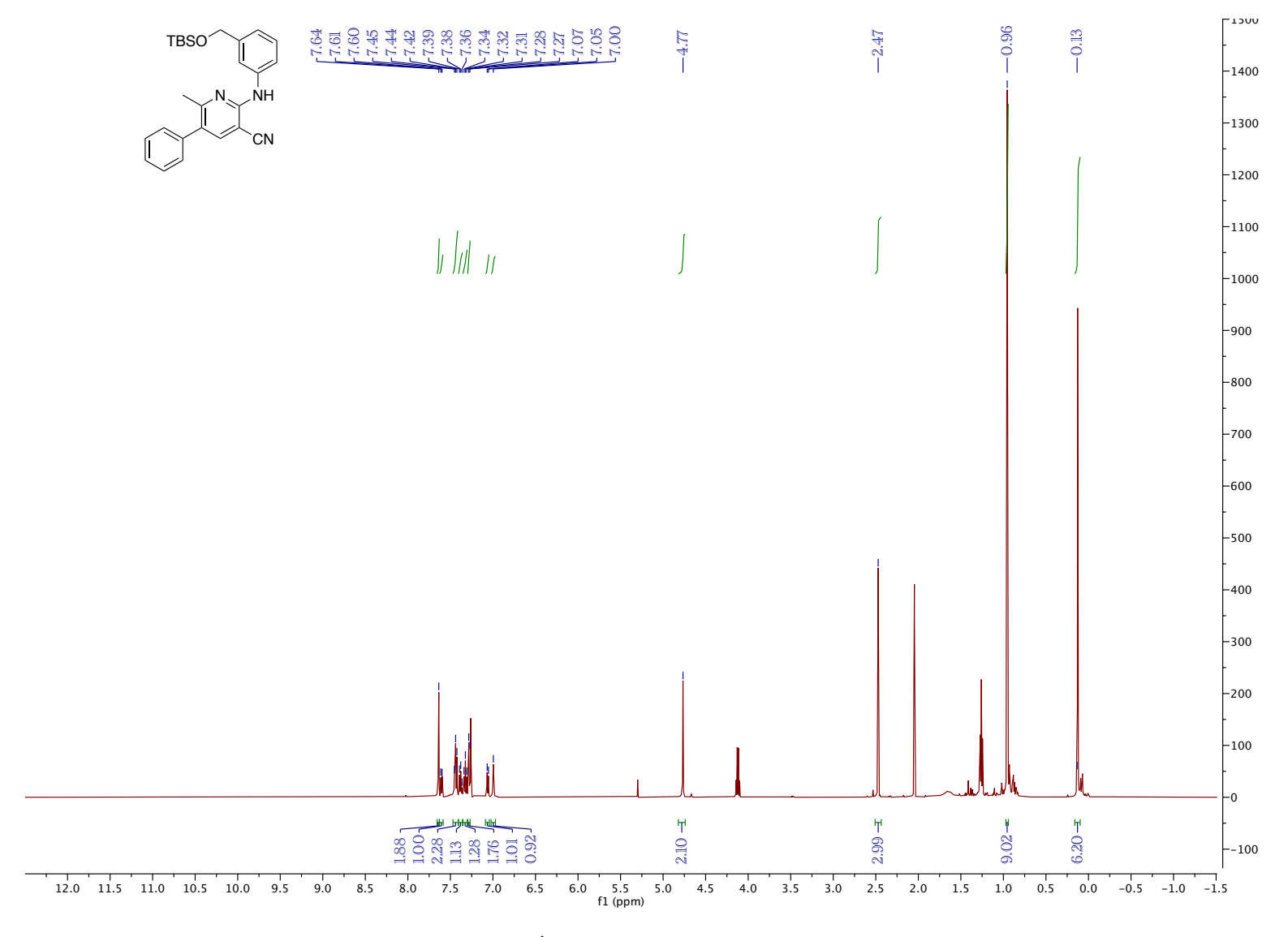


Figure 5.25. ¹H NMR (CDCl₃, 500 MHz, 25 °C)

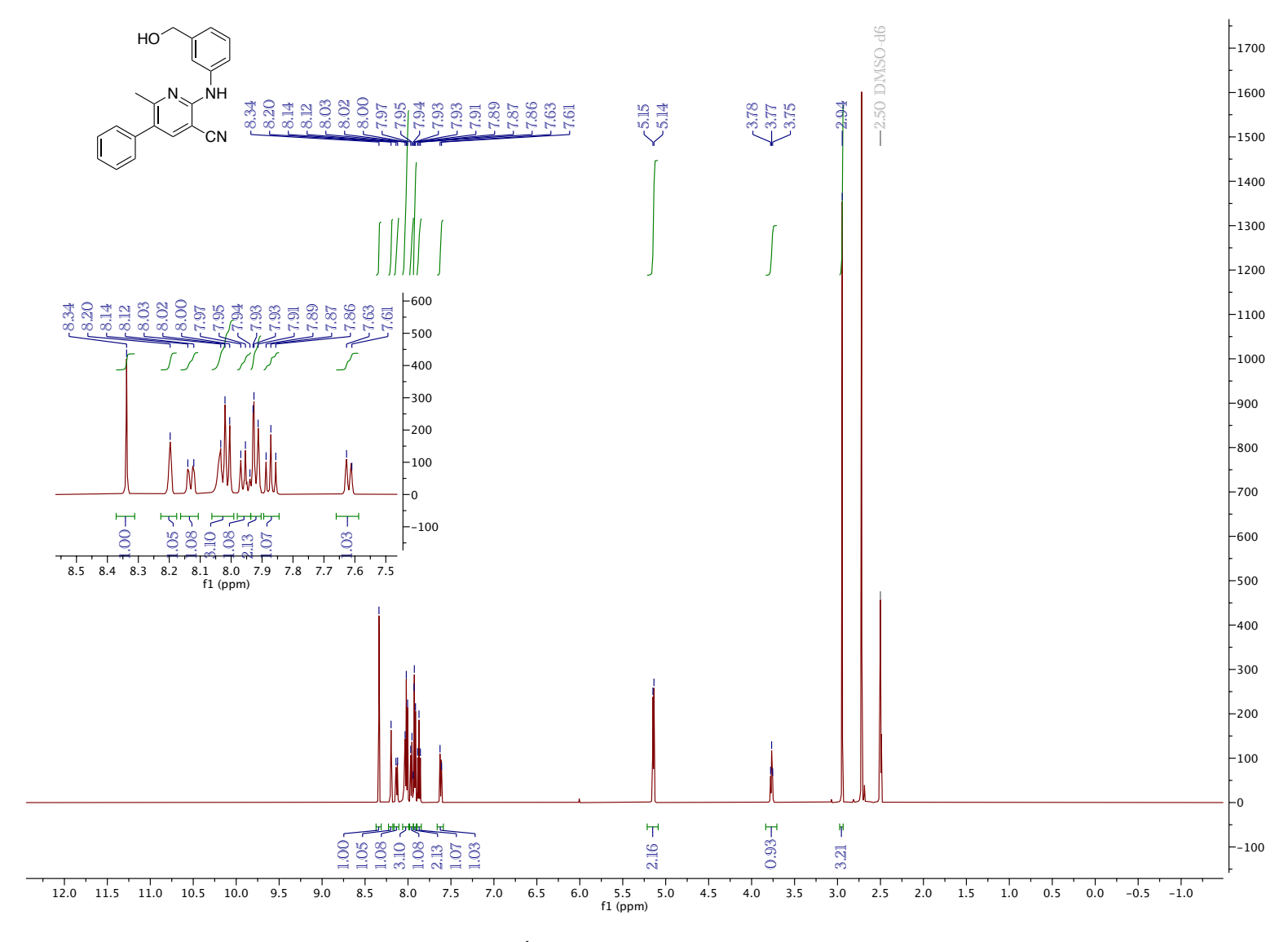


Figure 5.26. ¹H NMR (500 MHz, DMSO-d₆, 25 °C)

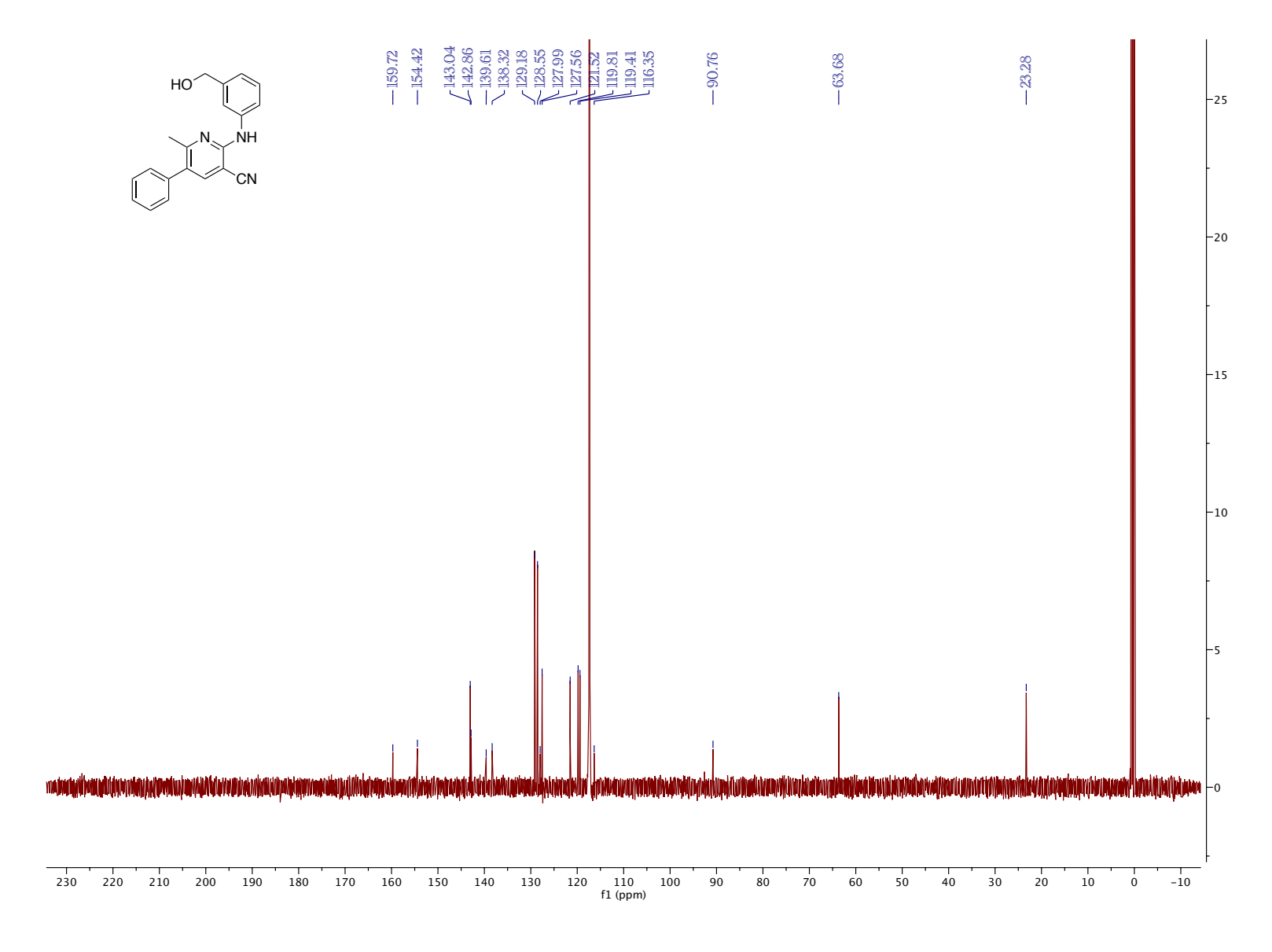


Figure 5.27. ¹³C NMR (DMSO-d₆, 126 MHz, 25 °C)

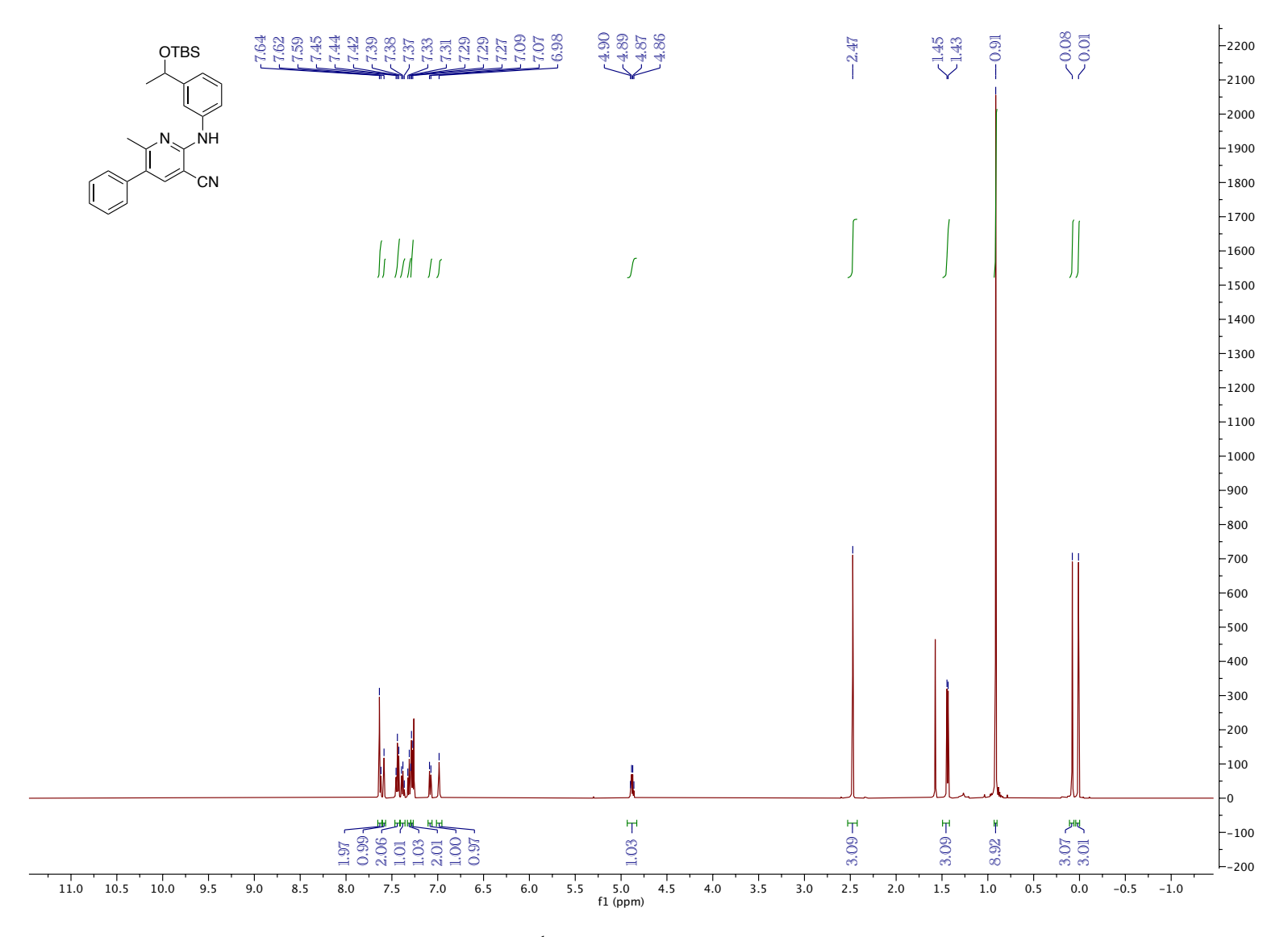


Figure 5.28. ¹H NMR (CDCl₃, 500 MHz, 25 °C)

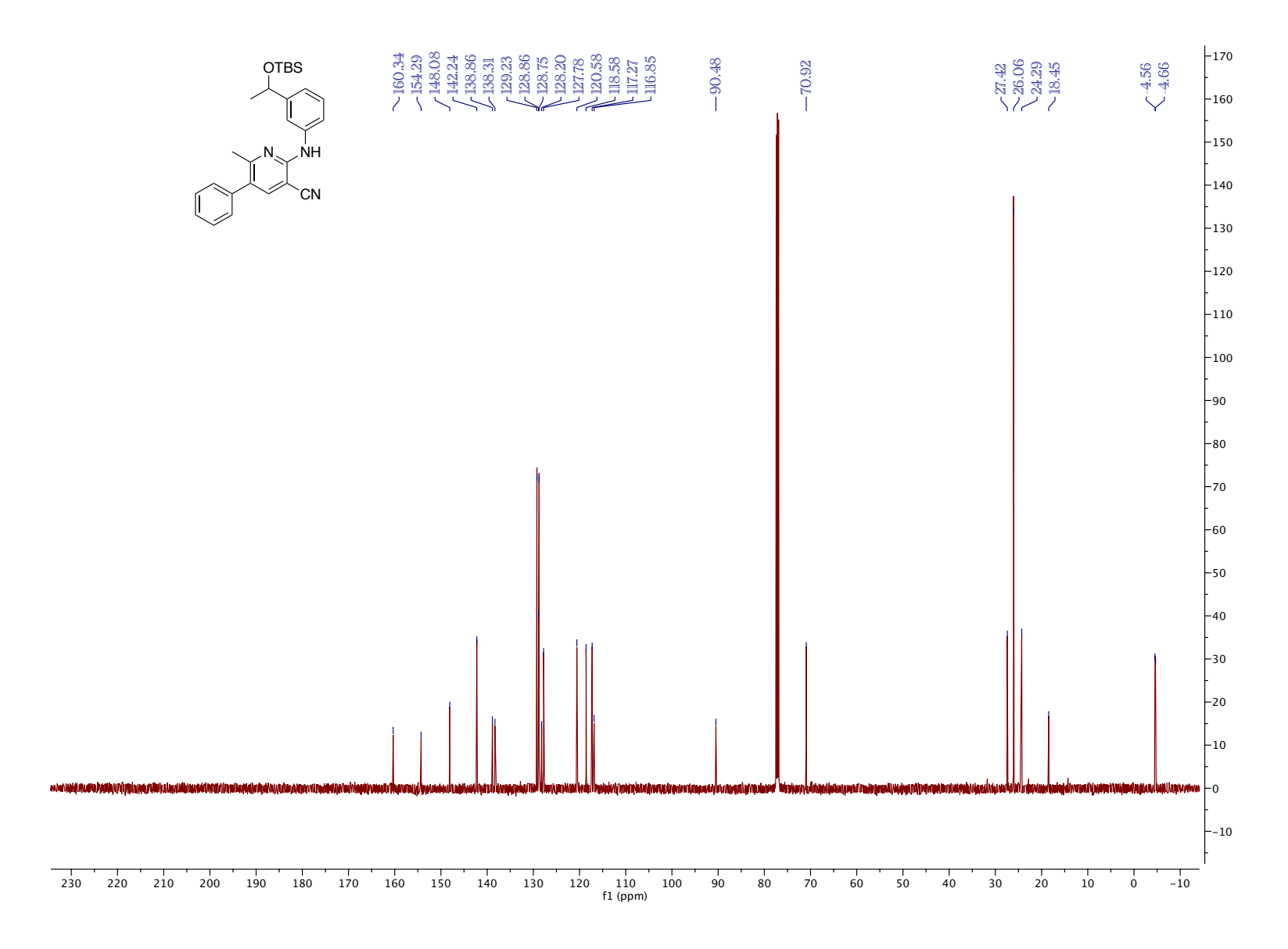


Figure 5.29. ¹³C NMR (CDCl₃, 126 MHz, 25 °C)

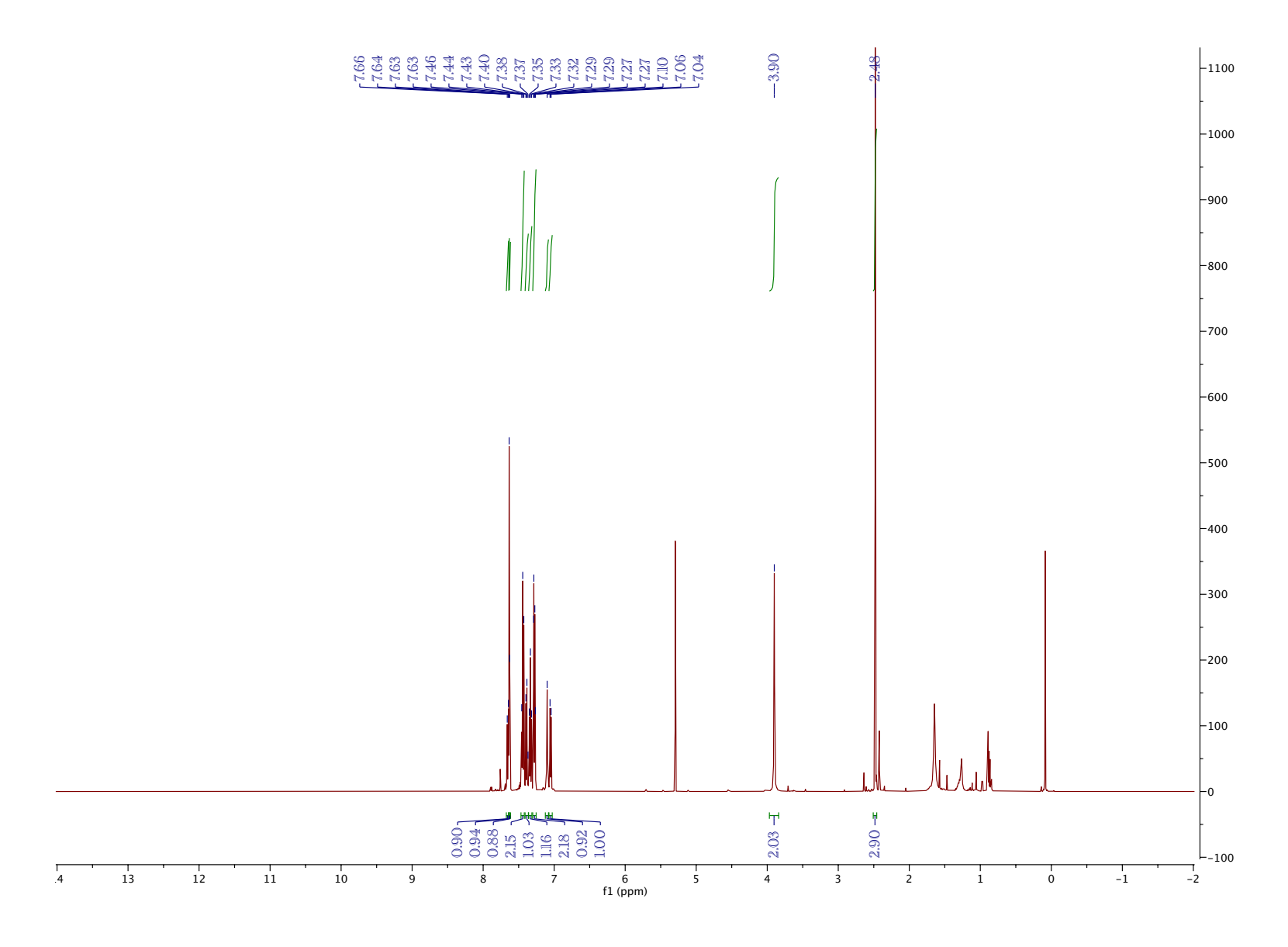


Figure 5.30. 1 H NMR (CDCl₃, 500 MHz, 25 $^{\circ}$ C)

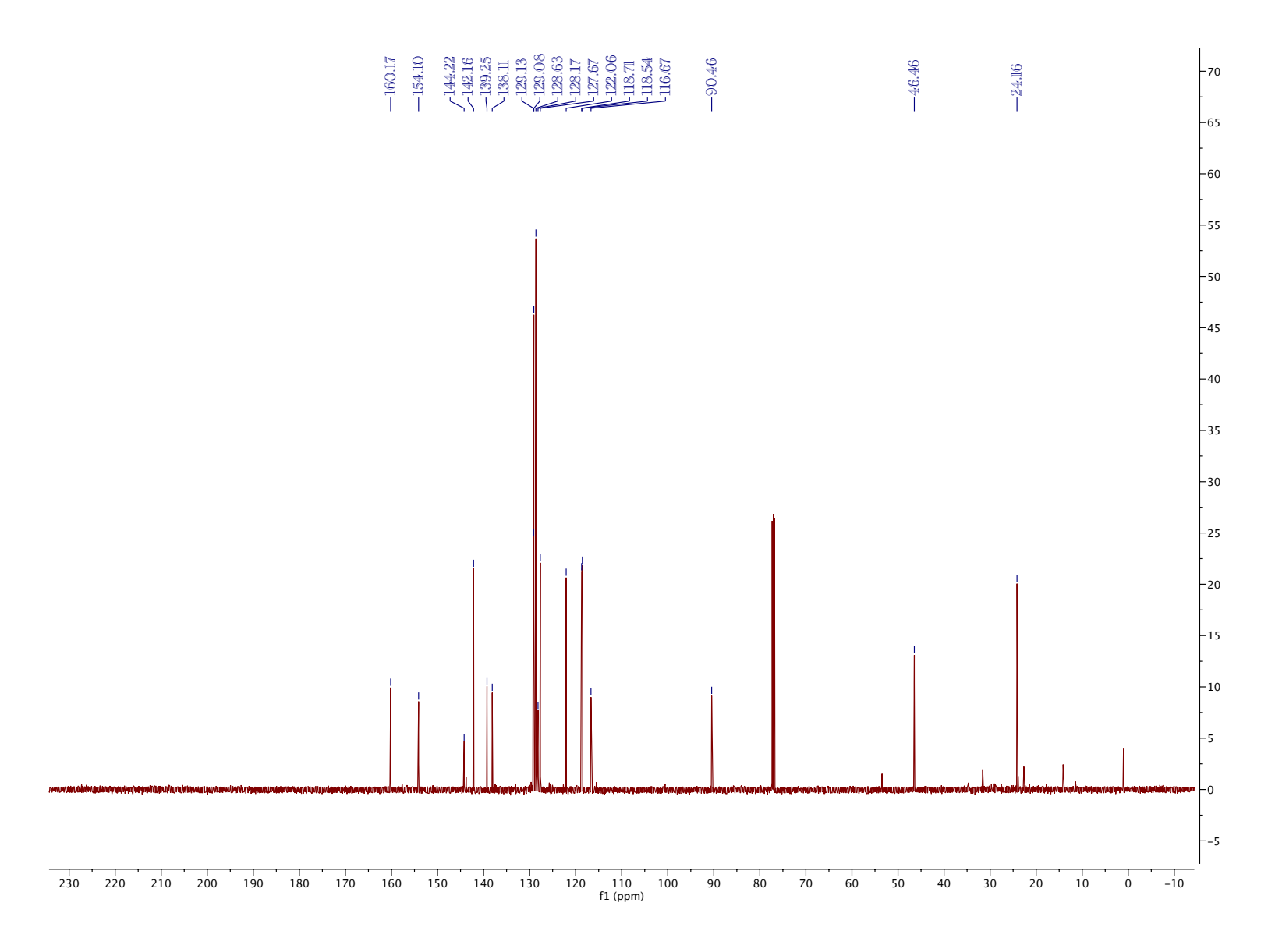


Figure 5.31. ¹³C NMR (CDCl₃, 126 MHz, 25 °C)

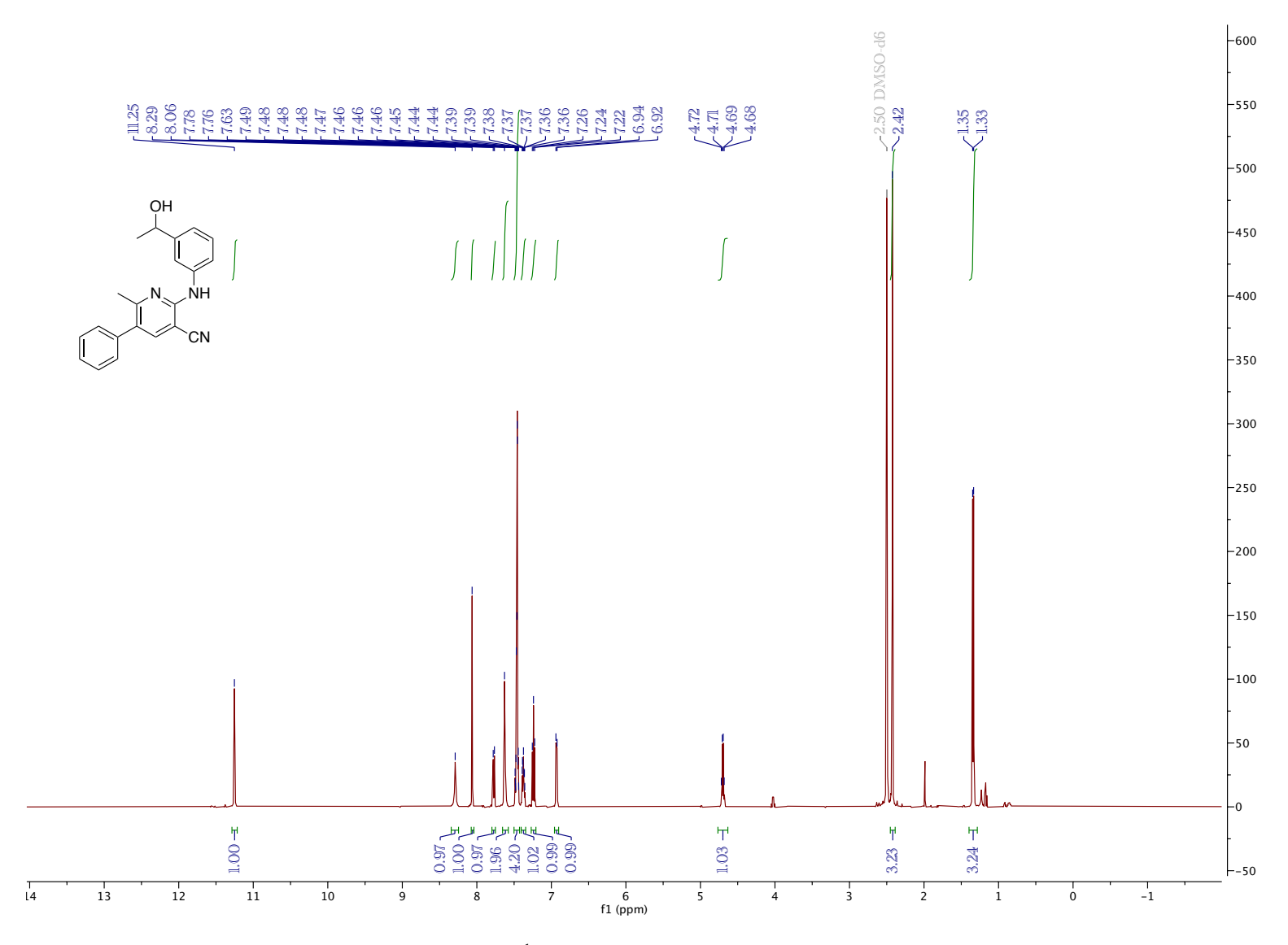


Figure 5.32. ¹H NMR (500 MHz, DMSO-d₆, 25 °C)

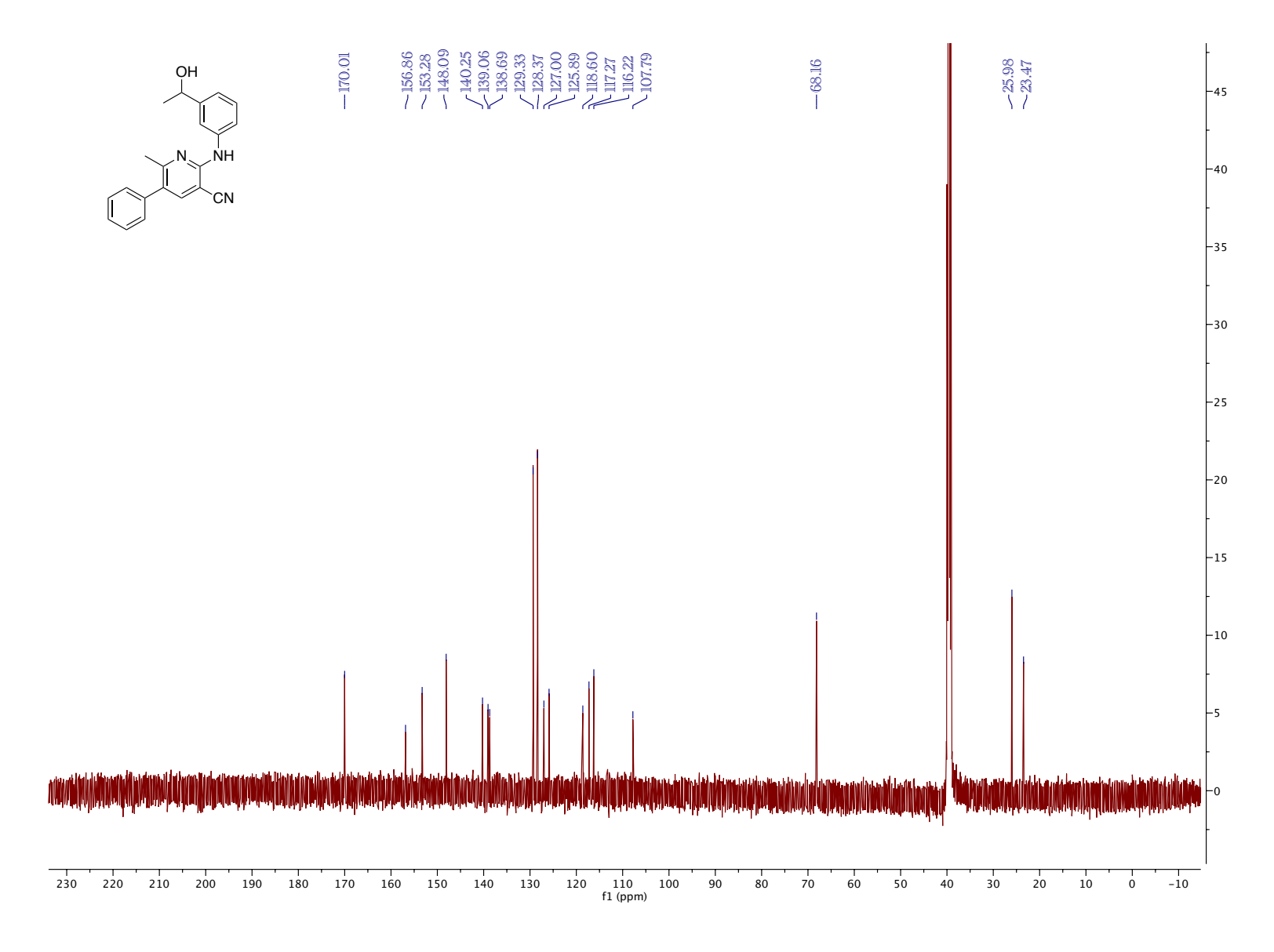


Figure 5.33. ¹³C NMR (DMSO-d₆, 126 MHz, 25 °C)

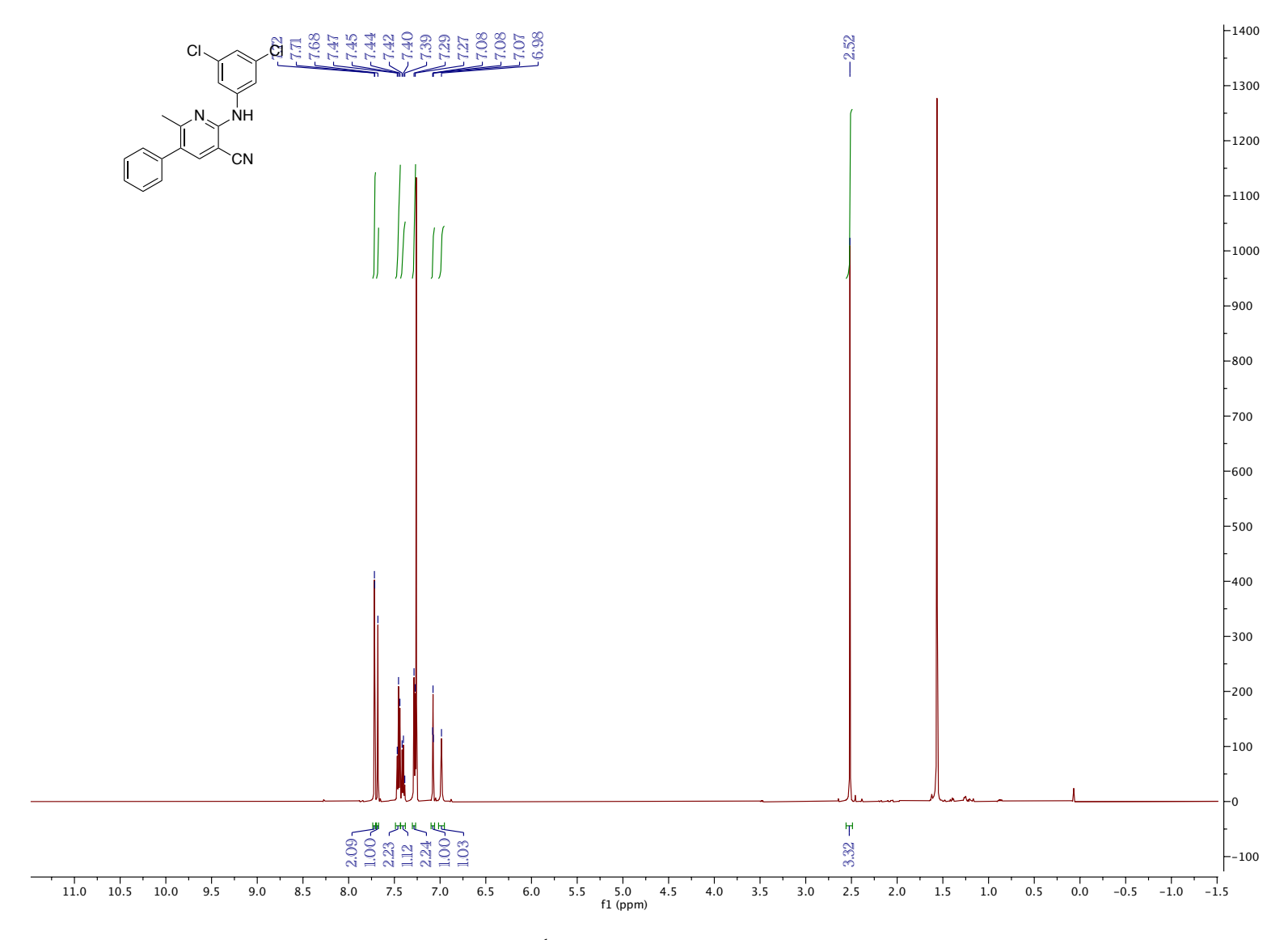


Figure 5.34. ¹H NMR (CDCl₃, 500 MHz, 25 °C)

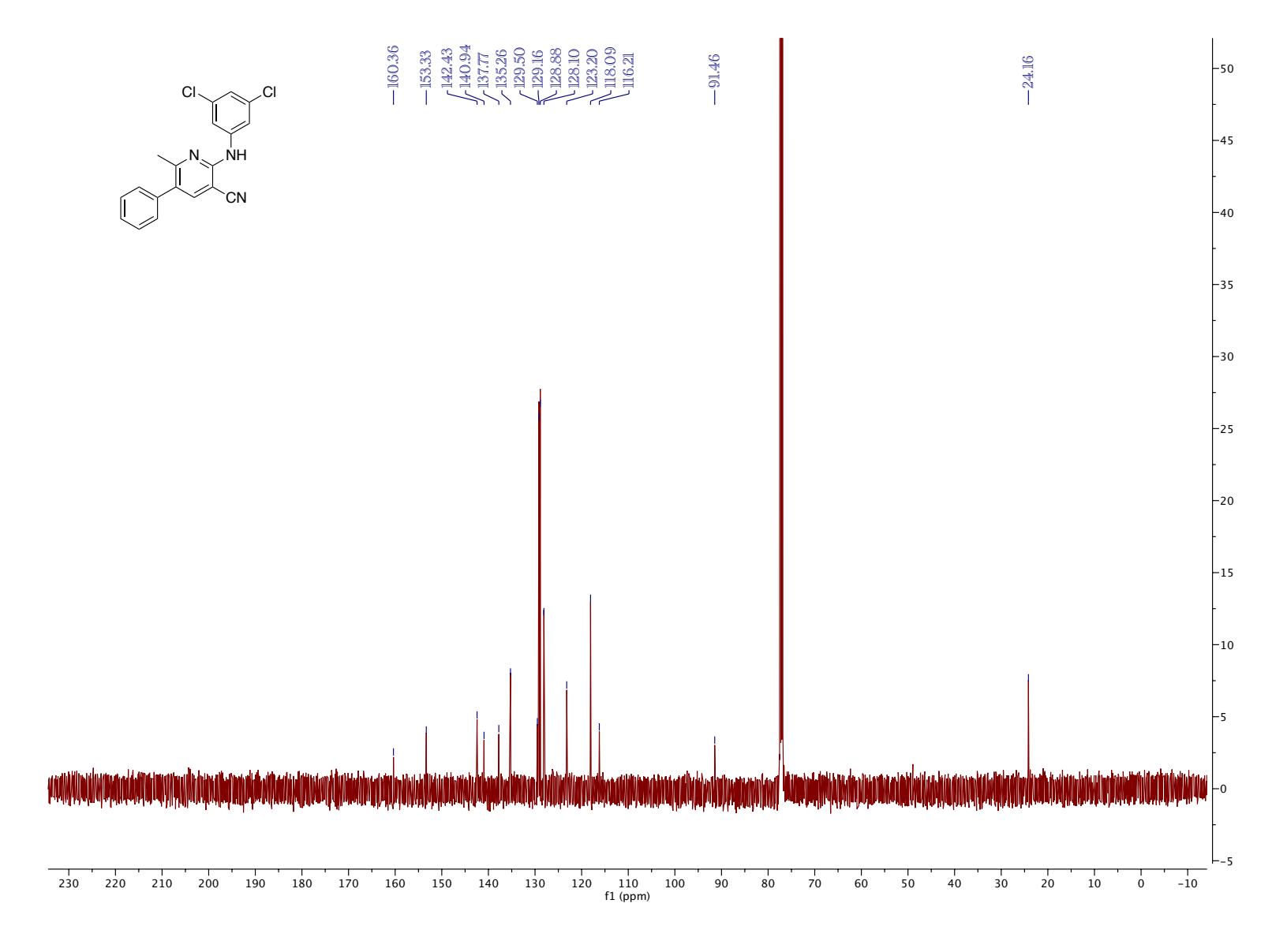


Figure 5.35. ¹³C NMR (CDCl₃, 126 MHz, 25 °C)

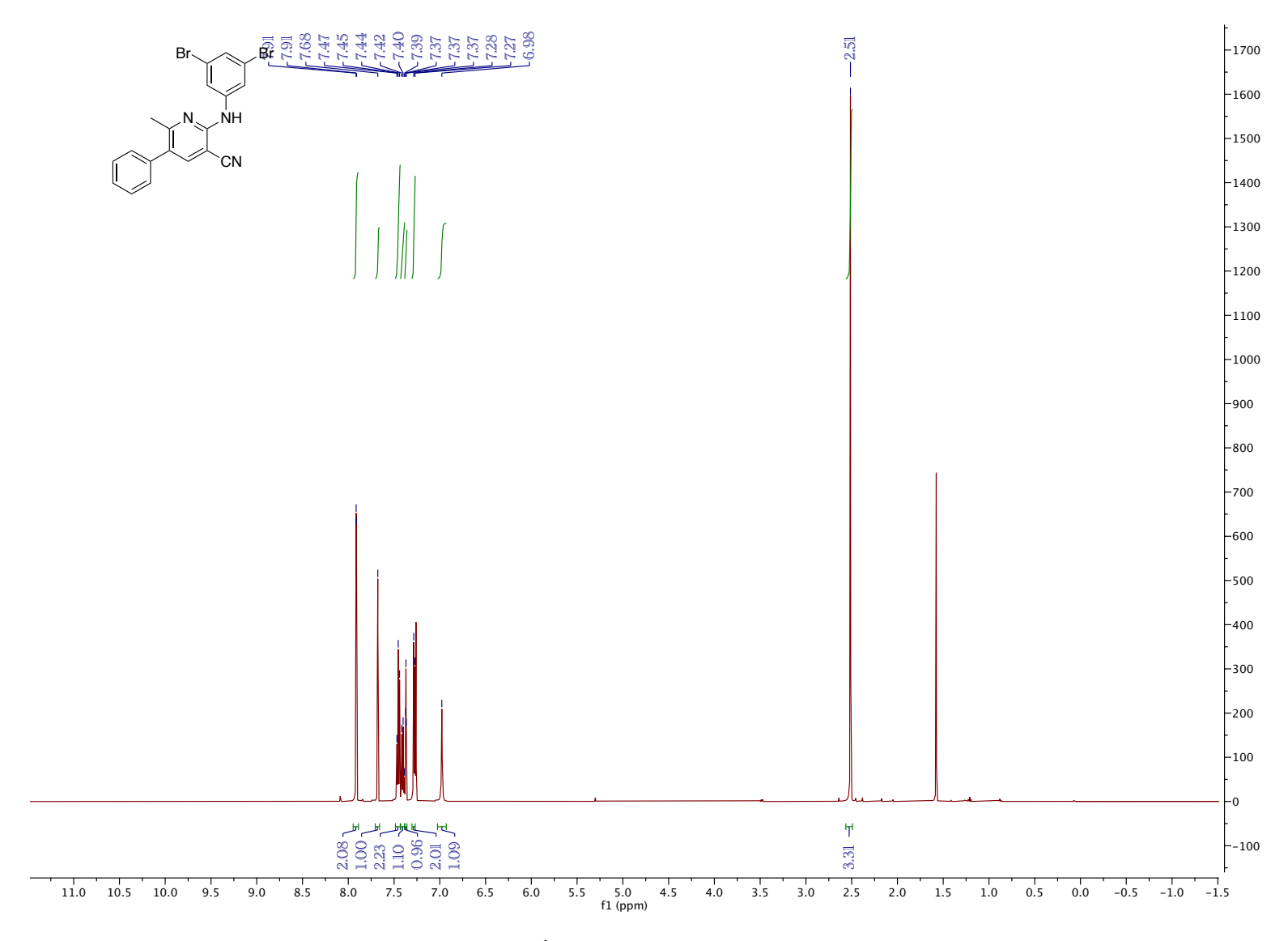


Figure 5.36. ¹H NMR (CDCl₃, 500 MHz, 25 °C)

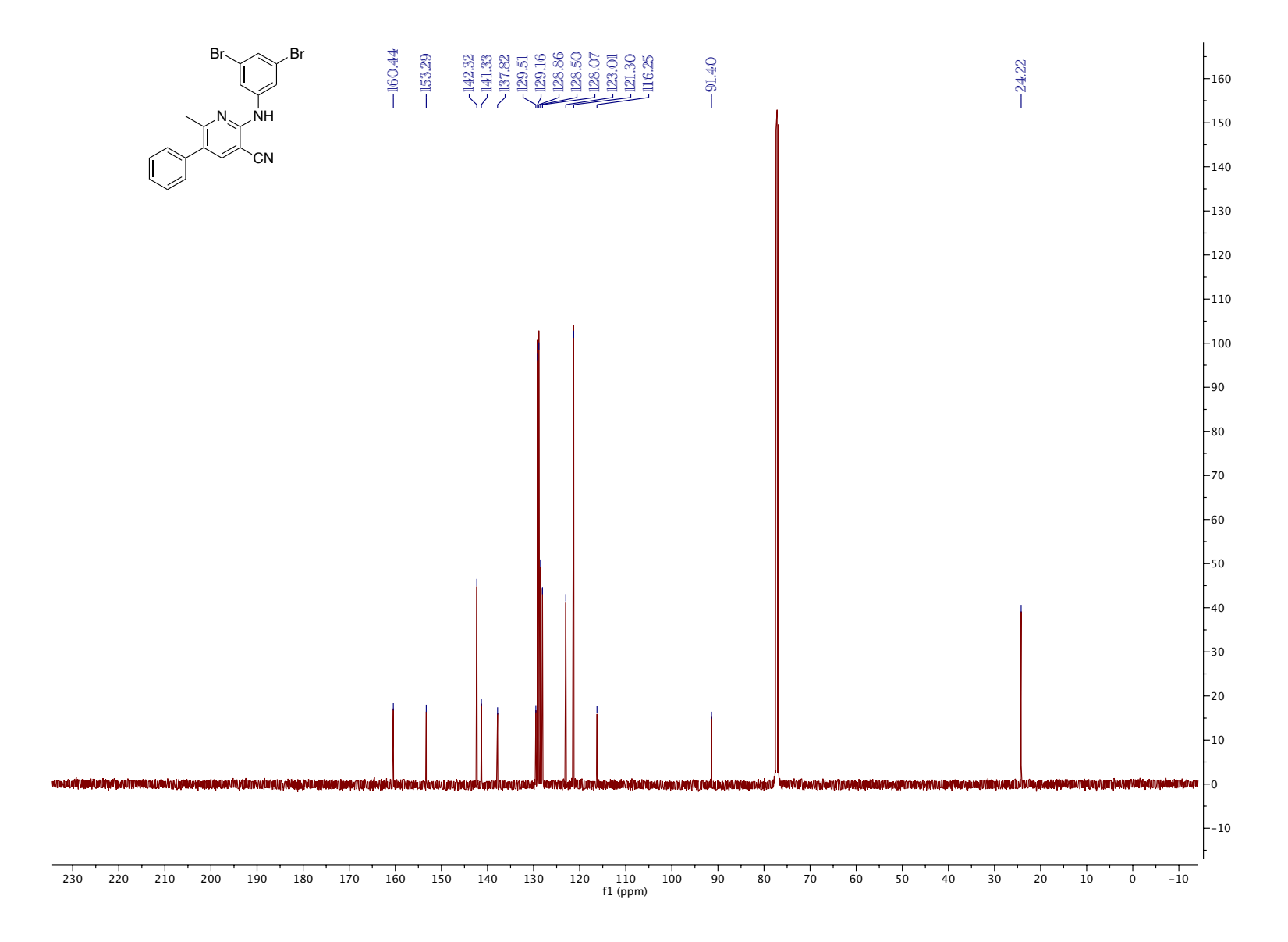


Figure 5.37. ¹³C NMR (CDCl₃, 126 MHz, 25 °C)

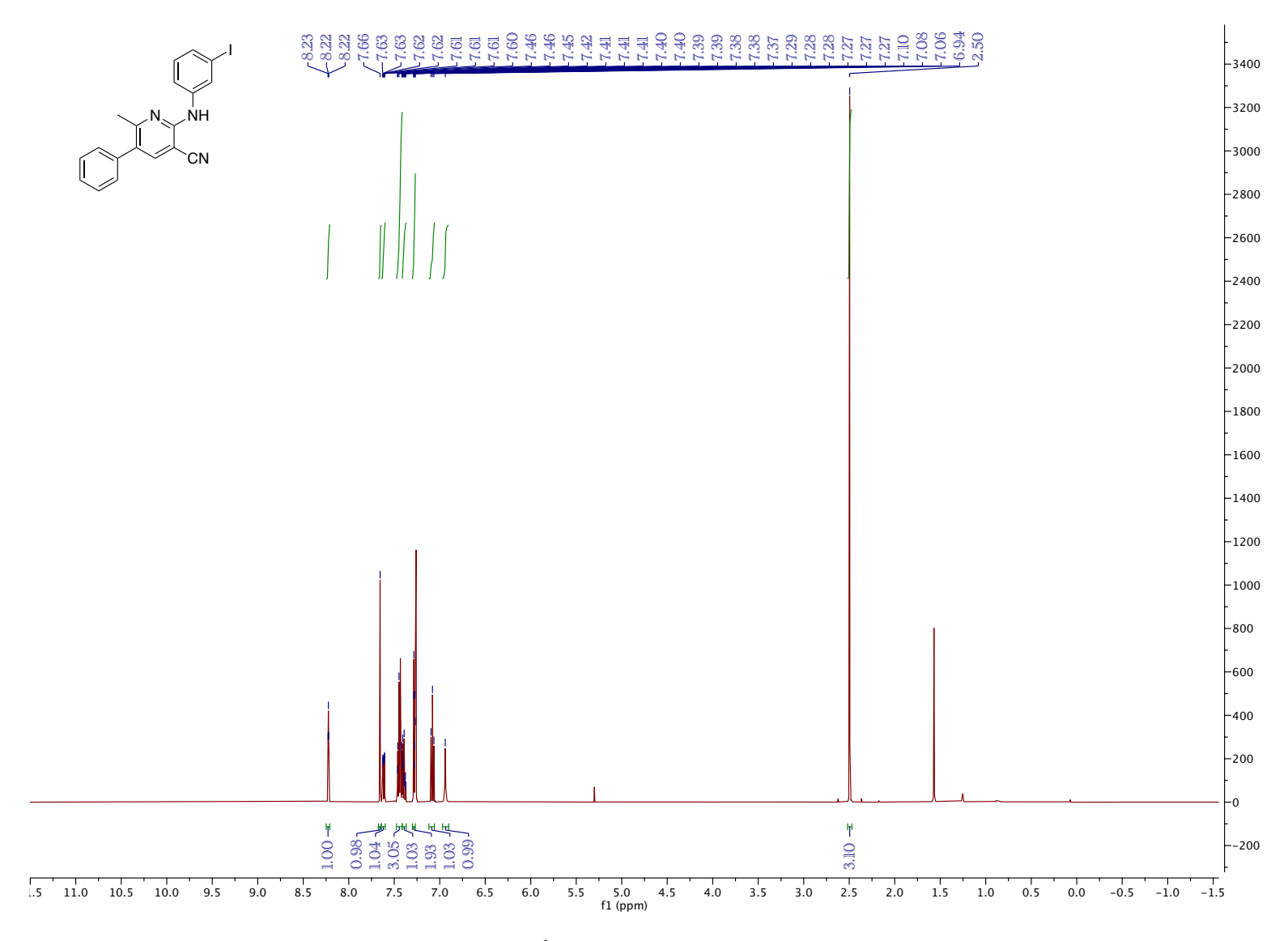


Figure 5.38. ¹H NMR (CDCl₃, 500 MHz, 25 °C)

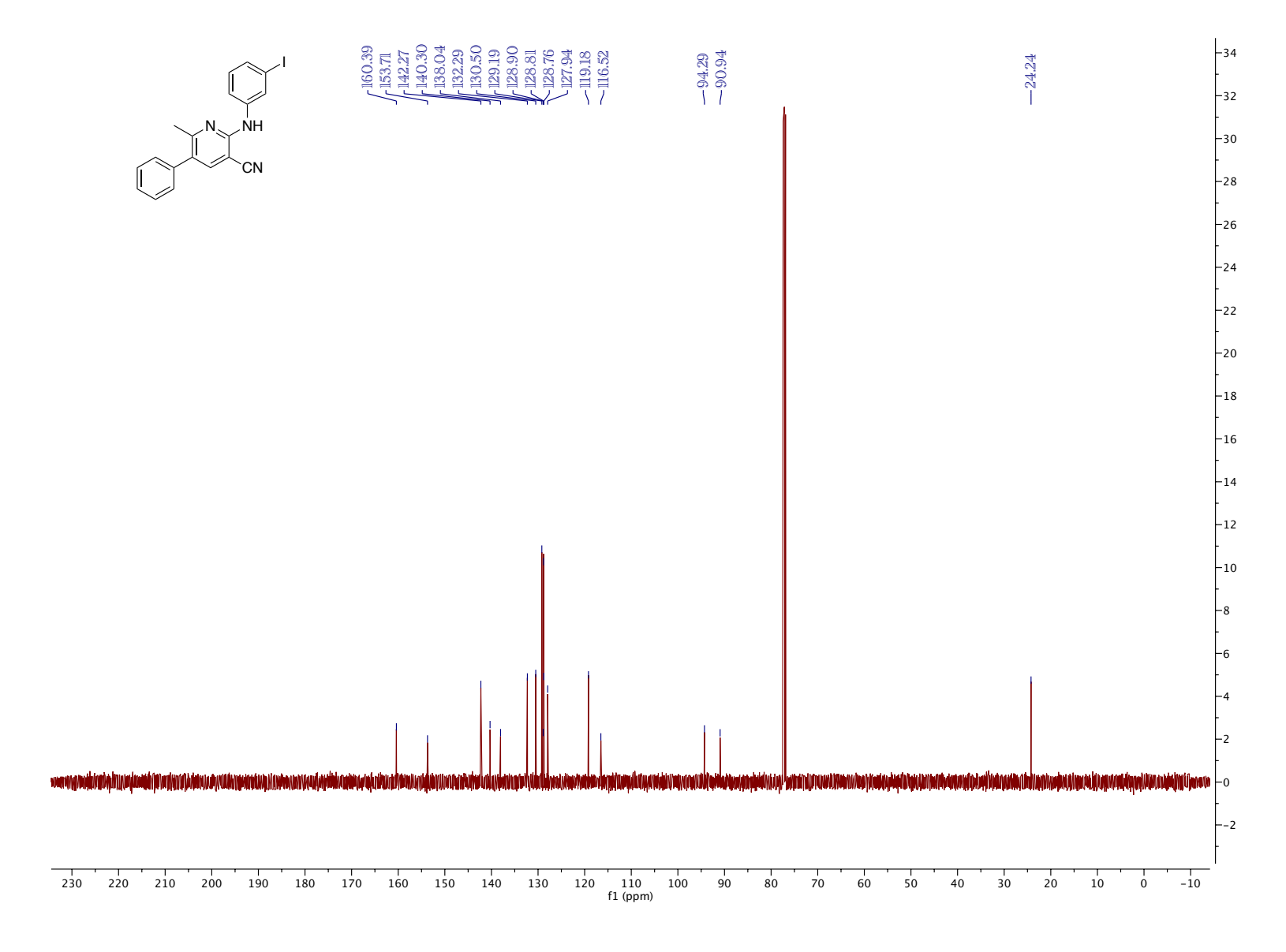


Figure 5.39. ¹³C NMR (CDCl₃, 126 MHz, 25 °C)

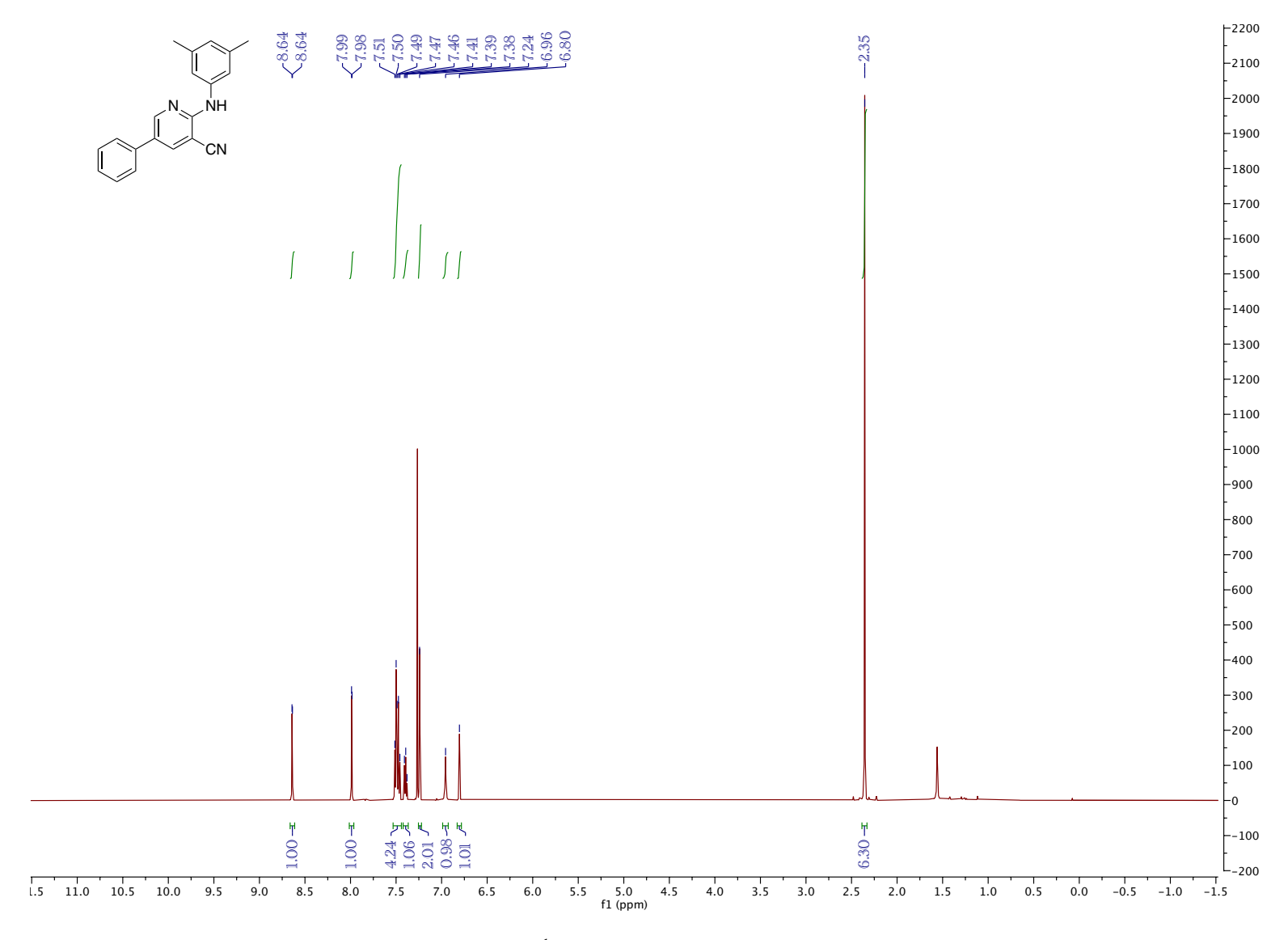


Figure 5.40. ¹H NMR (CDCl₃, 500 MHz, 25 °C)

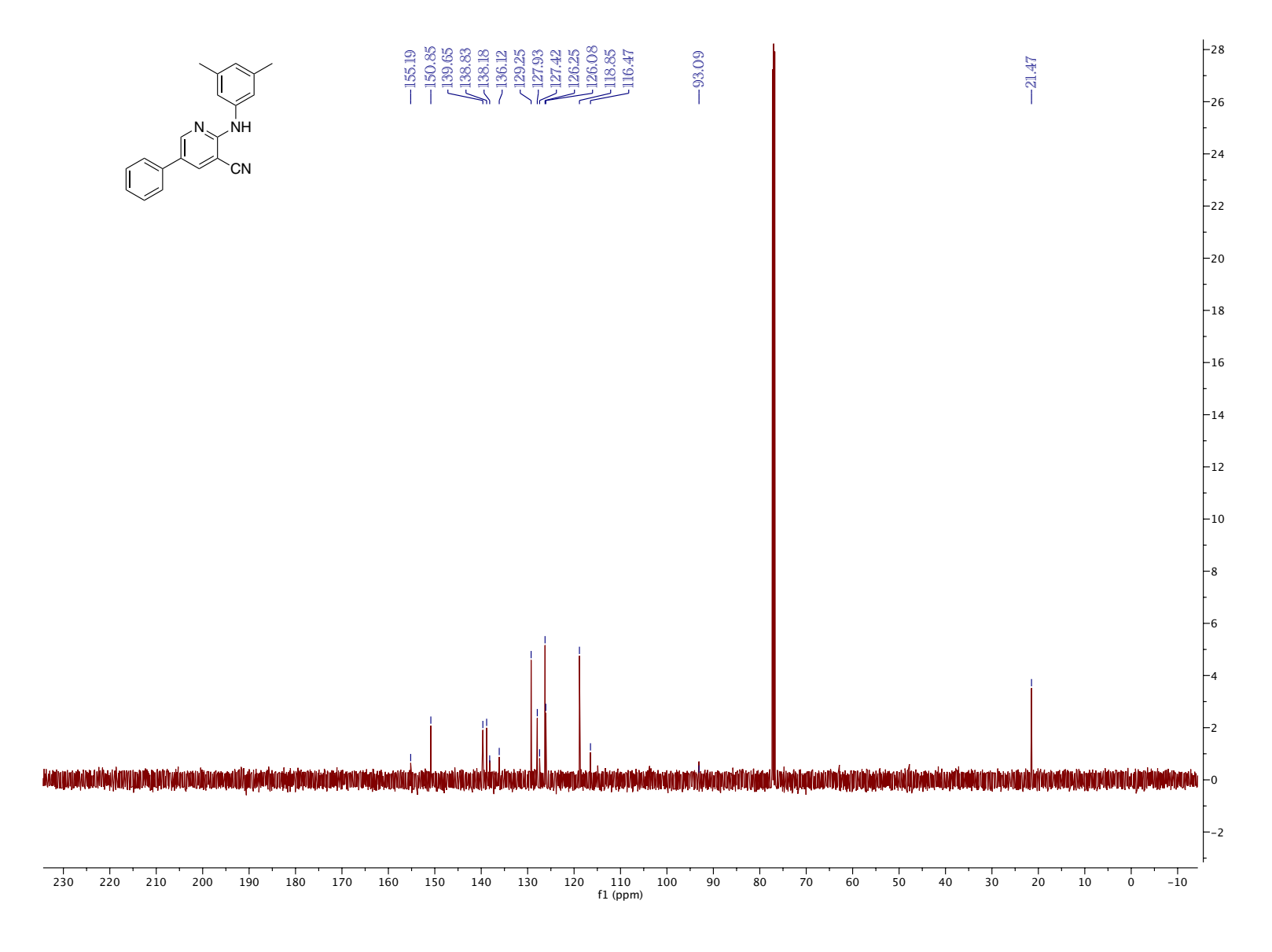


Figure 5.41. ¹³C NMR (CDCl₃, 126 MHz, 25 °C)

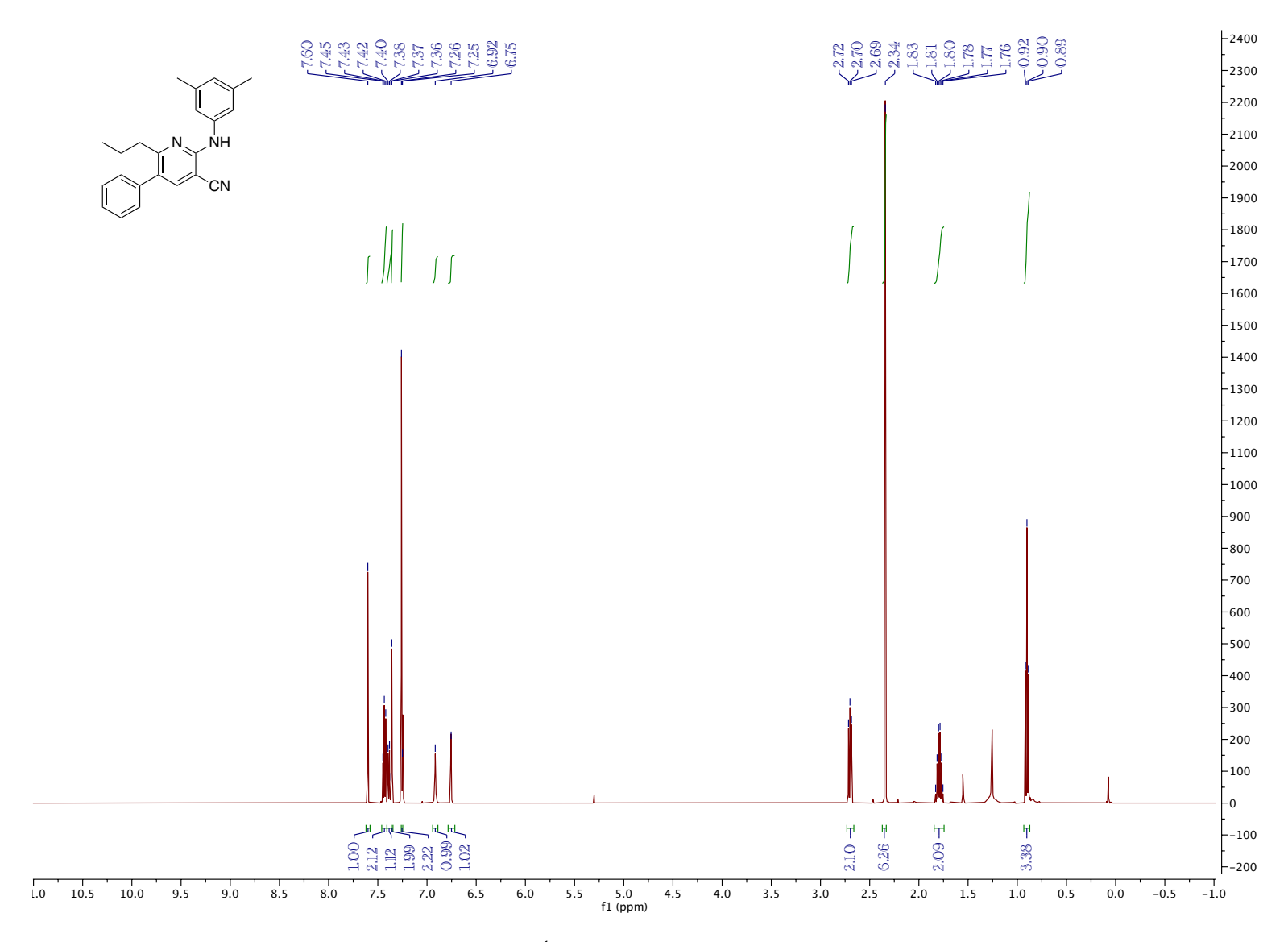


Figure 5.42. ¹H NMR (CDCl₃, 500 MHz, 25 °C)

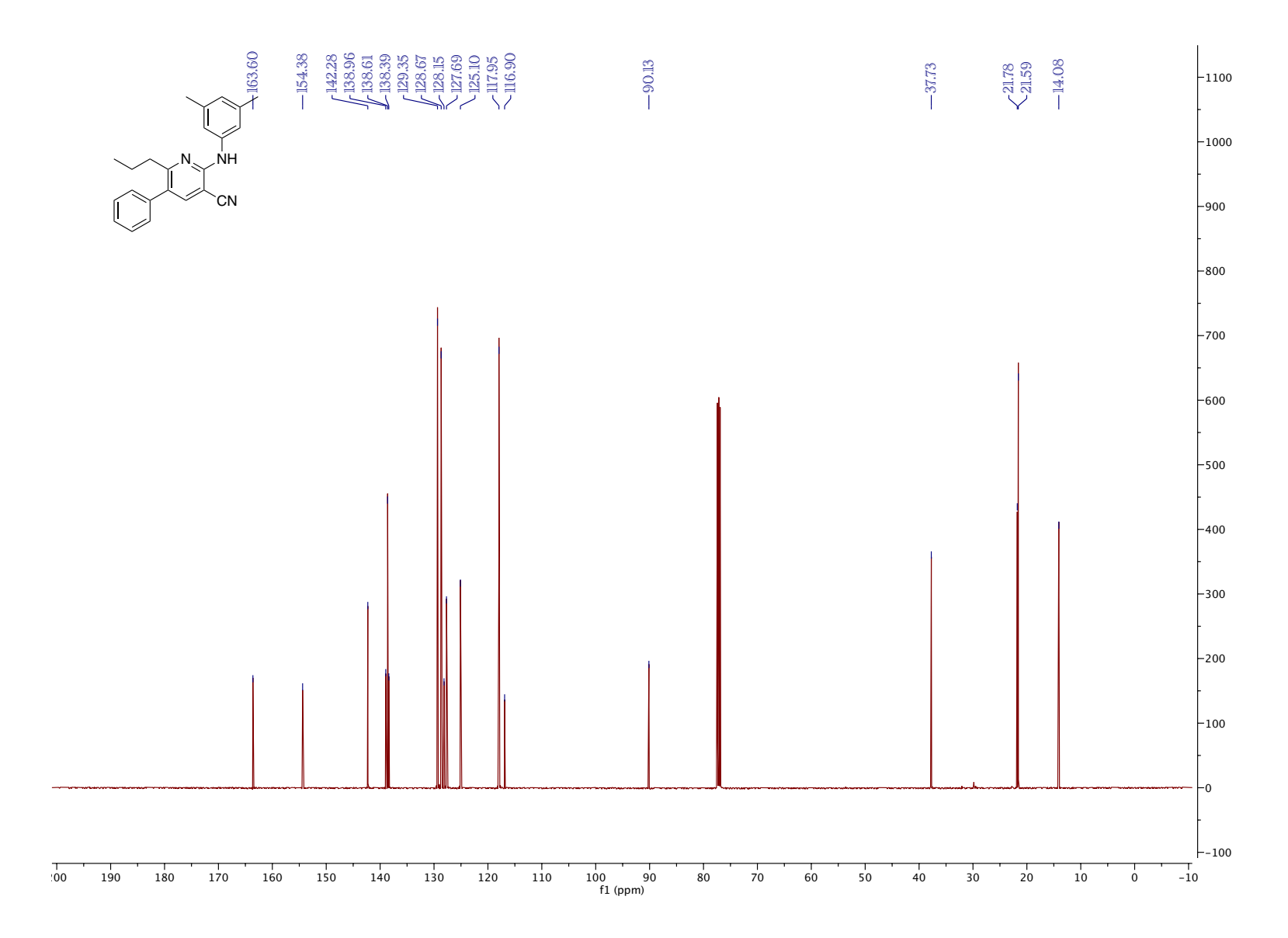


Figure 5.43. 13 C NMR (CDCl₃, 126 MHz, 25 $^{\circ}$ C)

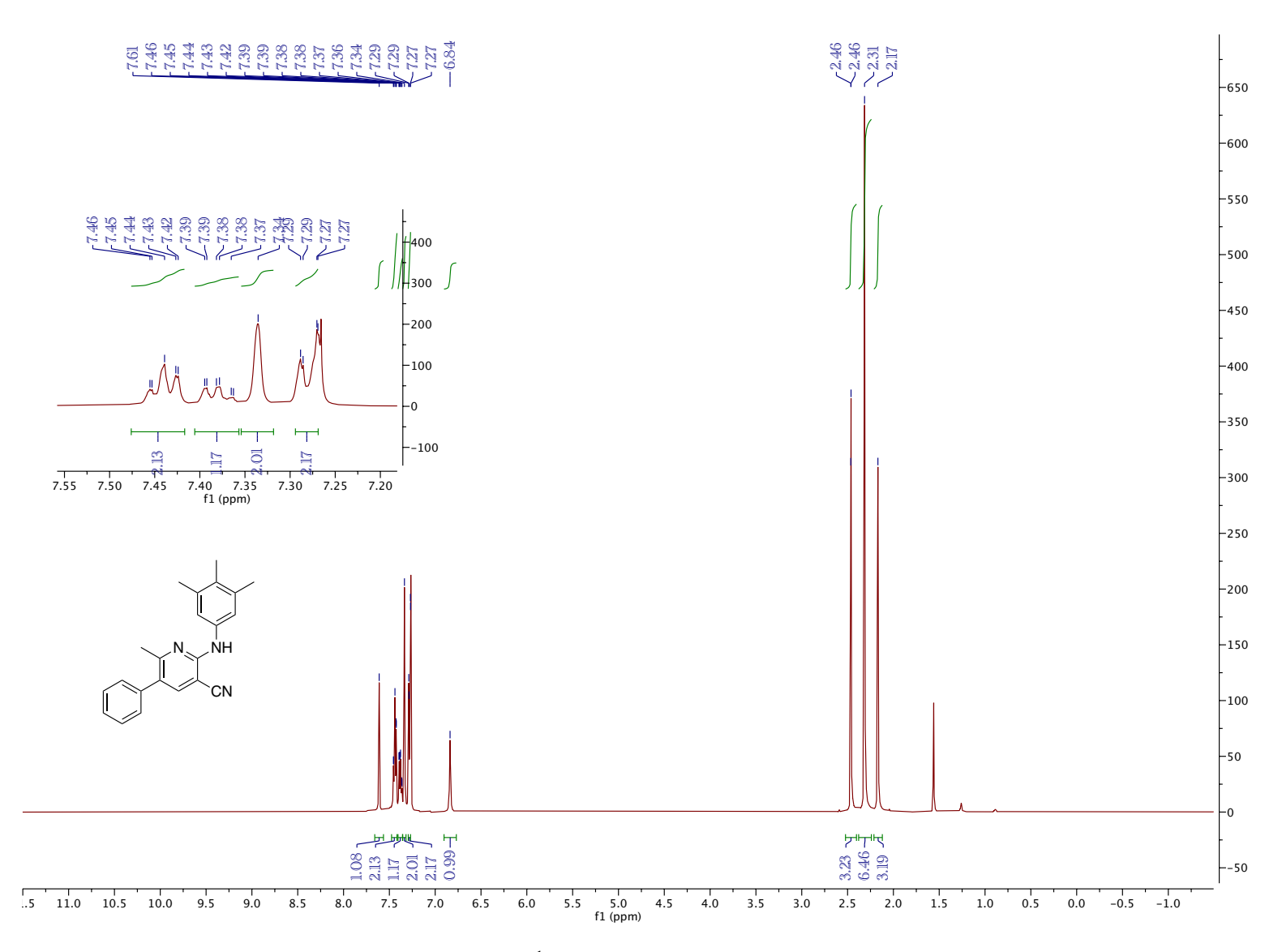


Figure 5.44. ¹H NMR (CDCl₃, 500 MHz, 25 °C)

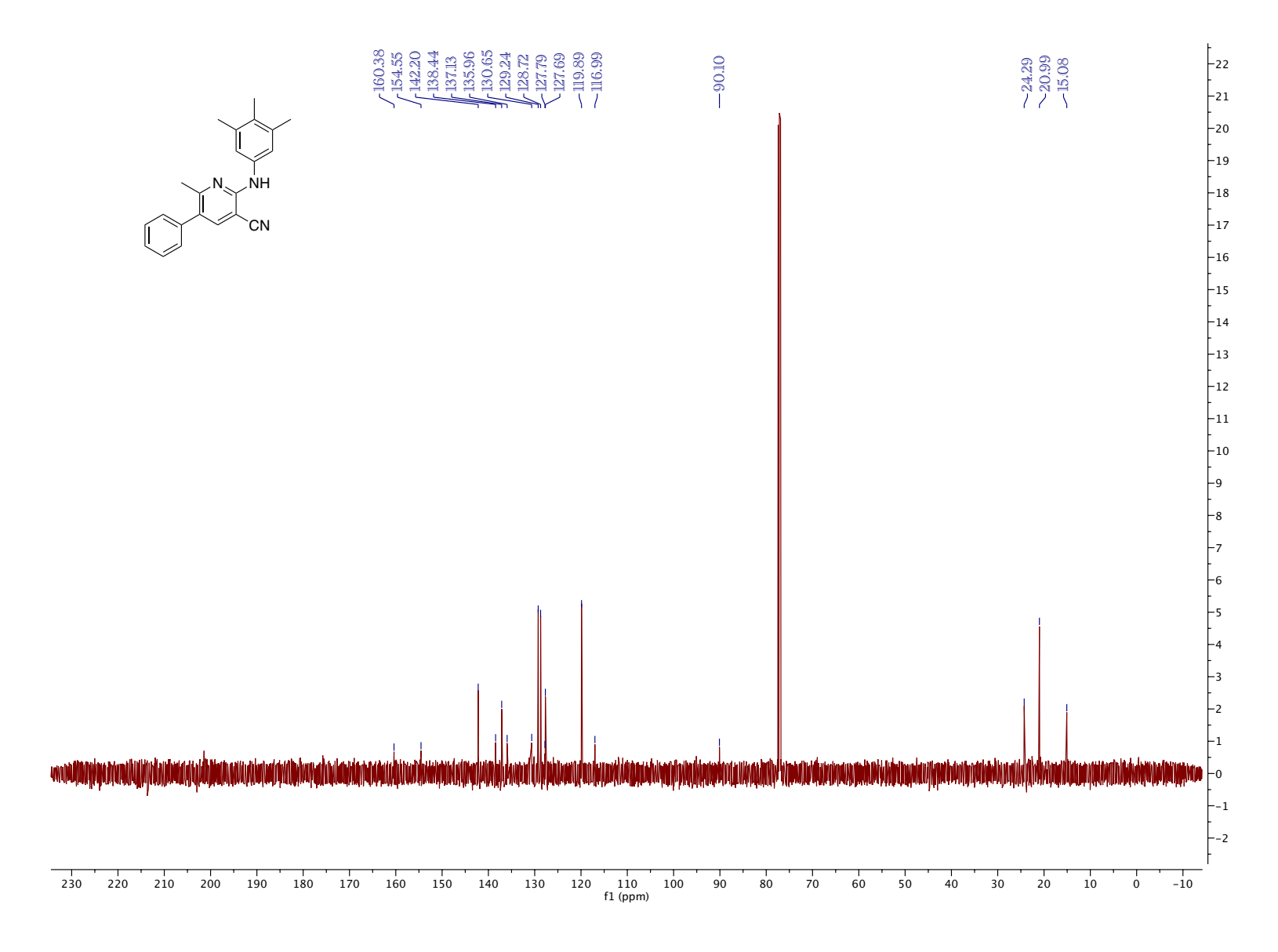


Figure 5.45. ¹³C NMR (CDCl₃, 126 MHz, 25 °C)

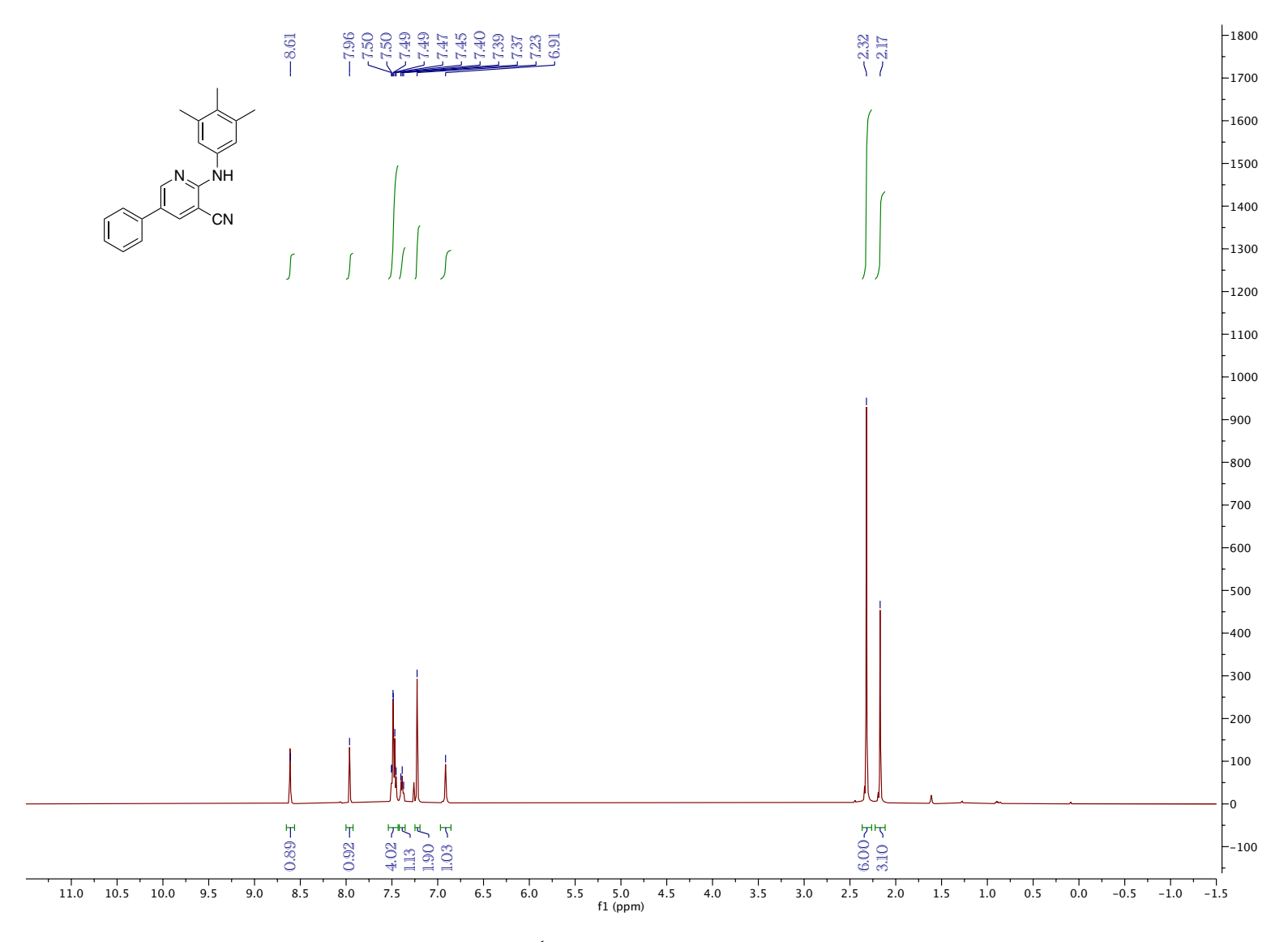


Figure 5.46. ¹H NMR (CDCl₃, 500 MHz, 25 °C)

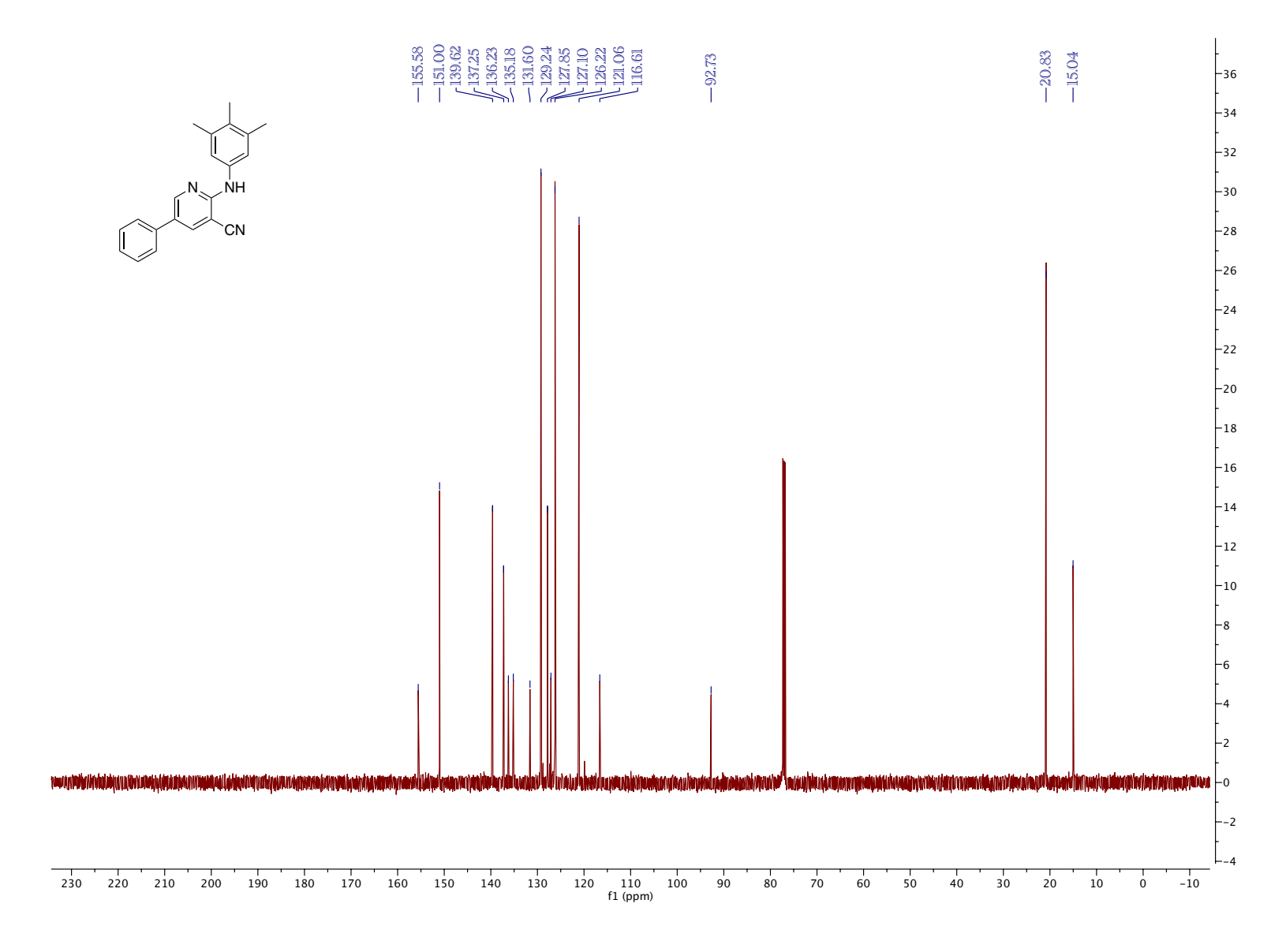


Figure 5.47. 13 C NMR (CDCl₃, 126 MHz, 25 $^{\circ}$ C)

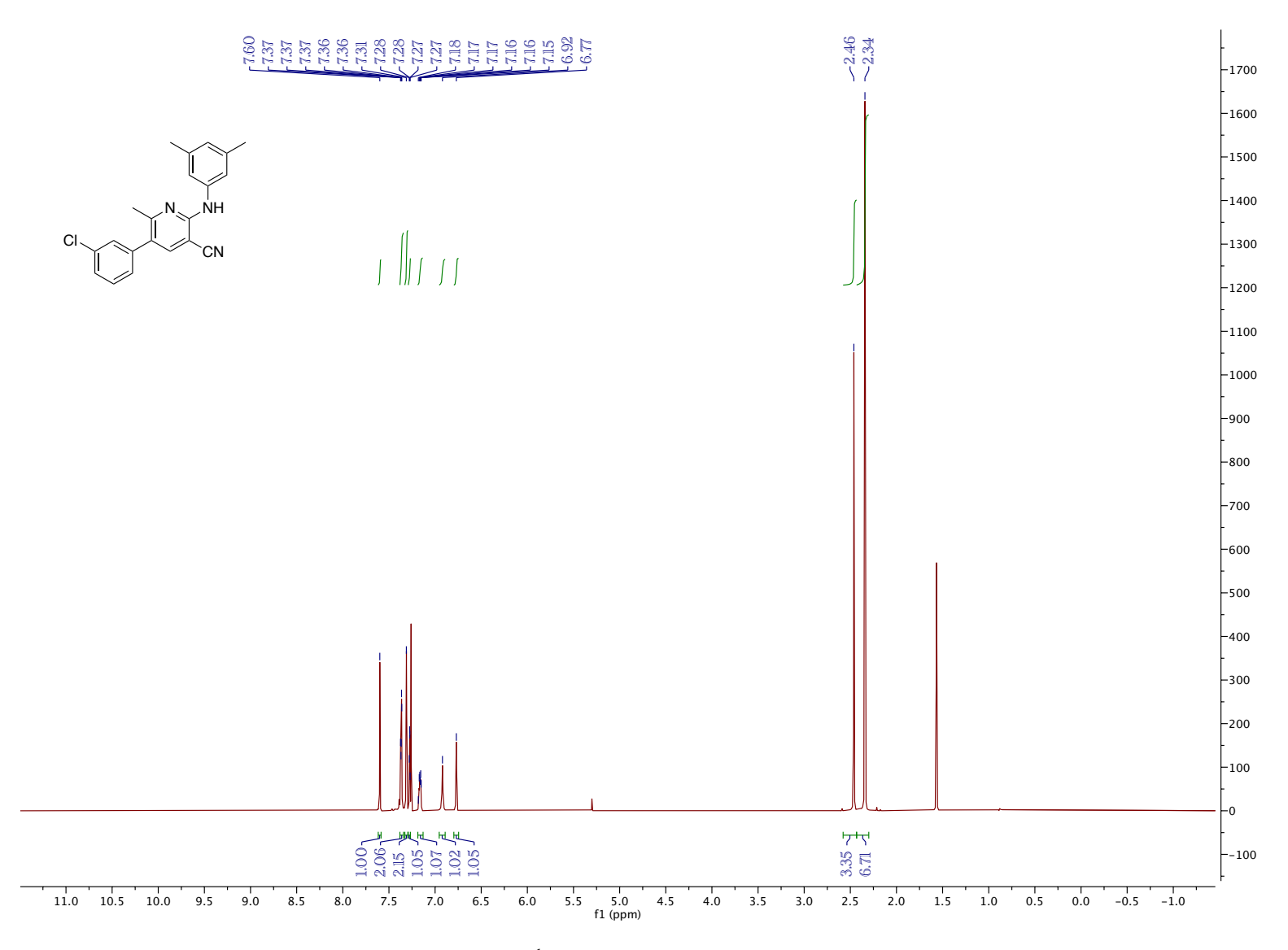


Figure 5.48. ¹H NMR (CDCl₃, 500 MHz, 25 °C)

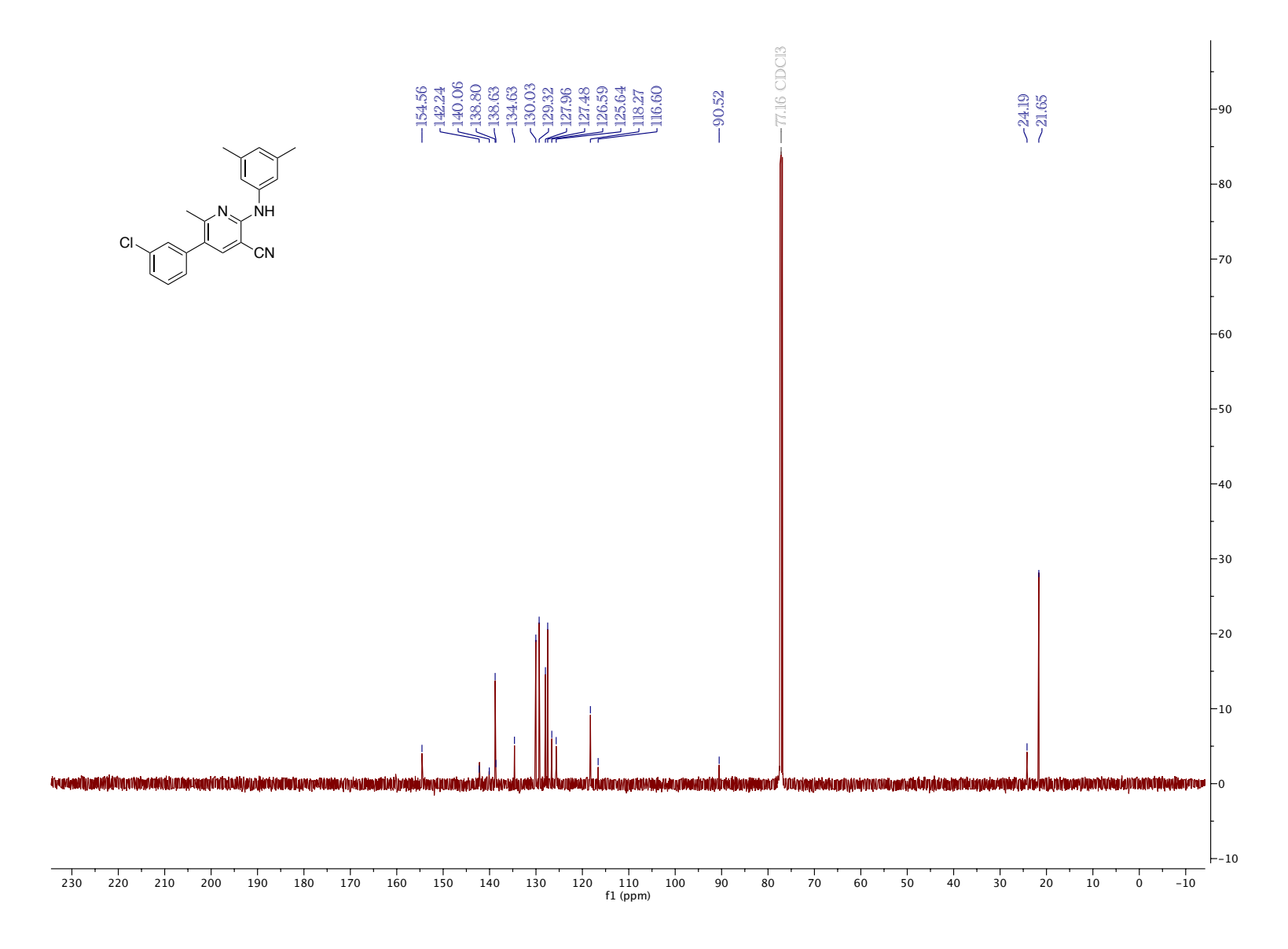


Figure 5.49. ¹³C NMR (CDCl₃, 126 MHz, 25 °C)

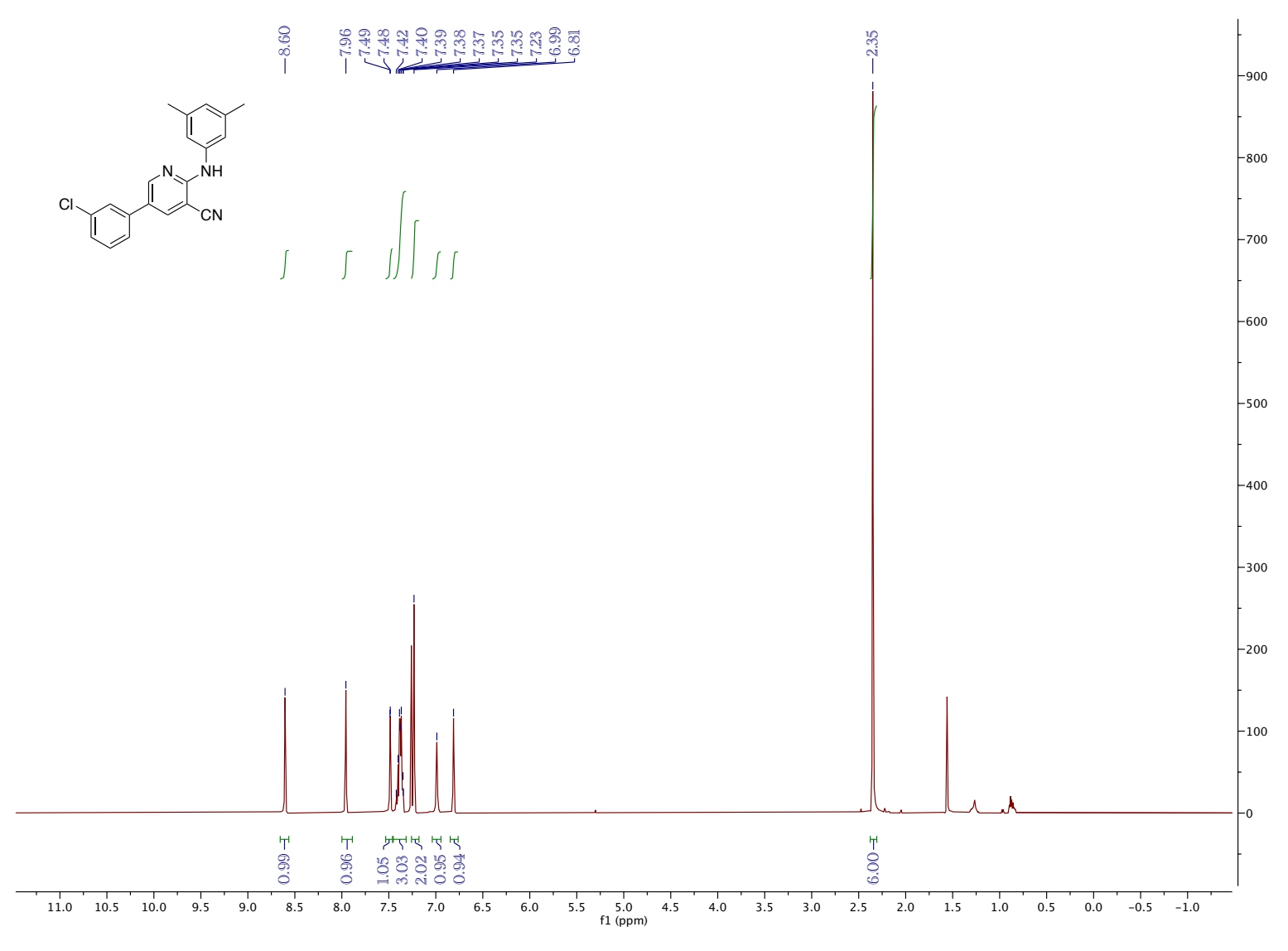


Figure 5.50. ¹H NMR (CDCl₃, 500 MHz, 25 °C)

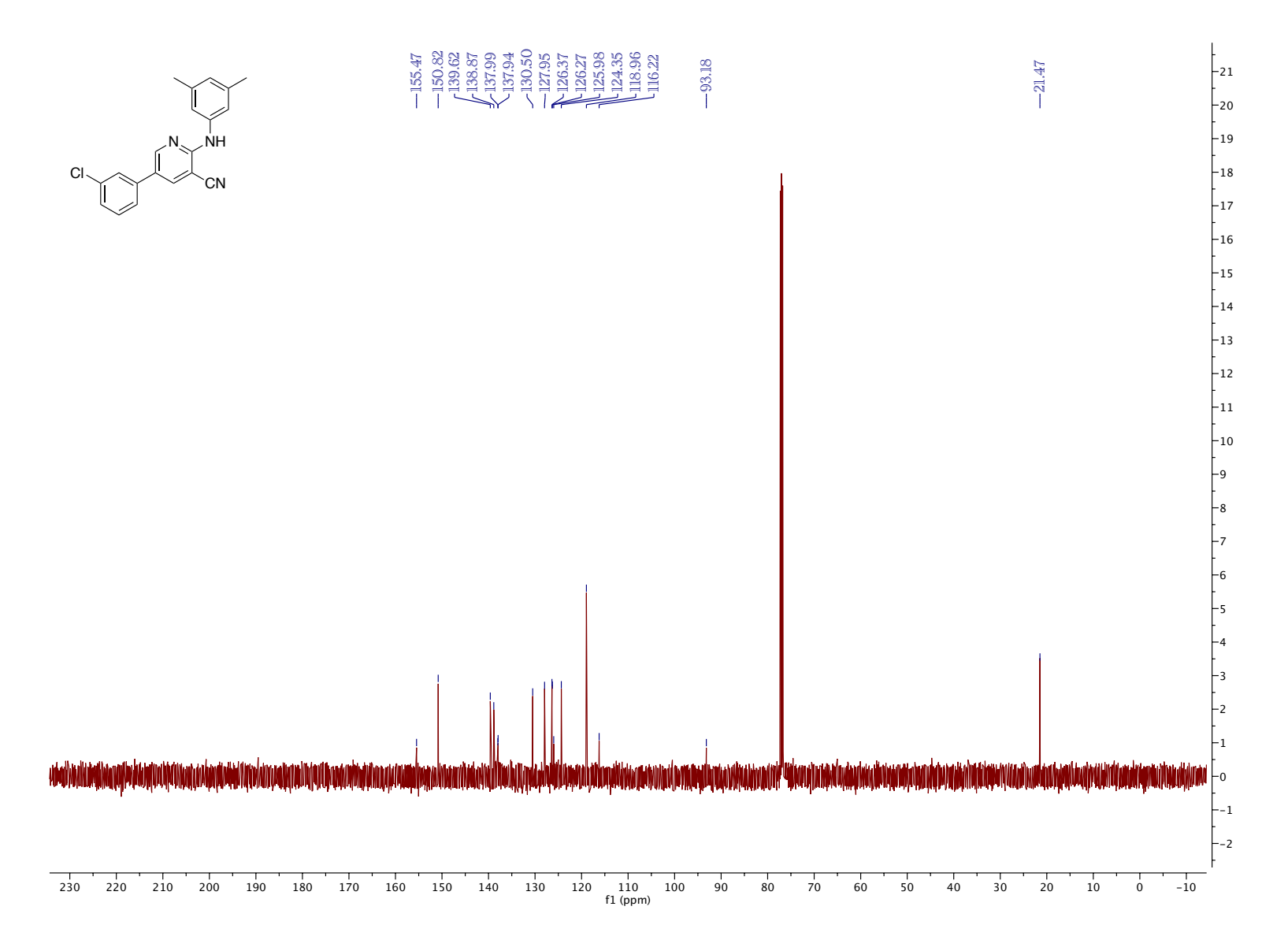


Figure 5.51. ¹³C NMR (CDCl₃, 126 MHz, 25 °C)

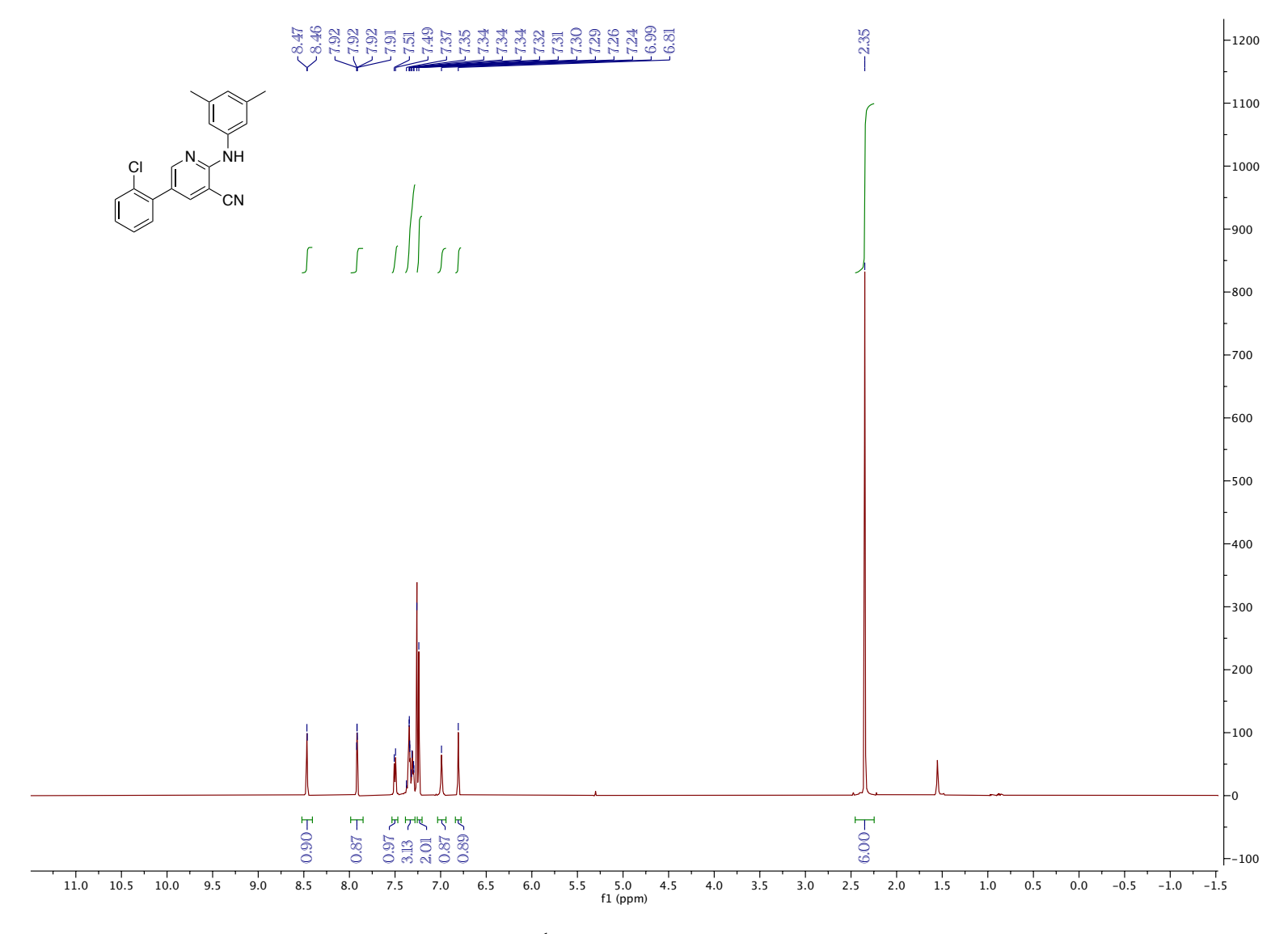


Figure 5.52. ¹H NMR (CDCl₃, 500 MHz, 25 °C)

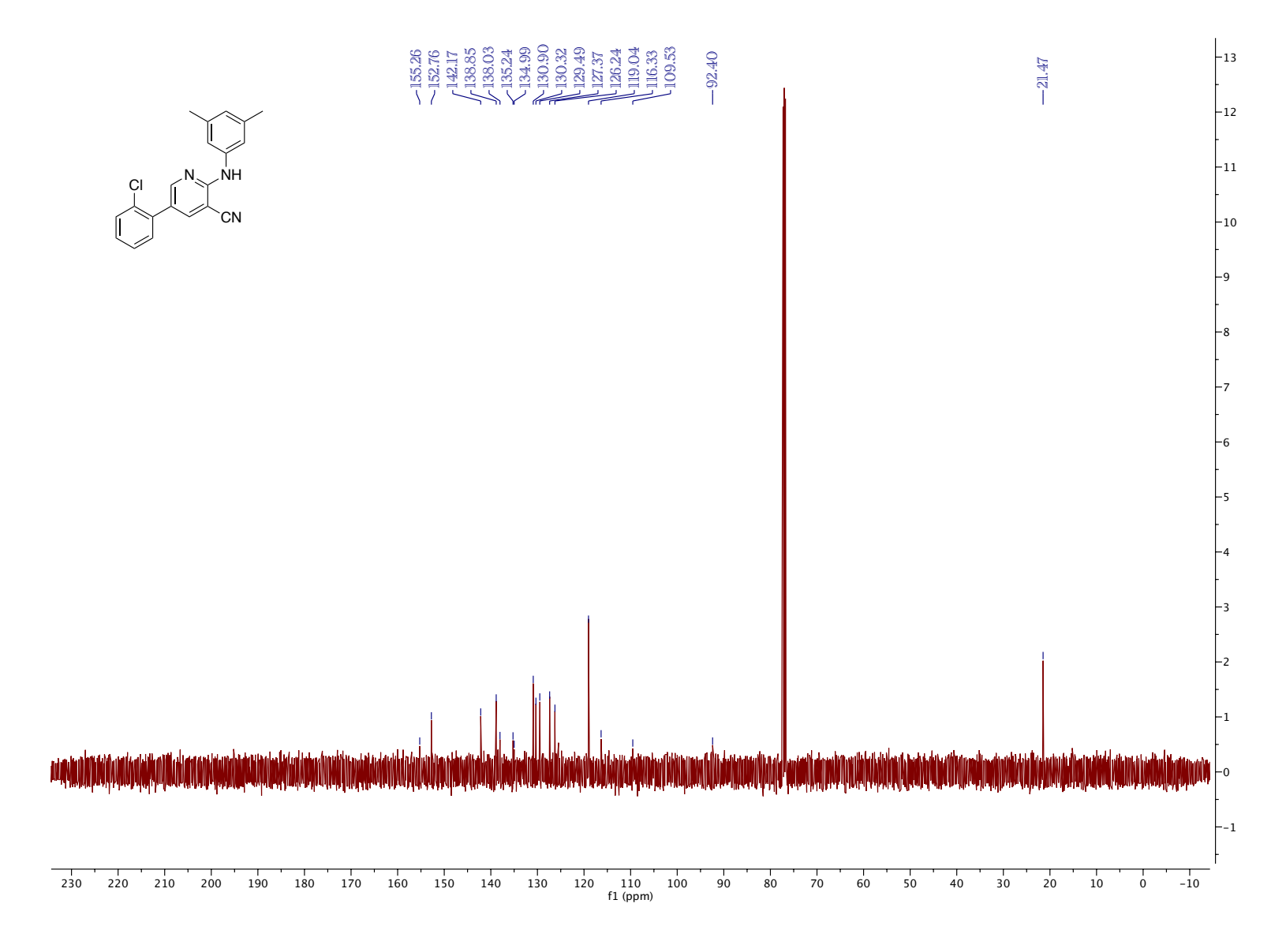


Figure 5.53. ¹³C NMR (CDCl₃, 126 MHz, 25 °C)

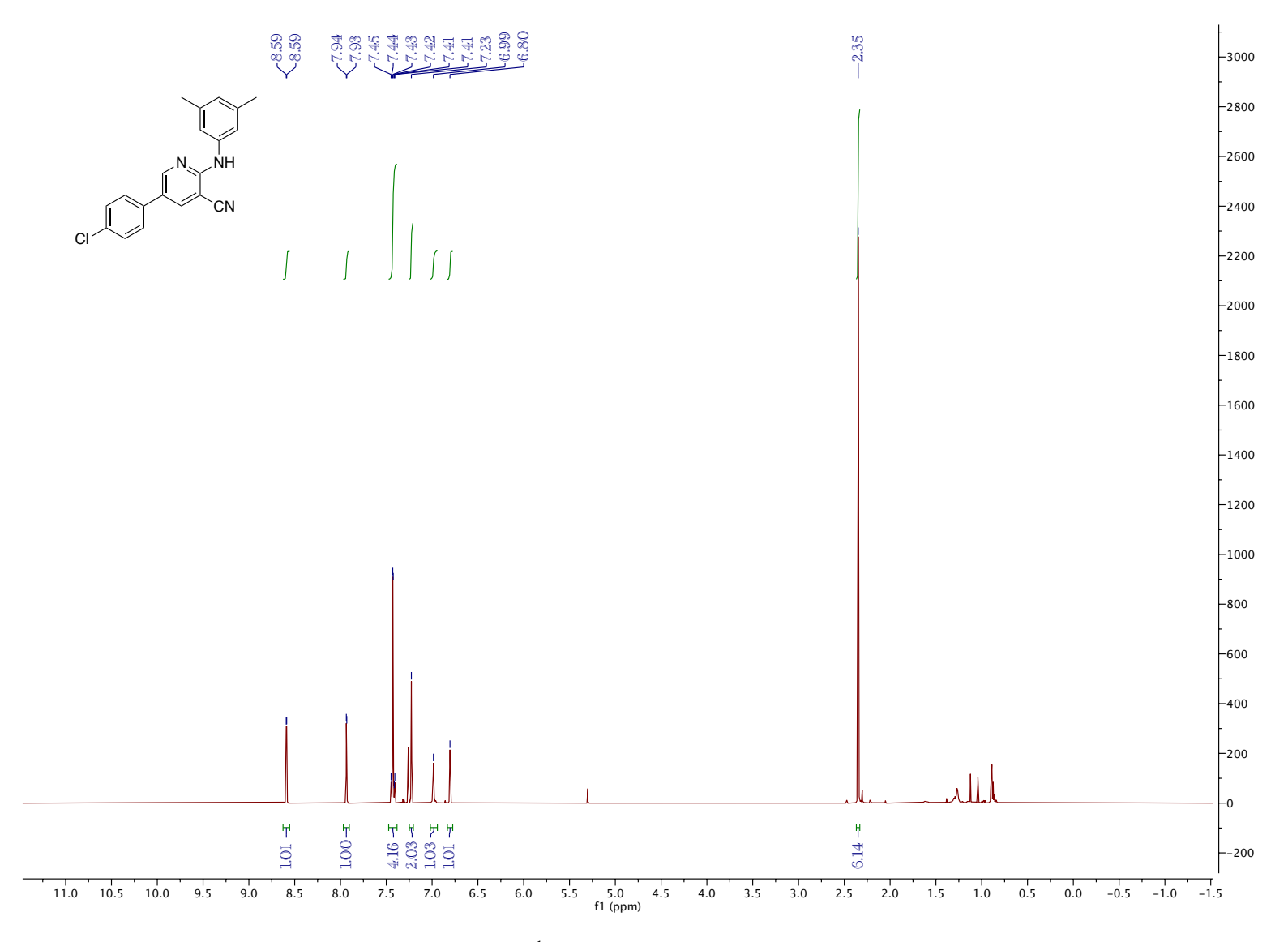


Figure 5.54. ¹H NMR (CDCl₃, 500 MHz, 25 °C)

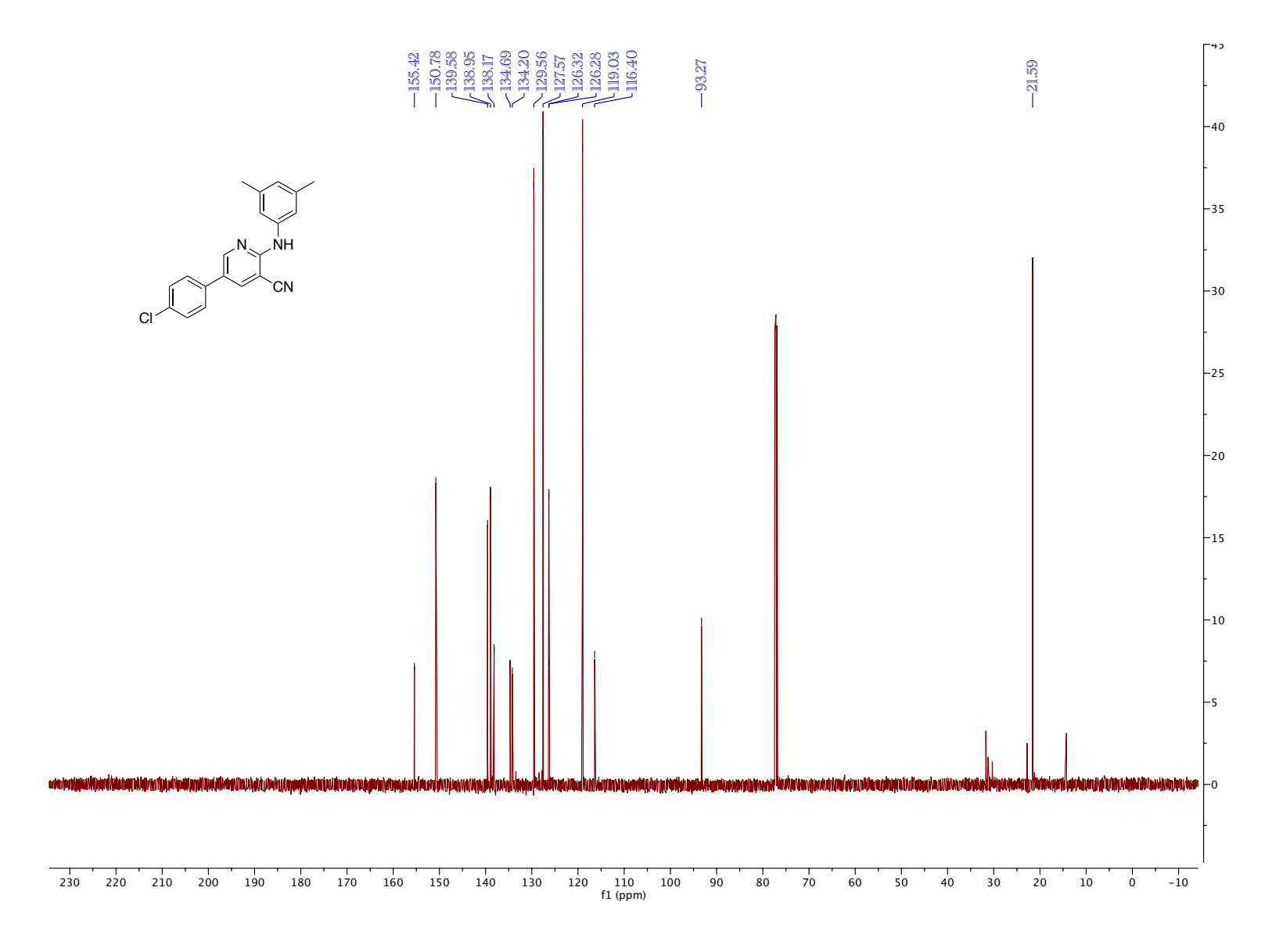


Figure 5.55. ¹³C NMR (CDCl₃, 126 MHz, 25 °C)

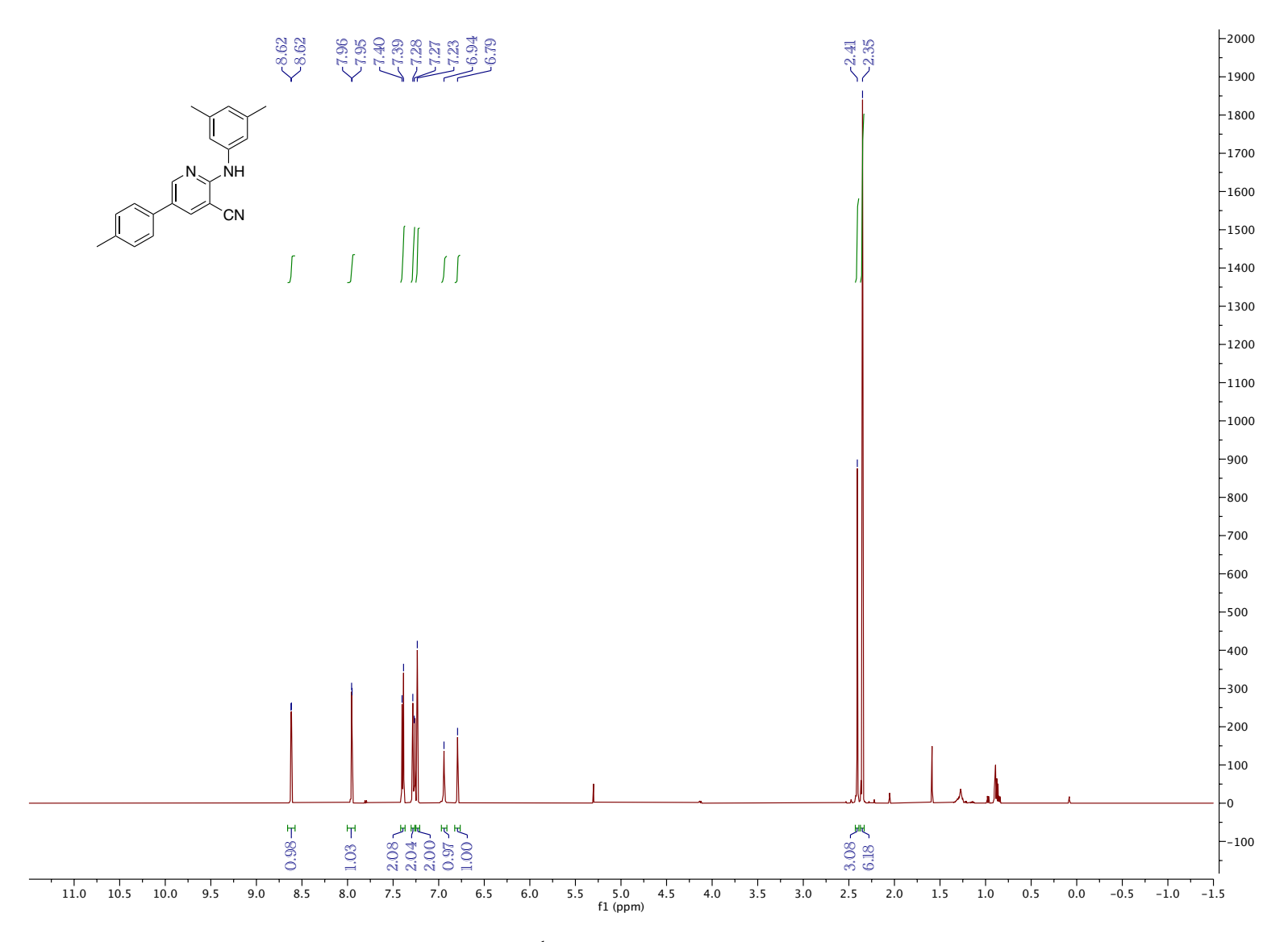


Figure 5.56. ¹H NMR (CDCl₃, 500 MHz, 25 °C)

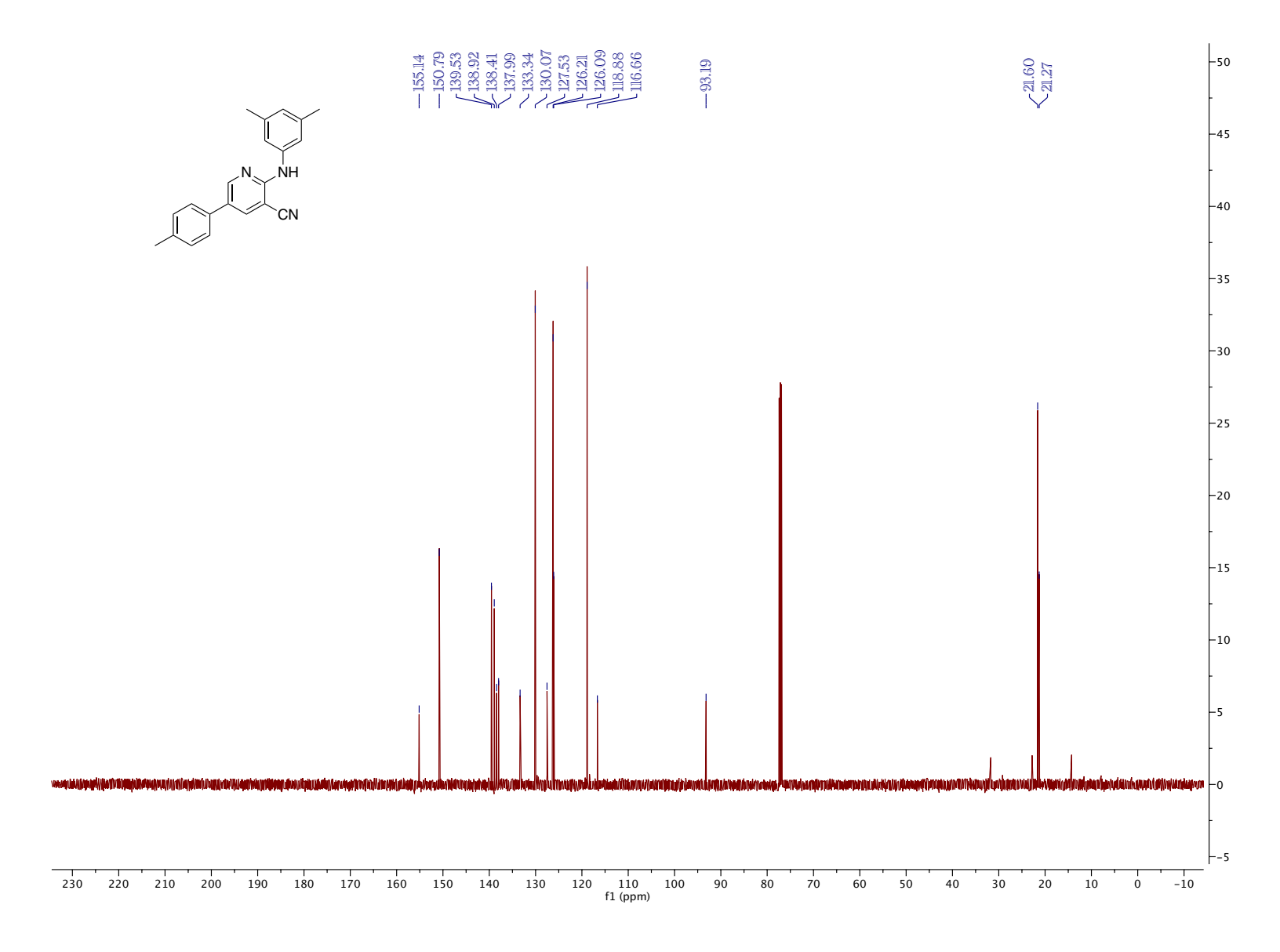


Figure 5.57. ¹³C NMR (CDCl₃, 126 MHz, 25 °C)

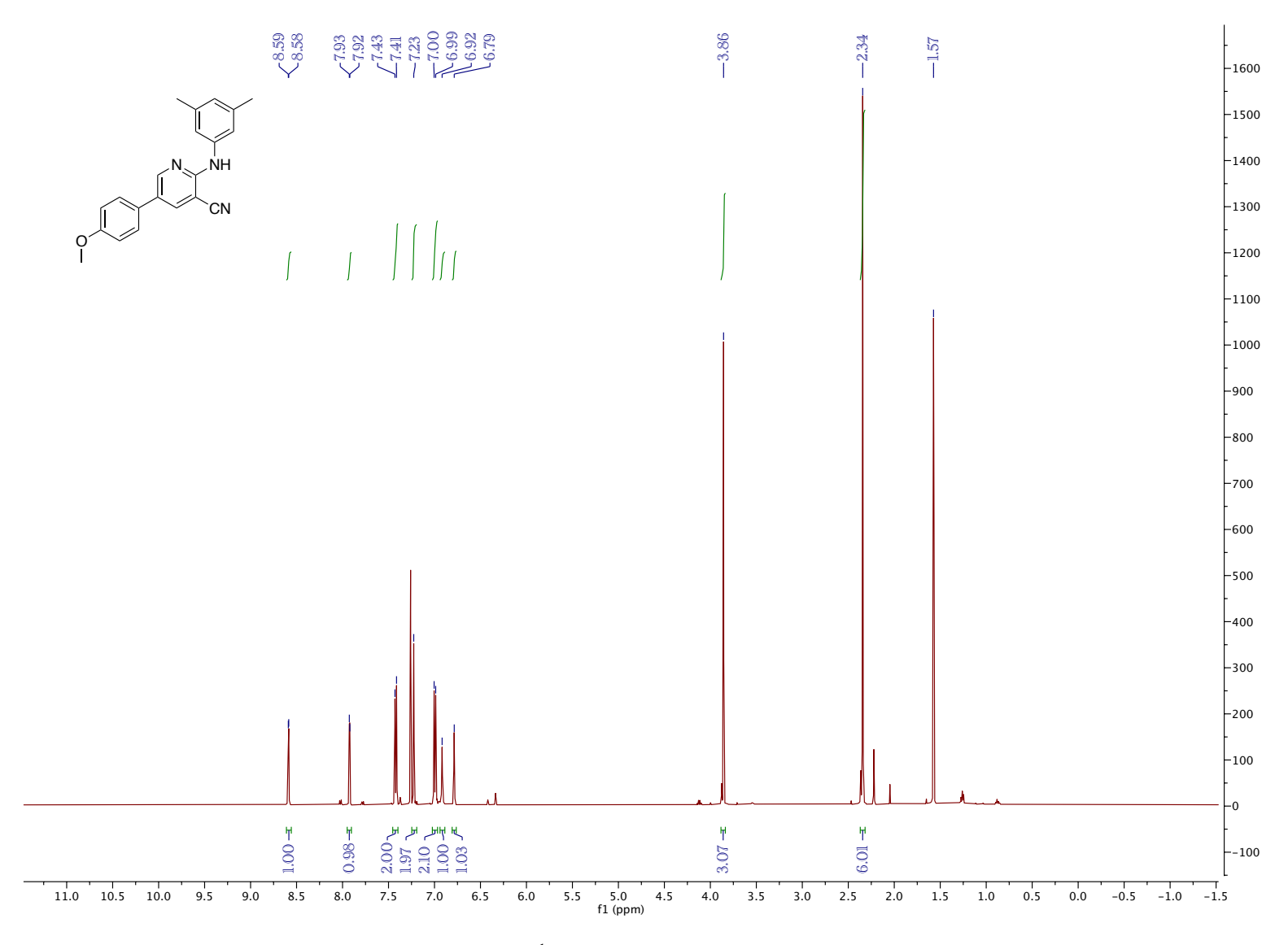


Figure 5.58. ¹H NMR (CDCl₃, 500 MHz, 25 °C)

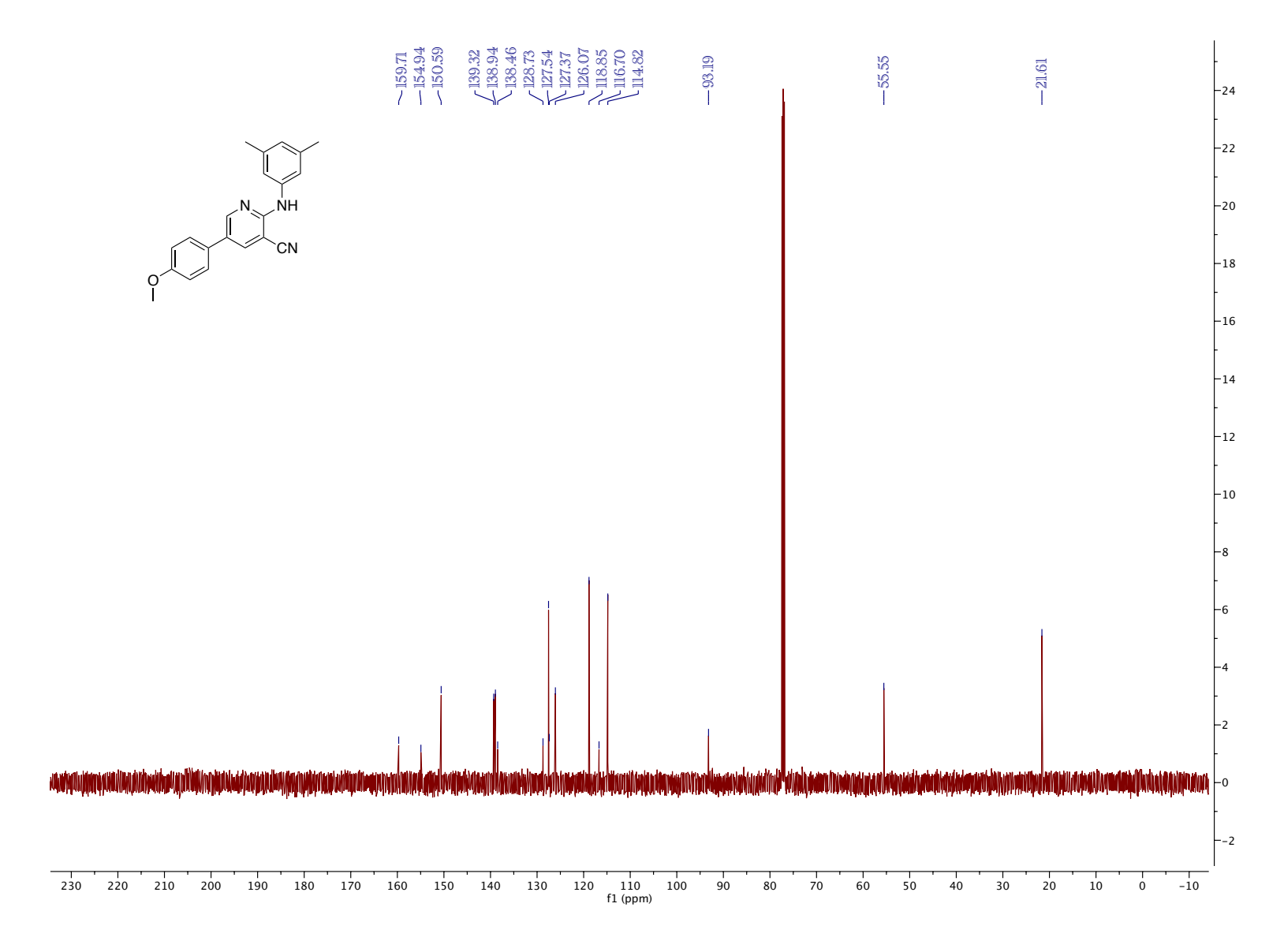


Figure 5.59. ¹³C NMR (CDCl₃, 126 MHz, 25 °C)

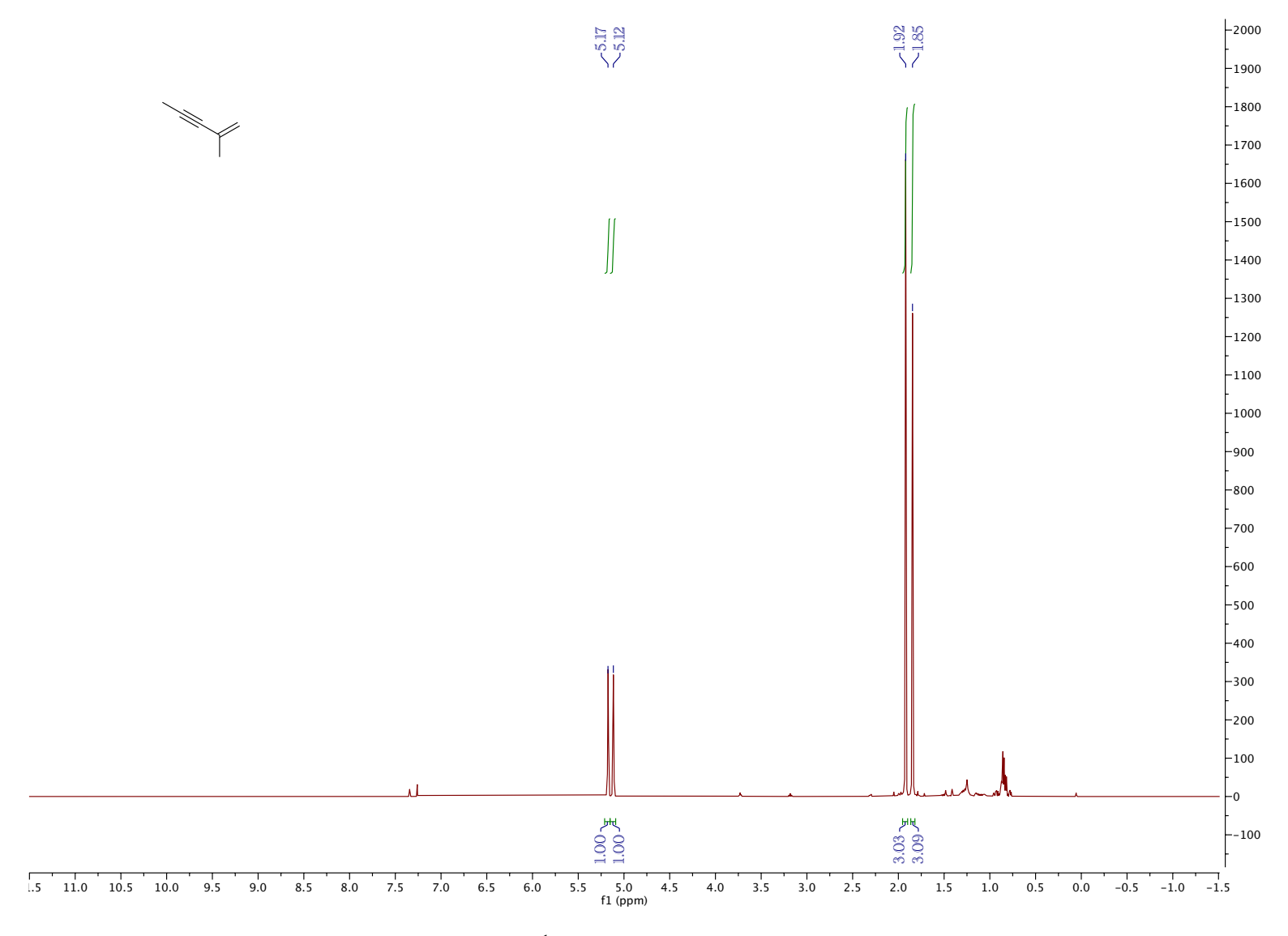


Figure 5.60. ¹H NMR (CDCl₃, 500 MHz, 25 °C)

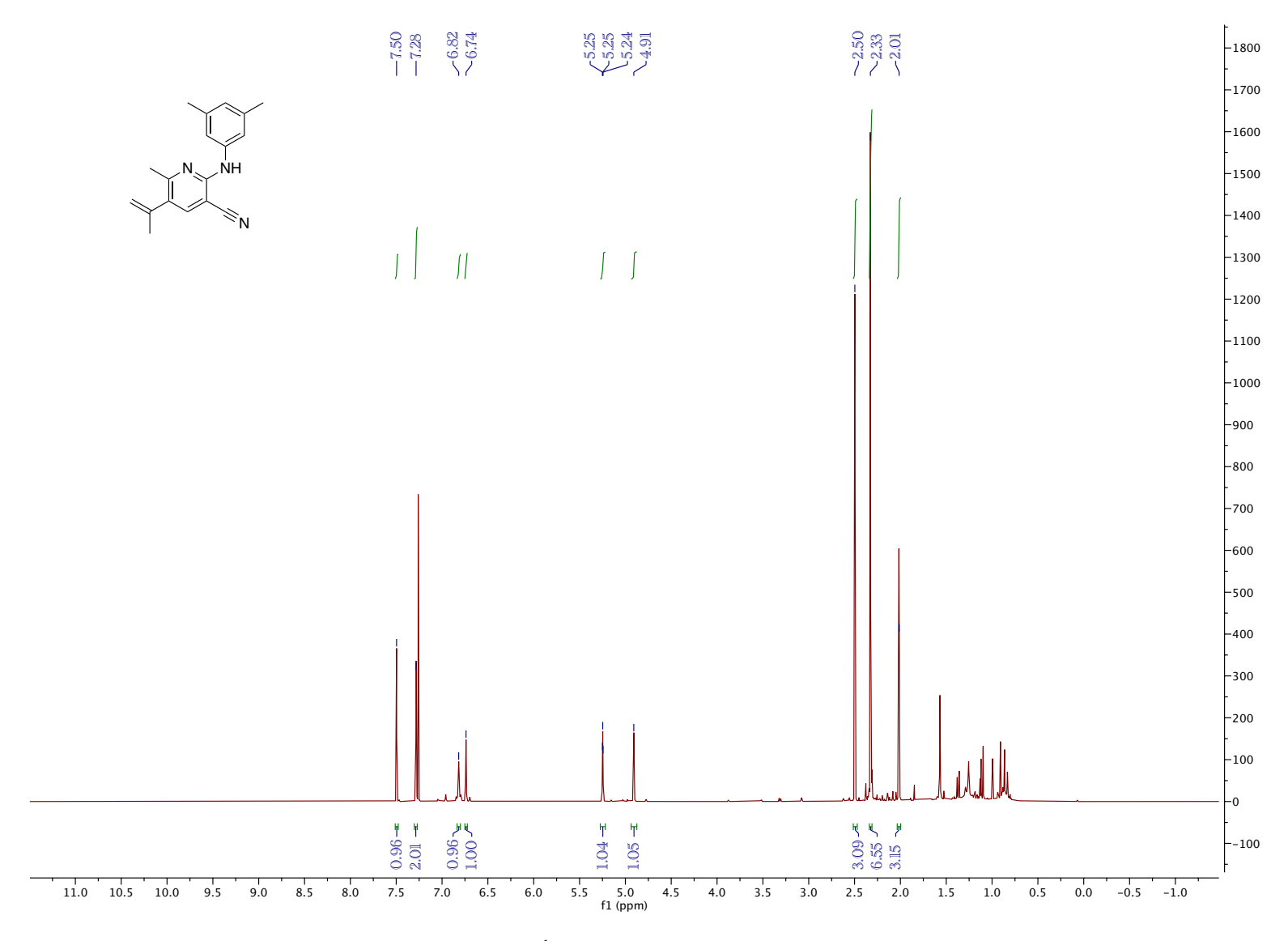


Figure 5.61. ¹H NMR (CDCl₃, 500 MHz, 25 °C)

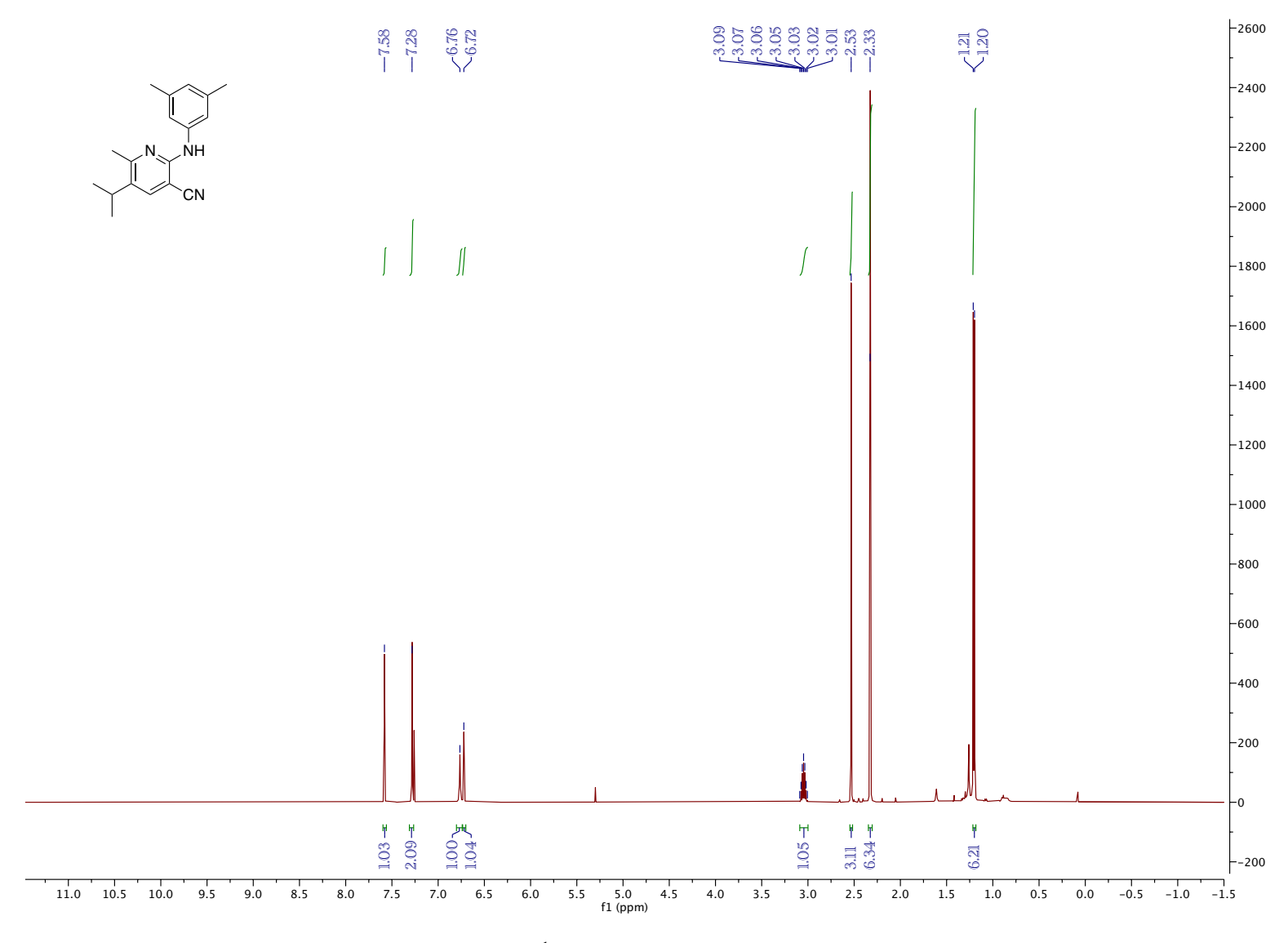


Figure 5.62. ¹H NMR (CDCl₃, 500 MHz, 25 °C)

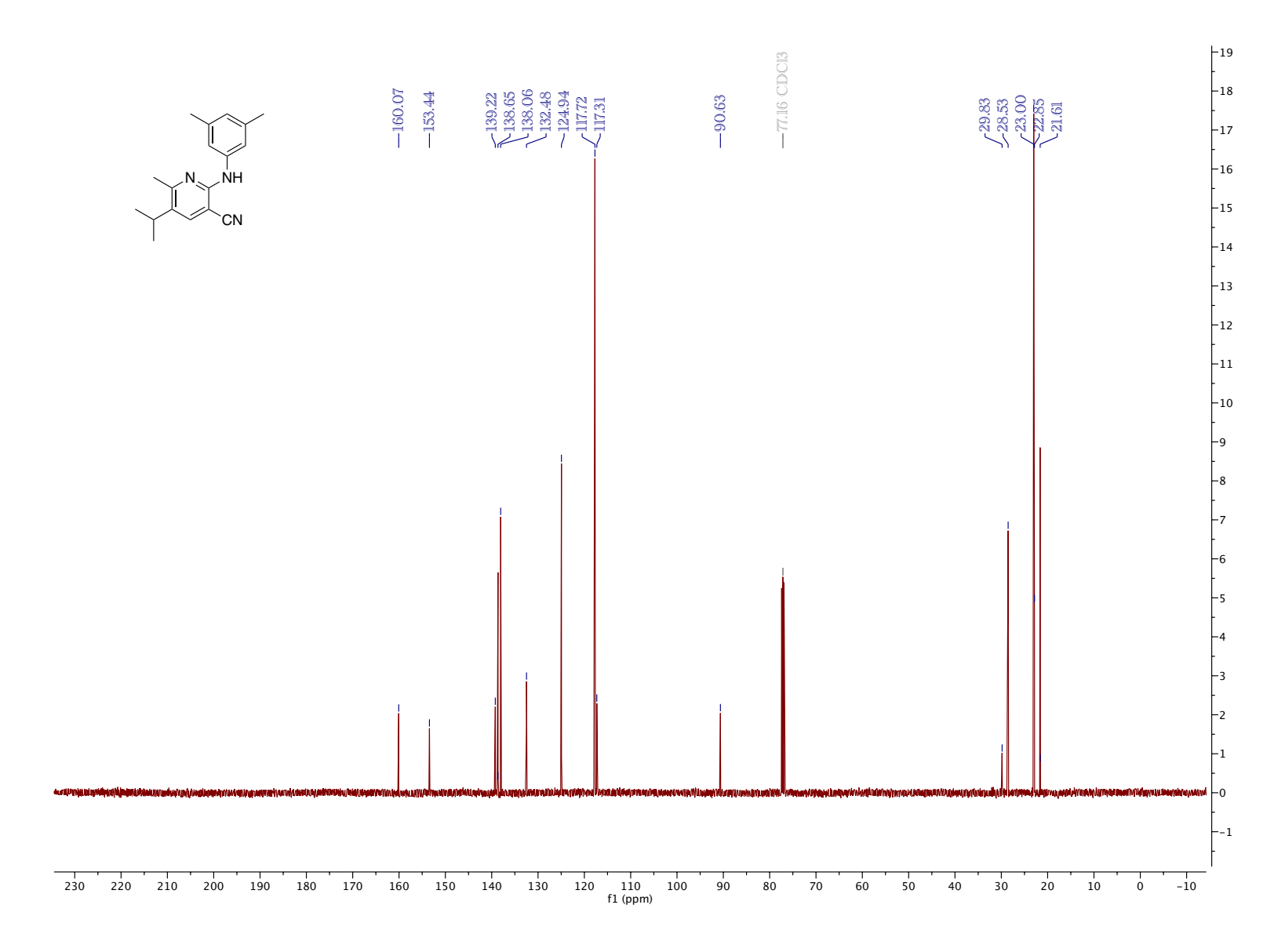


Figure 5.63. 13 C NMR (CDCl₃, 126 MHz, 25 $^{\circ}$ C)

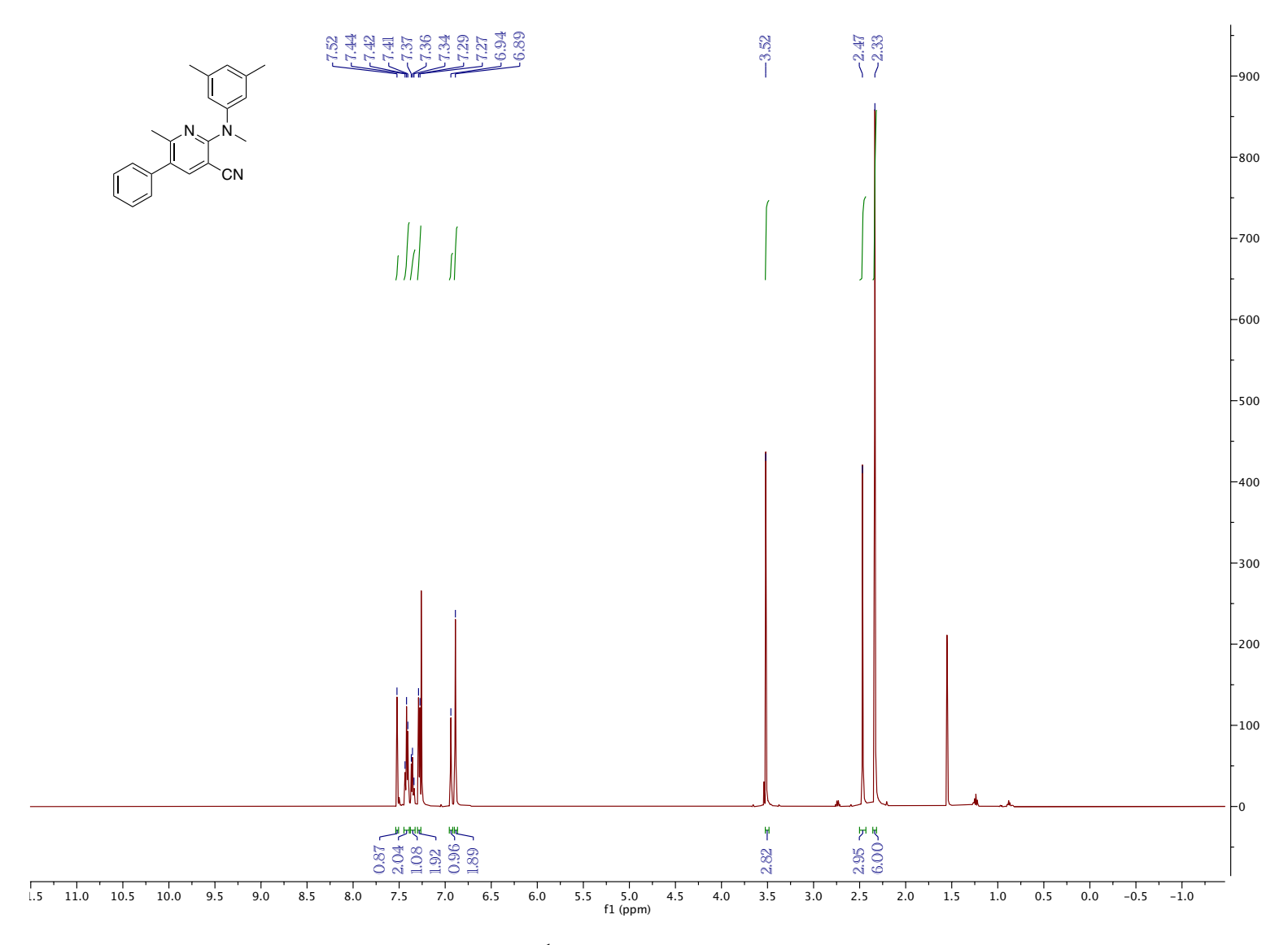


Figure 5.64. ¹H NMR (CDCl₃, 500 MHz, 25 °C)

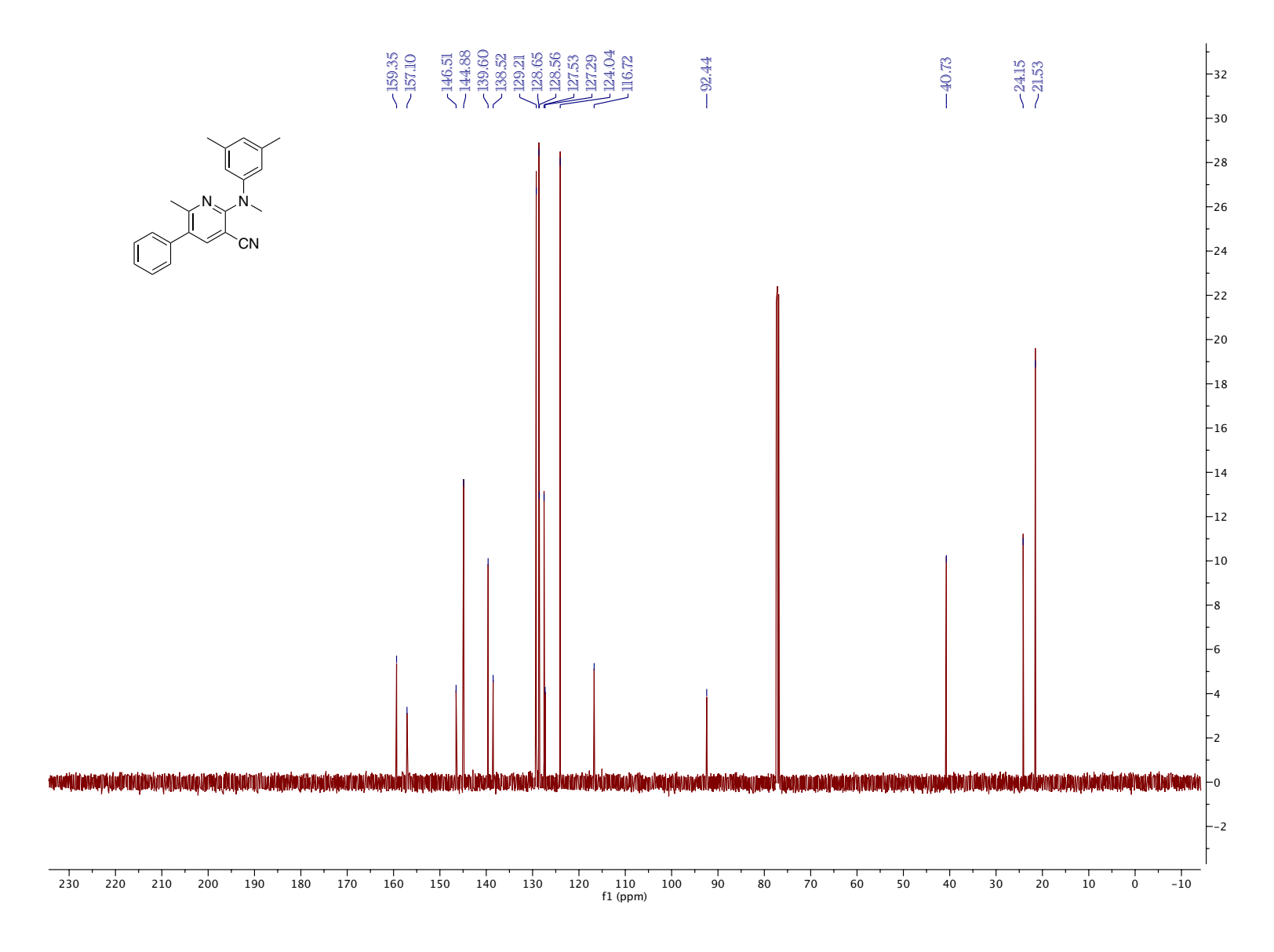


Figure 5.65. 13 C NMR (CDCl₃, 126 MHz, 25 $^{\circ}$ C)

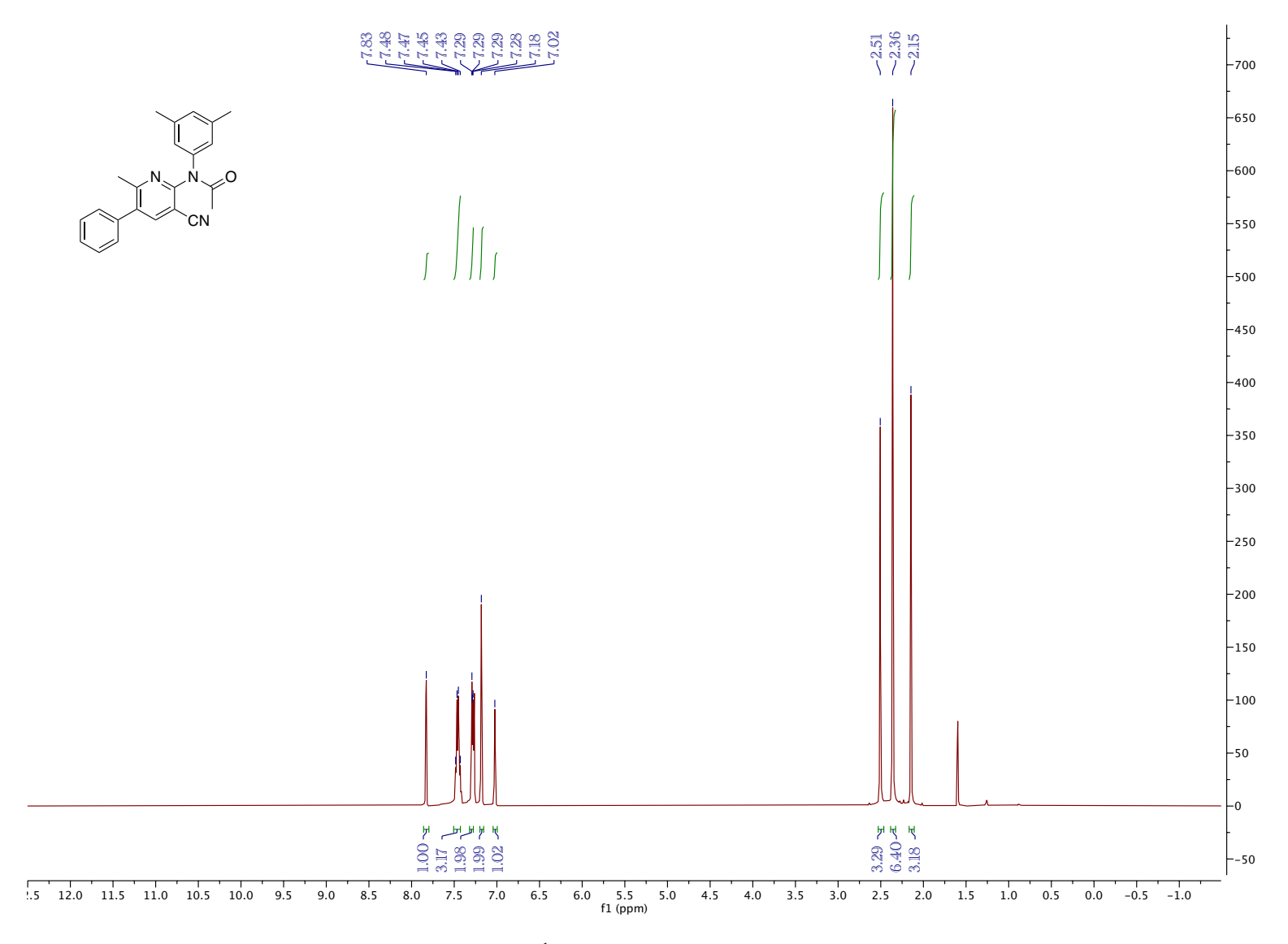


Figure 5.66. ¹H NMR (CDCl₃, 500 MHz, 25 °C)

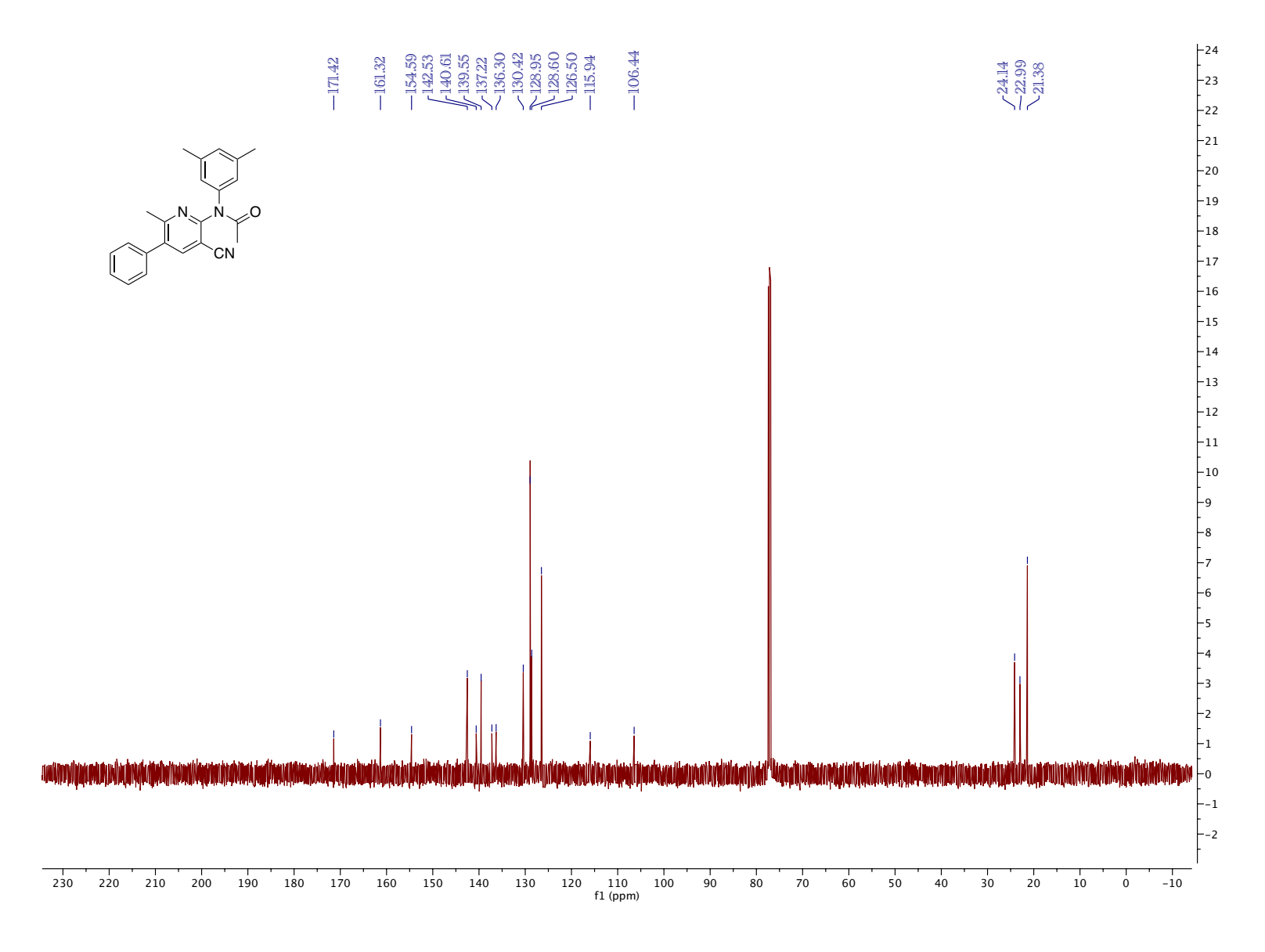


Figure 5.67. 13 C NMR (CDCl₃, 126 MHz, 25 $^{\circ}$ C)

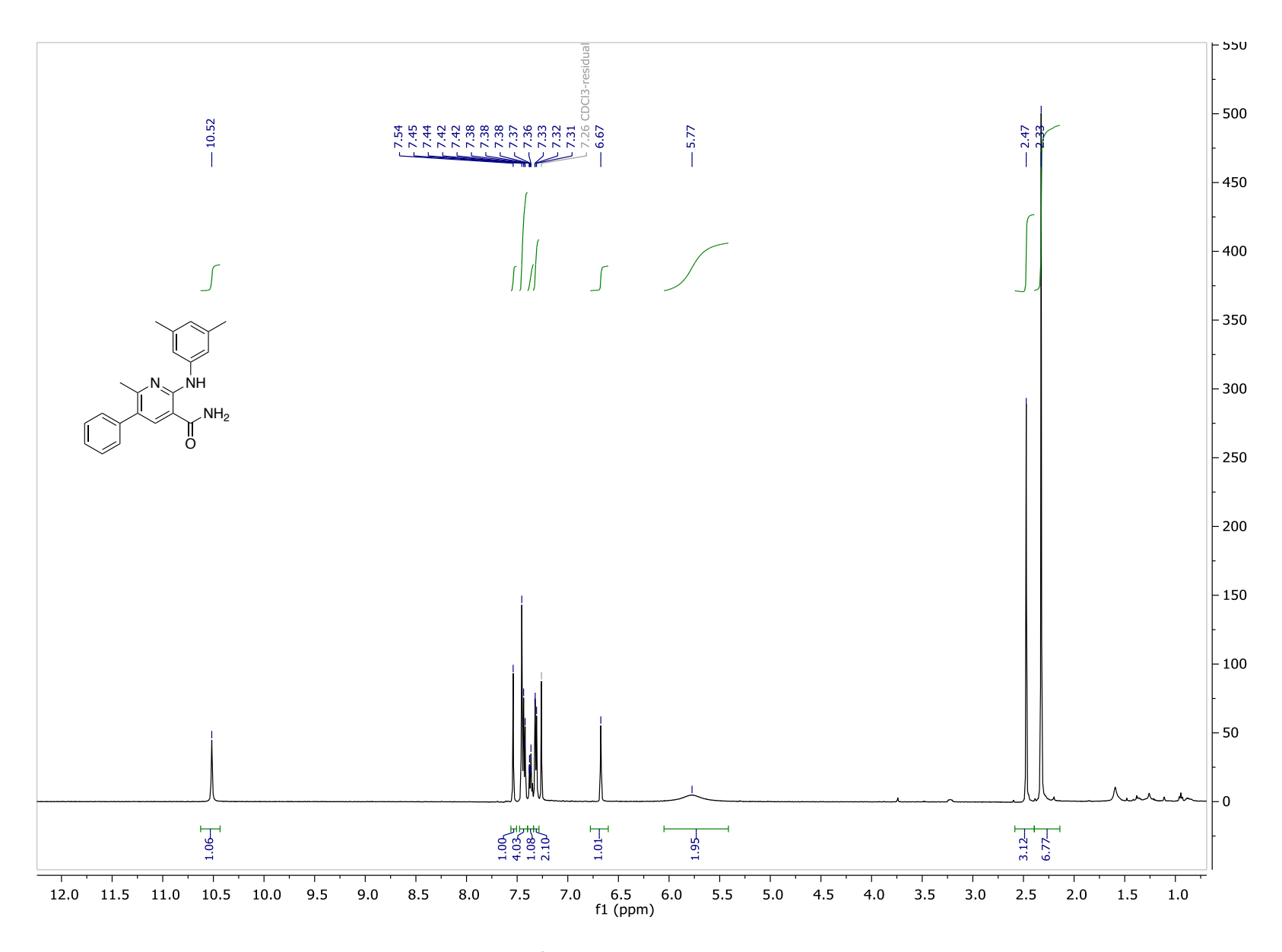


Figure 5.68. ¹H NMR (CDCl₃, 500 MHz, 25 °C)

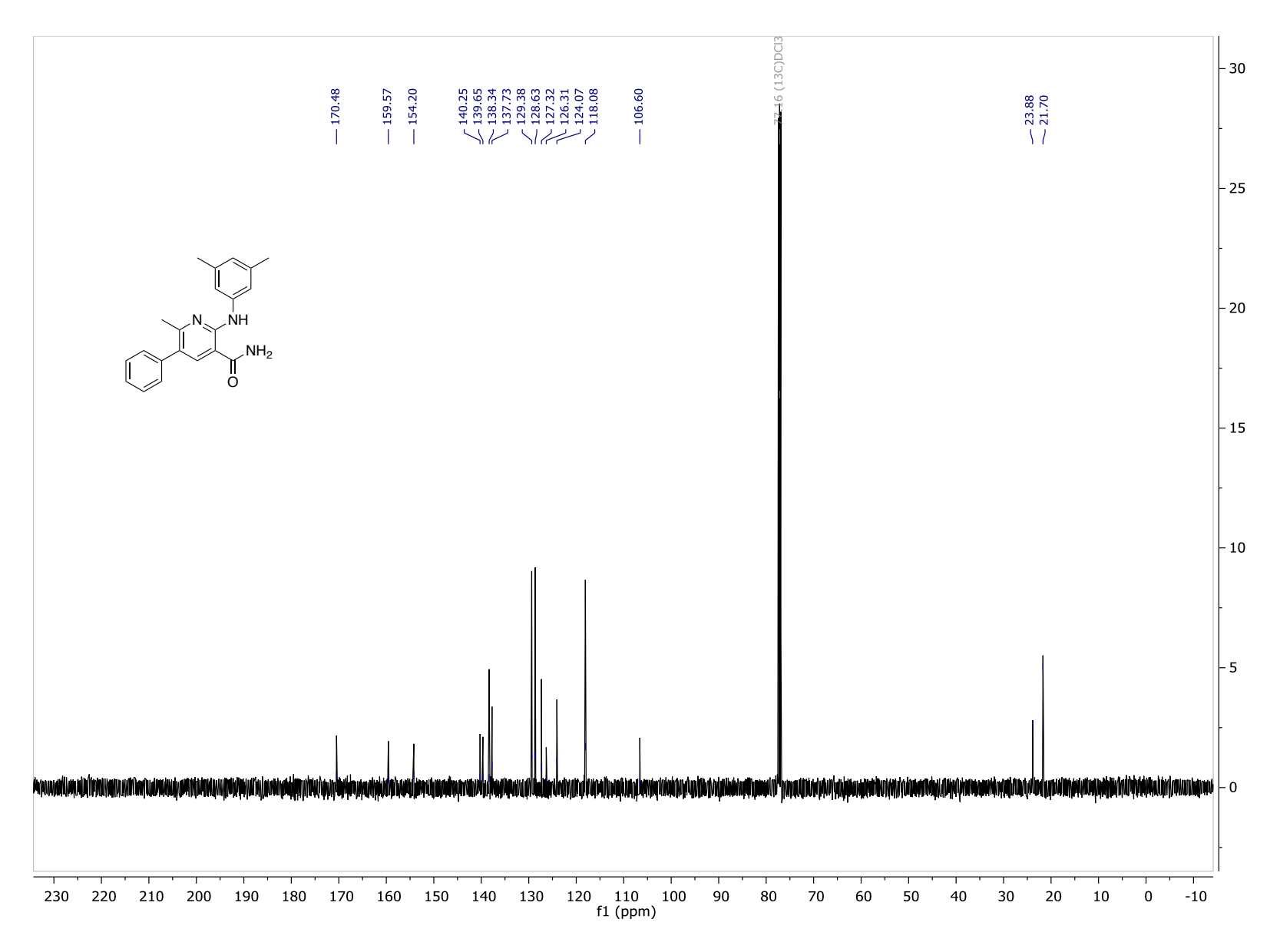


Figure 5.69. ¹³C NMR (CDCl₃, 126 MHz, 25 °C)

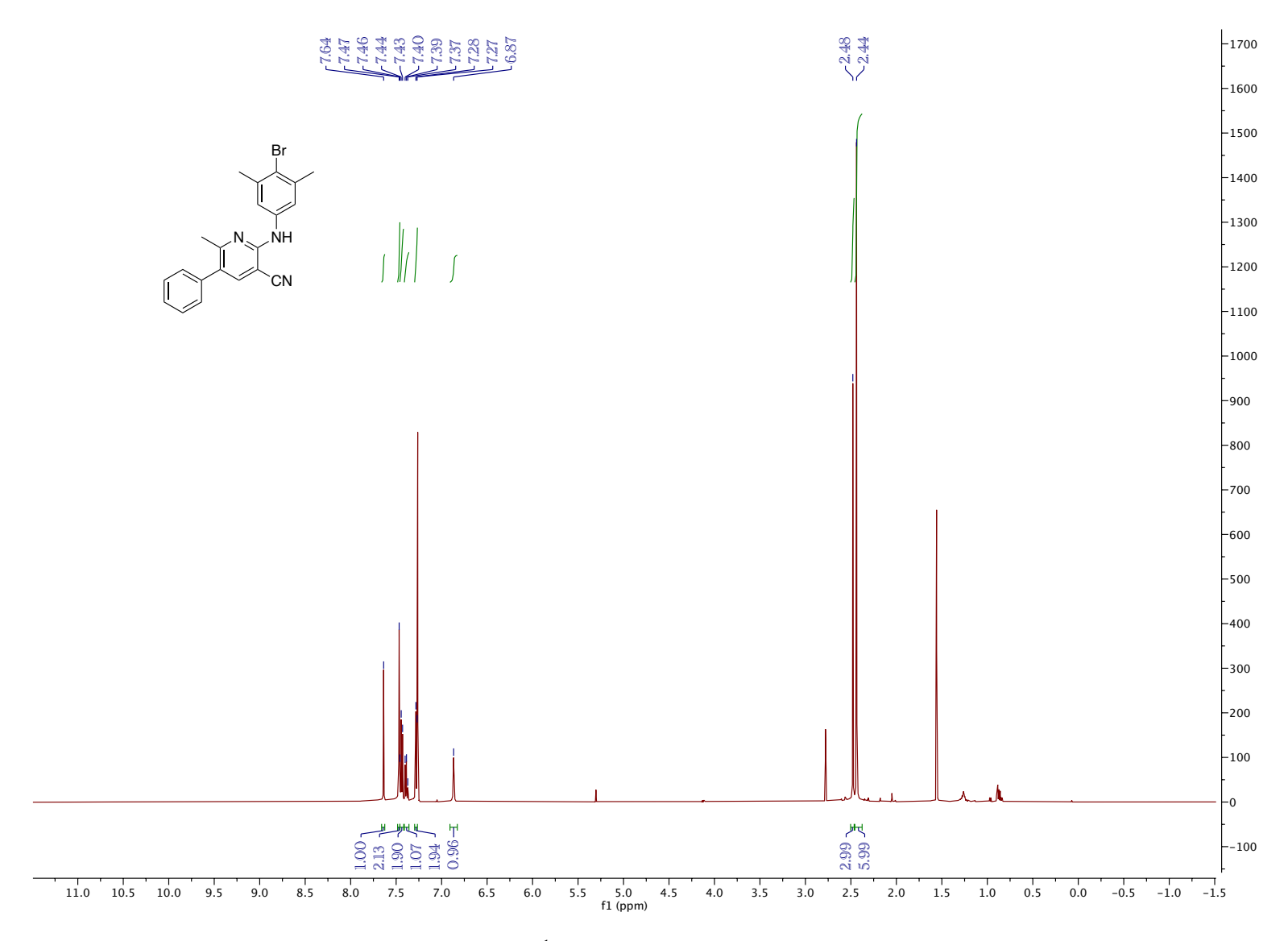


Figure 5.70. ¹H NMR (CDCl₃, 500 MHz, 25 °C)

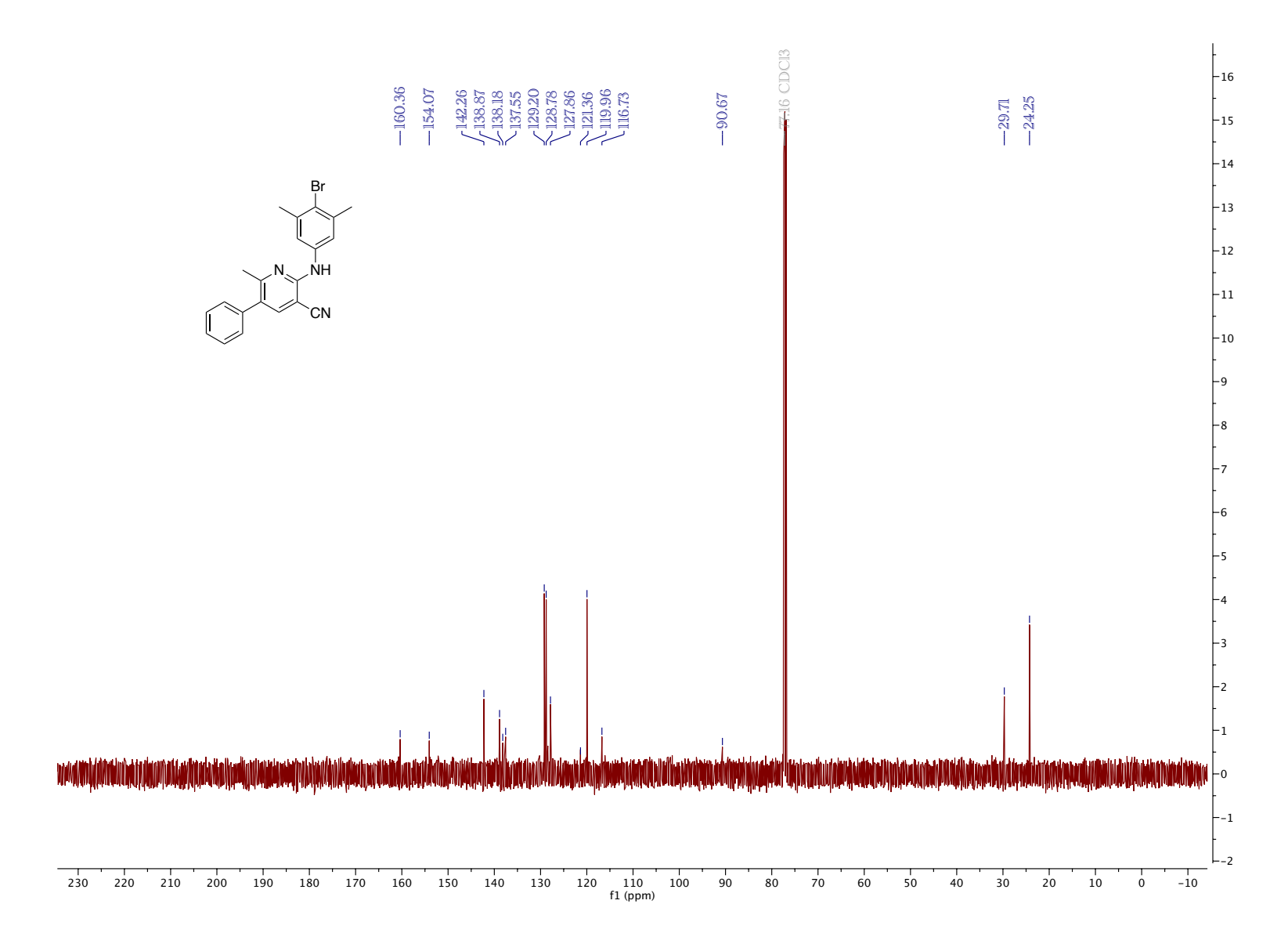


Figure 5.71. ¹³C NMR (CDCl₃, 126 MHz, 25 °C)

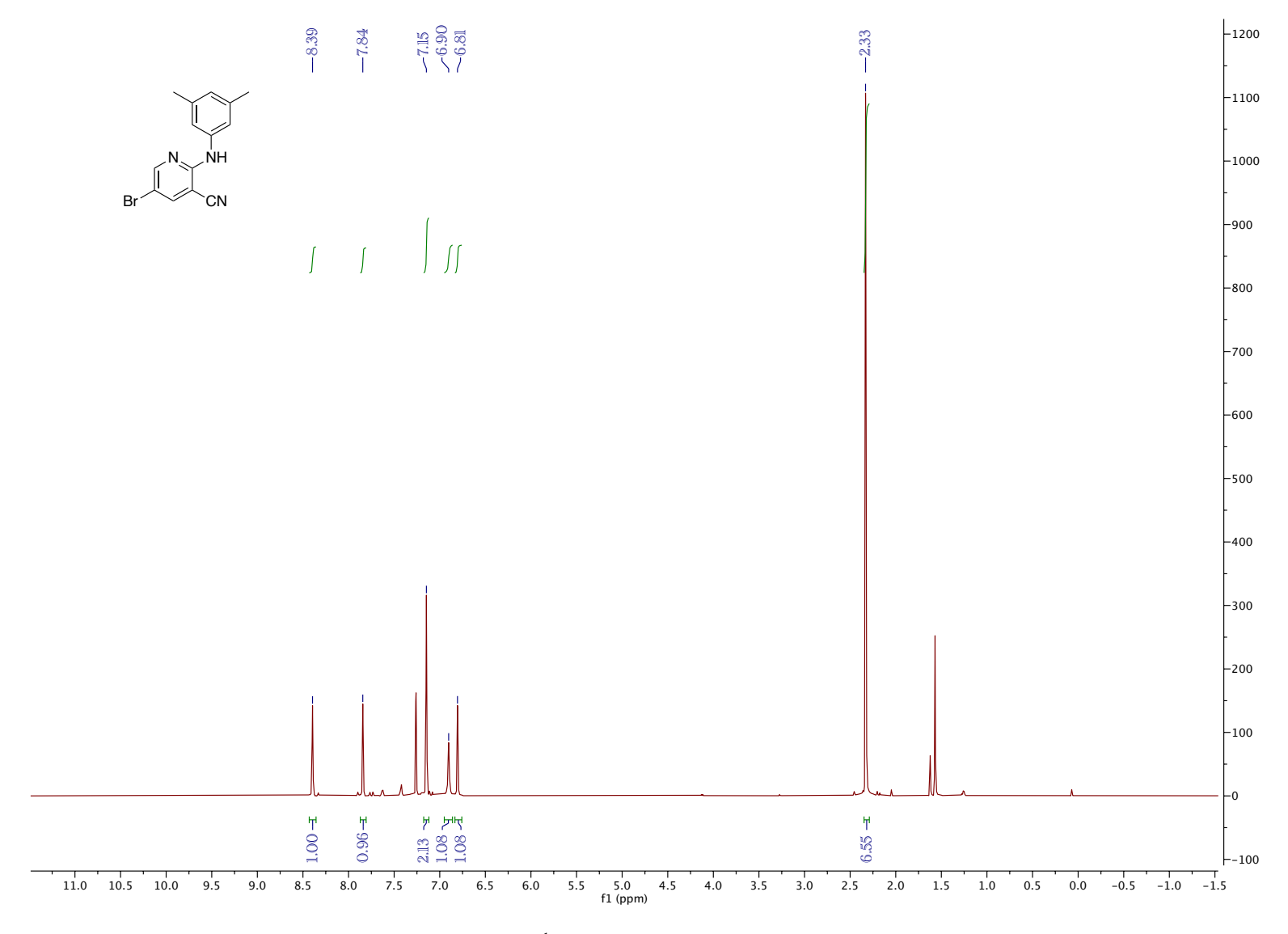


Figure 5.72. ¹H NMR (CDCl₃, 500 MHz, 25 °C)

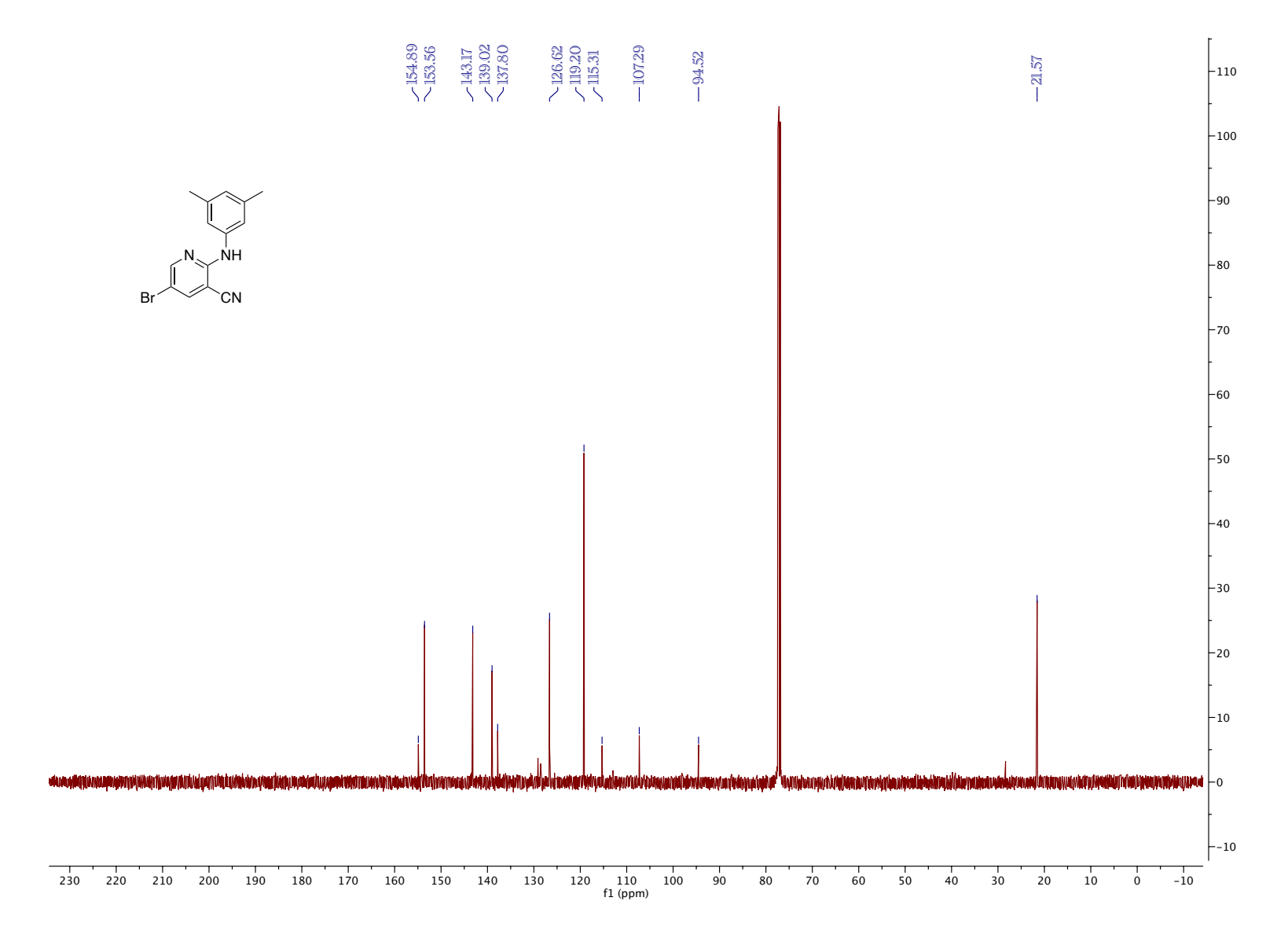


Figure 5.73. ¹³C NMR (CDCl₃, 126 MHz, 25 °C)

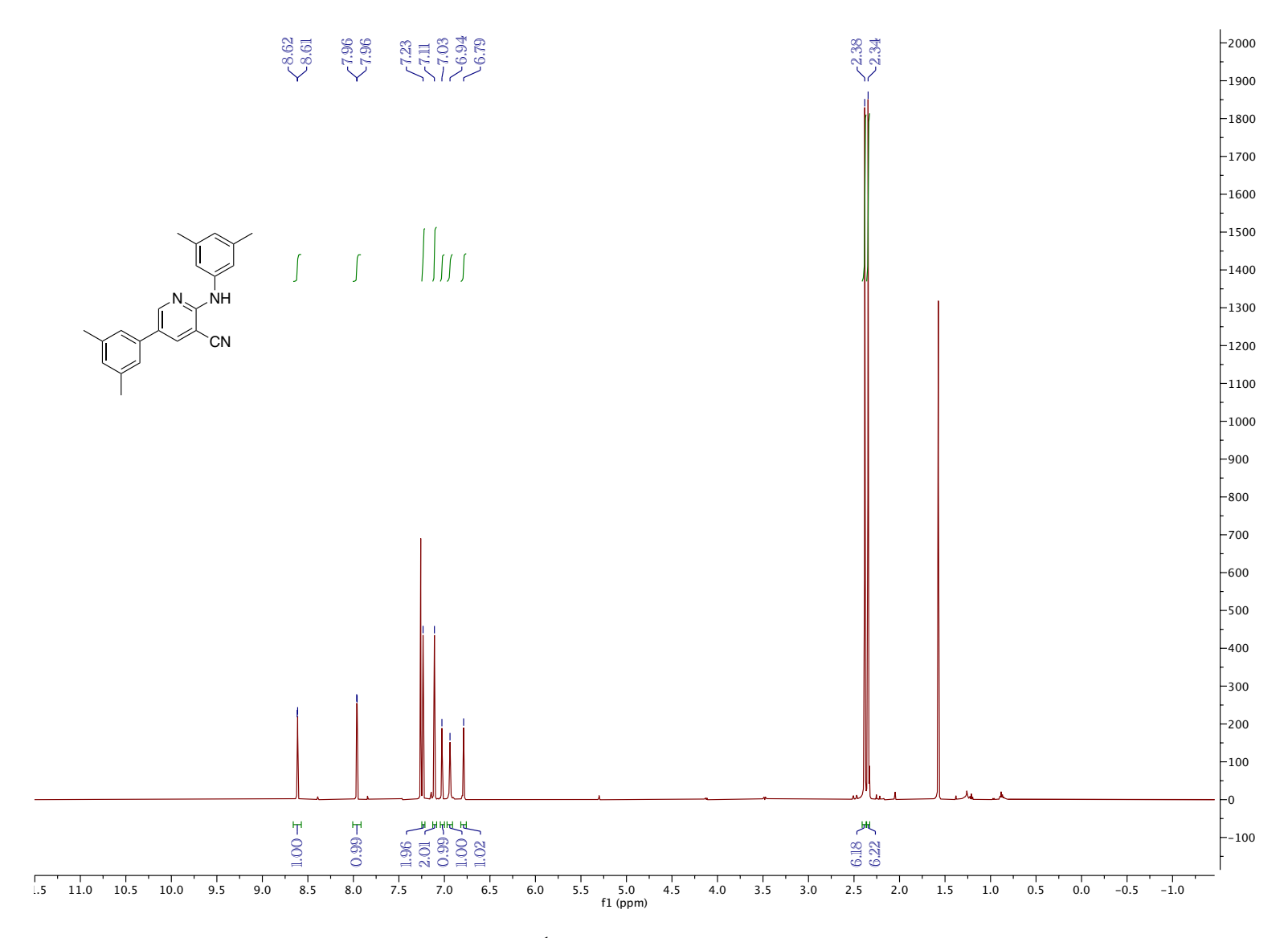


Figure 5.74. ¹H NMR (CDCl₃, 500 MHz, 25 °C)

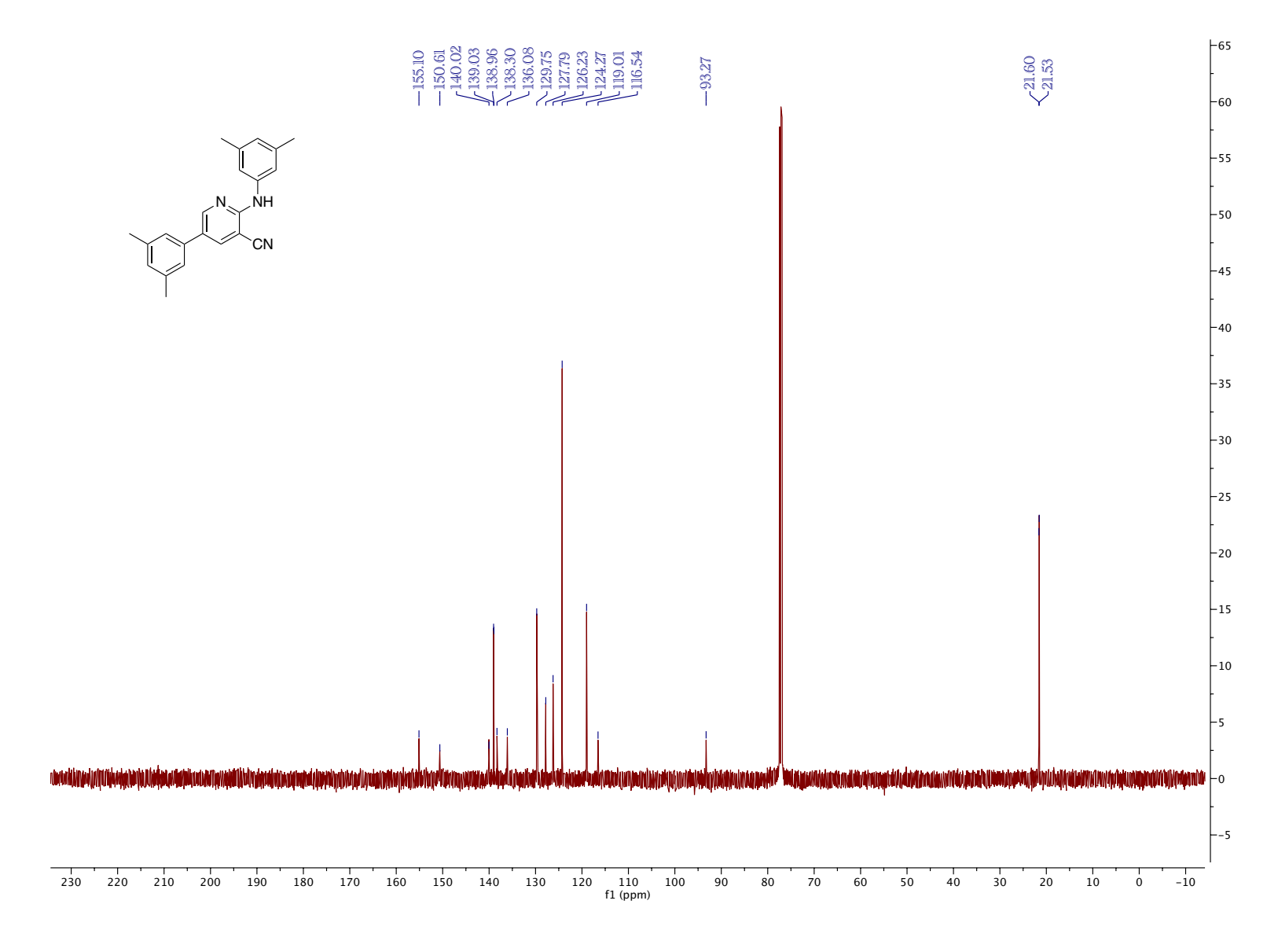


Figure 5.75. ¹³C NMR (CDCl₃, 126 MHz, 25 °C)

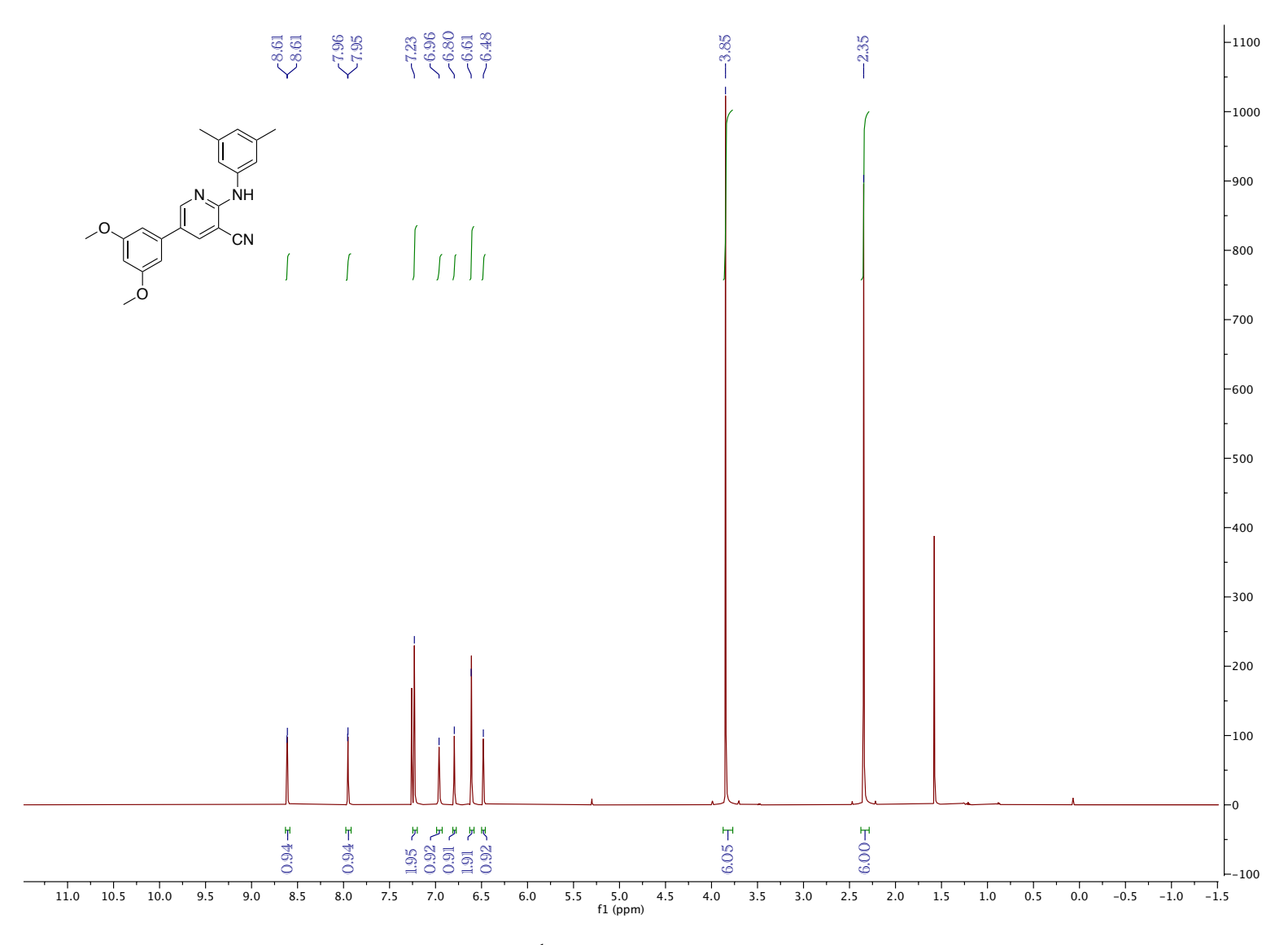


Figure 5.76. 1 H NMR (CDCl₃, 500 MHz, 25 $^{\circ}$ C)

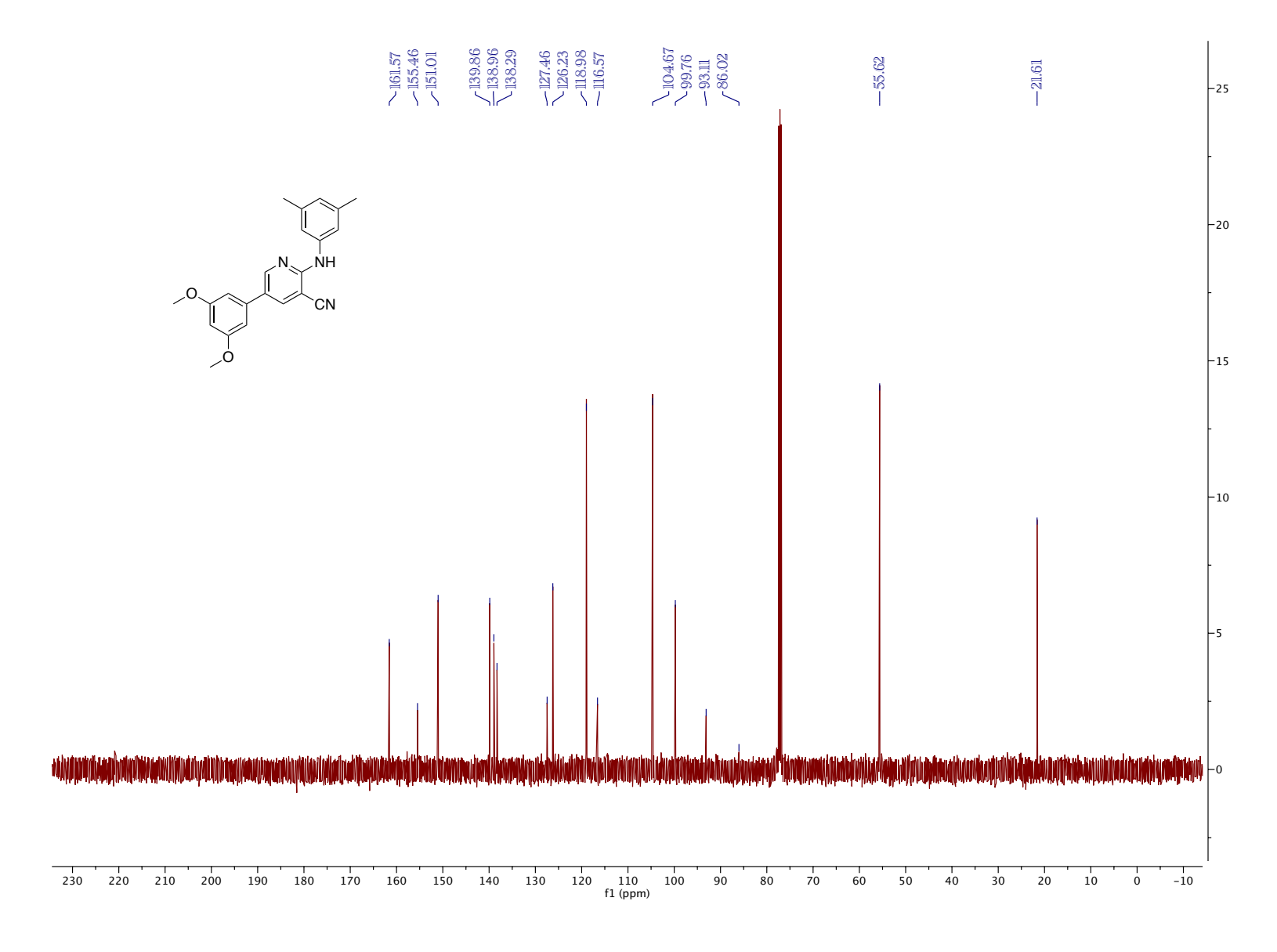


Figure 5.77. ¹³C NMR (CDCl₃, 126 MHz, 25 °C)

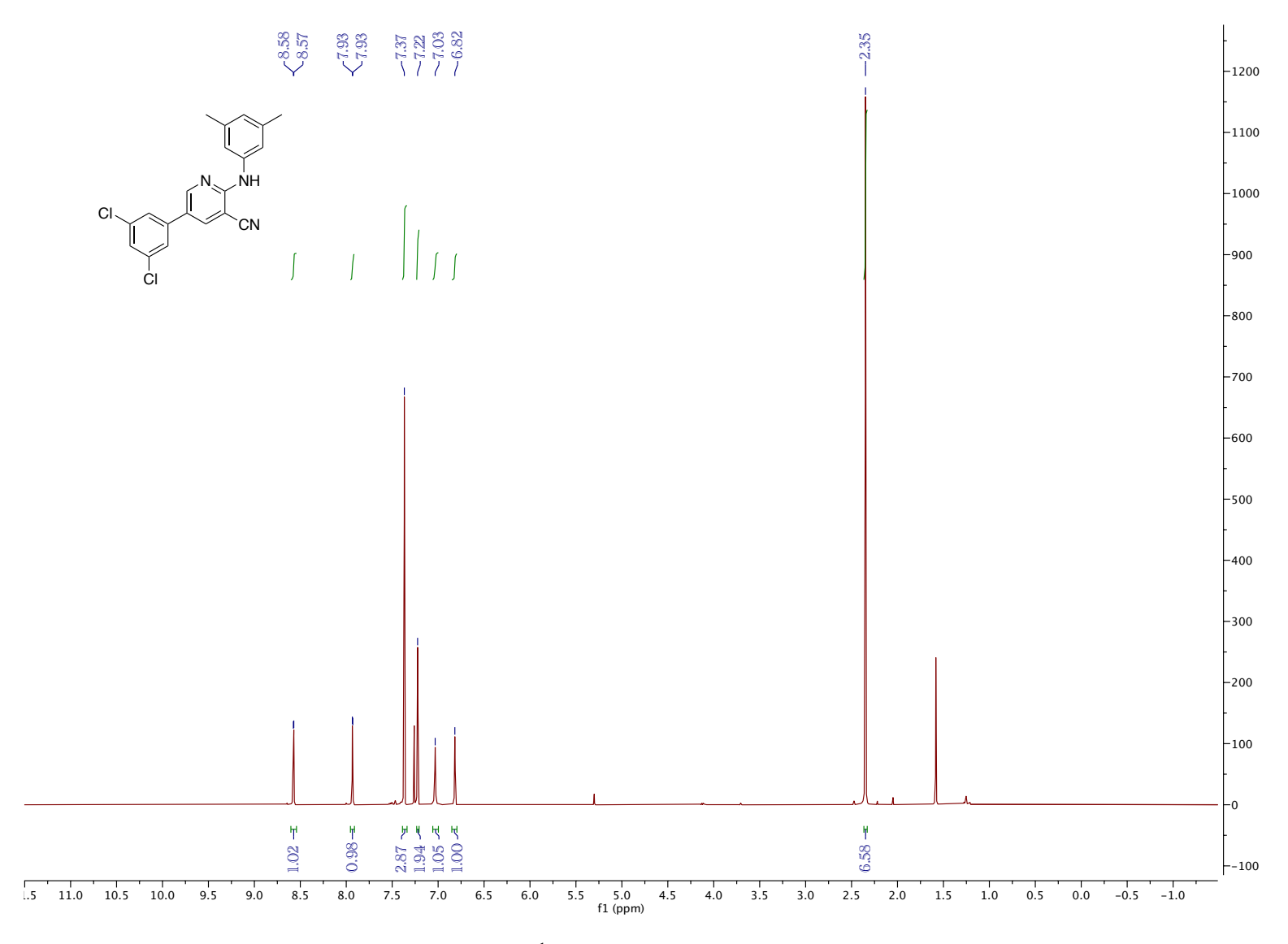


Figure 5.78. ¹H NMR (CDCl₃, 500 MHz, 25 °C)

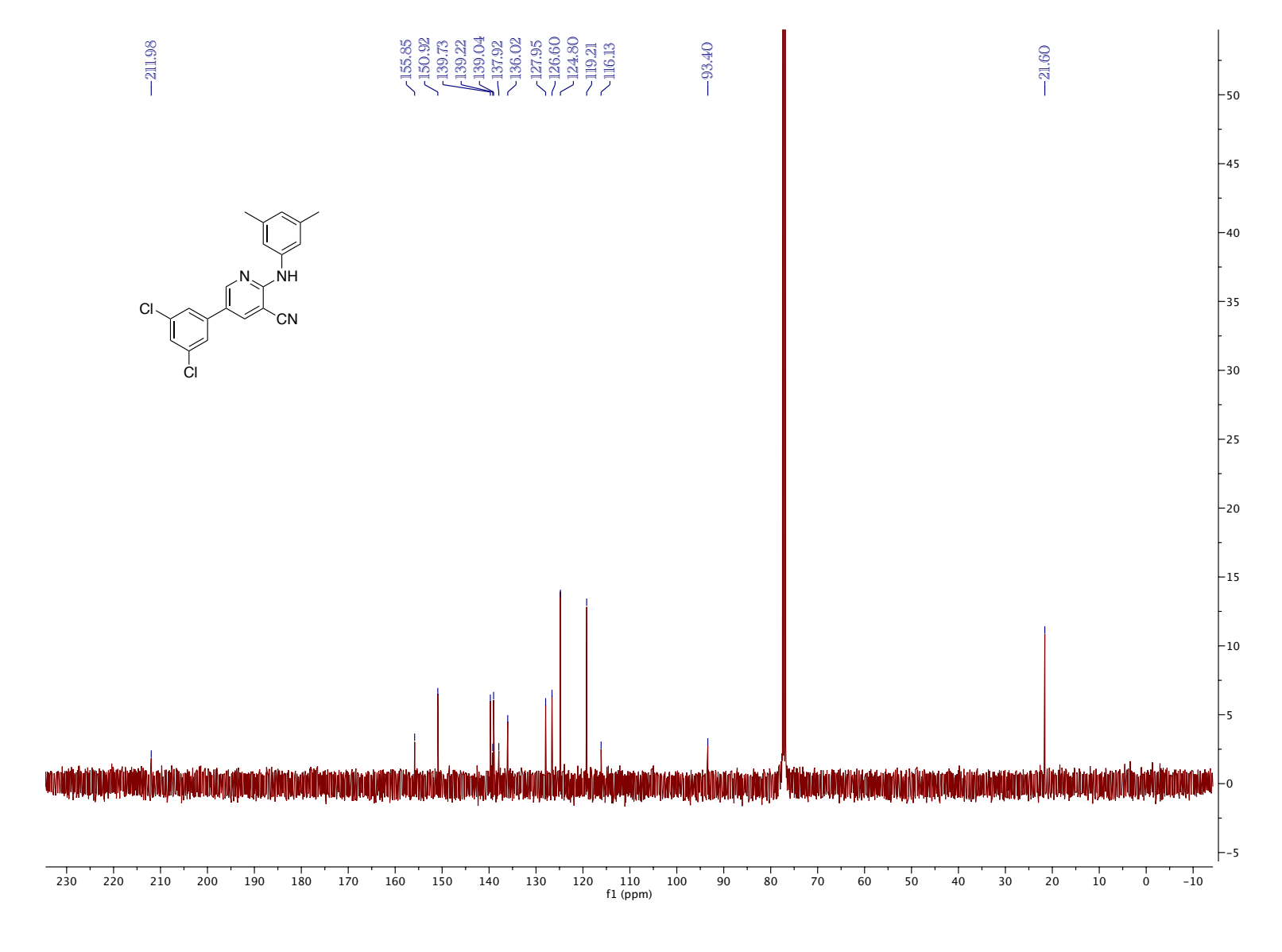


Figure 5.79. ¹³C NMR (CDCl₃, 126 MHz, 25 °C)

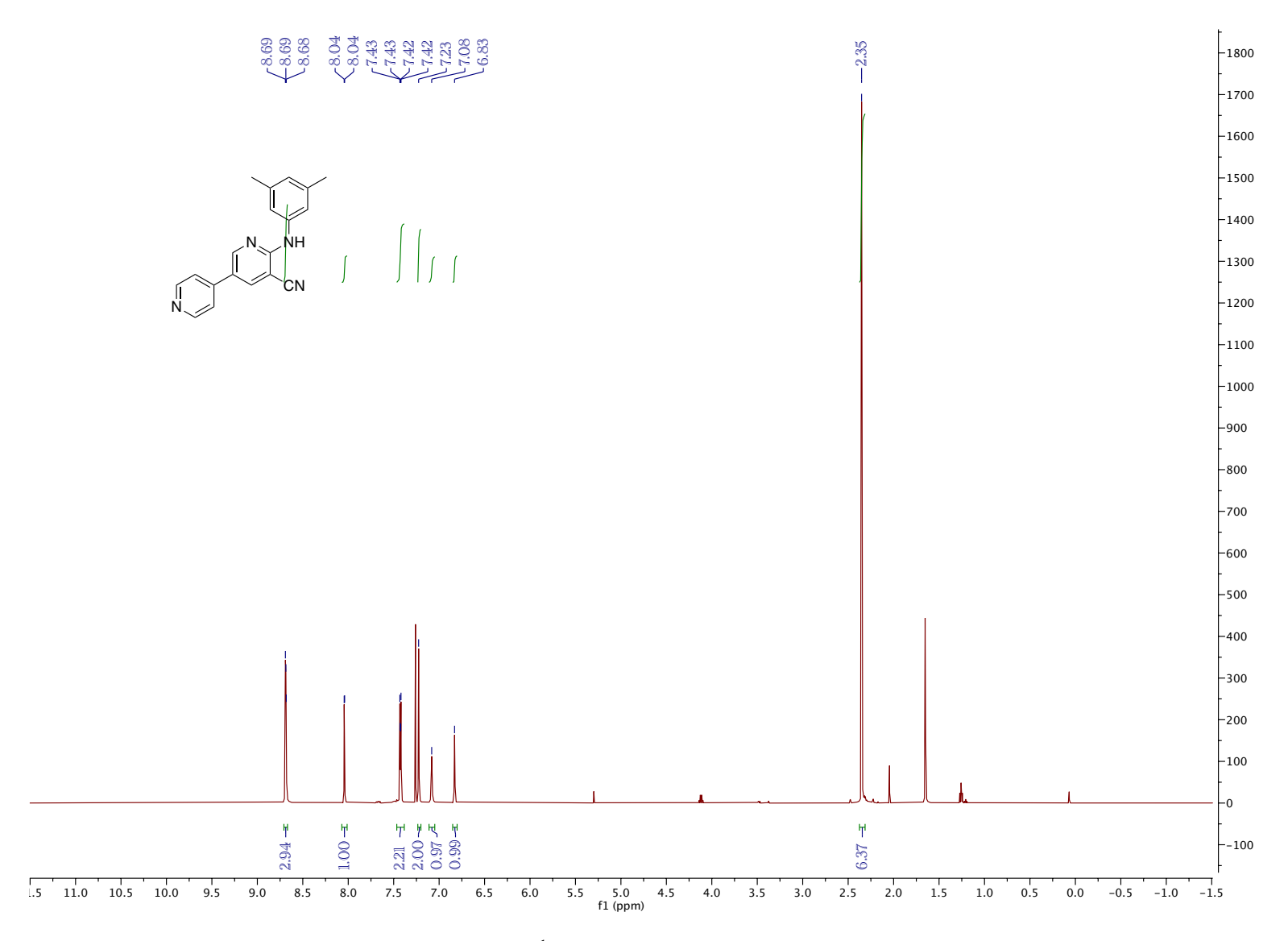


Figure 5.80. ¹H NMR (CDCl₃, 500 MHz, 25 °C)

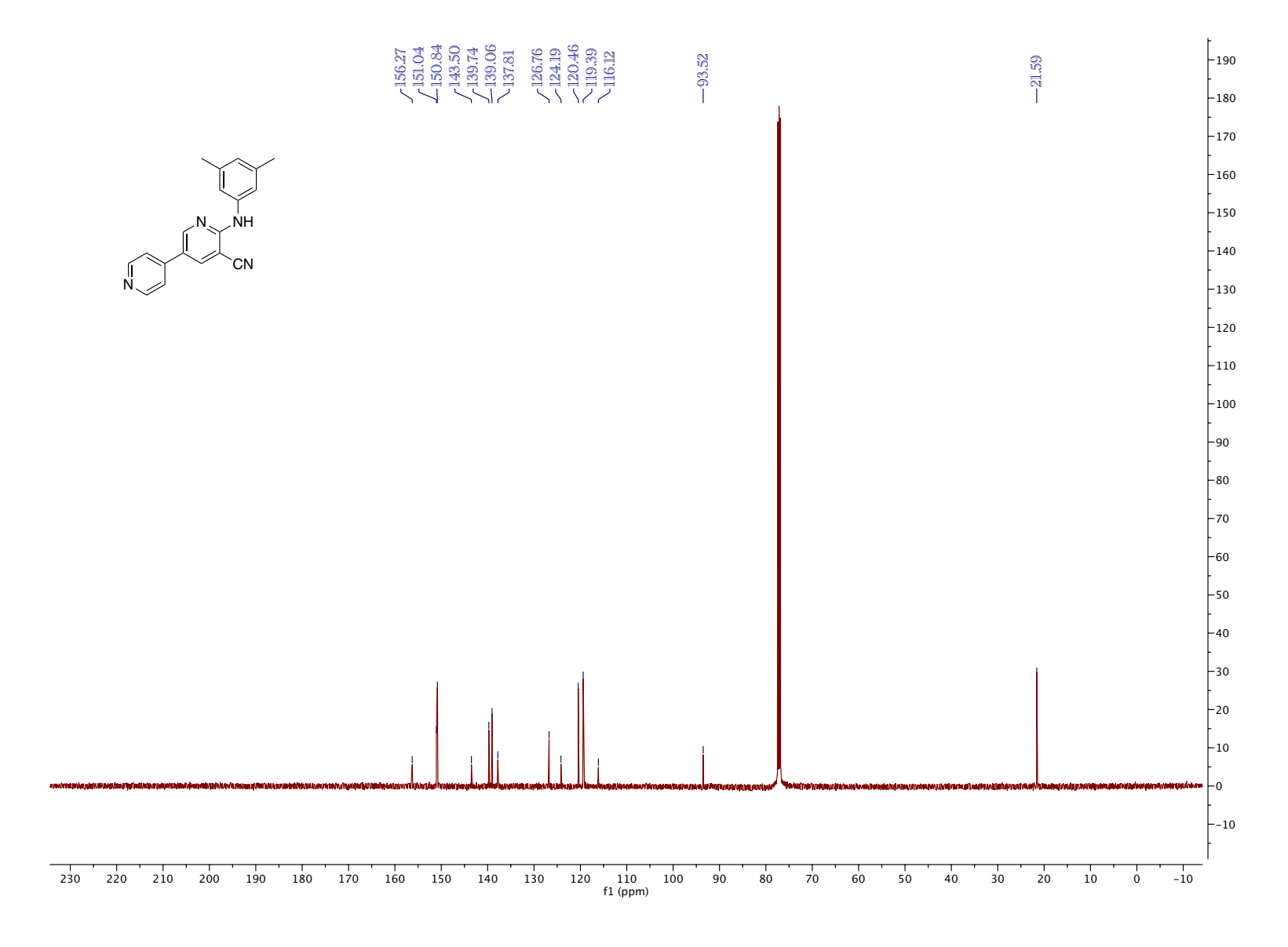


Figure 5.81. ¹³C NMR (CDCl₃, 126 MHz, 25 °C)

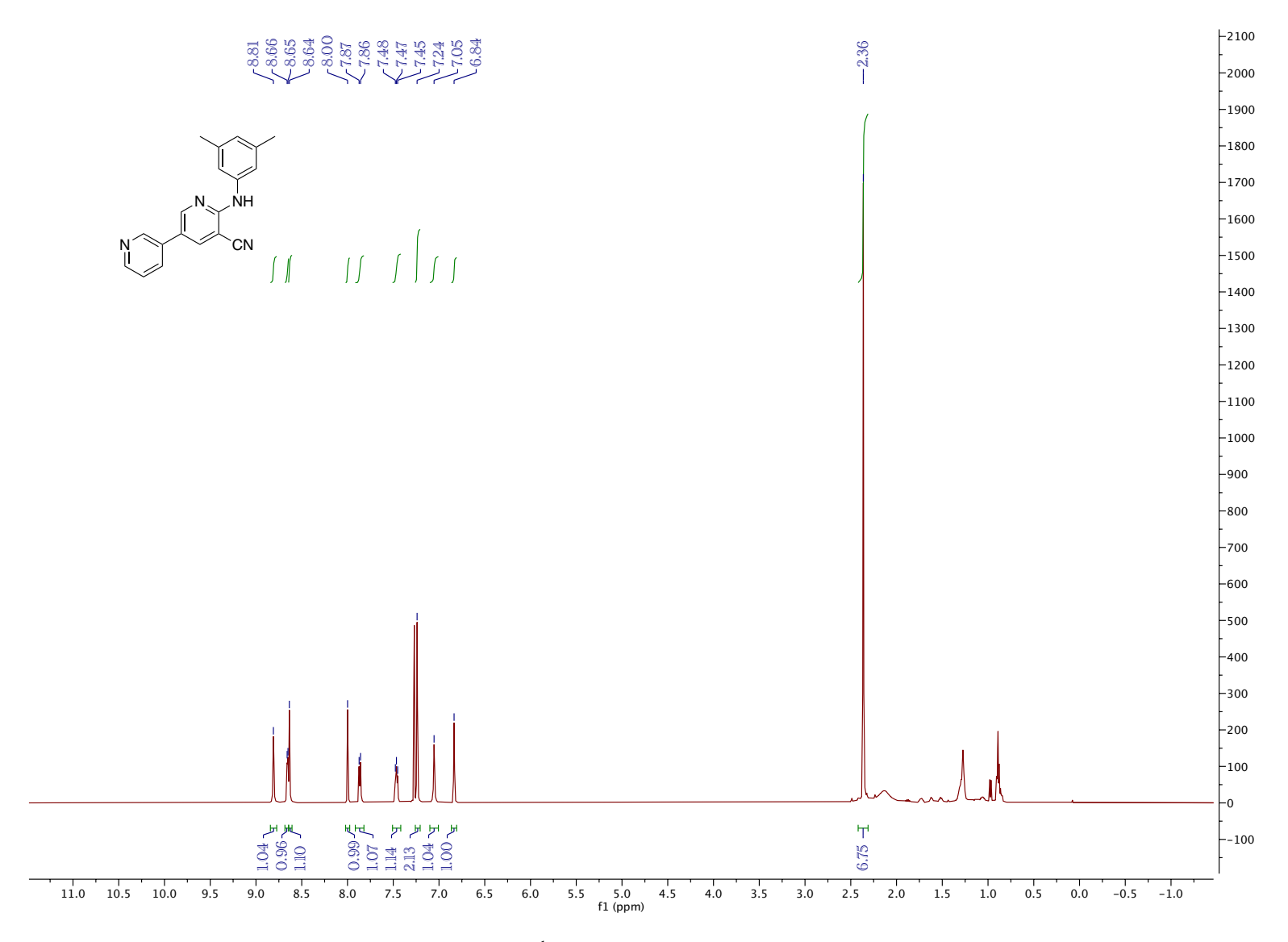


Figure 5.82. ¹H NMR (CDCl₃, 500 MHz, 25 °C)

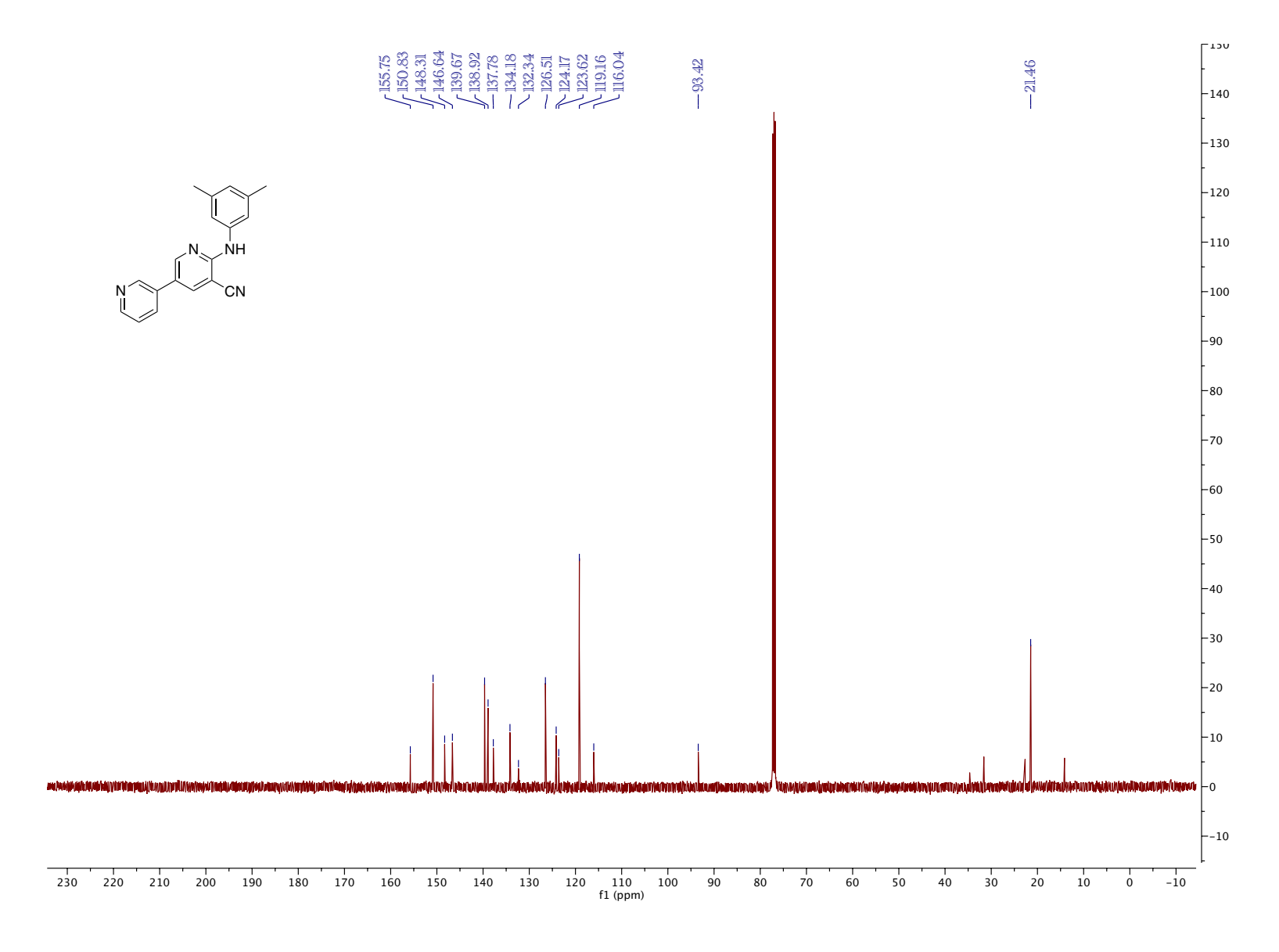


Figure 5.83. ¹³C NMR (CDCl₃, 126 MHz, 25 °C)

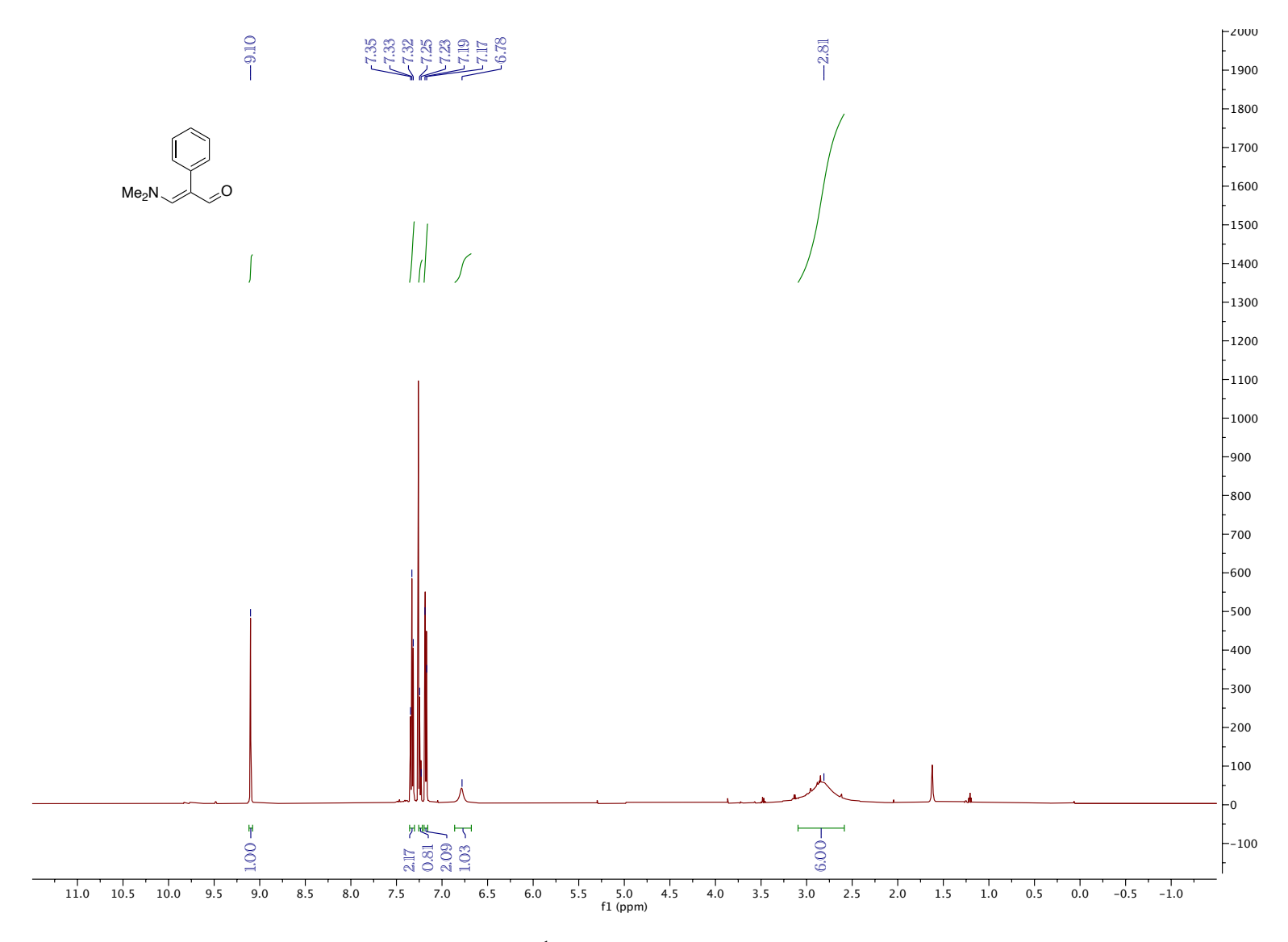


Figure 5.84. ¹H NMR (CDCl₃, 500 MHz, 25 °C)

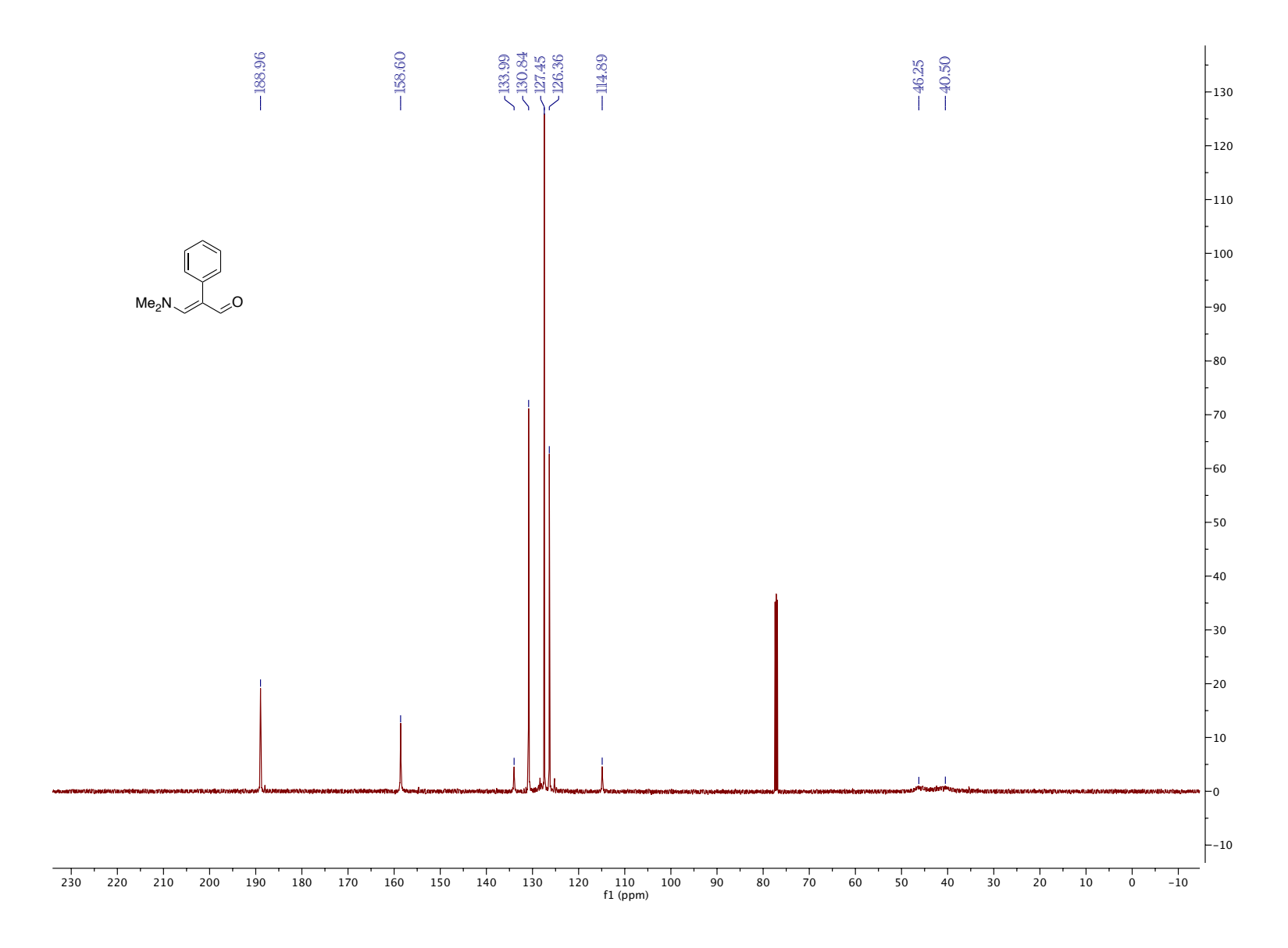


Figure 5.85. ¹³C NMR (CDCl₃, 126 MHz, 25 °C)

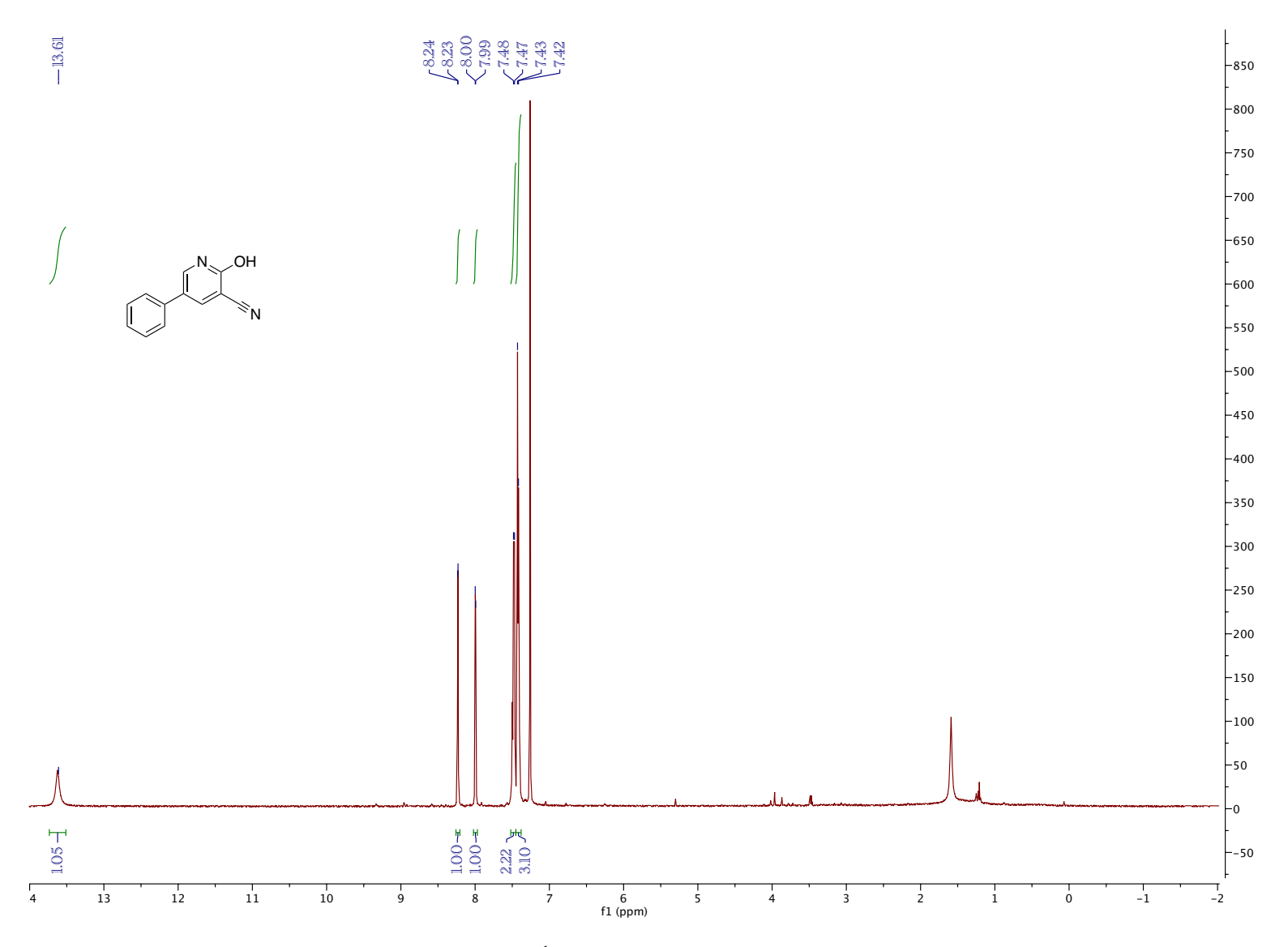


Figure 5.86. 1 H NMR (CDCl₃, 500 MHz, 25 $^{\circ}$ C)

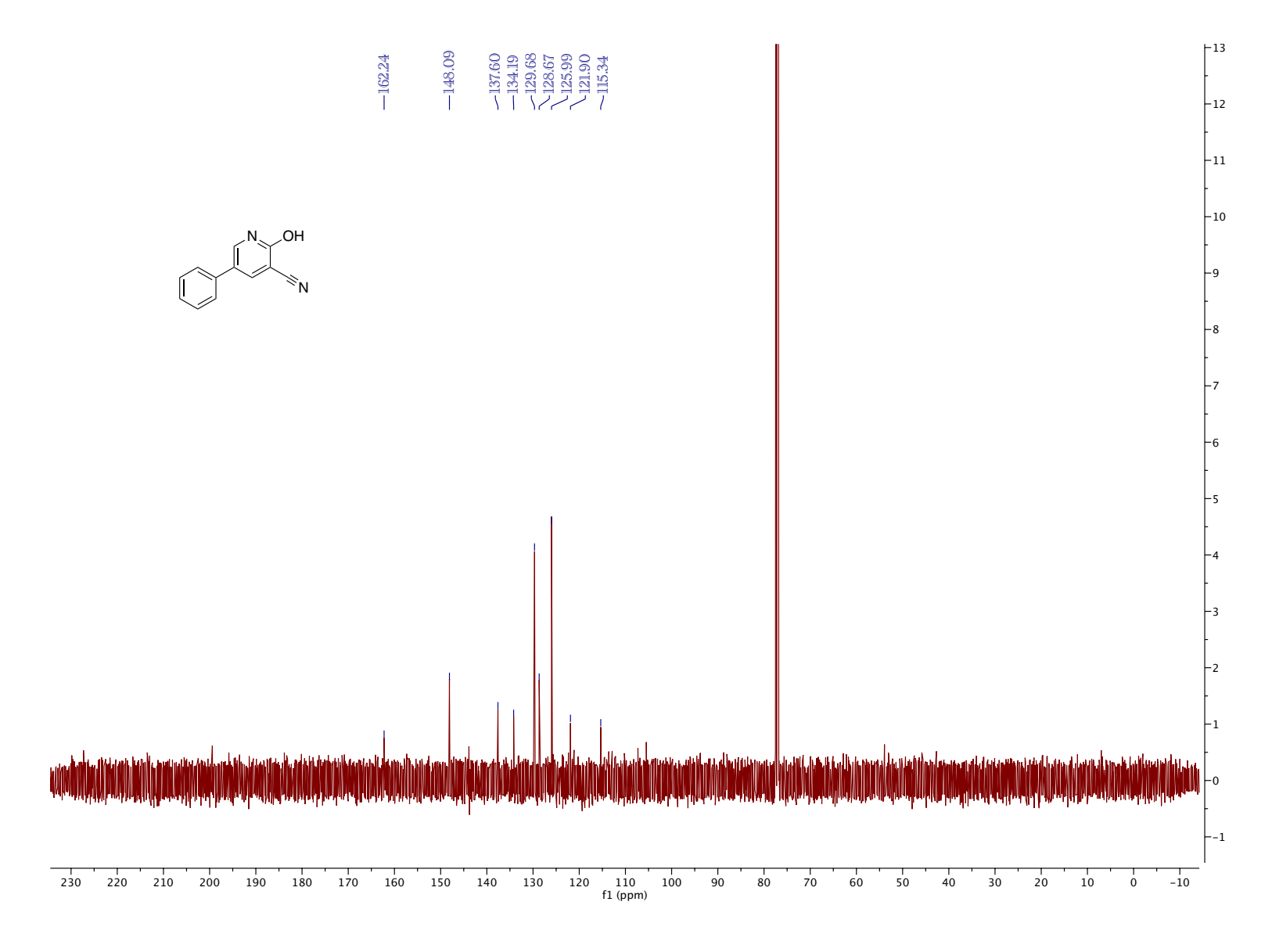


Figure 5.87. ¹³C NMR (CDCl₃, 126 MHz, 25 °C)

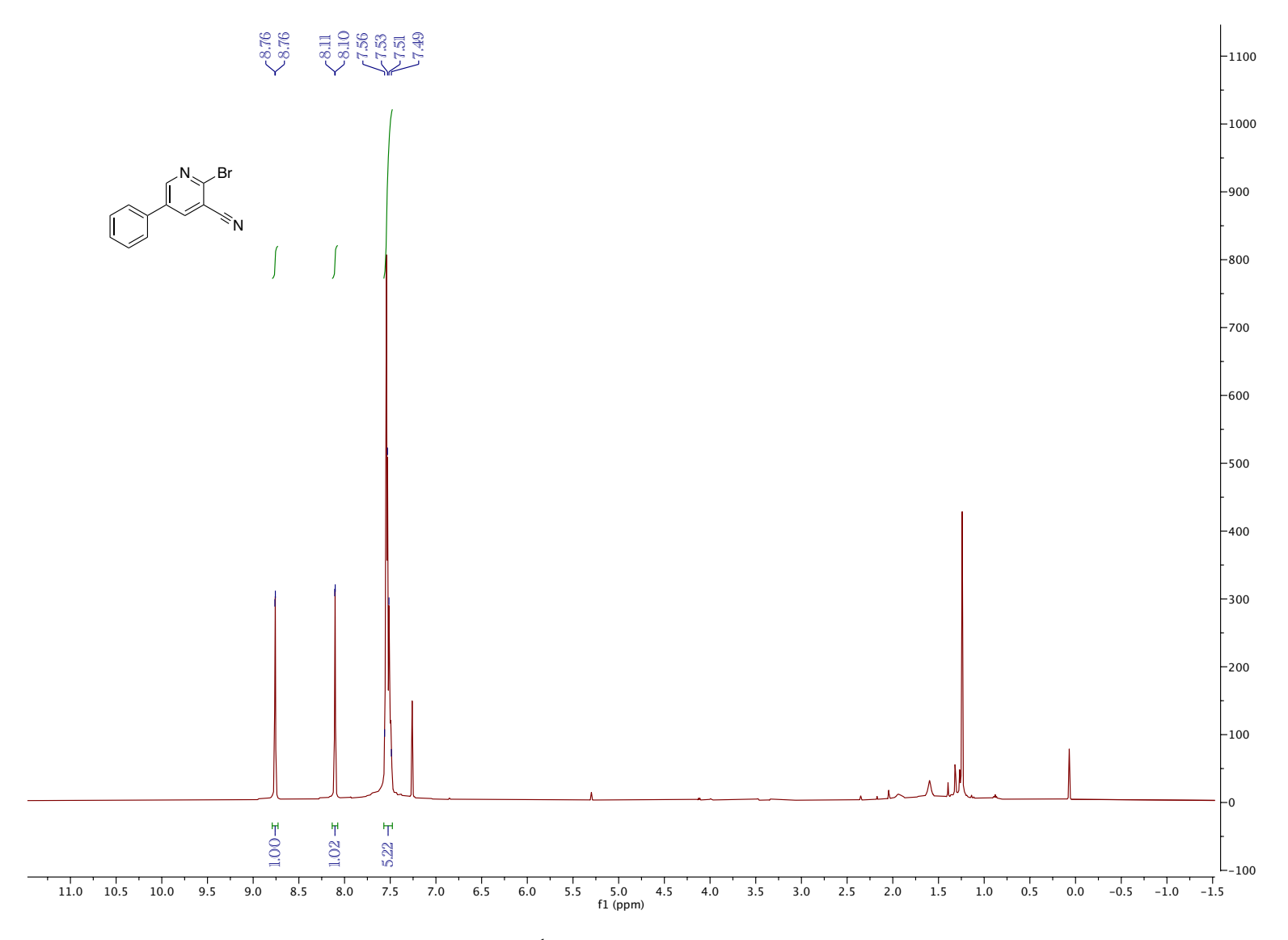


Figure 5.88. ¹H NMR (CDCl₃, 500 MHz, 25 °C)

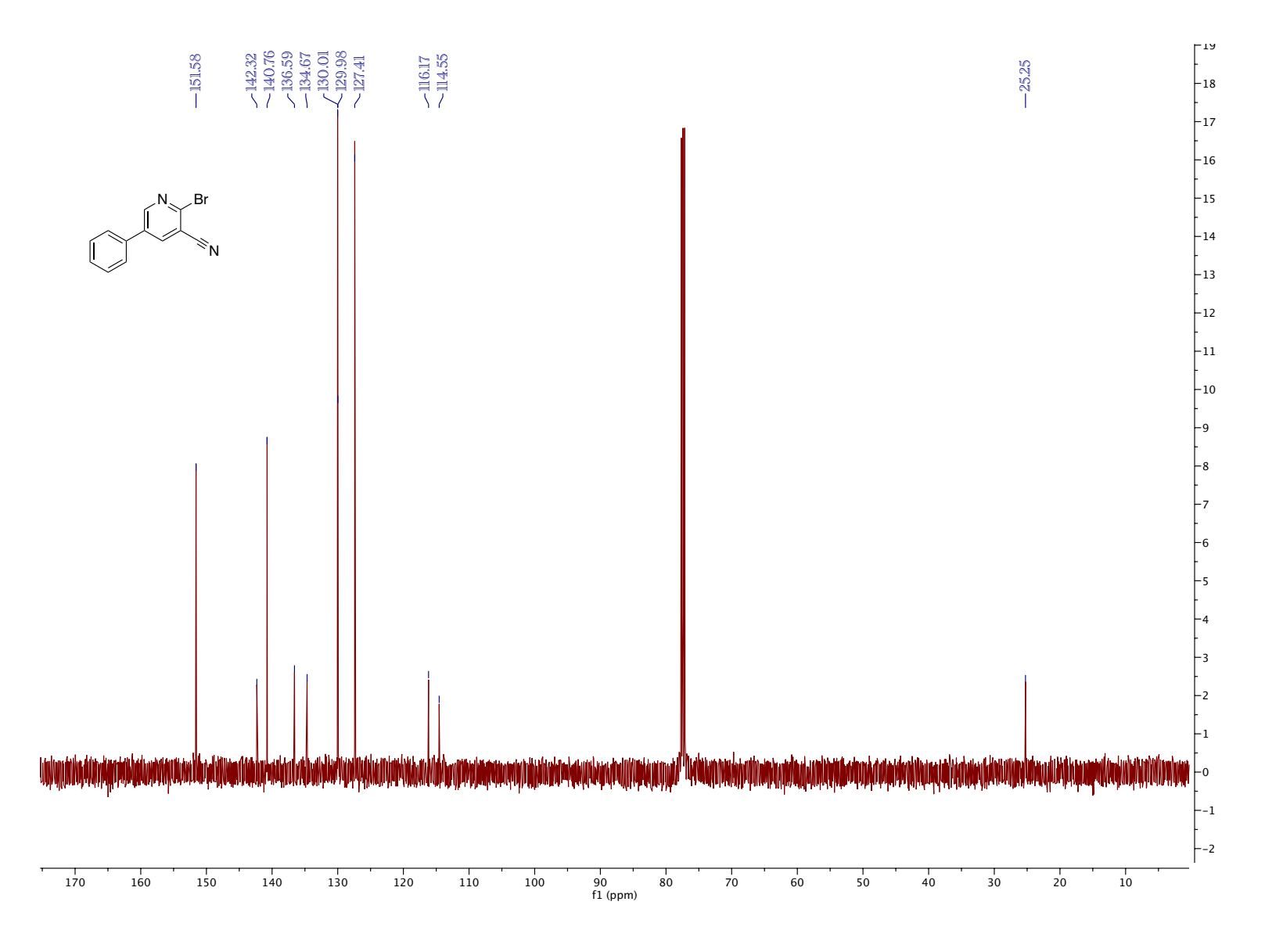


Figure 5.89. 13 C NMR (CDCl₃, 126 MHz, 25 $^{\circ}$ C)

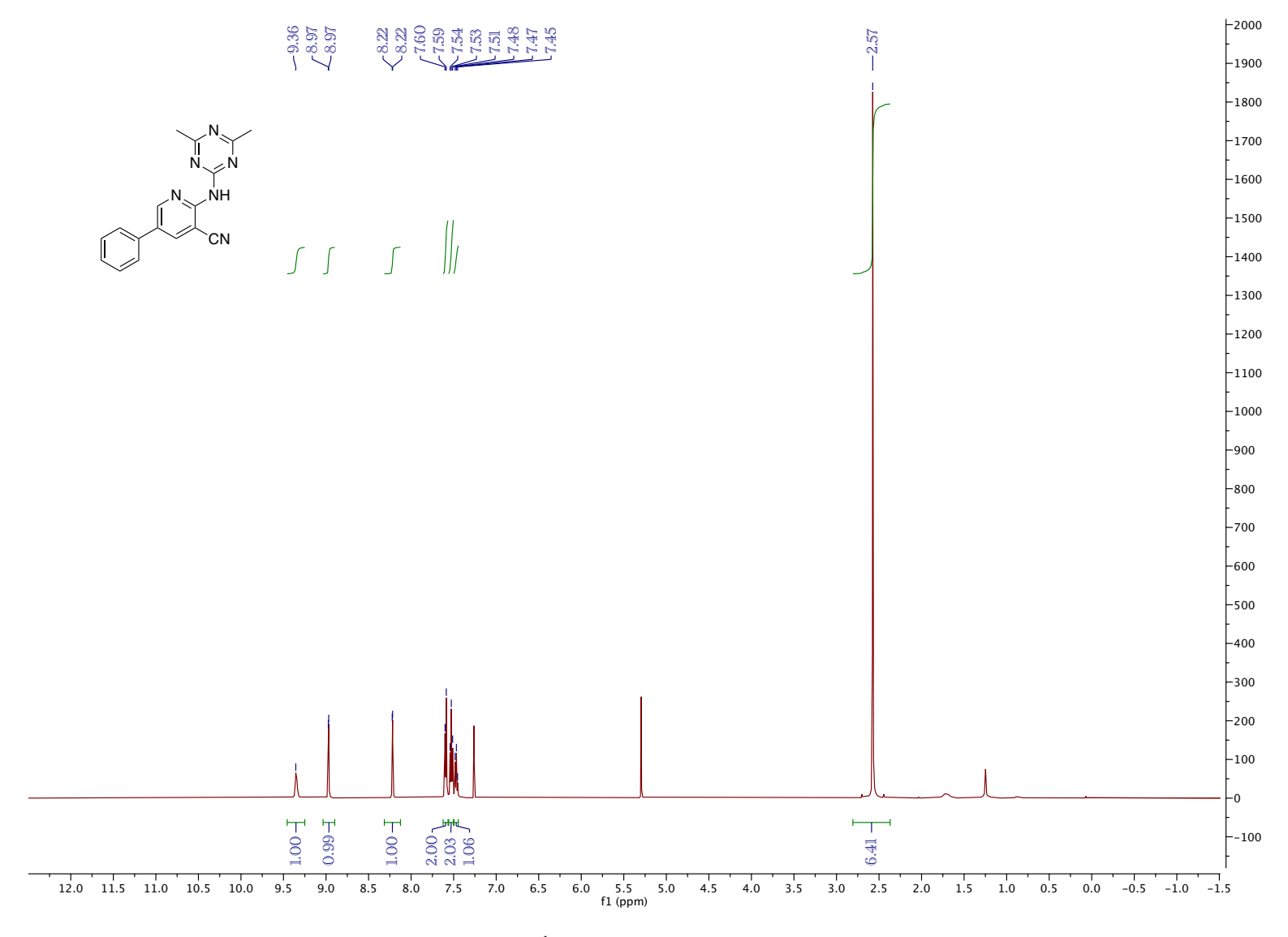


Figure 5.90. ¹H NMR (CDCl₃, 500 MHz, 25 °C)

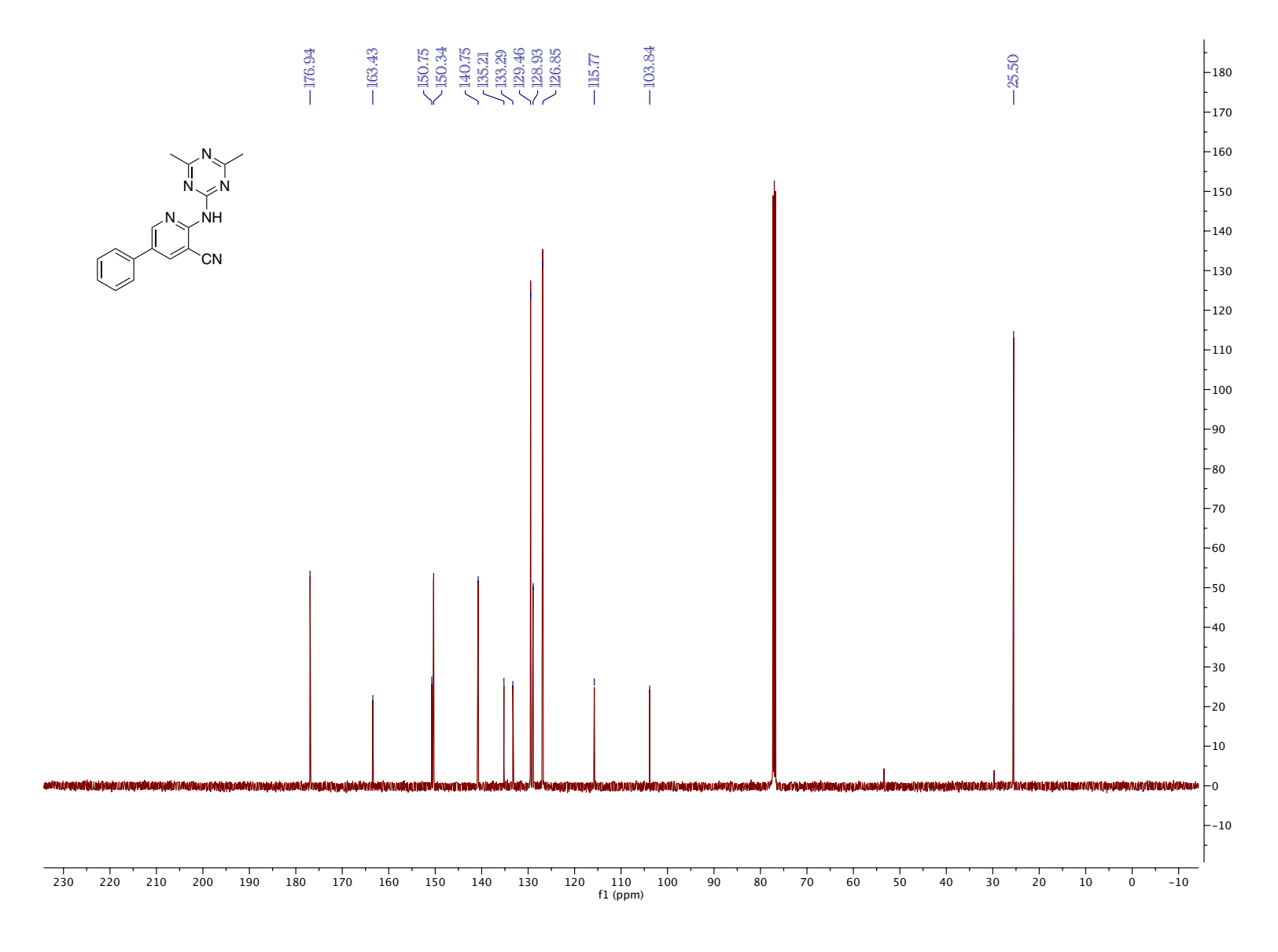


Figure 5.91. ¹³C NMR (CDCl₃, 126 MHz, 25 °C)

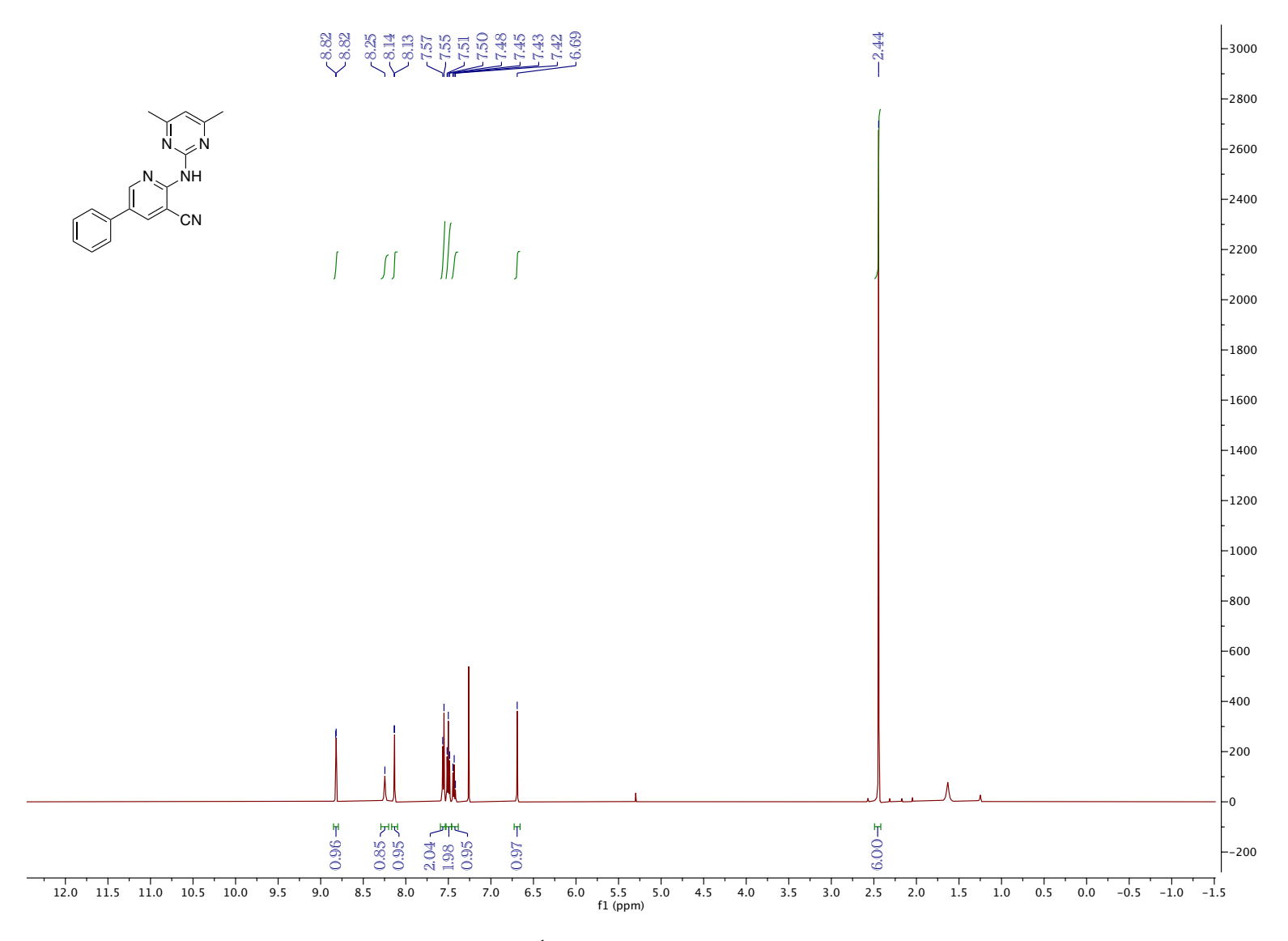


Figure 5.92. ¹H NMR (CDCl₃, 500 MHz, 25 °C)

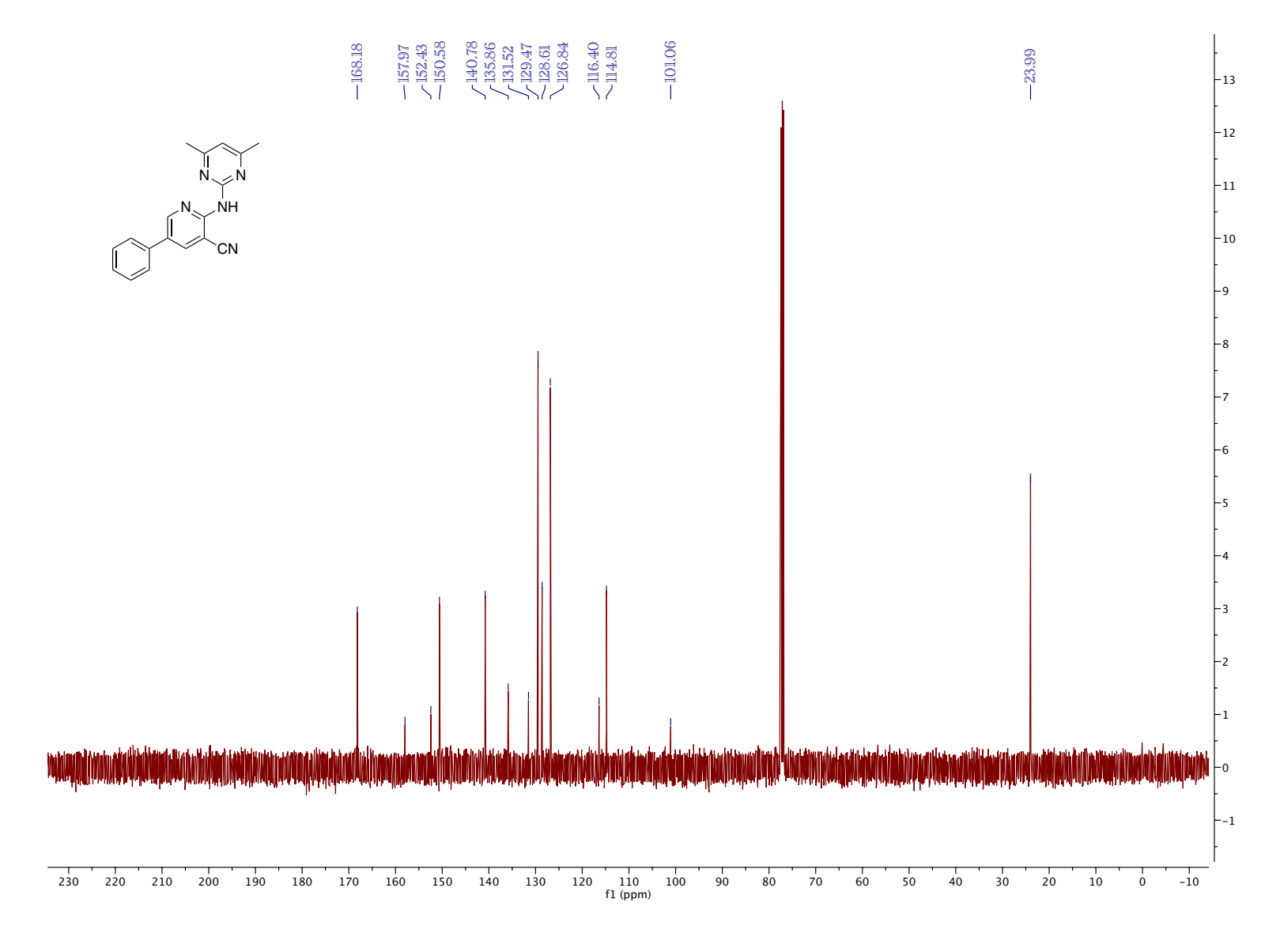


Figure 5.93. ¹³C NMR (CDCl₃, 126 MHz, 25 °C)

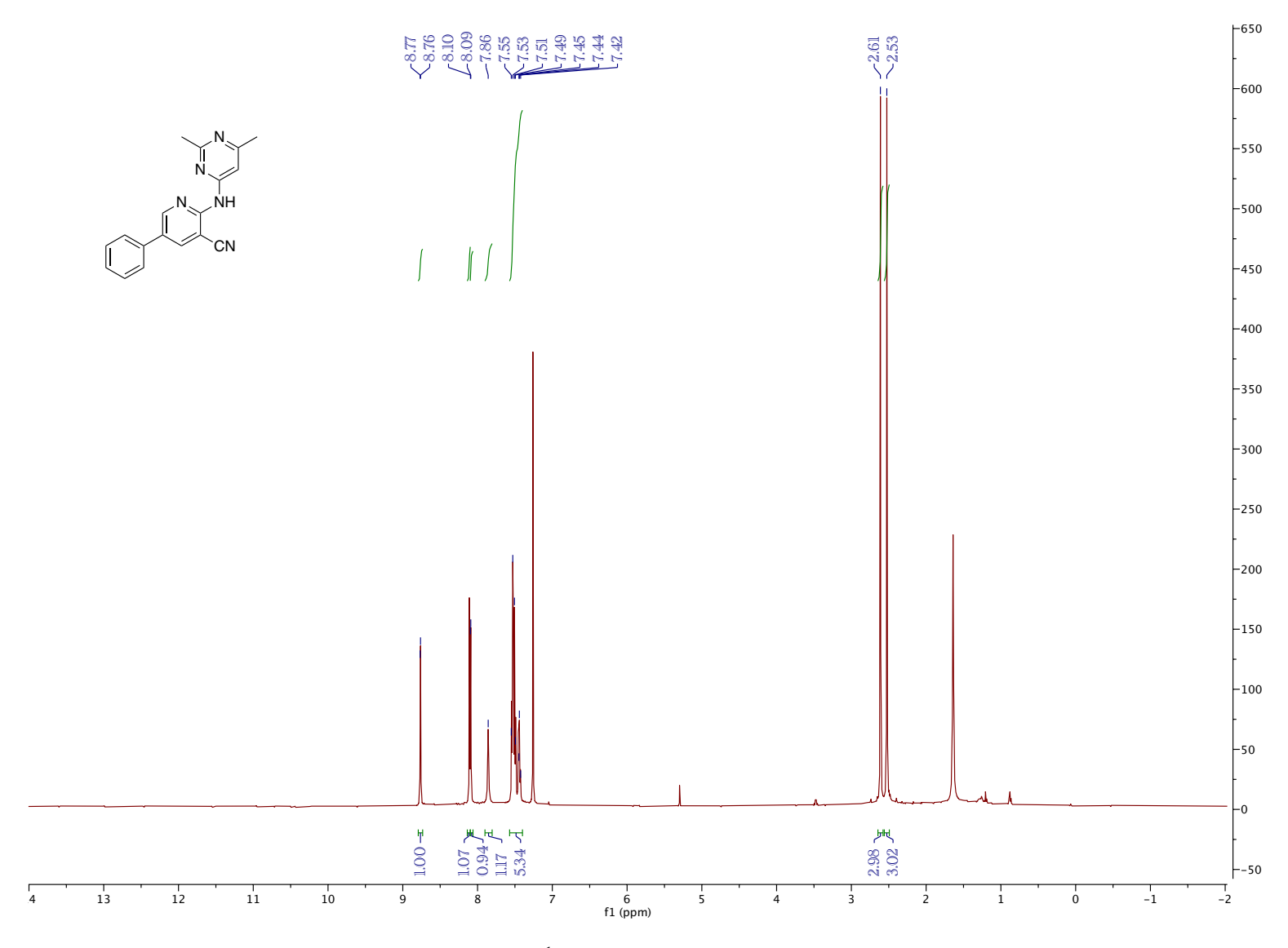


Figure 5.94. 1 H NMR (CDCl₃, 500 MHz, 25 $^{\circ}$ C)

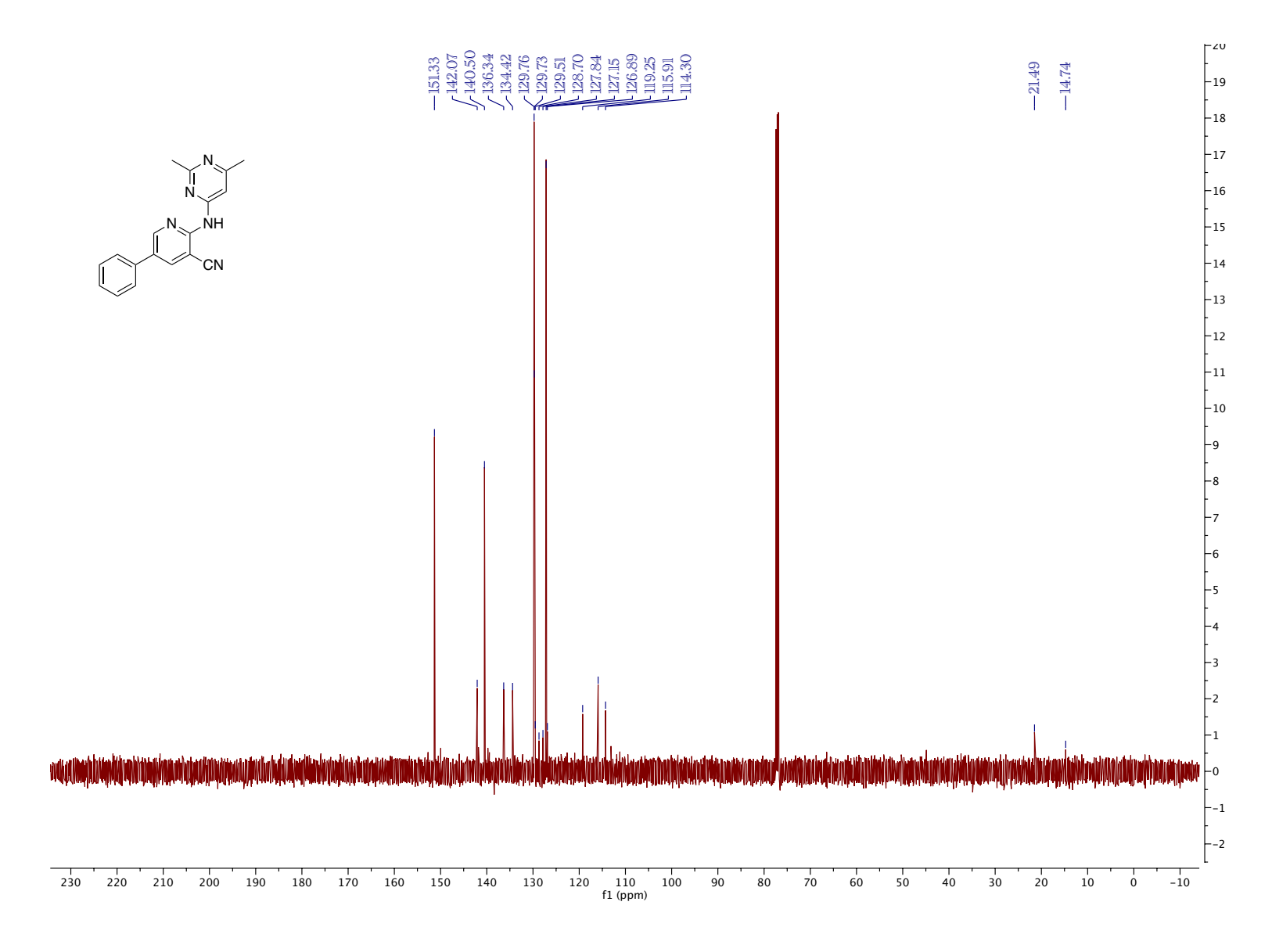


Figure 5.95. ¹³C NMR (CDCl₃, 126 MHz, 25 °C)

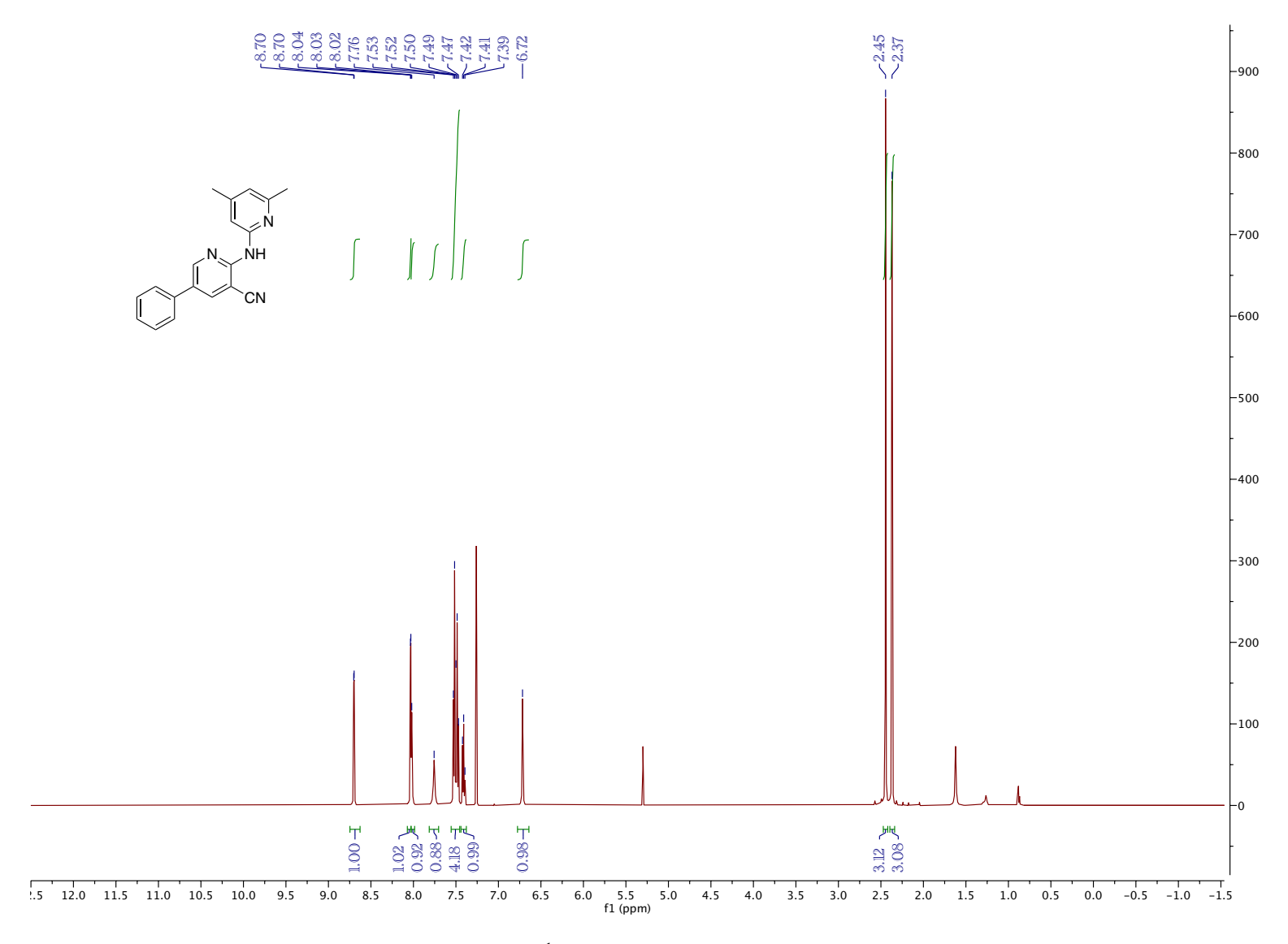


Figure 5.96. ¹H NMR (CDCl₃, 500 MHz, 25 °C)

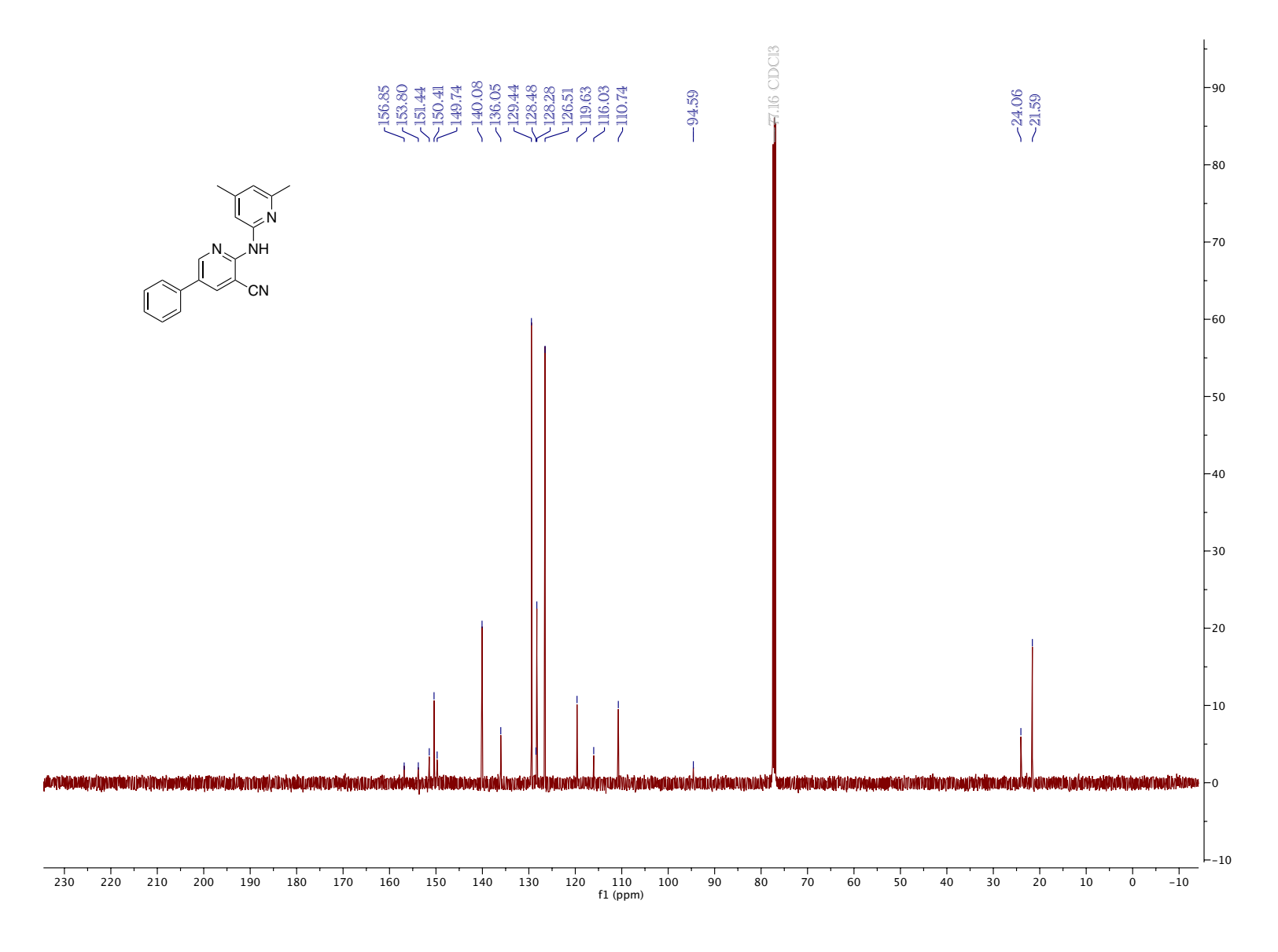


Figure 5.97. ¹³C NMR (CDCl₃, 126 MHz, 25 °C)

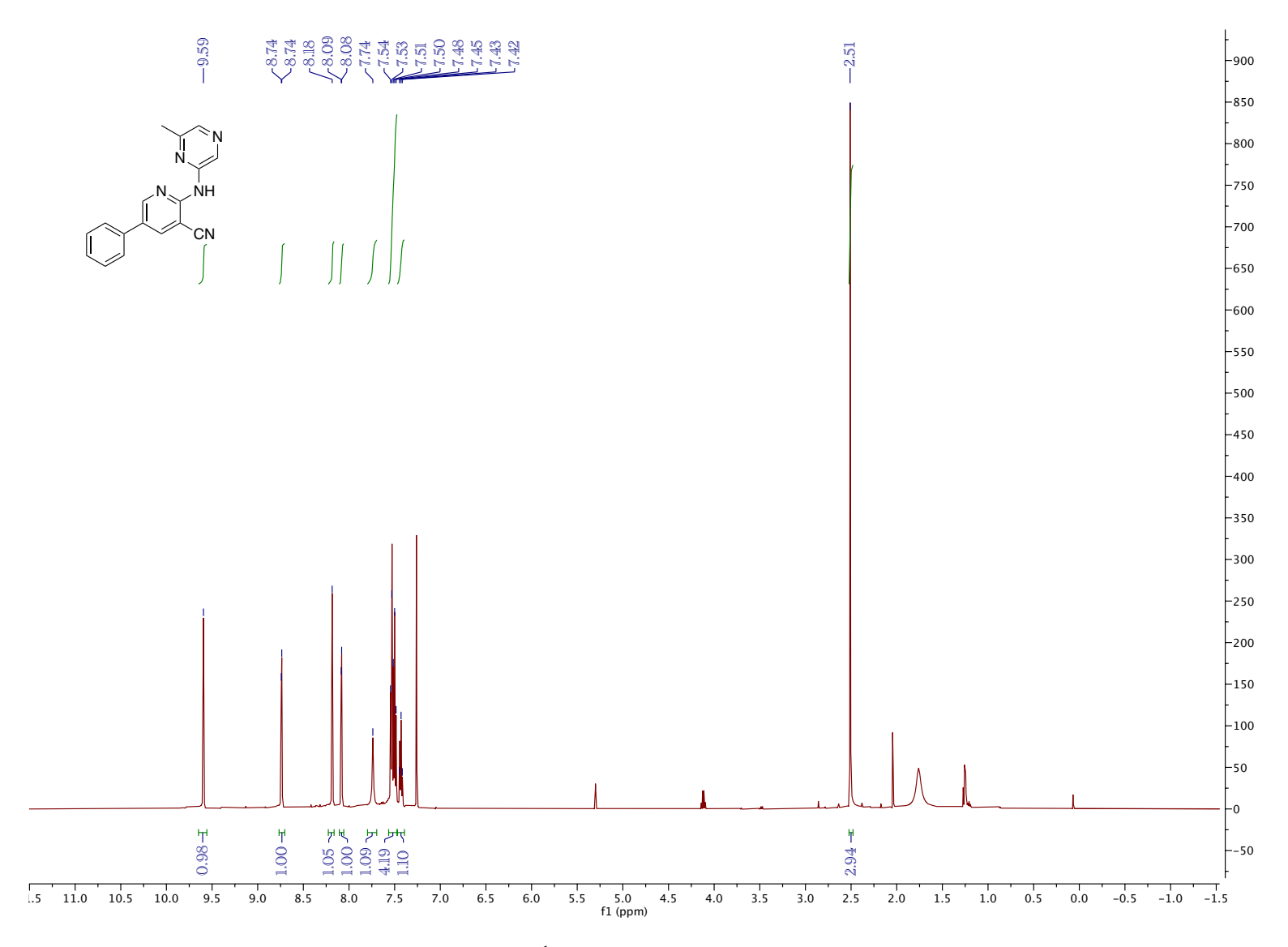


Figure 5.98. ¹H NMR (CDCl₃, 500 MHz, 25 °C)

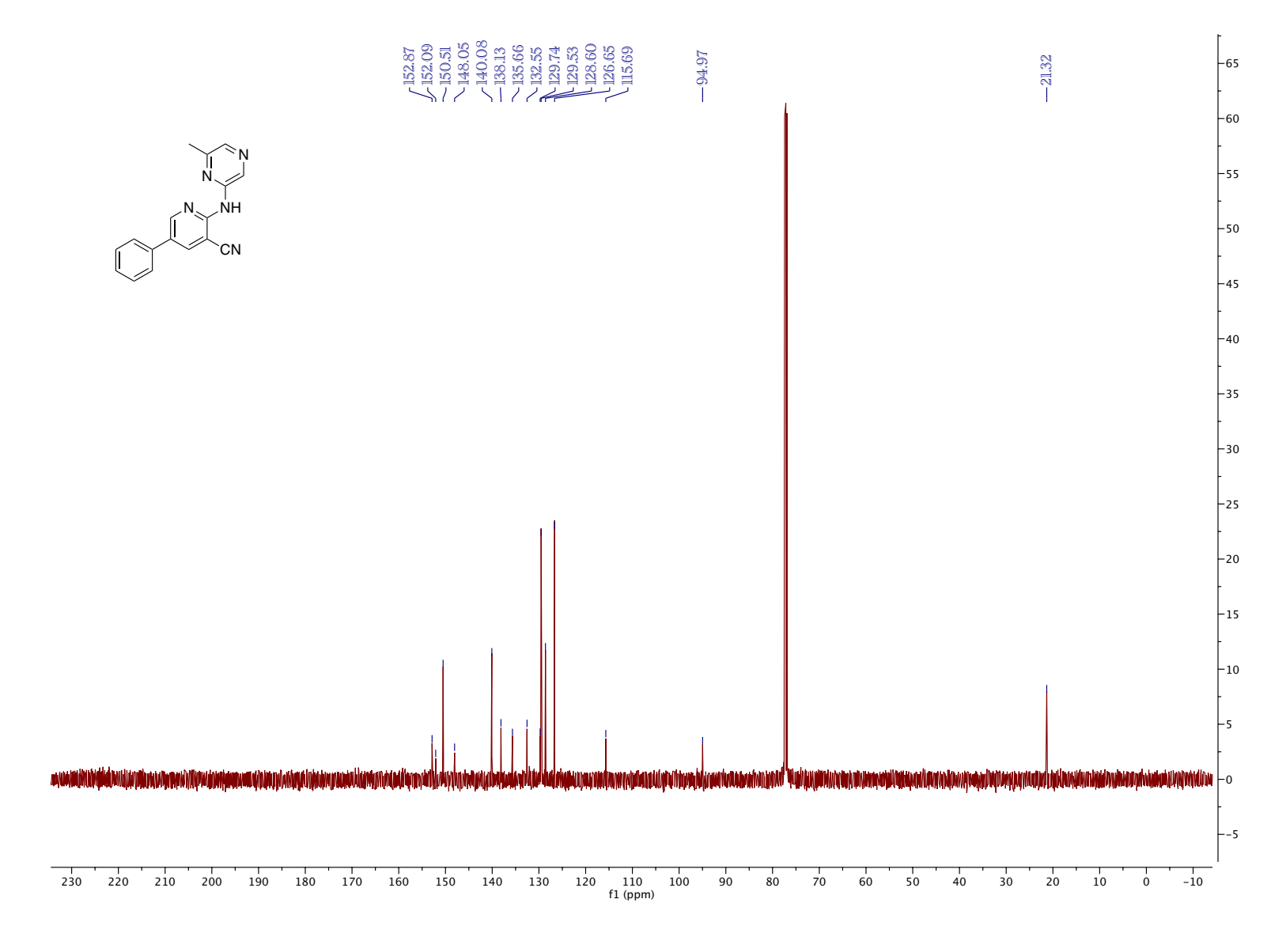


Figure 5.99. ¹³C NMR (CDCl₃, 126 MHz, 25 °C)

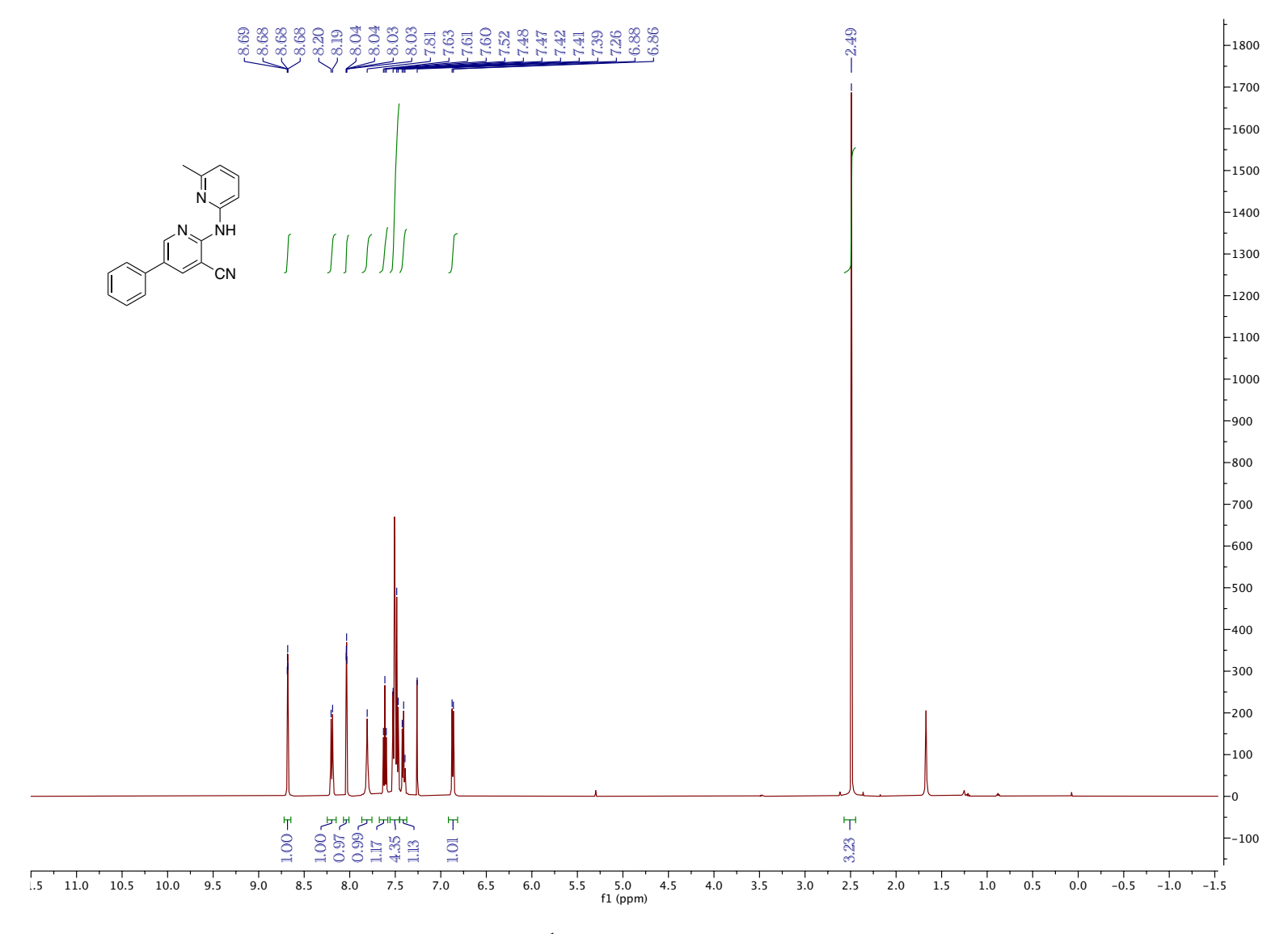


Figure 5.100. ¹H NMR (CDCl₃, 500 MHz, 25 °C)

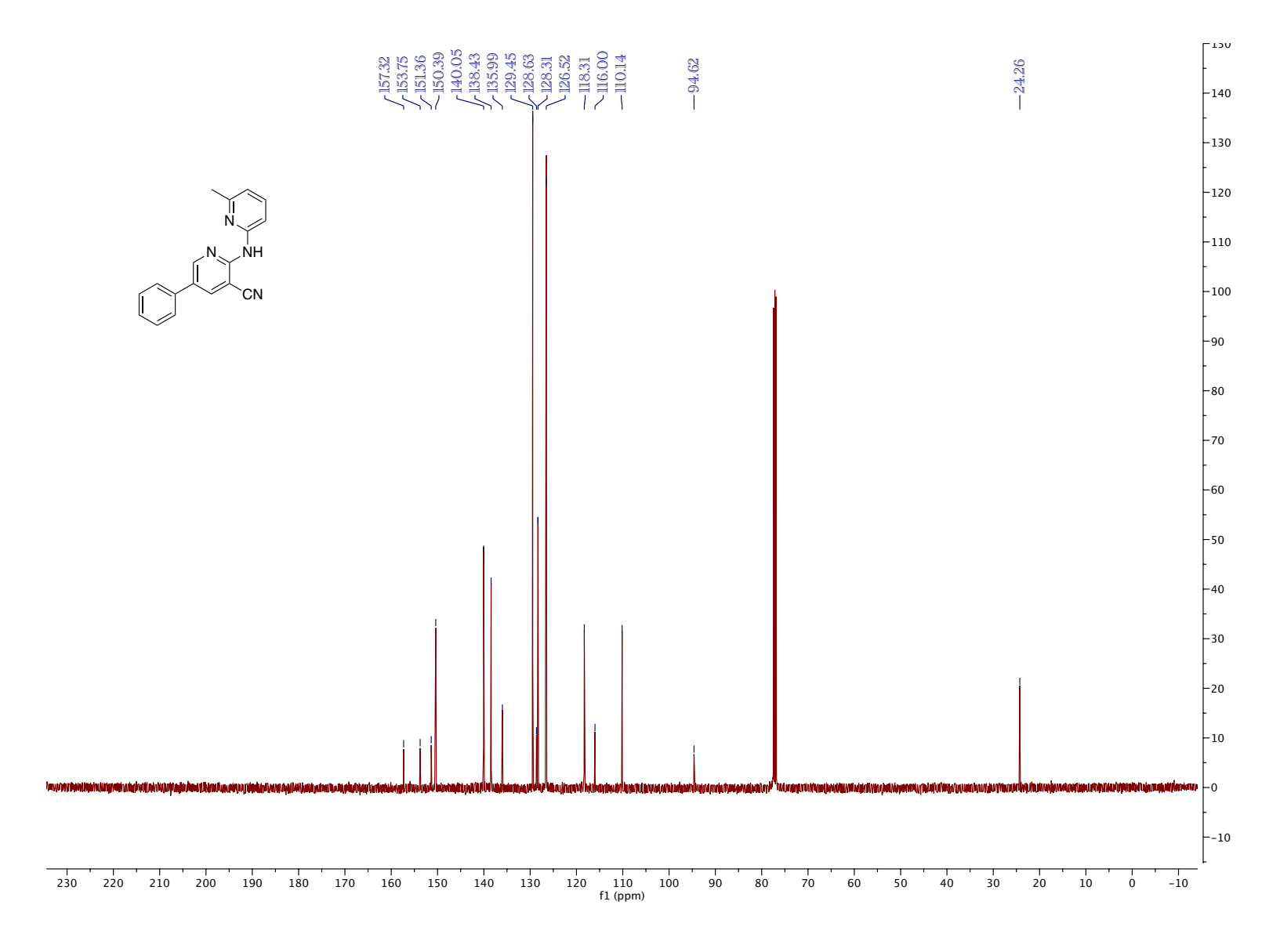


Figure 5.101. ¹³C NMR (CDCl₃, 126 MHz, 25 °C)

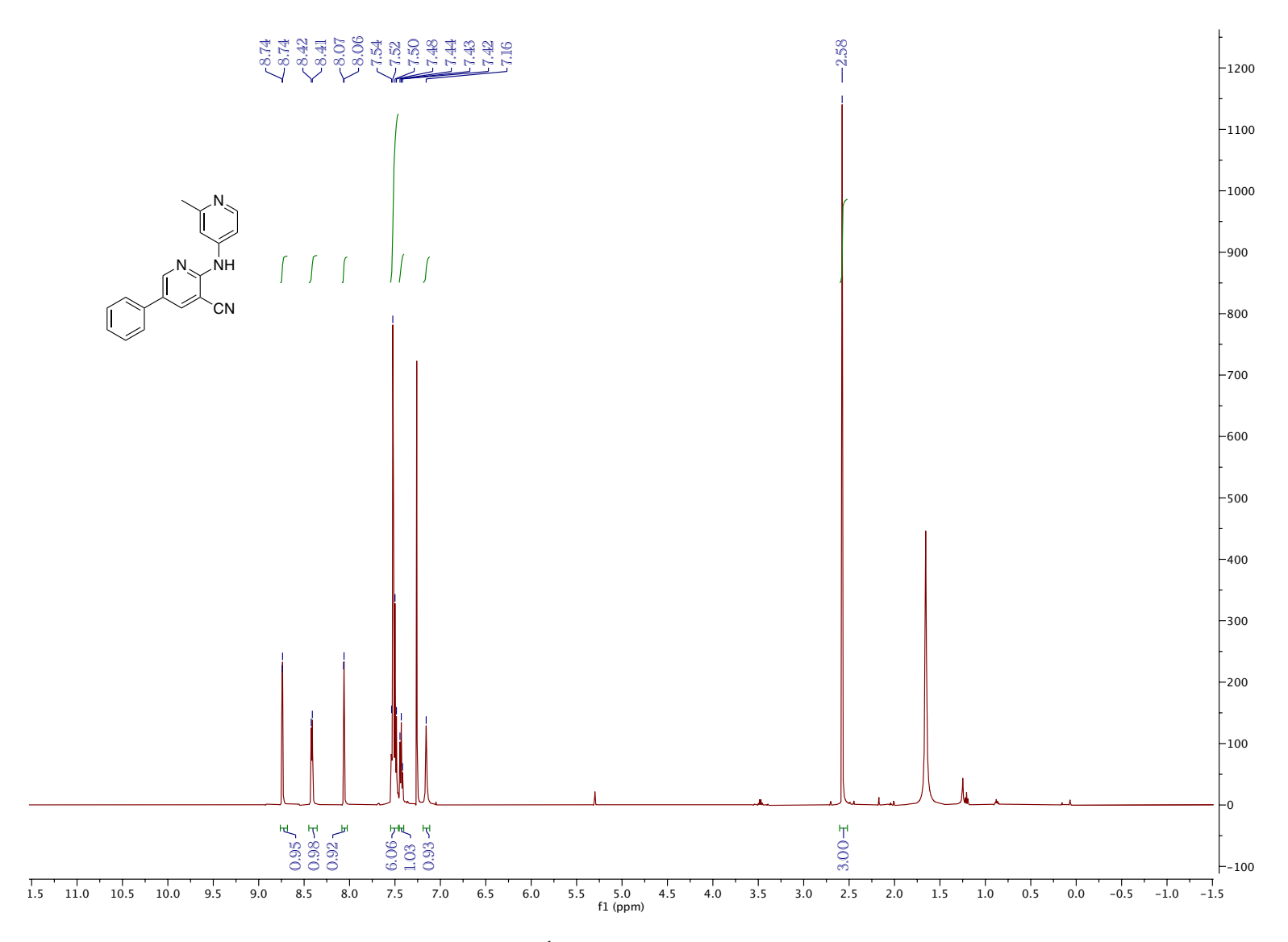


Figure 5.102. ¹H NMR (CDCl₃, 500 MHz, 25 °C)

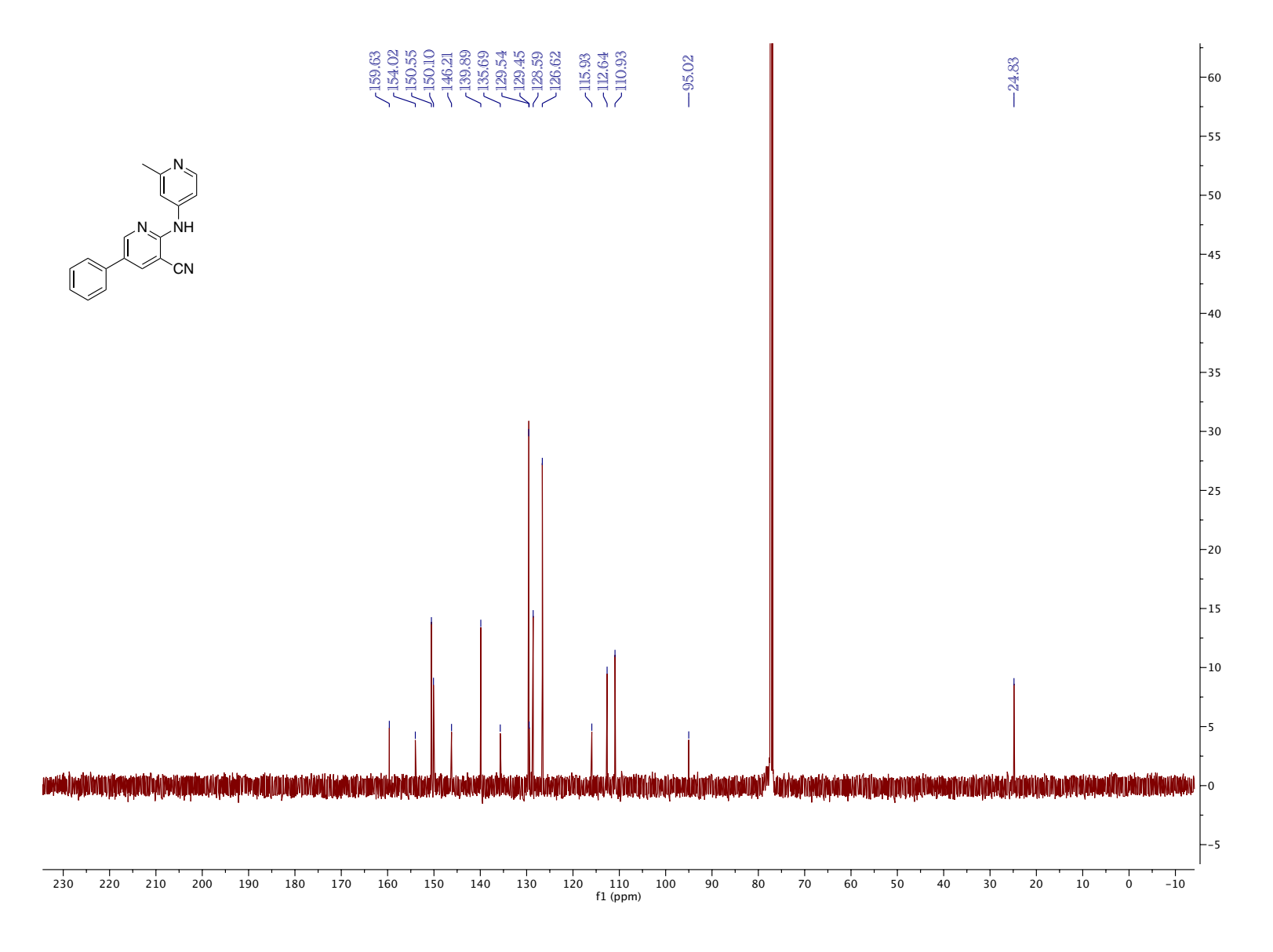


Figure 5.103. ¹³C NMR (CDCl₃, 126 MHz, 25 °C)

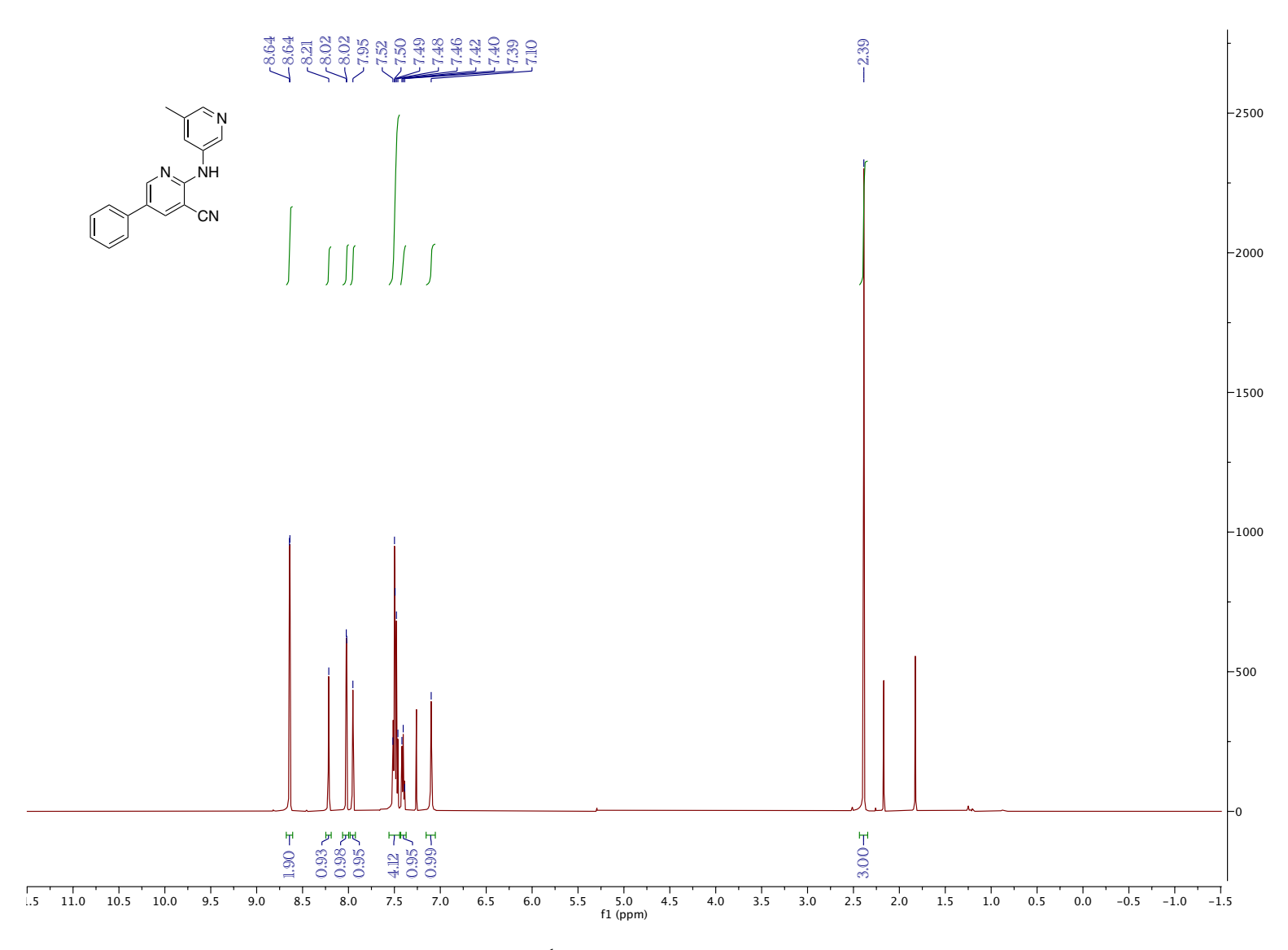


Figure 5.104. ¹H NMR (CDCl₃, 500 MHz, 25 °C)

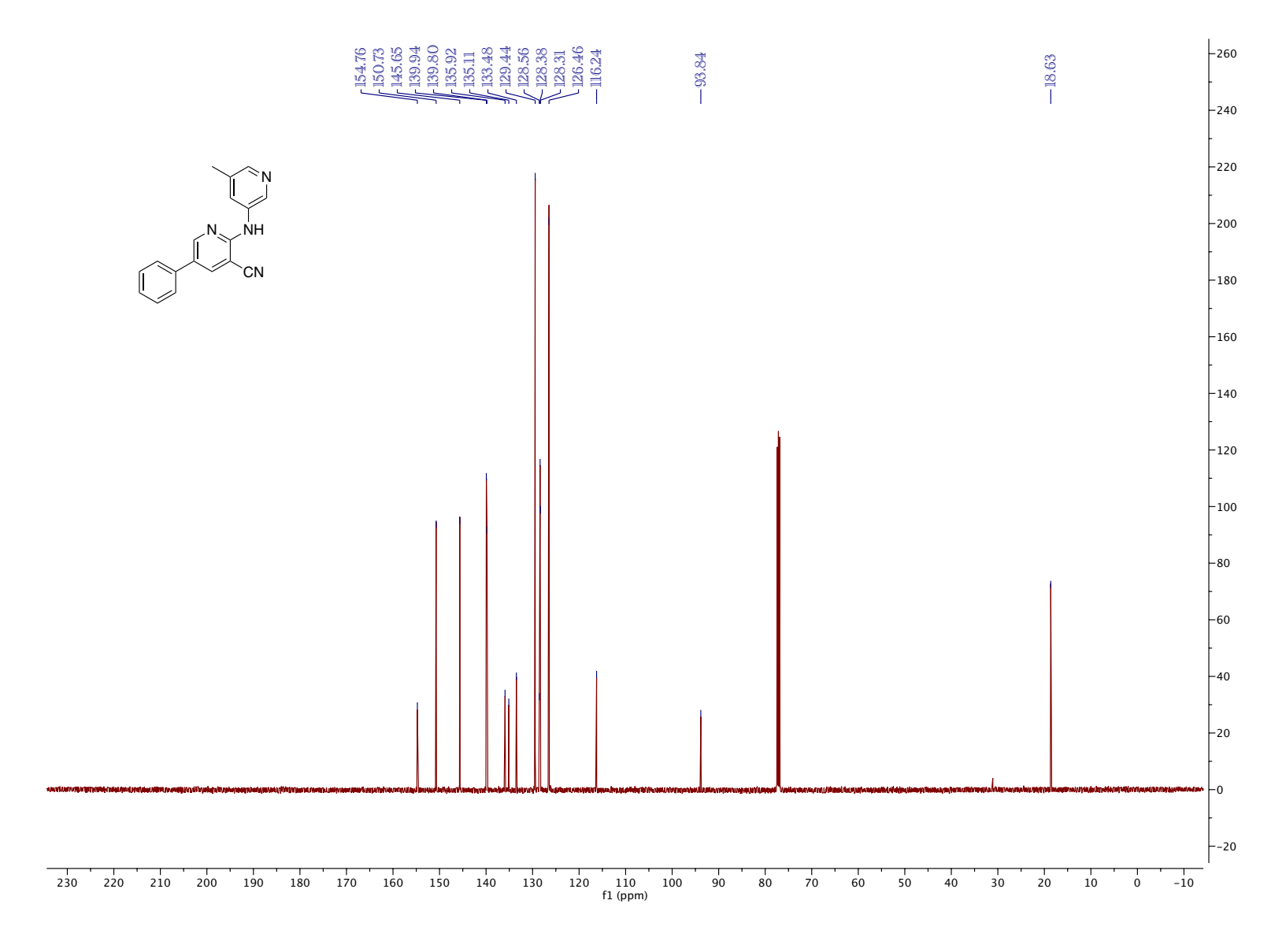


Figure 5.105. ¹³C NMR (CDCl₃, 126 MHz, 25 °C)

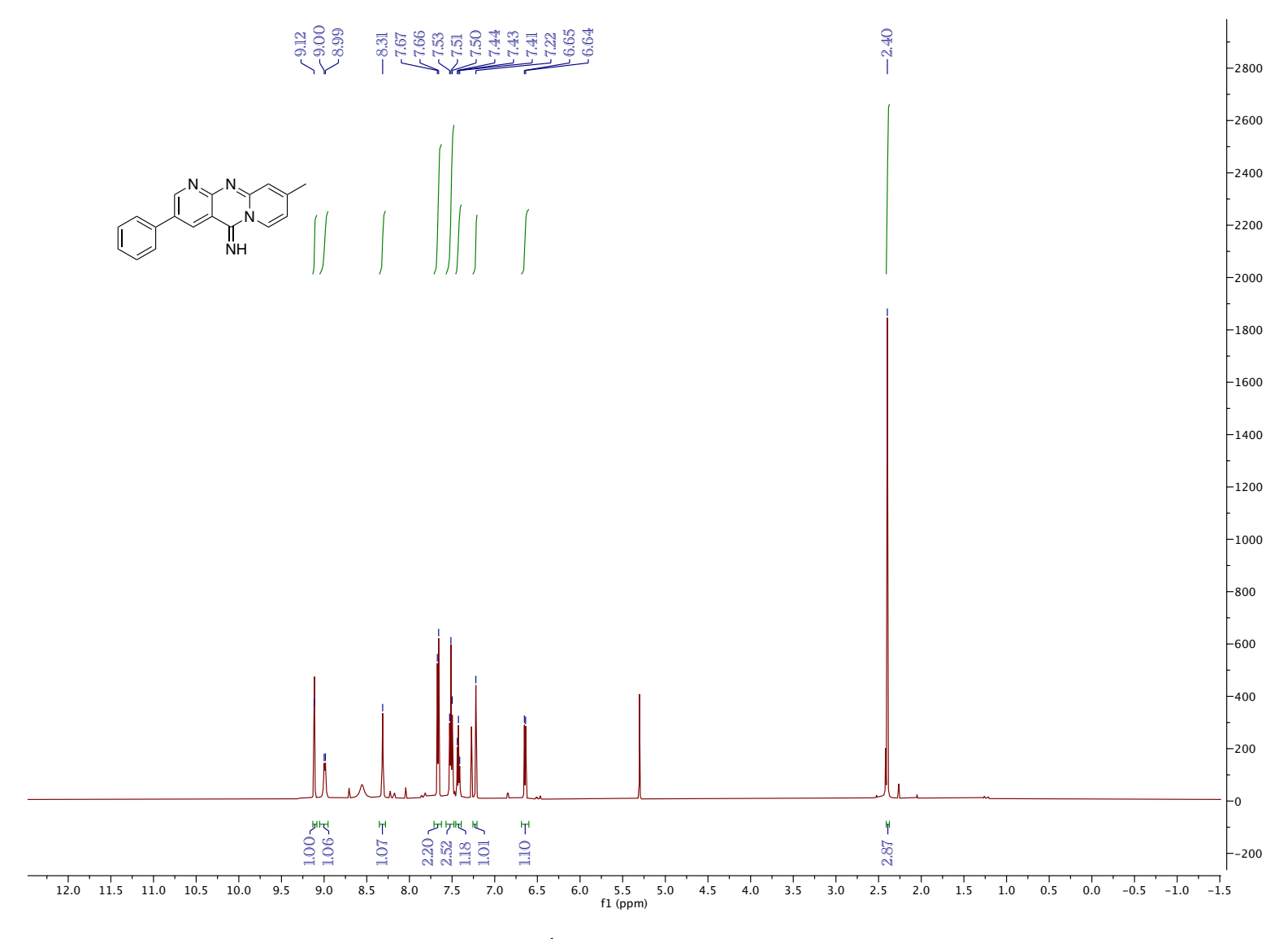


Figure 5.106. ¹H NMR (CDCl₃, 500 MHz, 25 °C)

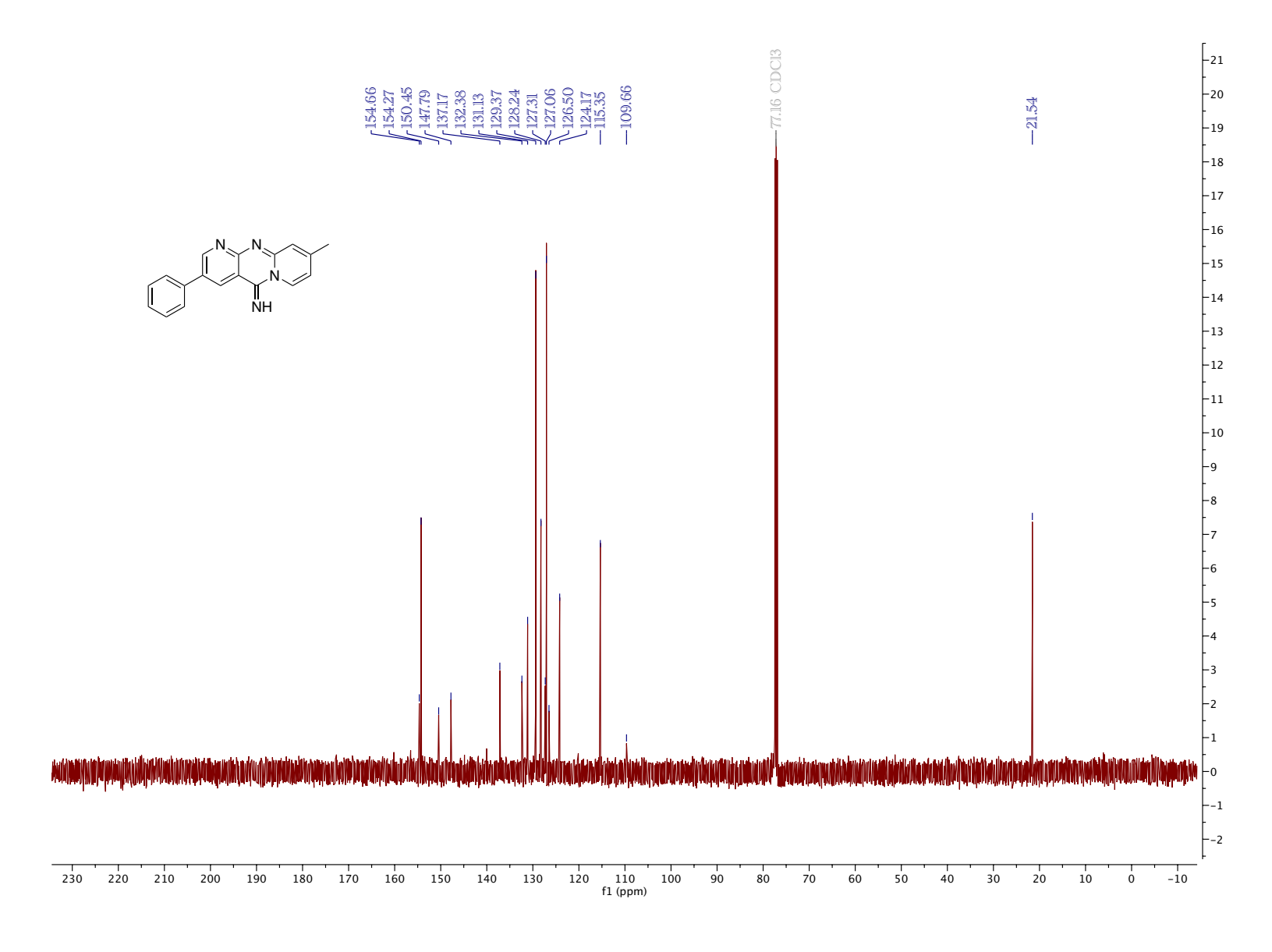


Figure 5.107. ¹³C NMR (CDCl₃, 126 MHz, 25 °C)

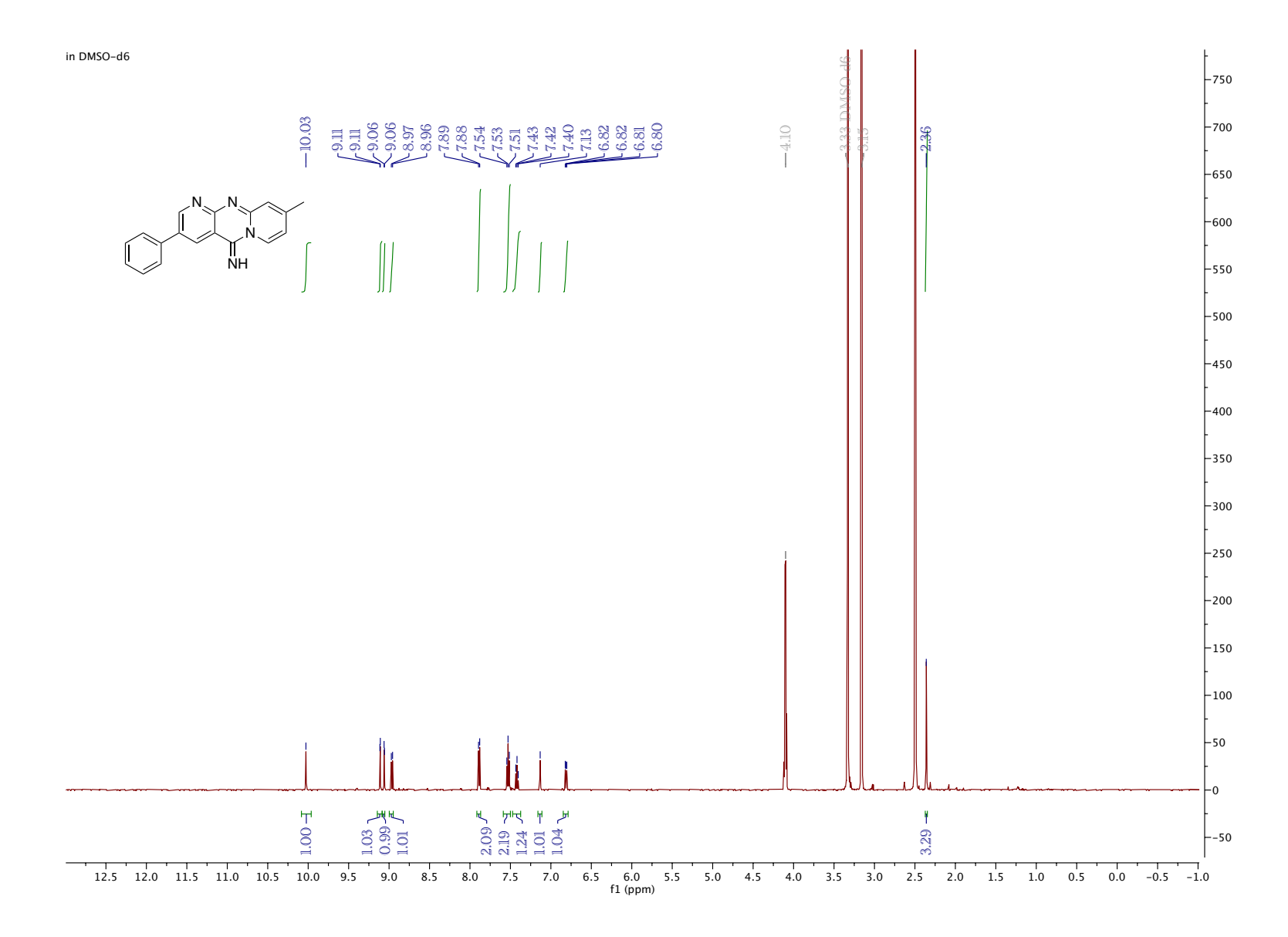


Figure 5.108. 1 H NMR (500 MHz, DMSO-d₆, 25 $^{\circ}$ C)

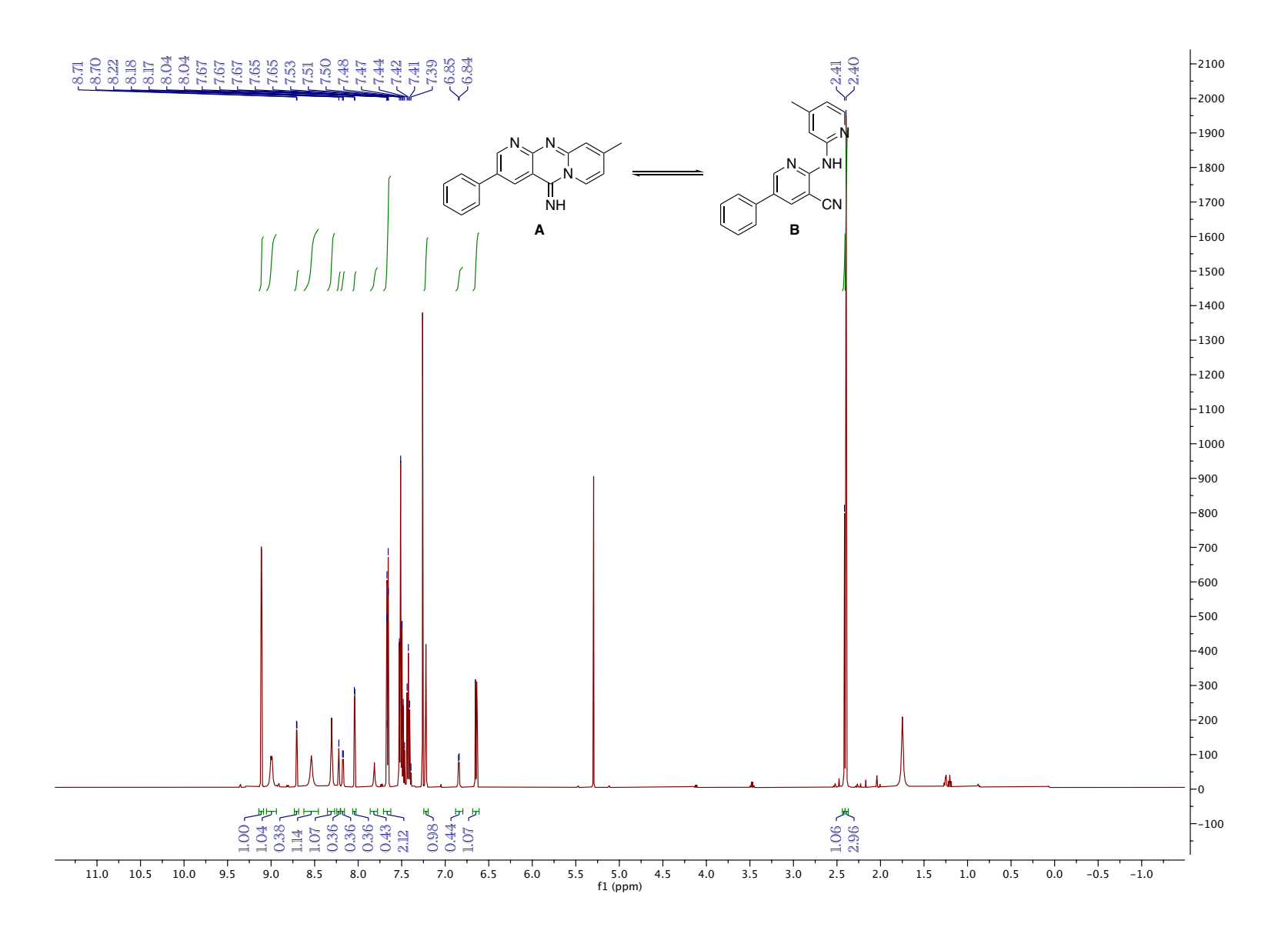


Figure 5.109. ¹H NMR (CDCl₃, 500 MHz, 25 °C)

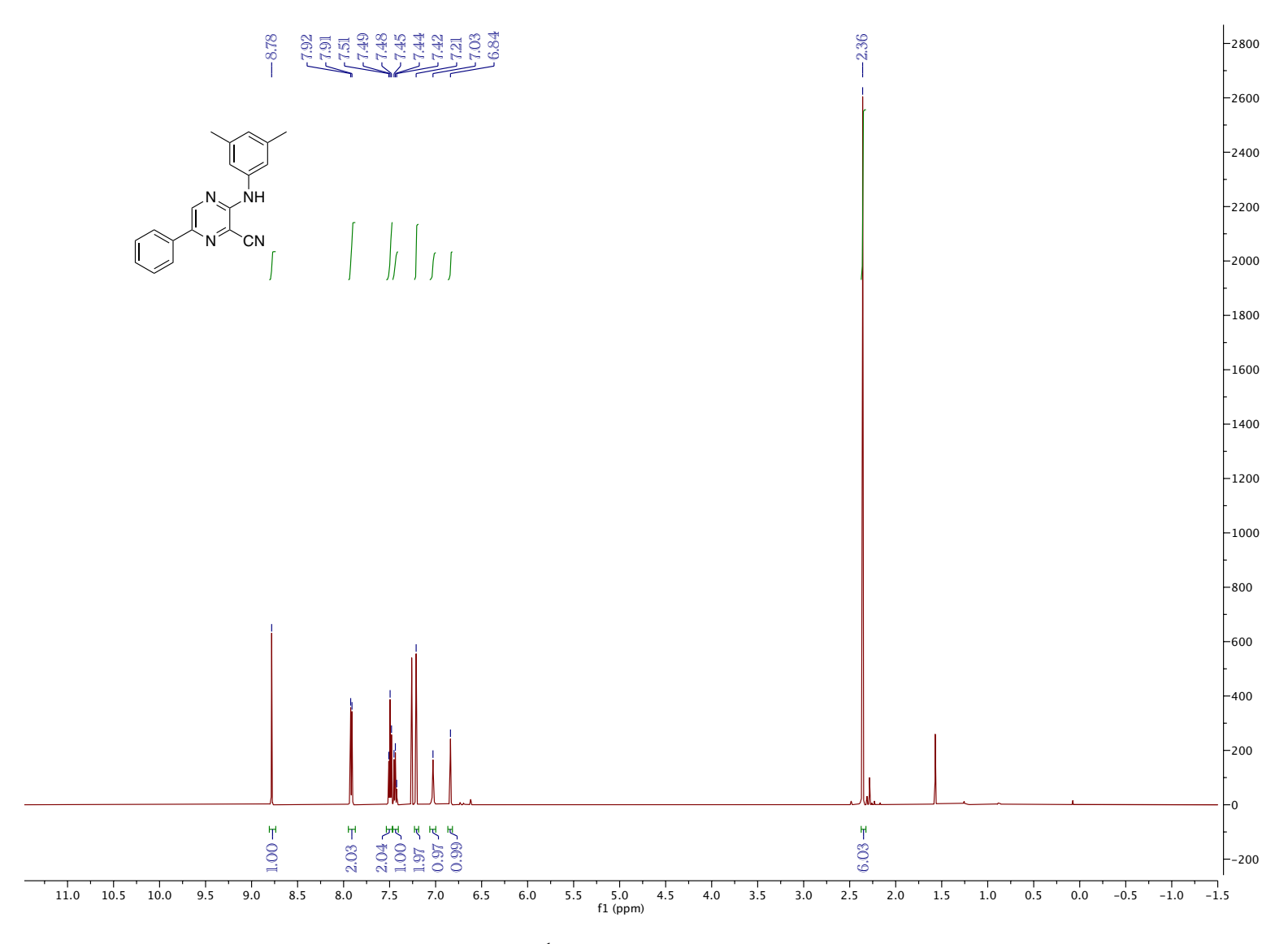


Figure 5.110. ¹H NMR (CDCl₃, 500 MHz, 25 °C)

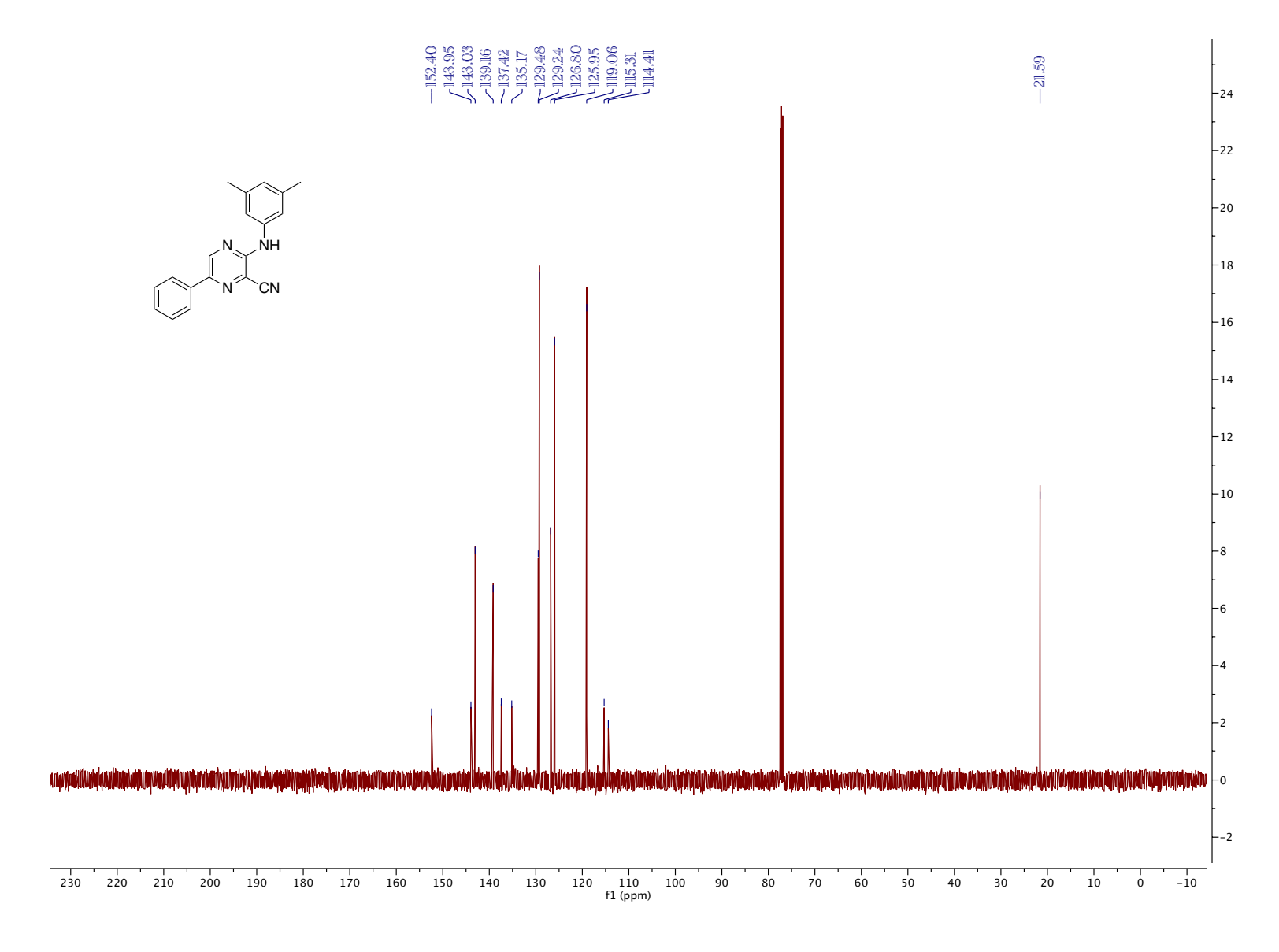


Figure 5.111. ¹³C NMR (CDCl₃, 126 MHz, 25 °C)

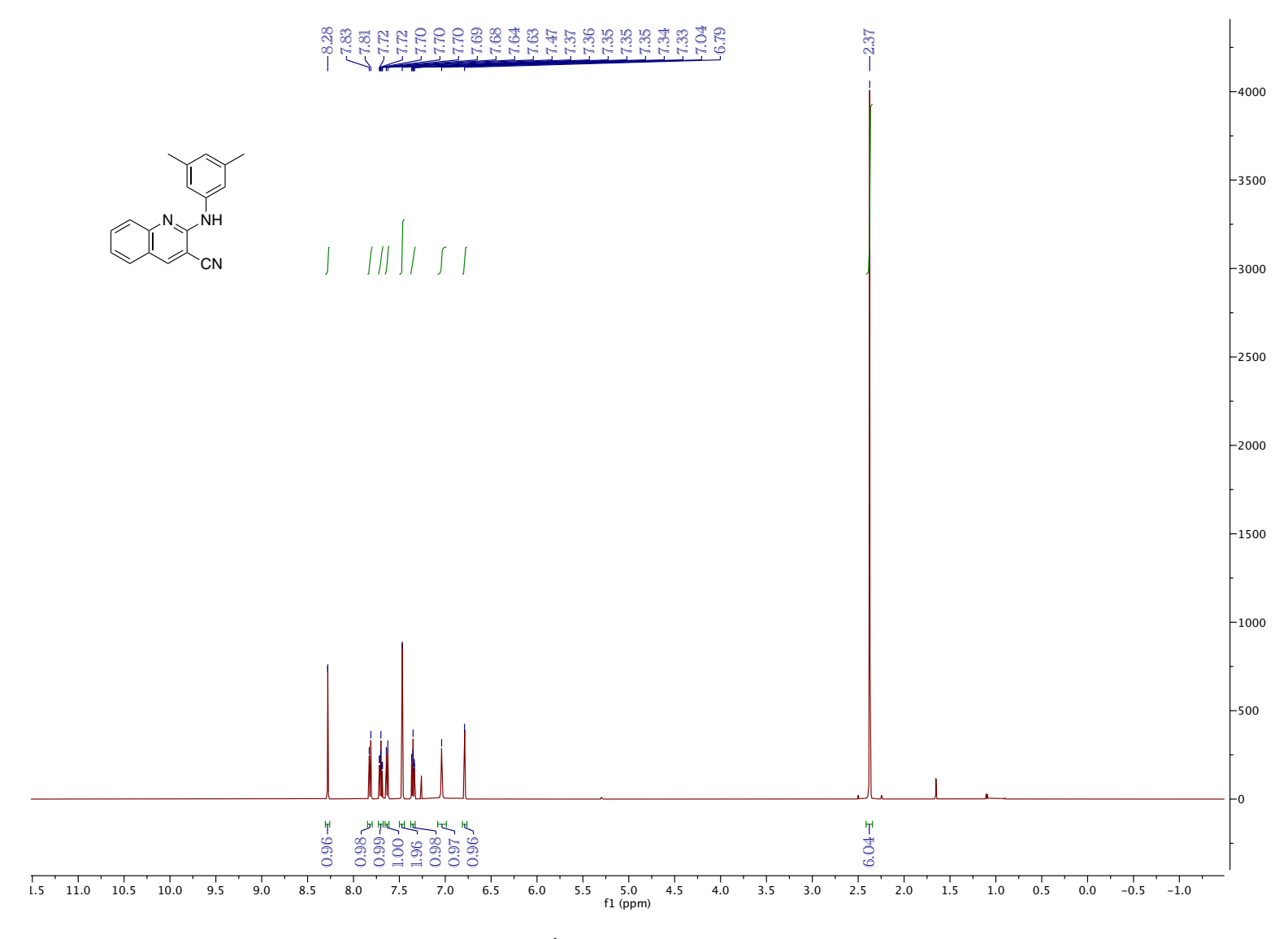


Figure 5.112. 1 H NMR (CDCl₃, 500 MHz, 25 $^{\circ}$ C)

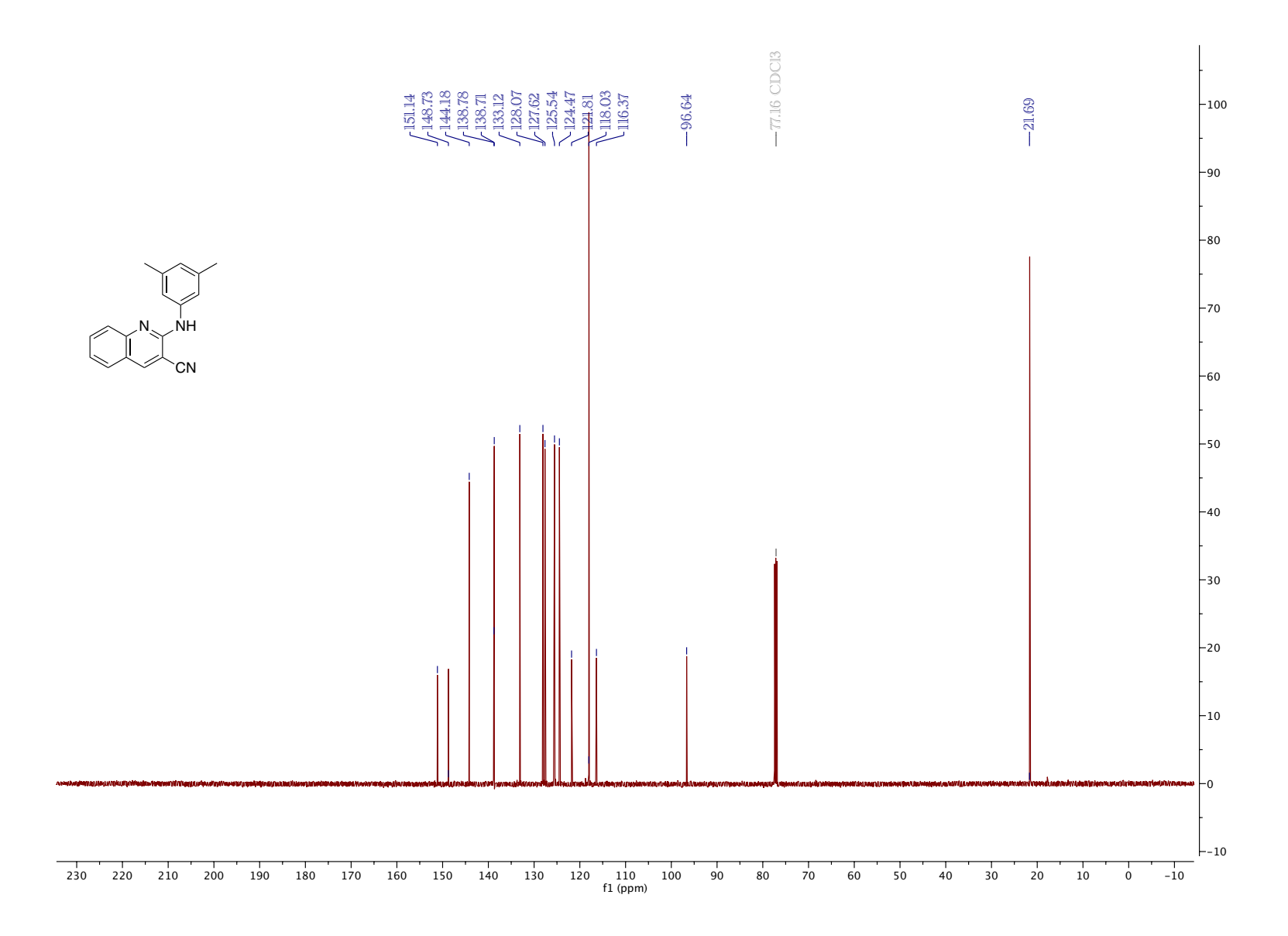


Figure 5.113. 13 C NMR (CDCl₃, 126 MHz, 25 $^{\circ}$ C)

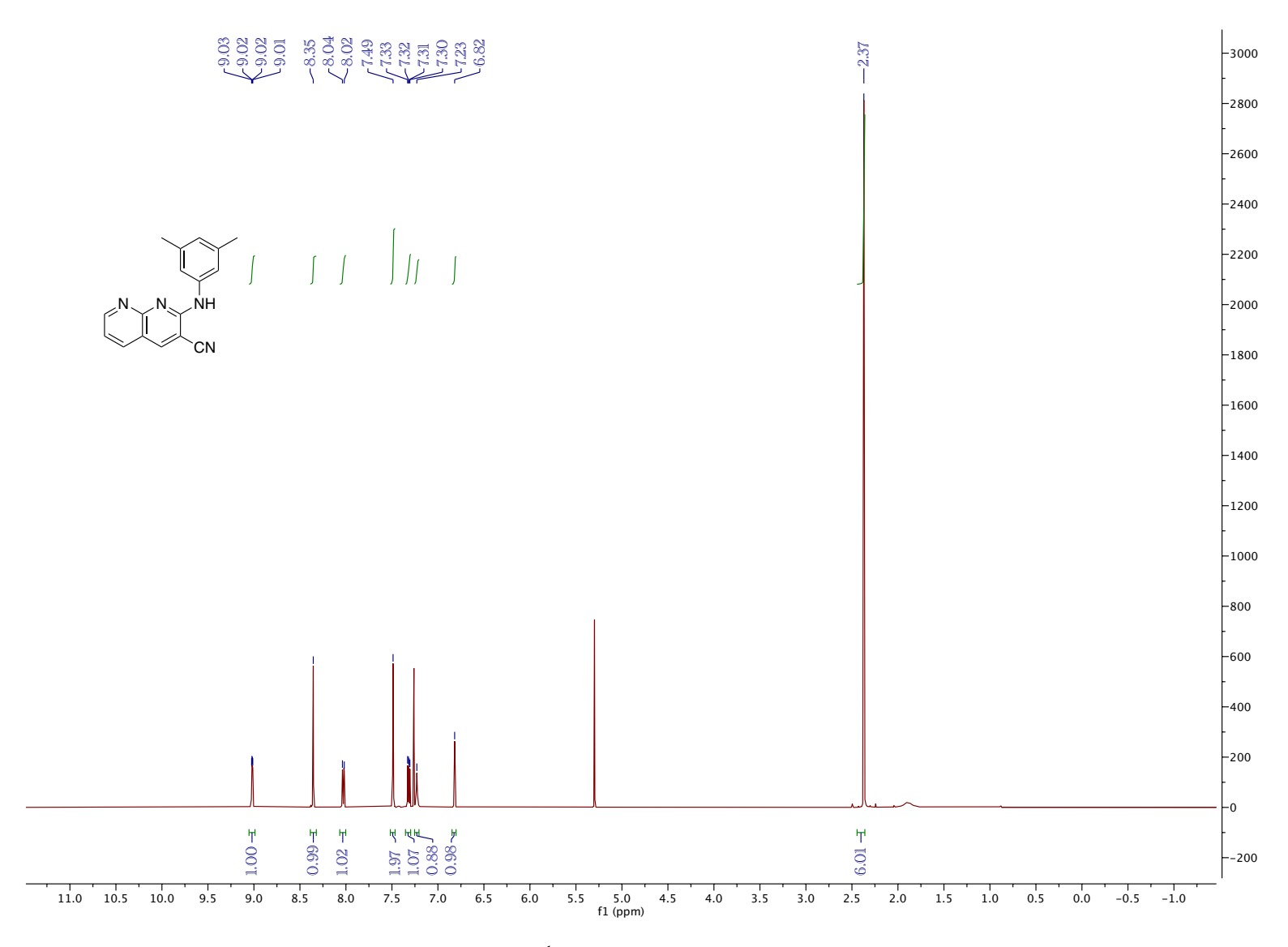


Figure 5.114. ¹H NMR (CDCl₃, 500 MHz, 25 °C)

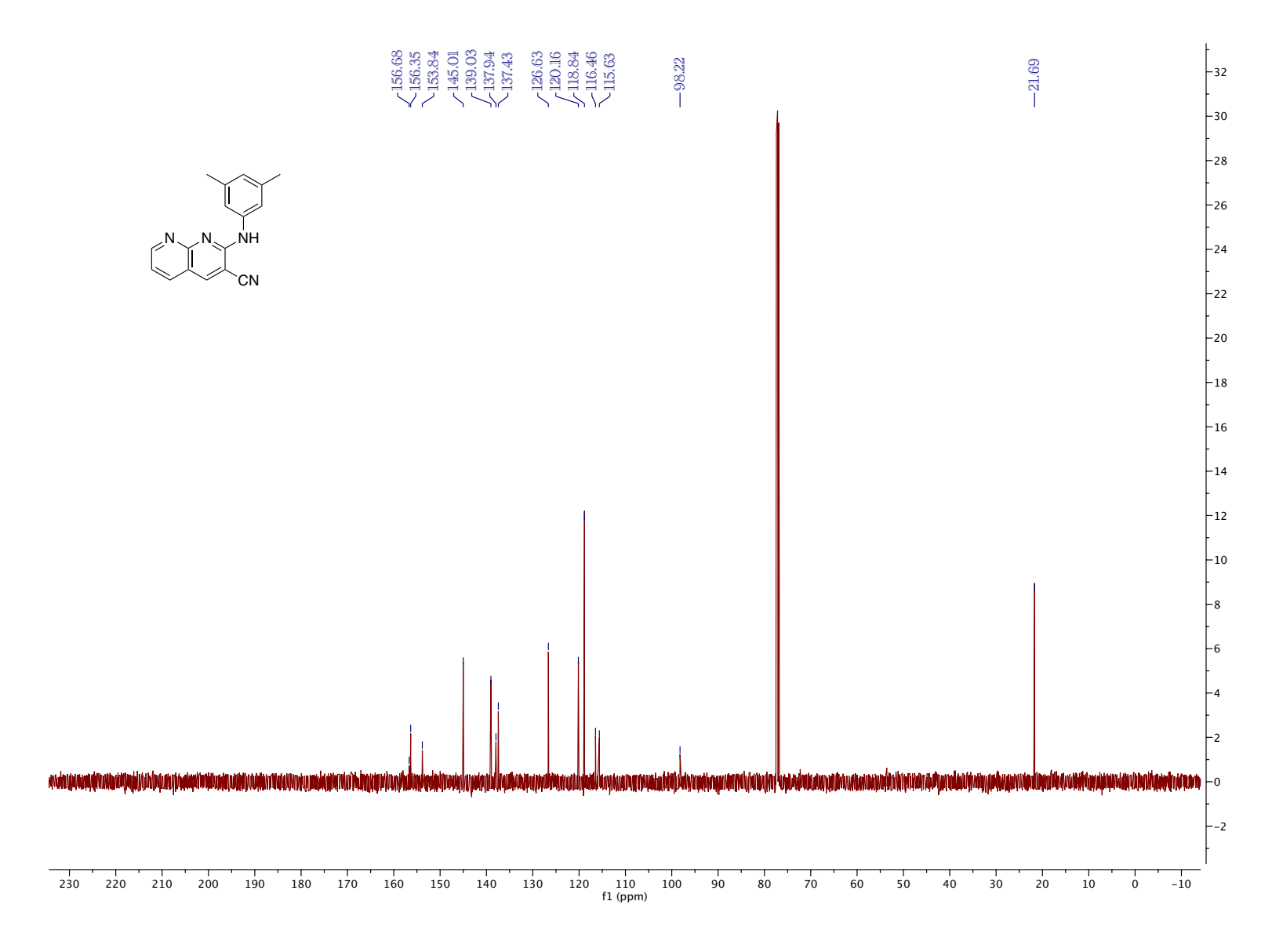


Figure 5.115. ¹³C NMR (CDCl₃, 126 MHz, 25 °C)

APPENDIX B

NMR Spectra (Ruthenium Complexes)

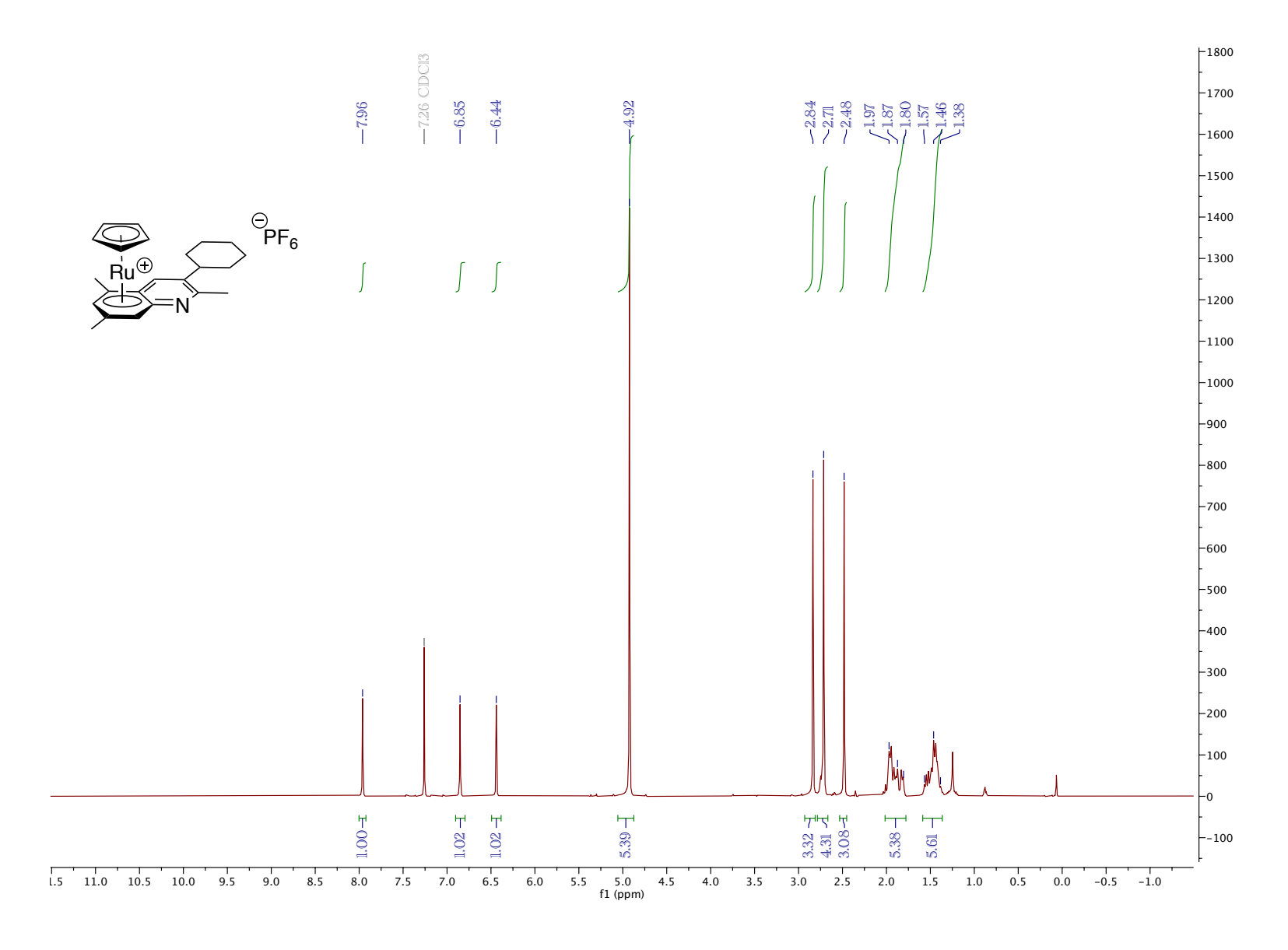


Figure 5.116. ¹H NMR (CDCl₃, 500 MHz, 25 °C)

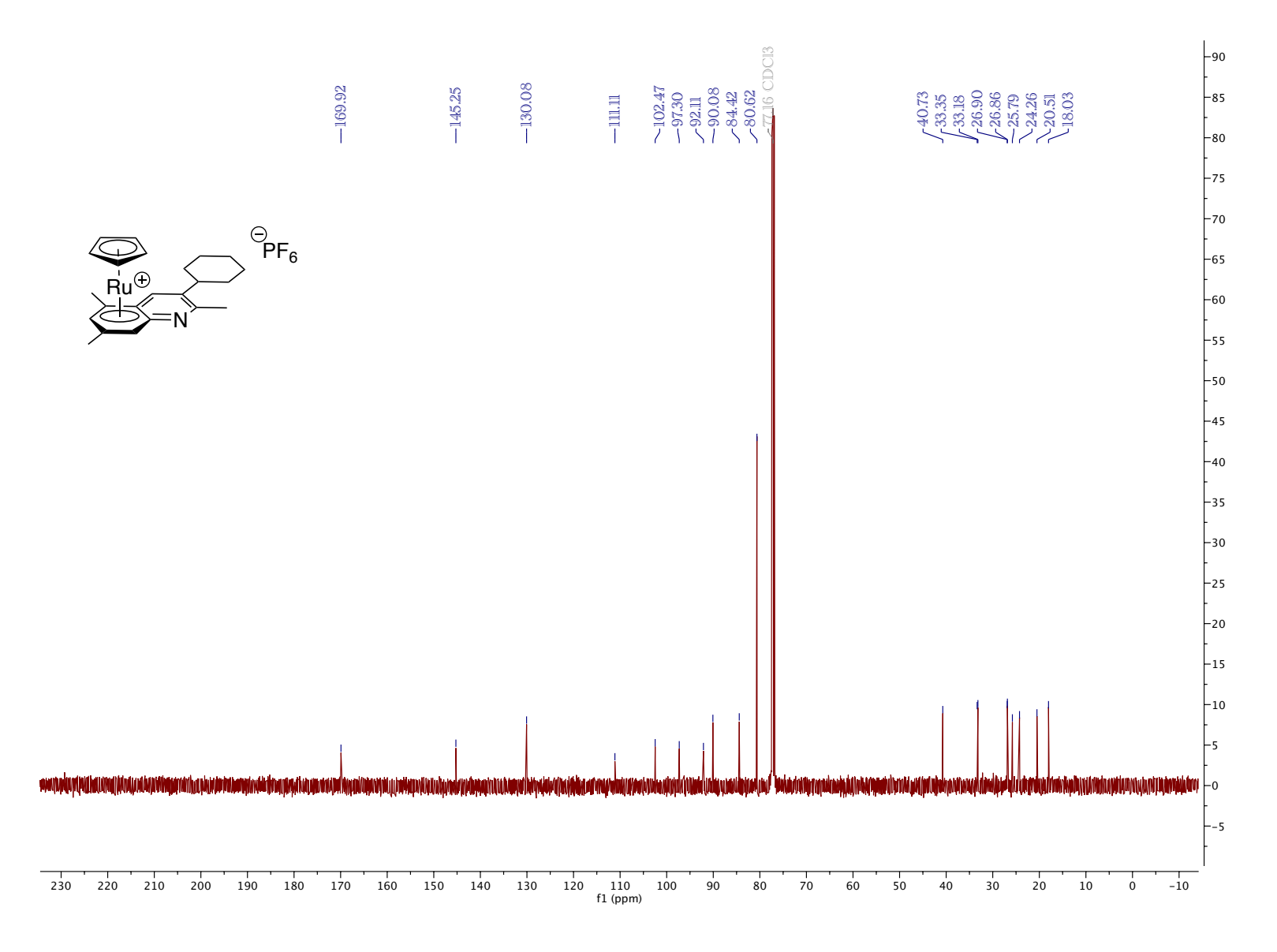


Figure 5.117. ¹³C NMR (CDCl₃, 126 MHz, 25 °C)

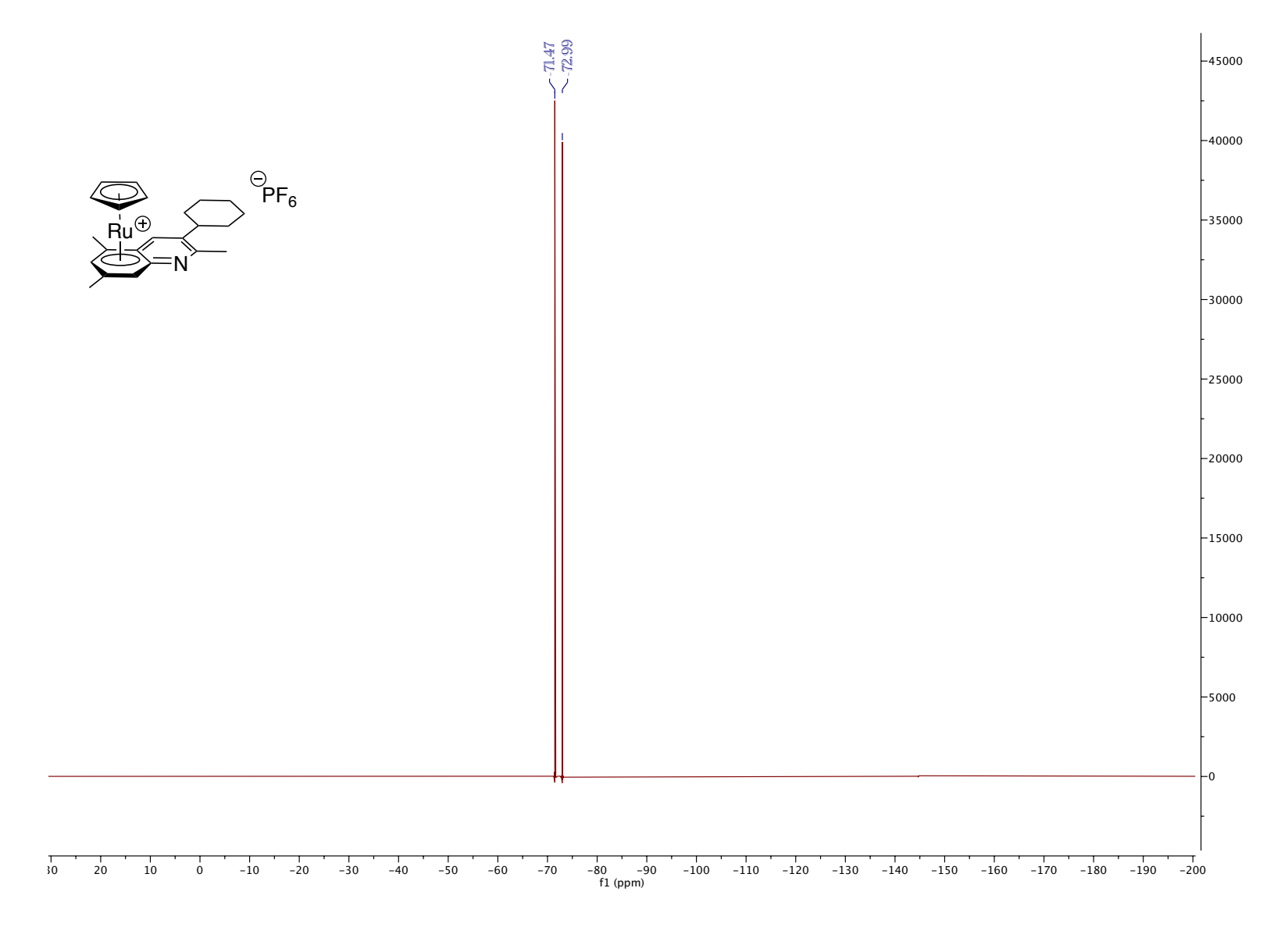


Figure 5.118. ^{19}F NMR (CDCl₃, 470 MHz, 25 $^{\circ}C)$

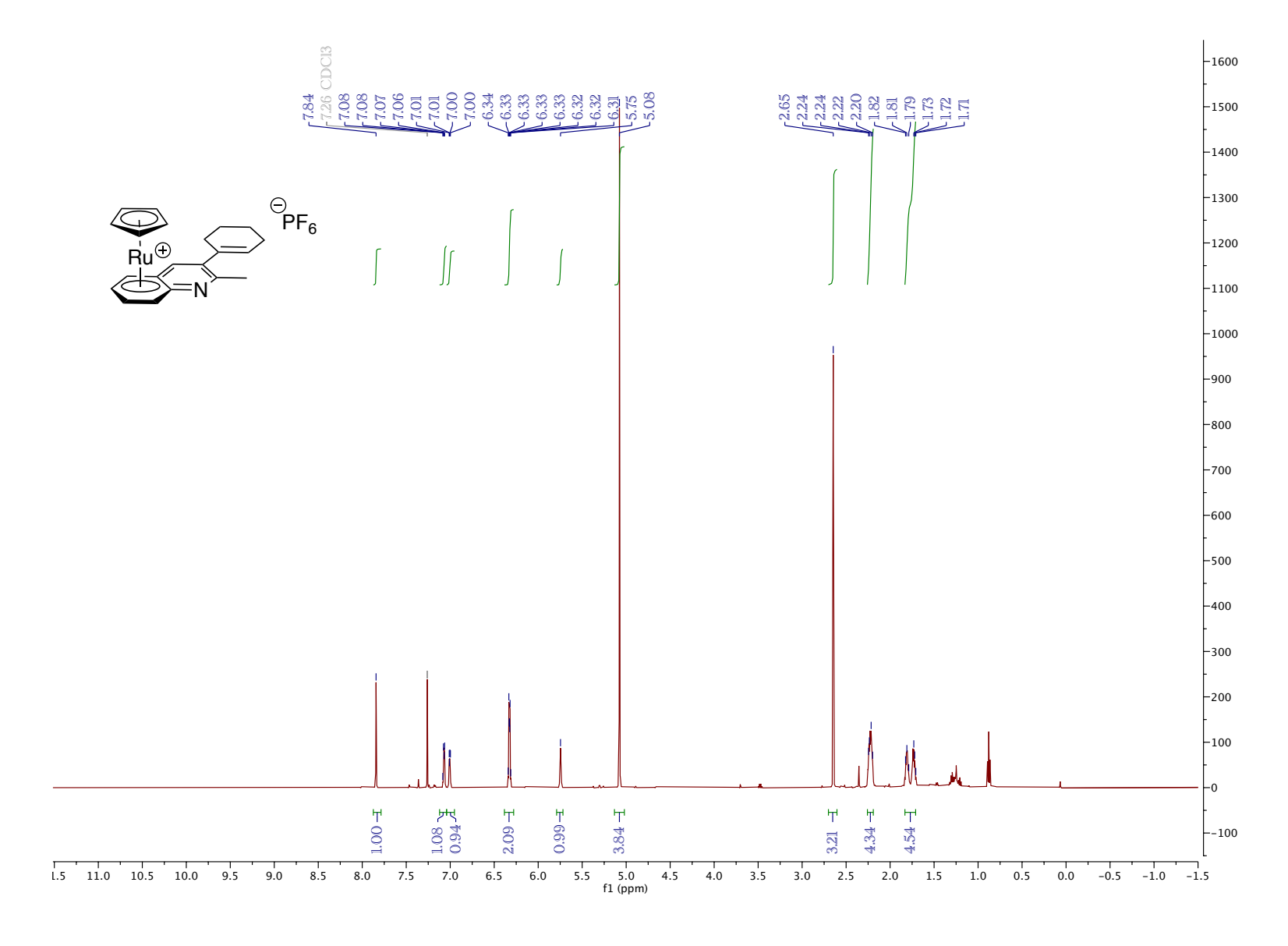


Figure 5.119. ¹H NMR (CDCl₃, 500 MHz, 25 °C)

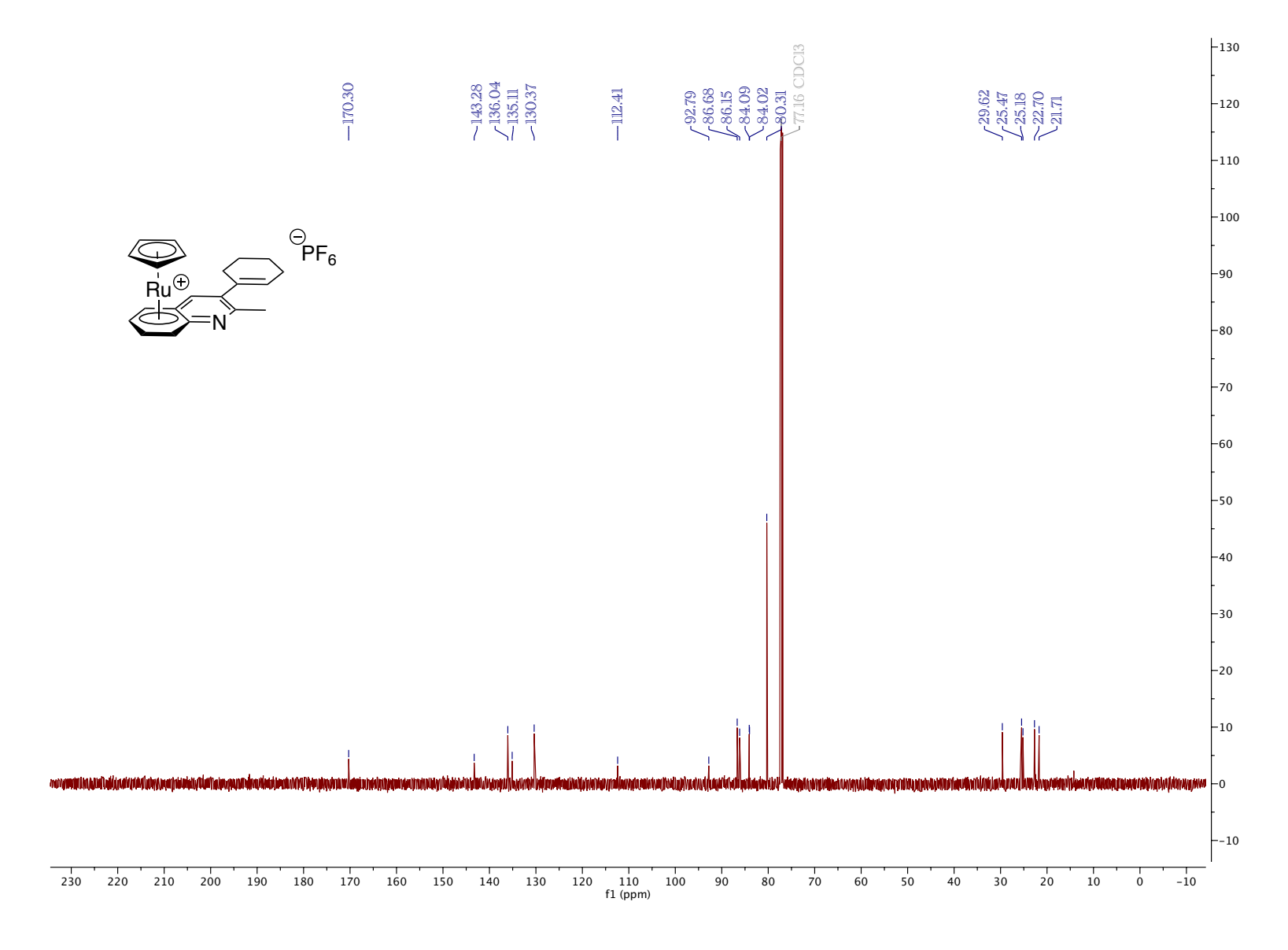


Figure 5.120. ¹³C NMR (CDCl₃, 126 MHz, 25 °C)

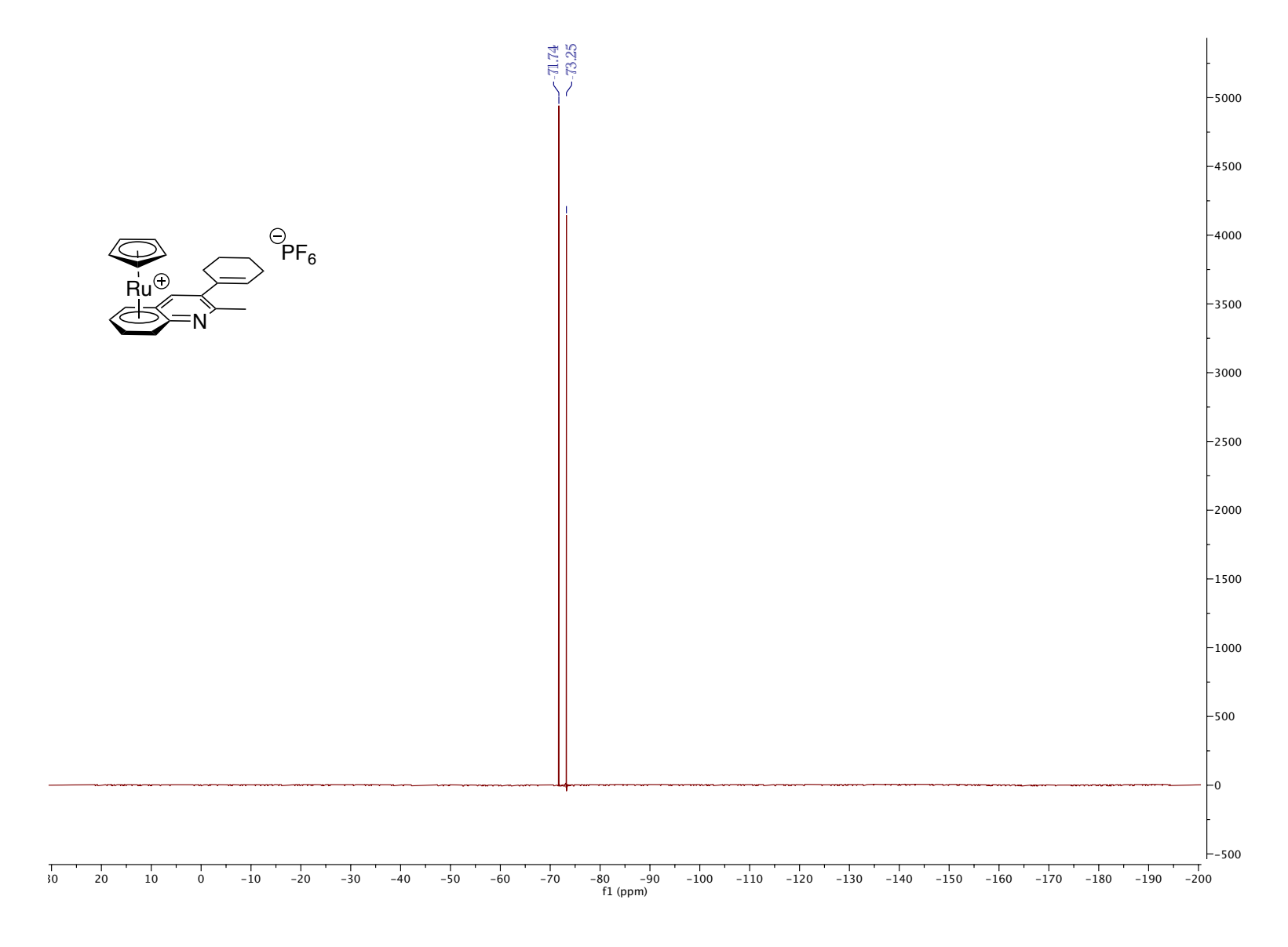


Figure 5.121. ^{19}F NMR (CDCl₃, 470 MHz, 25 $^{\circ}C)$

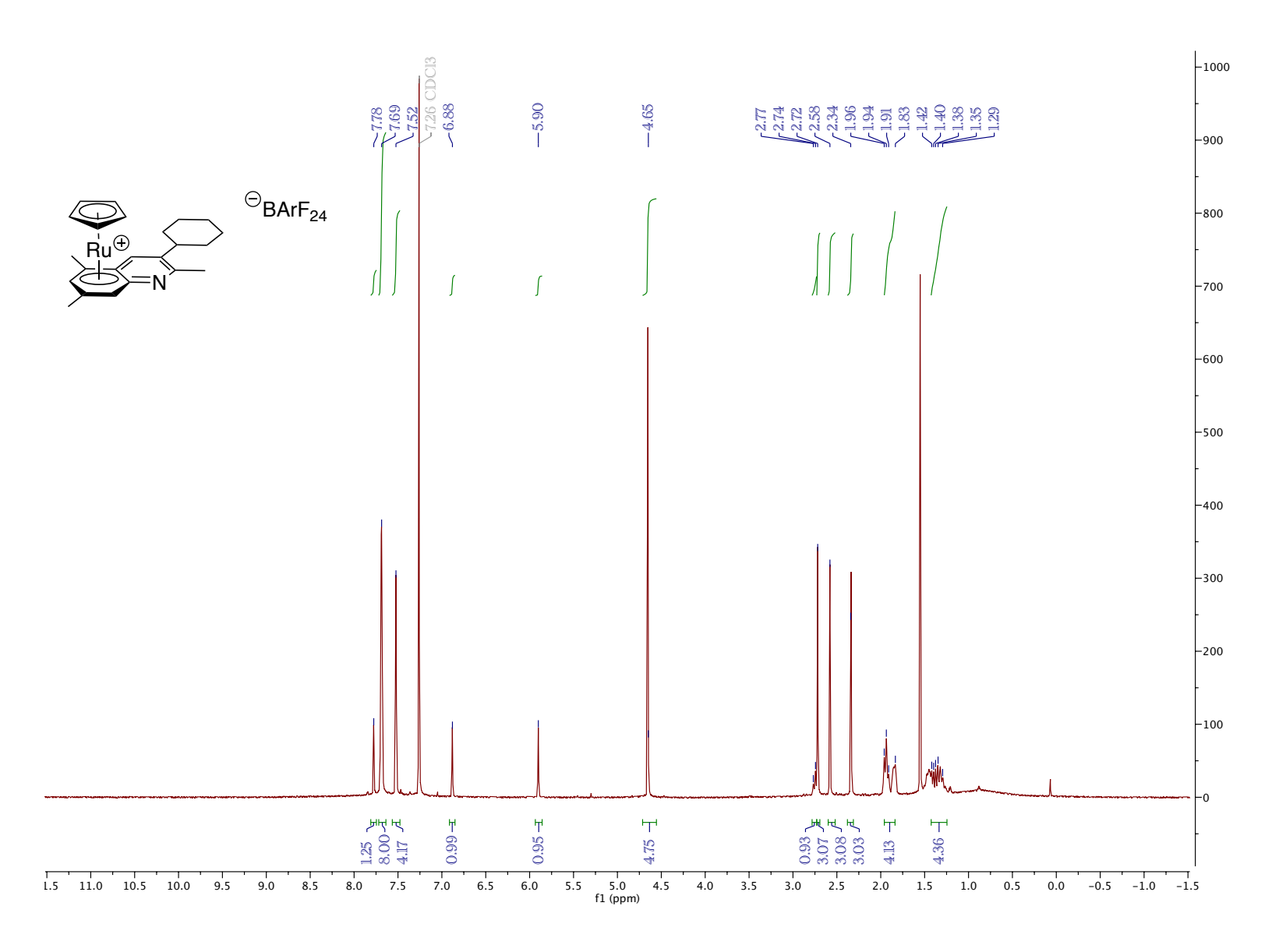


Figure 5.122. 1H NMR (CDCl₃, 500 MHz, 25 $^{\circ}$ C)

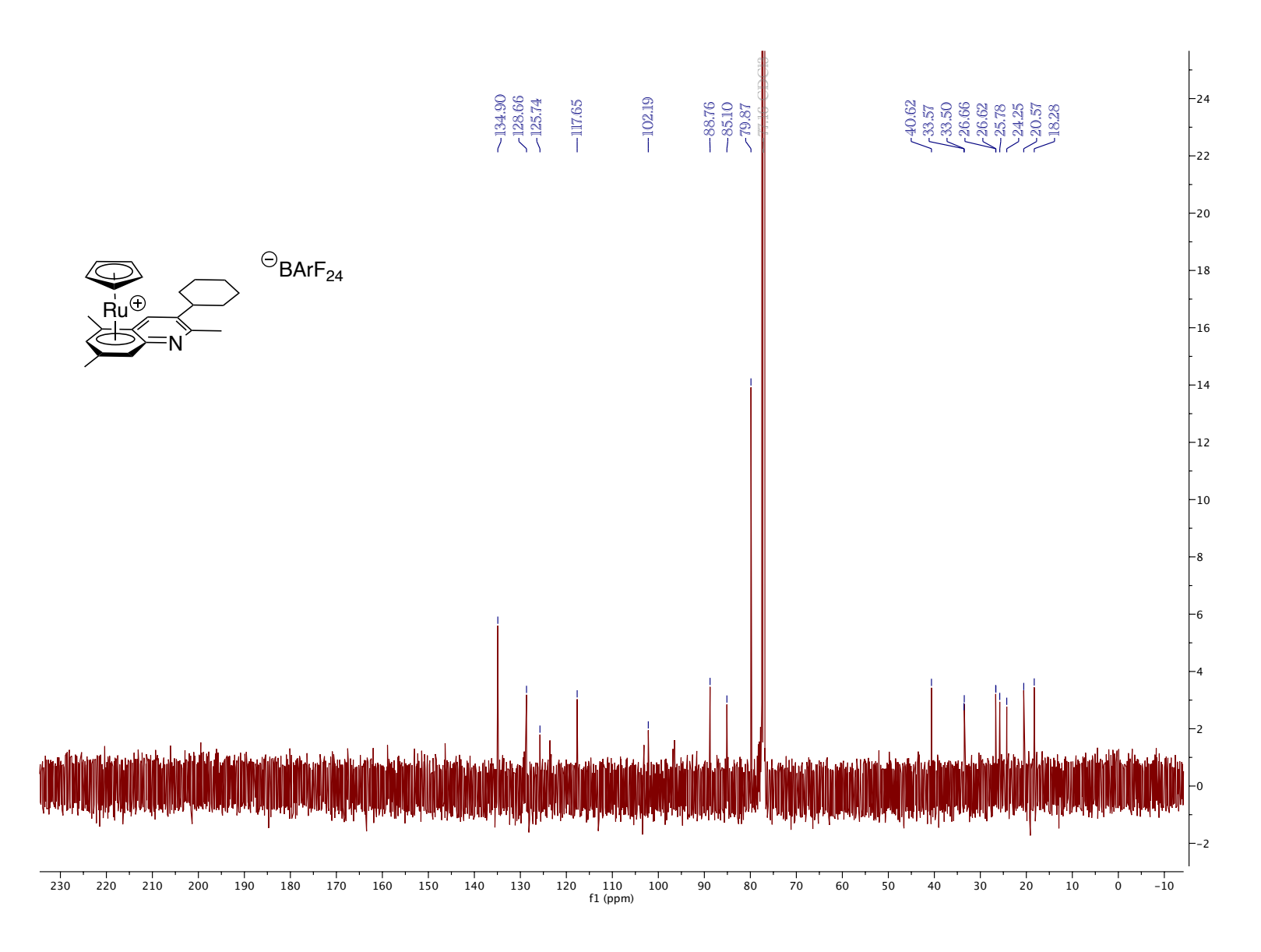


Figure 5.123. 13 C NMR (CDCl₃, 126 MHz, 25 $^{\circ}$ C)

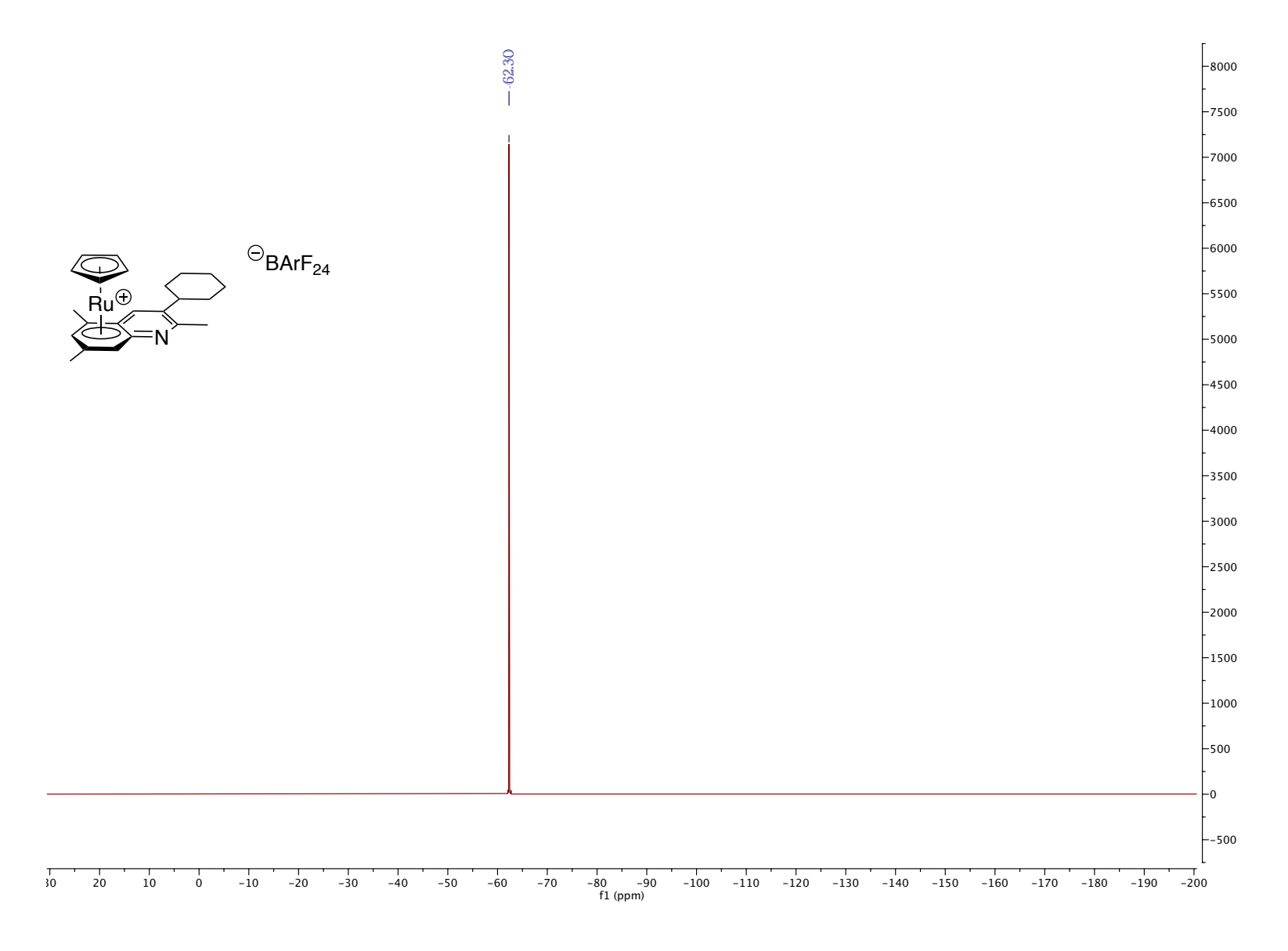


Figure 5.124. ^{19}F NMR (CDCl₃, 470 MHz, 25 $^{\circ}C)$

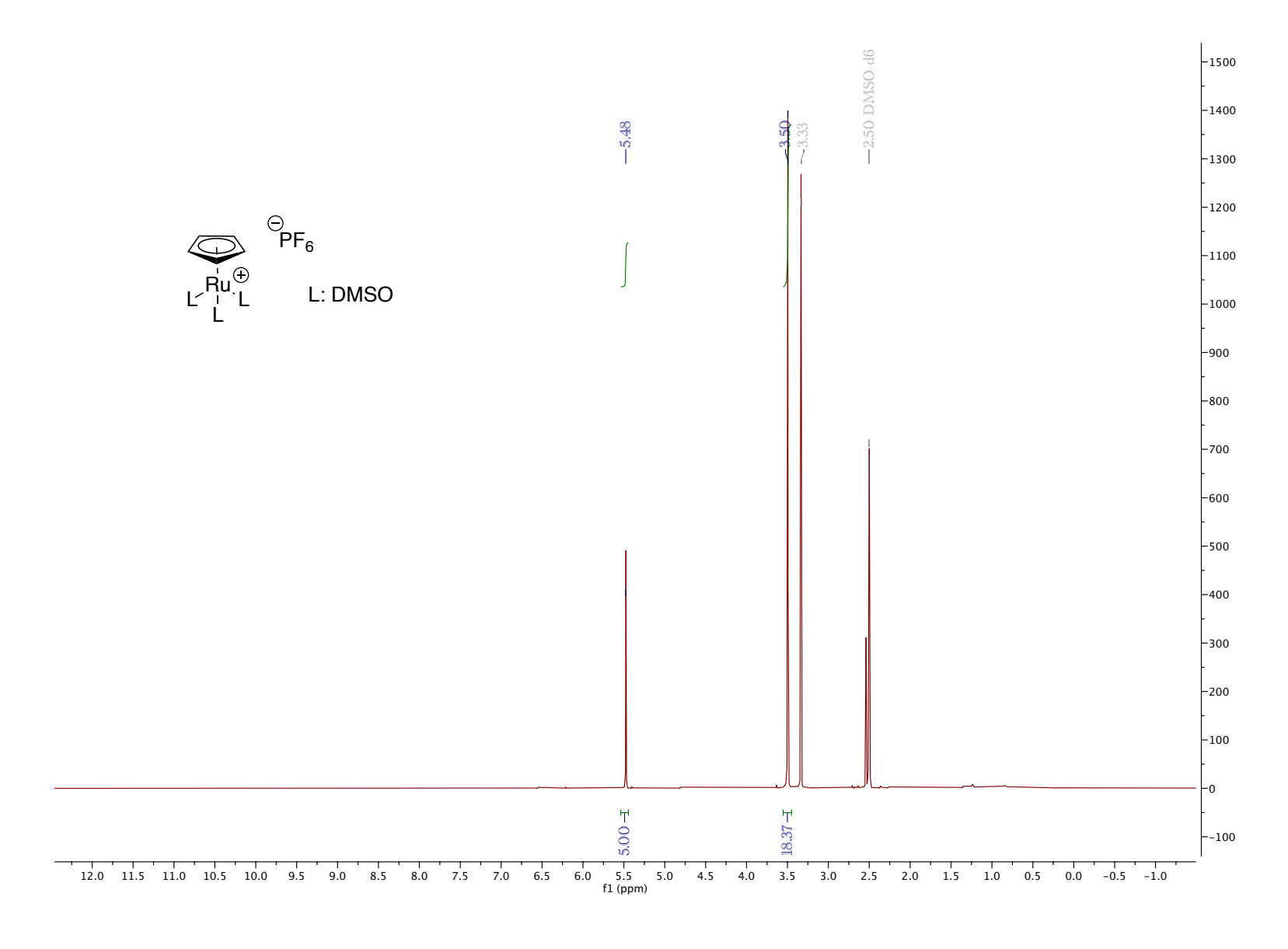


Figure 5.125. ¹H NMR (CDCl₃, 500 MHz, 25 °C)

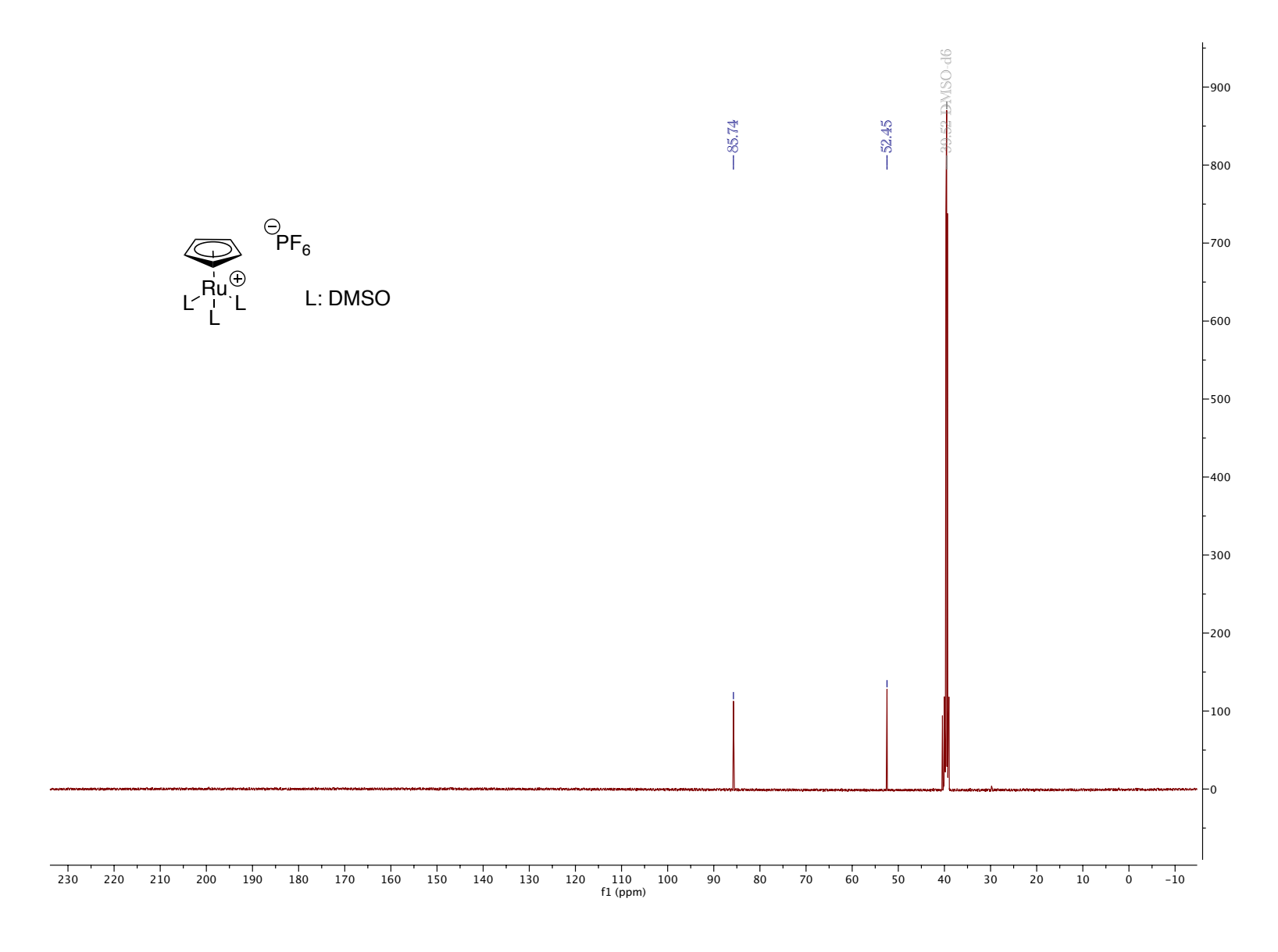


Figure 5.126. ¹³C NMR (CDCl₃, 126 MHz, 25 °C)

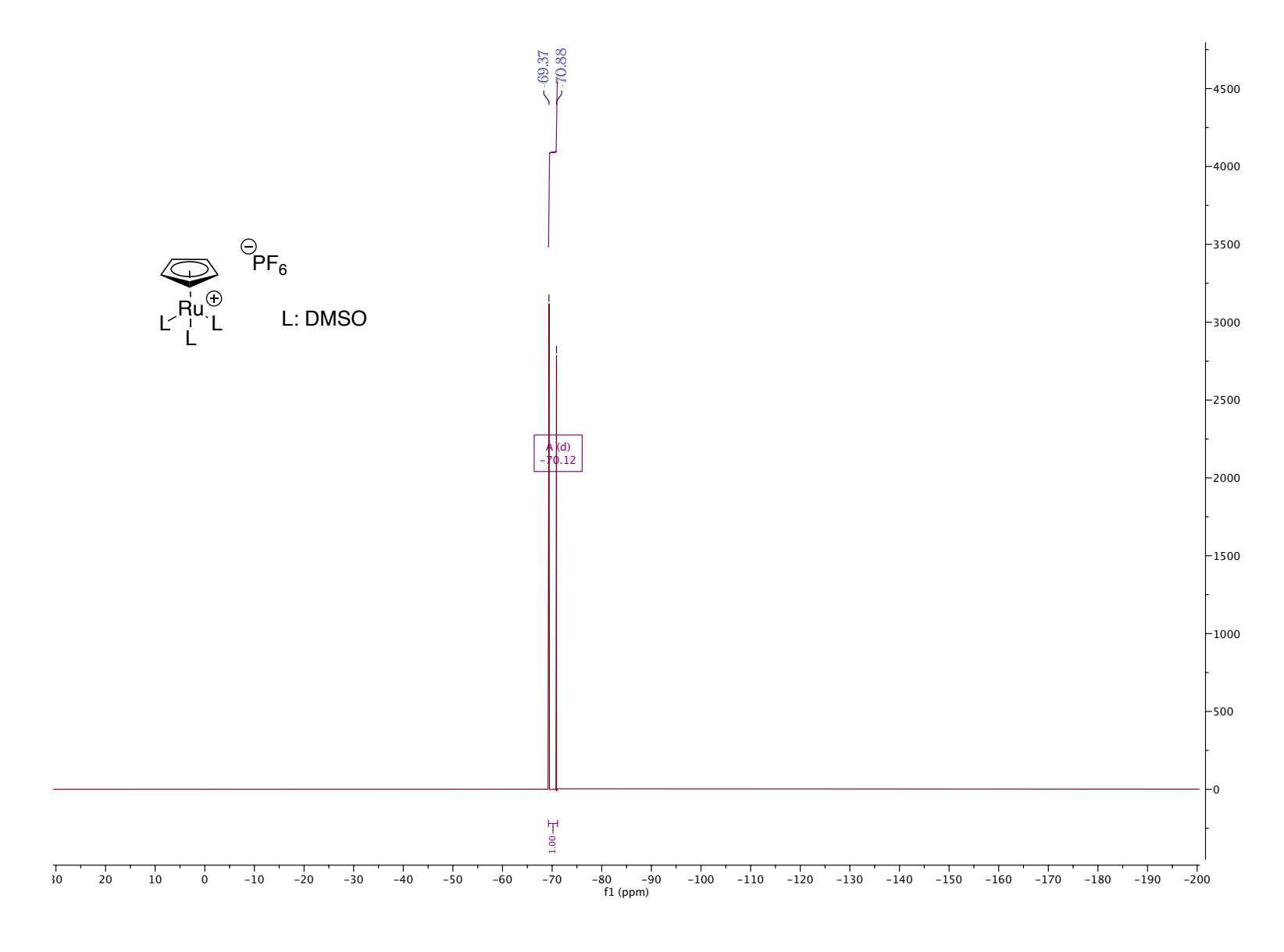


Figure 5.127. 19 F NMR (CDCl₃, 470 MHz, 25 $^{\circ}$ C)

APPENDIX C

NMR Spectra (Unsymmetrical Ligands and Titanium Catalysts)

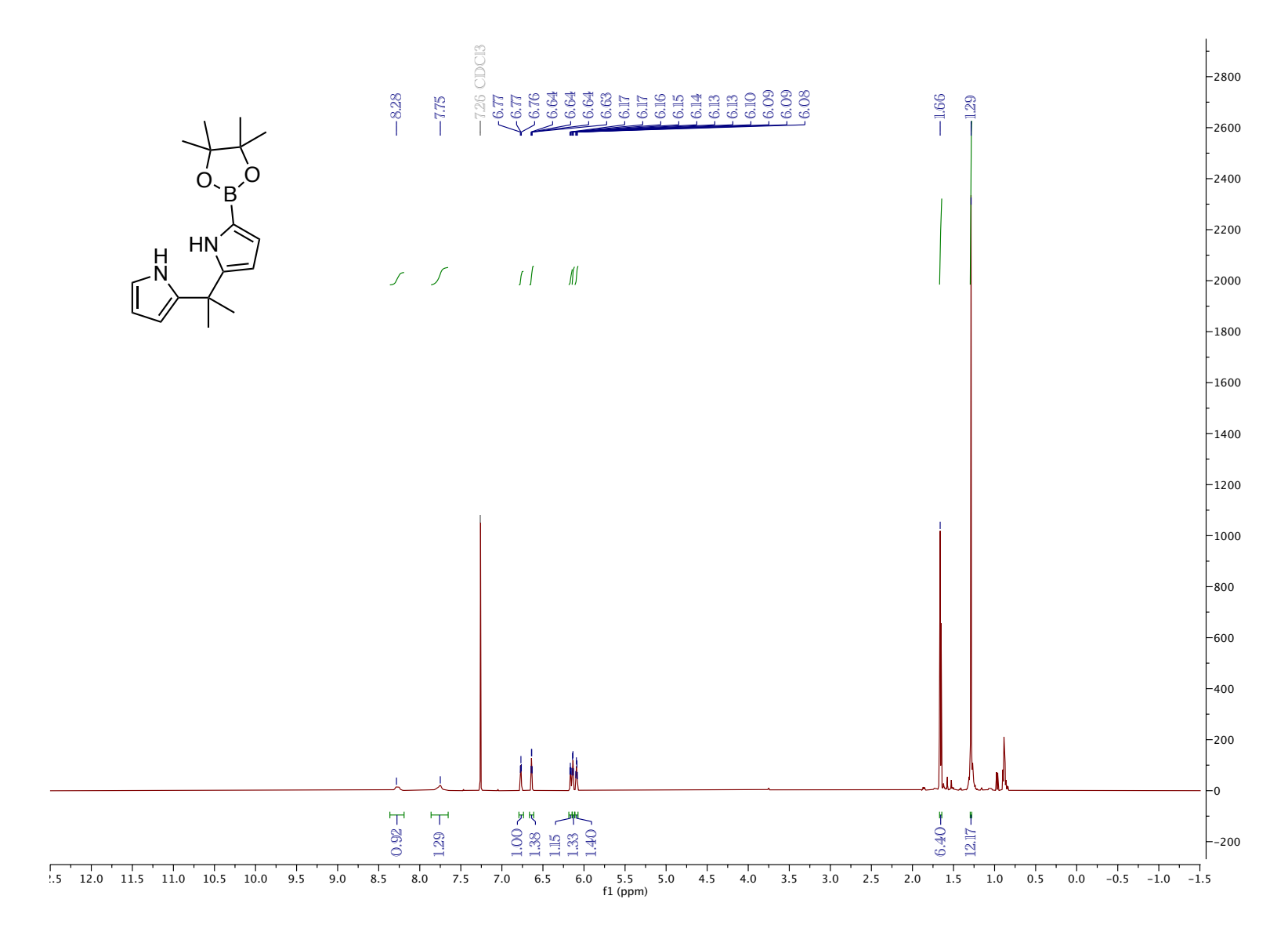


Figure 5.128. ¹H NMR (CDCl₃, 500 MHz, 25 °C)

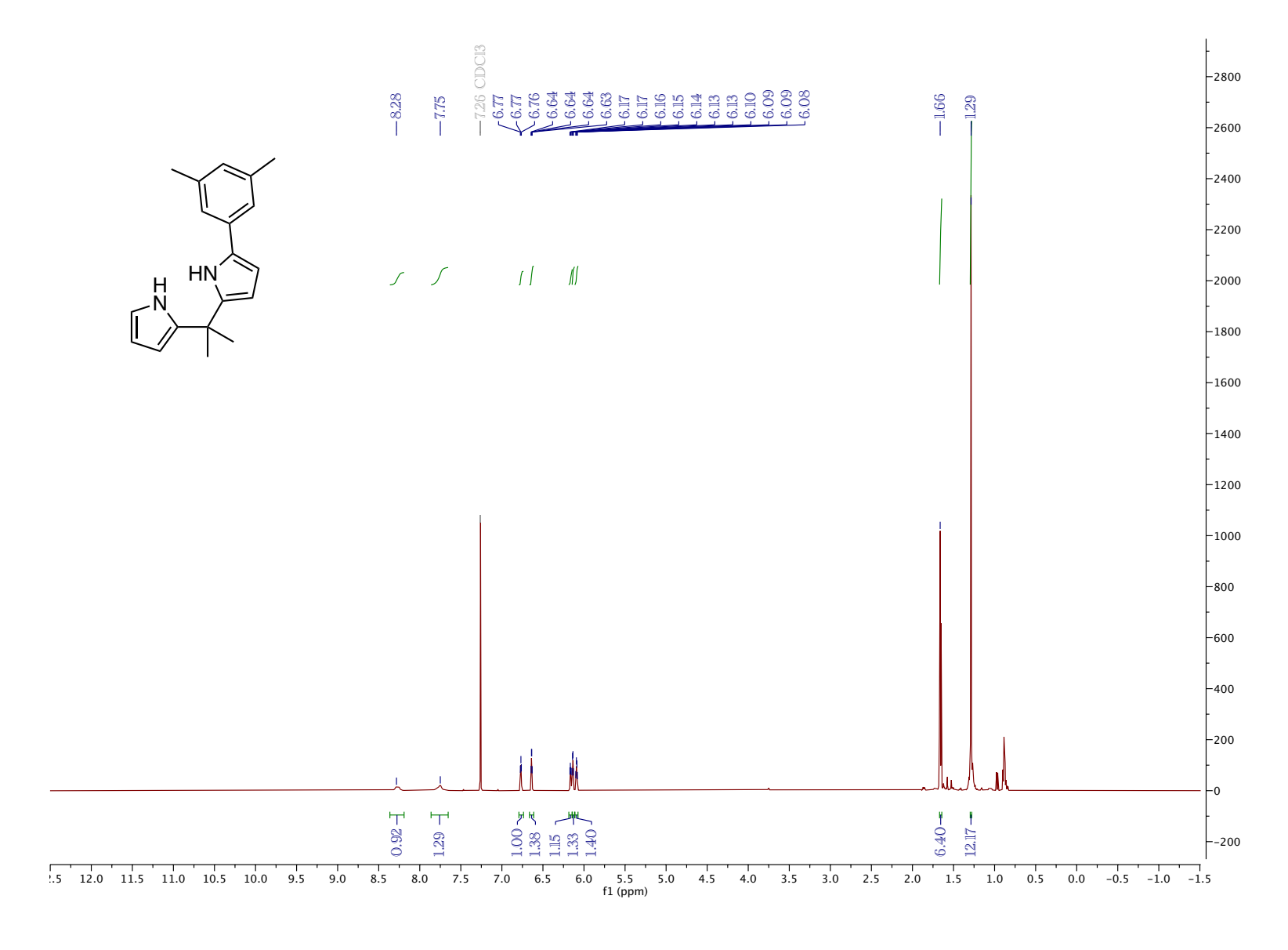


Figure 5.129. ¹H NMR (CDCl₃, 500 MHz, 25 °C)

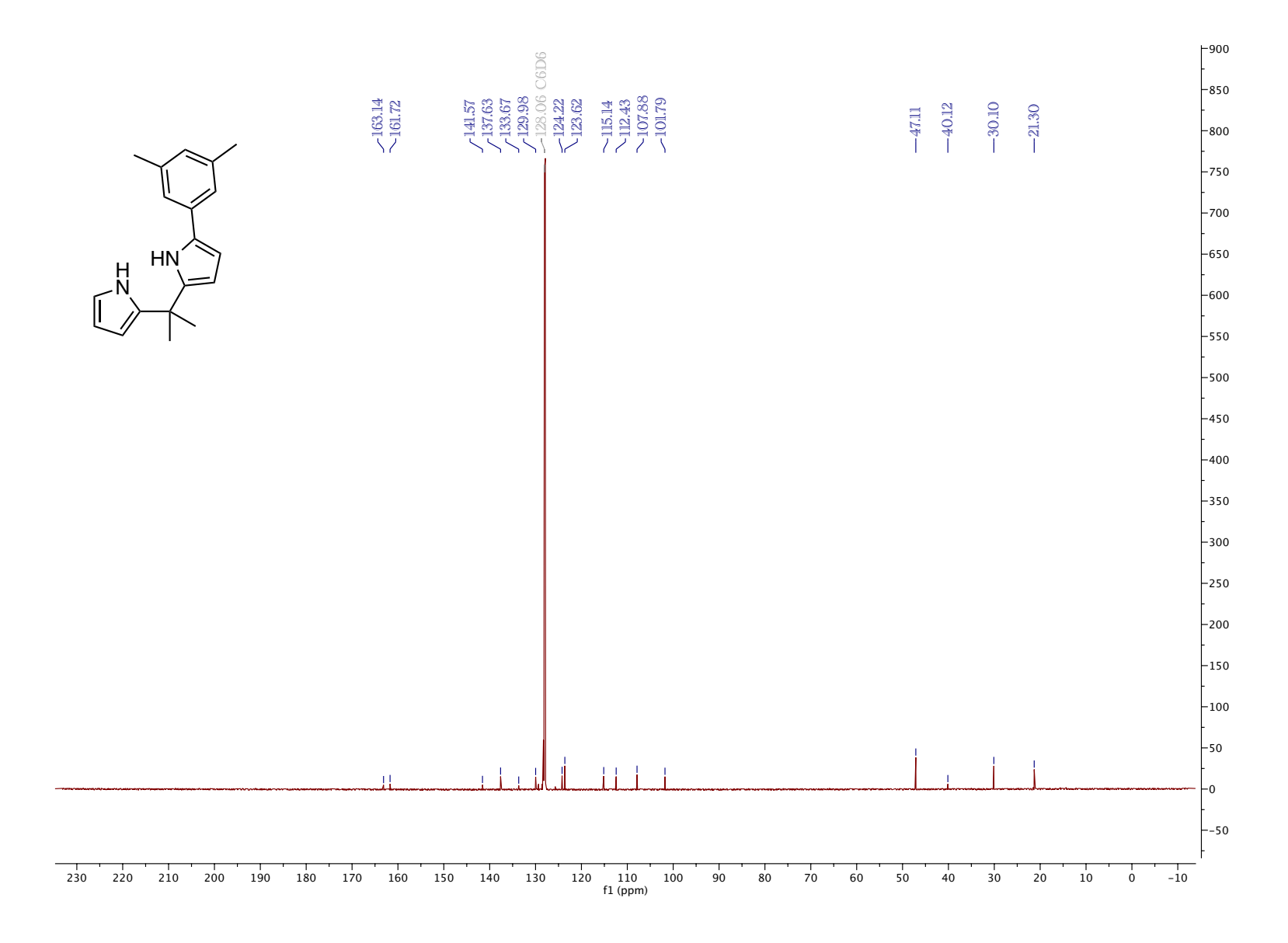


Figure 5.130. ¹³C NMR (CDCl₃, 126 MHz, 25 °C)

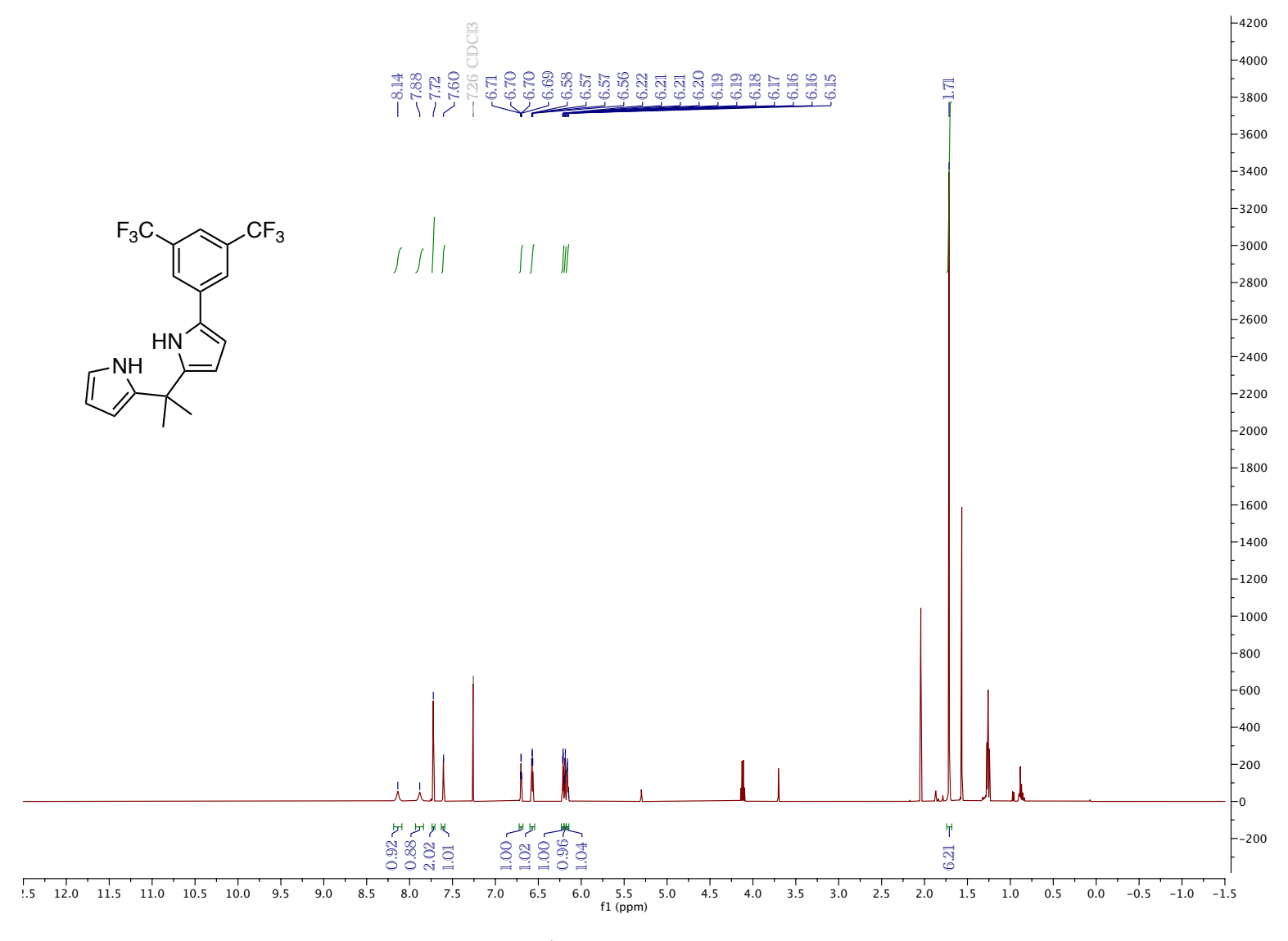


Figure 5.131. ¹H NMR (CDCl₃, 500 MHz, 25 °C)

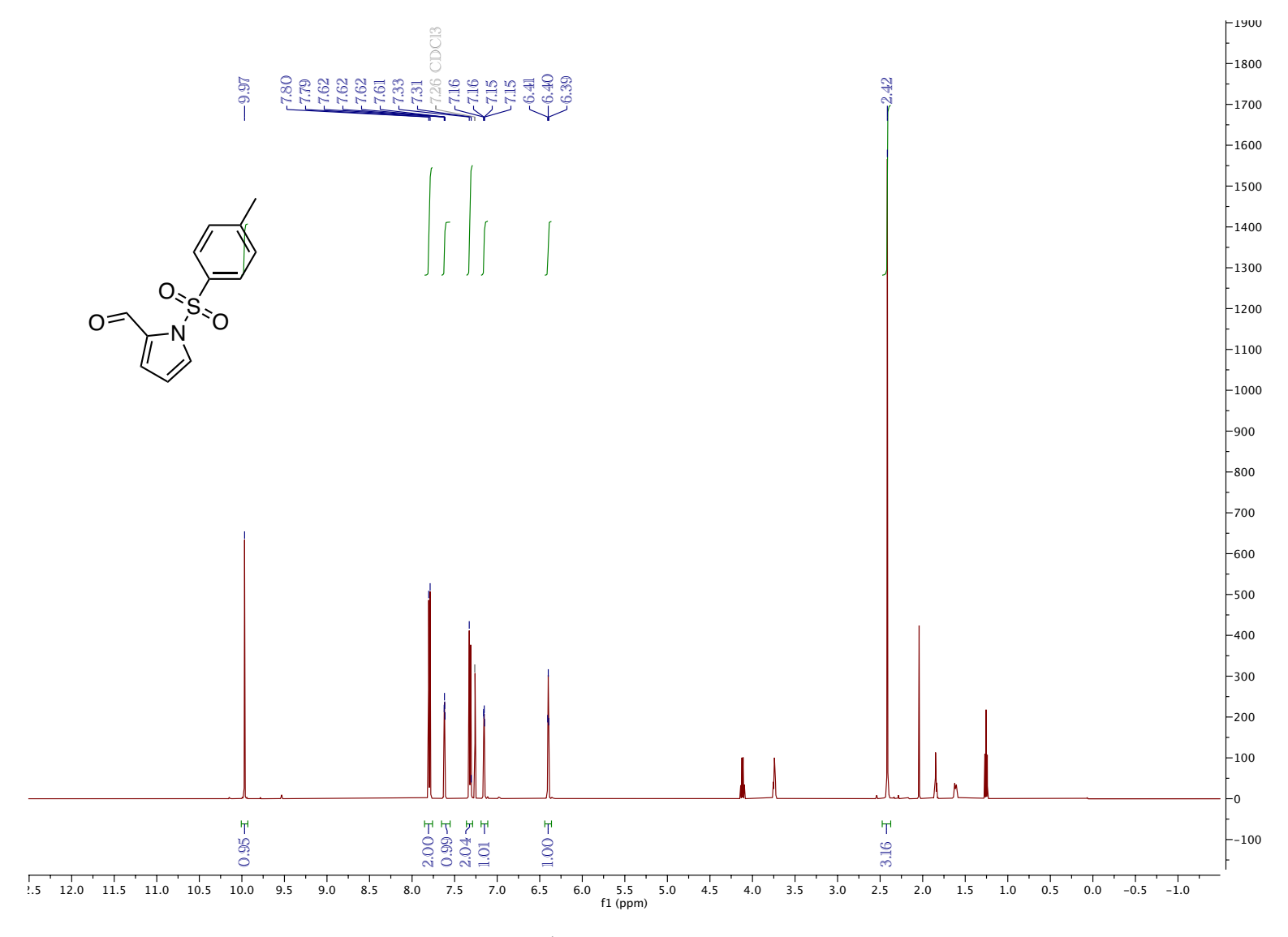


Figure 5.132. ¹H NMR (CDCl₃, 500 MHz, 25 °C)

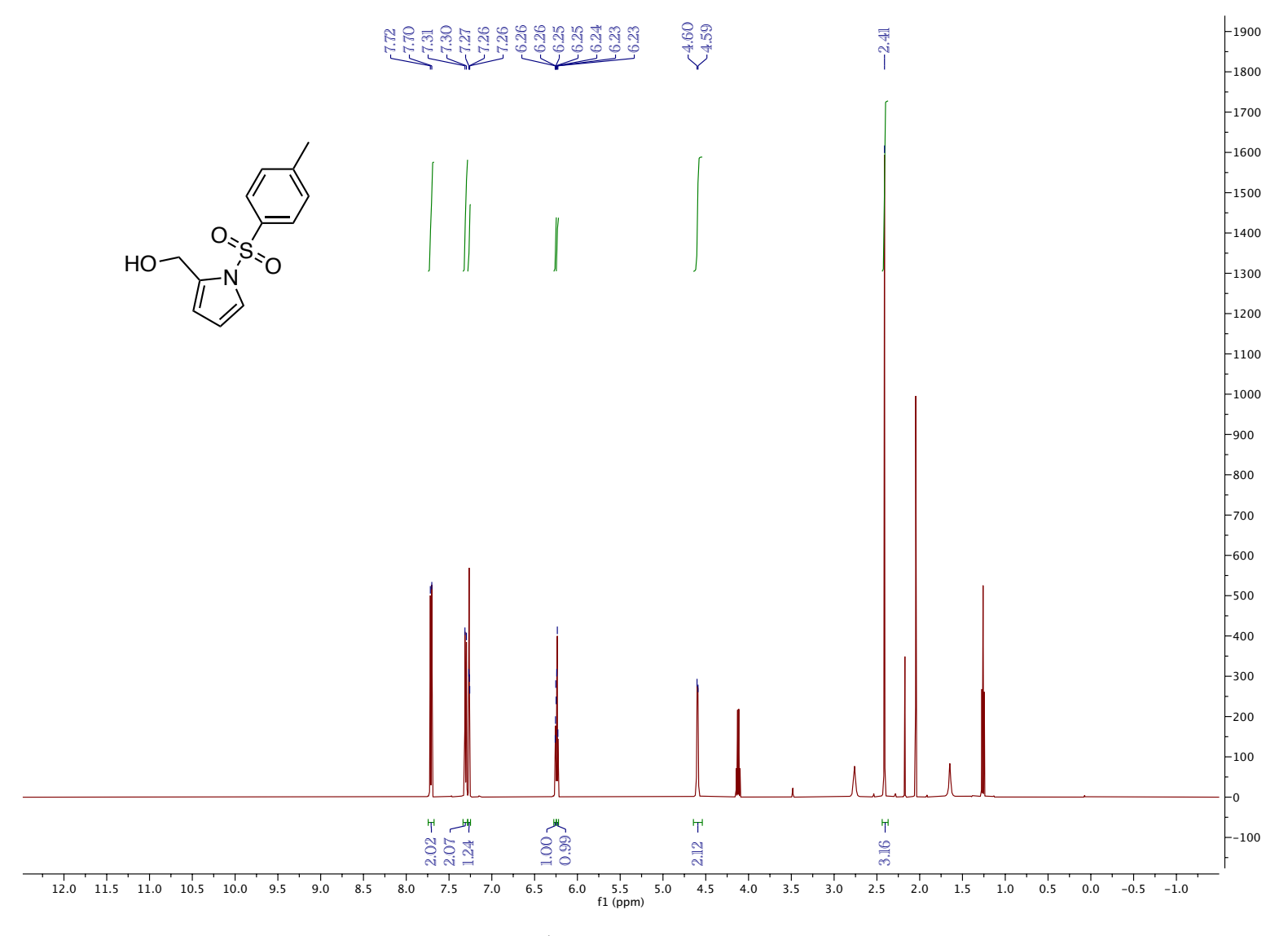


Figure 5.133. ¹H NMR (CDCl₃, 500 MHz, 25 °C)

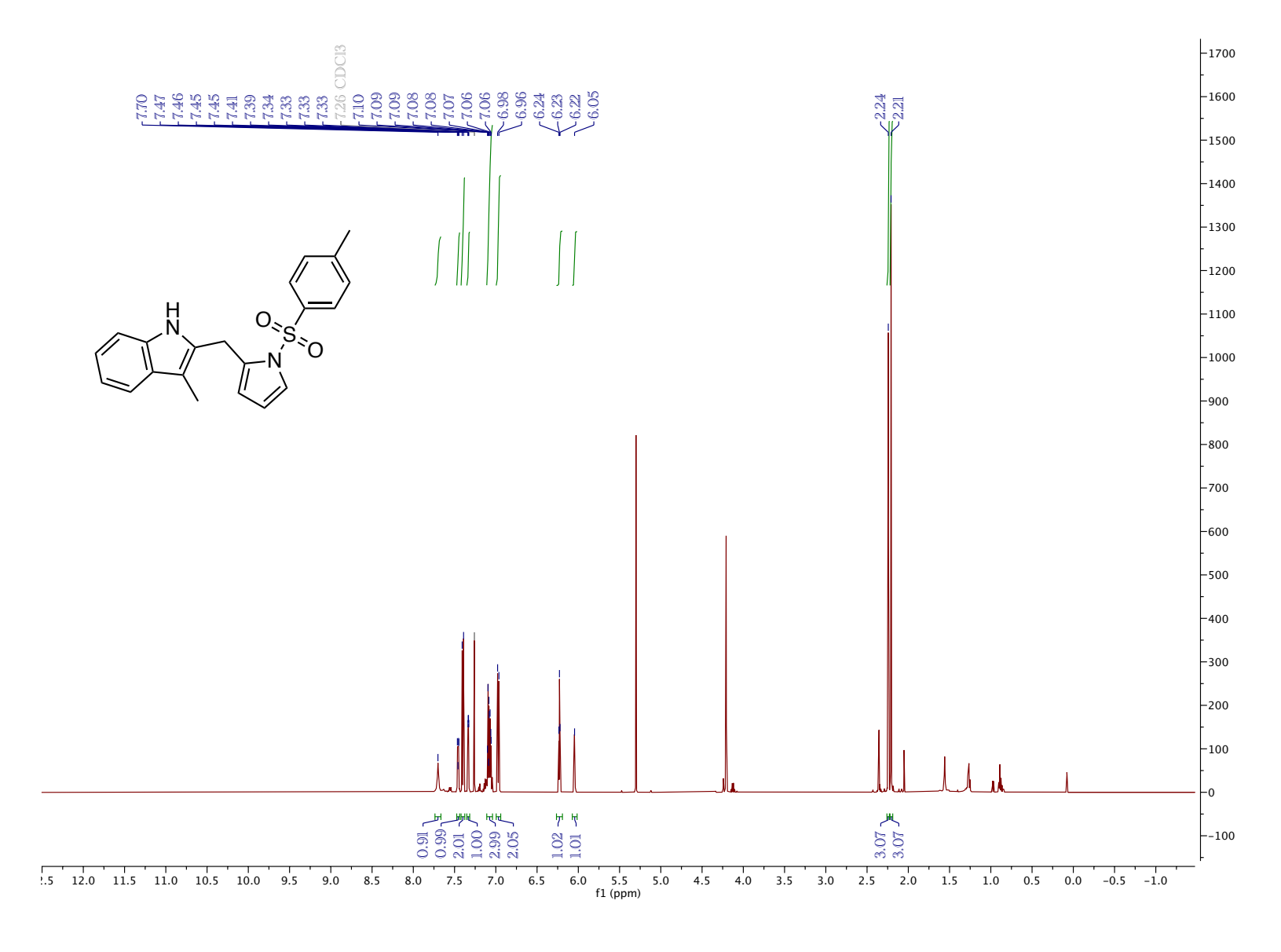


Figure 5.134. Figure 5.134. 1 H NMR (CDCl₃, 500 MHz, 25 $^\circ$ C)

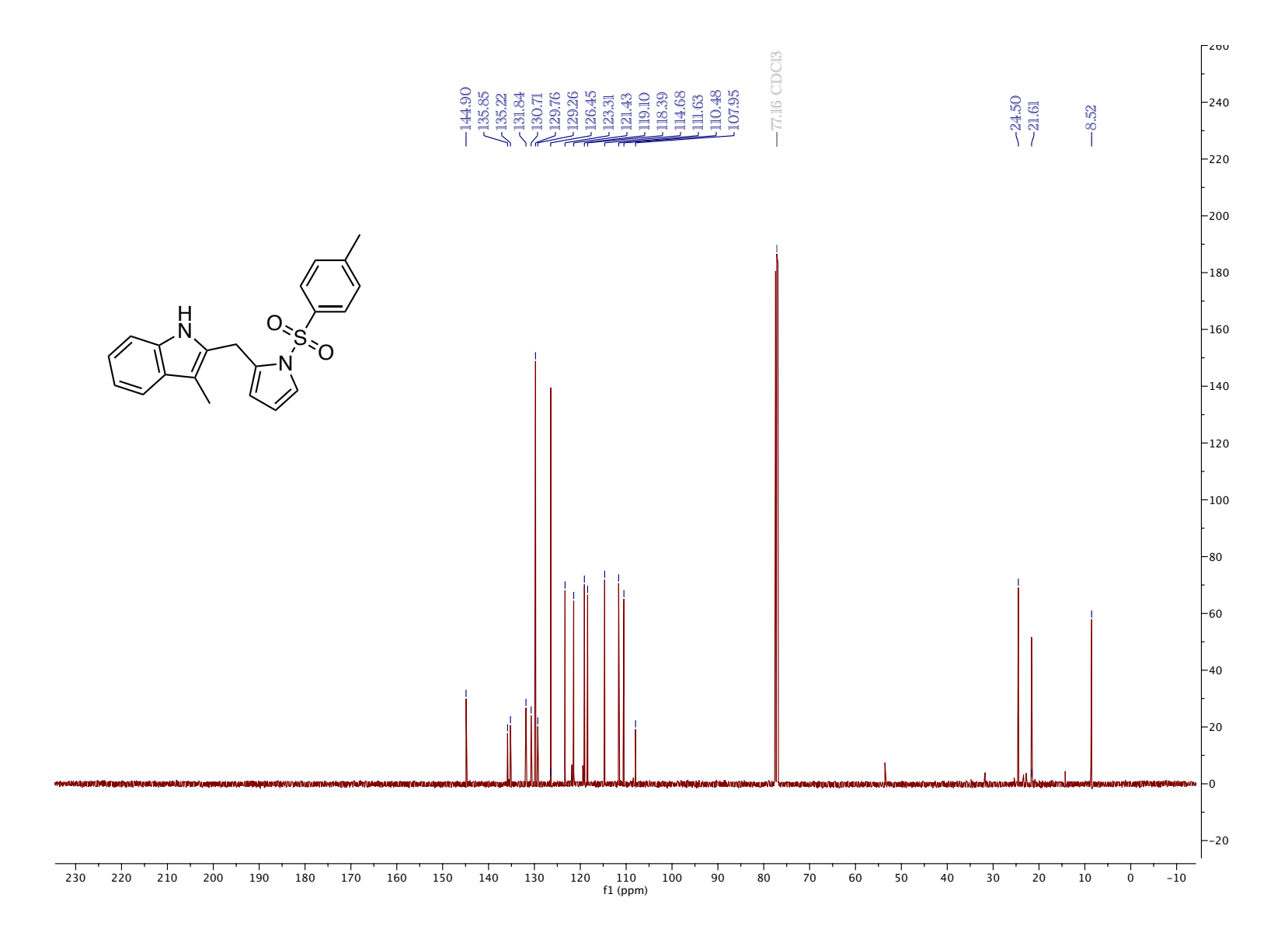


Figure 5.135. ¹³C NMR (CDCl₃, 126 MHz, 25 °C)

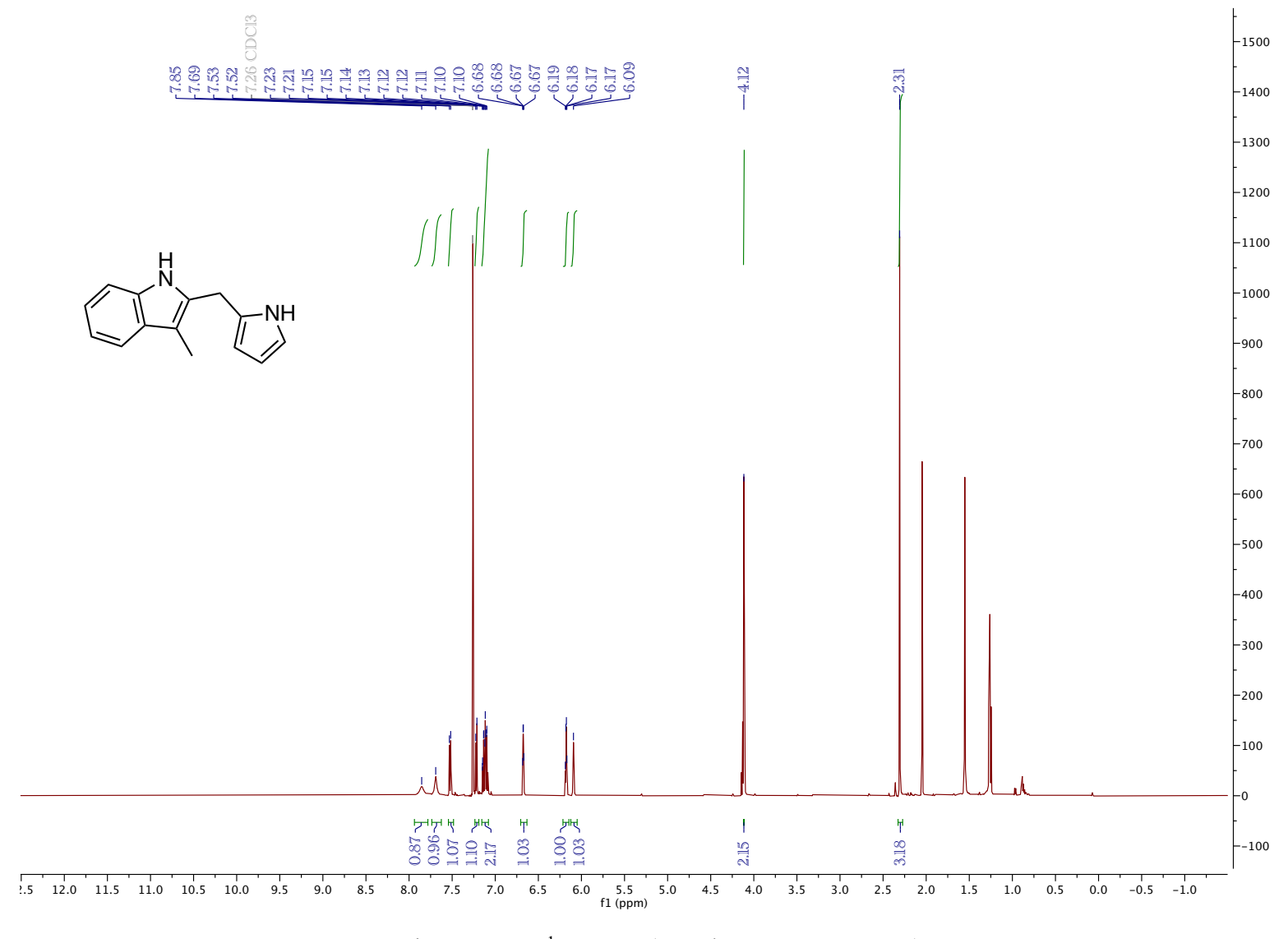


Figure 5.136. ¹H NMR (CDCl₃, 500 MHz, 25 °C)

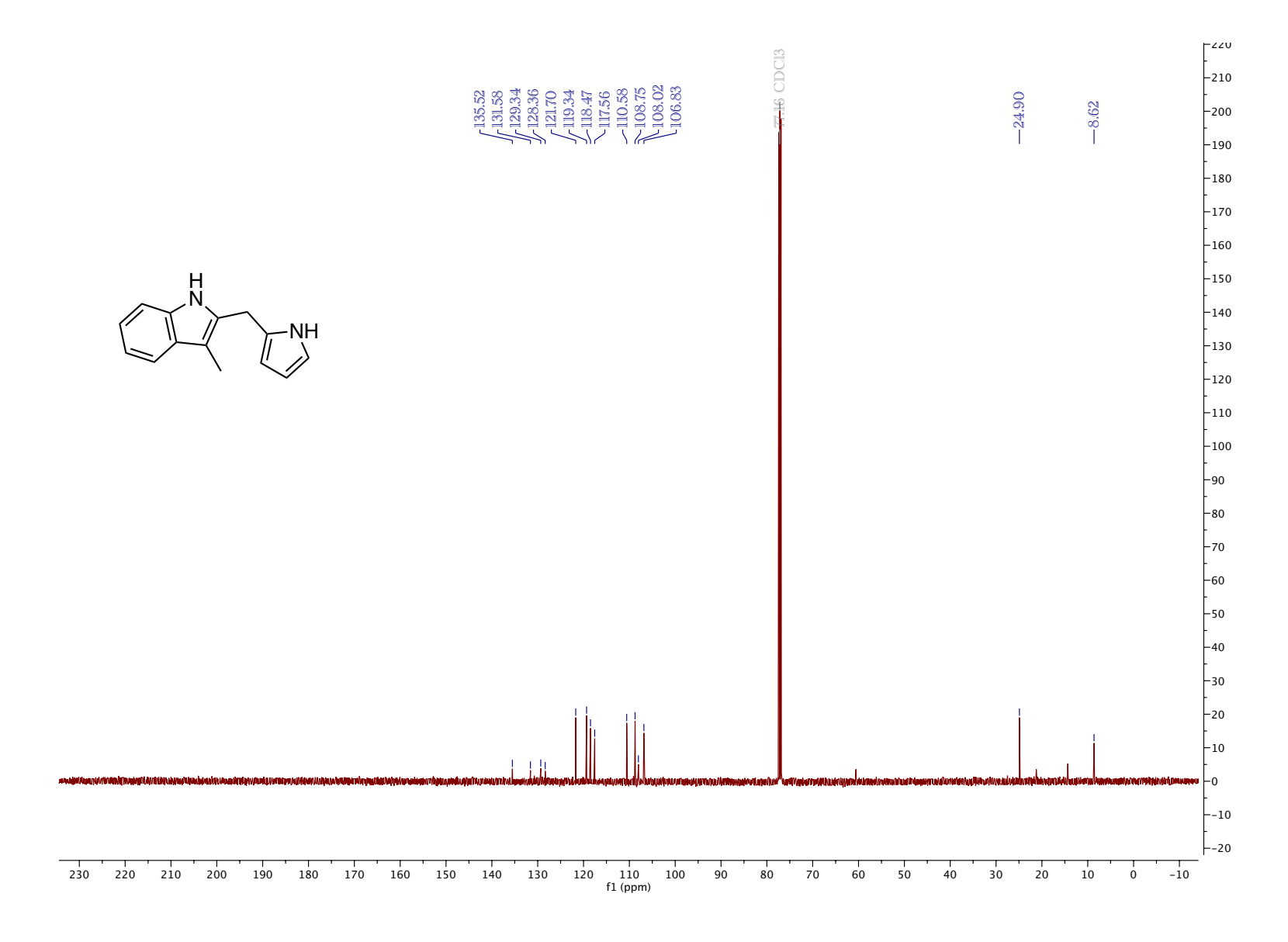


Figure 5.137. ¹³C NMR (CDCl₃, 126 MHz, 25 °C)

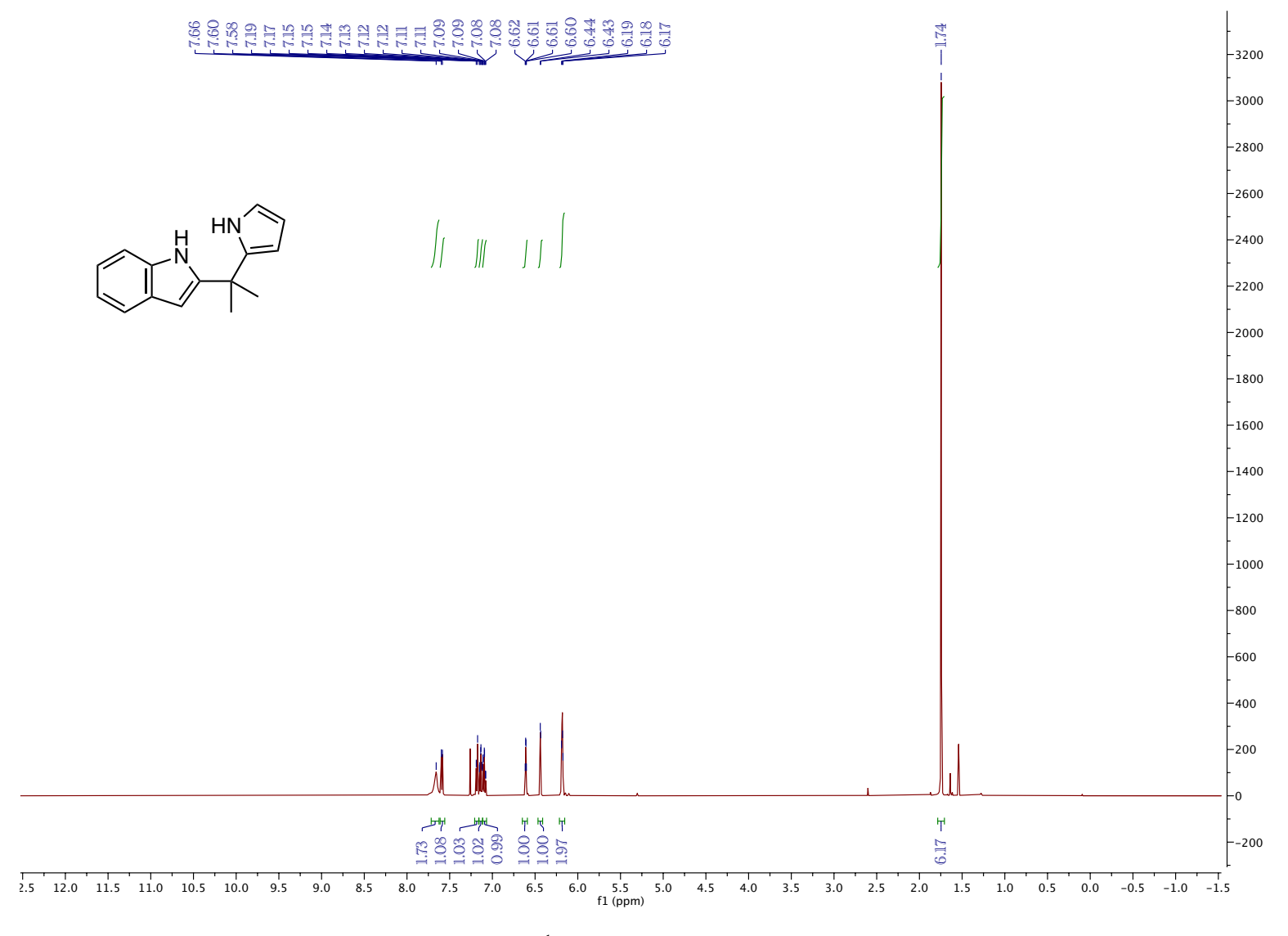


Figure 5.138. ¹H NMR (CDCl₃, 500 MHz, 25 °C)

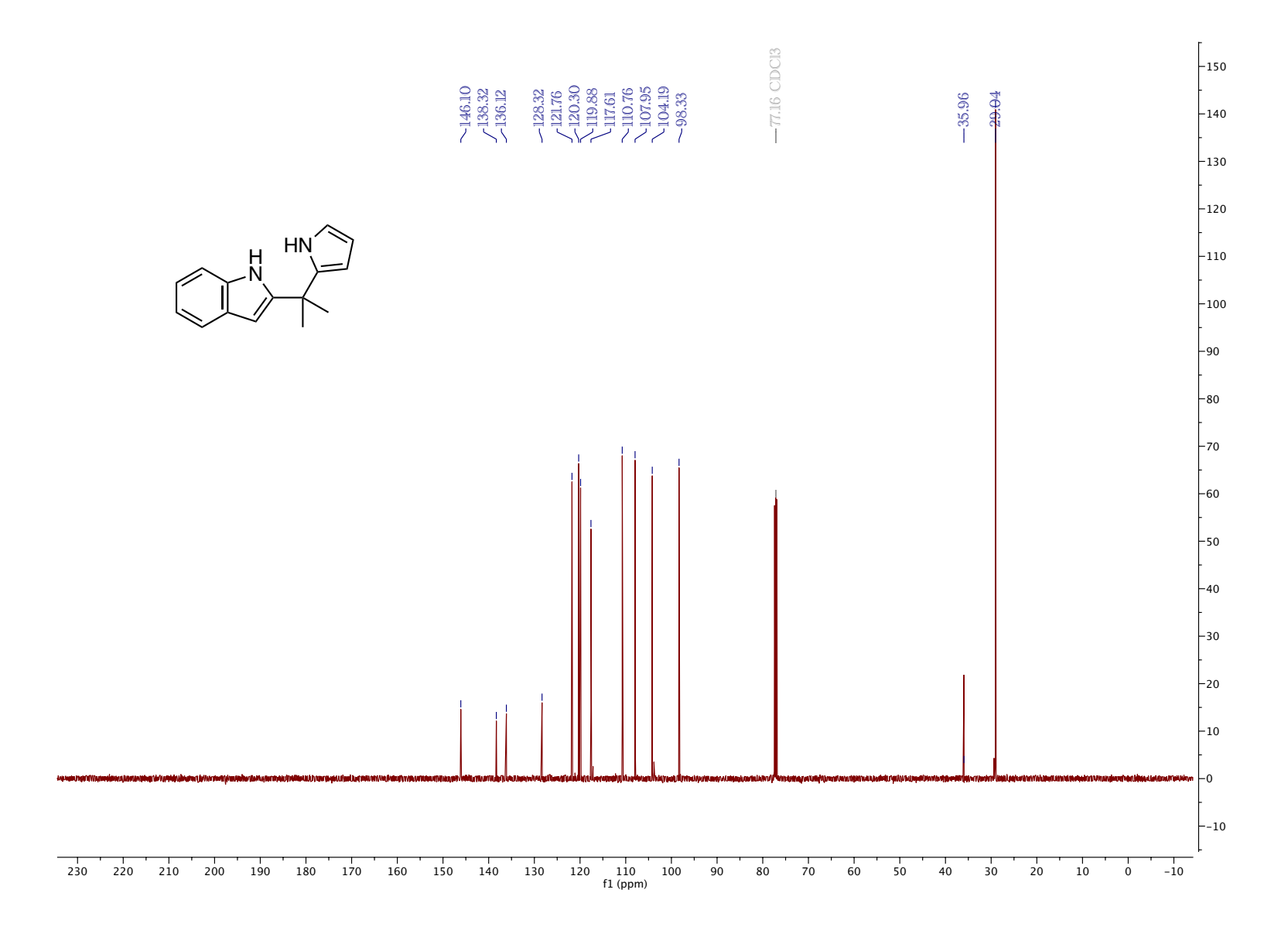


Figure 5.139. 13 C NMR (CDCl₃, 126 MHz, 25 $^{\circ}$ C)

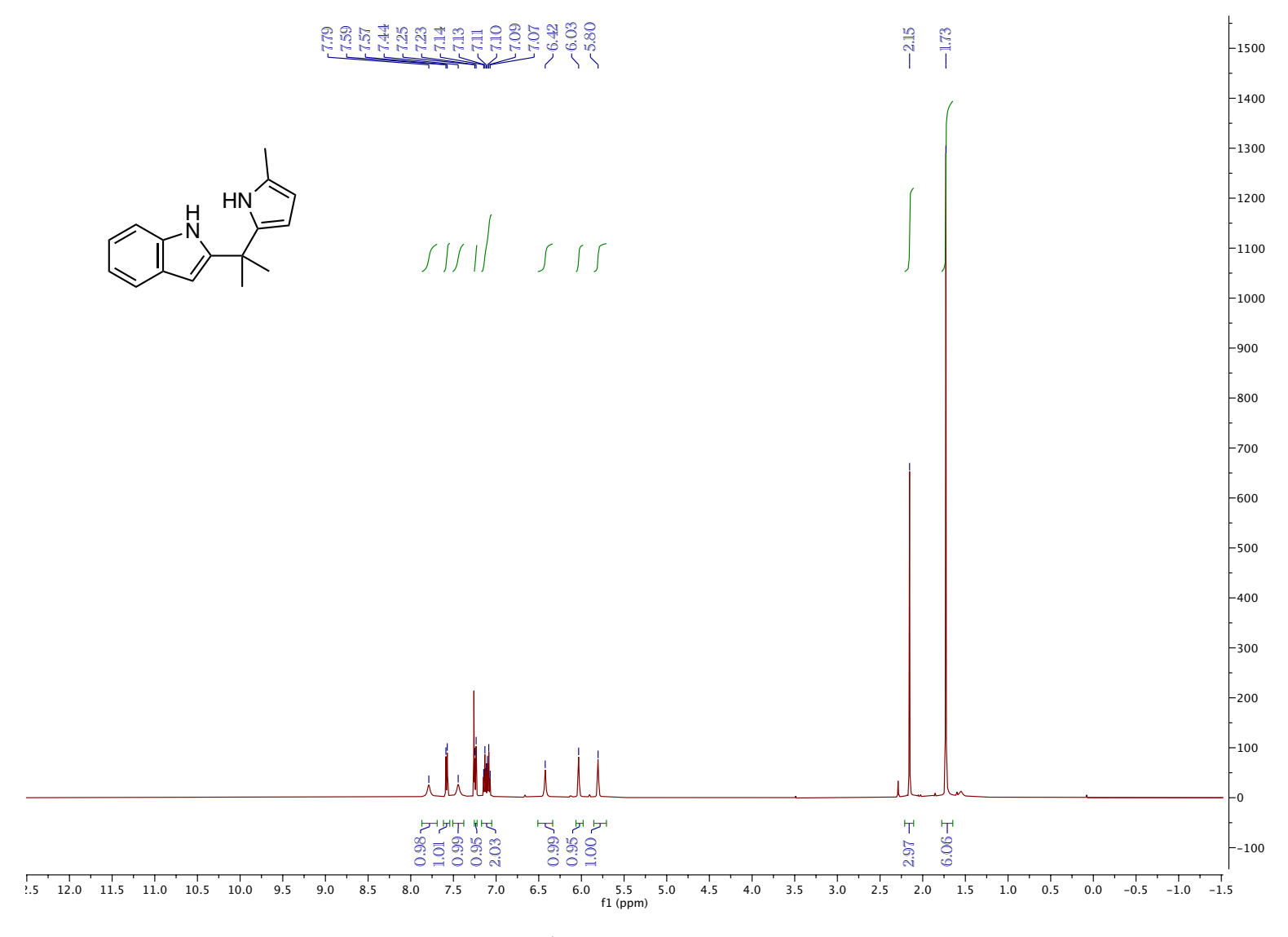


Figure 5.140. 1 H NMR (CDCl₃, 500 MHz, 25 $^{\circ}$ C)

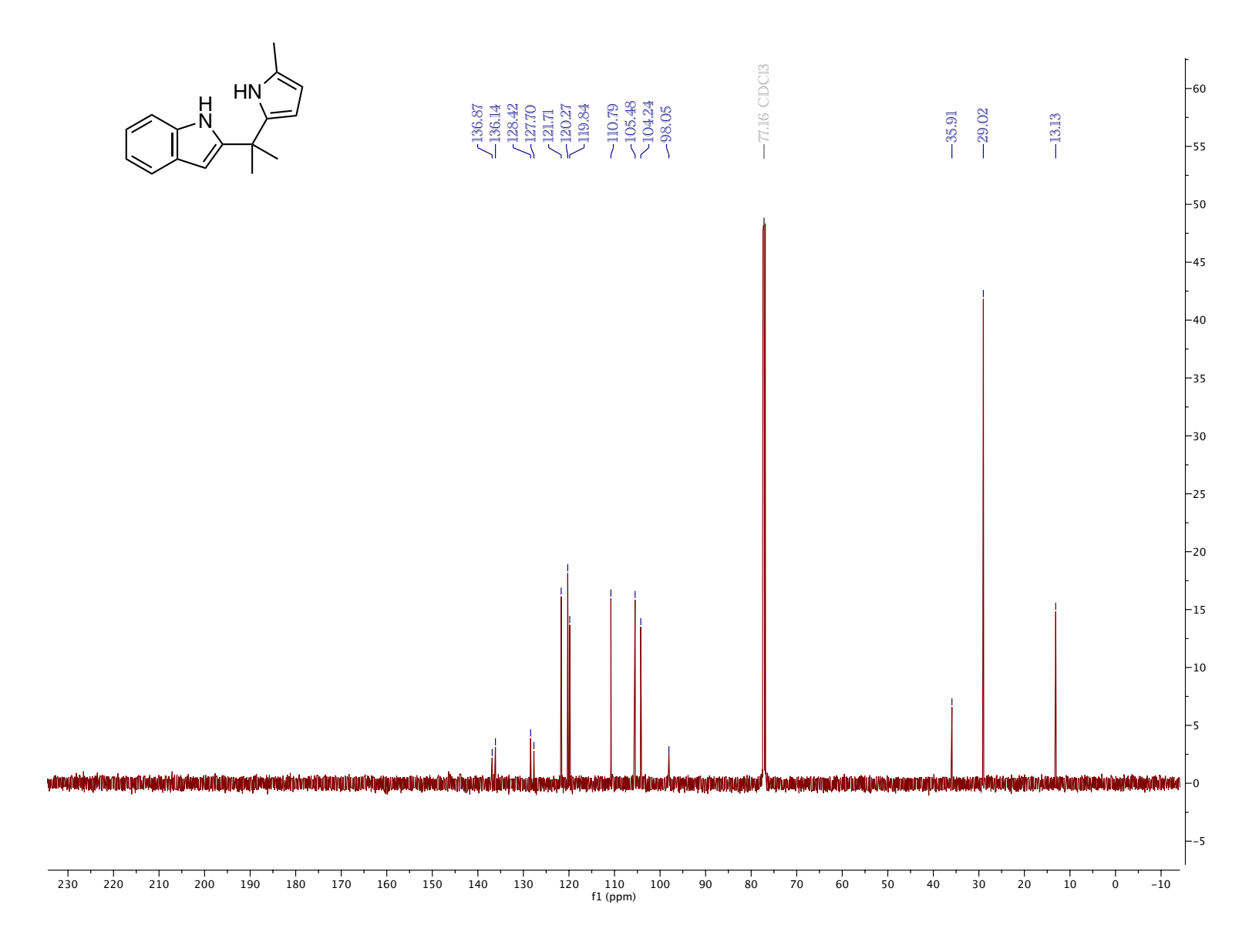


Figure 5.141. ¹³C NMR (CDCl₃, 126 MHz, 25 °C)

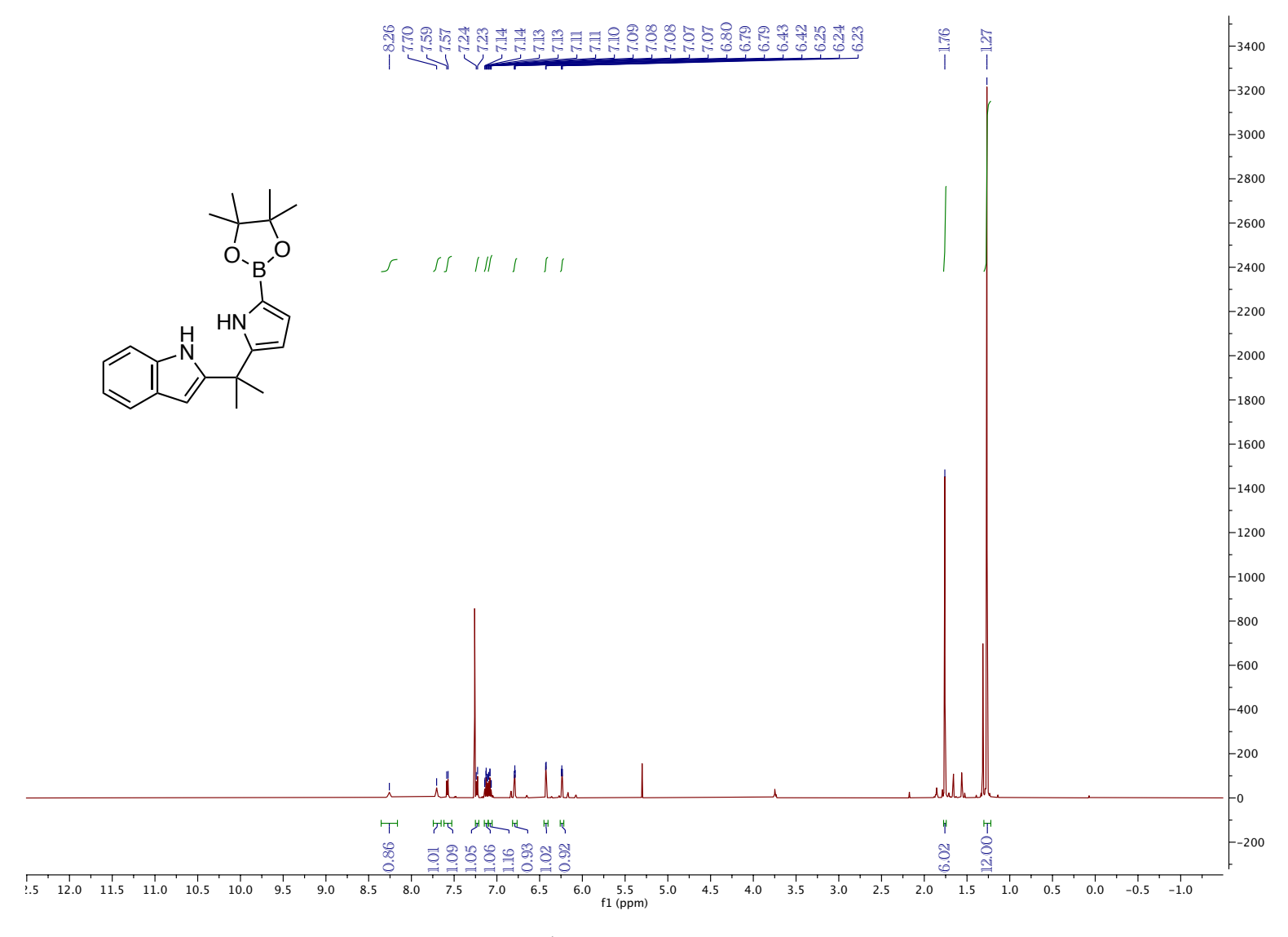


Figure 5.142. ¹H NMR (CDCl₃, 500 MHz, 25 °C)

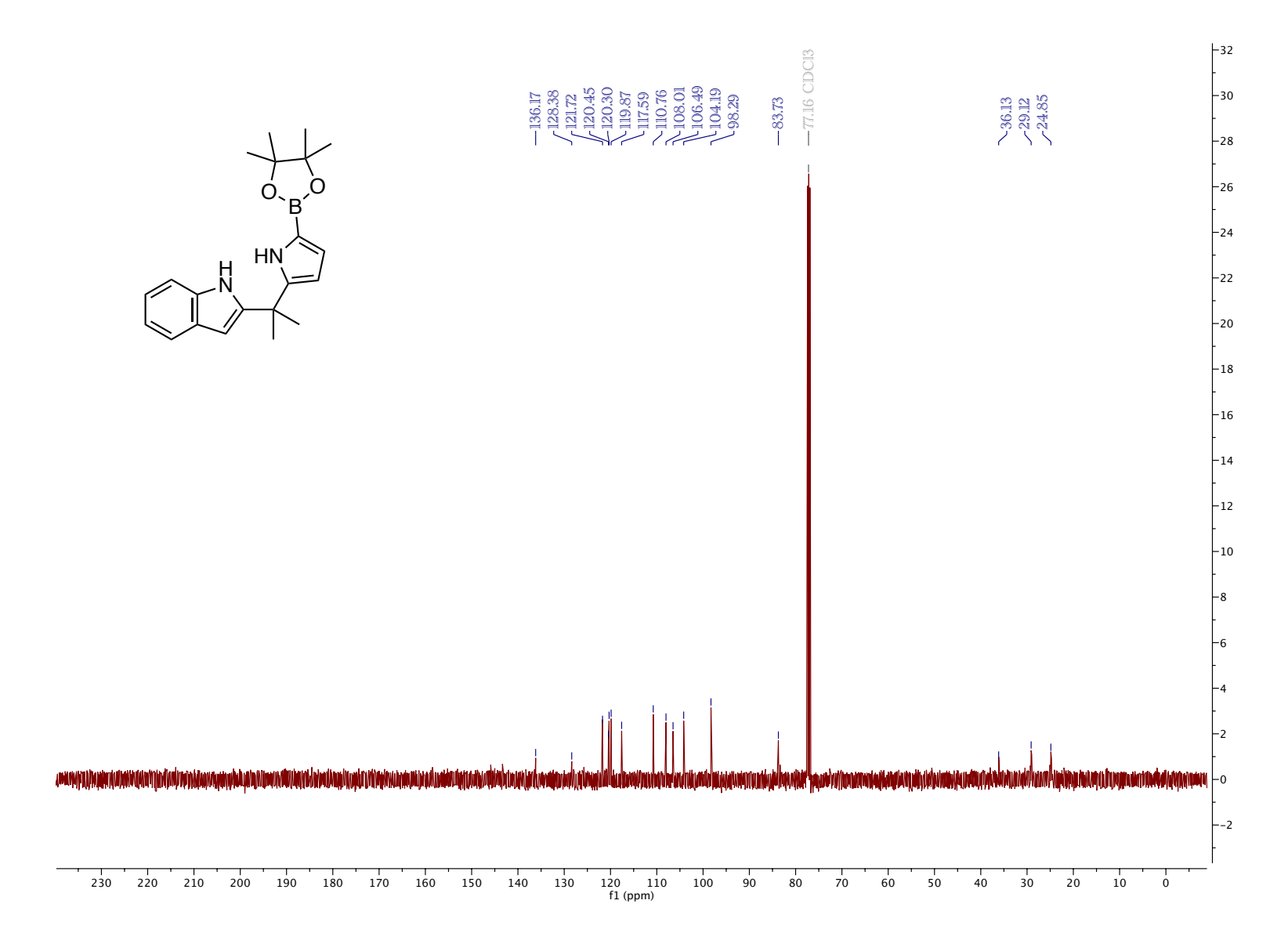


Figure 5.143. ¹³C NMR (CDCl₃, 126 MHz, 25 °C)

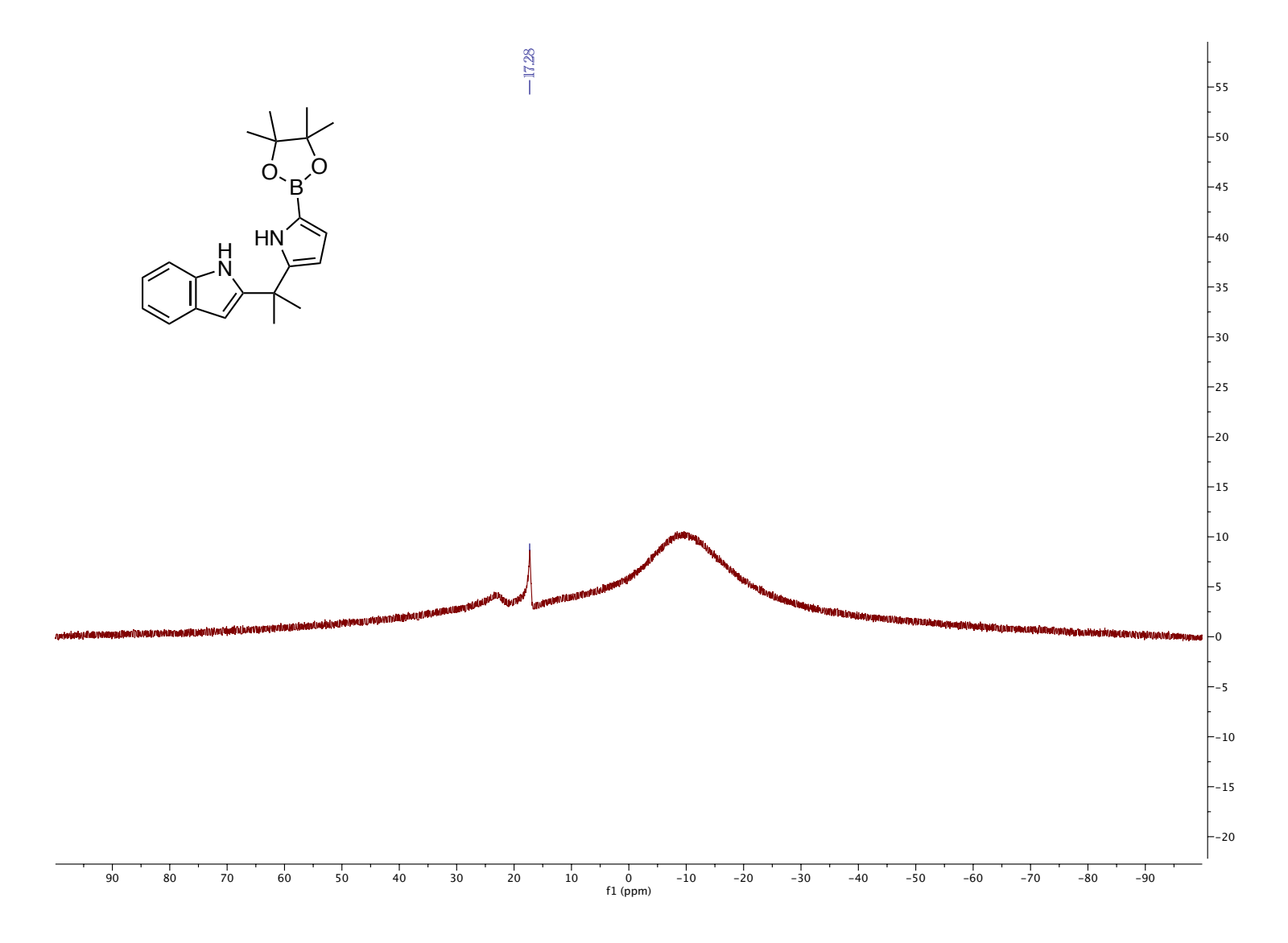


Figure 5.144. 11B NMR (CDCl₃, 160 MHz, 25 °C)

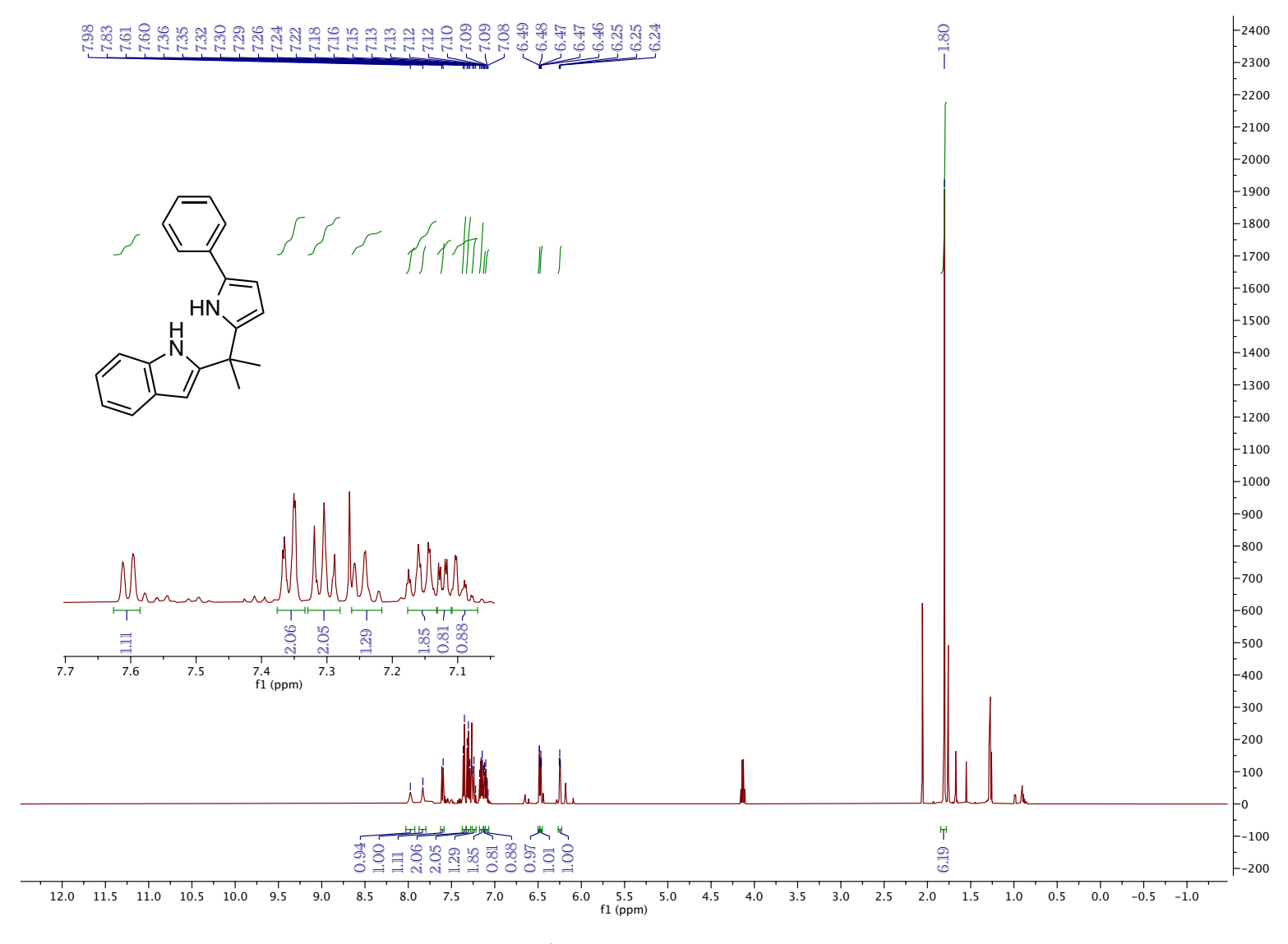


Figure 5.145. ¹H NMR (CDCl₃, 500 MHz, 25 °C)

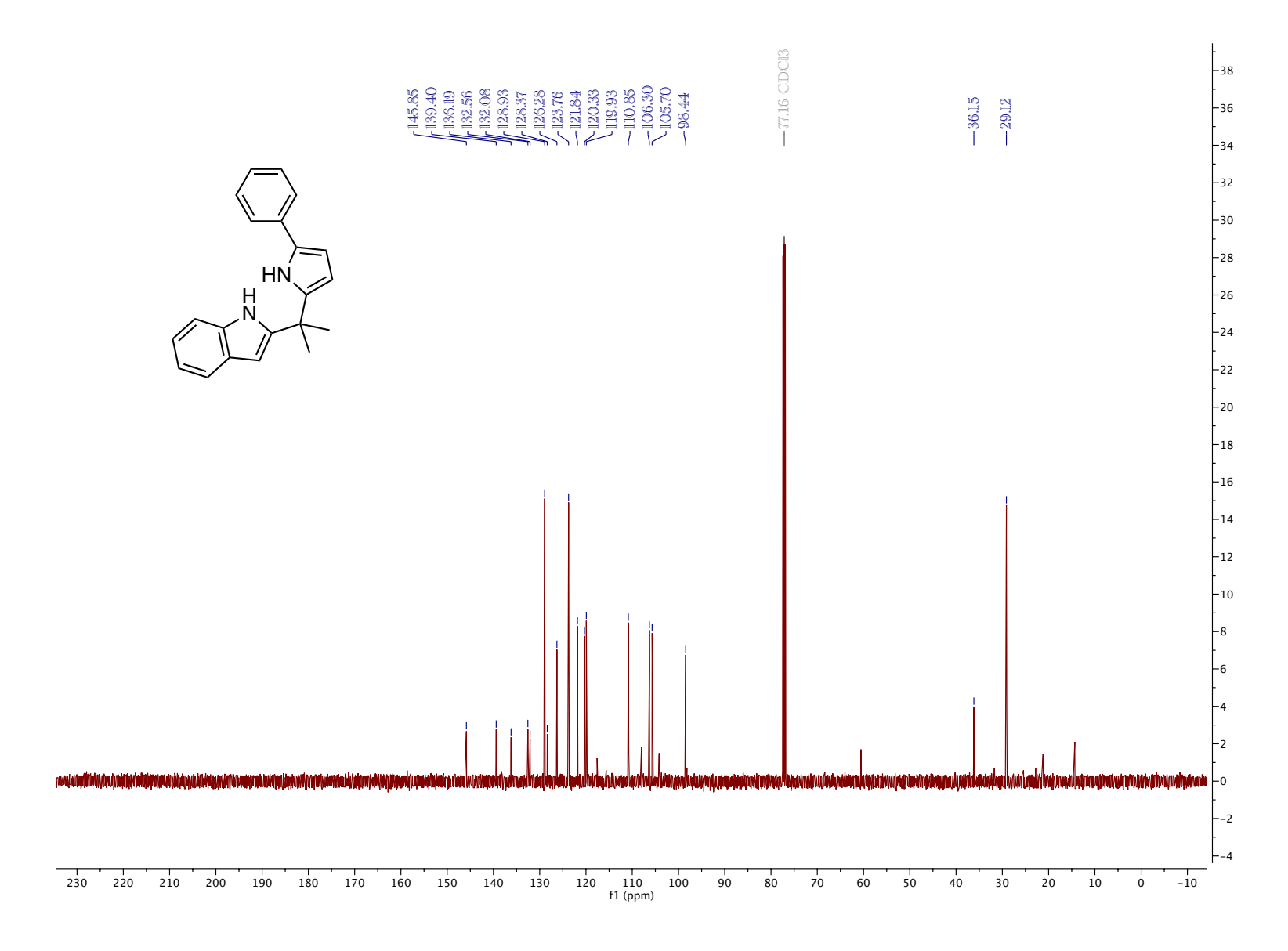


Figure 5.146. ¹³C NMR (CDCl₃, 126 MHz, 25 °C)

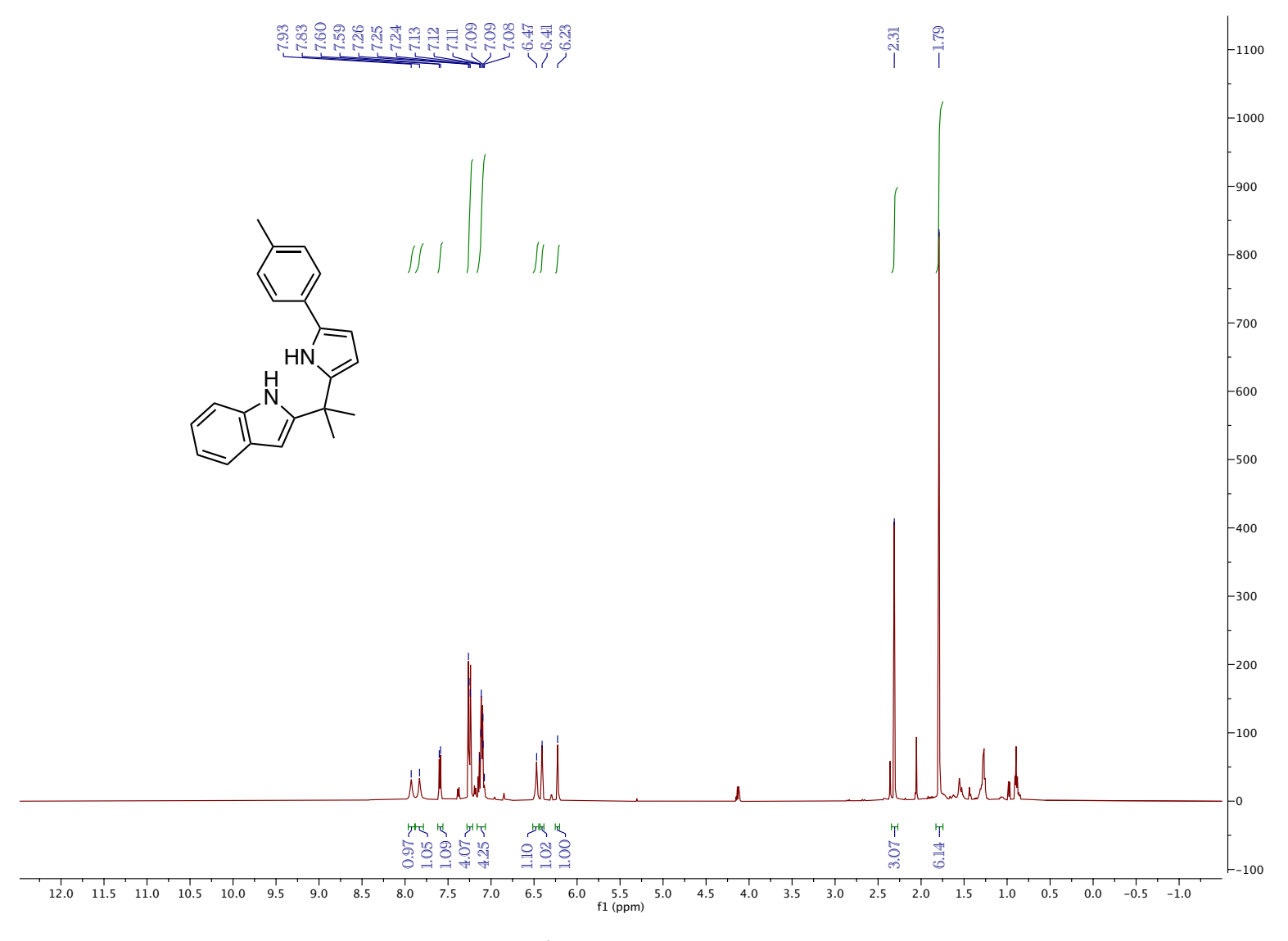


Figure 5.147. ¹H NMR (CDCl₃, 500 MHz, 25 °C)

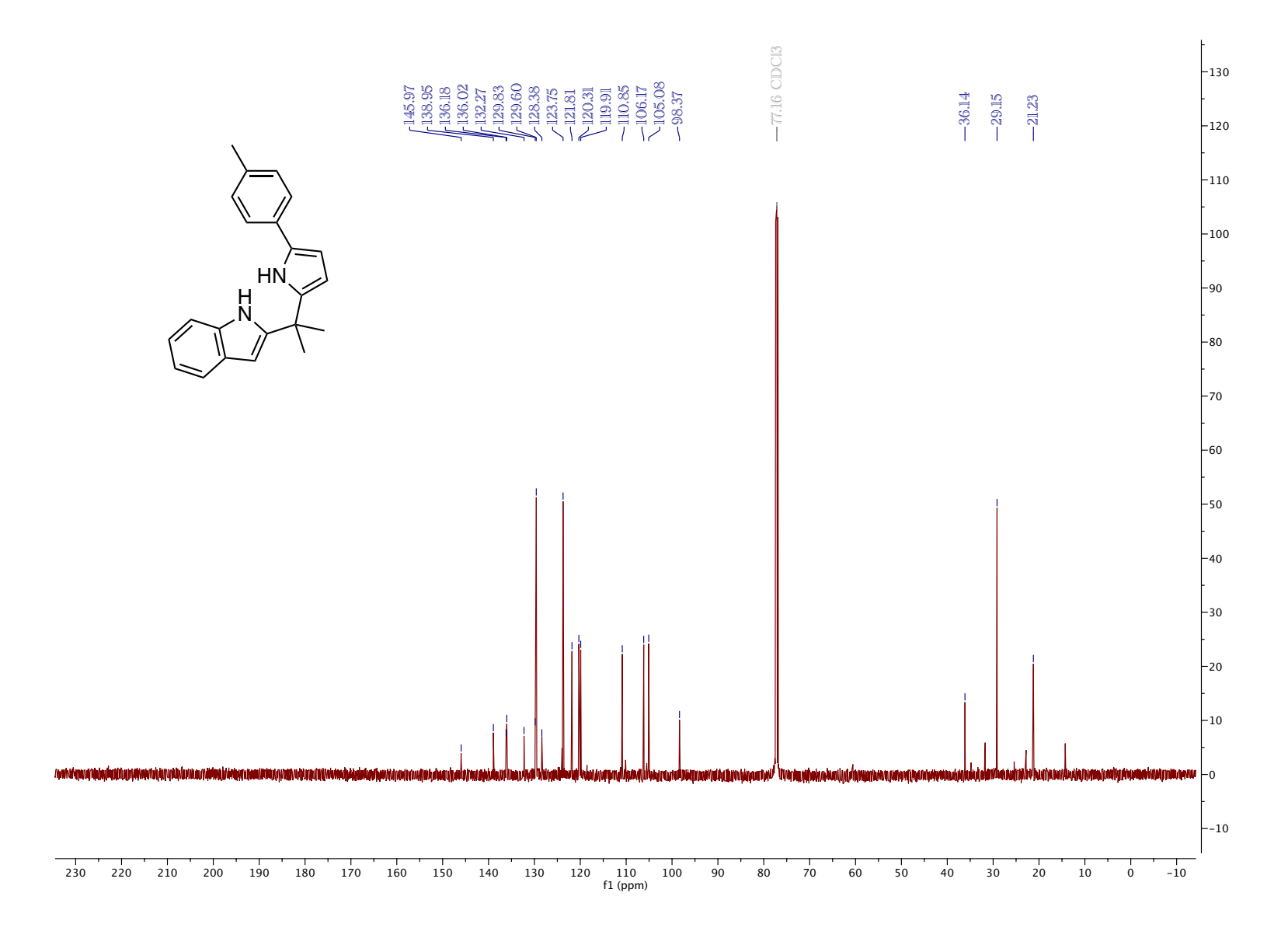


Figure 5.148. ¹³C NMR (CDCl₃, 126 MHz, 25 °C)

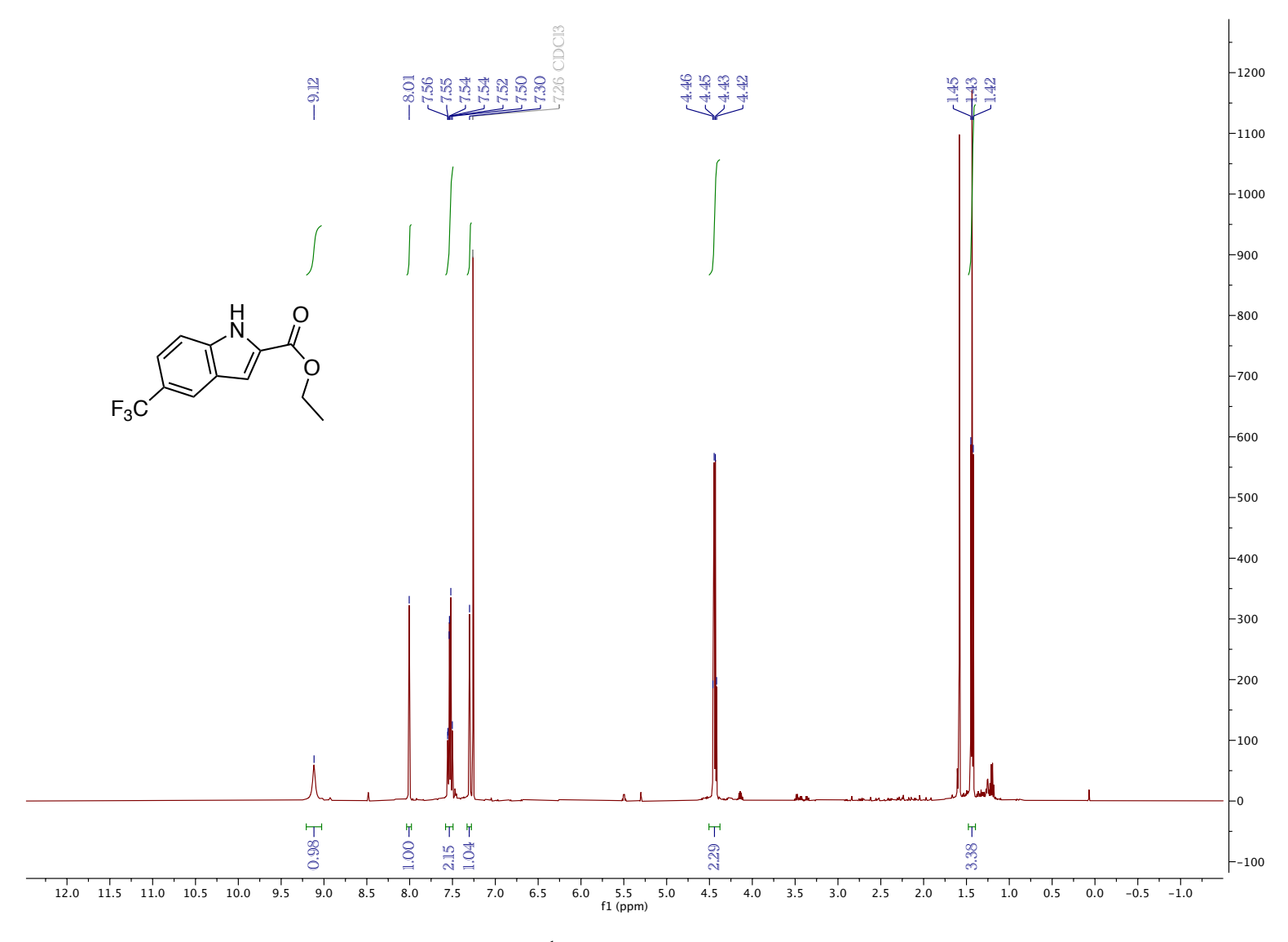


Figure 5.149. ¹H NMR (CDCl₃, 500 MHz, 25 °C)

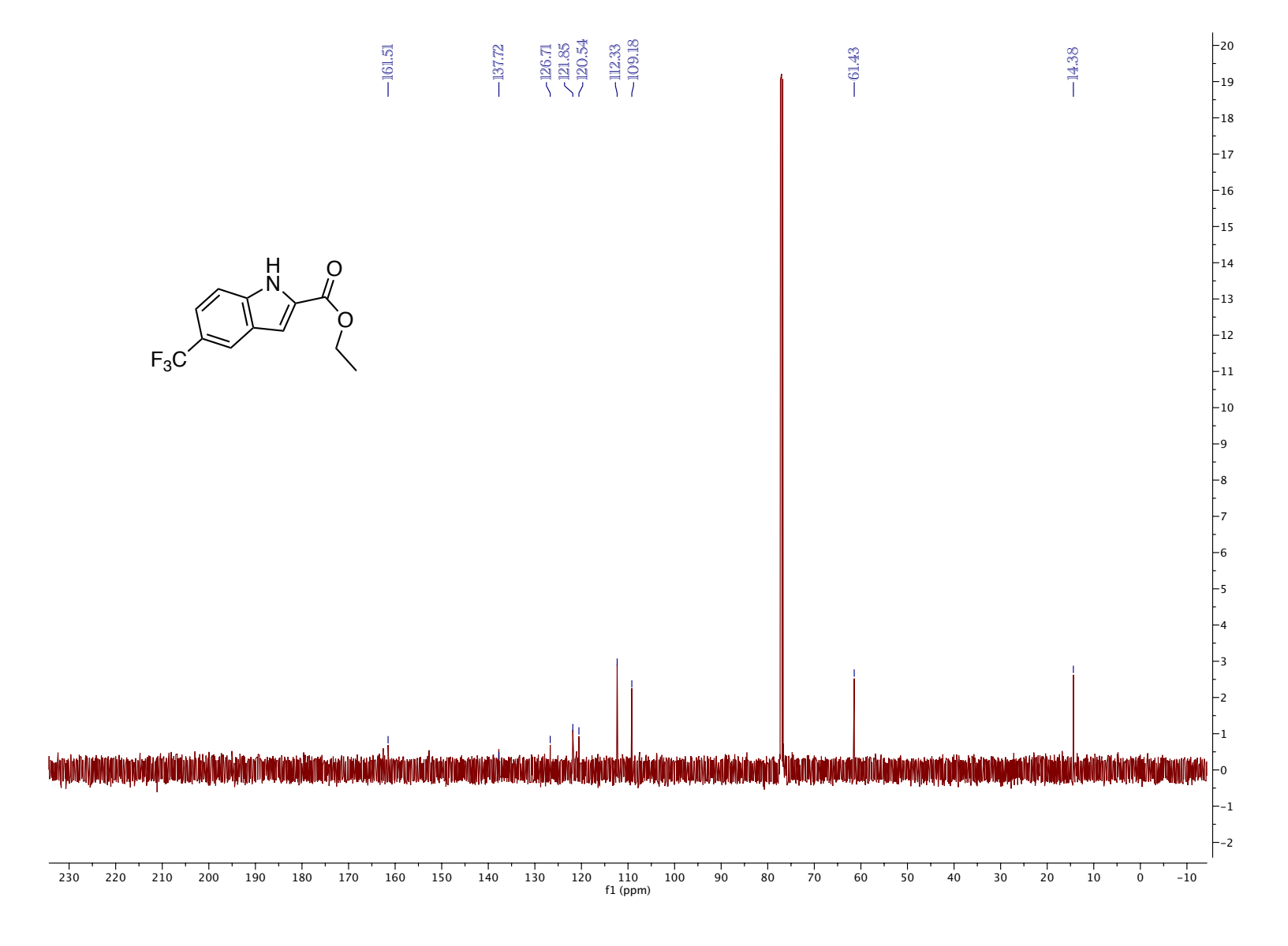


Figure 5.150. 13 C NMR (CDCl₃, 126 MHz, 25 $^{\circ}$ C)

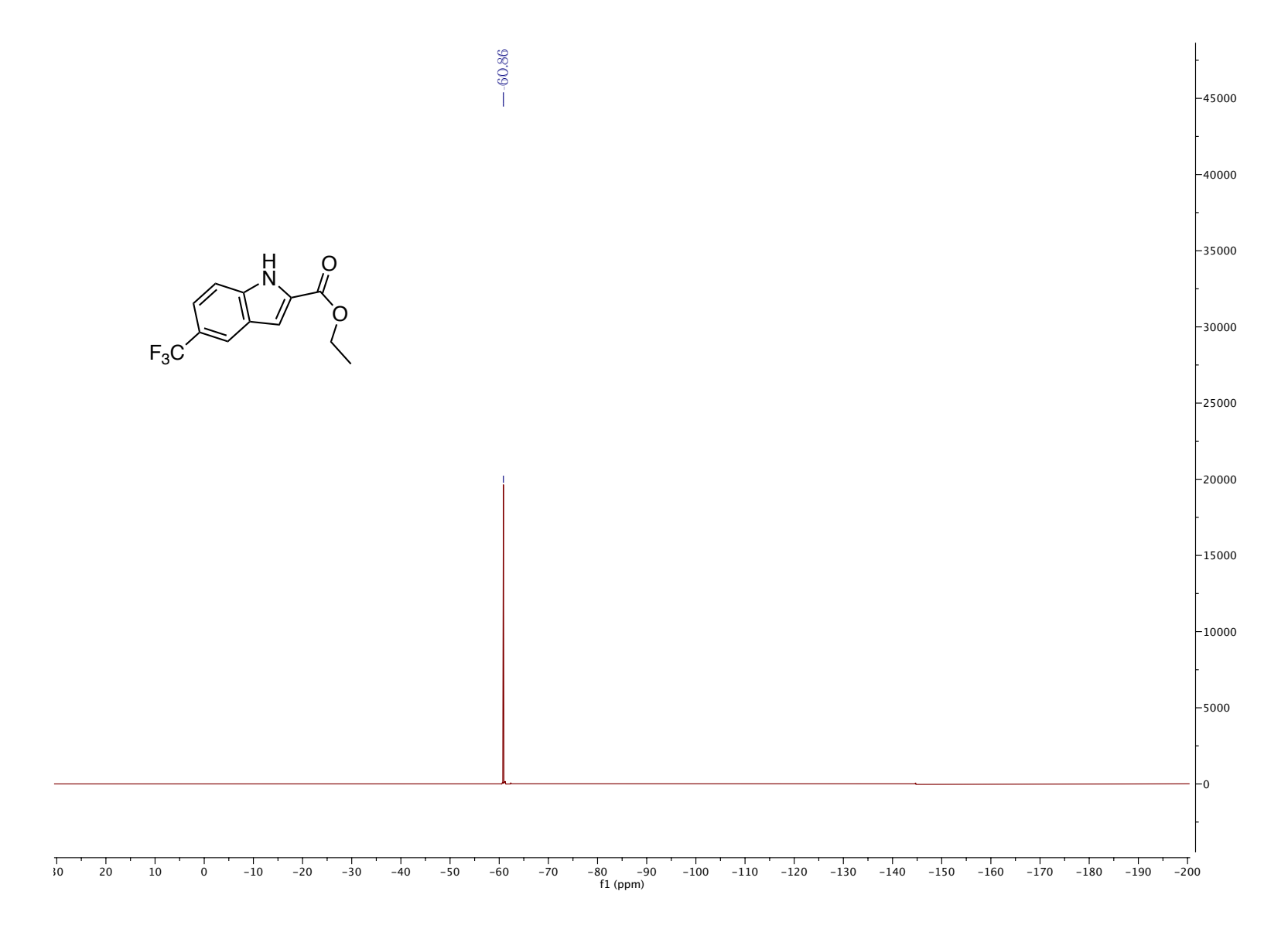


Figure 5.151. 19 F NMR (CDCl₃, 470 MHz, 25 $^{\circ}$ C)

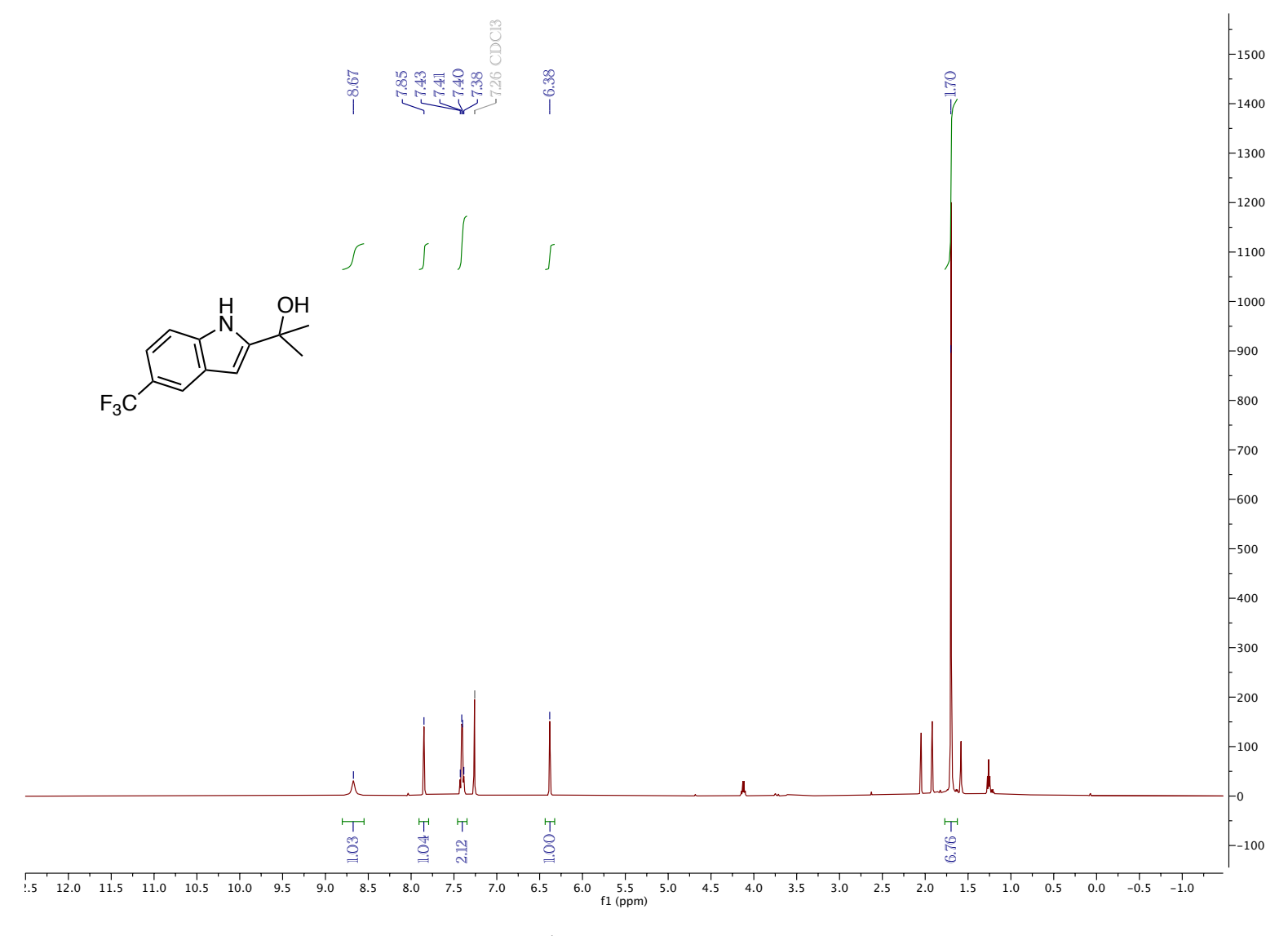


Figure 5.152. ¹H NMR (CDCl₃, 500 MHz, 25 °C)

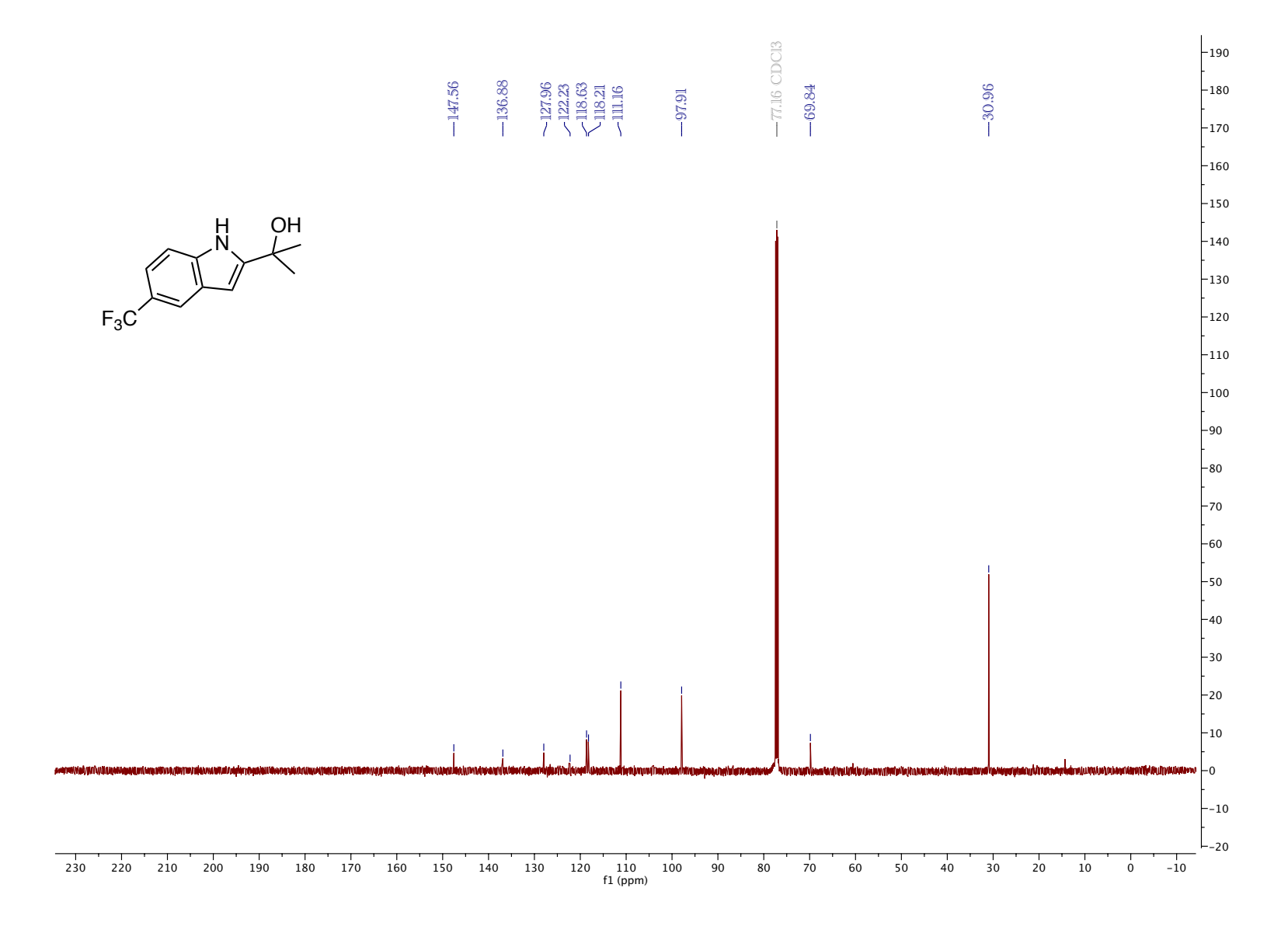


Figure 5.153. ¹³C NMR (CDCl₃, 126 MHz, 25 °C)

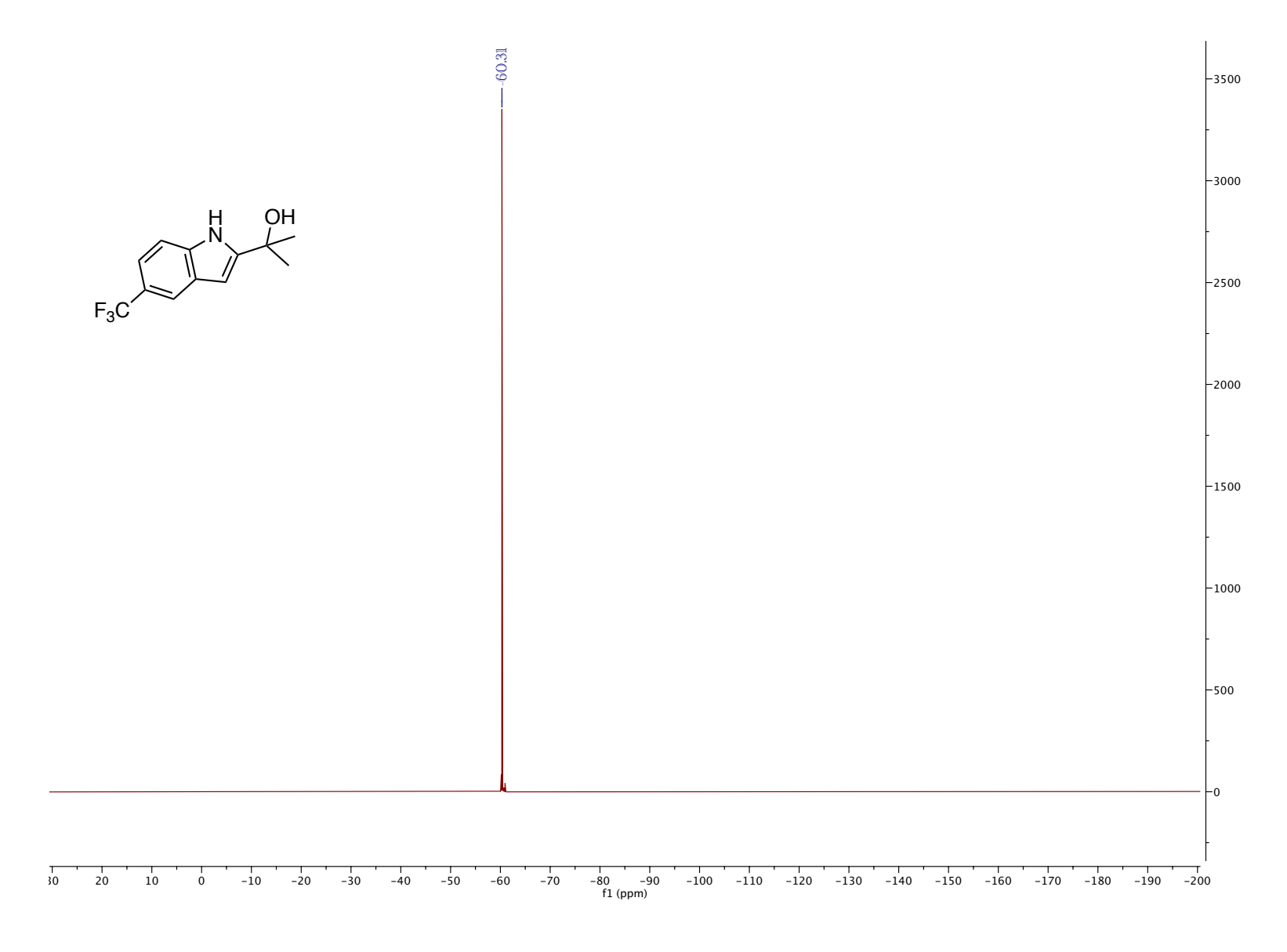


Figure 5.154. 19 F NMR (CDCl₃, 470 MHz, 25 $^{\circ}$ C)

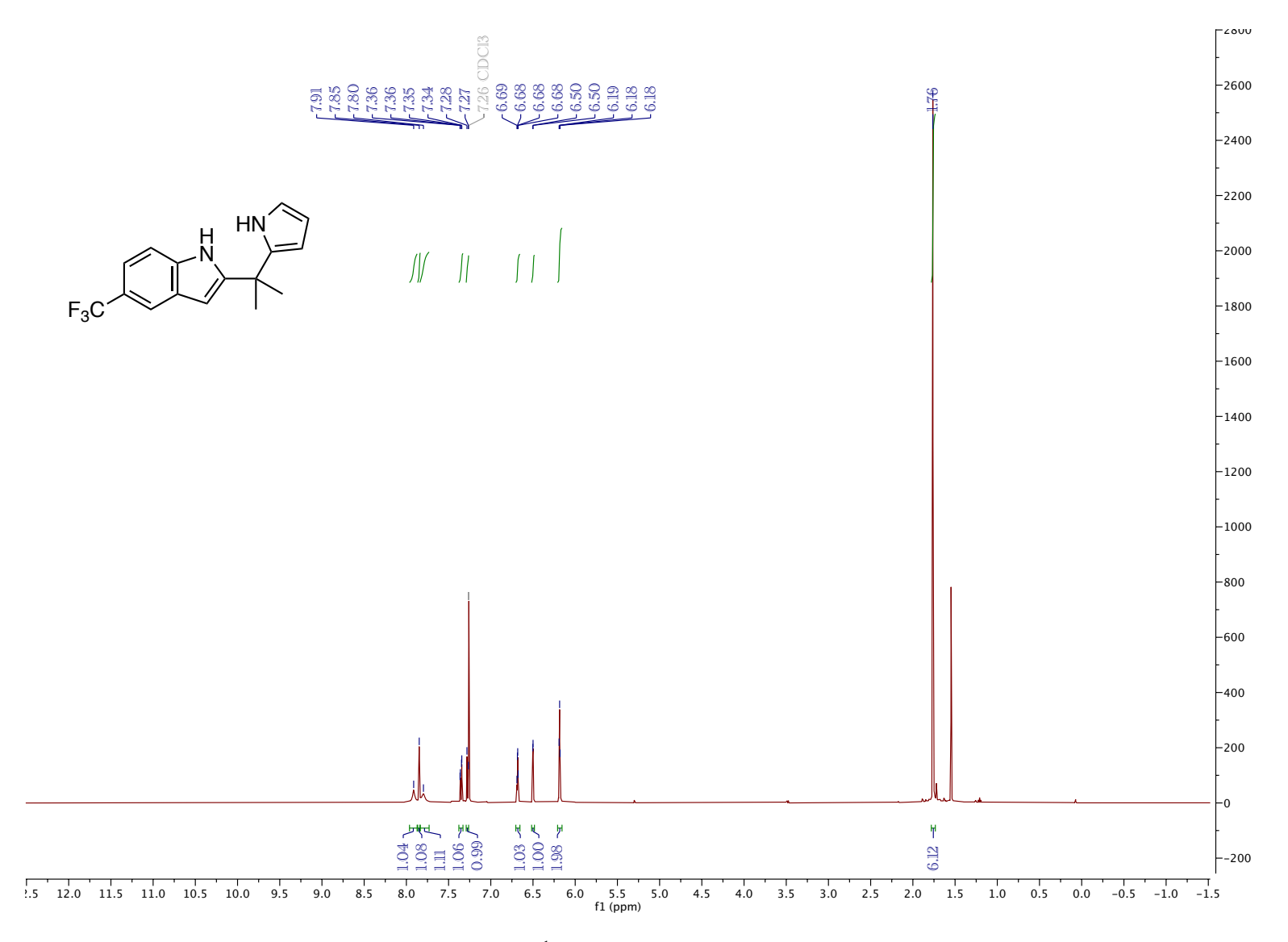


Figure 5.155. ¹H NMR (CDCl₃, 500 MHz, 25 °C)

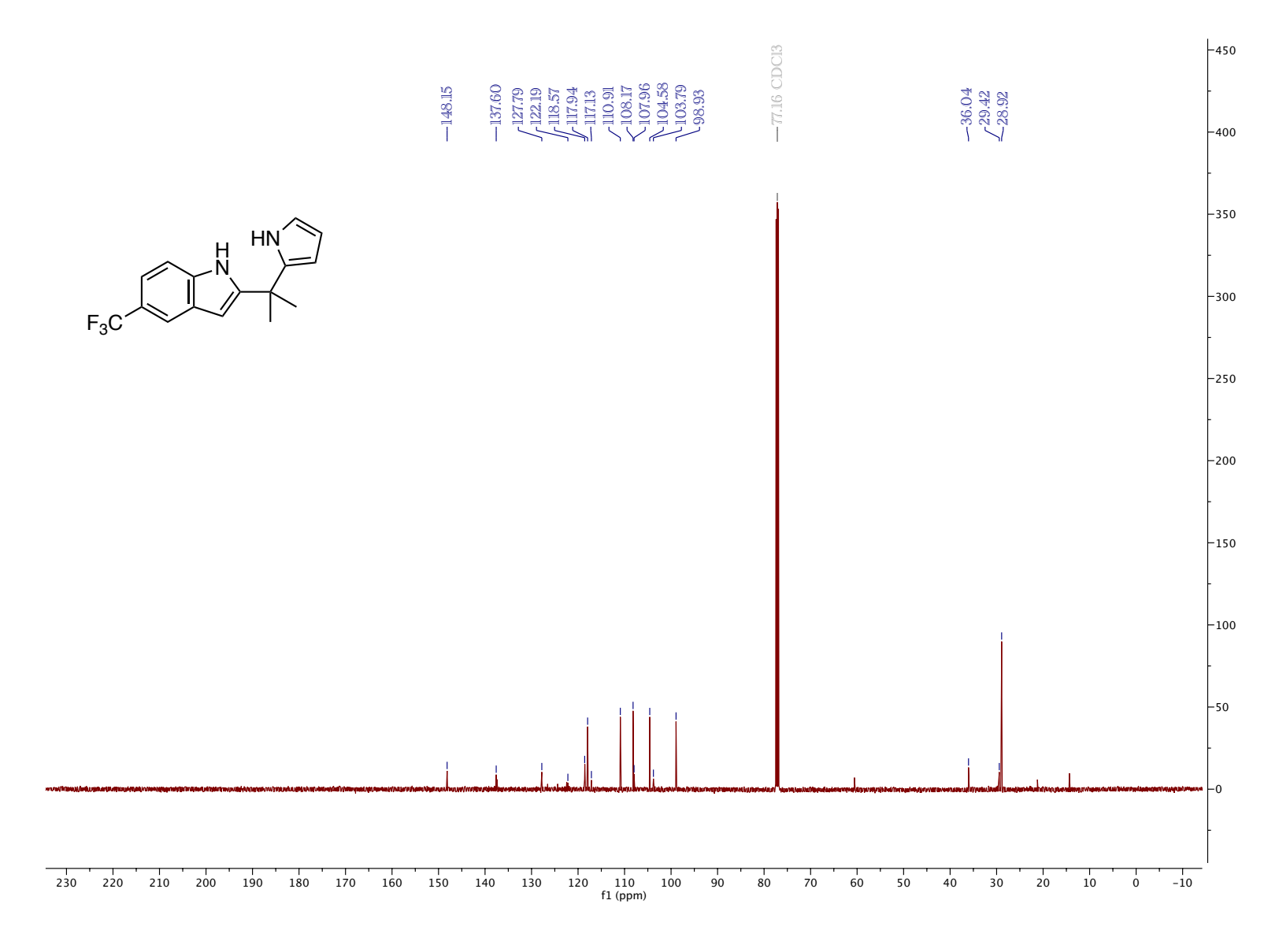


Figure 5.156. 13 C NMR (CDCl₃, 126 MHz, 25 $^{\circ}$ C)

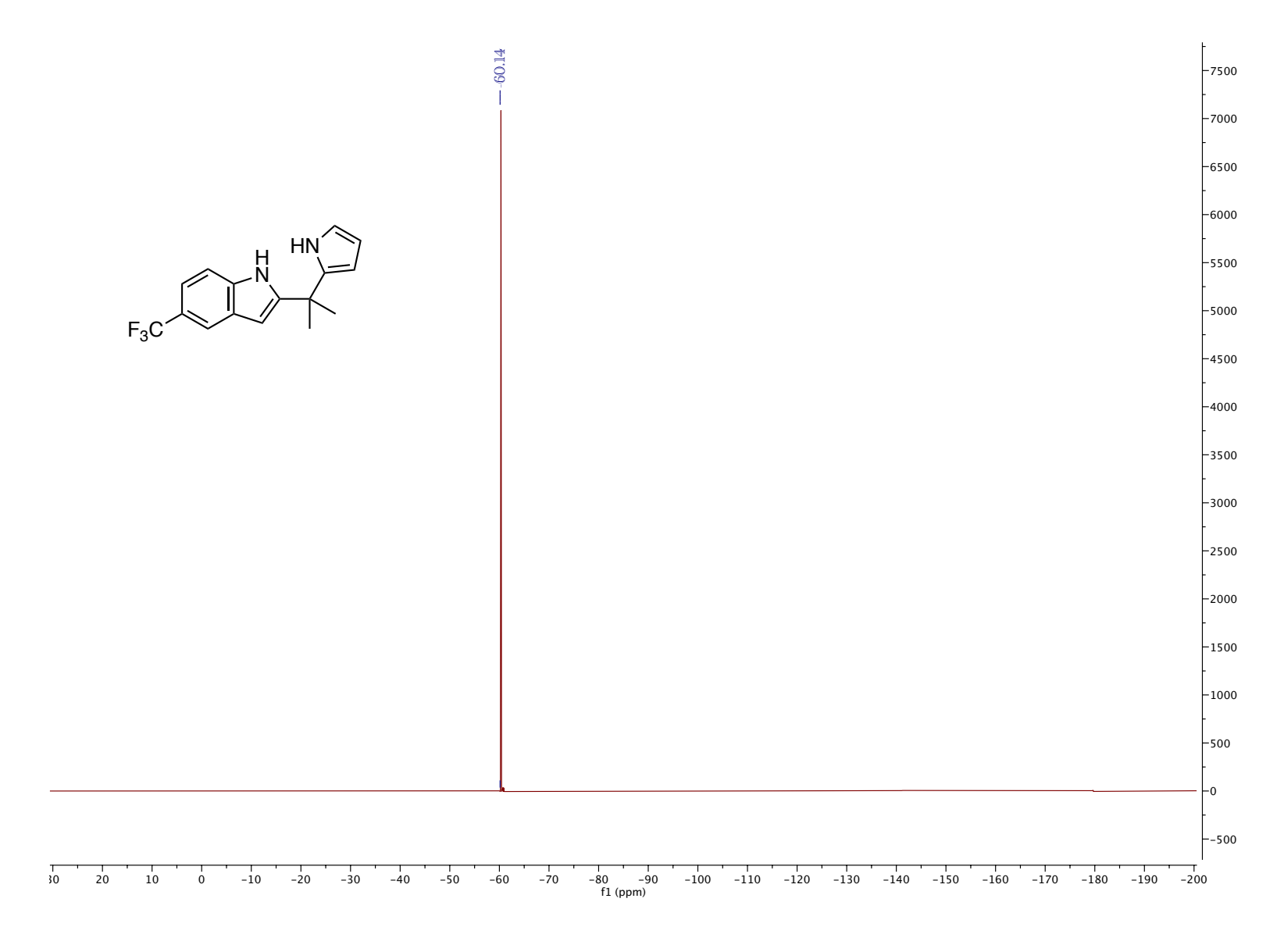


Figure 5.157. 19 F NMR (CDCl₃, 470 MHz, 25 $^{\circ}$ C)

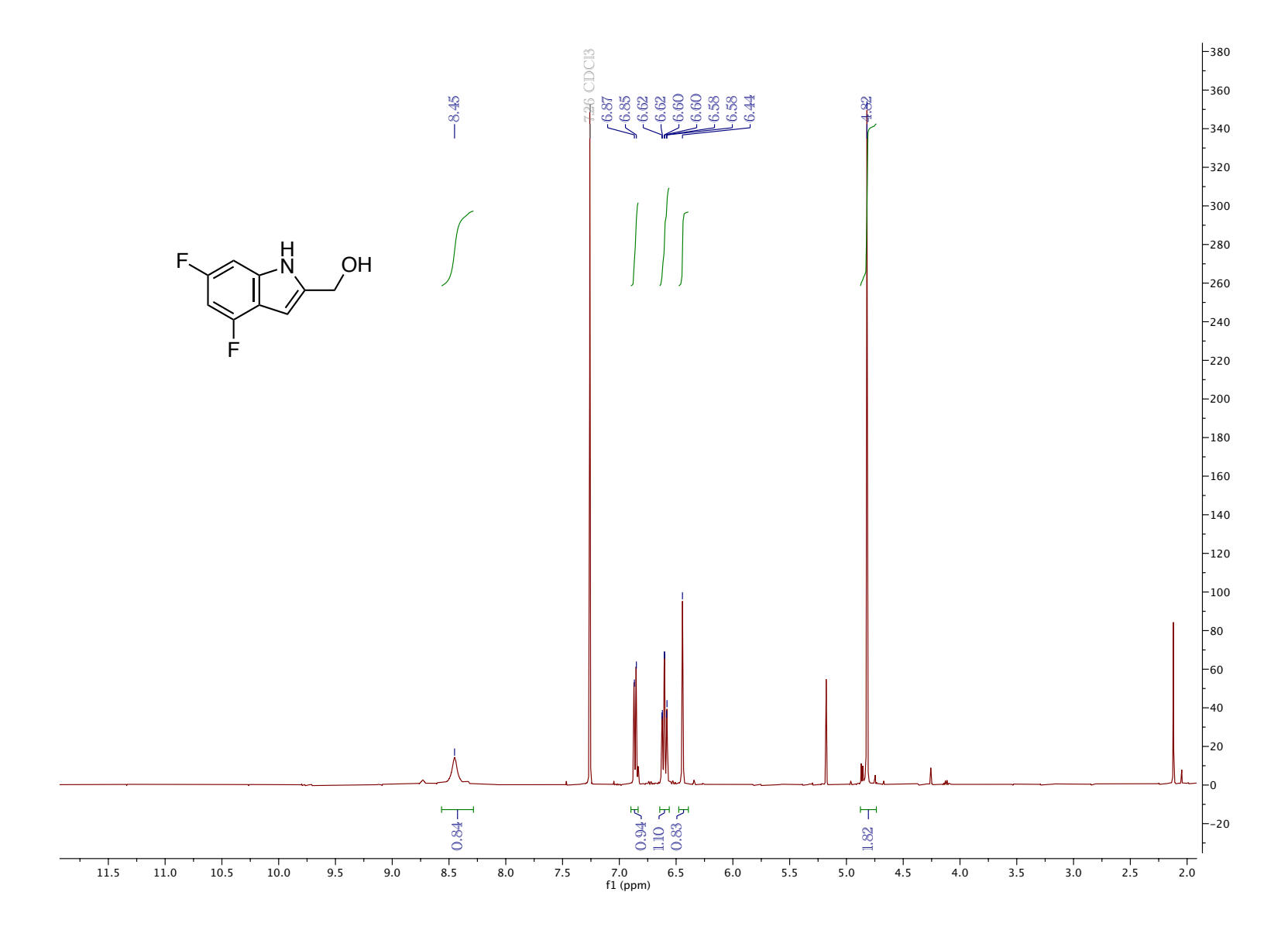


Figure 5.158. ¹H NMR (CDCl₃, 500 MHz, 25 °C)

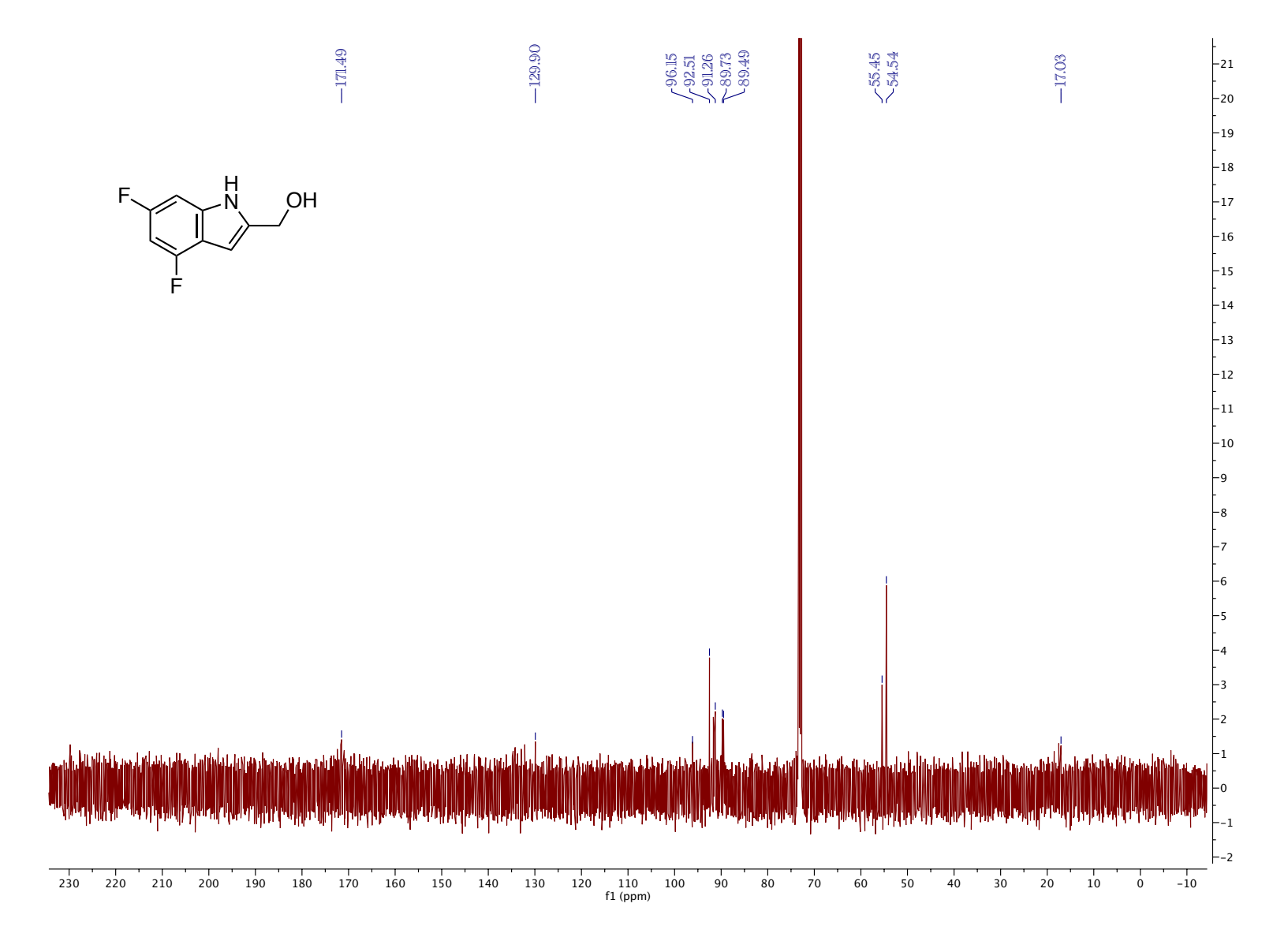


Figure 5.159. 13 C NMR (CDCl₃, 126 MHz, 25 $^{\circ}$ C)

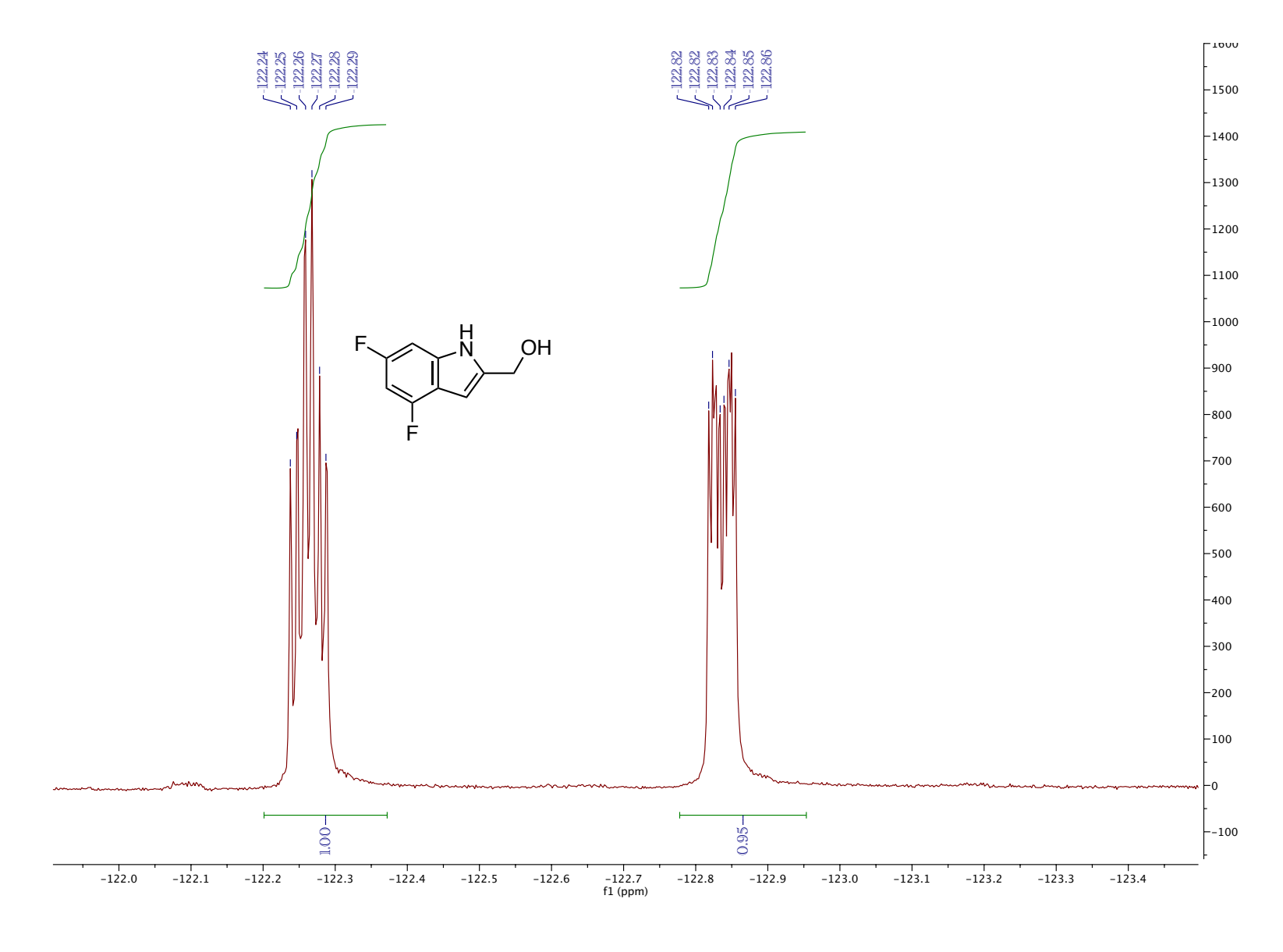


Figure 5.160. ^{19}F NMR (CDCl₃, 470 MHz, 25 $^{\circ}C)$

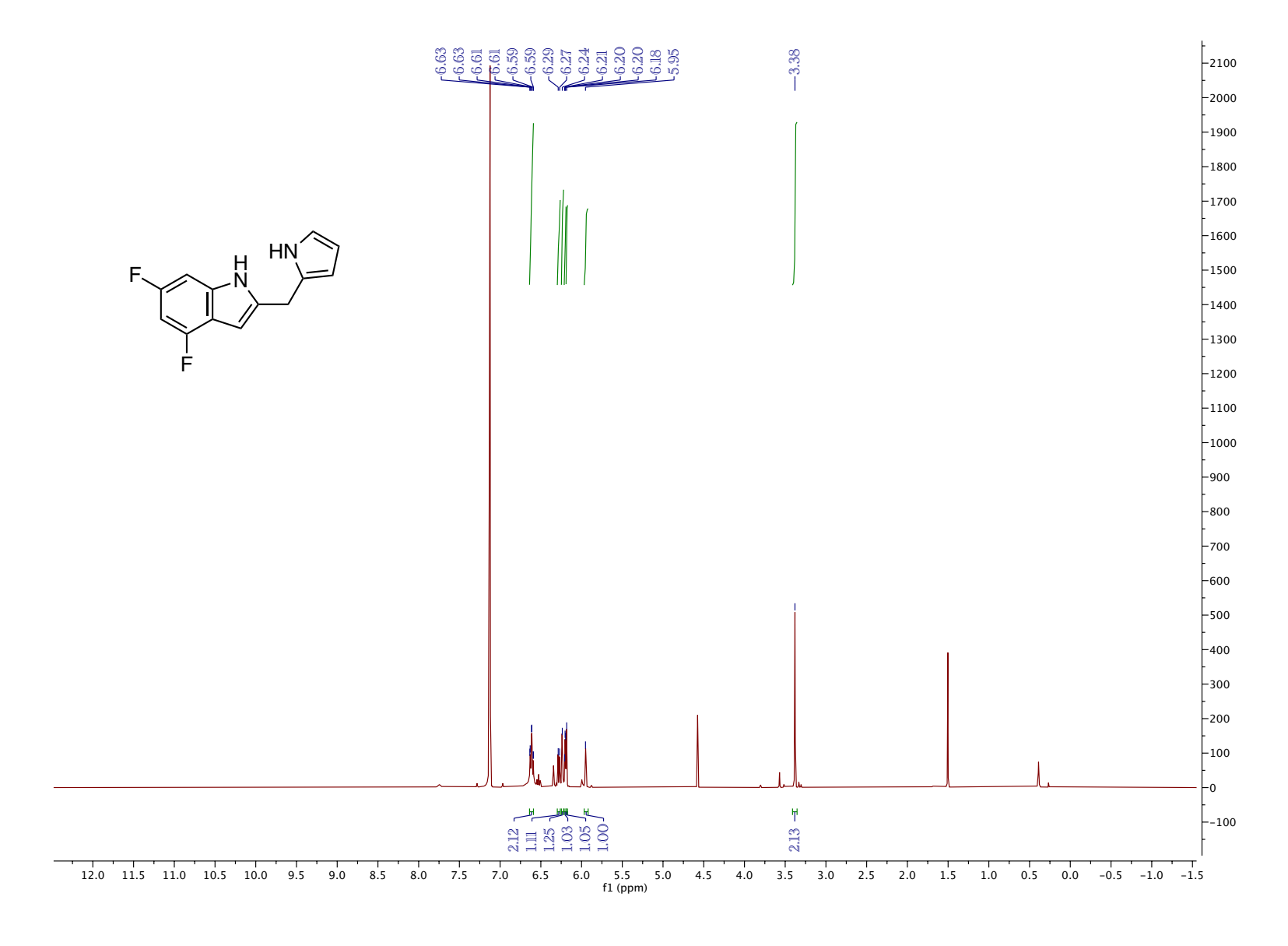


Figure 5.161. ¹H NMR (CDCl₃, 500 MHz, 25 °C)

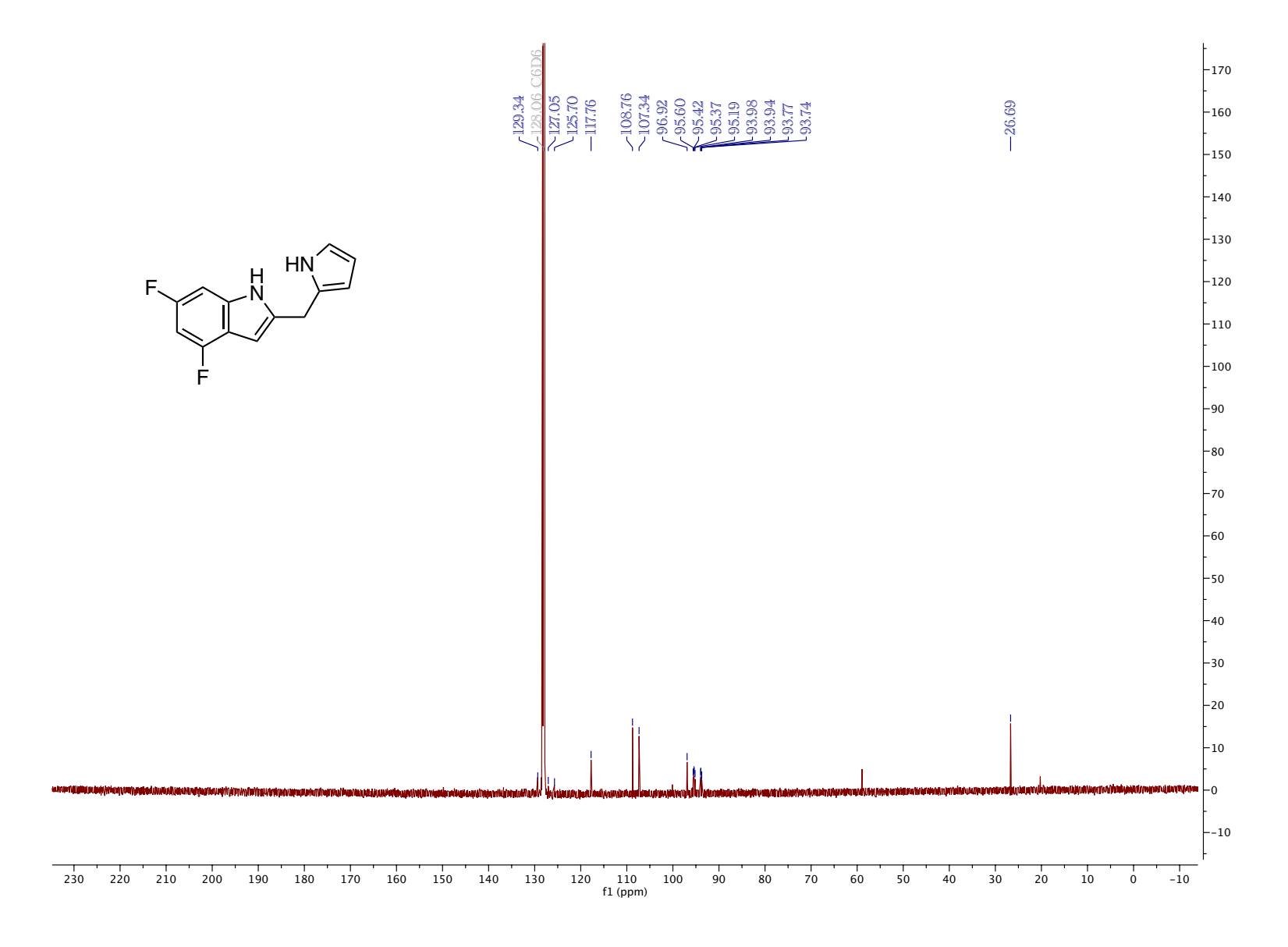


Figure 5.162. ¹³C NMR (CDCl₃, 126 MHz, 25 °C)

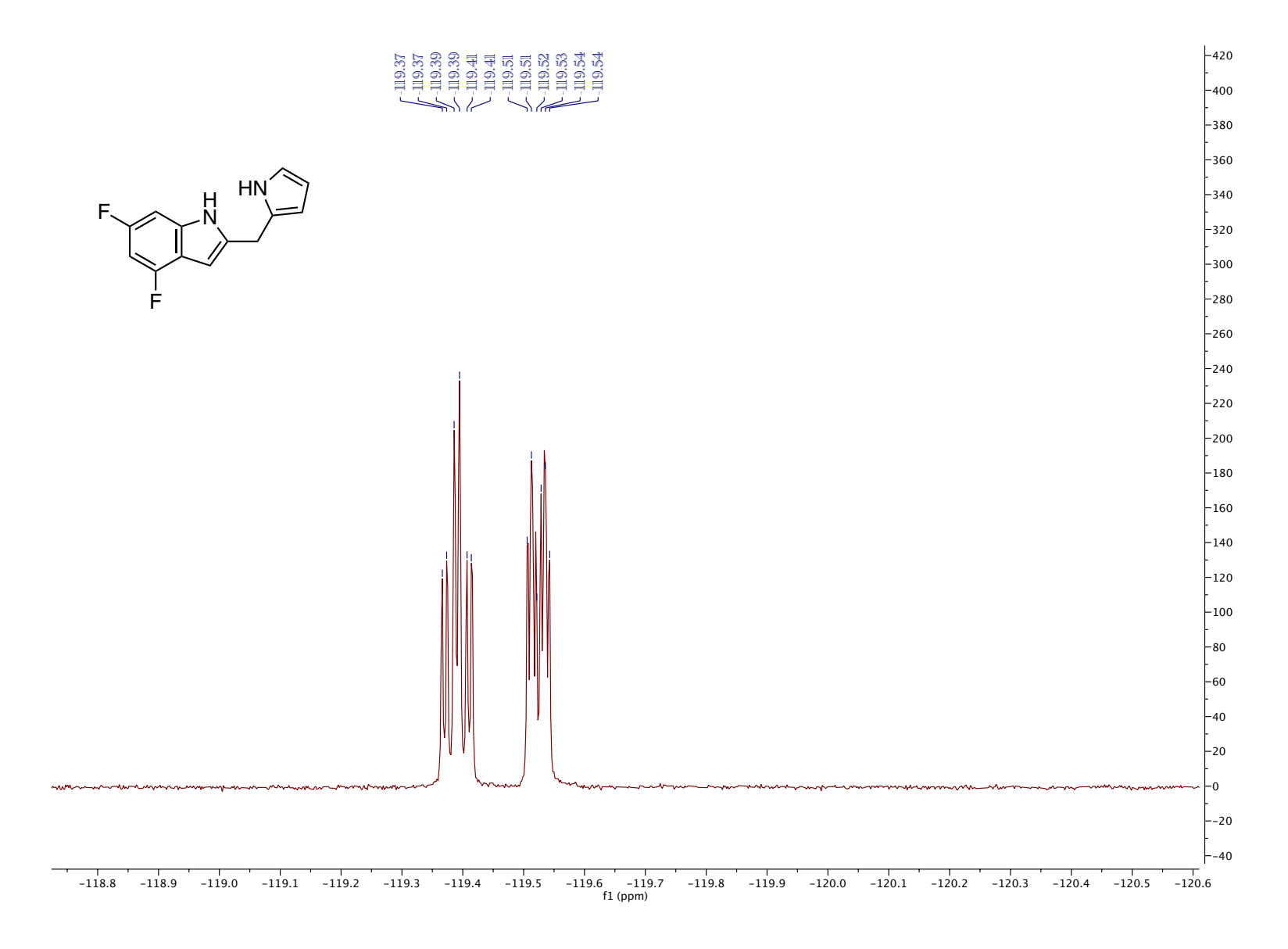


Figure 5.163. 19 F NMR (CDCl₃, 470 MHz, 25 $^{\circ}$ C)

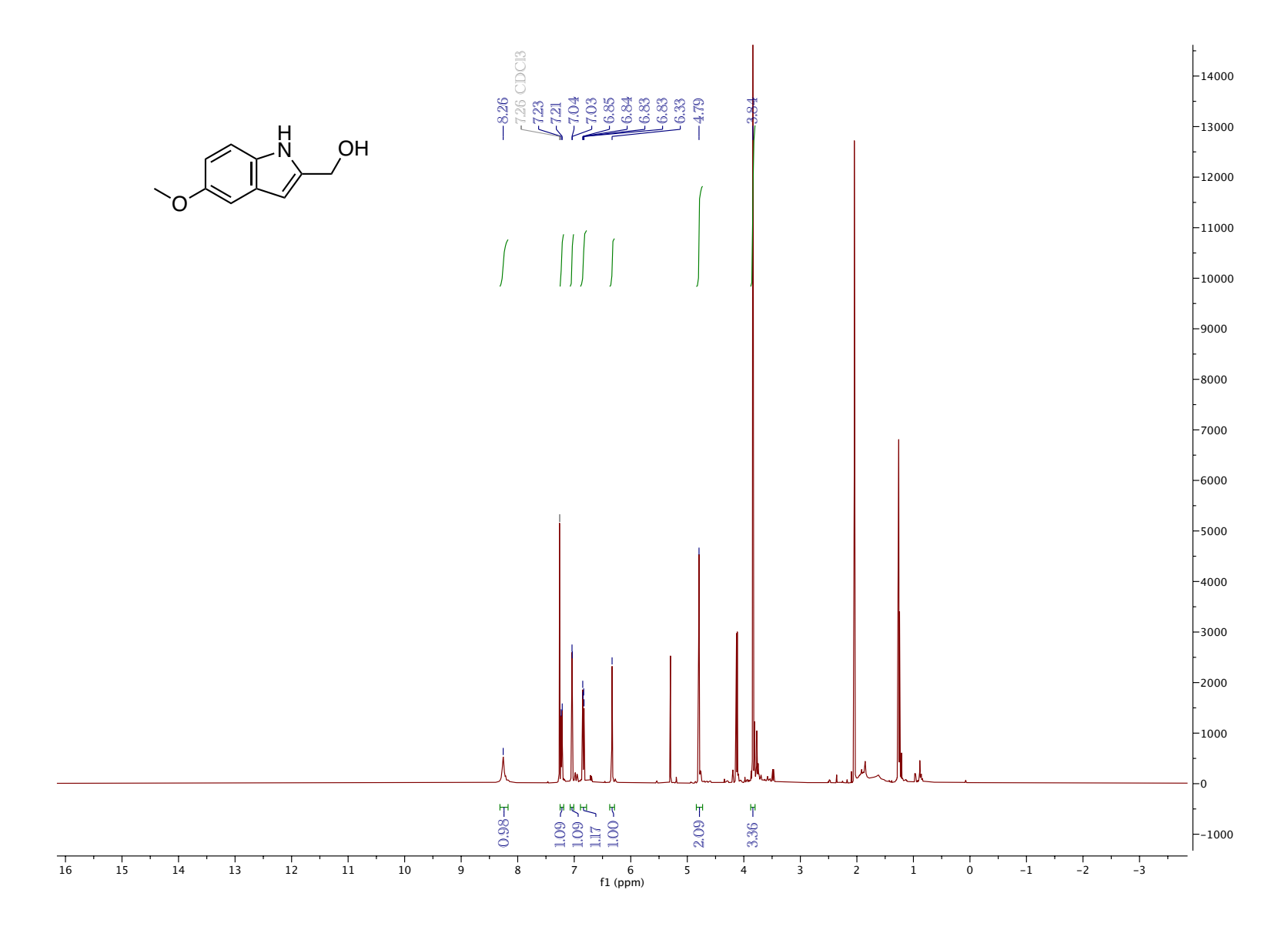


Figure 5.164. ¹H NMR (CDCl₃, 500 MHz, 25 °C)

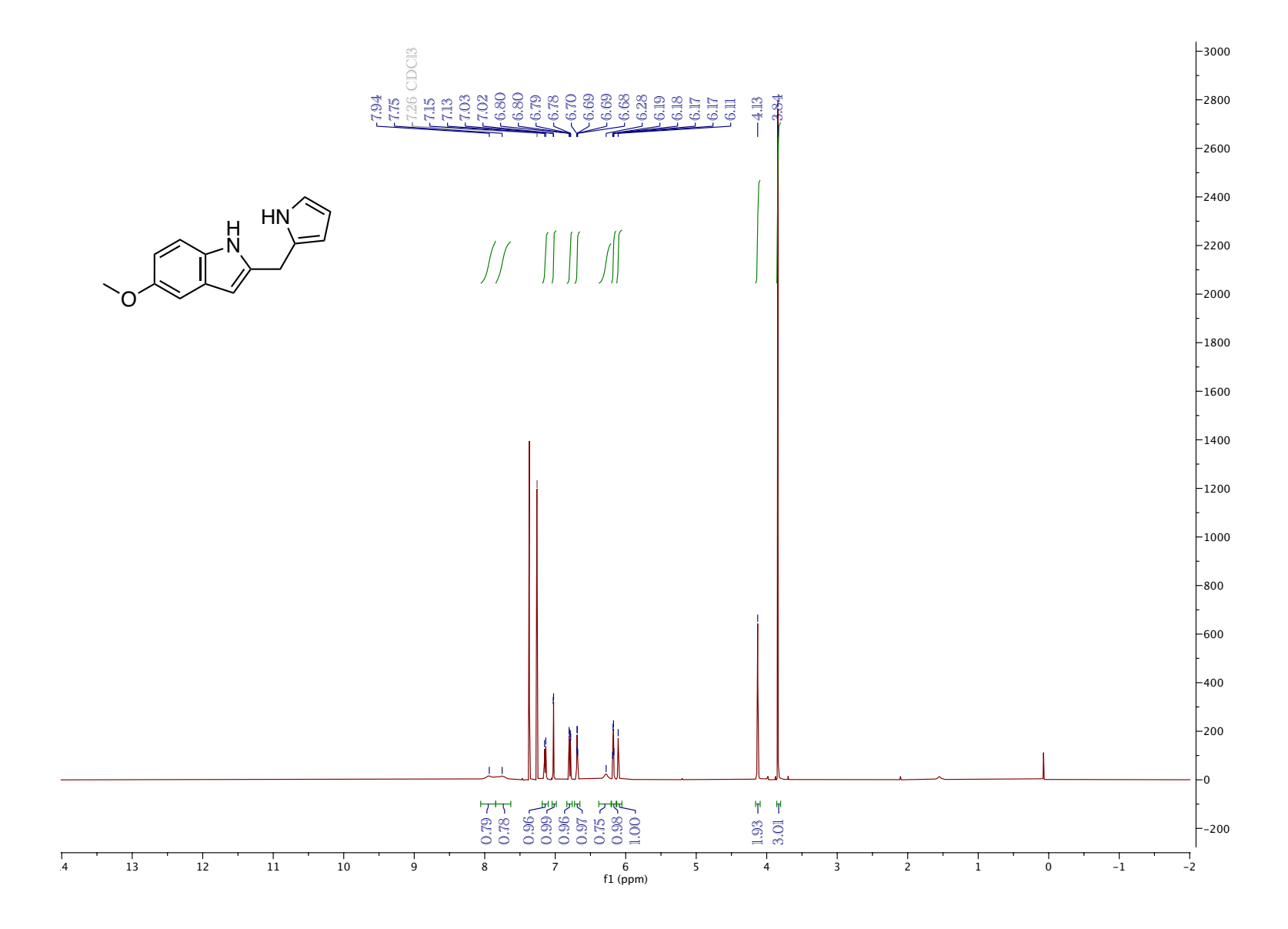


Figure 5.165. ¹H NMR (CDCl₃, 500 MHz, 25 °C)

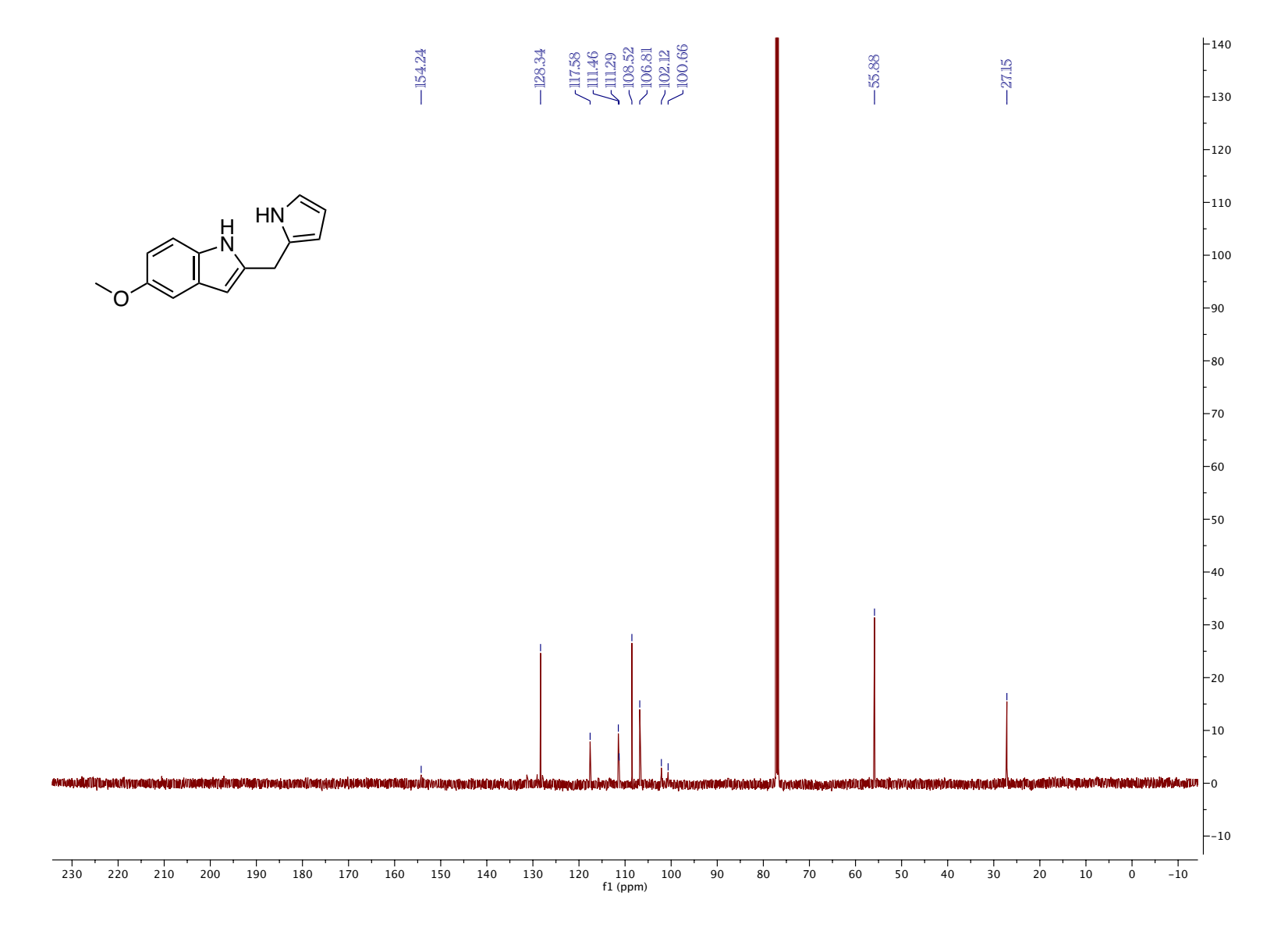


Figure 5.166. ¹³C NMR (CDCl₃, 126 MHz, 25 °C)

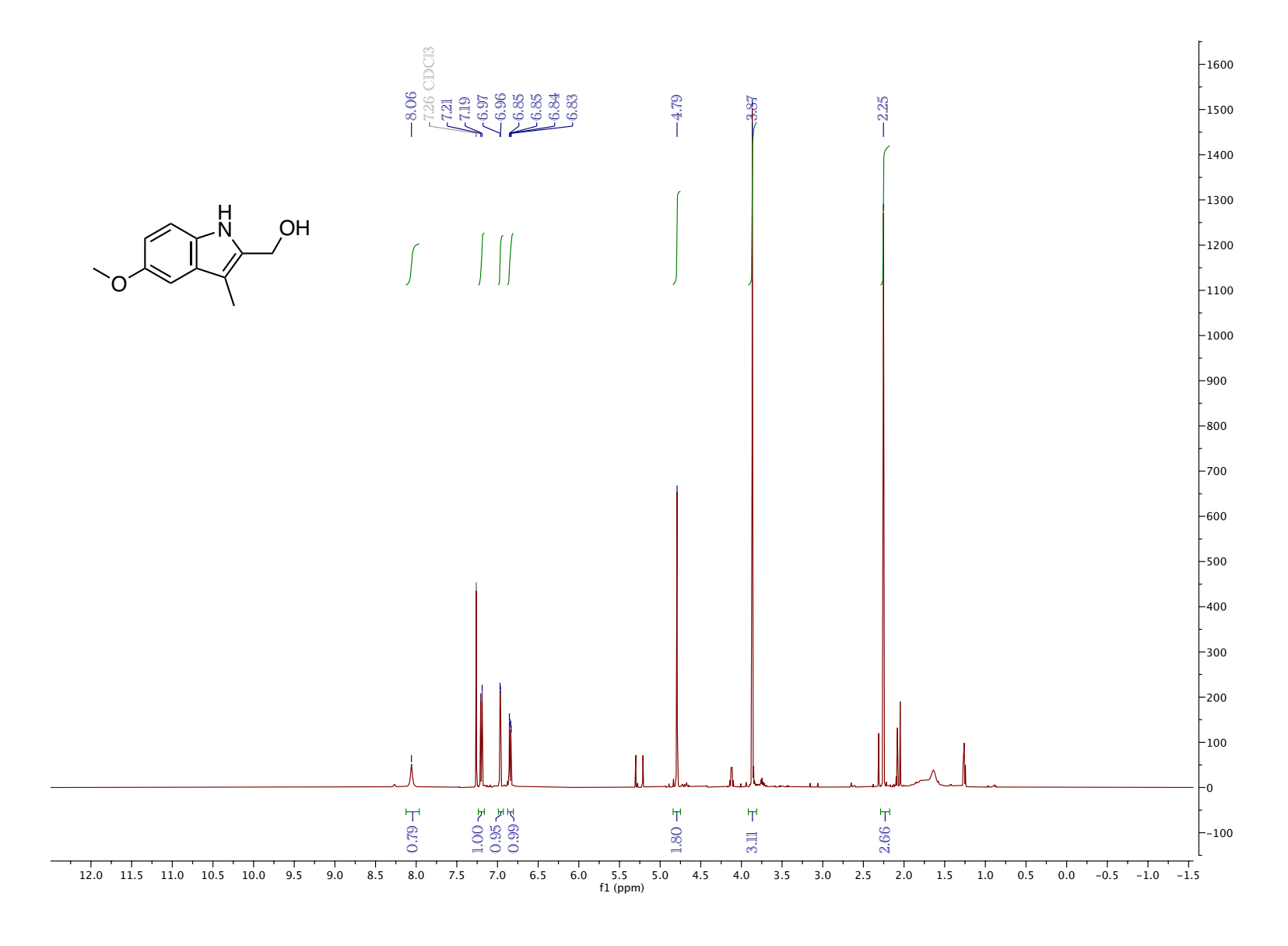


Figure 5.167. ¹H NMR (CDCl₃, 500 MHz, 25 °C)

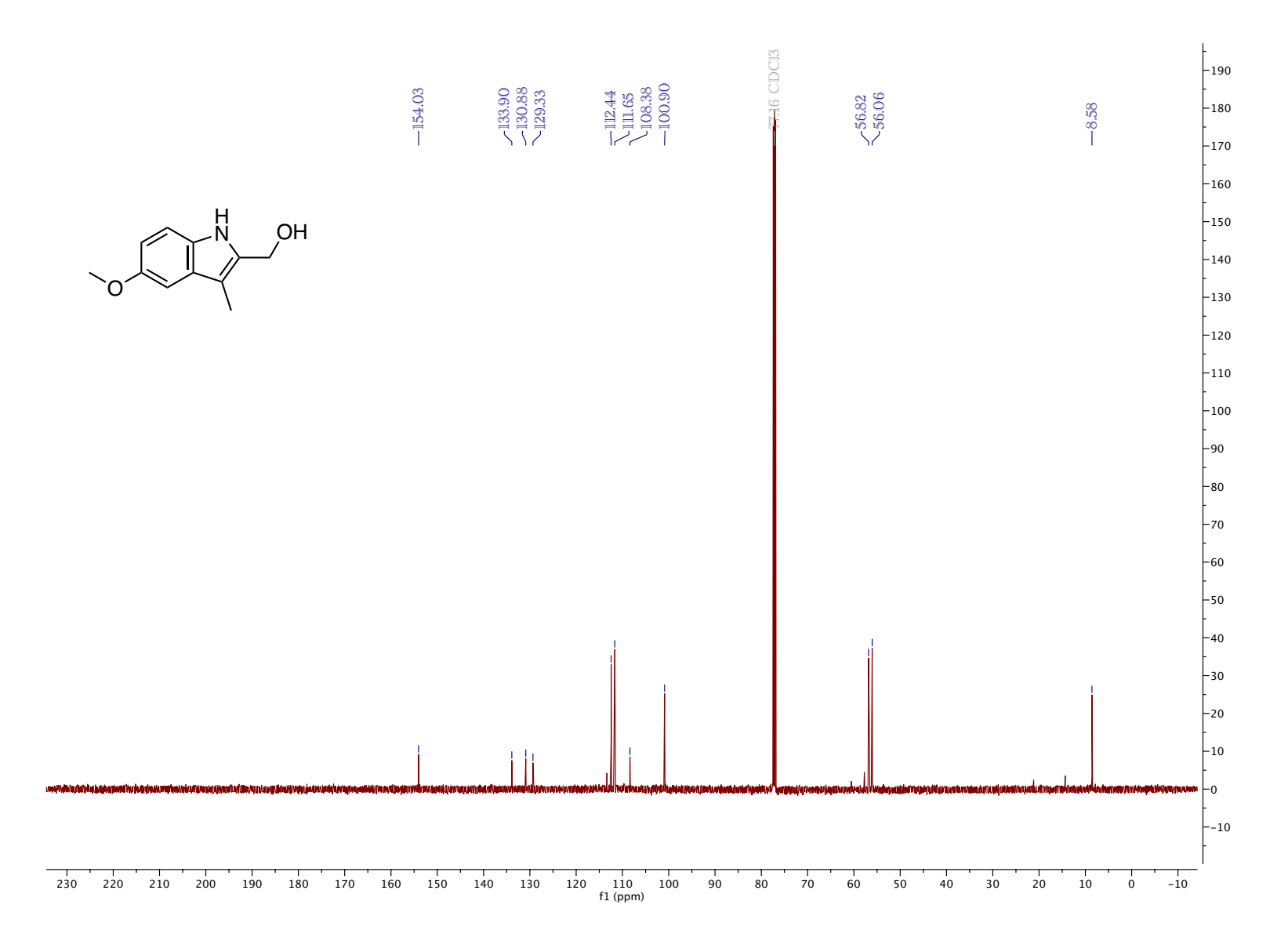


Figure 5.168. ¹³C NMR (CDCl₃, 126 MHz, 25 °C)

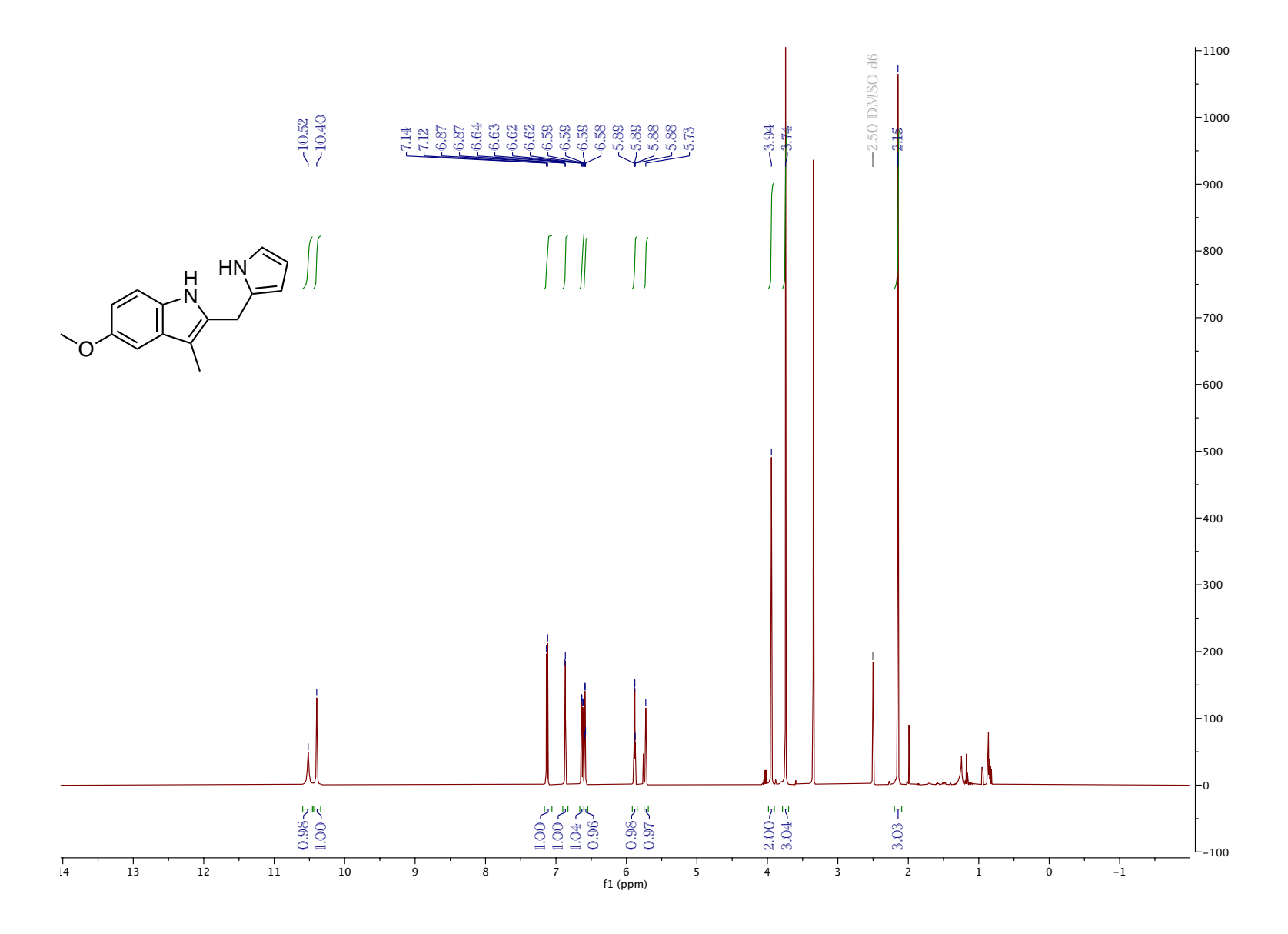


Figure 5.169. ¹H NMR (DMSO-d₆, 500 MHz, 25 °C)

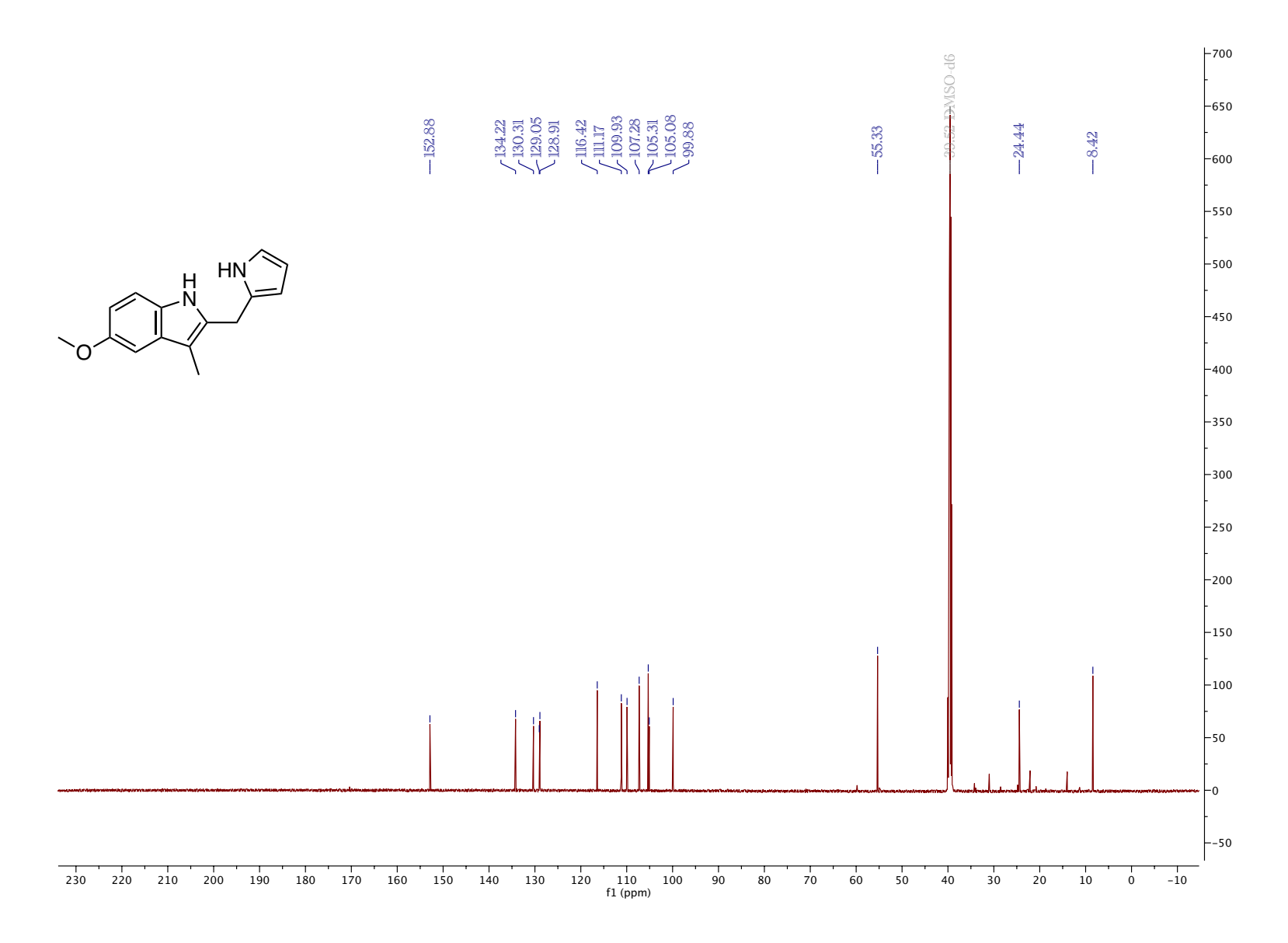


Figure 5.170. ¹³C NMR (DMSO-d₆, 126 MHz, 25 °C)

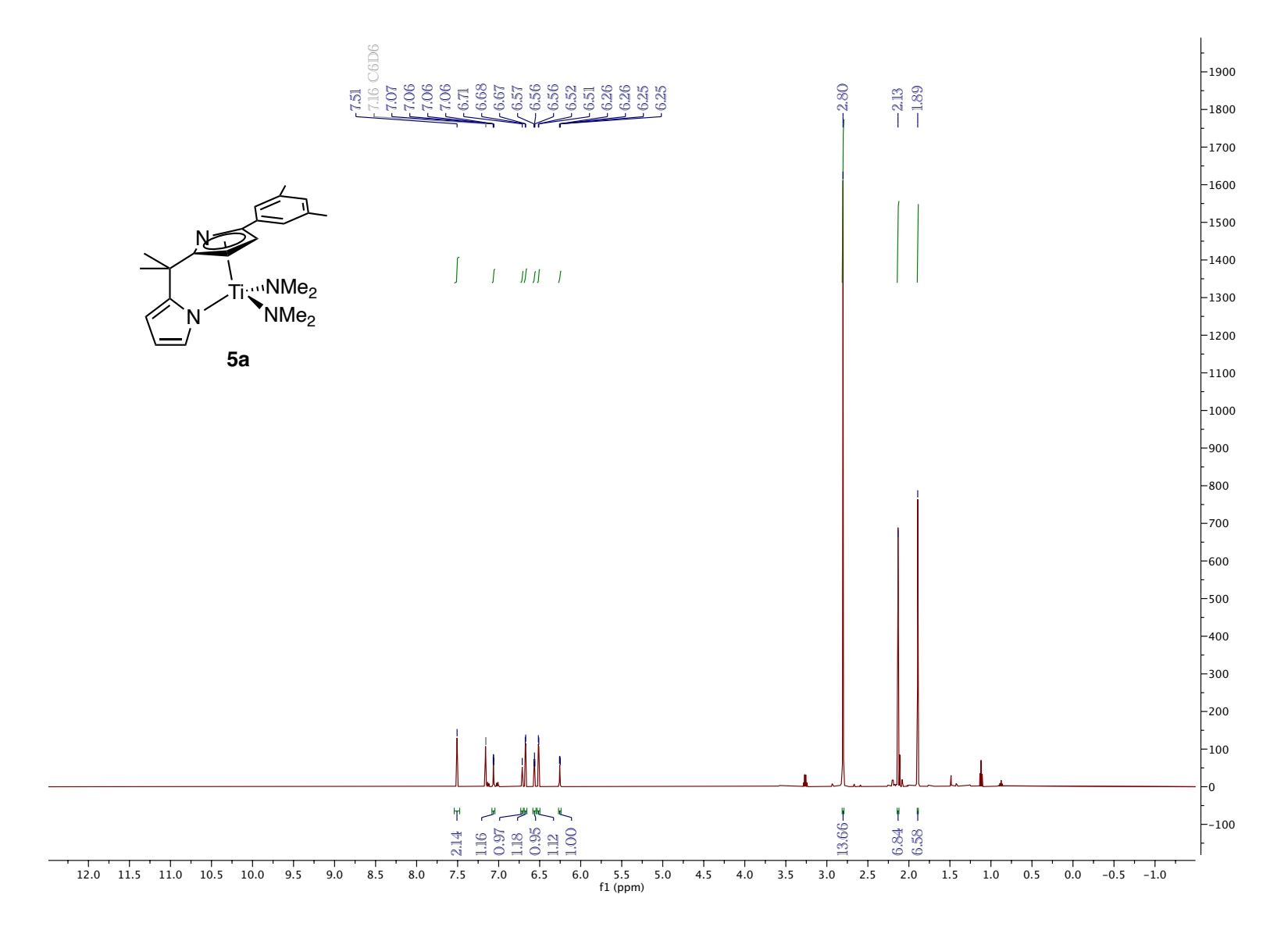


Figure 5.171. ¹H NMR (C₆D₆, 500 MHz, 25 °C)

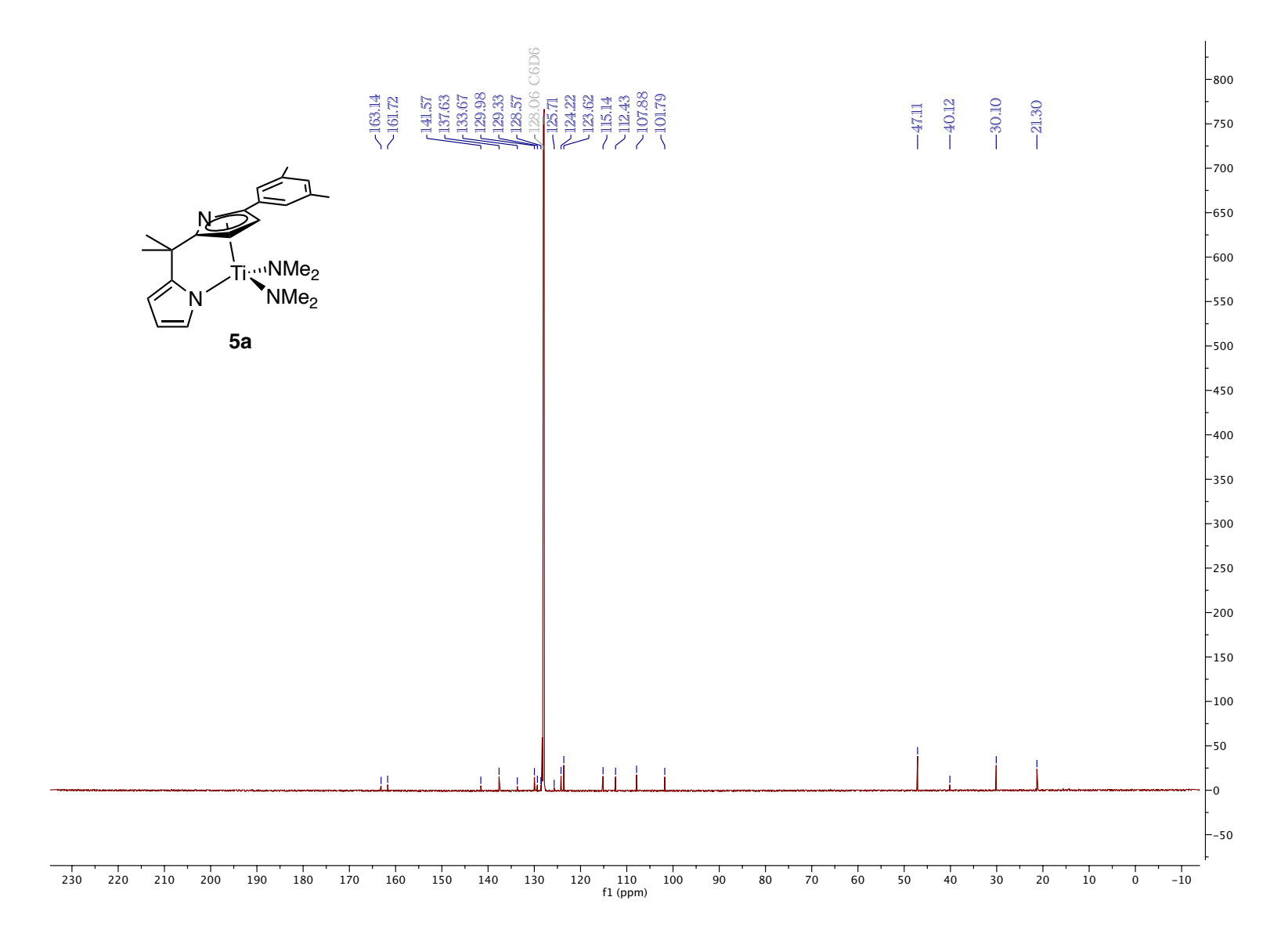


Figure 5.172. ¹³C NMR (C₆D₆, 126 MHz, 25 °C)

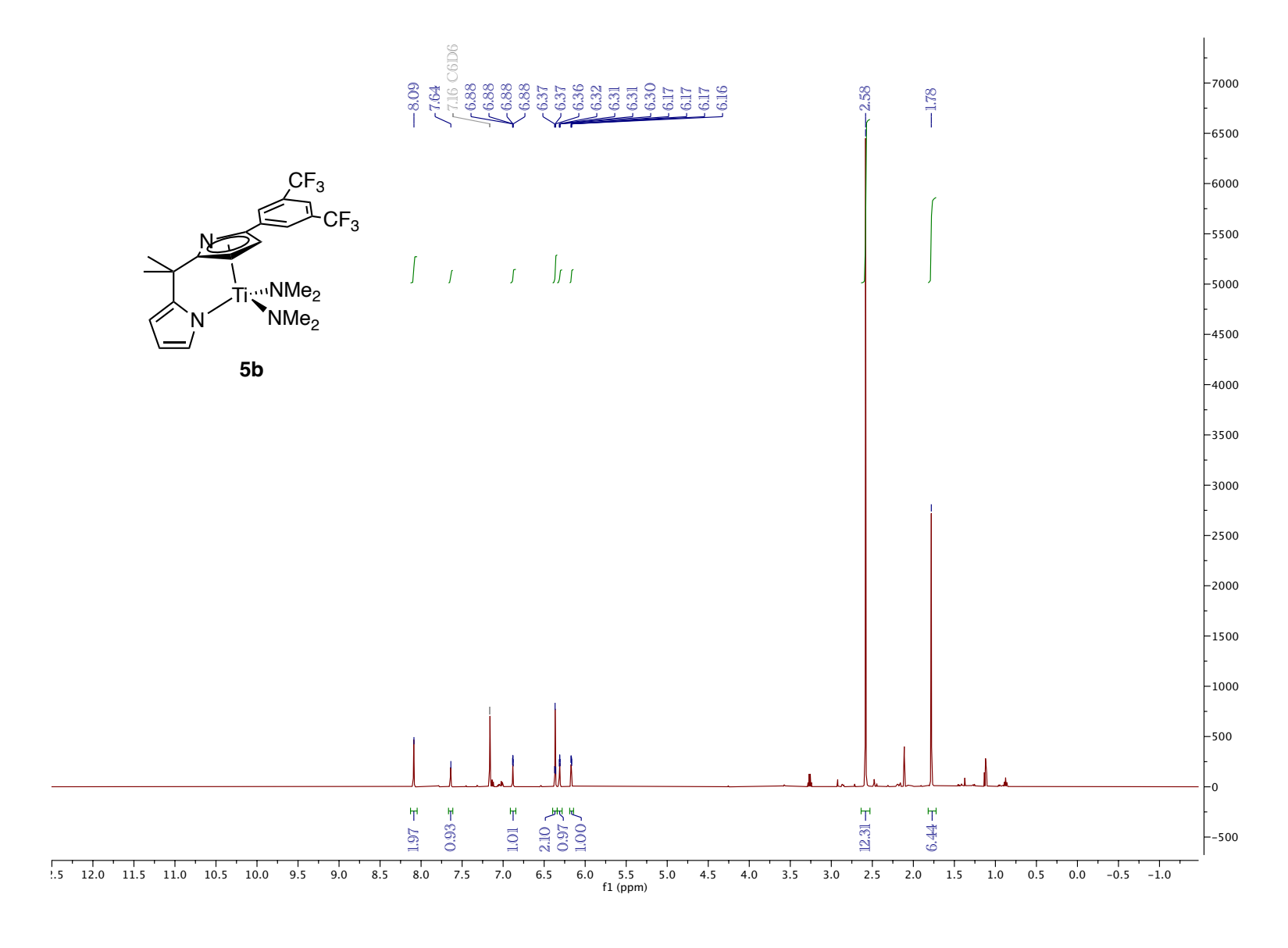


Figure 5.173. 1 H NMR (C_6D_6 , 500 MHz, 25 $^{\circ}$ C)

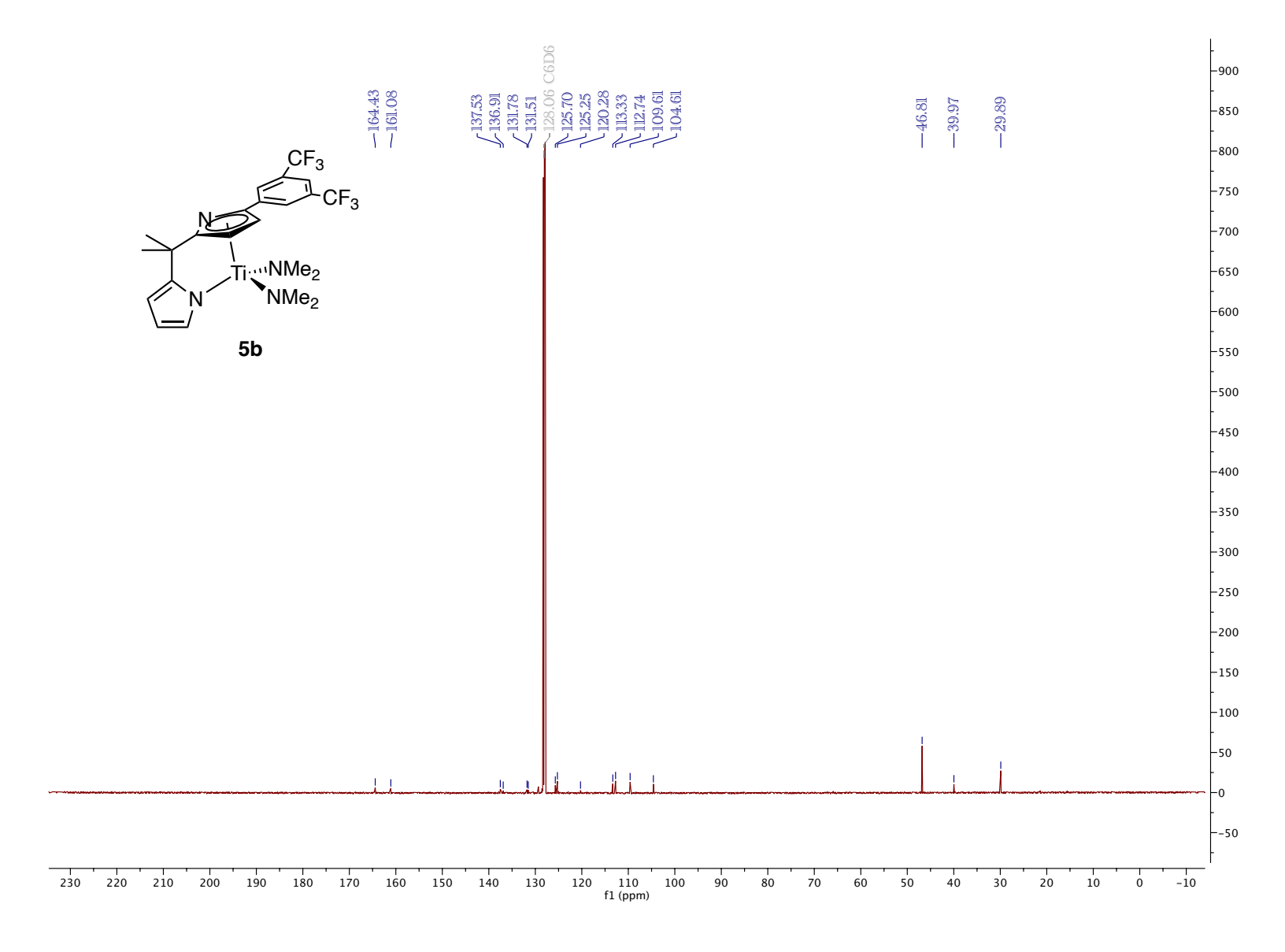


Figure 5.174. ¹³C NMR (C₆D₆, 126 MHz, 25 °C)

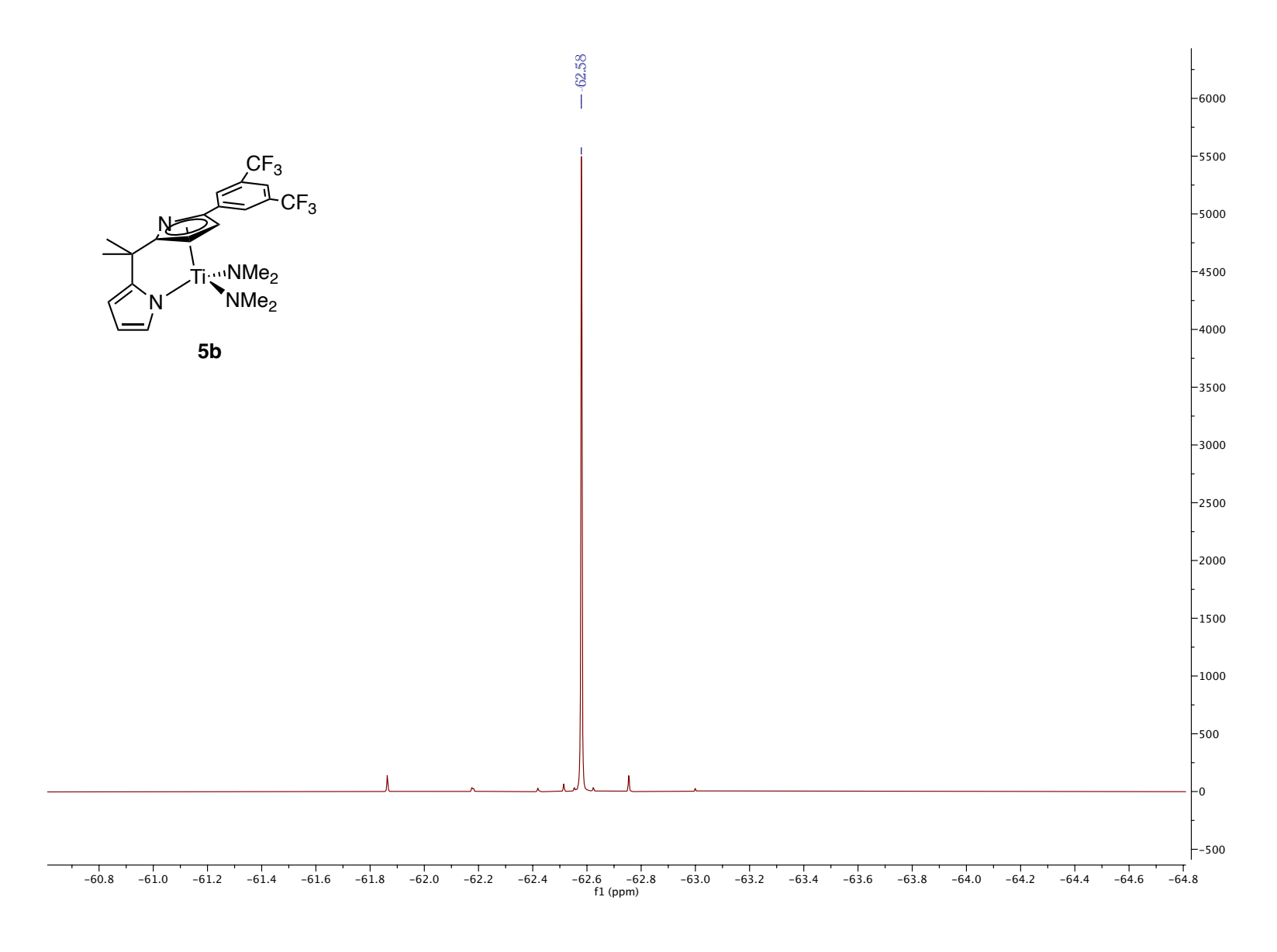


Figure 5.175. ¹⁹F NMR (470 MHz, C₆C₆, 25 °C)

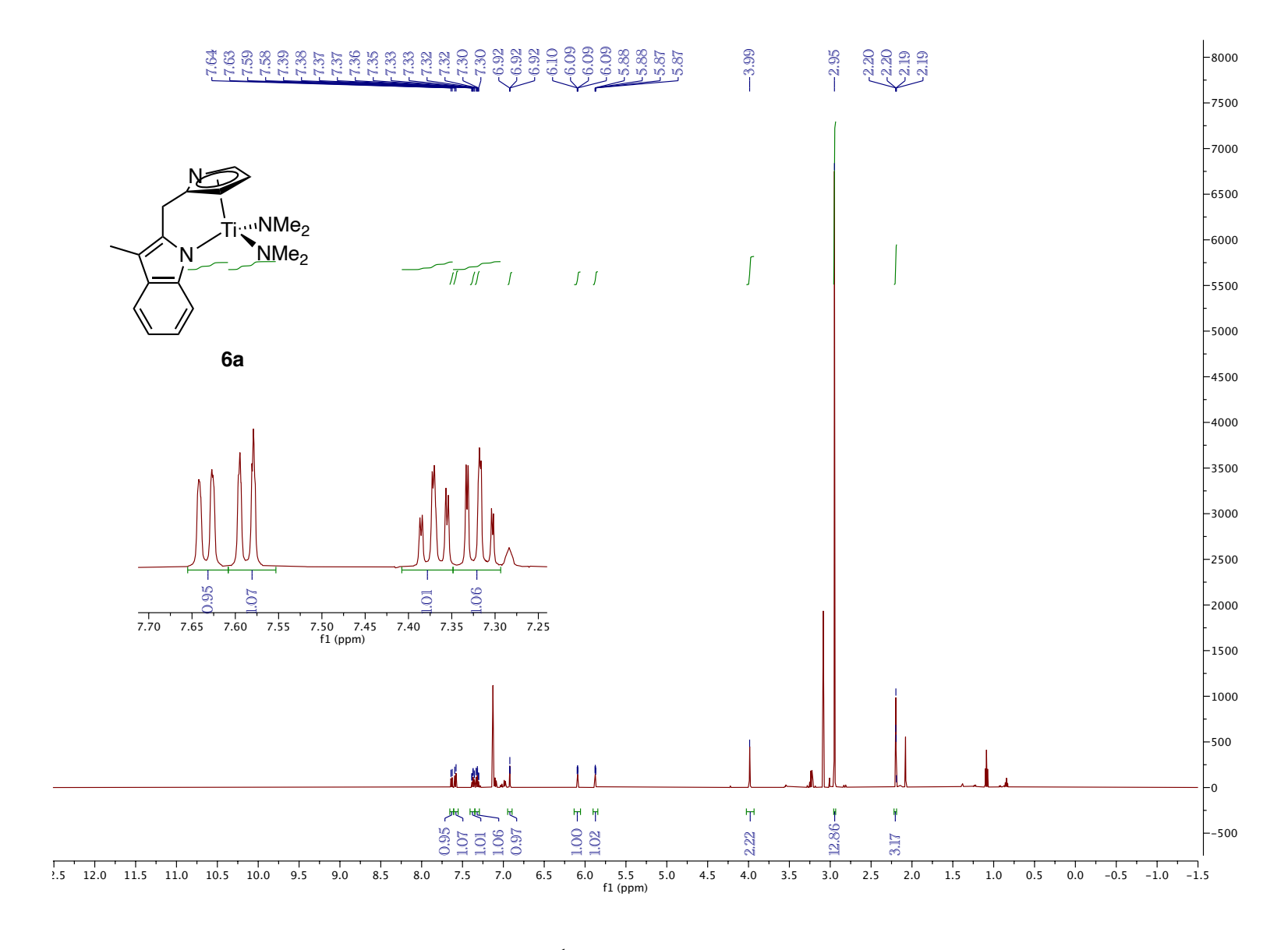


Figure 5.176. ¹H NMR (C₆D₆, 500 MHz, 25 °C)

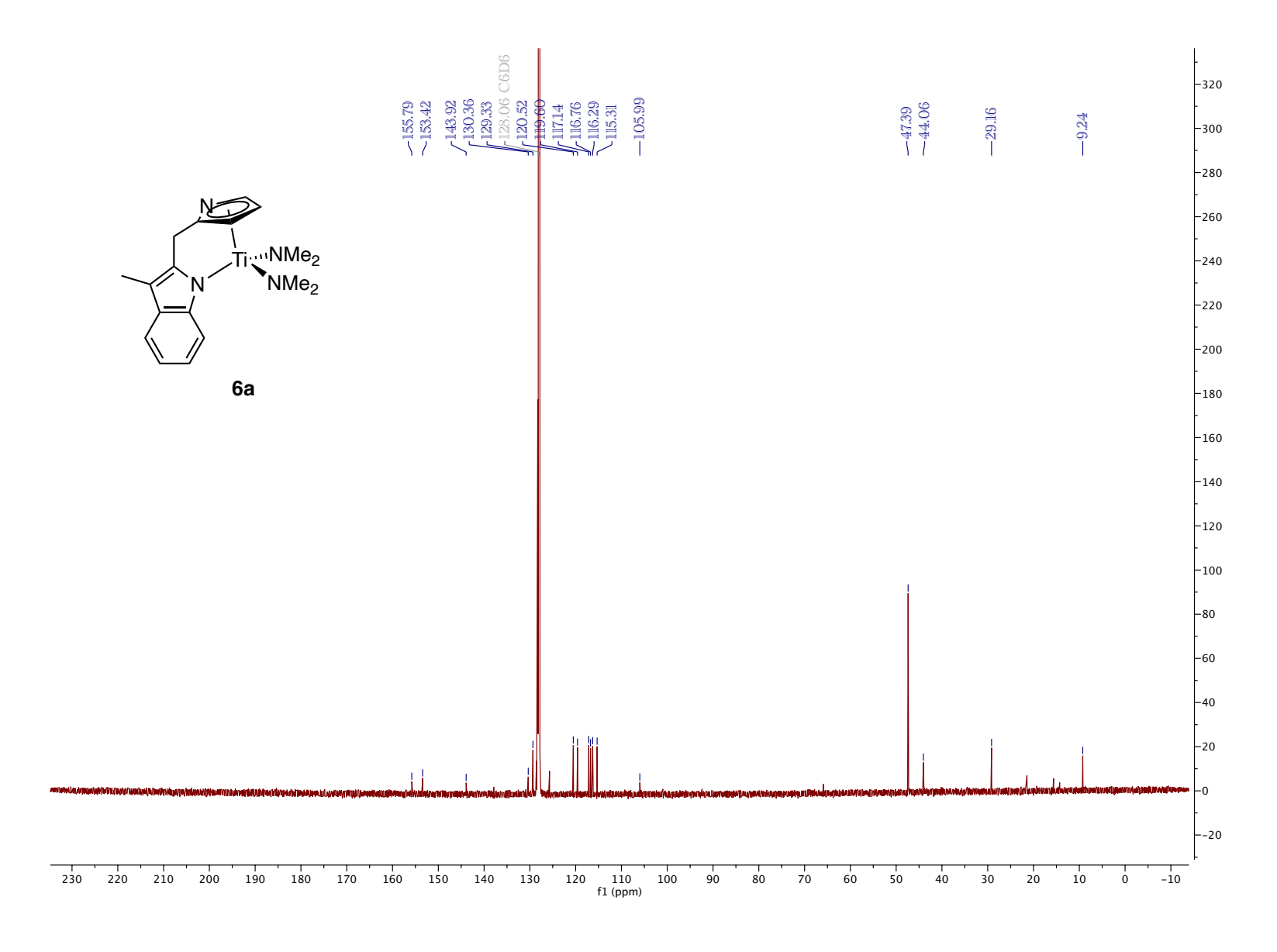


Figure 5.177. ¹³C NMR (C₆D₆, 126 MHz, 25 °C)

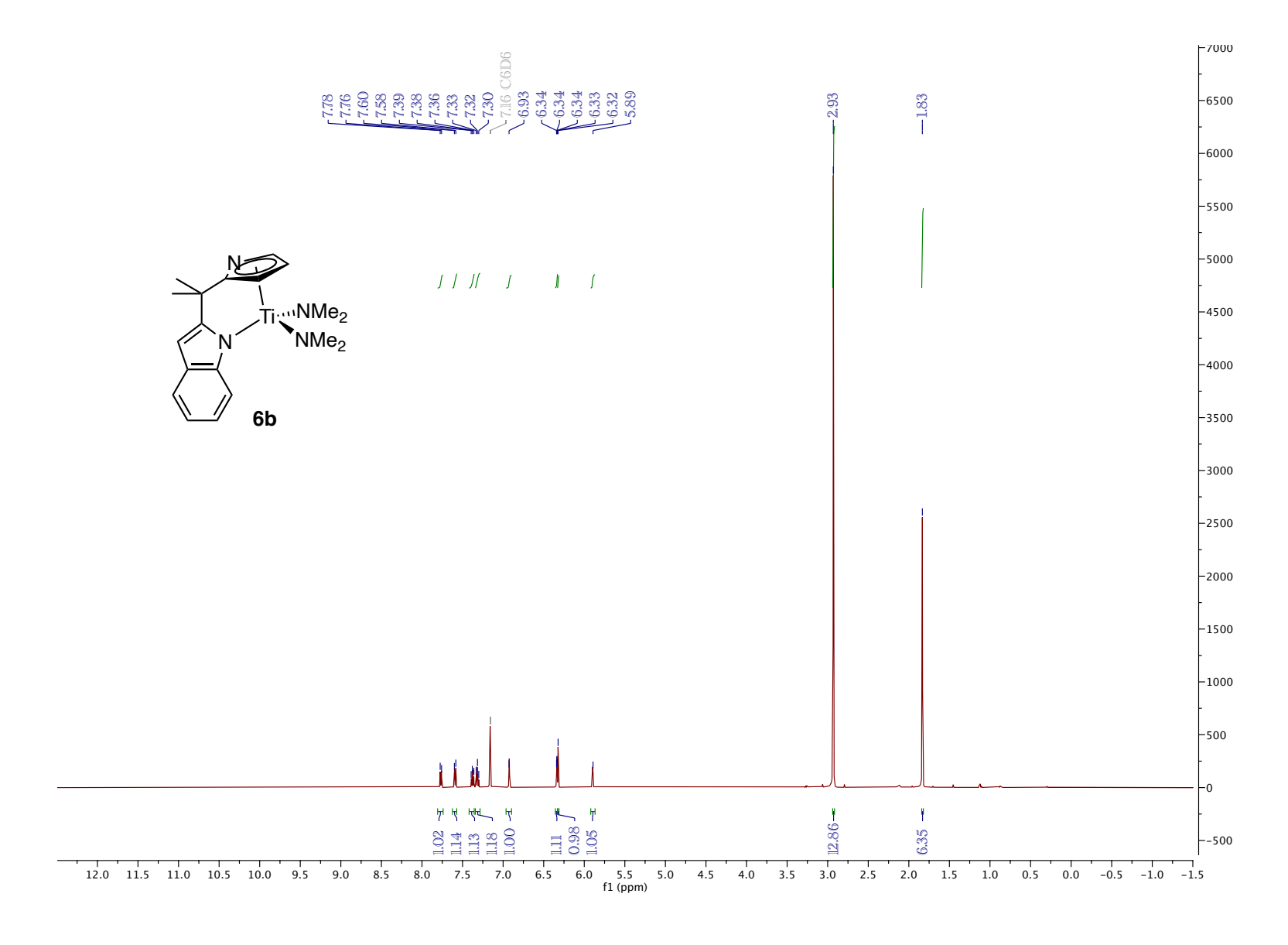


Figure 5.178. 1 H NMR (C_6D_6 , 500 MHz, 25 $^{\circ}$ C)

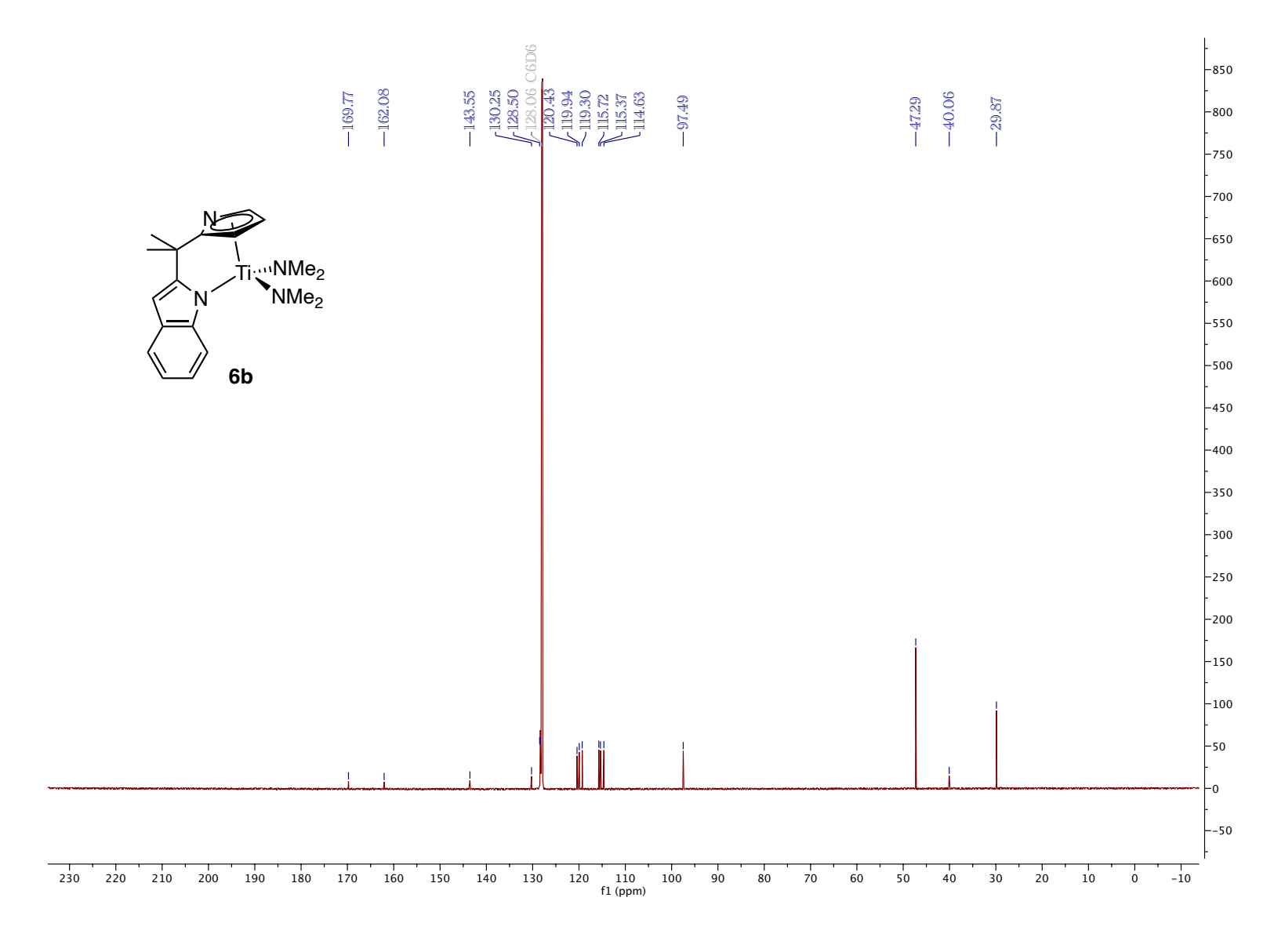


Figure 5.179. ¹³C NMR (C₆D₆, 126 MHz, 25 °C)

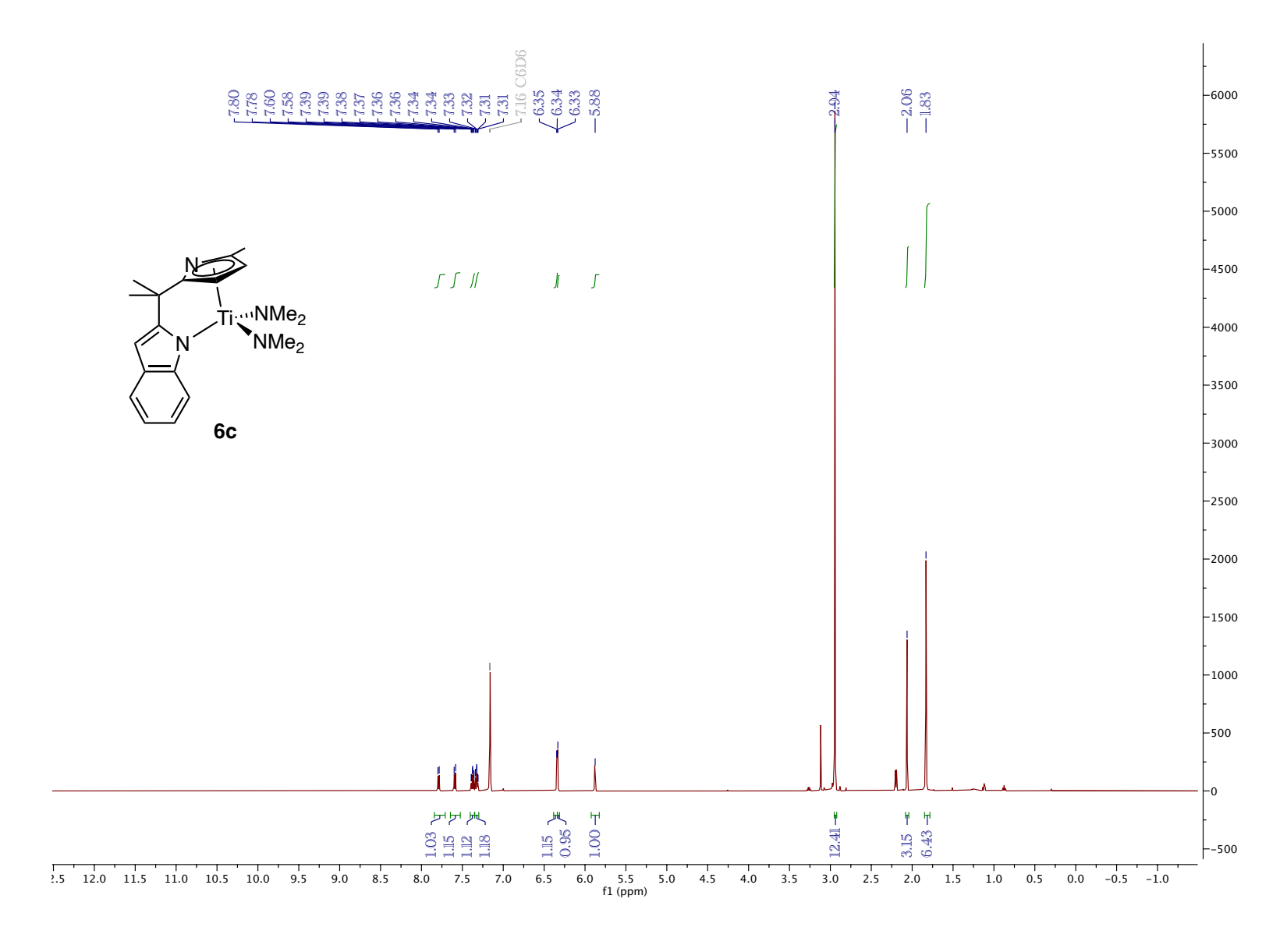


Figure 5.180. 1 H NMR (C_6D_6 , 500 MHz, 25 $^{\circ}$ C)

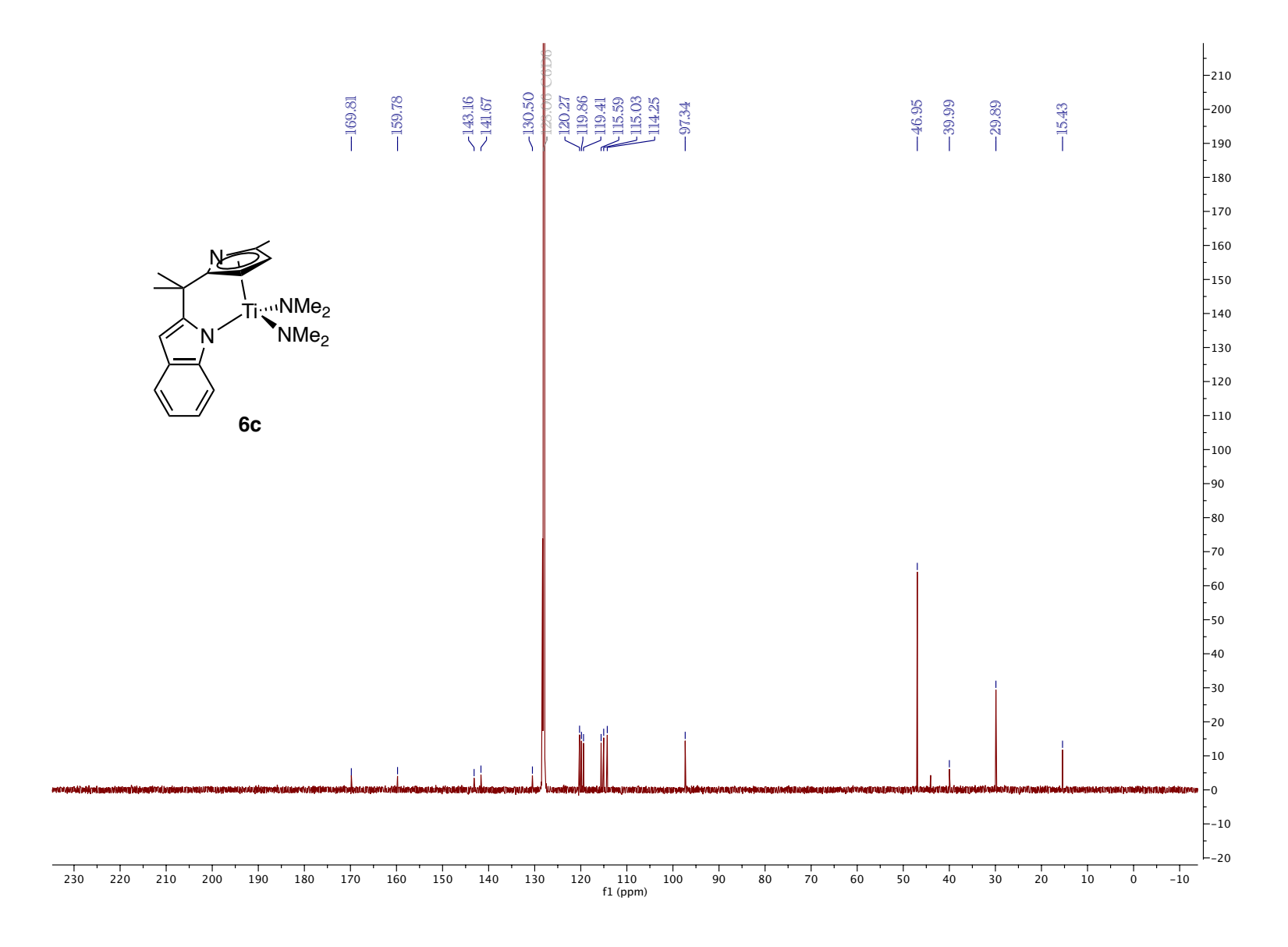


Figure 5.181. ¹³C NMR (C₆D₆, 126 MHz, 25 °C)

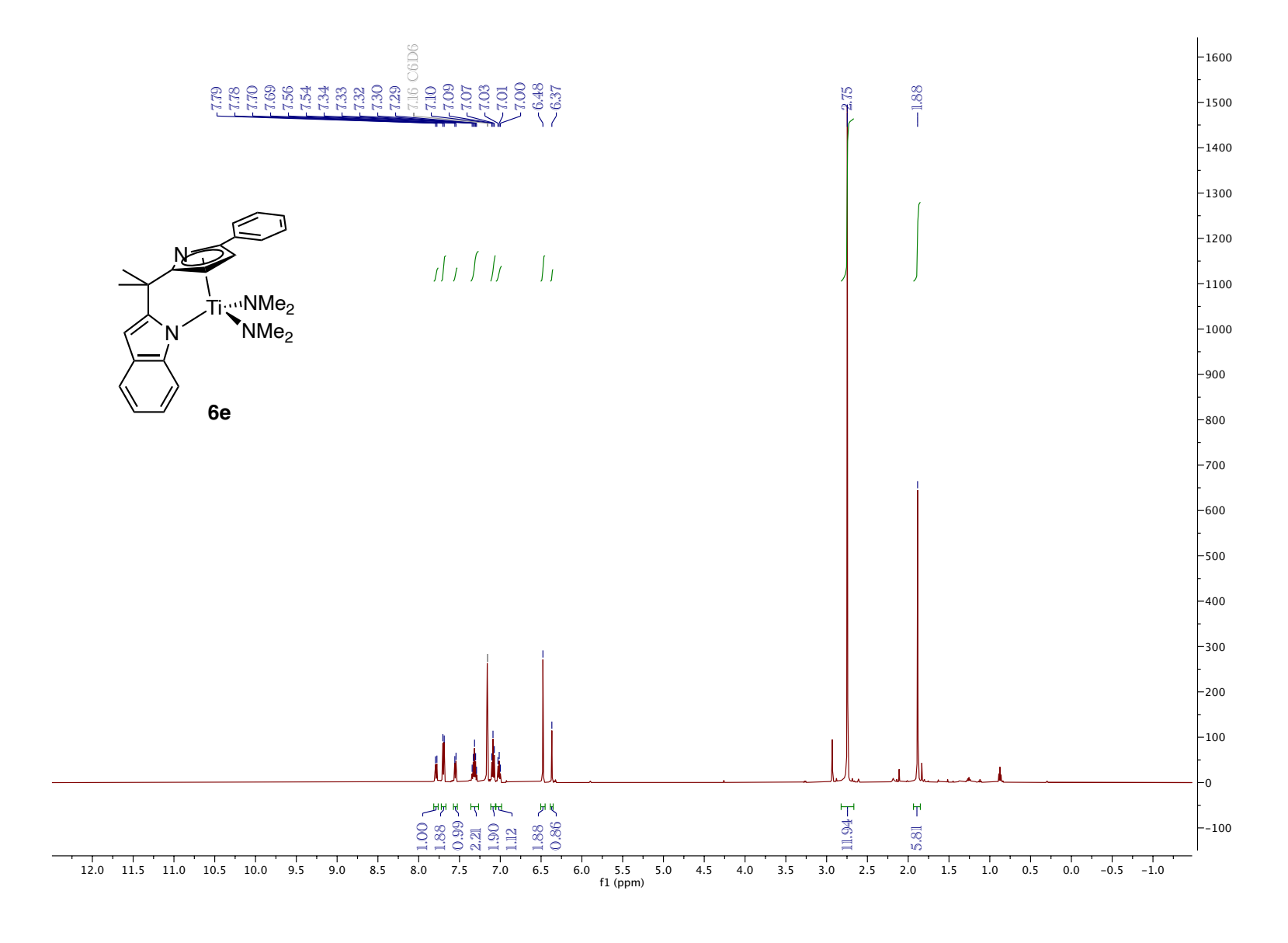


Figure 5.182. 1 H NMR (C_6D_6 , 500 MHz, 25 $^{\circ}$ C)

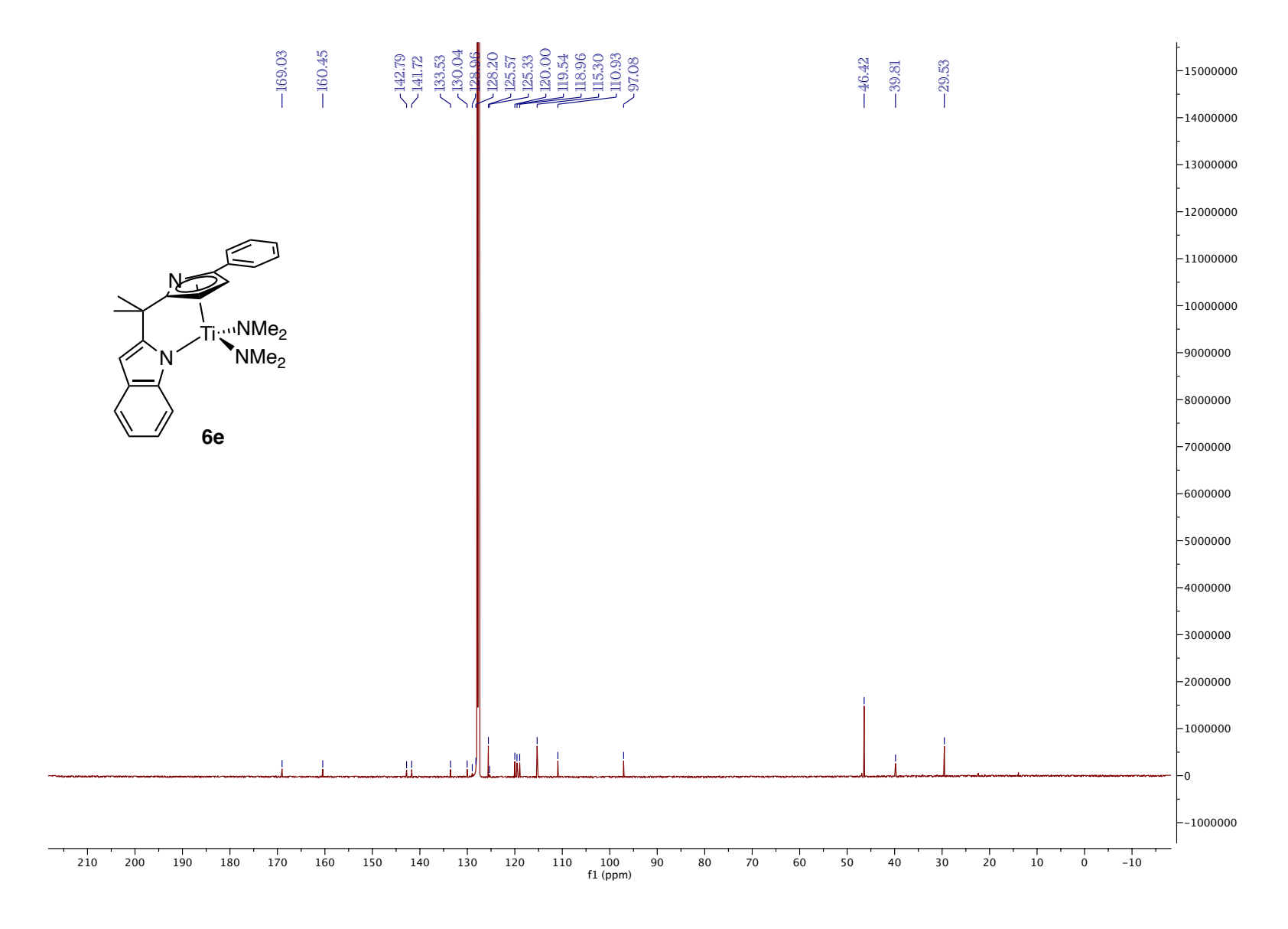


Figure 5.183. ¹³C NMR (C₆D₆, 126 MHz, 25 °C)

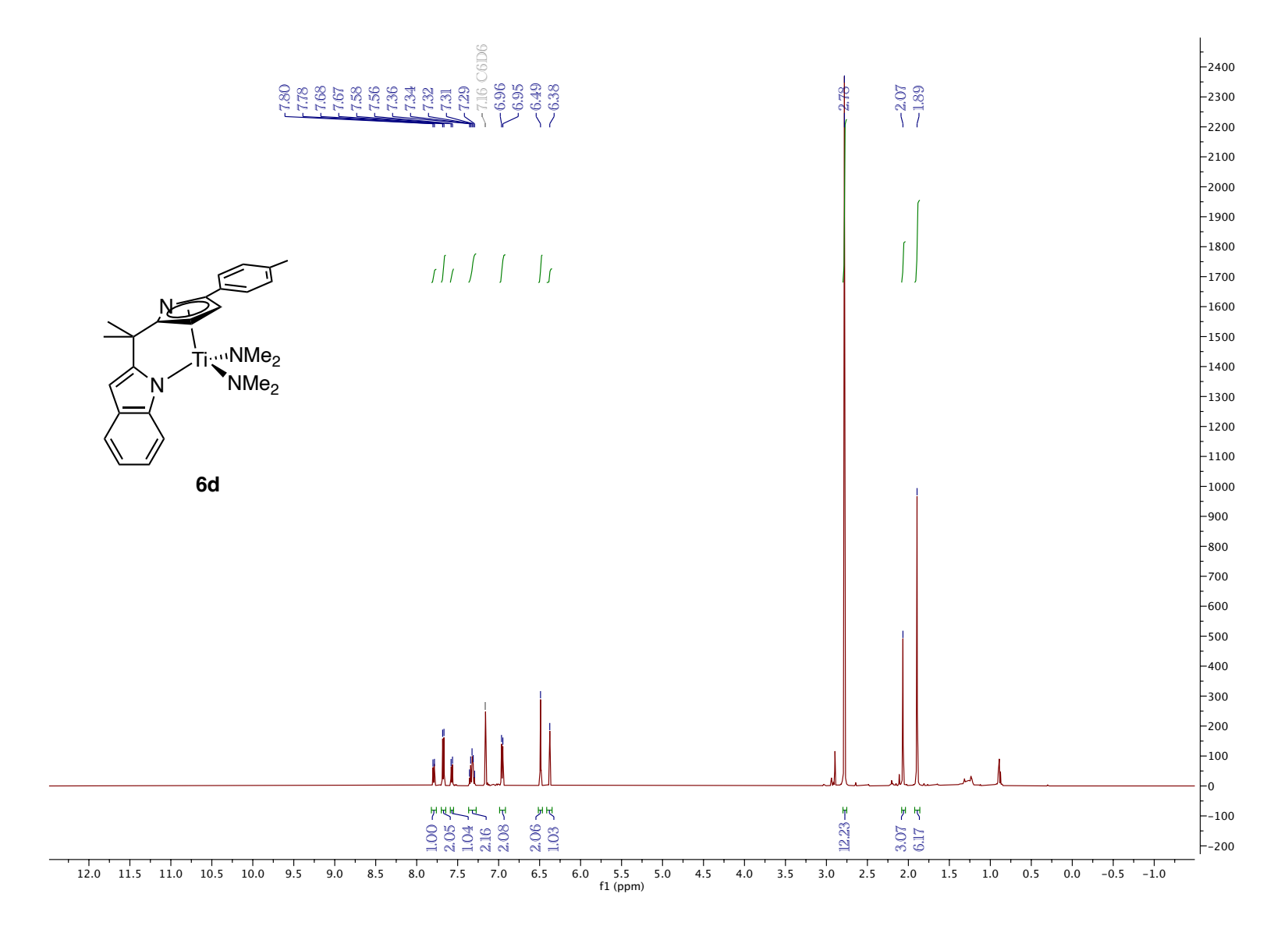


Figure 5.184. 1 H NMR (C_6D_6 , 500 MHz, 25 $^{\circ}$ C)

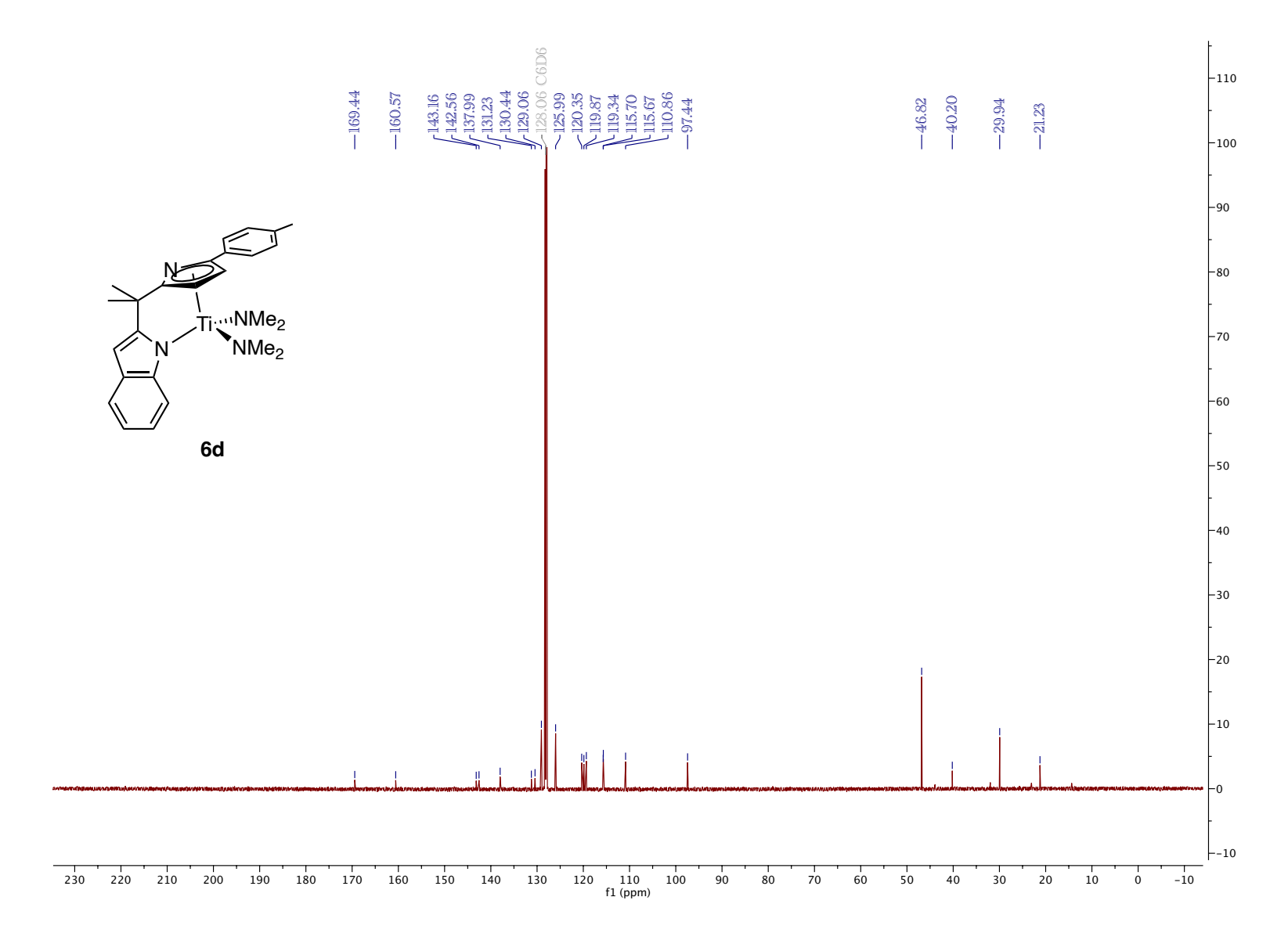


Figure 5.185. ¹³C NMR (C₆D₆, 126 MHz, 25 °C)

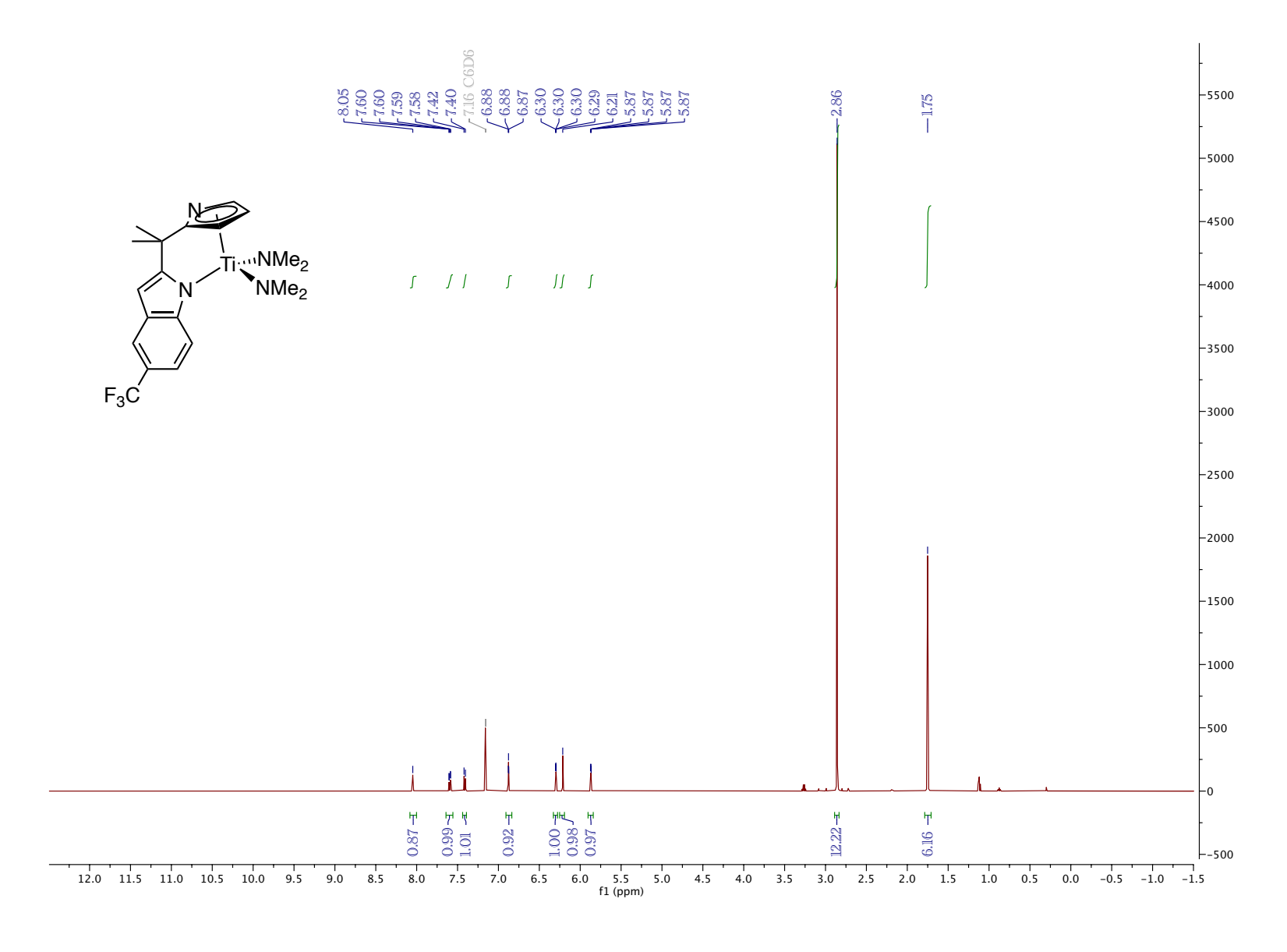


Figure 5.186. 1 H NMR (C_6D_6 , 500 MHz, 25 $^{\circ}$ C)

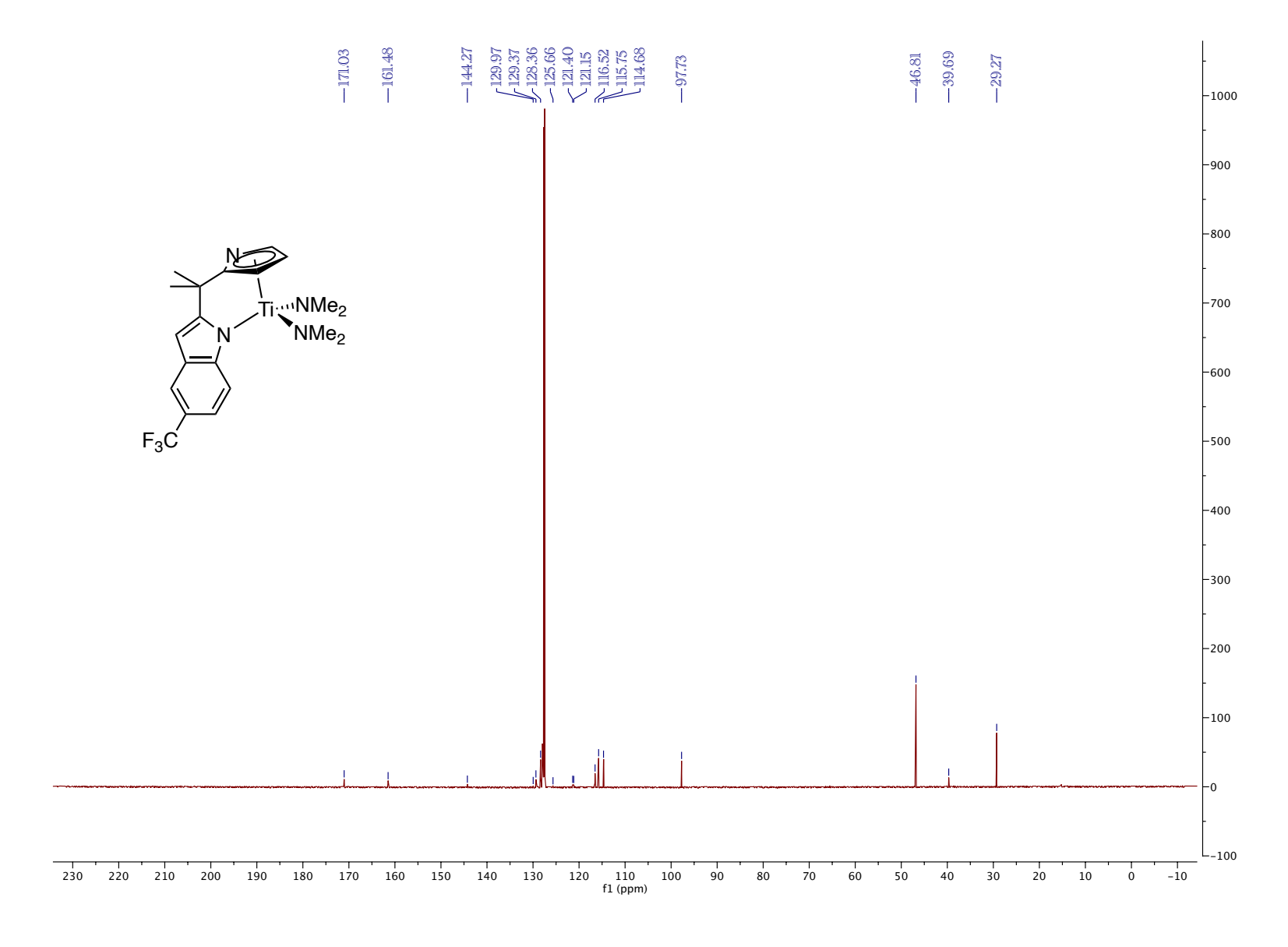


Figure 5.187. ¹³C NMR (C₆D₆, 126 MHz, 25 °C)

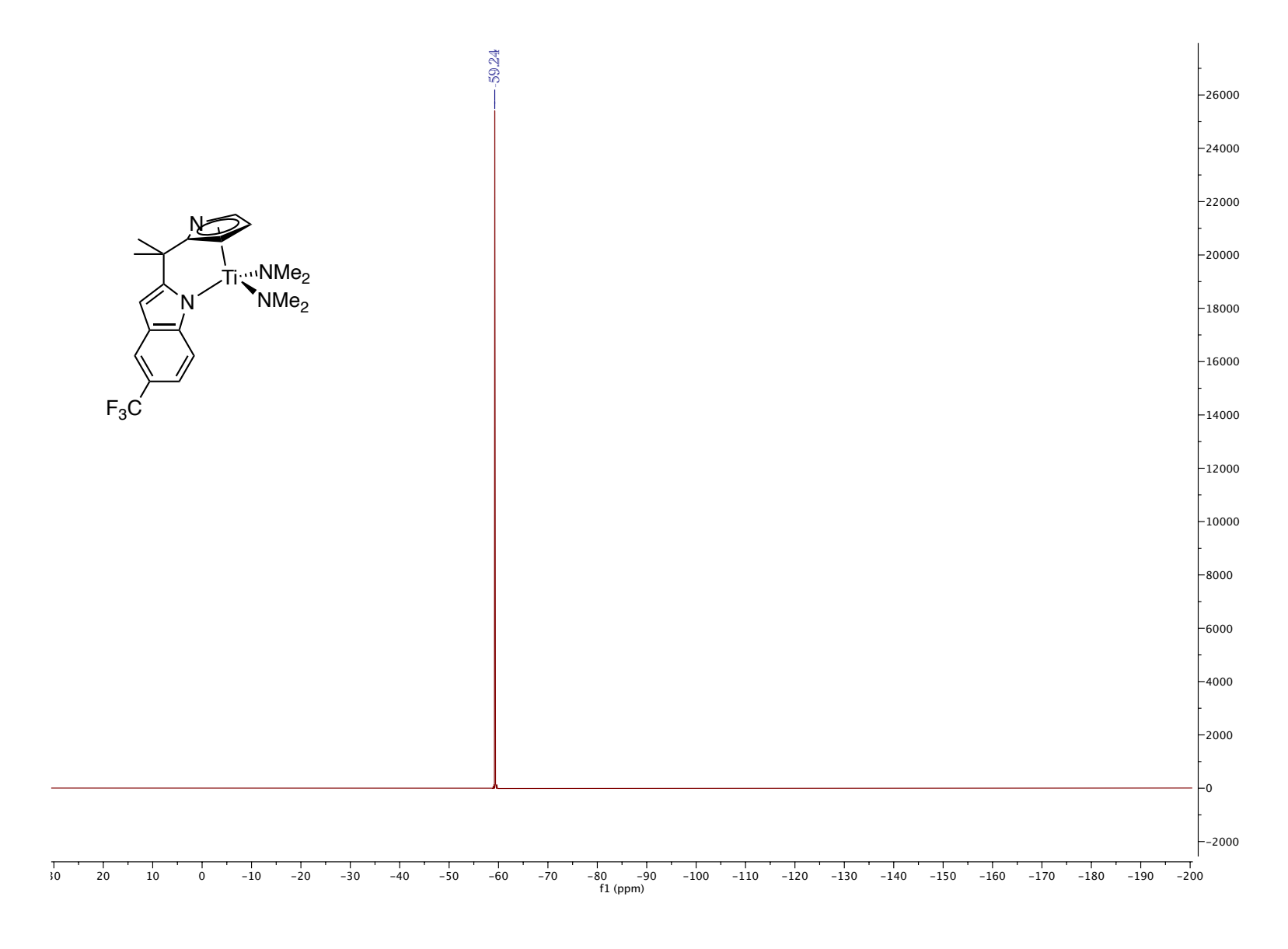


Figure 5.188. ¹⁹F NMR (470 MHz, C₆C₆, 25 °C)

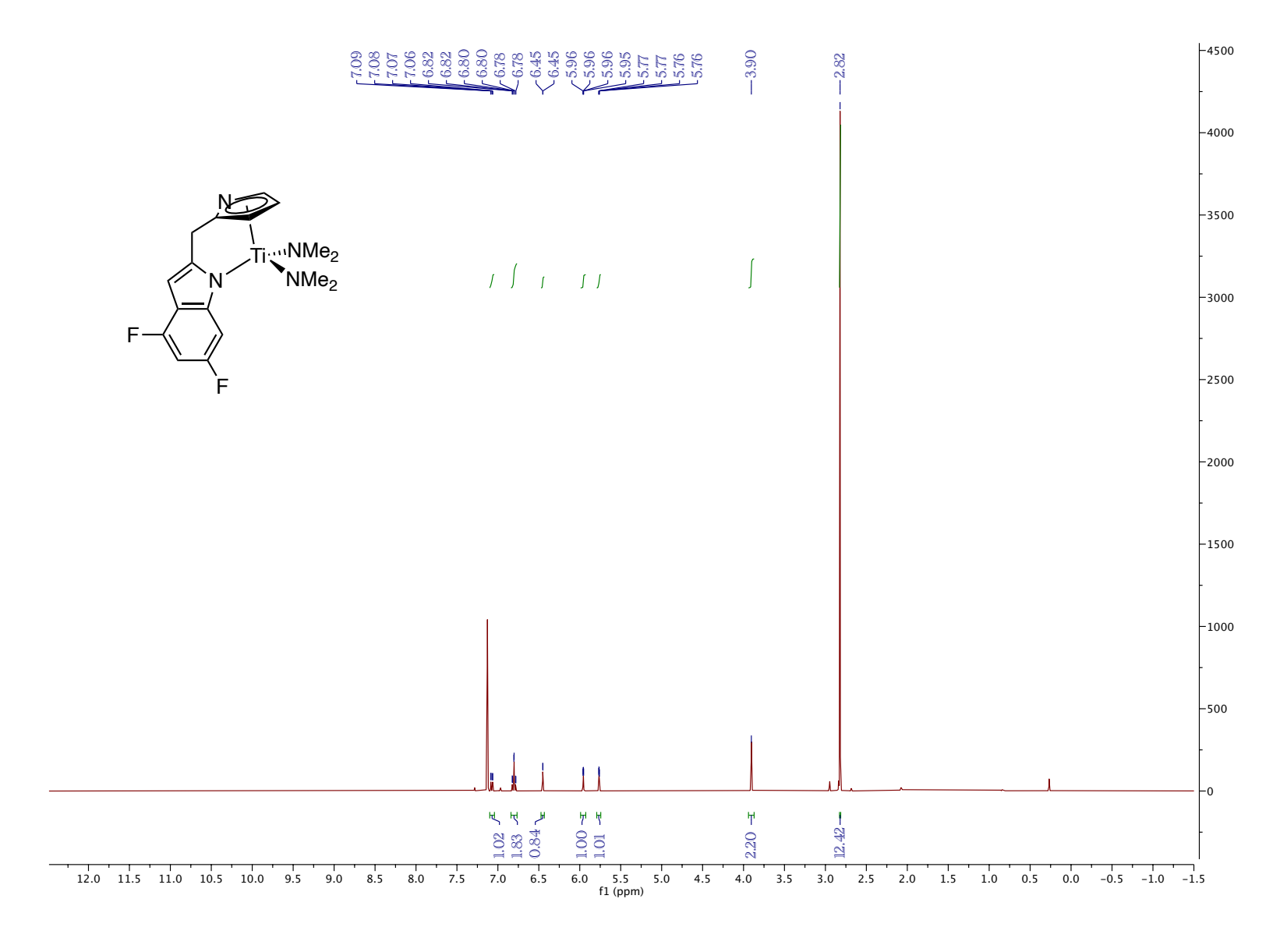


Figure 5.189. 1 H NMR (C_6D_6 , 500 MHz, 25 $^{\circ}$ C)

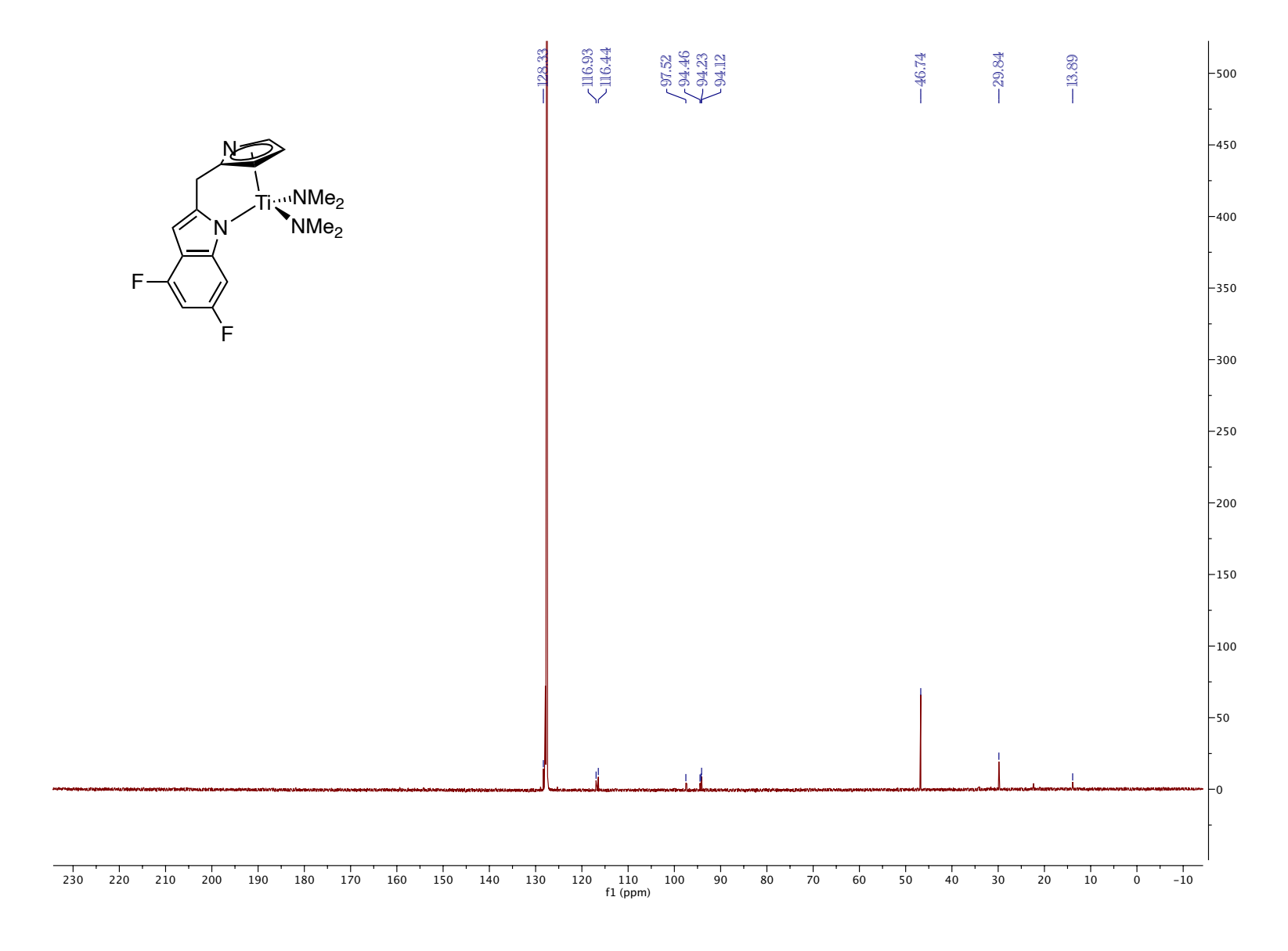


Figure 5.190. ¹³C NMR (C₆D₆, 126 MHz, 25 °C)

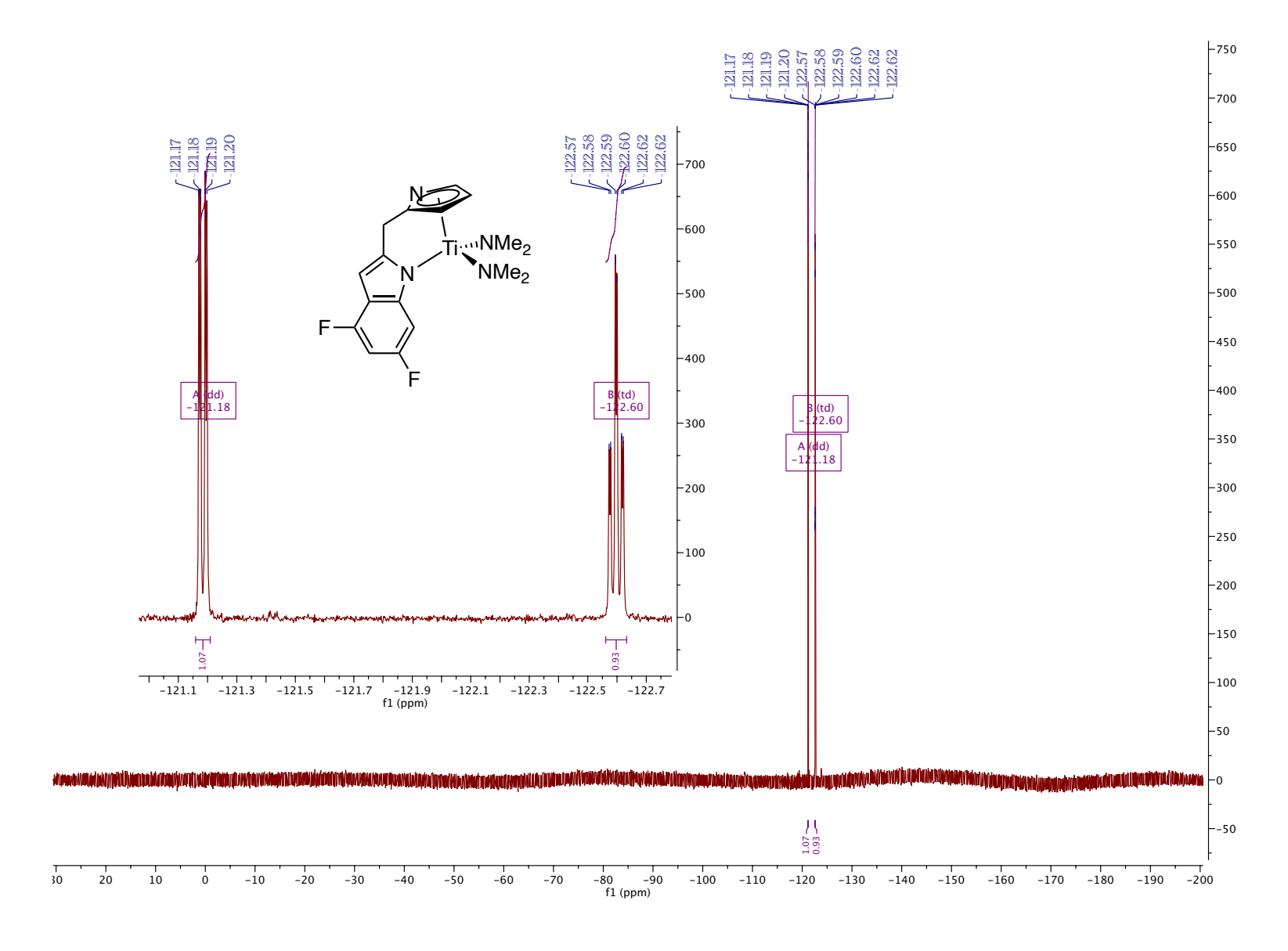


Figure 5.191. ¹⁹F NMR (470 MHz, C₆C₆, 25 °C)

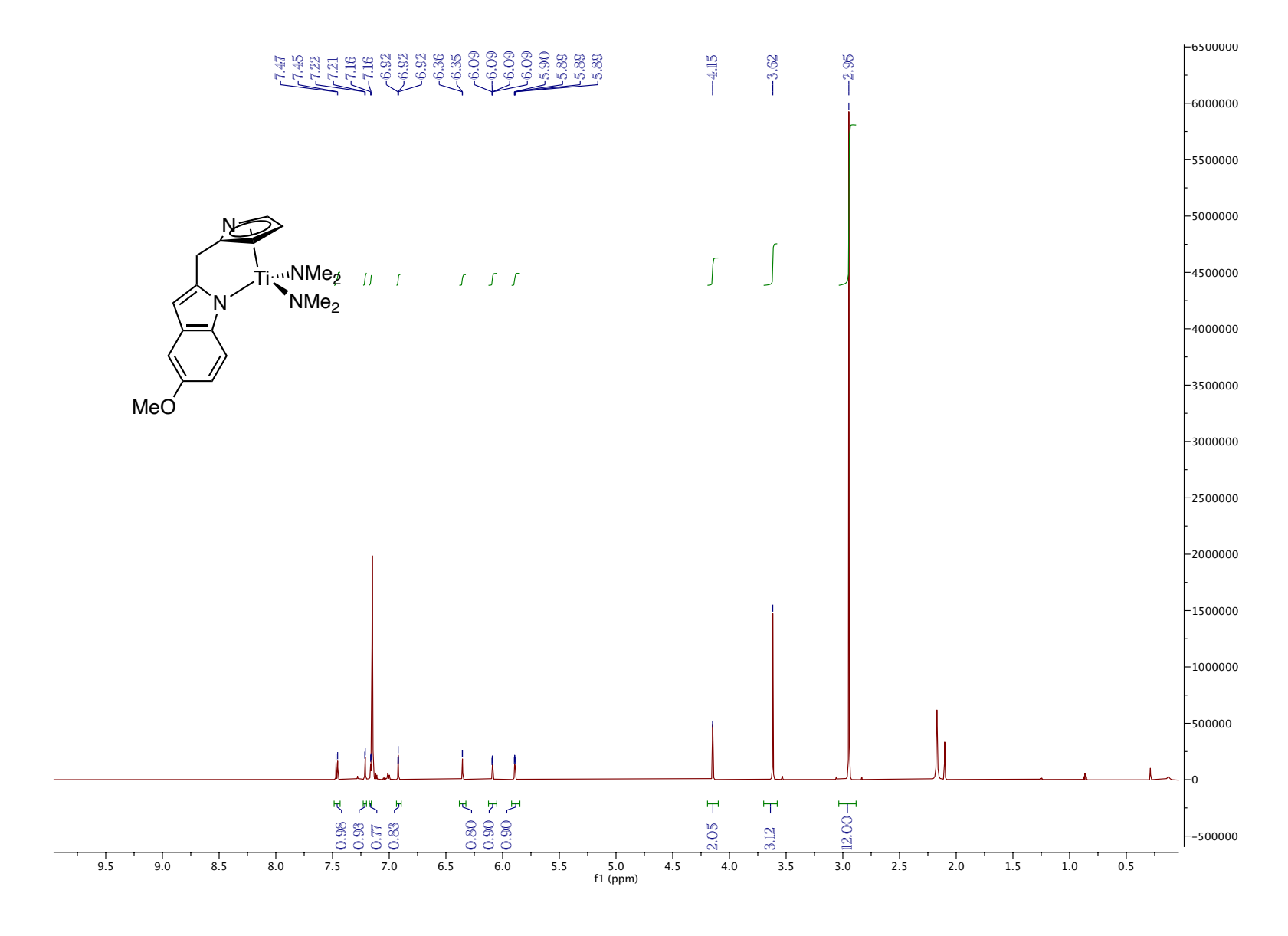


Figure 5.192. ¹H NMR (C₆D₆, 500 MHz, 25 °C)

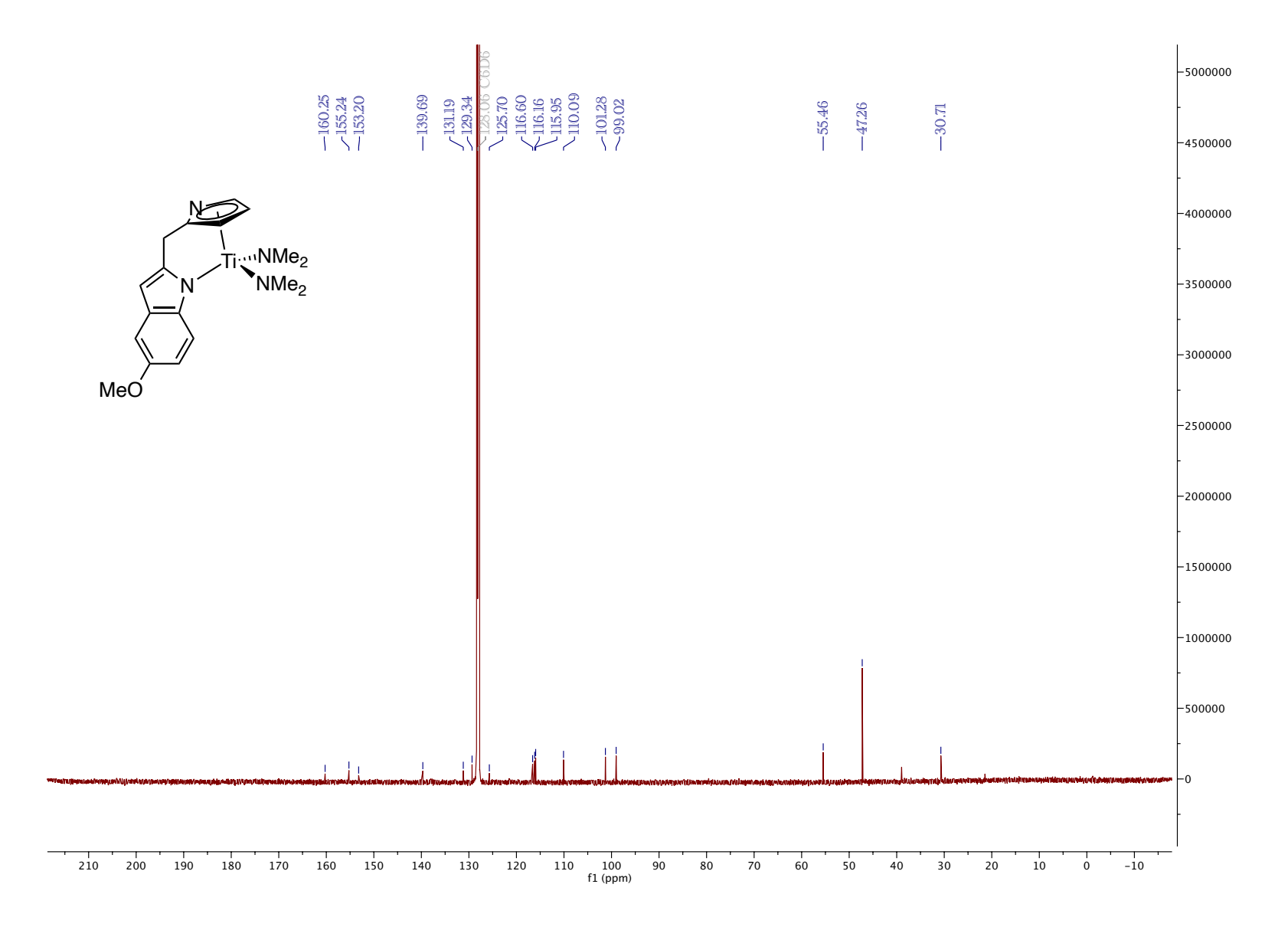


Figure 5.193. ¹³C NMR (C₆D₆, 126 MHz, 25 °C)

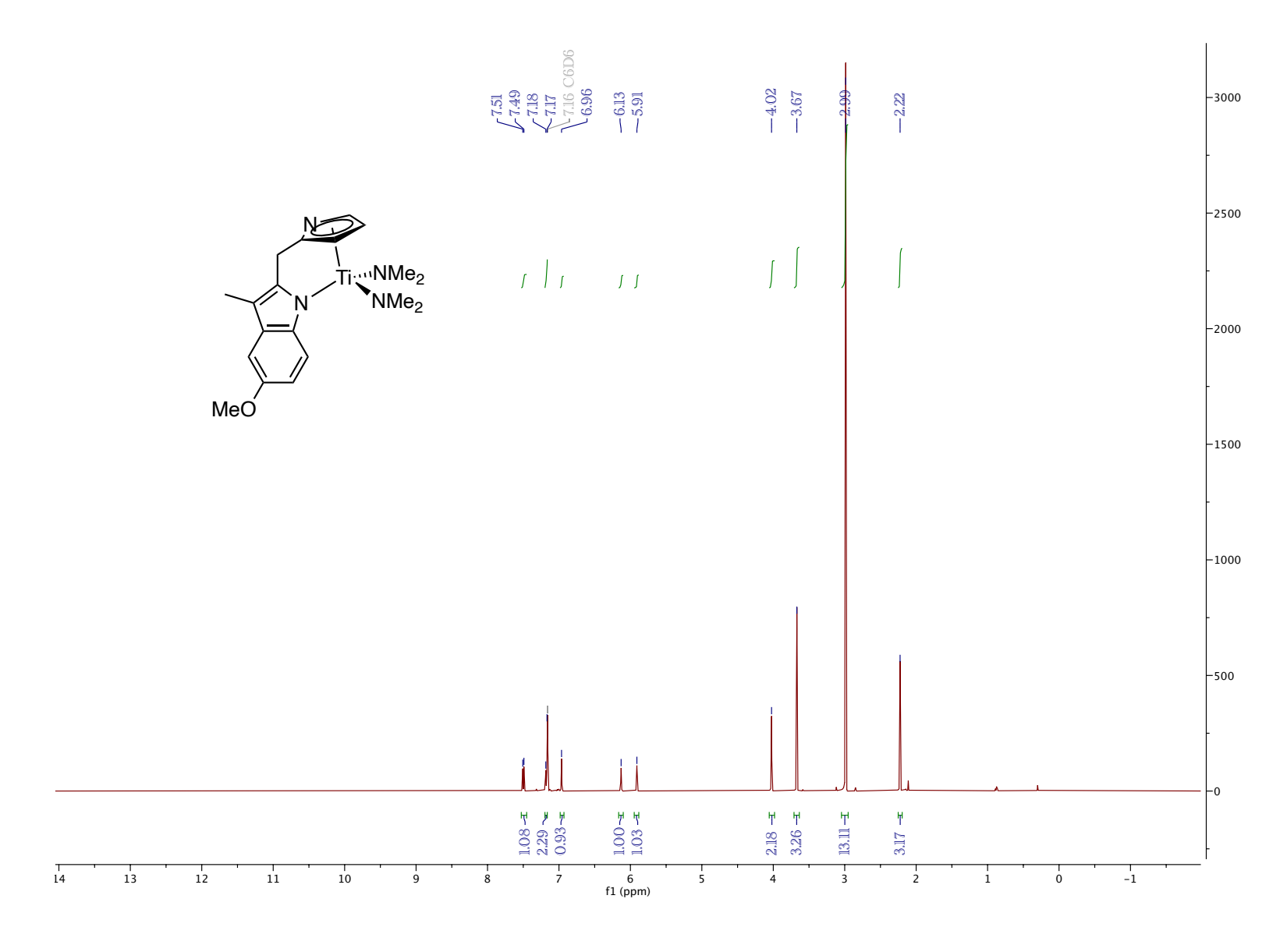


Figure 5.194. 1 H NMR (C₆D₆, 500 MHz, 25 $^{\circ}$ C)

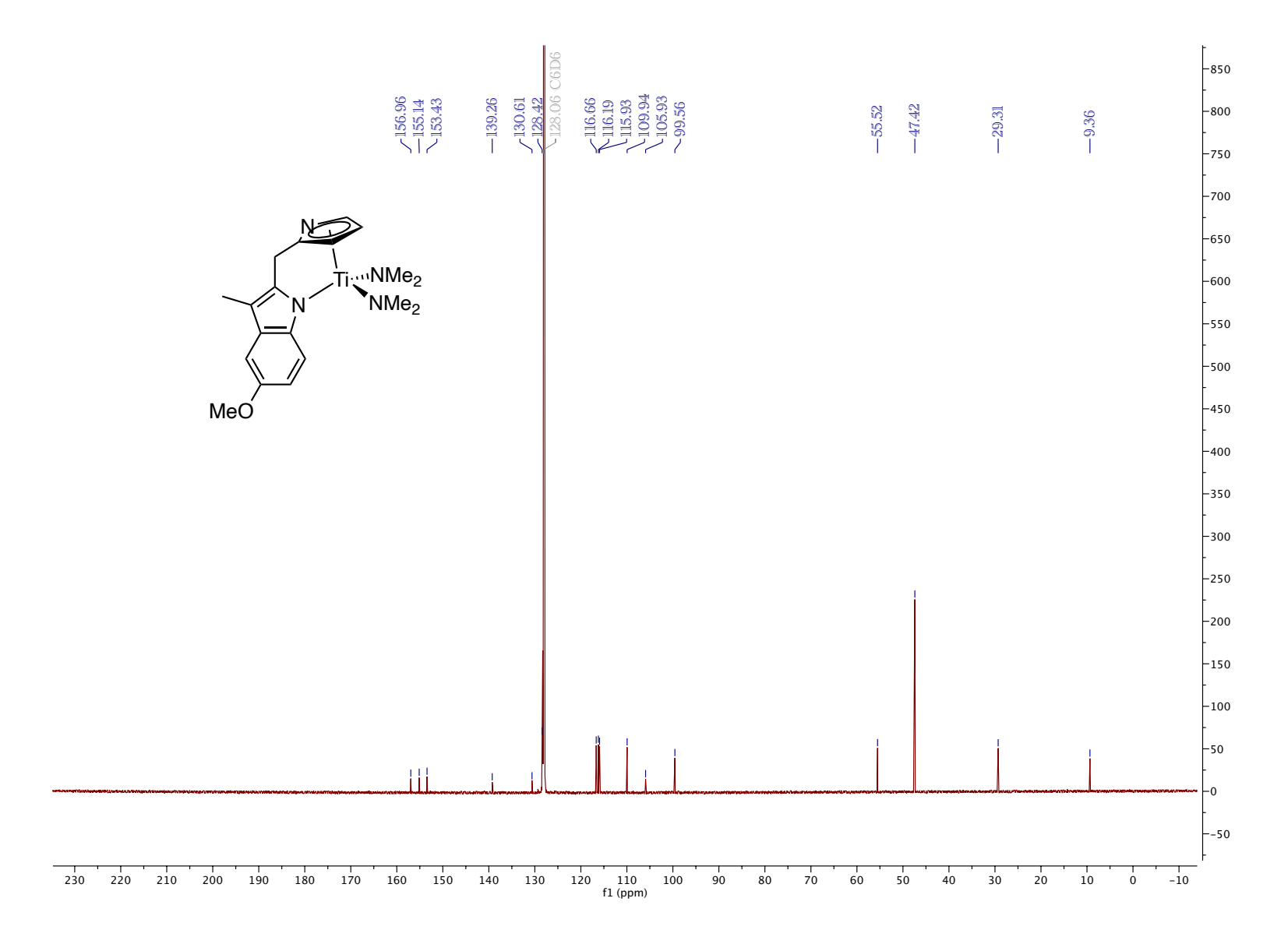


Figure 5.195. ¹³C NMR (C₆D₆, 126 MHz, 25 °C)

REFERENCES

REFERENCES

- 1. Catlow, C. R.; Davidson, M.; Hardacre, C.; Hutchings, G. J. Catalysis making the world a better place. *Philosophical Transactions of the Royal Society a-Mathematical Physical and Engineering Sciences* **2016**, *374* (2061).
- 2. Tolman, C. A. Steric effects of phosphorus ligands in organometallic chemistry and homogeneous catalysis. *Chemical Reviews* **1977**, 77 (3), 313-348.
- 3. Fernandez, A.; Reyes, C.; Prock, A.; Giering, W. P. Exploring ligand effects through isoequilibrium phenomena: The quantitative analysis of ligand effects. *Organometallics* **1998**, *17* (12), 2503-2509. Fernandez, A. L.; Reyes, C.; Prock, A.; Giering, W. P. The stereoelectronic parameters of phosphites. The quantitative analysis of ligand effects (QALE). *Journal of the Chemical Society-Perkin Transactions* **2 2000**, *5*, 1033-1041.
- 4. Delferro, M.; Marks, T. J. Multinuclear Olefin Polymerization Catalysts. *Chemical Reviews* **2011**, *111* (3), 2450-2485. Pelletier, J. D. A.; Basset, J. M. Catalysis by Design: Well-Defined Single-Site Heterogeneous Catalysts. *Accounts of Chemical Research* **2016**, *49* (4), 664-677.
- 5. Zhang, D.; Hou, Z. L.; Aldrich, K. E.; Lockwood, L.; Odom, A. L.; Liby, K. T. A Novel Nrf2 Pathway Inhibitor Sensitizes Keap1-Mutant Lung Cancer Cells to Chemotherapy. *Molecular Cancer Therapeutics* **2021**, *20* (9), 1692-1701.
- 6. DiFranco, S. A.; Maciulis, N. A.; Staples, R. J.; Batrice, R. J.; Odom, A. L. Evaluation of Donor and Steric Properties of Anionic Ligands on High Valent Transition Metals. *Inorganic Chemistry* **2012**, *51* (2), 1187-1200.
- 7. Billow, B. S.; Bemowski, R. D.; DiFranco, S. A.; Staples, R. J.; Odom, A. L. Synthesis and Structure of Chromium(VI) Nitrido Cyclopentadienyl Complexes. *Organometallics* **2015**, *34* (18), 4567-4573. Beaumier, E. P.; Billow, B. S.; Singh, A. K.; Biros, S. M.; Odom, A. L. A complex with nitrogen single, double, and triple bonds to the same chromium atom: synthesis, structure, and reactivity. *Chemical Science* **2016**, *7* (4), 2532-2536.
- 8. Bemowski, R. D.; Singh, A. K.; Bajorek, B. J.; DePorre, Y.; Odom, A. L. Effective donor abilities of E-t-Bu and EPh (E = O, S, Se, Te) to a high valent transition metal. *Dalton Transactions* **2014**, *43* (32), 12299-12305.
- 9. Billow, B. S.; McDaniel, T. J.; Odom, A. L. Quantifying ligand effects in high-oxidation-state metal catalysis. *Nature Chemistry* **2017**, *9* (9), 837-842.
- 10. Falivene, L.; Credendino, R.; Poater, A.; Petta, A.; Serra, L.; Oliva, R.; Scarano, V.; Cavallo, L. SambVca 2. A Web Tool for Analyzing Catalytic Pockets with Topographic Steric Maps. *Organometallics* **2016**, *35* (13), 2286-2293.

- 11. Odom, A. L.; McDaniel, T. J. Titanium-Catalyzed Multicomponent Couplings: Efficient One-Pot Syntheses of Nitrogen Heterocycles. *Accounts of Chemical Research* **2015**, *48* (11), 2822-2833.
- 12. Sattely, E. S.; Meek, S. J.; Malcolmson, S. J.; Schrock, R. R.; Hoveyda, A. H. Design and Stereoselective Preparation of a New Class of Chiral Olefin Metathesis Catalysts and Application to Enantioselective Synthesis of Quebrachamine: Catalyst Development Inspired by Natural Product Synthesis. *Journal of the American Chemical Society* **2009**, *131* (3), 943-953.
- 13. Shi, Y.; Hall, C.; Ciszewski, J. T.; Cao, C.; Odom, A. L. Titanium dipyrrolylmethane derivatives: rapid intermolecular alkyne hydroamination. *Chemical Communications* **2003**, (5), 586-587.
- 14. Ishiyama, T.; Takagi, J.; Yonekawa, Y.; Hartwig, J. F.; Miyaura, N. Iridium-catalyzed direct borylation of five-membered heteroarenes by bis(pinacolato)diboron: Regioselective, stoichiometric, and room temperature reactions. *Advanced Synthesis & Catalysis* **2003**, *345* (9-10), 1103-1106.
- 15. Cuny, G. D.; Yu, P. B.; Laha, J. K.; Xing, X.; Liu, J.-F.; Lai, C. S.; Deng, D. Y.; Sachidanandan, C.; Bloch, K. D.; Peterson, R. T. Structure–activity relationship study of bone morphogenetic protein (BMP) signaling inhibitors. *Bioorganic & Medicinal Chemistry Letters* **2008**, *18* (15), 4388-4392.
- 16. Loughlin, W. A.; Jenkins, I. D.; Karis, N. D.; Schweiker, S. S.; Healy, P. C. 2-Oxo-1,2-dihydropyridinyl-3-yl amide-based GPa inhibitors: Design, synthesis and structure-activity relationship study. *European Journal of Medicinal Chemistry* **2016**, *111*, 1-14.
- 17. Fu, J.; Wurzer, N.; Lehner, V.; Reiser, O.; Davies, H. M. L. Rh(II)-Catalyzed Monocyclopropanation of Pyrroles and Its Application to the Synthesis Pharmaceutically Relevant Compounds. *Organic Letters* **2019**, *21* (15), 6102-6106.
- 18. Xu, J.; Rawal, V. H. Total Synthesis of (-)-Ambiguine P. *Journal of the American Chemical Society* **2019**, *141* (12), 4820-4823.
- 19. Gowri Sreedevi, K. C.; Thomas, A. P.; Salini, P. S.; Ramakrishnan, S.; Anju, K. S.; Derry Holaday, M. G.; Reddy, M. L. P.; Suresh, C. H.; Srinivasan, A. 5,5-Diaryldipyrromethanes: syntheses and anion binding properties. *Tetrahedron Letters* **2011**, *52* (45), 5995-5999.
- 20. Walsh, P. J.; Baranger, A. M.; Bergman, R. G. Stoichiometric and catalytic hydroamination of alkynes and allene by zirconium bisamides Cp2Zr(NHR)2. *Journal of the American Chemical Society* **1992**, *114* (5), 1708-1719.
- 21. Du, P.; Zhao, J. Y. Comparative DFT study of metal-free Lewis acid-catalyzed C-H and N-H silylation of (hetero)arenes: mechanistic studies and expansion of catalyst and substrate scope. *Rsc Advances* **2019**, *9* (64), 37675-37685.

- 22. Pohlki, F.; Doye, S. The mechanism of the Cp2TiMe2 -catalyzed intermolecular hydroamination of alkynes. *Angewandte Chemie-International Edition* **2001**, *40* (12), 2305-+.
- 23. Robertson, W. M.; Kastrinsky, D. B.; Hwang, I.; Boger, D. L. Synthesis and evaluation of a series of C5'-substituted duocarmycin SA analogs. *Bioorganic & Medicinal Chemistry Letters* **2010**, *20* (9), 2722-2725.
- 24. Espenson, J. H. Chemical kinetics and reaction mechanisms; McGraw Hill, 2002.